UNIVERSIDADE D
COIMBRA

Beatriz Theresa Ruth Büschbell

CHARACTERIZATION OF PROTEIN-PROTEIN INTERACTIONS INVOLVING G PROTEIN-COUPLED RECEPTOR 143 BY COMPUTATIONAL AND PHARMACOLOGICAL METHODS

VOLUME 1

Doctoral Thesis submitted for the PhD degree in Experimental Biology and Biomedicine - Development of Cellular and Molecular Biology supervised by Professor Irina de Sousa Moreira, PD Dr. Anke C. Schiedel and Professor Prashiela Manga and presented to the Institute of Interdisciplinary Research of the University of Coimbra

August 2023

Institute of Interdisciplinary Research of the University of Coimbra

CHARACTERIZATION OF PROTEIN-PROTEIN INTERACTIONS INVOLVING G PROTEIN-COUPLED RECEPTOR 143 BY COMPUTATIONAL AND PHARMACOLOGICAL METHODS

Beatriz Theresa Ruth Büschbell

Doctoral Thesis submitted for the PhD degree in Experimental Biology and Biomedicine - Development of Cellular and Molecular Biology supervised by Professor Irina de Sousa Moreira, PD Dr. Anke C. Schiedel and Professor Prashiela Manga and presented to the Institute of Interdisciplinary Research of the University of Coimbra

VOLUME 1

August 2023

UNIVERSIDADE D
COIMBRA

STATEMENT OF INTEGRITY

I declare that I have conducted this academic work with integrity. I confirm that I have not used plagiarism or any form of undue use of information or falsification of results along the process leading to its elaboration.

I further declare that I have fully acknowledged the Code of Ethical Conduct of Universidade de Coimbra.

Acknowledgements

I would first like to thank the Fundação para a Ciência e Tecnologia for the PhD scholarship I was awarded (SFRH/BD/149709/2019), without which this work would not be possible.

I also thank my main host institution, the Center for Innovative Biomedicine and Biotechnology, the Institute for Interdisciplinary Research, and the PhD Program for Experimental Biology and Biomedicine.

In addition, I would like to thank my secondary host institution, the Department of Pharmaceutical & Medicinal Chemistry at the Pharmaceutical Institute in Bonn, for granting me access to their laboratories, which special thanks to Christa E. Müller.

Furthermore, I would like to thank the European Regional Development Fund, COMPETE2020 – Operational Program for Competitiveness and Internationalization and the Fundação para a Ciência e Tecnologia which supported the contributions of my supervisor Dr. Irina S. Moreira and my co-authors during this time: LA/P/0058/2020, UIDB/04539/2020, UIDP/04539/2020, PTDC/QUI- OUT/32243/2017, DSAIPA/DS/0118/2020, UIDB/04046/2020, UIDP/04046/2020,, CEECIND/02300/2017, SFRH/BD/145457/2019 and the German Federal Ministry of Education and Research (BMBF) for supporting my supervisor PD Dr. Anke C. Schiedel.

In addition, I would like to thank the Laboratory for Advanced Computing at the University of Coimbra for providing access to the computing cluster. Parts of this work were conducted under the Advanced Computing Project CPCA/A2/7219/2020, which I also thank for their support.

I wish to express my deepest gratitude to my three supervisors Dr. Irina S. Moreira, PD Dr. Anke C. Schiedel and Dr. Prashiela Manga for supporting me during this time and always providing help and expertise whenever needed. I thank them all for offering this opportunity and working together throughout this project.

I would also like to thank all of my colleagues from the Moreira Lab and the Schiedel Lab for the cheerful and productive working environment and for all the help with the experiments, useful comments and the great time we had together.

I would like to thank Andhika B. Mahradhika for cloning and sharing the pE-YFP-N1-GPR18.
I would also like to thank Dr. Miguel Machuqueiro and Pedro R. Magalhães for having me in their lab and for the help with the analysis of chapter 3.2.

I would like to thank Agnieszka A. Kaczor for sharing the tcl script and Tiago Barbosa for his help with scripting parts of the analysis workflow.

Finally, I thank my family and friends for their encouragement. Knowing that I always had their back in any situation, their endless love and support have made these 3.5 years really special for me.

Resumo

Os recetores acoplados à proteína G (GPCRs) desempenham funções críticas no desenvolvimento e progressão de diversas patologias. Muitos membros da família GPCR são expressos no cérebro e exercem as suas funções através de neurotransmissores conhecidos, como a dopamina, a noradrenalina e outras moléculas. Também têm sido considerados determinantes estruturais e biológicos de doenças neurodegenerativas.

Para além do facto de que GPCRs individuais podem contribuir para condições patológicas através de desregulação ou ativação aberrante, agora é amplamente aceite que os GPCRs são capazes de formar homodímeros e heterodímeros funcionais, bem como oligómeros que consistem em mais de dois recetores. A interação e comunicação cruzada, também denominadas interações proteína-proteína (PPIs), levam a mudanças nas vias de sinalização e resultados fisiológicos complexos. Estas PPIs também foram relatadas como tendo um impacto significativo nos processos de doença.

Neste estudo, foram investigados dois tipos de GPCRs, ambos provavelmente relevantes para condições neurológicas e patologias consequentes: o recetor de dopamina D2 (D_2R) e o recetor acoplado à proteína G 143 (GPR143). Embora os recetores de dopamina, especialmente o D2R, tenham sido correlacionados com muitas doenças neurológicas e neurodegenerativas, a função precisa do órfão GPR143 ainda não foi descoberta.

Determinámos uma PPI relevante entre o GPR143 e os recetores de dopamina (DR), especialmente o D_2R e o D_3R, e mostrámos que o GPR143 modula negativamente a atividade do DR em resposta à dopamina. Além disso, fomos capazes de localizar complexos GPR143-DR em vesículas intracelulares. Este efeito não foi influenciado pela coexpressão de GPR143, que geralmente não é encontrado na membrana plasmática, ou pela variante GPR143 localizada na membrana plasmática, pmGPR143, quando coexpressa. Estudámos o efeito do GPR143 nos DRs através do recrutamento de β-arrestina e visualizámos os complexos utilizando Transferência de Energia de Ressonância de Fluorescência (FRET).

Seguidamente, estudámos a homodimerização PPI do conhecido alvo D_2R. Foi relatado que os homodímeros D2R estão envolvidos no desenvolvimento de esquizofrenia e no stress de derrota social. Construímos diferentes configurações de homodímeros D_2R, onde os monómeros tinham conformações diferentes, por exemplo, ativa (ligada ao agonista de D_2R bromocriptina), inativa e ligada à β-arrestina. Depois de construir uma pipeline computacional para gerar os dímeros de GPCR, os modelos de homodímeros D_2R foram submetidos a simulações de dinâmica molecular. A partir destas simulações, pudemos concluir que os domínios transmembranares 4 e 5 (TM4 e TM5, respetivamente) são os mais proeminentes na interface do dímero. Além disso, identificámos um subconjunto de resíduos-chave que eram principalmente apolares em

TM4 e TM5. Outros TMs, como o TM2 e o TM3, também se mostraram relevantes para certas combinações de monómeros D_2R. Para algumas configurações, a conformação inativa de um monómero levaria a uma mudança da conformação ativa para inativa do seu recetor parceiro. Também observámos que a conformação β-arrestina apresentaria propriedades de um recetor ativo, mesmo na ausência de um agonista, quando complexada com outro recetor. Sugerimos que este comportamento reflete uma mudança para outro meta-estado após a dimerização. Os resultados deste estudo computacional são consistentes com os dados experimentais.

No geral, este estudo fornece informações profundas sobre a dimerização de GPCRs no contexto de problemas neurológicos. Conseguimos elucidar a arquitetura dos homodímeros D_2R de uma perspetiva computacional. Além disso, determinámos as funções potenciais do GPR143 na sinalização dopaminérgica usando PPIs determinados experimentalmente. Os nossos resultados sobre a dimerização de GPCRs são promissores como novas oportunidades para o desenvolvimento futuro de medicamentos para doenças neurodegenerativas.

Palavras-chave: Doenças neurodegenerativas, receptores acoplados à proteína G (GPCRs), receptores de dopamina, D_2R, D_3R, receptor acoplado à proteína G 143, doença de Parkinson, interações proteína-proteína, interface dímero, homodímeros, cross-talk, seletividade, classe A, classe C.

Abstract

G protein-coupled receptors (GPCRs) play a critical role in the development and progression of various pathologies. Many members of the GPCR family are expressed in the brain and exert their functions through known neurotransmitters, such as dopamine and noradrenaline. They have also been considered structural and biological determinants of neurodegenerative diseases.

Apart from the fact that single GPCRs can contribute to pathological conditions through dysregulation or aberrant activation, it is now widely accepted that GPCR can form functional homo- and heterodimers, as well as oligomers consisting of more than two receptors. Crosstalk and interaction, also termed protein-protein interactions (PPIs), lead to changes in signaling pathways and complex physiological outcomes. Such PPIs have also been reported to have a significant impact on disease progression.

In this study, two types of GPCRs were investigated, both of which are probably relevant to neurological conditions and consequent pathologies: dopamine receptor D2 (D_2R) and G protein-coupled receptor 143 (GPR143). While dopamine receptors, especially D2R, have been correlated with many neurological and neurodegenerative diseases, the precise role of orphan GPR143 is yet to be discovered.

We determined a relevant PPI between GPR143 and dopamine receptors (DR), especially D_2R and D_3R, and showed that GPR143 negatively modulated DR activity in response to dopamine. Moreover, we were able to localize GPR143-DR-complexes in vesicles of the intracellular vesicles. This effect was not influenced by co-expression of wild-type GPR143, which is usually not found in the plasma membrane, or the plasma membrane-localized GPR143 variant pmGPR143. We studied the effect of GPR143 on DRs via β-arrestin recruitment and visualized the complexes using Fluorescence Resonance Energy Transfer (FRET).

Next, we studied PPI homodimerization of the well-known target D_2R. D_2R homodimers have been reported to be involved in the development of schizophrenia and social defeat stress. We constructed different setups of D_2R homodimers, where the protomers had different conformations, such as active (bound to the D_2R-agonist bromocriptine), inactive, and β-arrestin-bound. After constructing a computational pipeline for generating, scoring, and docking GPCR dimers, D2R homodimer models were subjected to molecular dynamics simulations. From these simulations, we can conclude that transmembrane domains 4 and 5 (TM4 and TM5, respectively) were the most prominent at the dimer interface. Furthermore, we identified a subset of key residues that were mostly non-polar in TM4 and TM5. Other TMs such as TM2 and TM3 are also relevant to certain combinations of D2R-monomers. In some setups, the inactive conformation of a protomer leads to a switch from the active to the inactive conformation of its partnered receptor. We also observed that the β-arrestin conformation would display the properties

of an active receptor, even in the absence of an agonist, when complexed with another receptor. We suggest that this behavior reflects a switch to another meta-state upon dimerization. The findings of this computational study are consistent with the experimental data.

Taken together, this study provides profound insights into GPCR dimerization in the context of neurological disorders. We elucidated the architecture of D_2R homodimers from a computational perspective. Furthermore, we determined the potential role of GPR143 in dopaminergic signaling using experimentally determined PPIs. Our results on GPCR dimerization hold promise as novel opportunities for future drug development for neurodegenerative diseases.

Keywords: Neurodegenerative diseases, G protein-coupled receptors (GPCRs), dopamine receptors, D_2R, D_3R, G protein-coupled receptor 143, Parkinson's disease, protein-protein interactions, dimer interface, homodimers, cross-talk, selectivity, class A, class C.

Table of contents

Acronyms

3D – Three-dimensional
5HT - 5-hydroxytryptamine
Ab – Amyloid b
AC – Adenylate cyclase
AD – Alzheimer's disease
ADH – Antidiuretic hormone
ADHD – Attention deficit hyperactivity disorder
AR – Adenosine receptors
ASD – Autism spectrum disorder
ATP – Adenosine triphosphate
BD – Brownian dynamics
BiFC – Biomolecular fluorescence complementation
BRET – Bioluminescence resonance energy transfer
BSA – Bovine serum albumin
CaMKIIa – Calcium/calmodulin kinase IIa
cAMP – cyclic adenosine monophosphate
CaSR – Calcium-sensing receptor
CCK – Cholecystokinin
CFP – Cyan fluorescent protein
CHO – Chinese Hamster Ovary
CNS – Central nervous system
Co-IP – Co-immunoprecipitation
CRD – Cysteine rich domain
CREB – cAMP response element-binding protein
Cryo-EM – Cryogenic electron microscopy
CUD – Cannabis use disorder
DFT – Density Functional Theory
DMEM – Dulbecco's modified eagle medium
DMSO – Dimethyl sulfoxid
DR – Dopamine receptor
D_2R/DRD_2 – Dopamine receptor D2
D_3R/DRD_3 – Dopamine receptor D3
ECL1-3 – Extracellular loop 1-3
ECS – Endocannabinoid system
EPSC – Excitatory postsynaptic current
ERK – Extracellular signal-regulated kinase
FEP – Free-energy perturbation
FDA – Food and drug administration
FF – Force field
FFR – far red fluorescent protein
FFT – Fourier transform algorithm
FK – Forskolin

FLIM-FRET - Fluorescence lifetime-imaging-microscopy-based fluorescence resonance energy transfer
FRET – Fluorescence/Förster Resonance Energy Transfer
FTD – Frontotemporal dementia
FUS – fused in sarcoma
FZD – Frizzeled receptor family
GA – Generic algorithm
GABA - γ-Aminobutyric acid
GAL – Galanin
GASP – GPCR-associated sorting protein
GFP – Green fluorescent protein
GHS-R – Growth Hormone Secretagogue Receptor
GIP – GPCR interacting protein
GPCR – G protein-coupled receptor
GPR143 – G protein-coupled receptor 143
GRAFS – Glutamate, Rhodopsin, Adhesion, Frizzeled/Taste, Smoothened families
HEK – Human embryonic kidney
HD – Huntington's disease
HR – Histamine receptor
HRP – Horseradish peroxidase
HTS – High-throughput screenings
ICL1-3 – Intracellular loop 1-3
IFP – infra-red fluorescent protein
IGF-1 – Insulin-like growth factor 1
KO – knockout
L-DOPA – Levodopa
LIE – Linear interaction energy
MAP – Mitogen-activated protein
MAPK – Mitogen-activated protein kinase
MART-1 – Melanoma antigen recognized by T cells-1
MC – Monte Carlo
MD – Molecular Dynamic
MDD – Major depressive disorder
MITF - Microphthalmia transcription factor
MM – Molecular mechanics
MOR – Mor-opioid receptor
MS – Multiple sclerosis
MT – Melatonin
NAc – Nucleus accumbens
NAM – Negative allosteric modulator
NMDA - N-Methyl-D-Aspartate
NMR – Nuclear magnetic resonance
NOP – Nociceptin receptor
NT – Neurotensin
OA1 – Ocular albinism type 1
OCD – Obsessive-compulsive disorder
OR – Opioid receptor

OT – Oxytocin
PAM – Positive allosteric modulator
PBS – Phosphate-buffered saline
PD – Parkinson’s Disease
PDB – Protein data bank
PDZ - PSD-95/Discs-large/ZO-1 domain-containing protein
PFC – Prefrontal cortex
PKA – Proteinkinase A
PLA – Proximity ligation assay
PLC – Phospholipase C
PME – Particle Mesh Ewald
PMEL – Premelanosome protein
PNS – Peripheral nervous system
PPD – Protein-protein docking
PPI – Protein-protein interaction
QM – Quantum mechanics
R – Receptor
RAAS – Renin-Angiotensin-Aldosterone-System
RAMH – (R)-α-methylhistamine
RFD – Red fluorescent protein
RMSD – Root-mean-square-distance
ROI – Region of interest
SASA – Solvent-accessible surface area
SCN – Suprachiasmatic nucleus
SMO – Smoothened receptor family
SPME – Smooth Particle Mesh Ewald
SST – Somatostatin
TAAR – Trace amine-associated receptor
TDP-43 – Transactive response DNA-binding protein
THC - Δ-tetrahydrocannabinol
TM – Transmembrane helix
TrkBR – Tyrosine protein kinase B receptor
VaD – Vascular dementia
VFT – Venus flytrap
VTA – Ventral tegmental area
YFP – Yellow fluorescent protein

List of Figures

List of Tables

List of Equations

Chapter 1: Introduction

This chapter is an unmodified version of a review article published in Current Neuropharmacology, written in co-authorship with Ana B. Caniceiro, Anke C. Schiedel and Irina S. Moreira. The manuscript was up-to-date at the time of submission (March 2022).

1.1. Biological Background: Class A and Class C dimers in neurodegenerative diseases

1.1.1. Scope of review

Neurodegenerative diseases, characterized by progressive neuronal dysfunction, toxicity and death [1] are prevalent among the worldwide elderly population [2]. These diseases cause irreversible damage to all types of brain functions and it is estimated that over 30 million individuals suffer from them worldwide [3,4]. Parkinson's disease (PD), Alzheimer's disease (AD), Vascular dementia (VaD), Frontotemporal dementia (FTD), and Huntington's disease (HD) are the most prevailing ones [5,6]. Among those, AD and PD have an earlier average onset between 50 and 60 years [5,7,8].

Impaired cognitive function, memory loss and negative personality are common traits associated with people suffering from AD [9–11]. The accumulation of amyloid b (Ab) in amyloid plaques and hyperphosphorylated aggregates of the microtubule-associated protein tau in neurofibrillary tangles, which slowly progress from the frontal and temporal lobes to other areas of the neocortex are the pathological features observed in AD patient [9].

PD is predominantly characterized by motor impairments such as bradykinesia, rigidity, tremor and gait disorder [12]. Also non-motor impairments like cognitive impairment and neuropsychiatric symptoms are observed among PD patients [12]. The pathology of PD has been well-studied over the years. The loss of dopaminergic neurons in the substantia nigra is the major feature observed in PD patients, but also the deposition of Lewy bodies and abnormal aggregates of the a-synuclein protein in several brain regions, such as the substantia nigra and temporal cortex, have been described to play a role in PD [12].

In contrast to AD, VaD has a variable onset age and is the second most common cause of dementia [5]. Disturbance in the frontal executive function and multiple cerebral pathologies including arteriosclerosis and various forms of arteritis, aneurysms or vessel occlusion are characteristic for VaD [13,14]. Under the age of 65, FTD is known to be the mayor responsible for dementia [5,15]. FTD patients display neuropsychiatric symptoms and cognitive, motor and behavioral impairments as well as the abnormal

deposition of the three major proteins tau, transactive response DNA-binding protein 43 (TDP-43) and fused in sarcoma (FUS) protein in the brain [16].

As for PD, HD symptoms can be divided into motor and non-motor symptoms such as chorea, bradykinesia, impaired coordination, rigidity, which are motor symptoms, whereas depression and slowed cognitive function are described as non-motor symptoms [17]. The root-cause of HD is genetic, unlike the other diseases described here. HD is caused by a CAG trinucleotide repeat expansion in the *Huntingtin (Htt)* gene [5,17]. In unaffected individuals the CAG repeats vary from 6 to 35 nucleotides, while > 36 repeats are present in HD patients [18]. The number of repeats inversely correlates with the age of onset [5,18]. Consequently, Huntingtin protein (HTT) is deposited in the brain, typically in the cerebral cortex, but also in other regions such as striatum, hippocampus, and cerebellum [19].

Some of the structural and biological determinants of neurodegenerative diseases have already been revealed [20–24]. However, the turning point of when a pathological condition becomes chronic and leads to neurodegeneration remains elusive for most of the diseases. In this review we focus on G protein-coupled receptor (GPCRs) heterodimers, which are known to play significant roles in the brain [25–29].

1.1.2. G protein-coupled receptors

1.1.2.1. General mode of action

GPCRs are the mediators of almost all (patho)physiological responses in the human body and comprise the largest family of membrane proteins [30,31]. GPCRs share a common architecture of seven transmembrane helices (7TM), connected through 3 intra- and extracellular loops (ICL1-3, ECL1-3) with an extracellular N-terminus and intracellular C-terminus [32,33]. Around 800 genes encode for GPCRs in the human genome [34,35] and about 370 of them are non-sensory GPCRs, ~90% of each expressed in the brain [1,5]. They play important roles in regulating mood, appetite, pain,vision, immune responses, cognition, and synaptic transmissions [5,30,33]. Most of these functions are mediated via endocrine and neurological pathways [1,5,29,35].

In the brain, neurotransmitters signal via GPCRs to modulate the activity of muscles and neurons [36,37]. Dopamine, serotonin, noradrenaline and other derivatives of amino acids and amines, but also oligopeptides like oxytocin or endorphins as well as purines constitute some of known GPCRs ligands [38–45]. Furthermore, an individual small-molecule neurotransmitter might target a dozen different GPCRs. Neurons expressing certain types of receptors are then formed as entire systems. The five main transmission systems are: the noradrenaline, dopamine, histamine, serotonin, and the acetylcholine system [46–50]. Strong imbalances or disruption of these systems have been associated with many mental disorders and neurological conditions such as depression, schizophrenia, attention deficit hyperactivity disorder (ADHD), anxiety, memory loss, pain perception as well as dramatic changes in weight and addictions, aside from neurodegenerative diseases [51–58]. Some studies were also able to connect malfunctioning of the dopaminergic system to multiple sclerosis (MS) [59]. Genetics may also play a role [60].

Vertebrate GPCRs were classified through the GRAFS (Glutamate, Rhodophsin, Adhesion, Frizzeled/Taste, Smoothened families) system that uses a phylogenetic tree of approximately 800 human GPCR sequences to assign the receptors to a specific family[61–64]. Another system, the A-F system, classifies GPCRs by their amino acid sequences and functional similarities (e.g. fingerprints of the characteristic 7TM domains) [64–66]. Here, GPCRs are categorized into six classes: Class A—rhodopsin-like receptors, Class B—secretin family, Class C—metabotropic glutamate receptors, Class D—fungal mating pheromone receptors (non-vertebrate receptors), Class E—cAMP receptors (non-vertebrate receptors, and Class F—frizzled (FZD) and smoothened (SMO) receptors [67,68]. The difference between the GRAFS system and the A-F system is the further division of class B from the A-F system into the secretin and adhesion family in the first system based on preliminary findings that these two families evolved distinct from each other [64].

From these, the classes A and C receptor families comprise the relevant members involved in neurodegenerative diseases and neurological pathologies. These receptors also show a higher amount of relevant data regarding alternative signalling pathways through the formation of GPCR dimers.

1.1.2.2. Dimerization

For a long time it was believed that the functional entity of GPCRs was monomeric: an extracellular signal, such as the binding of a ligand, would lead to conformational rearrangements within the protein, so that the signal was further transmitted intracellularly via heterotrimeric G proteins, arrestin proteins and different downstream signalling cascades [69,70]. This concept was then extended by findings that the receptors can also function as homo- and/or heterodimers or even higher-order oligomers with relevant biological value [71–74]. It was also reported that GPCRs can also form heterodimers with ionotropic receptors and receptor tyrosine kinases and henceforth, modulate their function [75]. In addition, adaptor proteins were described to interact with receptor protomers, modulating their interactions [75]. Consequently, GPCR signalling is not only determined by conformational changes induced by ligand-binding, but also by interaction with other proteins [76], which diversifies and fine-tunes their signalling, rendering it highly dynamic nature [76–79].

For instance, it was reported that the physiological consequences of GPCR-dimerization results in the modulation of downstream signalling, trafficking, and regulation as well as negative and positive cooperativity on ligand-binding [71,79,80]. Furthermore, allosteric dimerization between a monomer and another GPCR can influence ligand recognition by modulation of the orthosteric and allosteric binding sites. This can influence G protein-coupling and selectivity and may cause switching from G protein- to β-arrestin-coupling [79,81]. Additionally, dimerization may lead to the appearance of novel allosteric sites that can again alter different pharmacological properties [81]. However, the structural basis behind such interactions is not fully understood yet.

While class C GPCRs function as dimers only, there is also evidence for the existence of homodimers, heterodimers, and/or higher-order oligomers in other GPCR classes through a variety of reports describing biophysical studies: single-molecule fluorescence-based approaches, X-ray crystallography, nuclear magnetic resonance (NMR)

spectroscopy, and cryogenic electron microscopy (cryo-EM) - as well as computational studies [82–88]. Furthermore, the knowledge about GPCR-dimers being involved in pathological conditions increased in the last years [71]. Such an impact has been reported for asthma, cardiac failure, preeclampsia, schizophrenia and PD [71]. Several studies have shown that GPCR heterodimers elicit a significant role in various diseases at different stages, by regulating the pathological condition towards its progression, or modulating selective downstream signalling cascades [71]. It was already hypothesized that learning and memory occurs at a molecular level by the reorganization of homo- and heterodimers in the postsynaptic membrane [75]. According to the authors Borroto-Escuela and Fuxe, disbalances of homo- and heterodimers are linked to diseases and targeting heterodimers represents a novel strategy for the treatment of brain disorders [75,89].

The understanding of the pharmacological and functional properties of GPCR classes A and C dimers can be crucial for the treatment of mental disorders and neurological conditions, due to evidence suggesting that these macromolecular structures may play an important role. Additionally, the large number of GPCRs and their ability to form different complexes, suggests the existence of a high number of possible GPCR heterodimers in the CNS. This also indicates that heterodimers constitute a unique signalling in such that different neurons with different heterodimers may respond differently to the same ligand [90]. Here, we review the latest advances in obtaining and understanding GPCR dimers (classes A and C) structure and function and, consequently, their role in neurodegenerative diseases. Listing of these complexes can be found on **Table 1** (found at the end of chapter 1.1.8). Until now, 56 dimers were identified as expressed in the brain. Out of these, 48 were from class A-class A dimers, 3 from class C-class C dimers and 5 were class A-class C dimers (**Figure 1**).

In the next sections, we will describe brain-relevant class A GPCRs and known heterodimers followed by class C. A few examples for interclass heterodimers, comprising of class A and class C as well as receptor mosaics will be also listed.

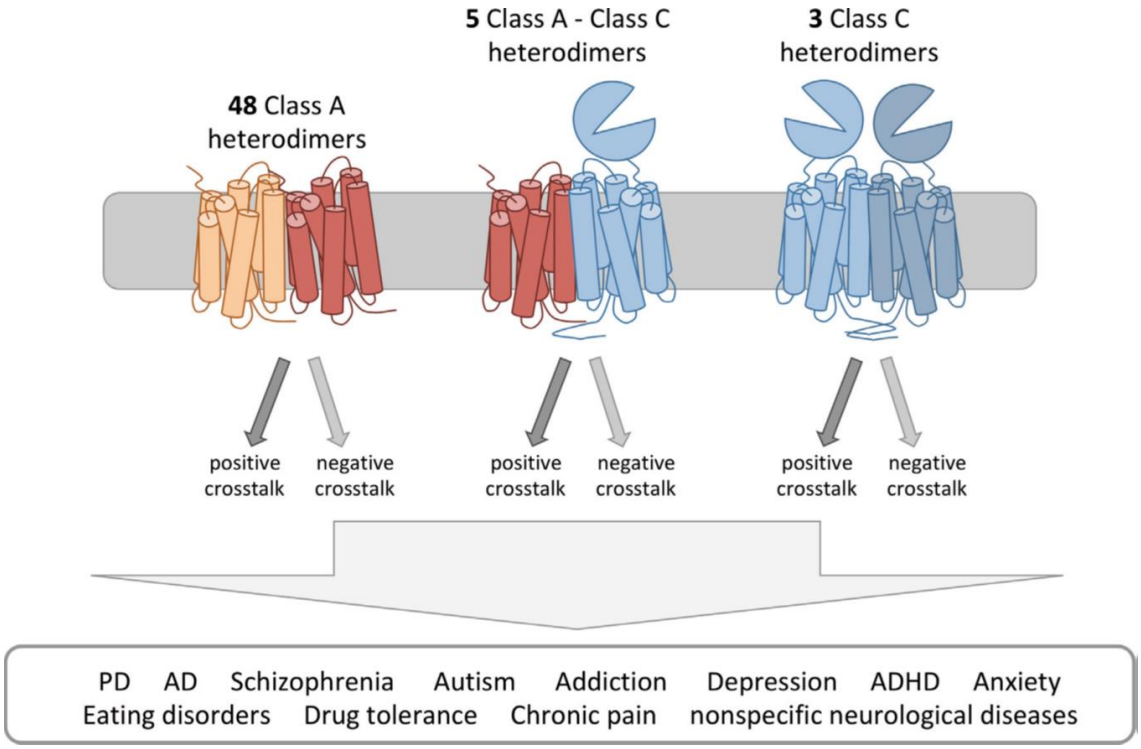

Figure 1. Overview of neurodegenerative-relevant GPCR heterodimers of classes A and C.

1.1.3. Class A G protein-coupled receptors

1.1.3.1. Class A receptors in the brain

The family of class A GPCRs, also referred to as rhodopsin receptors, is a very large and diverse group of receptors. They mediate signalling processes in all kinds of physiological actions such as cell communication, the senses of sight, smell and taste, sensory perception, chemotaxis and neurotransmission [70,91]. In those processes, there is involvement of a wide array of different ligands including light, peptides, lipids, proteins and small molecules such as biogenic amines, nucleotides and ions [70,92]. The activation mechanism of class A GPCRs is the prime example for studying how monomeric GPCRs transduce extracellular signals into intracellular ones. All members of class A GPCRs share a sequence identity of more than 20% in their TM domains, so they are expected to have evolved from a common ancestor [93]. Hence, the growing number of structure-function studies and the increase in resolved crystal structures, suggests that there are common structural and functional motifs responsible for the activation of this family of GPCRs [70,94,95]. In order to make the localization of such structural and functional motifs easy to compare between the different GPCR families, all GPCR residues are usually numbered according to the Ballesteros & Weinstein nomenclature [96]. Hereby, the first digit identifies the TM helix and the second digit

identifies the position of the residues in relation to the most conserved residue in the TM helix which is assigned the index number 50 (numbers decrease towards the N-terminus and increase towards the C-terminus) [70,96]. As already summarized by Moreira [70] and Zhou *et al*. [97] the most important motifs are: (i) the interaction of the cytoplasmic "ionic lock" on TM3 with the consensus "(D/E)R(Y/M)" (3.49-3.51) with D/E (6.30) on TM6, which is disrupted when the receptor is activated [98–107]; (ii) the hydrophobic arginine cage around the conserved arginine (R3.50) of the DRY motif, which restrains its conformation in inactive state of the receptor consisting of two hydrophobic amino acids (such as L, V, I or M) on TM3 and TM6 (3.46, 6.37) [108–110]; (iii) the NPxxYxF motif on TM7,responsible for interaction of a tyrosine (7.53) on TM7 with the phenylalanine (7.60) on HX8 together with the side chain and backbone of an arginine on TM2 (2.40) via a water molecule [101,111–122]; (iv) the Rotamer Toggle Switch, a coordinated change upon ligand coupling of aromatic residues in TM6 around a very conserved tryptophan (6.48) that leads to disruption of the ionic lock [109,114,123,124]; (v) the CWxP motif, the cluster around the conserved tryptophan on TM6, which is part of the Rotamer Toggle Switch and also undergoes a conformational rearrangement upon activation from pointing towards TM7 in the inactive state to pointing towards TM5 in the active state [112,119–127]; (vi) the PIF motif [96,101,128,129], and (vii) the Na^+-pocket [113,119,127,130–136]. It is well established that the outward movement of TM6 upon ligand binding is another common feature of class A GPCR activation. However at the residue level, the changes that triggers such a movement can be individual for each receptor subfamily as it requires a global rearrangement of residue contacts and water-mediated interactions [97,107,137,138].

5-Hydroxytryptamine receptors

Serotonin, also called 5-hydroxytryptamine (5-HT), is an important neurotransmitter responsible for anxiety, aggressive behaviour, stress, blood pressure regulation, peristaltic movements, heart rate, and the coagulation system [139–141][142] This family comprises many members: 5-HT_{1A}R, 5-HT_{1B}R, 5-HT_{1D}R, 5-HT_{1e}R, 5-HT_{1F}R, 5-HT_{2A}R, 5-HT_{2B}R, 5-HT_{2C}R, 5-HT_4R, 5-HT_{5A}R, 5-HT_{5b}R, 5-HT_6R, 5-HT_7R [143]. Many of them, such as 5-HT_{1A}R, 5-HT_{1D}R, 5-HT_{1E}R are drug targets of numerous disorders [144]. Currently, alterations in the serotoninergic neurotransmission and disturbances in the level of 5-HT have been described to be associated with migraine, epilepsy, PD, MS, amyotrophic lateral sclerosis (ALS), ADHD and autism spectrum disorder (ASD) [139,140,145–149]. Especially for migraine, disturbances in the serotoninergic system are the hallmark of this disorder, which affects 11% of adults worldwide [139]. Chronically low 5-HT disposition due to malfunction of its biosynthesis leads to the development of migraine [139].

Adenosine receptors

Adenosine receptors (AR) are another family of class A GPCRs that are activated by their endogenous ligand, adenosine [151]. The four members A_1R, A_{2A}R, A_{2B}R, A_3R have been considered potential targets for several disorders such as PD, schizophrenia,

analgesia, ischemia and cancer [151,152]. Some studies also reported effects of adenosine on neuronal protection and neuronal viability as well as in inflammatory processes [153]. Combined effects may lead to considerations for ARs and possible roles in Lesch-Nyhan syndrome, Creutzfeldt-Jakob disease, Huntington's disease, PD and AD and multiple sclerosis, as well as the brain damage associated with stroke [152,153].

Adrenoceptors

The noradrenergic system in the brain has the global function of neuronal modulation, controlling vigilance, attention, the sleep-wake cycle and to some extent also in learning and memory processes [154–157]. In addition, depression, anxiety and sensory information processing, such as pain or touch, mediated through the sympathetic nervous system, are processes regulated by noradrenaline and the neurohormone epinephrine through the noradrenergic system [154,156–158]. All these ligands bind to the nine members of the adrenoceptor family, all expressed in the brain: α_{1A}AR, α_{1B}AR, α_{1D}AR, α_{2A}AR, α_{2B}AR, α_{2C}AR, β_1-AR, β_2-AR and the β_3-AR [71,158,159]. The adrenoceptors are further classified into three subgroups: the α1 group which comprise α_{1A}AR, α_{1B}AR and α_{1D}AR since they couple to G_q; the α2 group containing α_{2A}AR, α_{2B}AR and α_{2C}AR, in which all couple to G_i and the β group which consists of the β_1-AR, β_2-AR and the β_3-AR, all able to couple to G_s. However, β_2-AR and β_3-AR also couple to G_i [160]. Disruption in the noradrenergic system was reported to be connected to a number of neurological diseases such as AD, epilepsy, ADHS, PD, depression, schizophrenia, and posttraumatic stress disorder [154].

Cannabinoid receptors

The two cannabinoid receptors CB_1R and CB_2R together with their endogenous ligands, anandamide, 2-arachidonoylglycerol and other endocannabinoids, were discovered in the late 80s and resulted in a major effort in understanding the mechanisms and physiological roles of the endocannabinoid system (ECS) [143,150]. The ECS regulates a variety of physiological processes such as appetite, mood, memory and pain sensation [151]. This complex system is also believed to play a neuroprotective role during traumatic brain injury, and may be part of a natural compensatory repair mechanism, relevant also during neurodegeneration [152–155]. The modulation of this new neuronal network has been proposed to target many neurological conditions including epilepsy, cognitive deficits and neurodegenerative diseases [152,156,157]. While CB_1R is mainly expressed in the brain, CB_2R can be found in diverse parts of the immune system and partially in the brain [158–160]. Interestingly, CB_1R is a promiscuous protein, able to couple to different G proteins, activate signalling pathways mediated by β-arrestins and signal from intracellular compartments, adding another level of complexity to this system [150,161,162]. Therefore, CB_1R has an impact in brain disorders including basal ganglia disorders such as AD, MS and HD [157,163].

The expression pattern of CB_2R contrasting to CB_1R is more defined and increased in microglia and macrophages of the central nervous system (CNS) [160,164]. The CB_2R is mainly associated with inflammation, and due to its selective localization, it is a promising target for AD and other basal ganglia disorders [157,165–167].

Cholecystokinin receptors

Cholecystokinin (CCK) is a gastrin-like peptide found in the brain and the gastrointestinal tract [168]. CCK triggers the signalling cascade by activating two GPCRs, CCK_1R/CCKAR and CCK_2R/CCKBR, also found in similar regions of the human body [143,169]. The CCK_2R has been associated with the neurobiology of anxiety and panic attacks since the 90s [170]. The CCK_1R is mainly known as physiologic mediator of pancreatic enzyme secretion and smooth muscle contraction of the gallbladder and stomach [171]. Yet, at minor levels, CCK_1R is also present in different regions of the brain, where it mediates the anorectic action of CCK [172–174]. Besides this function, CCK_1R also facilitates dopamine neurotransmission, regulates hypothalamic neurotransmitters, increases the excitability of the cortex and regulates endocrine secretions [171]. For instance, there is accumulating evidence that about 70% of PD patients have experienced diverse non-motor symptoms, most commonly gastrointestinal problems, before the onset of motor dysfunctions [175,176]. Such findings suggest that neuropeptides derived from the gastrointestinal tract may be related to the onset of PD. This is further supported by the fact that CCK and several other neuropeptides are expressed in dopaminergic neurons of the substantia nigra, and galanin or opioid neuropeptides are also released from the hypothalamic neurons [175,177,178]. In PD patients or experimental models, significant changes in brain neuropeptides have already been observed [175].

Dopamine receptors

The dopamine receptor family consists of five receptors (DRD_1-DRD_5) [179] which are divided into two subclasses (D1-like and D2-like) based on their coupling to G proteins. DRD_1 and DRD_5 couple to $G_{S,olf}$ and belong to the D1-like class, while DRD_2, DRD_3 and DRD_4 couple to $G_{i/o}$ and belong to the D2-like class [179–182]. Additionally, for DRD_2 two splicing variants exist, DRD_{2long} and the 29 amino acids shorter DRD_{2short} [179]. While DRD_{2long} is mostly located in the intracellular part, DRD_{2short} is primarily found at the plasma membrane [183]. DRs are associated with many pathological conditions and mental disorders, most prominently PD, schizophrenia, Tourette's syndrome, depression, bipolar disorder, hypertension, gastroparesis and nausea, as well as others [179,182,183].

Galanin receptors

The neuropeptide galanin (GAL) is widely found in the human brain and gastrointestinal tract and couples to three GPCRs: GAL_1R, GAL_2R and GAL_3R [184]. In the past, several physiological effects were attributed to galanin signalling including smooth muscle contraction, inhibition of insulin release and stimulation of growth hormone release [185–187]. However, it was revealed that the galanin-like immunoreactivity in the CNS and peripheral nervous system (PNS) leads to the regulation of numerous biological processes such as learning and memory, neurogenesis and neuroprotection, seizure activity, pain threshold, neurotransmitter and hormone release and many more [187–198]. Consequently, the role of galanin in mood disorders has attracted a lot of interest [187,191,199]. Neurological disorders have also been linked to galanin signalling such as AD, epilepsy, depression, eating disorders and addiction [194,200].

Histamine receptors

The histamine receptor (HR) family comprises four members, H_1R, H_2R, H_3R, H_4R [201]. Histamine itself is known to be involved in local immune responses as well as regulating functions in the gastrointestinal tract [202]. For a long time it has been considered as a local hormone, as it lacks the endocrine glands to secrete it, but it has now been recognized as neurotransmitter [202,203]. The HRs exert diverse functions in the brain. Whereas H_1R promotes wakefulness, nociception, endocrine homeostasis and appetite, the role of H_2R has not been established yet, since most known ligands are unable to cross the blood-brain barrier in sufficient concentrations [62,201,204–207]. The H_3R is described as an "autoreceptor" with constitutive activity and decreases the release of histamine, acetylcholine, serotonin and norepinephrine [201,208]. Lastly, H_4R is not located in the brain, but rather in basophils and in the bone marrow [201]. Especially H_1R and H_3R orchestrate disparate behaviours and homoeostatic functions [207]. Recent evidence suggested that aberrant neuronal histamine signalling may also be a key factor in degenerative diseases such as PD, AD, sleep disturbance and MS, as well as in addictive behaviours [207,209–211]. Moreover, the concentration of metabolites of histamine was shown to be increased in the cerebrospinal fluid of schizophrenia patients compared to normal patients [212,213]. In addition, a decrease in the binding sites of H_1R was observed in schizophrenia patients [212,213].

Opioid receptors

The oldest and most potent drugs used for the treatment of moderate-severe acute and chronic pain are opioids [214,215]. Actions of opioids are mediated through opioid receptors (ORs), widely distributed across the skin, digestive tract, spinal cord and in the brain [69,216–218]. There are four major classes of receptors: delta receptor (DOR), kappa receptor (KOR), mu receptor (MOR) and the nociceptin (NOP) receptor [217,219,220]. ORs are activated by their endogenous opioid ligands that are released by neurons such as dynorphins, enkephalins, endorphins, endomorphins and nociceptin, but also by exogenous opiate drugs [221–227]. Since the ORs are all coupled to G_i proteins, their activation characteristically inhibits neuronal firing as well as neurotransmitter and hormone release [221,228–231]. The opioid system plays an important role in hedonic homeostasis, mood and well-being, including a large number of sensory, motivational, emotional and cognitive functions and addictive behaviours [221,232]. The ORs are also known to regulate peripheral functions including endocrine, gastrointestinal, immune and respiratory functions and responses to stress [232]. Due to its main role in the control of pain, the opioid system is also associated with multiple adaptations in the nervous, endocrine and immune system which can lead to the development of pathologic, chronic pain [228,233,234]. In addition, ORs may play a pivotal role in the development of AD, since ORs are known to regulate the neurotransmitters acetylcholine, γ-Aminobutyric acid (GABA), glutamate, norepinephrine and serotonin that have been implicated in the pathogenesis of AD [221].

Somatostatin receptors

The peptide somatostatin (SST) consists of two bioactive forms, SST-14 and SST-28, produced in neuroendocrine cells in the periphery and in the brain that modulate cell secretion and proliferation as well as neurotransmission [235–238]. Five GPCRs, SST_1R, SST_2R, SST_3R, SST_4R and SST_5R mediate the actions of SST which are variably expressed in the brain [236,238,239]. SST_2R, SST_3R, SST_4R and SST_5R undergo rapid endocytosis, induced by the binding of agonists, while SST_1R does not internalize but is rather up-regulated when continuously exposed to agonists [240,241]. The types of active SST isoforms, SST-14 and SST-28 vary in their distribution: SST-14 is more predominant in the CNS, whereas SST-28 is more abundant in peripheral organs [242,243]. Both bind to the SSTR in nanomolar affinity. However, SST_5R has a higher affinity for SST-28 over SST-14, while for the other SSTRs the contrary is true [256]. In the cortex, SST is a protein marker of inhibitory interneurons, as SST is expressed mainly in a subset of GABAergic neurons [242]. SST and SSTRs contribute to cortical processing and in the striatum SST-positive interneurons are able to co-release glutamate and GABA [242]. This co-release generates excitation-inhibition sequences in postsynaptic neurons, which is interpreted as the glutamatergic response and persists for a shorter time than a usual inhibitory response would [242,244,245]. The involvement of SSTR in neurodegenerative and neuropsychiatric disorders such as AD, OD, HD, bipolar disorder, schizophrenia and major depressive disorder (MDD) has been linked to a decrease in the amount of expressed SST [242].

Vasopressin and oxytocin receptors

Arginine-vasopressin, also known as antidiuretic hormone (ADH), and oxytocin (OT) are hormones derived from the neurohypophysis. These are similar nonapeptides that differ only at residues 3 and 8 [246]. ADH is essential for cardiovascular homeostasis (water body balance), key for shock states [246,247]. OT is also known as the “quick birth” hormone, because it facilitates reproduction in vertebrates at several levels, due to its uterine-contracting properties. This hormone is the one that responds to sexual activity and during labour where oxytocin controls the highly potent uterotonic activity, induces milk production and it additionally induces the first onset of maternal behaviour [246–250]. The actions of ADH are mediated by tissue specific GPCRs and known as V1 vascular ($V_{1A}R$), V2 renal (V_2R) and V3 pituitary ($V_{1B}R$, previously known as V_3R) [251–253]. The $V_{1A}R$ has been shown to be ubiquitously expressed in the brain [246], and therefore plays a role in many physiological functions including cell contraction and proliferation, platelet aggregation, liver glycogenolysis, vascular smooth muscle, aldosterone secretion by the adrenals and subserve neurotransmitter-like actions of ADH in the CNS [254–258]. Species-typical social behaviours (e.g., affiliative behaviour) in rodents and humans may be associated with the pattern of $V_{1A}R$ expression in the brain [259–262]. The $V_{1B}R$ mediates the release of ADH and beta-endorphin from the anterior pituitary through the mobilization of intracellular calcium by phosphatidylinositol hydrolysis [246,263]. However, the receptor was also found in other organs including the adrenals, the brain and the pancreas [264–266]. In 2002, SSR149415, a $V_{1B}R$-antagonist, was developed with antidepressant- and anxiolytic-like properties [246,267]. Since then, it has been hypothesized that $V_{1B}R$ may play an important role in major depressive disorder (MDD) and chronic stress. In addition it has been shown that a small subset of MDD patients display an impaired hypothalamus-pituitary-adrenal (HPA) axis function, which was also present in patients with treatment-resistant depression or

severe depression [268–277]. This led to the assumption that V_{1B}R-antagonists would improve the treatments of such conditions, and several selective and potent antagonists have been developed and their potential as antidepressants has been verified in animal models [277].

The main endocrine function of ADH, the facilitation of water reabsorption in the kidney through inhibition of the diuresis, is mediated by the V_2R [246]. The deployment of ADH analogous (dDADH, desmopressin) as selective V_2R-agonists has been successful for the treatment of central diabetes insipidus, patients suffering from hemophilia A and Von Willebrand's disease, the most frequent congenital bleeding disorders [278–282]. In summary, the key function of the V_2R is to regulate fluid homeostasis [283].

The last member of this family, the oxytocin receptor (OTR), is activated by the neurotransmitter oxytocin (OT) which regulates emotional, parental, affiliative and sexual behavioural functions, including mother-infant bonding [246,284]. The OTR is expressed in the brain and body, especially in reproductive organs [284]. Also, the number of receptors varies in different periods of life such as birth and postpartum [284,285]. In the brain, OT induces the suppression of GABAergic neurons [286,287]. It has also been reported that OT has an anti-inflammatory effect, observable in wound healing and pain relief [288,289]. Besides this function, anti-depressant effects have been described for OT [290,291]. OT might also have anti-anxiety effects mediated by the HPA axis [292]. Recently, increased methylation levels in the OTR have been linked to obsessive-compulsive disorder (OCD) [293]. Another study demonstrated that substantial loss of hypothalamic oxytocin-producing neurons occurs in amyotrophic lateral sclerosis [294].

Trace Amine-associated Receptors

Trace amine-associated receptors (TAARs) were discovered in 2001 [295,296] and are activated by a diverse group of aminergic compounds. In mammalian, the nine TAAR members are divided into two sub-families: $TAA_{1\text{-}4}$R and $TAA_{5\text{-}9}$R [297,298]. In humans, there are six functional TAAR genes (TAA_1R, TAA_2R, TAA_5R, TAA_6R, TAA_8R and TAA_9R) and three pseudogenes (TAA_3R, TAA_4R and TAA_7R) [299]. TAA_1R is the most well-characterized member and a potential target for psychiatric disorders, such as schizophrenia [299] and drug abuse [300], as well as for metabolic disorders [301]. The endogenous trace amines p-tyramine, β-phenylethylamine, tryptamine and octopamine bind to TAARs [302–304], essentially to TAA_1R and TAA_4R, and they induce effects in CNS. For example, phenylethylamine acts as a postsynaptic neuromodulator of dopamine and noradrenaline neurotransmission [305]. Tryptamine potentiates neural responses to dopamine and causes an increased response to norepinephrine in cortical neurons [306]. Octopamine increases depressive and excitatory responses to norepinephrine in the rat cerebral cortex [307]. 3-Iodothyronamine may have a pro-learning anti-amnesia effect [306]. With the exception of TAA_1R, all TAARs have been detected in olfactory sensory neurons [321]. TAA_1R is coupled to G_s protein [295,302], recruits the β-arrestin-2 cascade [308,309] and increases the opening of inwardly rectifying K^+-channels that have the characteristics of G protein-coupled inwardly-rectifying potassium channels (GirK) channels [310,311]. All the other TAARs within the olfactory epithelium are coupled to G_{olf} to regulate cyclic adenosine monophosphate (cAMP) accumulation [312]. TAA_5R is also coupled to G_s cascade [313], $G_{q/11}$ cascade and $G_{12/13}$ dependent mitogen-activated protein (MAP) kinase pathways [314]. In

contrast, TAA_8R is G_i-coupled [315]. The signal transduction events of TAA_6R and TAA_9R are still unknown.

Neurotensin receptors

The central and peripheral effects of tridecapeptide neurotensin (NT) are mediated through interaction with three identified neurotensin receptors: NTS_1, NTS_2 and NTS_3 (Sortilin 1) [316]. Whereas NTS_1 and NTS_2 receptors have seven transmembrane helices and are G protein-coupled, the Sortilin 1 receptor is a single transmembrane domain receptor [316]. NTS_1R are found in the brain and intestine of rats and humans [317]. In the brain, the NTS_1R is mainly found in in neurons of the diagonal band of Broca, medial septal nucleus, nucleus basalis magnocellularis, suprachiasmatic nucleus, supramammillary area, substantia nigra and ventral tegmental area, as well as in the small dorsal root ganglion neurons of the spinal cord [318,319]. NTS_2R are mostly expressed in brain [320–322] and mainly localized in the olfactory system, the cerebral and cerebellar cortices, the hippocampal formation and selective hypothalamic nuclei of the mouse [323] and rat [324] brain. NTS_1R are G_q-coupled [316,325,326], but some other studies demonstrated that NTS_1R are also $G_{i/o}$ and G_s-coupled [316,327–329]. In contrast, signal transduction of NTS_2R receptors is still unclear. The role of neurotensin and its receptors is related with analgesic effects, which could be an alternative to opioids [330–332].

Angiotensin receptors

The actions for angiotensin II, which is an important peptide hormone in the renin–angiotensin–aldosterone system (RAAS), are mediated through angiotensin receptors AT_1R and AT_2R [333–335]. The RAAS system involves different peptides and proteins with opposing effects in order to function [336]. On the one hand vasoconstrictive, pro-inflammatory and pro-proliferative are mediated by angiotensin II, AT_1R and angiotensin-converting enzyme (ACE), while on the other hand cardio-protective effects are mediated by Ang(1-7), AT_2R and ACE2 [336]. However, angiotensin II displays ubiquitous actions by activation of different pathways by the binding to AT_1R and AT_2R in order to initiate the RAAS system or to further get cleaved into shorter peptides such as Ang IV, Ang(1-7) and almandine [336–339]. Besides, angiotensin II, angiotensin I and angiotensin III are endogenous ligands of ATRs [335]. The AT_1R is clinically relevant as it is targeted by a large class of sartans, AT_1R blockers [335]. The AT_1R is mainly expressed in the brain, heart, blood vessels, lungs and kidneys [340,341] and known to bind to $G_{q/11}$, $G_{i/o}$ proteins, G_{12} and G_{13} proteins as well as tyrosine kinases [336,342]. Functions involving AT_1R are cardiac hypertrophy, vasoconstriction, aldosterone synthesis and secretion, increased vasopressin secretion, decreased renal blood flow and renin inhibition, central and peripheral sympathetic nervous system activity and osmocontrol [343]. In the brain, AT_1R antagonists were shown to reduce fear memory recall in mice [344,345].

AT_2R was shown in *in vitro* and *in vivo* studies to counterbalance the effect of AT_1R, however this is still speculative [334,335,338,346–348]. AT_2R are highly expressed in fetus and neonate and induce fetal tissue development, and so, although controversially, it is assumed they are involved in vascular growth, [349,350]. However, some studies could show that AT_2R was upregulated after vascular injury, cardiac failure, myocardial infarction or wound healing, suggesting that this possibly reflects the re-activation of this

fetal genetic programme [334,338,351,352]. The expression of AT_2R in humans is therefore developmentally regulated. In adults AT_2R is expressed in lower density in the adrenal medulla, brain and reproductive tissues [349,350]. AT_2R expression in the cerebellum has been associated with inhibition of cell growth differentiation, neuronal regeneration and ventricular hypertrophy [353]. Also, it was suggested that AT_2R-mediated effects in other tissues require the local conversion of angiotensin II to II [354–356]. The downstream signalling transduction of the AT_2R is poorly understood. It is known that the receptors possesses important structural motifs which are typical for class A GPCR activation; however several modalities can result in AT_2R activation [357–375].

The existence of AT_3R and AT_4R was also proven, but only AT_4R remained to be relevant [376,377]. AT_4R was shown to be the mammalian selective receptor for angiotensin IV (Ang3.8) as well as a receptor for insulin-regulated membrane aminopeptidase [378–381]. It has been proposed that the AT_4R may be relevant in the regulation of the extracellular matrix of the CNS and modulation of oxytocin release [378,382–386].

Growth Hormone Secretagogue Receptors

The Growth Hormone Secretagogue Receptor (GHS-R) is a GPCR that binds growth hormone secretagogues (GHSs), like ghrelin. GHS-R is G_q and G_s-coupled and the binding of ghrelin or synthetic peptidyl and non-peptidyl ghrelin mimetic agents leads to increased intracellular calcium content [387,388]. GHS-R and its ligand ghrelin have special influence in food intake, gut motility, sleep, memory, behaviour, lipid and glucose metabolism, and cardiovascular effects [389]. GHS-R is expressed by growth hormone-releasing hormone (GHRH) neurons in the pituitary [390], but also in hypothalamus, pancreas, adipose tissue, immune cells and cardiovascular system [391,392]. GHS-R has two isoforms, GHS-R_{1a} and GHS-R_{1b}, but only $GHSR_{1a}$ transduces ghrelin signalling by binding the active form of ghrelin [393]. GHS-R_{1a} agonist and antagonist reveal to have benefits in cancer, cachexia [394–396], aging related cognitive decline [397,398], obesity [399] and diabetes [400–402].

Melatonin receptors

The melatonin receptors MT_1R and MT_2R are expressed in several areas in the human body such as brain, retina, cardiovascular system, organs or skin are activated by their endogenous ligand melatonin [403–407]. An additional MT_3R has been identified in birds and amphibians [407]. MT_3R was later identified in humans as a cytoplasmic enzyme, involved in the detoxification by reduction of quinones and also binds with low affinity to melatonin [408,409]. Melatonin is a hormone mainly produced in a circadian rhythm in the pineal gland, with low levels during day and high levels at night [405,410–412]. This circadian secretion was found to be regulated by the suprachiasmatic nucleus (SCN) in a negative feedback-loop by melatonin binding to MT_1R and MT_2R, which then decreases SCN firing [413]. Melatonin is mainly known as a sleep promoter and regulator of circadian rhythms. Still, more effects such as antioxidants, reproduction-stimulation, analgesic and suppression of tumors have been attributed to it [407,414].

It has been identified that the sleep promoting effects for melatonin are mainly regulated by MT_1R [415]. MT_1R was also shown to be involved in adaptation to the light/dark-circle, phase-shifting activity and prolactin secretion [407,415]. MT_1R and also MT_2R exert their

signals by binding to $G_{i/o}$ proteins [416]. However, they are also able to bind to other G proteins such as G_q and to soluble guanylate cyclases [405,415–417]. In contrast to MT_1R, the MT_2R was shown to regulate a variety of functions in the body. It is known that melatonin inhibits through MT_2R the Ca^{2+}-dependent release of dopamine in the retina [418] as well as light-dependent phagocytosis and photopigment disc shedding [419]. MT_2R were also shown to be expressed in a higher amount on differentiating osteoblasts [420].

In many studies melatonin improved the treatment of PD, AD, alcoholism, depression or traumatic brain injuries [403,421,422]. For instance, addictive behaviours have been associated with an increased MTR-related cAMP concentration in the mesolimbic dopaminergic system [407]. Mostly, melatonin is used as a treatment for different types of insomnia, jet lag or shift work due to its sleep-promoting function [413]. MT_1R and MT_2R were also found to exist as homo- and heterodimers *in vivo* and *in vitro [406,423–425]*. In mice rod photoreceptors, *in vivo* melatonin mediated the light sensitivity by formation of heterodimers, which led to heterodimer-specific activation of phospholipase C and protein kinase C [425]. This effect was abolished in MT_1R knockout (KO) mice, MT_2R KO mice and in mice overexpressing a non-functional mutant of MT_2R, that also interfered with the formation of functional heterodimers [425].

1.1.3.2. Orphan class A receptors

The orphan receptor GPR139, was first discovered in 2002 [426], further curated in full-length in 2005 and classified into the class A GPCR family, right next to its closest relative, GPR142 [427–429]. As GPR139 is still considered an orphan receptor, a precise function remains to be determined. However, some reports suggest a role for GPR139 in locomotor activity, metabolism, alcohol addiction and hyperalgesia and phenylketonuria [430]. Lastly, genetic analysis has linked GPR139 to depression, schizophrenia and ADHD [430–435].

1.1.3.3. Class A receptor heterodimers

While class C GPCRs are obligate dimers, for a long time it was not clear if class A GPCR were also able to dimerize, and what was the importance of such macromolecular structures. However, as GPCRs exhibit a high tendency to aggregate, some authors raised the question: What are the criteria for a minimal functional unit? [436,437]. Indeed, for example, it was found for the $5\text{-}HT_4R$ that two monomers were associated with one G protein [438]. In this case, one $5\text{-}HT_4R$ was enough to simulate the G protein, but positive receptor crosstalk was observed upon co-activation, leading to the conclusion that $5\text{-}HT_4R$ would rather function as homodimers [437]. This was also the case for the DRD_2. In a study by Han *et al.* 2009 [439] it was shown that the maximal activity of the DRD_2 was achieved upon agonist-binding to one monomer but was modulated by the constitutive activity of the second monomer indicating asymmetric functional interaction [437]. Hence, the minimal functional unit of class A receptors, which can either be a monomer or a homodimer, appears to be receptor dependent [72]. In addition to these findings, heterodimers have been intensively studied using cotransfected cells in biochemical, biophysical and pharmacological experiments with wildtype or often also using mutant receptors [440–442].

Since the family of class A GPCRs comprises many receptor subfamilies such as dopamine, adenosine or serotonin receptors that mediate diverse functions in the human body transduced by only one endogenous ligand, it becomes patent that heterodimerization is indeed also required for this GPCR class [443,444]. Many prominent examples have been intensively studied, such as the A_1R–$A_{2A}R$ complex, able to couple to G_i at low concentrations of adenosine and to G_s at high concentrations [445–447]. Another example is the DRD_1–DRD_2, which couples to G_q, whereas as monomers the DRD_1 and DRD_2 couple to G_s or G_i, respectively [448–451]. Lastly, the finding that opioid receptors are also able to form heterodimers resolved many questions about atypical behaviour of targeting drugs, which apparently were selective for such heterodimers [452–459].

However, the idea of dimerization/oligomerization of GPCRs for neurotransmitters was already formulated by Fuxe *et al.* in the 80s [444,460–462]. Since then and until 2014 the number of protein-protein interactions between GPCRs was found to be 537 according to Borroto-Escuela *et al*., indicating that class A GPCR dimers are an important and relevant discovery [463].

Dopamine - Dopamine receptor heterodimers

The five members of the dopamine receptor family are known to form dimers among their family and with other class A GPCRs [464–467]. Besides homodimers DRD_2–DRD_2 [77,468], DRD_3–DRD_3 [469], DRD_4–DRD_4 [467], also many heterodimer combinations were identified such as DRD_5–DRD_2 [470], DRD_1–DRD_2 [465], DRD_1–DRD_3 [464] or DRD_2–DRD_3 [471]. More combinations were reviewed in Schiedel *et al.* [79], displaying the dopamine signalling heterogeneity [466,472].

DRD_1 and DRD_2 receptors are mainly expressed in the dorsal (caudate-putamen) and ventral striatum (nucleus accumbens, NAc) areas [473]. DRD_1–DRD_2 was discovered using co-immunoprecipitation (Co-IP) and confocal Förster-Resonance-Energy-Transfer (FRET) experiments performed in brain tissues [451,465,474] and later by protein complementation studies [475]. More recent studies demonstrated the existence of the heterodimer in the dorsal striatum and NAc of mammalian species, including mouse, rat, nonhuman primate, and human, with a higher extent in the ventral than in the dorsal striatum [476–478]. In 2020, a study showed that the heterodimer is also found in cortical brain regions, such as piriform, medial prefrontal, and orbitofrontal, and claustrum, amygdala, and lateral habenula [479]. Many studies using signalling assays were able to show that the heterodimer formation might induce a change in the pattern of G protein-coupling (**see Figure 2A**) [448,474,478,480]. Monomeric DRD_1 couples to G_s and DRD_2 to $G_{i/o}$, but DRD_1–DRD_2 was found to be associated with $G_{q/11}$ and activate the phospholipase C cascade in the striatum [451]. However, in order to conduct such actions and subsequent intracellular Ca^{2+} release, the specific DRD_1 agonist SKF83959 had to bind to both receptors: it acted as full agonist at DRD_1 and high-affinity partial agonist for a pertussis toxin-resistant at DRD_2 [451]. Furthermore, the intracellular calcium increase was associated with an increase in striatal calcium/calmodulin kinase IIa (CaMKIIa) phosphorylation [481]. The DRD_1–DRD_2 was reported to be upregulated in individuals suffering from depression [482,483], while it was diminished in schizophrenia patients (**Figure 2B**) [484]. In striatal neurons, the DRD_1–DRD_2 heterodimer activity resulted in rapid activation of cytosolic and nuclear CaMKII with an

increase in brain-derived neurotrophic factor (BDNF) expression, which was the first evidence by then, linking dopamine receptors and endogenous GPCR heterodimers to neuronal maturation [449].

Regarding the potential interface of the DRD_1–DRD_2, a comprehensive study by O'Dowd *et al. [485]*, showed that it involves a pair of adjacent glutamic acids in the C-terminus of the DRD_1 and a pair of adjacent arginine residues in ICL3 of the DRD_2, oppositely charged residues, able to form stable electrostatic interactions [448],498]. When SKF83959, which apparently is an agonist to the DRD_1–DRD_2, was administered to rats, activation of the heterodimer generated aversion in conditioned place preference studies, while disruption of it was rather rewarding [448]. Schizophrenia is known to be associated with hyperdopaminergia in subcortical dopamine projections [448]. Compared to globus pallidus tissue from normal subjects, the number of agonist-detected high-affinity state DRD_1–DRD_2 was found to be increased in globus pallidus tissue of schizophrenia patients [448]. According to George *et al.*, these findings possibly reflect the hyperdopaminergic state associated with schizophrenia, similarly to what was observed upon amphetamine administration [448,476].

A recent study revealed that genetic variations of DRD_2 (Val96Ala, Pro310Ser, and Ser311Cys) affect the heterodimerization between DRD_1 and DRD_2 [465]. In addition, the Ser311Cys variant seems to be a risk factor in schizophrenia [499] and shows a better response to the schizophrenia' treatment [486]. Once this DRD_2 variant forms less heterodimeric interactions with DRD_1 than DRD_2 native, targeting the DRD_1-DRD_2 heterodimer under excessive dopaminergic firing will result in antipsychotic actions, with minimal side effects [465]. Another recent study showed that DRD_1-DRD_2 heterodimers play a role in cocaine dependence [487] and repeated cocaine administration of rats increase DRD_1-DRD_2 heterodimer expression [478]. The cocaine-induced biochemical changes, such as accumulation of ΔFosB, phosphorylation of extracellular signal-regulated kinases (ERK), and phosphorylation of Thr34-DARPP-32 in NAc are blocked by heterodimer activation [487]. Similar to what happens with cocaine, heterodimer expression is also increased after chronic administration of Δ-tetrahydrocannabinol (THC) in rhesus monkeys [478]. Consequently, the DRD_1-DRD_2 heterodimer would also be a good pharmacological target in cannabis use disorder (CUD) and the THC-induced changes in the dopamine signalling are also implicated in behavioural despair disorders [478,479,488,489].

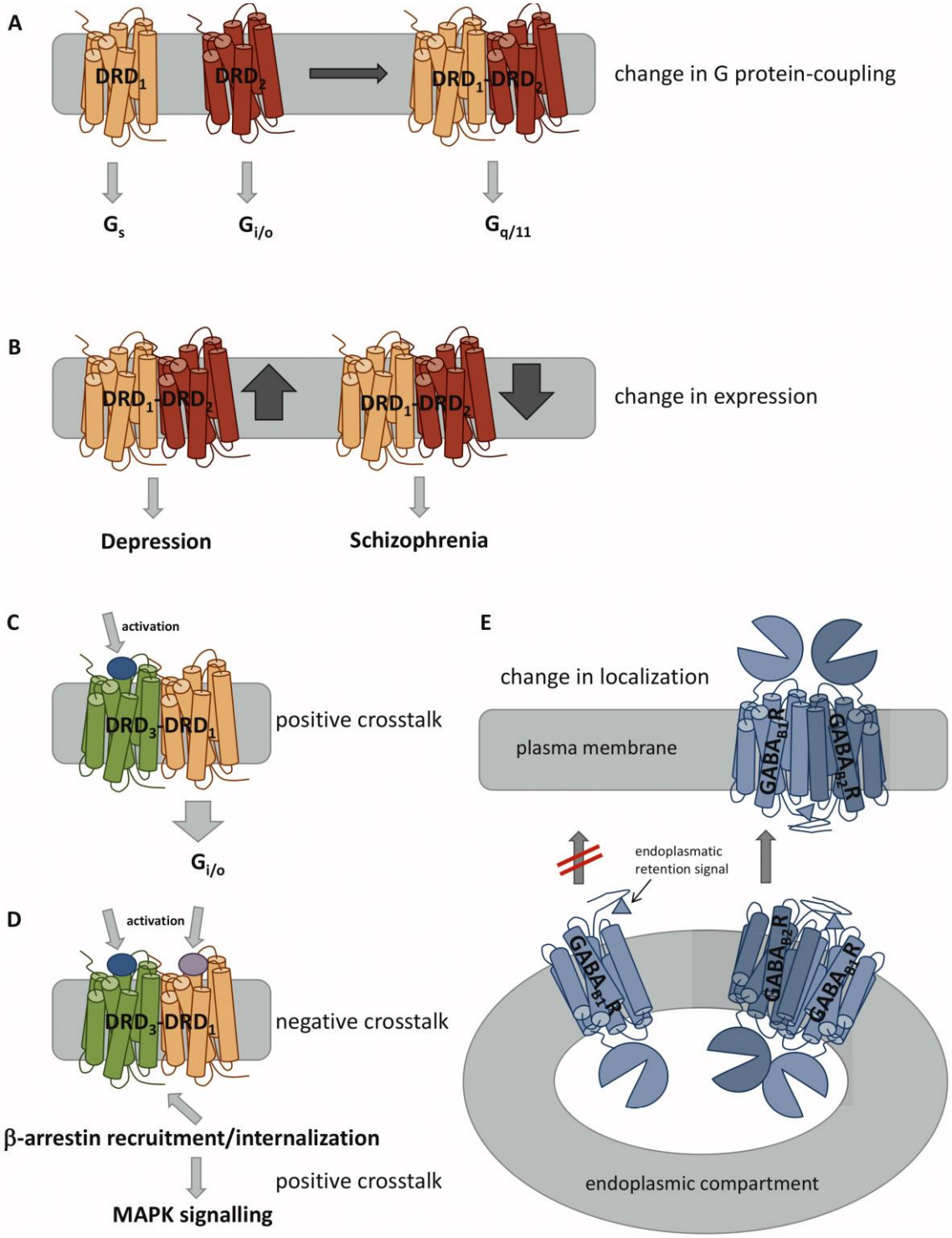

Figure 2. Possible modulations upon GPCR dimer formation. (A) Heterodimerization can induce a change of G protein-coupling. (B) Different expression levels of heterodimers are associated with distinct diseases. (C) Activation of one receptor can promote signalling of the other receptor via positive crosstalk. (D) Activation of both receptors can lead to b-arrestin recruitment and internalization via negative crosstalk. This can lead to intracellular signalling via mitogen-activated protein kinase (MAPK). (E) Dimerization can be necessary for plasma membrane localization, e.g. by masking an endoplasmic retention signal, which will prevent the transport to the plasma membrane as monomers.

Another dopamine receptor heterodimer, DRD_1–DRD_3 was also found to be expressed in the ventromedial striatum by FRET and bioluminescence resonance energy transfer

(BRET) techniques [464,490–493]. One of the first studies about DRD_1–DRD_3 heterodimer's mechanism, reported in 2008 that DRD_3 activation amplified DRD_1-mediated adenylate cyclase (AC) signalling in the DRD_1–DRD_3 heterodimer (**Figure 2C**) [493]. However, in 2014, Ferré and co-workers reported that co-activation of both receptors had antagonistic effects at the level of the AC, due to DRD_3-mediated inhibition [490]. Therefore, co-activation of both receptors led to the canonical negative interaction at the level of AC signalling, to the recruitment of β-arrestin-1 and selective activation of MAPK signalling, which was mediated by a G protein-independent mechanism (**Figure 2D**) [490,491]. Furthermore, this positive crosstalk through β-arrestin-1 recruitment and MAPK signalling, induced by DRD_3 and DRD_1 agonists, respectively, was counteracted by DRD_1 and DRD_3 antagonists. Moreover, the DRD_1-DRD_3 heterodimer was implicated in L-DOPA-induced dyskinesia [490,494–496]. Some studies reported that DRD_1 super-sensitivity during L-Dopa induced dyskinesia was accompanied by DRD_3 up-regulation [494–496], and mice with DRD_3 knockout displayed reduced L-Dopa-induced dyskinesia [496,497]. *In vitro* studies performed by Cortés and colleagues using transfected human embryonic kidney 293 (HEK293) cells [490] and *in vivo* studies conducted by Bishop and colleagues (using hemi-parkinsonian rats) [495] demonstrated that DRD_1–DRD_3 heterodimers influenced the cooperative effect of both receptors in L-Dopa-induced dyskinesia. The co-activation with the DRD_1 and DRD_3 agonists SKF38393 and PD128907, respectively, generated an exacerbated dyskinetic effect, and an increase of downstream signalling of ERK phosphorylation, which is specific to dyskinesia as general locomotor effects or pERK were not observed in non-responders [495].

In 2001, evidence based on Co-IP studies in cultured cells pointed to DRD_2 and DRD_3 heterodimerization [471]. DRD_2 and DRD_3 were found to colocalize on dopaminergic neurons as autoreceptors and at postsynaptic loci to dopaminergic projections in the globus pallidus, nucleus accumbens and in the frontal cortex on pyramidal cells and/or GABAergic interneurons [498,499]. In a study by Maggio and colleagues, [500], it was shown that some antiparkinsonian agents (pramipexole and ropinirole) with a preference for DRD_3, displayed amplified potency at DRD_2-DRD_3 heterodimers. In COS-7 cells cotransfected with DRD_2 and DRD_3, together with a chimeric AC AC-V/VI, these same agents were able to suppress forskolin (FK)-stimulated cAMP production with higher potencies as compared to cells only transfected with DRD_2 or DRD_3 receptors and without exposure to the ligands [500,501]. Furthermore, the binding of this heterodimer may be responsible for the antipsychotic actions of DRD_2 partial agonists and DRD_3 agonists, such as aripiprazole and N-desmethylclozapine [500,502]. The characterization of the pharmacological properties of the DRD_2-DRD_3 heterodimer by Novi and co-workers [502] showed that the agonist quinpirole potently suppresses FK-induced cAMP accumulation in recombinant cell lines transfected with DRD_2 receptors and AC-V/VI, while the partial agonists aripiprazole, S33592, bifeprunox, NDMC, and preclamol less strongly reduce FK-stimulated cAMP accumulation. On the other hand, all these compounds failed to modify FK-induced cAMP accumulation in cells transfected with DRD_3 and the chimeric DRD_3-insensitive AC-V/VI [502]. However, in cells transfected with DRD_2 and an excess of DRD_3, together with AC-V/VI, quinpirole diminished FK-induced cAMP accumulation with a potency and efficacy comparable to cells transfected solely with DRD_2, and the partial agonists were inactive [502]. These results suggest that an excess of DRD_3 receptors can modify the functional status of

DRD_2 receptors, since partial agonists of DRD_2 are transformed into antagonists at the DRD_2-DRD_3 heterodimers [500,503]. Thus, this could justify the low incidence of extrapyramidal side effects of the partial agonists, as the extent of the DRD_2-DRD_3 heterodimer formation is low in the dorsal striatum [500,503]. Knowledge about the structure and action mechanism of this heterodimer provides insights into cellular processes associated with diseases such as schizophrenia, PD, and ADHD.

DRD_4 is also expressed in the brain, but its expression is lower than other types of dopamine receptors [504,505]. However, human DRD_4 has polymorphic variants [506] that are more abundant: $DRD_{4.2}$, $DRD_{4.4}$ and $DRD_{4.7}$ [463]. DRD_2 and DRD_4 receptors partially co-distribute in the dorsal striatum and appear to play a fundamental role in complex behaviours and motor function. In 2011, based on BRET and *in situ* proximity ligation assay (PLA) in cotransfected HEK293T cells showed the coupling between DRD_2 and DRD_4 [463]. Specifically, they showed that the long form of human DRD_2 (DRD_{2long}) was able to interact and form heterodimers with the three human DRD_4 isoforms, with the $DRD_{4.7}$ variant being the least effective [463]. Upon co-activation by the DRD_4 agonist PD168077, DRD_2 agonist-induced ERK phosphorylation was enhanced in cells co-expressing DRD_2 with $DRD_{4.2}$ and $DRD_{4.4}$, but not in cells co-expressing DRD_{2long} with $DRD_{4.7}$ [463]. The $DRD_{4.7}$ variant showed reduced ability to form a heterodimer with DRD_{2long}, as no additive effect was observed after combined treatment with DRD_2 and DRD_4 agonists (quinerolane and PD, respectively) on MAPK activity when these receptors were expressed together [463]. Furthermore, the short form of DRD_2 (DRD_{2short}) was reported to form heterodimer complexes with $DRD_{4.2}$ and $DRD_{4.4}$, while the $DRD_{4.7}$ failed to interact with DRD_{2short} in BRET studies, using cotransfected HEK293T cells [463]. So, the biochemical crosstalk between DRD_{2short} and cotransfected DRD_4 variants potentiates DRD_4-mediated MAPK activation and ERK phosphorylation by DRD_2 and not the inverse [507]. This biochemical crosstalk was not observed in striatal slices taken from gene knock-in mice carrying the human $DRD_{4.7}$, confirming that DRD_2 and $DRD_{4.7}$ do not form heterodimers [507]. Solely DRD_2-$DRD_{4.2}$ and DRD_2-$DRD_{4.4}$ heterodimers exist in the striatum and they may be a potential target for antiparkinsonian drugs [508].

Finally, O'Dowd and colleagues also demonstrated the existence of the DRD_5-DRD_2 heterodimer in HEK293T cells co-expressing both receptors, through FRET analyses [480]. The authors reported that co-activation of both receptors of the DRD_5-DRD_2 heterodimer resulted in the generation of a calcium signal [480]. DRD_5 was able to activate a strong calcium signal when it was expressed alone. These calcium signals resulting from activation of DRD_5 alone or within a heterodimer, require $G_{q/11}$ and phospholipase C (PLC) activity, and the presence of extracellular calcium [480]. However, DRD_5 and DRD_2 heterodimerization negatively modified the functional unit of calcium signalling, attenuating the ability of the DRD_5 receptor to trigger a calcium signal. DRD_5 and DRD_2 receptors have been shown to cooperate functionally to facilitate motor activity and striatal long-term depression [509].

Dopamine - Adenosine receptor heterodimers

Besides neuronal dopaminergic transmission regulation through different heterodimers compositions, dopamine can also be regulated by adenosine. According to George *et*

al., two mechanisms of adenosine receptor-mediated neuromodulation of dopamine exist in cells: (i) adenosine counteracts cAMP levels, which are modulated by dopamine; (ii) adenosine-dopamine receptor dimers exert a different signal then when they are activated as monomers [448].

Co-expression of adenosine and dopamine receptors in different basal ganglia pathways and pathways that control motor behaviour, underlined that different heterodimers exist in neuronal subpopulations [448]. In 2000, Gines and co-workers showed the existence of A_1R-DRD_1 heterodimer, using Co-IP in cotransfected fibroblast cells and cortical neurons in culture [510]. The expression of the A_1R-DRD_1 heterodimer in the brain was demonstrated by Franco and co-workers, using FRET and BRET techniques [511]. A_1R and DRD_1 were found to colocalize in soma and dendritic regions of cortical neurons [512,513]. One of the first evidence found was that A_1R agonists can reduce oral dyskinesias induced by levodopa in rabbits [514]. Adenosine agonists inhibited the motor responses of dopamine in basal ganglia and vice-versa, suggesting their functional antagonist action [515]. While DRD_1 is predominantly coupled to G_s protein, which in turns stimulates AC, A_1R is coupled to $G_{i/o}$ protein, which has inhibitory effects [514]. A_1R antagonist 1,3-dipropyl-8-cyclopentylxanthine lead to an increase in the DRD_1-induced cAMP response, which can be related to their regulation of G proteins having offsetting activities [516]. Thus, co-activation of A_1R-DRD_1 heterodimer induces a decrease of the affinity of DRD_1 for agonist and, consequently, decrease of the DRD_1-induced cAMP accumulation [510,516]. Kalivas and co-workers demonstrated that A_1R-DRD_1 heterodimer can also be involved in the pathophysiology of addiction [517]. They reported that cocaine, a potent stimulant of the CNS, targets the A_1R-DRD_1 heterodimer in rat nucleus accumbens, inhibiting the physical interaction between A_1R and DRD_1 [517]. This evidence emphases the therapeutic relevance of this heterodimer for cocaine addiction. Moreover, a recent study demonstrated the existence of A_1R-DRD_1 heterodimers in the spinal motoneuron, using PLA experiments, and that adenosine tonically inhibited DRD_1-mediated signalling in the spinal motoneuron [518]. Given the importance of controlling motoneuron excitability, the A_1R-DRD_1 heterodimer may also be a potential target for the treatment of spinal cord injury, motor aging-associated disorders, and restless legs syndrome.

$A_{2A}R$-DRD_2 heterodimer was among the first heterodimers reported, involving two different neurotransmitters [448,519,520]. The existence of $A_{2A}R$-DRD_2 was proven by Co-IP, BRET and FRET analyses [521,522]. Later on, PLA studies located the $A_{2A}R$-DRD_2 in the mice striatum [523,524]. A functional association between $A_{2A}R$ and DRD_2 was also reported to exhibit a negative allosteric cooperativity in which the activation of the $A_{2A}R$ by CGS21680 ($A_{2A}R$ agonist) leads to a decrease of DRD_2 of dopamine binding affinity [519,525–527]. Furthermore, the activation of $A_{2A}R$ was shown to decrease coupling of DRD_2 to its $G_{i/o}$ protein and stimulation of DRD_2 was shown to decrease the coupling of $A_{2A}R$ to its G_s protein [520,528]. The effect of the $A_{2A}R$-DRD_2 heterodimer on ligand binding of the monomers and G protein-coupling was also associated with cross-desensitization mechanisms, which function via agonist-induced coaggregation and co-internalization of both receptors [520]. The $A_{2A}R$-DRD_2 is also a promising candidate target for the treatment of PD, schizophrenia and addiction [515,521,528,529]. For instance, the $A_{2A}R$-DRD_2 has been considered as a potential target to reduce L-DOPA-induced dyskinesia in PD treatment [71,530]. Behavioural and microdialysis experiments

in mouse, rat, dog and human models suggested a mechanism that involves a co-expression of $A_{2A}R$-DRD_2 in striatopallidal GABAergic neurons and nucleus accumbens [531–534]. Consequently, selective and potent $A_{2A}R$ antagonists are able to reduce DRD_2-dependent signalling in these areas and enhance therapeutic effects, as it was demonstrated in animal models of PD [526,535–537].

Indications that DRD_3 can heterodimerize with $A_{2A}R$ emerged in 2005, based on confocal microscopy and FRET studies using transiently cotransfected HeLa cells [538]. Results from confocal microscopy showed that $A_{2A}R$ and DRD_3 colocalize in the plasma membrane, and results from FRET experiments showed that $A_{2A}R$ and DRD_3 receptors can form heterodimers in the transiently cotransfected HeLa cells [538]. Also, saturation analysis of [^{3}H]dopamine binding in the $A_{2A}R$-DRD_3, a CHO cell line was generated, indicating that $A_{2A}R$ agonist CGS-21680 is able to significantly reduce the affinity of the high affinity binding state of the DRD_3 receptors for dopamine [538]. Moreover, A_{2A} and DRD_3 receptors seem to interact at the G protein coupling level, since the CGS-21680 $A_{2A}R$ agonist fully counteracted the dopamine mediated strong inhibition of forskolin-induced cAMP accumulation. So, when both receptors are co-expressed in the same cells, the antagonistic interaction of $A_{2A}R$–DRD_3 is verified, that is, A_{2A} receptors antagonistically modulate both, the affinity and the signalling of DRD_3 receptors [538]. Since DRD_3 is involved in the treatment of schizophrenia, the DRD_3–$A_{A2}R$ receptor interactions could provide an alternative antischizophrenic treatment.

<u>Dopamine receptor and other GPCR heterodimers</u>

Besides the intensive relationship between dopamine and adenosine receptors, DRs may also form heterodimers with GPCRs from other families. For instance, H_3R is found in striatal medium spiny neuron that express post-synaptic DRD_1 and obtain histaminergic input from hypothalamic asynaptic varicosities [539]. The receptors were then shown to form DRD_1-H_3R heterodimers by BRET and binding assays in transiently transfected human embryonic cells [540], Co-IP experiments in rats [541] and PLA studies in mice striatum [542]. Upon DRD_1 and H_3R receptors activation by their respective agonists (SKF38393 and (R)-α-methylhistamine (RAMH)), DRD_1 and H_3R lead to the coupling to the $G_{i/o}$ protein and MAPK cascades, respectively [540]. The unique biochemical function of this heterodimer is supported by the fact that, when each receptor is activated alone, DRD_1 leads to the coupling to the $G_{s/olf}$ protein, while H_3R does not signal through the MAPK pathway, and they are unable to induce ERK1/2 phosphorylation in mice with either receptor knockout [540,541,543]. In addition, DRD_1 and H_3R antagonists, such as SCH23390 and thioperamide, can block the distinct signalling mediated by the heterodimer [540]. An antagonist of one of the receptor units in the DRD_1–H_3R heterodimer is able to induce conformational changes in the other receptor and block specific signals originating in the heterodimer [540]. One of the last studies on this heterodimer, performed in rats and mice, reported that cocaine inhibited the bidirectional cross antagonism and the inhibitory effect of the DRD_1 and H_3R signalling [542]. McCormick and co-workers reported that σ1R binds DRD_1-H_3R heterodimers in transfected cells and in mouse and rat striatum. Authors also postulated that cocaine, a σ1R-agonist, modifies the structure and counteract the biochemical properties of the DRD_1-H_3R heterodimer, such as heterodimer signalling through G_i protein, the ability of H_3R activation to signal through MAPK, and the ability of H_3R

ligands to inhibit the effects of DRD_1-mediated signalling, including cell death [542]. They also reported that blockade of H_3R-mediated inhibition of DRD_1 function in the σ1R-DRD_1-H_3R complexes plays a key role in the effects of cocaine [542]. So, σ1R-DRD_1-H_3R may be a new target for the treatment of cocaine abuse.

Besides the DRD_1, also DRD_2 was found to form a heterodimer with H_3R, which was discovered by Ferrada and co-workers in 2008 using BRET in cotransfected HEK293 cells [544]. Heterodimerization of DRD_2 and H_3R was also demonstrated *in vivo* by Moreno and co-workers, using Co-IP studies in rat striatal tissues [541]. DRD_2 and H_3R can colocalize in GABAergic striatal efferent neurons and in specific DRD_2-expressing GABAergic enkephalinergic neurons [545]. The study from Ferrada and co-workers reported the existence of behaviourally significant antagonistic postsynaptic interactions [546] between H_3R and DRD_2 receptors in reserpinized mouse model [544]. Whereby the stimulation of the H_3R significantly decreased the ability of agonists to bind to the DRD_2, while antagonists were unaffected [544]. Thus, this heterodimer may play a role in the function of the GABAergic enkephalinergic neuron [544]. Beyond Parkinson's disease, a therapeutic approach based on H_3R receptor-mediated negative modulation of DRD_2 receptor function may emerge and play a role in disorders involving the cortico-striatal-thalamo-cortical circuits, such as Huntington's disease, Tourette syndrome, obsessive– compulsive disorder, schizophrenia and addiction [544].

DRD_2 was also found to colocalize with SST_5R in transfected HEK293 cells, using FRET [547]. The heterodimerization of both receptors was promoted by application of antidepressant drugs (desipramine and citalopram) [547]. The physical evidence of DRD_2-SST_5R heterodimer was then proven with PLA studies in the striata of mice and striatal neuronal cultures [548]. It was suggested, that the DRD_2-SST5R may be a potential mediator of antidepressant effects, since the heterodimerization of these receptors appeared to occur in native brain tissue and in primary striatal neuronal cultures [548]. Furthermore, prolactin is a neurotransmitter regulated by those two receptors and its excessive excretion was reported in cases of depression [549]. In addition, a study by Szafran-Pilch *et al.* suggested that the stimulation of DRD_2-SST_5R may enhance the inhibition of this prolactin [548]. Proceeding with the promiscuous DRD_2, another interaction partner was reported in a BRET study using transfected HEK293T cells: NTS1R [550]. Recently, Friedland *et. al.* reported the existence of DRD_2-NTS1R heteroreceptor complexes in the accumbens core and shell, especially in the dorsal striatum, using PLA assays [551]. The NTS1R was shown to negatively modulate DRD_2 signalling through immediate receptor-receptor crosstalk, that is, based on CRE luciferase gene assay, NTS1R activation generates a blockade of the DRD_2 induced inhibition of the AC-PKA-CREB pathway [552–554]. Also, the NTS1R agonist NT(8-13) reduces the $G_{\alpha q}$-mediated calcium signal in the DRD_2-NTS1R heterodimer compared to the NTS1R monomer, which can also be reversed by DRD_2 antagonists [551]. The heterodimer activation by CS148, a NTS1R agonist and also DRD_2 antagonist, increases the calcium response, dependable with the effect of the monovalent ligands indicating an allosteric DRD_2-mediated modulation [551]. This provides the evidential basis of functional association of DRD_2 and NTS1R in brain areas that closely linked to the pathophysiology of schizophrenia [551,555].

Another partner for DRD_2 is the TAA_1R, a member of class A GPCRs, not yet well investigated. The DRD_2-TAA_1R heterodimer was found in dopaminergic innervated areas and provides a mechanism for dopamine neurotransmission modulation via TAA_1R [556,557]. Different studies could show that TAA_1R may affect the DRD_2 function and firing rate of dopaminergic neurons [310,556,558]. The DRD_2- TAA_1R heterodimer exerts its effect through the cAMP pathway, and haloperidol was found to promote cAMP-mediated TAA_1R signalling [556]. With haloperidol as a known antipsychotic, the DRD_2-TAA_1R may have a role in the treatment of schizophrenia [299]. The DRD_2-OTR was identified in cotransfected HEK293 cells using PLA [559,560]. Further studies on the DRD_2-OTR suggested the existence of allosteric reciprocal interactions endowed with the ability to enhance signalling of DRD_2-OTR. The heterodimer is excreted upon OT activation, facilitating DRD_2 signalling via allosteric receptor-receptor interactions [560]. It was also reported that the dysfunction of the DRD_2-OTR in the central amygdala may lead to anxiety development [560]. Therefore, restoration of its activity may be a new therapeutic approach against anxiety [560].

Another DRD_2 interaction partner represents the growth hormone secretagogue receptors (GHS-R), also known as Ghrelin receptors [561,562]. GHS-R_{1a} is a transcript variant of GHS-R and encodes the functional protein, which defines a neuroendocrine pathway for growth hormone release [563]. GHS-R signals via $G_{\alpha q/11}$ cascade to mobilize calcium from intracellular stores [564] and plays a role in the regulation of feeding behaviour [565]. Similarly, DRD_2 are also known to control physiological functions like food consumption [566,567]. Henceforth, it was very likely that a DRD_2-GHS-R_{1a} exists, which was eventually discovered by Smith and co-workers, using immunofluorescence and time-resolved FRET experiments in hypothalamic neurons of rodents [568]. Within the DRD_2-GHS-R_{1a}, the apo-ghrelin (unliganded) GHS-R_{1a} was reported to modulate DRD_2 signalling from the normal $G_{\alpha i/o}$ subunit mediated inhibition of cAMP to $G_{\beta\gamma}$ subunit mediated PLC-IP3 cascade [568]. Also, in the absence of ghrelin, the endogenous ligand of GHS-R, dopamine and/or DRD_2 agonists were able to activate this biased $G_{\beta\gamma}$ subunit mediated PLC-IP3 signalling, suggesting that apo-GHS-R_{1a} acts as an allosteric modulator on DRD_2 [568]. In order to assess if the allosteric interaction between DRD_2 and GHS-R_{1a} could be pharmacologically targeted, the selective GHS-R_{1a} antagonist JMV2959 was applied in treated mice with the highly selective neutral GHS-R_{1a} antagonist JMV2959 prior to cabergoline treatment. It was shown that cabergoline-induced anorexia (selective DRD_2 agonist) was blocked upon binding to the DRD_2-GHS-R_{1a} [568]. Targeting heterodimers represents a therapeutic advantage for the treatment of eating disorders.

Adenosine - Adenosine receptor heterodimers

The endogenous purine nucleoside adenosine is obtained by the breakdown of adenosine triphosphate (ATP) and consists of a ribose sugar and adenine attached by a glycosidic linkage [569]. The importance of ATP and its metabolites is further underlined as they are the main energetic molecules in living organisms. The actions of adenosine through the four specific ARs are found in every single mammalian cell [569]. The first heterodimer consisting of A_1R and $A_{2A}R$ was found in 2006 by a study using Co-IP, BRET and time-resolved FRET techniques from Ciruela *et al*. [445]. It was shown that A_1R-

$A_{2A}R$ exists in striatal glutamate neurotransmission at the presynaptic level [445]. Interestingly, both monomers are known to couple to different G proteins, A_1R couples to $G_{i/o}$ whereas $A_{2A}R$ couples to G_s [570]. Ciruela and co-workers were able to demonstrate that depending on the concentration of adenosine, the regulation of glutamate release by cortical glutamatergic terminals would be opposite [445,569]. A_1R-$A_{2A}R$ was shown to regulate the GABA uptake through adenosine in astrocytes. Hence, it was suggested that A_1R-$A_{2A}R$ acts as a sensor of adenosine concentration as consequent fine-tuning modulation of striatal glutamatergic neurotransmission, in a manner that there is either A_1R or $A_{2A}R$-mediated signalling [569]. Elevated extracellular levels of adenosine activate the $A_{2A}R$ protomer in this complex, producing an antagonist allosteric receptor-receptor interaction inhibiting A_1R protomer signalling. Thus, activation of the $A_{2A}R$ in A_1R-$A_{2A}R$ heterodimers produces an increase of glutamate release, while the activation of A_1R leads to the opposite effect [445,546,571]. Upon G protein-coupling to the heterodimer, the long C-terminus of $A_{2A}R$ is the key region that determines the dominant $A_{2A}R$-mediated signalling [569,572]. A_1R-$A_{2A}R$ heterodimers may exist in glutamate projections that regulate GABA striatal pallidal neurons, mediating motor inhibition. In the case of this heterodimer, $A_{2A}R$-induced glutamate release should neutralize movement inhibition, making it a therapeutic target for neurological diseases associated with motor activity [573]. Other studies determined caffeine as a new ligand for A_1R–$A_{2A}R$, which when chronically applied, led to strong tolerance to the psychomotor effects of caffeine mediated by A_1R–$A_{2A}R$ [574].

<u>Adenosine receptor and other GPCR heterodimers</u>

The frequency of 'spontaneous' (non-electrically evoked) excitatory postsynaptic currents (EPSCs) in layer V pyramidal neurons increases after 5-HT_2A receptor activation [575] and leads to an increase in late components of EPSCs evoked by electrical stimulation [576]. Since A_1R and 5-HT_2AR receptors are both localized in the prefrontal cortex, a study about how A_1R receptor modulate 5-HT_2A-enhanced 'spontaneous' and electrically evoked excitatory postsynaptic currents in layer V pyramidal neurons in the medial prefrontal cortex was done by Aghajanian and co-workers [577]. They showed that A_1R-agonist (N^6-cyclopentyladenosine) suppressed the frequency of EPSCs generated via 5-HT_2A receptor-induced glutamate release in the medial prefrontal cortex. As it did not generated large postsynaptic currents, the suppression mechanism was thought to be predominantly presynaptic [577]. Also, in 2009, Marek studied the effects of the A_1R receptor agonist N^6-cyclohexyladenosine on phenethylamine hallucinogen DOI-induced head shakes in order to examine a behaviour induced by activation of 5-HT_2A receptors in the rat prefrontal cortex [578]. The results showed that while N^6-cyclopentyladenosine suppressed head shakes, induced by activation of 5-HT_2A receptors with the DOI, an A_1R receptor antagonist (DPCPX) enhanced DOI-induced head shakes and blocked the suppressant action of an A_1R agonist on DOI-induced head shakes [578]. This mechanism of action of A_1R agonists on the 5-HT_2A receptor suggests a novel therapeutic approach for schizophrenia as well as psychosis and anxiety disorders [577,578].

In 2018, an $A_{2A}R$-H_3R heterodimer was discovered for the first time in recombinant cell systems and in rat striatal nerve terminals, based on functional complementation and

Co-IP assays in HEK293T cells [579]. $A_{2A}R$ and H_3R were found to be co-expressed in the cortico-striatal glutamatergic afferents and the GABAergic medium-sized spiny neurons that originate from the indirect pathway of the basal ganglia [579]. Therefore, both monomers can regulate the striatal GABAergic and glutamatergic transmission. It was reported that the co-activation of $A_{2A}R$ and H_3R leads to enhancement of $A_{2A}R$ signalling and decrease of H_3R functionality via their coupled G proteins [579]. As a protomer, H_3R is coupled to $G_{i/o}$ proteins and, consequently, inhibits AC activity. When RAMH, a H_3R agonist, activates the H_3R receptor, it leads to a decrease in cAMP formation. However, the expression of $A_{2A}R$ leads to an increase of the H_3R-mediated cAMP formation [579]. In addition, the endogenous ligand histamine cannot signal through the heterodimer, unlike the exogenous agonist RAMH, suggesting that RAMH can lead to conformational changes in the H_3R, allowing heterodimerization. On the other hand, the histamine-induced changes may not be sufficient to signal the heterodimer [579]. Based on binding studies with striatal membranes and histamine, it was demonstrated that H_3R activation by histamine resulted in an increase of the binding affinity of the $A_{2A}R$ for its agonist CGS-21680, while RAMH resulted in a decrease of the binding affinity, indicating that histamine and RAMH lock the H_3R in different conformational states that affect its interaction with the $A_{2A}R$ [579]. It is possible that the H_3R-$A_{2A}R$ heterodimer plays a role with key physiological implications.

Opioid - Opioid receptor heterodimers

As referred, the most effective analgesics in clinical pain management are opioids such as morphine, codeine, hydrocodone, oxycodone, fentanyl, and tramadol [580]. However, they are also commonly prescribed and frequently abused [581,582]. Among the intricacy of opioid receptor pharmacology, opioid receptor heterodimers represent another important layer of signalling complexity and provide an opportunity for the development of analgesics with fewer side effects [583]. Dimerization was already reported for homodimers MOR-MOR [584] and heterodimers containing only opioid receptors such as MOR-DOR [585–587], MOR-KOR [588] and DOR-KOR heterodimer [589], were proven to exist both *in vitro* and *in vivo*. OR heterodimers are often expressed in limited and specific brain regions and are involved in adverse effects induced by chronic opioid therapy, underlining the importance to develop therapeutic strategies to target these heterodimers [108,590].

Selective agonists and antagonists were developed to target MOR-DOR [591]. Devi and Rozenfeld reported that the MOR agonist Tyr-D-Ala-Gly-*N*-Me-Phe-Gly-ol (DAMGO) activates $G_{i/o}$-mediated signalling in MOR-expressing cells as well as β-arrestin-2-mediated signalling for changing the dynamics of ERK-mediated signalling in MOR-DOR heterodimer-expressing cells [592]. In MOR-DOR expressing cells, using a chimeric G protein-mediated calcium fluorescence assay, it was shown that the DOR selective agonist SNC80 induces intracellular Ca^{2+} release [593]. Another example is CYM51010, a selective MOR-DOR agonist, able to induce the recruitment of β-arrestin-2 and GTPγS binding, which could then be blocked by a MOR-DOR selective antibody (mAb) [594]. Here, the DOR was shown to have an antagonistic allosteric influence on MOR activity within the heterodimer [590]. The DOR peptide antagonist TIPPΨ was shown to enhance the binding of morphine to MOR, $G_{i/o}$ coupling and inhibition of cAMP levels [587]. Furthermore, the MOR-DOR may also have specific intracellular trafficking. According to

studies by Milan-Lobo and Whistler, MOR and DOR are only able to dimerize when both are present at the plasma membrane [595]. Controversly, Hasbi *et al.*, stated that MOR-DOR are located in the endoplasmic reticulum, where they recruit the G_{az} protein [596]. Another study by Décaillot *et al.* reported that the agonists DAMGO, Deltorphin (Delt) II, SNC80 and methadone can induce MOR-DOR endocytosis, but others such as DADPE were not able to do so [597]. In the same study, Décaillot and co-workers identified RTP4, a Golgi chaperone as an important regulator of MOR-DOR levels at the cell surface [597]. This was found to be in concordance with a study by He *et al.*, where the application of DOR-selective agonists Delt I, Delt II and SNC80 induced endocytosis and further procession of degradation of DOR and MOR, resulting in a reduced MOR surface expression in double-transfected HEK293 cells [598]. This effect was also achieved when DAMGO, a selective MOR agonist, was applied [598]. The effect was then only diminished when an interfering peptide D-Phe-Cys-Tyr-D-Trp-Om-Thr-Pen-Thr-NH2 (CTOP) or the antagonist naloxone was added [598]. In order to perform a whole-brain dual receptor mapping study, RedMOR/ greenDOR double knock-in mice were generated. MOR and DOR were colocalized in subcortical neuronal networks, responsible for eating actions, sexual behaviours or response to aversive stimuli [599]. In 2018, Wang *et al.* found that the co-expression of MOR and DOR is restricted to small populations of spinal cord neurons and yet is rare in the parabrachial, amygdala and cortical regions of the brain for pain processing [600]. In another study carried out by Gomes *et al*., they showed, using tail-flick assays in mice, that the CYM51010 ligand for the heterodimer MOR-DOR has analgesic activity identical to the one from morphine [594]. Also, CYM51010-induced analgesia was abrogated in MOR knockout mice and still persisted in morphine-tolerant mice [594]. The evidence of these heterodimers in CNS pain circuits suggests that MOR-DOR heterodimers cellular interactions are important for the development of novel opioid analgesics.

The MOR-KOR heterodimer was discovered in 2010 by Chakrabarti and co-workers [588]. The results of their study showed that MOR-KOR was more prevalent in the spinal cord of proestrus (with high estrogen receptor levels) vs. diestrus females and vs. males [588,601]. It was then concluded that dynorphin would serve a potential female-specific KOR-ligand within the MOR-KOR. Furthermore, gender- and ovarian steroid-dependent recruitment of MOR-KOR was seen as a way to balance the actions of anti-nociceptive and pro-nociceptive functions of the dynorphin/KOR opioid system in the spinal cord. Lastly, various types of chronic pain states that are significantly more common in women than men, could be the result of impaired formation of MOR-KOR and therefore this holds promise for the development of a special ligands to target the MOR-KOR [590].

Opioid receptor and other GPCR heterodimers

The main goal of studying OR heterodimers is to understand their existence and physiological function under the perspective of pain transmission. Once resolved, potent analgesics with fewer side effects could be developed. Studies by Vilardaga *et al.* and Yang *et al.* showed that a conformational antagonistic crosstalk exists between MOR and α_{2A}AR [602,603]. FRET microscopy studies showed that MOR and α_{2A}AR communicate via a switch of conformations within the monomers that leads to inhibition of one monomer by the other [602]. Morphine binding to MOR within the MOR-α_{2A}AR

was reported to induce a conformational change in the norepinephrine-bound α_{2A}AR, which then inhibits $G_{\alpha i}$ signalling and the downstream MAP kinase responses [602]. Hence, MOR activation mediates the rapid inactivation of its coupled partner α_{2A}AR. Already in the 90s it was reported that combined agonist acting on MOR and α_{2A}AR would act synergistically when co-administered into the spinal cord and would have an analgesic effect [604]. Furthermore, it was also reported that norepinephrine or clonidine, which are both agonists of α_{2A}AR, were able to reduce significantly the release of glutamate, substance P and calcitonin gene related peptides from spinal cord synapses [605,606]. MOR and α_{2A}AR were both located in the superficial layers of the dorsal horn of the spinal cord, and in the rat spinal cord, α_{2A}AR was located on the terminals of capsaicin-sensitive, SP-containing primary afferent fibers in immunostaining studies [605]. Both receptors were reported to affect the nociceptive system and are particularly involved in depression of neurotransmitter release in the spinal cord [607,608]. However, the synergy of MOR and α_{2A}AR agonists in the MOR-α_{2A}AR in analgesia remains unclear [590].

In 2019, Wang and co-workers identified the MOR-GPR139 heterodimer in which the orphan GPR139 negatively regulates the opioid receptor function, signalling and trafficking [590,609]. By using *C. elegans* as a model organism, it was shown that mammalian MOR was expressed in the nervous system of nematodes (tgMOR), and that application of morphine and fentanyl leads to a decrease in locomotion in nematodes expressing tgMOR [590,609]. By applying a large-scale genetic screening and whole genome sequencing, Wang *et al.* identified the orphan receptor FRPR-13, the homolog of the human GPR139, as negative regulator of MOR *in vivo* [590,609]. The functional relationship between MOR and GPR139 was further investigated in MOR and GPR139 transfected HEK293 cells, where MOR activation was shown to cause an opening of G protein-coupled inwardly rectifying potassium channels (GIRKs). This lead to hyperpolarization of membrane potential, which could be inhibited by GPR139 expression [590,609]. In addition, Zhang *et al.* were able to show that MOR and GP139 could be co-immunoprecipitated. They also showed that when GPR139 was highly overexpressed, the cell surface expression of MOR was reduced, suggesting that GPR139 is able to regulate MOR trafficking to the plasma membrane or internalization [590]. Furthermore, GPR139 was found to bind directly to MOR *in vitro* and promote the recruitment of β-arrestin-2 and inhibit GIRK and G protein activation [590]. More evidence for MOR-GPR139 was generated in *in situ* hybridization experiments, where MOR and GPR139 are co-expressed in similar brain regions [590]. Zhang *et al.* also provided electrophysiological evidence, where in cultured brain slices GPR139 deficiency reduced the basal firing rate and increased opioid sensitivity in neurons [590]. Lastly Wang *et al.* investigated the relationship between MOR and GPR139 in *in vivo* animal studies in mice. GPR139 knockout (KO) mice had normal baseline learning, nociception, locomotor activities, and motor coordination, but showed sensitivity to morphine-induced analgesia and reward effects [590,609]. When JNJ-63533054, an GPR139-agonist, was administered, morphine-induced analgesia and rewards was inhibited in mice [590,609]. Also, GPR139 KO mice did not show explicit opioid withdrawal reactions [590,609]. Hence, GPR139 was identified as a novel anti-opioid system in the brain.

In 2018, Koshimizu and co-workers identified the MOR-V_{1B}R heterodimer [610]. The endogenous ligand of V_{1B}R, ADH (or also AVP) was reported to regulate morphine tolerance and sensitivity [590]. Koshimizu *et al.* revealed in V_{1B}R KO mice, the nociceptive thresholds and morphine sensitivity is enhanced. Also, the development of analgesic tolerance to morphine was significantly delayed in these mice, when V_{1B}R-subtype-selective antagonist SSR149415 was administrated [610]. Furthermore, application of SSR149415, a selective V_{1B}R-antagonist but not a V_{1A}R-antagonist, into the lateral ventricle of the mice also reduced the development of morphine tolerance [590,610]. In *in situ* hybridization experiments, Koshimizu *et al.* discovered that MOR and V_{1B}R colocalized in the rostral ventromedial medulla [590,610]. By using cotransfected HEK293 cells, a functional interaction between MOR and V_{1B}R was observed as well as in single cells BRET analysis (close proximity of both receptors <10 nm) [590,610]. In another experiment, using a radioligand binding assay and cyclic AMP assay, morphine binding to MOR was shown to be significantly influenced by MOR-V_{1B}R formation [590,610]. Also, ADH-enhanced morphine-induced super activation of the AC triggered by the MOR-V_{1B}R, was indicated to be dependent on β-arrestin-2 and ERK phosphorylation [590,610]. Koshimizu and co-workers also discovered that a leucine-rich segment in the C-terminal tail of the V_{1B}R is responsible for binding of β-arrestin-2, which when deleted through genome editing, increased morphine analgesia and reduced ADH-mediated AC super activation increased [590,610]. Taking all findings together, it was suggested that the MOR-V_{1B}R is indeed another mechanism to alter opioid receptor function such that morphine-induced analgesia could be potentiated, and morphine tolerance could be delayed.

The formation of a MOR-GAL_1R was identified by Moreno *et al.*, in transfected cells and in neurons in the rat ventral tegmental area (VTA) [611]. Previous *in vivo* studies showed that behavioural effects of MOR agonists were counteracted by galanin [590]. According to Moreno *et al.* the MOR-GAL_1R mediates antagonist interactions between MOR- and GAL_1R-selective ligands and is a key player in the functioning of dopaminergic neurons [611]. In another study by Cai *et al.* it was discovered that methadone potency for stimulating dopamine release and euphoria was reduced through MOR-GAL_1R heterodimers in the rat VTA [590,612]. Such alterations of opioid receptor functions in opioid-induced rewarding were not observed for other opioids such as morphine and fentanyl [590,612]. These data suggest that MOR-GAL_1R mediates dopaminergic effects of opioids and that pharmacological differences between methadone and other opioids may provide a way to dissect the euphoric from therapeutic effects of methadone-like compounds [590,612]. Consequently, novel methadone-like compounds with reduced potency, able to activate MOR-GAL_1R may be a possibility to develop safer opioid analgesics [590,612].

Early studies in 2001, identified MOR and CB_1R co-localization in lamina II neurons in the spinal cord [613]. Synergistic interactions between the opioid and the cannabinoid system in analgesia were already known, as the CB_1R is also present in the brain on primary sensory neurons in the DRGs, spinal cord, and some brain regions related to pain processing [590,614,615]. Rios *et al.* were able to show MOR-CB_1R heterodimers in transfected HEK293 cells using biophysical methods, such as BRET [616]. Additionally, they demonstrated that co-activation of MOR-CB_1R would lead to

antagonistic allosteric interactions, which was determined by cross-inhibition of neurite outgrowth involving inhibition of the Src-STAT3 pathway [590,616]. In 2016, Manduca *et al.* identified MOR-CB_1R heterodimers in rodents nucleus accumbens core (NAcC) and studied the importance of MOR-CB_1R heterodimers to control social behaviour in adolescent rodents [617]. They studied, in particular, the role of the endocannabinoid 2-arachidonoylglycerol (2-AG) in social play [617]. 2-AG is released in the brain of adolescent rats during social play [618] and 2-AG levels are high in the NAc of socially stimulated mice [619]. Systemic administration of the JZL184 (a 2-AG hydrolysis inhibitor) or morphine (MOR agonist) increased social play behaviour in adolescent rats [617]. However, these social play-enhancing effects were blocked by direct infusion of SR141716 (CB_1R antagonist) and naloxone (MOR antagonist) into the NAcC [617]. Neuronal plasticity and socioemotional behaviours could be modulated by MOR-CB_1R.

Already in the 90s it was discovered that the cholecystokinin octapeptide (CCK8) antagonises opioid analgesia [620]. Furthermore, using L-365,260, a CCK_2R/CCKBR-selective antagonist, it was shown that CCK-8 inhibited opioid analgesia through CCKBR [621]. In 2018, Yang *et al.* identified the MOR-CCKBR heterodimer, which they believed may underlie the CCK8-antagonism of opioid analgesia [590,602]. Co-localization studies using double-labelling immunofluorescence staining showed that MOR and CCKBR colocalize in neurons in spinal cord dorsal horn and DRGs. Using Co-IP and fluorescence lifetime-imaging-microscopy-based fluorescence resonance energy transfer (FLIM-FRET) assays, Yang *et al.* showed heterodimerization of MOR and CCKBR in HEK293 cells [590,602]. They also validated that the TM3 of MOR plays a key role in the formation of MOR-CCKBR [590,602]. The MOR-CCKBR functions include a decrease in MOR affinity for ligands and reduction of agonist-mediated phosphorylation of ERK1/2 in transfected HEK293 cells [590,602]. In their study Yang and co-workers developed a cell-penetrating interfering peptide by adding the TAT sequence (RKKRRQRRR) to the C terminal of the entire TM3 (TM3MOR-TAT), which disrupted the MOR-CCKBR [590,602]. In transfected cells TM3MOR-TAT was shown to enhance MOR signalling and in rats it prevented CCK8-induced antagonism against morphine analgesia, rendering TM3MOR-TAT as a promising target for increasing morphine analgesia without applying increasing amounts of morphine [590,602].

Suzuki *et al.* demonstrated that MOR and chemokine receptor CCR5 can also form heterodimers in the cell membrane of lymphocytes, using Co-IP and chemical crosslinking experiments [622]. In this study, the authors demonstrated that the MOR-CCR5 heterodimer is functional, since the co-activation of receptors with morphine (MOR agonist) and MIP-1beta (CCR5 agonist) suppresses the inhibitory effect of MIP-1beta and increases the stimulatory effect of morphine on CCR5 expression [622]. Also in 2002, based on behavioural test in rats' PAG (the brain area that is the focus of opioid analgesic actions), Szabo *et al.* found the ability of CCR5 receptors to desensitize MOR receptors [623]. They demonstrated that chemokine ligands for CCR5 (CCL5) can inactivate the normal neuronal signalling pathway involved in reducing the sensation of pain [623].. Thus, activation of MOR-CCR5 increased nociception.

In 2008, immunohistochemistry experiments by Juhasz *et al.* demonstrated that MOR and DRD_1 colocalized in neurons of the cortex and caudate nucleus and in living cells

[638]. They showed within the cellular nuclear translocation pathway that MOR-DRD_1 formation resulted in a significantly enhanced surface expression of MOR [624]. Another study by Tao *et al.* by performing Co-IP, BRET and cross-antagonism assays, confirmed the existence of MOR-$DRD_{1\ [625]}$. Furthermore, they could show that SCH23390, a DRD_1-selective antagonist, was able to inhibit the agonist-induced activation of MOR and downstream signalling in transfected cells and in striatal tissues from wild-type but not DRD_1 KO mice [625].. Similarly, to what has been described for heterodimers so far, antagonizing one monomer within the dimer, also inhibits the signalling of the partnered monomer, although the latter was activated by its own ligand [625]. In addition, the MOR-DRD_1 was identified *in vivo* through biochemical and biophysical assays [625]. Here it was shown, that by destruction of the dopaminergic projection from the ventral tegmental area to the striatum, dopamine release was abolished, and SCH23390 was still able to significantly inhibit agonist-induced MOR behavioural responses in rats [625]. Lastly, Tao *et al.* demonstrated that MOR or DRD_1 KO mice were not able to show locomotor sensitization to morphine, because they were unable to form MOR-$DRD_{1\ [625]}$. Hence, MOR-DRD_1 may be involved in the dopamine-independent expression of locomotor sensitization to opiates [625].

MOR and DRD_2 receptors are colocalized in the spinal cords of mice, confirmed by Co-IP assays [626]. In 2019, Stove and co-workers proved the existence of MOR-DRD_2 heterodimers using HEK293T and HeLa cells, both cotransfected, by Co-IP, BRET, FRET and functional complementation of a split luciferase techniques [627]. MOR activation by its agonists (DAMGO and fentanyl) resulted in a recruitment of β-arrestin to the receptor and, consequently, caused internalization of the receptor [628,629]. This β-arrestin recruitment is associated with the unwanted effects of opioids [630,631]. Based on time-lapse imaging technique, the effect of heterodimerization of MOR-DRD_{2long} on the internalization characteristics of MOR, indicated a decrease in the internalization of MOR-YFP (MOR associated with Yellow fluorescent protein) with the co-expression of DRD_{2long}, when stimulated upon addition of DAMGO [627]. This suggests that the heterodimer may be a potential therapeutic target associated with diseases such as addiction.

Serotonin - serotonin receptor heterodimers

5-HT_{1A} and 5-HT_{2A} receptors, which have inhibitory actions via $G_{i/o}$ and excitatory actions via $G_{q/11}$, respectively, are the two major known 5-HT receptors in the brain [632]. The evidence that 5-HT_{1A} and 5-HT_{2A} receptors can form a heterodimer was demonstrated by Borroto-Escuela *et al.* in the dorsal hippocampus and the anterior cingulate cortex using *in situ* PLA assay and BRET saturation assay in cotransfected HEK293T cells [633]. Based on a 5-HT_{1A} radioligand binding assay, Borroto-Escuela *et al.* showed that TCB2 (5-HT_{2A} agonist) reduced the binding affinity of the 5-HT_{1A} agonist ipsapirone in membranes of the frontal lobe of the cortex [633]. However, this action seems to be blocked by ketanserin, a 5-HT_{2A} antagonist. These results suggest that 5-HT_{1A}-5-HT_{2A} heterodimers perform inhibitory interactions of the allosteric type, with a dominant effect of 5-HT_{2A} over 5-HT_{1A} protomer [633]. In 2018, another study with this heterodimer was performed to understand how antipsychotic drugs, such as clozapine, ketamine and haloperidol, affect the formation of the heterodimer [634]. Clozapine and ketamine

showed an impact on heterodimer formation. Whereas ketamine exhibited high affinity only for 5-HT_{2A}, clozapine only had an effect on heterodimers in low dosage [634]. Since both receptors are known to be involved in depression [635], this heterodimer may play a role in this disease.

5-HT_{2A}, 5-HT_{2B} and 5-HT_{2C} receptors are both $G_{q/11}$-coupled receptors, which mediate excitatory neurotransmission [636]. These receptors are co-expressed in GABAergic interneurons and in a subpopulation of pyramidal neurons of the prefrontal cortex (PFC) [637,638], and in dopaminergic neurons of the ventral tegmental area [639,640]. Using Co-IP and BRET techniques, Moutkine and co-workers demonstrated that 5-HT_{2A}-5-HT_{2B} and 5-HT_{2A}-5-HT_{2C} heterodimers can be formed, when co-expressed in heterologous expression systems [641]. In 5-HT_{2C}-containing heterodimers, ligands bind and activate only the 5-HT_{2C} protomer. The same authors also demonstrated that 5-HT_{2A}-5-HT_{2B} and 5-HT_{2A}-5-HT_{2C} heterodimers exhibit an asymmetry in G_q-protein coupling, and that signalling from 5-HT_{2A} and 5-HT_{2B} protomers is blunted, as only the 5-HT_{2C} protomer is able to activate the G_q protein [641]. Thus, there is a dominance of 5-HT_{2C} on 5-HT_{2A} and 5-HT_{2B} receptor binding. Also, this dominant effect was validated *in vivo* (observed in neurons), which resulted in an exogenous expression of an inactive form of the 5-HT_{2C} receptor in the locus ceruleus associated with a decreased 5-HT_{2A}-dependent noradrenergic transmission [[641]. As such, these heterodimers must be considered for depression and addiction conditions.

Heterodimerization between 5-HT_{1A} and 5-HT_7 receptors was demonstrated by Ponimaskin and colleagues, using Co-IP and immunoblotting techniques and FRET assays in cotransfected neuroblastoma N1E-115 cells [642]. The 5-HT_{1A} receptor is $G_{i/o}$-coupled, which induces inhibition of AC and decrease of intracellular cAMP [643,644], and the 5-HT_7 receptor is $G_{\beta\gamma}$-coupled, which activates K^+ channels and MAPK Erk2 [643]. 5-HT_{1A}-5-HT_7 heterodimerization decreases the 5-HT_{1A}-receptor-mediated activation of G_i protein without affecting 5-HT_7-receptor-mediated G_s protein activation. Also, authors discovered that 5-HT_{1A}–5-HT_7 heterodimers reduce the ability of 5-HT_{1A} receptors to activate GIRK channels, an effect mediated through the Gβγ subunits of inhibitory G proteins [643]. This phenomenon may result from 5-HT_7 interacting with and directly modulating 5-HT_{1A}. In addition, MAP kinases ERK1/2 phosphorylation is induced by 5-HT_{1A} agonists, and this signal is enhanced when 5-HT_7 receptors are co-expressed, which suggests that heterodimerization favours activation of 5-HT_{1A}-receptor-mediated ERK signalling whereas it prevents 5-HT_{1A}-mediated activation of $G_{i/o}$-GIRK channel activity [643]. The differences in desensitization patterns between pre- and postsynaptic 5-HT_{1A} receptors can be explained by the differences in relative concentration of 5-HT_{1A}-5-HT_7 heterodimers on presynaptic serotonergic neurons and postsynaptic neurons. Besides, regulated and balanced ratio of homo- and heterodimerization on pre- and postsynaptic neurons may be involved in both the onset and the response to the treatment of neurological conditions, such as depression, anxiety, schizophrenia and drug abuse [645,646].

Serotonin receptor and other GPCR heterodimers

It is well established that the dopaminergic and the serotonin system play an important role in neurotransmission, and thus their malfunctioning is suggested to be linked to the development of psychiatric disorders such as schizophrenia [634]. Łukasiewicz and co-workers identified in HEK293 cells the presence of 5-HT_{1A}R-DRD_2 heterodimers [647]. The heterodimerization was shown to be mainly enhanced by exposure of clozapine but also by other antipsychotics such as olanzapine, aripiprazole, and lurasidone [647]. Functional assays like as cAMP and IP1 and ERK activation, indicated that the different antipsychotics exhibited diverse effects on the 5-HT_{1A}R-DRD_2 [661]. For instance, Łukasiewicz *et al*. demonstrated that clozapine and 8-OH-DPAT potentiated postsynaptic effects, especially ERK activation [647]. Furthermore, 5-HT_{1A}R activation by 8-OH-DPAT along with the DRD_2-blockade by clozapine led to a conformal change within the heterodimer and consequently change their signalling via $G_{\alpha q/11}$-mediated activation of ERK1/2 [647]. In 2018, a study by Szlachta *et al.* investigated the role of well-known antipsychotic drugs, clozapine and haloperidol, in the formation of 5-HT_{1A}R-DRD_2 heterodimers in mouse cortex [634]. By using PLA, in *in vitro* and *ex vivo* experiments co-localization of 5-HT_{1A}R and DRD_2 was confirmed [634]. Also, Szlacht and co-workers demonstrated that low-dose administration of clozapine increased the levels of 5-HT_{1A}R-DRD_2, while administration of haloperidol decreased their level in mouse cortices [634]. Different studies located the 5-HT_{1A}R-DRD_2 in the dorsal and ventral striatum using *in situ* PLA and FRET as well as in cellular models using BRET [648–650]. The 5-HT_{1A}R-DRD_2 has developed as an important therapeutic target due to a well-documented serotonin-dopamine interaction and its relevance to schizophrenia [651].

A study by Albizu *et al.*, using radioligand-binding and inositol phosphate production assays, identified a functional crosstalk between 5-HT_{2A}R and DRD_2 in the mouse brain and in HEK293 cells [649]. They were able to show that DRD_2 activation increases the hallucinogenic agonist affinity for 5-HT_{2A}R and decreases the 5-HT_{2A}R induced inositol phosphate production [649]. Albizu and co-workers demonstrated that the inhibition of MK-801-induced locomotor activity by DRD2 antagonist haloperidol requires the 5-HT_{2A}R expression [649]. MK-801, a potent and selective non-competitive NMDA receptor antagonist also known as dizocilpine, serves as a pharmacological model for schizophrenia in mice [652]. It was reported that MK-801 increases the locomotor activity of mice, a behaviour that is suppressed by the DR-antagonist haloperidol [653]. In Co-IP studies Albizu *et al*. showed that 5-HT_{2A}R and DRD_2 are able to interact physically in HEK293 cells [649]. Lastly, they suggested that depending on the treatment combination, different actions could be achieved by application of DRD_2-ligands such as quinpirole or butaclamol and 5-HT_{2A}R-ligands such as DOI and ketanserin [649]. DRD_2 expression was shown to increase the efficacy of DOI to activate the 5-HT_{2A}R-induced phosphoinositol $G_{q/11}$ signalling pathway [649]. Only the hallucinogenic partial agonist DOI seemed to promote this effect on 5-HT_{2A}R signalling [649].

The 5-HT_{1A}R and GAL_1R are both known to couple to $G_{i/o}$ proteins and transduce their signals mainly by inhibitions of the AC, calcium channel activity and neurotransmitter release [643,654,655]. In 2010, a study by Borroto-Escuela *et al.* discovered 5-HT_{1A}R-GAL_1R heterodimers in double-transfected mammalian cells with PLA and FRET techniques [654]. The presence of 5-HT_{1A}R-GAL_1R, induced either MAPK or AC

signalling pathways, indicating a allosteric cross-inhibition mechanism in order to block the excessive activation of $G_{i/o}$ and an exaggerated inhibition of AC or stimulation of MAPK activity [654]. By using reporter gene assays, CRE-luciferase and SRE-luciferase assays, it was possible for Borroto-Escuela *et al.* to further assess possible antagonistic allosteric receptor-receptor interactions 5-HT_{1A}R-GAL_1R [654]. In the brain, previous biochemical, cardiovascular and behavioural work has given additional proof for the existence of antagonistic 5-HT_{1A}R-GAL_1R interactions [656–661].

Only recently, in 2019, Chruścicka *et al*. discovered the existence of 5-HT_{2A}R-OTR heterodimers *in vitro* in living cells using a flow cytometry-based FRET approach and confocal microscopy [662]. The 5-HT_{2A}R and OTR were found to be expressed in similar brain regions modulating central pathways critical for social and cognition-related behaviours [663–666]. Therefore, Chruścicka *et al.* applied the PLA technique *ex vivo* in order to observe the formation and location of the 5-HT_{2A}R-OTR, which were found in limbic regions such as hippocampus, cingulate cortex and nucleus accumbens [662]. These were identified as key regions associated with cognition and social-related behaviours [662]. Functional crosstalk was observed in 5-HT_{2A}R-OTR using cellular-based assays, when a reduction in potency and efficacy of oxytocin, carbetocin and WAY267464 (synthetic OTR-agonists) was observed on OTR-mediated $G_{\alpha q}$ signalling [662]. Likewise, 5HT-induced activation of 5-HT_{2A}R also revealed attenuation in $G_{\alpha q}$-mediated signalling. According to Chruścicka *et al.* co-trafficking of 5-HT_{2A}R and OTR within the cell was also demonstrated [662].

Chruścicka *et al.* pointed towards the existence of 5-HT_{2C}-OTR heterodimer, based on FRET and confocal microscopy *in vitro* in a heterologous cell expression system and further using PLA assays in the rat brain [667]. 5-HT_{2C}R and OTR co-expression resulted in an attenuation of OTR-mediated G_q-signalling and significant changes in receptor trafficking. This attenuation was specifically caused by 5-HT_{2C}R protomer activation [667]. It seems likely that 5-HT_{2A}R-OTR and 5-HT_{2C}-OTR heterodimers can be involved in the development of depression and other types of psychiatric diseases involving disturbances in social behaviours.

To date, a functional link between the serotoninergic and melatoninergic system has only been sparsely reported. In a study by Prosser *et al.*, functional crosstalk between those two systems was reported, revealing that melatonin inhibits the ability of 5-HT to phase shift the suprachiasmatic circadian clock [668]. In addition, melatonin is synthetically derived from 5-HT, and therefore a close relationship is probable [669]. Furthermore, the clinically proven antidepressant ago-melatine, the first *non*-monoaminergic therapeutic, was shown to act as agonist at MT_1R and MT_2R, which are coupled to G_i proteins, while it is a neutral antagonist at the $G_{q/11}$-coupled 5-HT_{2C}R system [670,671]. According to Racagni, the affinity of agomelatine was reported to be substantially lower at 5-HT_{2C}R compared to MT_1R and MT_2R *in vitro*, suggesting that it may exert its actions “synergistically” [672]. It was also discovered that 5-HT_{2C}R, MT_1R and MT_2R are necessary for expression of the antidepressant actions of agomelatine, which cannot be reproduced either by melatonin or by selective 5-HT_{2C}R antagonists alone [669,672]. However, Kamal *et al.* presented evidence that 5-HT_{2C}R and MT_2R are able to form a heterodimer, by using Co-IP, BRET and pharmacological techniques, in transfected cells

and in human cortex and hippocampus [669]. The 5-HT_{2C}R-MT_2R was also discovered in the mouse brain [673]. The 5-HT_{2C}R-MT_2R was reported to be composed of G_i-coupled melatonin MT_2R and G_q-coupled serotonin 5-HT_{2C}R [669,673]. The activation of 5-HT_{2C}R-MT_2R was shown to amplify the activation of 5-HT-mediated G_q/phospholipase C response and trigger melatonin-induced unidirectional transactivation of the 5-HT_{2C}R [669,673]. According to Kamal *et al.*, agomelatine (antidepressant) has a distinctive profile on 5-HT_{2C}R-MT_2R. Whereas melatonin is able to activate both G_i and G_q pathways, agomelatine tends to activate the G_i/cAMP pathway and has an allosteric antagonistic effect on 5-HT-induced G_q pathway activation [669]. Lastly, a beneficial involvement of agomelatine in 5-HT_{2C}R-MT_2R heterodimer was suggested for the treatment of major depression and generalized anxiety disorder [669].

MOR and 5-HT_{1A} receptors are co-expressed in discrete areas of brain, such as, dorsal raphe nucleus, periaqueductal grey neuron, dorsal horn of the spinal cord, amygdala and primary afferent nociceptive fibers [674–676]. Also, both receptors are coupled to $G_{i/o}$ protein, which induces the inhibition of AC, the opening of K^+ channels, the closing of Ca^{2+} channels and the stimulation MAPK ERK1/2 pathways [677]. 5-HT_{1A}-MOR heterodimers were detected by Cussac *et al.* using Co-IP and by BRETmax determination in transiently cotransfected COS7, HEK293 or CHO-K1 cells [678]. To demonstrate the functional transactivation in GPCR heterodimers, they used receptor-G_α-protein fusions, consisting in the application of fusion proteins of protomers with a subtype of G_α protein, and that it is only activated by protomers if they are not in a free form [679]. As a result, by co-expressing the MOR and 5-HT_{1A}-$G_{\alpha o}$ fusion protein as well as MOR and 5-HT_{1A}-$G_{\alpha 15}$ fusion protein, they demonstrated that both receptors can induce transactivation of the G_α protein fused to its partner protomer in membrane preparations and in live cells, respectively [678]. In addition, MOR and 5-HT_{1A} receptors can co-exert control in the ERK1/2 pathway. However, the MOR receptor-induced EKR1/2 phosphorylation was selectively desensitized by prolonged stimulation and activation of 5-HT_{1A} receptor with 8-OH-DPAT agonist [678]. This heterodimer could have interesting therapeutic influences, since MOR and 5-HT_{1A} are involved in pain control.

Cannabinoid - Cannabinoid receptor heterodimers

One of the most important inhibitory regulation mechanisms acting in the CNS is the cannabinoid system [680,681]. The two cannabinoid receptors, CB_1R and CB_2R, share around 44% sequence similarity [682,683]. Until 2012 it was not clear if cannabinoid receptors were able to form heterodimers, despite the fact, that CB_1R and CB_2R have overlapping expression tissues and that they have been shown to regulate similar cellular processes [684]. Heteromerization of CB_1R and CB_2R was then demonstrated in a large study by Callén *et al*. [684]. In this study the receptors were investigated using cotransfected cells and in a variety of brain tissues, including pineal gland, nucleus accumbens, and globus pallidus and BRET technique and *in situ* PLA [684]. Another study by Sierra and co-workers identified the first CB_1R-CB_2R heterodimers in pallidothalamic projection neurons in the monkey, using PLA [685]. Both, CB_1R and CB_2R are coupled to G_i proteins, which is particular interesting as within the CB_1R-CB_2R heterodimer the CB_1R-antagonist AM251 was reported to block the effect of the CB_2R-

agonist JWH133 and *vice versa*, the CB_2R-antagonist AM630 was reported to inhibit the effect of the CB_1R-agonist ACEA [684,686]. Furthermore, agonist co-activation by ACEA and JWH133 of the CB_1R-CB_2R heterodimer was shown to lead to negative crosstalk in Akt phosphorylation and neurite outgrowth [684,686].. Recently, a study by Narvarro *et al.* showed that CB_1R-CB_2R heterodimers are expressed in LPS/IFN-γ-activated microglia [687]. When compared to resting cells, it was visible that CB_2R became robustly coupled to G_i in activated cells if CB_1R-CB_2R were also present, suggesting a potentiation effect by CB_1R-CB_2R [687]. In addition, an upregulated expression of CB_1R-CB_2R was observed in primary microglia cultures from the hippocampus of mutant β-amyloid precursor protein ($APP_{Sw,Ind}$) mice, a transgenic AD model [687]. Lastly, Navarro and co-workers identified a correlation between the increased expression of CB_1R-CB_2R in the striatum of in 6-hydroxy-dopamine-lesioned rat model for PD and dyskinesias by chronic levodopa (L-DOPA) treatment [687].

Cannabinoid receptor and other GPCR heterodimers

The cannabinoid and the dopaminergic system are known to display complex interactions within the basal ganglia [688–690]. The CB_1R was shown to be co-expressed with DRD_2 in the soma and dendrites of the ventral striatopallidal GABAergic neurons [691]. Meschler *et al.* also reported interactions between CB_1R and DRD_2 (and DRD_1) in the rat and monkey striatum [692].

CB_1R and DRD_1 receptors colocalize in the basal ganglia circuitry, sharing the same G protein transduction pathway and playing a main role in the control of motor activity in both systems [693,694]. In 2011, Tersian and colleagues provided the first evidence for a physiological crosstalk between CB_1R and DRD_1 receptors in the modulation of depression-like behaviour, social skills, and fear conditioning [695]. In this study, the authors revealed that conditional CB_1R knockout mice lacking CB_1Rs in neurons expressing DRD_1 exhibited significantly increased contextual and auditory-cued fear. This suggested that a specific reduction of endocannabinoid signalling in neurons that express simultaneously dopamine DRD_1 is indeed able to affect acute fear adaptation [695]. Serrani *et al.* studied the role of DRD_1 receptors in the behavioural responses induced by acute and repeated stimulation of cannabinoid CB_1R receptors, including the development of physical dependence, using female dopamine DRD_1 receptor-deficient mice and wild-type littermates treated with HU-210 (a synthetic cannabinoid agonist) [696]. The results of the study showed that the mutant mice, compared to wild-type females, exhibited an enhanced response to the acute motor and hypothermic effects of HU-210 [696]. Administration of SR141716A (CB_1R antagonist) precipitated a cannabinoid withdrawal syndrome in HU-210 tolerant female mice. Furthermore, the severity of the cannabinoid withdrawal syndrome was potentiated in female mice with DRD_1 deficiency [696]. Therefore, there is involvement in DRD_1 in the acute effects induced by HU-210, as well as in the somatic expression of cannabinoid withdrawal, supporting the functional interaction between the cannabinoid and dopaminergic systems in the development of cannabinoid dependence [696].

Some studies pointed out that CB_1R and DRD_2 receptors are colocalized in the basal ganglia, mainly in the striato-pallidal GABAergic neurons and in the cortico-striatal

glutamate neurons [697–699]. The first author to provide the evidence of CB_1R-DRD_2 heterodimerization was Kearn *et al.*, based on Co-IP studies in HEK293 cells [690]. Then, other studies confirmed this evidence in globus-pallidus and striatum of rodents and primates, using BRET, PLA and Co-IP assays [699–704]. In the study of Kearn *et al.,* it was demonstrated that stable expression of CB_1R and DRD_2 in HEK293 cells resulted in a pertussis toxin-insensitive component to CB_1R activation of ERK 1/2 and a stimulation of AC activity after simultaneous activation of both receptors by the agonists quinpirole (DR-agonist) and CP55940 (CB_1R-agonist) [690]. Furthermore, the study could show and confirm previous results [705,706] that DRD_2-activation together with the activation of CB_1R resulted in the complex coupling G_s instead of its preferred G-protein, $G_{i/o}$, which was observed in an increase in cAMP levels instead of an synergistic inhibition of AC activity [690,707,708]. In addition, recent studies revealed that CB_1R-DRD_2 heterodimerization requires the bidirectional allosteric interaction of the two receptors, as the expected effect was not observed when only one receptor was activated [701,702]. A recent study from Bagher *et al.* revealed that CB_1R-DRD_2 heterodimer formation in C57BL/6J mice is reduced when treated with the typical antipsychotic haloperidol [700]. In addition, the abundance of the heterodimer increased when treated with the nonselective cannabinoid receptor agonist (CP55,940), whereas the atypical antipsychotic olanzapine treatment had no effect [700]. These results suggest that this heterodimer has an influence in dopamine and cannabinoid-related disorders.

The expression of CB_1R and $A_{2A}R$ in corticostriatal glutamatergic terminals, suggests an interaction potential between those two receptors [709,710]. Indeed, it has been demonstrated that the ability of WIN 55212-2, a CB_1R-agonist, to increase DARPP32 phosphorylation and to inhibit motor activity, requires the presence and the activation of $A_{2A}R$, which then functions as a heterodimer [711,712]. The study of Carriba *et al.* also demonstrated, through Co-IP and BRET experiments in living cells and in rat striata, that CB_1R-$A_{2A}R$ heterodimers are functional since they were shown to mediate the cannabinoid-induced motor effects [709,712]. Another study by Tebano *et al.* using SH-SY5Y neuroglioblastoma cells in biochemical and cellular signalling assays as well as behavioural tests using wildtype and $A_{2A}R$ KO mice indicated that striatal CB_1R activation-induced synaptic effects depend on $A_{2A}R$ activation [710]. Indeed, CB_1R-agonist WIN55,212-2-induced motor depressant effects are inhibited by the $A_{2A}R$-antagonist ZM241385 [712]. Furthermore, Tebano and co-workers demonstrated that the blockade of $A_{2A}R$ reduces WIN55,212-2-induced depression of synaptic transmission in corticostriatal slices and that the synaptic effects of WIN 55212-2 are reduced in slices from $A_{2A}R$ KO mice. According to Tebano *et al.,* this suggests the occurrence of a permissive role of $A_{2A}R$s towards CB_1R effects [710,712]. In addition, this permissive role of the $A_{2A}R$ was reported to occur in postsynaptic effects [712].

The main psychoactive compound in *Cannabis sativa*, THC, a ligand of cannabinoid receptors, is known to induce a variety of behavioural responses and undesirable effects such as dependence, anti-anxiety effects and memory impairments [713–717]. Different studies have shown that THC and other cannabinoid-induced behaviours are typically mediated by 5-$HT_{2A}R$ [718–720]. CB_1R, that typically couples to G_i and 5-$HT_{2A}R$, which is coupled to G_q were found to be colocalized in brain structures involved in regulating emotions, learning, and memory, including the amygdala, cerebral cortex, and

hippocampus [721–723]. For the first time. In 2015, it was discovered that the anxiolytic and amnestic effects of the THC, a CB_1R-agonist, require the presence of 5-$HT_{2A}R$ [717]. Behavioural studies in 5-$HT_{2A}R$ KO mice, BRET, cAMP and calcium signalling assays using cotransfected HEK293T cells and *in situ* PLA using mouse brain slices, determined a remarkable 5-$HT_{2A}R$-dependent dissociation in the beneficial antinociceptive effects of THC and its detrimental amnesic properties, mediated by CB_1R-5-$HT_{2A}R$ [717]. Furthermore, their study showed that CB_1R and 5-$HT_{2A}R$ are expressed and functional in specific brain regions involved in memory impairment [717]. Moreover, it was shown that in CB_1R-5-$HT_{2A}R$ co-stimulation of both receptors by agonists WIN 55212–2 and DOI reduces cell signalling, antagonist binding to one receptor (either rimonabant or MDL 100907) blocks signalling of the interacting receptor, and heterodimer formation leads to a switch in G-protein coupling for 5-$HT_{2A}R$ from G_q to $G_{i\ [717]}$. Heterodimerization was shown to be disrupted *in vivo* by ICV infusion of synthetic peptides with the sequence of TM5 and TM6 of CB_1R, leading to blunted amnesic and anxiolytic, but not antinociceptive, effects of THC selectively in wild-type mice [717]. Later Galindo *et al.*, presented more evidence that CB_1R-5-$HT_{2A}R$ exists in *ex-vivo* primary cultures of human olfactory epithelial cells [724]. Furthermore, they observed a positive correlation between CB_1R-5-$HT_{2A}R$ heterodimer expression, and the amount of cannabis consumed. A negative correlation was observed between heterodimer expression levels and attention and working memory performance in cannabis users [724]. Galindo and co-workers also observed negative crosstalk between CB_1R and 5-$HT_{2A}R$ within the heterodimers in human olfactory epithelial cells when co-stimulated with WIN 55212–2 and DOI, which would lead to reduced activation of ERK1/2 signalling [724]. Furthermore, rimonabant and MDL 100907 blocked the effects induced by WIN 55212–2 and DOI, suggesting that CB_1R-5-$HT_{2A}R$ in control subjects and in cannabis users display bidirectional cross antagonism [724].

Diverse GPCR heterodimers

Besides the more common families described above, other class A GPCRs can form heterodimers. One example is the GAL_1R-GAL_2R heterodimer, identified in HEK293T cells using BRET and in the midbrain raphe-dorsal hippocampal pathways of rodents using *in situ* PLA [725]. In this study by Borroto-Escuela *et al.*, the hypothesis was formulated that the N-terminal galanin fragments preferring binding sites on galanin receptors are formed through the formation of GAL_1R-GAL_2R heterodimers. The galanin 1-15 fragment was shown to induce a disbalance in GAL_1R-GAL_2R signalling, where enhanced activation of $G_{i/o}$-mediated signalling via GAL_1R was observed, while no significant effects were induced by $G_{q/11}$-mediated signalling of GAL_2R [725]. By comparing the results of the study between the two galanin fragments galanin (1-15) and galanin (1-29), it was suggested that the orthosteric agonist binding site of GAL_1R may have an increased affinity for the galanin (1-15) vs galanin (1-29), leading to its demonstrated increase in potency to inhibit CREB vs galanin (1-29) in CRE luciferase reporter gene assays [725]. Furthermore, Borroto-Escuela and co-workers demonstrated that NFAT reporter gene assays galanin (1-29) shows a higher efficacy than galanin (1-15) in increasing $G_{q/11}$-mediated signalling over GAL_2R of GAL_1R-GAL_2R heterodimers [725]. The reported galanin(1-15)-mediated disbalance may contribute to depression and anxiety-related behaviours [726,727].

In 2020, a study by Rivas-Santisteban *et al.* discovered the existence of AT_1R and AT_2R heterodimer expression in hemilesioned 6-OH-DA rat model of PD [728]. AT_1R and AT_2R, which are part of the angiotensin-peptide producing RAS, and their endogenous ligand angiotensin are important regulators of motor control, have been suggested to be promising targets for PD and related conditions such as levodopa (L-DOPA)-induced dyskinesias [728–730]. In their study, Rivas-Santisteban and co-workers demonstrated that co-activation of AT_1R and AT_2R by Ang II and CGP-42112A within the AT_1R-AT_2R heterodimer was known to reduce the downstream signalling of angiotensin II [728]. However, a cross-potentiation was observed, as that application of AT_1R-antagonist candesartan increased the effect of the selective AT_2R-agonist CGP-42112A [728]. Regarding their relevance for PD, it was demonstrated that microglial AT_1R-AT_2R heterodimers are upregulated in parkinsonian conditions and in L-DOPA-induced dyskinesias and their activation was observed to exert neuroprotective effects [728]. Lastly, Rivas-Santisteban *et al.* suggested that the opposite action of AT_1R and AT_2R by AT_1R-antagonist-mediated cross-potentiation of AT_2R actions and the upregulation of AT_1R-AT_2R heterodimers in microglia may be beneficial to treat PD through AT_2R by this heterodimer signalling mechanism [728].

1.1.4. Class C G protein-coupled receptors

1.1.4.1. Class C receptors in the brain

Class C receptor family in humans is composed by γ-aminobutyric acid B receptors ($GABA_{B1}R$ and $GABA_{B2}R$ receptors), calcium-sensing receptor (CaSR), metabotropic glutamate receptors ($mGlu_{1\text{-}8}R$), sweet and amino acid taste receptors and several orphan receptors (GPR156, GPR158, GPR179, GPRC5A, GPRC5B, GPRC5C, GPRC5D, GPRC6) [143,430,731]. Among them CaSR, $GABA_BR$ and mGluR are highly expressed in the brain and represent an important class of drug targets for neurological diseases and calcium homeostasis [732–734].

mGluR and $GABA_BR$ receptors are particularly relevant as they constitute a comprehensive model for the allosteric regulation and cooperativity of receptor protomers, which can be tendentially transferred to other GPCR classes, such as class A receptors [88]. Despite the fact that their sequences and overcall structures differ significantly from other classes, some structural similarities have been reported between classes A and C receptors. The most significant similarities were found in the TM domains. In class A receptors the “ionic lock” is defined by a salt bridge between a conserved Arg3.50 and Glu(Asp)6.30, while this motif occurs via Lys3.50 and Glu6.35 in class C [735].

Aside from the common architecture of GPCRs, the class C receptors possess an extracellular domain that contains a Venus flytrap (VFT) module and a cysteine rich domain (CRD, except in the $GABA_BR$) [734]. This exceptionally large extracellular domain contains the orthosteric binding site for ligands, while in the 7TM region only allosteric binding sites are found [734]. Moreover, the C-terminus is highly variable and plays a role in scaffolding and signalling protein coupling [731]. Another unique characteristic of the class C receptor family is the fact that they only function as

homodimers (mGluR and CaSR) or heterodimers ($GABA_BR$) [734]. The structure of the VFT was first solved for the $mGlu_1R$ (PDB-id: 1EWV, 1EWT, 1EWK) [750] and it revealed that the VFT consists of a bilobed domain being separated by a cleft in which endogenous ligands are able to bind [736–738]. In absence of a ligand, the VFT oscillates between an open and closed conformation [734]. Agonists interact with lobe 1 in the open form of the VFT and stabilize the closed conformation through additional contacts with lobe 2, while antagonists inhibit the VFT closure [734,739]. Due to the necessary dimerization of class C receptors, the VFTs consequently interact with each other by forming constitutive dimers. Different studies found that a hydrophobic interaction between lobe 1 of each monomer is the driving force for VFT dimerization [740,741]. An additional disulphide bond linking the two VFTs was reported to further stabilize the dimer [741–743]. The CRD which is a segment of 80 amino acids, containing 9 conserved cysteines, connects the VFT and the 7TM domains [731,734]. Crystallography data shows that the CRD physically separates the VFT and 7TM modules (PDB-id: 2E4U, 2E4V, 2E4W,2E4X, 2E4Y, 2E4Z) [743]. Especially for mGluR, a conserved disulphide bond between the VFT and the CRD is necessary for receptor activation through allosteric interaction between VFT and 7TM [744]. CRD is also a mediator of receptor activation for CaSR [734,745].

Calcium-sensing receptor

CaSR is a unique receptor, highly sensitive to calcium ions (Ca^{2+}) and their concentration change in the extracellular space [734]. CaSR ensures calcium homeostasis and can consequently be activated by calcium itself without the cooperation of other ligands [732,746]. Pathological conditions involving CaSR are hyperparathyroidism, osteoporosis and different forms of hypocalcemia [746–748]. CaSR is pharmacologically targeted by positive allosteric modulators (PAMs), i.e., cinacalcet, evocalcet and etelcalcetide, for the treatment of secondary hyperparathyroidism and familial hypocalciuric hypercalcemia (FHH1). CaSR negative allosteric modulators (NAMs) act as calcilytics and are currently in phase II clinical trials for the treatment of Autosomal-Dominant Hypocalcemia Type 1 (ADH1) [749,750].

Although CaSR is mainly expressed in the parathyroid gland and in the renal tubules of the kidney, there is also a significant expression in the brain [751,752]. Calcium is one of the most abundant second messengers in the brain [753]. In the extracellular space calcium levels are maintained constant (between 1.1 and 1.4 mM), whereas in resting neurons calcium levels are strictly maintained around 100 nM [754,755]. Without a substantial calcium gradient neuronal functions, such as gene transcription, synaptic transmission, memory encoding, apoptosis, and many others may not be conducted [753,754]. The inability to maintain required calcium levels has been brought into context with neurodegenerative diseases such as PD, AD, HD, where this neuronal calcium dysregulation contributes to motor and/or cognitive dysfunctions [754,756–760].

γ-aminobutyric acid B receptors

γ-aminobutyric acid (GABA) is the major neurotransmitter for inhibitory signals in the mammalian CNS [734]. $GABA_BR$, which responds to GABA, regulates synaptic plasticity,

learning, and memory in the dentate gyrus [1], mediating a slow and prolonged synaptic inhibition [761]. They only function as obligate heterodimers of the two subtypes, $GABA_{B1}R$ and $GABA_{B2}R$ [762–767] with two distinct features: $GABA_{B1}R$ contains the GABA binding site [768], whereas $GABA_{B2}R$ activates the $G_{i/o}$ protein [769]. $GABA_B$ receptors are responsible for neuronal excitability and plasticity [734]. For instance, in a VaD rat hippocampus, it was observed a reduction in $GABA_BR$ expression, which resulted in spatial learning and memory deficits [1,770]. However, under certain conditions they may promote neuron survival such as metabolic stress, ischemia and apoptosis [734,771–773]. Consequently, these receptors are considered as promising targets for the treatment of many diseases including spasticity, neuropathic pain, drug addiction, schizophrenia, anxiety, depression or epilepsy [774–777].

Metabotropic glutamate receptors

L-Glutamate is the major neurotransmitter for most of the excitatory synapses in the mammalian CNS [8]. As L-glutamate is the endogenous ligand for mGluR, they participate in the neuronal excitability and modulation of synaptic transmission in the CNS [778,779]. The mGluR family comprises eight members, which are further classified based on their G protein coupling and sequence homology. The first group (Group I) consists of $mGlu_1R$ and $mGlu_5R$, which are coupled to G_q/G_{11} [1,780]. The second group consists of $mGlu_2R$ and $mGlu_3R$ (Group II) and the third group (Group III) of $mGlu_4R$, $mGlu_6R$, $mGlu_7R$ and$mGlu_8R$, of which all are coupled to G_i/G_o [778,780]. As such, mGlu receptors negatively regulate the adenylyl cyclase (AC) and were reported to also activate MAP kinase and PI-3-kinase pathways [778,780]. The $mGlu_5R$ has been reported to be involved in several neurodegenerative disorders [778]. Since $mGlu_5R$ is highly expressed in astrocytes, glial cells and neurons of the forebrain and hippocampus, several lines of evidence suggest a significant role of $mGlu_5R$ in developmental and neurodegenerative disorders such as Down Syndrome and AD [781,782]. Over the last years, several mGluR agonists, antagonists, PAMs and NAMs have been developed and studied *in vivo* animal models [1]. Comprehensive work from Chen *et al.* showed that LY341495 (Group I/II mGluR antagonist) was able to block amyloid β-enhanced long-term depression and improve synaptic plasticity [783]. In addition, the authors also showed that pre-treatment with an $mGlu_{1/5}R$ agonist, DHPG, decreased amyloid β-enhanced long-term depression [783]. Another study by Renner *et al.* demonstrated that SIB1757, a non-competitive antagonist of $mGlu_5R$, prevented amyloid β oligomer-induced synaptic N-Methyl-D-aspartic acid receptor NMDAR reduction [784]. Moreover, Caraci and co-workers demonstrated in their study that the $mGlu_2R$ PAM LY566332 amplified amyloid β-induced neurodegeneration, while treatment with the antagonist LY341495 of $mGlu_{2/3}R$ prevented this effect [785]. In a similar manner the dual $mGlu_{2/3}R$ agonist LY379268 exhibited neuroprotection by a paracrine mechanism mediated by transforming growth factor-β1 [785]. Consequently, negative modulation of the $mGlu_5R$ could be a promising strategy for treatment of PD and AD. Moreover, dual activation of Group II receptors, $mGlu_2R$ and $mGlu_3R$ could be a strategy for providing neuroprotection against amyloid β-induced toxicity [785].

1.1.4.2. Class C receptor heterodimers

Marshall and colleagues discovered already in 1998 that heterodimerization formation was crucial for a functional $GABA_BR$ [75,786]. Since then, the concept of GPCR dimerization has been widely accepted for class C receptors. The receptor-receptor cooperation has been found to be positive and negative and vital for signal transduction [88,787–790]. Class C GPCRs act as obligate dimers, since the VFTs of the single receptors have to interact with each other [740–742,791]. Therefore, homo- and heterodimerization is a common event among class C GPCRs.

In a recombinant system, it was found that $GABA_{B1}R$, cannot reach the cell surface without the presence of $GABA_{B2}R$, as $GABA_{B1}R$ contains a C-terminal endoplasmic retention motif, only masked when the heterodimer is formed (**Figure 2E**) [792,793]. Unexpectedly, all orthosteric agonist and antagonists rather bind to the VFT of the $GABA_{B1}R$. This coupling leads to the necessary conformational change in $GABA_{B1}R$, which crosstalks to $GABA_{B2}R$ leading to an active conformer able to bind to G protein and promoting functional physiological responses [794–797]. Also, additional GPCRs which can bind to $GABA_BR$ were identified: e.g., $GABA_AR$, $mGlu_1R$, N-methyl-D-aspartate (NMDA), insulin-like growth factor-1 (IGF-1), and tyrosine protein kinase receptor (TrkBR). It also has been shown that these GPCRs are able to form multi-complexes such as tetramers [798,799]. Such tetramers were described to exhibit negative cooperativity between the $GABA_BR$-heterodimers by decreasing the coupling efficiency towards G_i proteins [787,800]. Despite the large therapeutic potential and the development of many PAMs and NAMs which could help to investigate the relationship between the monomers of the $GABA_BR$, only Baclofen (Lioresal), a selective $GABA_BR$ agonist is available on the market [801,802].

Furthermore the well-known $GABA_BR$, the eight members of the mGluR family are key modulators of glutamatergic synaptic transmission of excitatory and inhibitory responses in the brain [779,803,804]. The structure of the mGluR contains special features such as a large cysteine enriched domain, which is linked to the transmembrane domain, and a large extracellular domain involving the VTF, where glutamate binds involving the VFT, which is also linked to the transmembrane domain, binding pocket to glutamate [75]. Many GPCRs are known to interact and regulate the mGluR subgroups such as the neuronal Ca^{2+} binding protein 2 that forms a co-assembly and coupling with activated Ca^{2+}-activated K^+-channels; and the contactin-associated protein 1, which appear to be important for the function of $mGlu_5R$ to control memory formation in the hippocampus [75,805–809].

For instance, the $mGlu_2R$-$mGlu_4R$ heterodimer, was already discovered in 2005 by Doumazane and co-workers using a technique to study plasma membrane receptor complexes and FRET [810]. Later, Kammermeier and co-workers elucidated that $mGlu_2R$-$mGlu_4R$ complexes are functional in neurons, only using both, $mGlu_2R$ specific and $mGlu_4R$ specific agonists [811]. Each individual receptor has two NAM binding sites and one PAM binding site. The activation of each receptor by NAMs was able to reverse the signalling of this heterodimer. Moreover, only one PAM per complex was needed for the full enhancement of the heterodimer complex activity[810].

Another example, the $mGlu_1R$-$mGlu_5R$ heterodimer in mice, was identified by Pandya and co-workers in 2016 [812]. The $mGlu_1R$-$mGlu_5R$ was found to be expressed in the cerebral cortex, hippocampus and hippocampal neurons using an interaction proteomics

strategy and super resolution microscopy [812]. The exact receptor complex composition is still unclear, but there is the indication that scaffolding proteins, phosphatases and kinases are involved in the process [813]. In synaptic and extra-synaptic locations, $mGlu_1R$-$mGlu_5R$ also appears to be in balance with the corresponding homodimers $mGlu_1R$-$mGlu_1R$ and $mGlu_5R$-$mGlu_5R$ [814]. The $mGlu_1R$-$mGlu_5R$ heterodimer may be a potential therapeutic target in autism spectrum disorders [812].

Although class C GPCRs, and especially mGluRs, are functional as constitutive dimers, the importance of dimerization remains unclear [804]. A study by El Moustaine *et al.* also demonstrated that the dimer formation is not required for G protein coupling, but rather for agonist activation and for limiting the agonist activity of PAMs [796,804]. This asymmetrical activation is also consistent with the asymmetric functioning reported for class A GPCR dimers [439,815,816].

1.1.5. Heterodimers class A-class C

GPCR heterodimers of the same classes such as class A - class A or class C - class C appear to be physiologically conclusive as they have the same activation mechanism despite the different ligands and G protein-coupling state. Also, their physiological functions appear coherently, notwithstanding that the partnered proteins often belong to different families. However, the existence of GPCR heterodimers of different classes such as class A - class C heterodimers, which will be described here, add another perspective to the complexity of GPCR signalling.

In 2020, Sebastianutto *et al.* discovered the DRD_1-$mGlu_5R$ heterodimer using BRET and bimolecular fluorescence complementation (BiFC) techniques at the plasma membrane in HEK293 cells, primary hippocampal neurons and in 6-OHDA lesion in mice and rats, which were used as PD models [817]. The dopaminergic and glutamatergic system are known to signal to the striatum where their crucial inputs control action selection and behavioural plasticity [818,819]. Hence, these basal-ganglia circuits represent an important target of L-DOPA-based therapy in PD [817]. Sebastianutto and co-workers demonstrated that the DRD_1-$mGlu_5R$ synergistically activates PLC signalling and intracellular calcium release in response to either glutamate or dopamine [817]. In addition, PLC signalling was seen to be responsible for a considerable proportion of striatal ERK1/2 activation in PD-model rodents which were treated with DRD_1-agonists SKF38393 or quinpirole [817]. Moreover, in the PD-model rodents, DRD_1-$mGlu_5R$ complexes were found to be strongly upregulated in the dopamine-denervated striatum [817]. DRD_1-$mGlu_5R$ -dependant PLC signalling was also linked to enhanced activation of extracellular signal–regulated kinases in striatal neurons, leading to dyskinesia in animals treated with L-DOPA or DRD_1-agonists SKF38393 or quinpirole [817]. It was concluded that DRD_1 appeared to engage in a preferential crosstalk with $mGlu_5R$- and G_q-related signalling components in dopamine-denervated striatal neurons [817].

Another example, A_1R-$mGlu_1R$, was discovered by Ciruela *et al.* already in 2001 using Co-IP, immunohistochemistry and ligand-binding experiments in HEK293 and rat cerebellum synaptosomes [820]. Furthermore, they showed that activation of A_1R and

$mGlu_1R$ would lead to a synergistic neuroprotection effect, since preincubation with quisqualic acid ($mGlu_1R$-agonist) and adenosine was much more effective than pre-treatment with any of the compounds used in their study. Later, more studies based on an analysis of non-neuronal cells using Co-IP and FRET by Kamikubo *et al.* supported the existence of A_1R-$mGlu_1R$ [821]. In a previous study, it was described that, in cerebellar Purkinje cells, the activation of A_1R attenuates neuronal responses to glutamate, as mediated by $mGlu_1R$ [821,822]. The $mGlu_1R$ is also known to regulate responses such as long-term depression of postsynaptic response to glutamate, which is a cellular basis for cerebellar motor learning [821]. Furthermore, Kamikubo and co-workers demonstrated that the activation of $mGlu_1R$ through glutamate inhibits A_1R signalling, which was measured in elevated cAMP signalling, since the A_1R is known to couple to $G_{i/o}$-proteins [821,823]. Kamikubo *et al.* concluded from their findings that $mGlu_1R$-mediated inhibition of A_1R signalling, which should activate PKA and cAMP response element-binding protein (CREB) may play a role in $mGlu_1R$-dependent cerebellar long-term depression and motor learning [821].

In 2008, González-Maeso *et al.* identified a physical and functional interaction between 5-$HT_{2A}R$ and $mGlu_2R$ in cortical pyramidal neurons using Co-IP, BRET and FRET in HEK293 cells and brain cortices from mice and humans [824,825]. Competition binding experiments showed that the $mGlu_2R$-agonist LY379268 was able to increase the affinity of hallucinogenic drugs such as DOI, DOM or for the 5-$HT_{2A}R$-binding site [825]. However, it was also shown that the 5-$HT_{2A}R$-agonist DOI decreased the affinity for $mGlu_2R$-agonists LY379268, DCG-IV, and L-CCG-I [825]. Hence, within the 5-$HT_{2A}R$-$mGlu_2R$, unique cellular responses are mediated when targeted by hallucinogenic drugs and activation of $mGlu_2R$ was shown to abolish hallucinogen-specific signalling and behavioural responses. González-Maeso *et al.* further supported those findings by showing that hallucinogens, including mescaline, psilocybin, and lysergic acid diethylamide (LSD) which profoundly affect perception, cognition, and mood and are known to activate 5-$HT_{2A}R$, but not all excerpt hallucinogenic behaviours [826]. It was shown that hallucinogenic and non-hallucinogenic 5-$HT_{2A}R$-agonists both regulate signalling in the same 5-$HT_{2A}R$-expressing cortical neurons. However different agonists were found to either regulate phospholipase C via coupling to $G_{q/11}$ proteins and/or bind to $G_{i/o}$ proteins and Src [826]. Fribourg *et al.* demonstrated that the signalling of the endogenous ligand on the associated protomer is suppressed or potentiated, by an agonist or an inverse agonist of one protomer, respectively [827]. Therefore, the 5-$HT_{2A}R$-$mGlu_2R$ heterodimer establishes an optimal $G_{i/o}$-G_q balance in response to serotonergic and glutamatergic drugs binding. The hallucinogenic agonists LY341495 ($mGlu_2R$ inverse agonist) and DOI (5-$HT_{2A}R$ receptor agonist) promote a decrease in $G_{i/o}$ and a strong increase in G_q. The opposite happens with the antipsychotics LY379268 ($mGlu_2R$ receptor agonist) and clozapine (inverse 5-$HT_{2A}R$ receptor agonist), which produce the opposite effect on $G_{i/o}$-G_q balance. Lastly, González-Maeso and co-workers identified that $mGlu_2R$ interacts via TM4 and TM5 with 5-$HT_{2A}R$ [825].

In 2009, Schröder *et al.* identified the MOR-$mGlu_5R$ heterodimer using Co-IP in HEK293 cells [828]. It was long hypothesized that opioid analgesia and tolerance can be modulated by metabotropic glutamate receptors [828–831]. Studies by Gabra *et al.* and Lee *et al.* were able to show that the $mGlu_5R$-antagonist MPEP inhibits hyperalgesia,

nociceptive behaviour and inflammation. Moreover, when co-administered with morphine, the morphine-induced antinociception development was suppressed [832,833]. The treatment of the cotransfected MOR and $mGlu_5R$ cells with DAMGO, a selective MOR-agonist, showed that co-expression of $mGlu_5R$ had no significant effect on the agonist binding sites and functional coupling of the MOR towards DAMGO, as DAMGO-induced inhibition of intracellular cAMP level was still observed [828]. However, when MPEP was co-administered, DAMGO-induced MOR phosphorylation, internalization, and desensitization was decreased, whereas non-selective competitive $mGlu_5R$-antagonists or -agonists had no effects [828]. According to Schröder *et al.* this allosteric modulation of $mGlu_5R$ on MOR displays a mechanistic basis how the MOR-$mGlu_5R$ functions, further supported by DAMGO-induced co-internalization of MOR and $mGlu_5R$ and the increase of MPEP bindings sites and a change of binding affinity of $mGlu_5R$ after the co-expression of MOR [828].

1.1.6. Heteroreceptor mosaics

The term “receptor mosaics” stands for assemblies of more than two receptors and was already introduced in the 80s to underline the role of topology in the highly dynamic life cycles of GPCRs [834–837]. Such mosaics may be the result of engrams of short-term memory, which are stored as a state of molecular circuit. They further suggested that these mosaics may be the representations of engrams of ultra-short memory in transient receptor mosaic formed in kiss-and-run encounters [836,838–840]. There are now many indications that heteroreceptor mosaics exist in nerve cells and throughout the brain [836,839,841].

The $A_{2A}R–CB_1R–DRD_2$ mosaic is one of the few examples where more than two receptors exhibit protein-protein interactions [519,712,834]. It also underlines the relevance of adenosine, dopamine and cannabinoid signalling and their pivotal contribution to various signalling mechanisms. The $A_{2A}R–CB_1R–DRD_2$ hetero-oligomer was identified for the first time in 2008 [842] using a method combining BiFC and BRET techniques [843–849]. In 2009, the $A_{2A}R$-DRD_2-$mGlu_5R$ was discovered in HEK293 cells, using BiFC and BRET approaches [850]. In addition to adenosine and dopamine transmission, glutamate transmission also plays an important role in the function of striatal GABAergic efferent neurons originating in the nucleus accumbens. In 2001 Popli *et al.* discovered the DRD_2-$mGlu_5R$ heterodimer and its association with $A_{2A}R$ receptor [851]. Authors used 6-OH-DA-lesioned rats as PD models to make behavioural and microdialysis experiments. In 6-OH-DA rats, the selective $mGlu_5R$-agonist (RS)-2-Cholro-5-Hydroxyphenylglycine (CHPG) was shown to inhibit the contralateral turning induced by quinpirole, a DR-agonist and less pronounced by the DR-agonist SKF 38393 [851]. The effect of CHPG on quinpirole-induced turning were significantly potentiated by CGS 21680, an $A_{2A}R$-agonist and attenuated by SCH 58261, an $A_{2A}R$-antagonist [851]. CHPG was shown to reduce the affinity of the high-affinity state of DRD_2 for quinpirole and this effect was again enhanced by CGS 21680 in rat striatal membranes [851]. $A_{2A}R$ and $mGlu_5R$ agonists (CGS 21680 and CHPG, respectively) synergistically increase ventral pallidal extracellular level of GABA in the nucleus accumbens promoting a potential stability of the inhibitory dopaminergic DRD_2 effects on the striato-pallidal GABA pathway [852]. In PD, where the dopaminergic nerve terminals are degenerated,

the DRD_2 on the glutamate nerve terminals can no longer appropriately inhibit glutamate release. Here, $A_{2A}R$ and $mGlu_5R$ antagonists could be successful to inhibit parkinsonian symptoms considering their increasing dominance, since the inhibitory DRD_2 lose their function [853]. Consequently, extracellular levels of adenosine and glutamate may increase, leading to a higher probability of formation of $A_{2A}R$-DRD_2, DRD_2-$mGlu_5R$ and $A_{2A}R$-DRD_2-$mGlu_5R$ that leads to further inhibition of PD symptoms. Lastly, $A_{2A}R$–CB_1R–DRD_2 and $A_{2A}R$-DRD_2-$mGlu_5R$ mosaics have recently been demonstrated in living cells using fluorescent techniques [846,850].

1.1.7. GPCR Interacting Proteins

Besides the binding of GPCRs to G proteins, β-arrestins and kinases, there exists a large numbers of GPCR interacting proteins (GIPs) [809,854–857]. GIPs can be other cytoplasmic or transmembrane proteins such as heat-shock proteins, PSD-95/Discs-large/ZO-1 (PDZ) domain-containing proteins or GPCR-associated sorting proteins (GASPs) [858–860], among many others. They excerpt multiple effects on GPCRs: interact with GPCRs in a more receptor-selective manner and can additionally mediate downstream signalling directly through binding to GPCRs, organize GPCR signalling through G proteins, promote receptor trafficking or anchor the receptors in certain subcellular areas [809,854,857,861]. In contrast to GPCRs, GIPs are capable of cluster various proteins and coordinate different types of signalling such as positive and negative feedback signals, graded or digital signals, transient or oscillatory signalling [809,862,863].

In terms of GPCR dimerization, it is known that the receptors influence each other through PPIs and subsequent conformational rearrangements upon the dimerization event that also influence the affinity for the binding of G proteins, alterations in ligand binding affinity and many other effects [71,79–81]. This also raised the question, how could dimerization affect the coupling to GIPs [856]. For instance, it was reported that MT_1R directly and constitutively bind to G_i proteins and RGS20 forming the MT_1R homodimers-RGS20-G_i protein complex [864]. Regulators of G-protein signalling (RGS) proteins bind to the activated form of G_α proteins and accelerate their GTPase activity [865,866]. By using BRET probes inserted at multiple sites of the complex and by homology modelling experiments, Maurice *et al.* suggested a model, where the G_i protein can bind to one MT_1R, while the RGS20 binds to the other MT_1R [864]. Similar observations were made for MT_1R/MT_2R-RGS20-G_i protein-complex, which was previously not known to bind to RGS20 [864]. Hence, it was concluded that the formation of asymmetric quaternary complexes involving GIP-binding and non-GIP-binding receptors may lead to sensitivity for GIPs, which is only present upon formation of such complexes [856,864].

Another example was recently discovered, involving mGluRs, known to be obligate dimers. The constitutive active $mGluR_1$ and $mGluR_5$, in absence of glutamate, were reported to form an interaction with Homer1a. This protein, part of the scaffolding protein family Homer, lacks dimerization capacity [867–870]. Usually, $mGlu_{1/5}R$ dimers are functionally physically linked to NMDA receptors via scaffolding proteins, which is then disrupted through the binding of Homer1a [867,871,872]. The $mGlu_{1/5}R$-Homer1a-

complex has been associated with several functions in synaptic plasticity of the visual system, in rewarded synapses, in chronically overactivated synaptic networks and sleep cycle [867].

Hence, the binding of GIPs to GPCR dimers adds another level of signalling complexity towards downstream signalling and indicates that its fine-tuning can be also context dependent [871,873].

1.1.8. Summary and concluding remarks

It has been widely accepted by now that GPCRs are able to couple to other GPCRs in order to alter their partner's signalling and/or their own, which furthermore diversifies and fine-tunes their physiological responses. Many studies have demonstrated that the nature of crosstalk within the heterodimer or oligomer can be either positive or negative. Hence, when GPCRs form a heterodimer, it was shown that this leads to the enhancement of each other's natural signalling pathways or inhibition of downstream signalling of either one receptor or both. Among all heterodimers described in this review, there was a clear balance between examples, which promoted either positive or negative crosstalk. In addition, there are still more options of alternate signalling by heterodimers to be investigated. Especially, when it comes to formation of oligomers, the signalling repertoire is even further increased.

The concept of GPCR dimers, which carry out physiological and pathophysiological actions in the brain, adds a new dimension to molecular signalling in the nervous system.

To be able to target both monomers within the dimer at the same time new concepts in drug design have been explored. Already in 1982 the concept of bivalent ligand was discovered and introduced for opioid heteromers by Philip Portoghese [874,875] and many have been developed over the years [876,877] to target other disease-relevant dimers. By definition bivalent ligands consist of two distinct pharmacophores that are connected by a linker/spacer, hence they are able to target two GPCRs simultaneously [878]. They can be further classified into either homobivalent ligands with two identical pharmacophores or heterobivalent ligands with two different pharmacophores [876].

The advantage of targeting both monomers of the dimer simultaneously provides insight into enhanced physiological responses and may help to understand the dynamic interactions of the two proteins, as usually either one of them is targeted by their ligands resulting in positive or negative crosstalk. Moreover bivalent ligands can be designed to either consist of two agonists, two antagonists or cross-overs which make them a helpful tool to understand the dynamics of dimerization and subsequent downstream signalling [876]. Considering the recent developments of bivalent ligands, most of them target class A heteromers including opioid receptors, dopamine receptors, serotonin receptors and cannabinoid receptors [876]. However one ligand described, was developed for an heterodimer between class A and class C, MQ-22a, which targets the DRD_2-$mGlu_5R$ heteromer [879]. Interestingly, an allosteric modulator 3-[(2-methyl-4-thiazolyl)ethynyl]pyridine (MTEP) was chosen for $mGlu_5R$, while for DRD2 ligands targeting the orthosteric binding pocket were selected, the DRD_2- and DRD_4-agonist 5-hydroxy-2-(dipropylamino)tetralin (DPAT) and the DRD_2-antagonist 1,4-disubstituted aromatic piperazine (DAP) [879]. Consequently also the level of binding property of the

selected pharmacophores provide an additional chemical space to be explored in terms of dimerization dynamics as it has been shown for monomers, that the physiological response also varies if ligands bind either to orthosteric or to the allosteric binding pockets [880–882]. Other bivalent ligands were also designed to induce dimerization as shown for the gastrin-releasing peptide receptor GRPR within 20-30Å [883].

Together with the growing numbers of GPCR crystal structures available and the improvement in computational techniques such as homology modelling, ligand docking and molecular dynamics, bivalent ligands are additional pharmacological tools for investigating the dimerization process and dynamics.

However there is still room for improvement as none of the bivalent ligands has made it to clinical trials yet, mostly due to their large size (> 700 kDa) and consequent unfavourable pharmaco-chemical properties, selectivity profiles and lacking *in vivo* studies [876].

Aside from bivalent ligands, nanobodies which are mostly derived from antibody fragments from the heavy chain-only antibodies of camelids, have emerged as promising alternatives due to their high target specificity [884,885]. Like bivalent ligands also nanobodies have been discovered in the 1980s but their utility was for long not recognized [886]. Nanobodies can be fused to fluorescent tags, radioisotopes or other biosensors to monitor cellular processes in living cells [885]. More recently fluorescently labeled conformation-specific nanobodies were utilized to monitor the activation of GPCRs upon ligand binding or rapid state transformation in living cells [885,887–890]. In another more recent study nanobodies were used to modulate the activity of $mGlu_4R$ in the brain but not Glu_4R heteromers with other GluRs, indicating that therapy of PD or pain could be improved through subtype-selective and blood-brain barrier permeable nanobodies [884]. While only biparatopic nanobody targeting different binding sites of the chemokine receptor CXCR2 entered phase 1 studies as potential new therapeutic for inflammation [891,892], nanobodies specifically targeting GPCR dimers (homo- and heterodimers) will be for sure a promising new therapeutic approach. Until now Ernumab, a monoclonal antibody, was recently approved for preventive treatment of chronic migraine as it binds to the calcitonin gene-related peptide receptor dimers [891,893,894].

All in all, future studies should be directed to identifying the dimer interface to design and develop interface-interfering molecules, able to specifically disrupt the dimer. This strategy will help to determine the functional role of the dimer as well as the allosteric receptor-receptor interaction within the dimer.

Herein, we provided a collection of neurodegenerative-relevant GPCR heterodimers of classes A and C, which appear to be promiscuous in their signalling. A detailed structural and functional characterization of these macromolecular machineries will be key to the development of new and improved drugs to treat neurodegenerative diseases.

Table 1. GPCR dimers and potential roles in neurodegenerative diseases.

HETERODIMER	GPCR CLASS	CLINICAL RELEVANCE	CROSSTALK	REFERENCES

DRD_1-DRD_2	Class A	PD Schizophrenia Autism Addiction Depression	Positive crosstalk	[448,449,451,465,473–475,482–484,487,895–897]
DRD_1-DRD_3	Class A	PD	Positive crosstalk	[464,490–496]
DRD_2-DRD_3	Class A	PD Schizophrenia Autism ADHD	Positive crosstalk	[471,499–503,897]
DRD_2-DRD_4	Class A	PD	Positive crosstalk	[463,507,508]
DRD_5-DRD_2	Class A	Depression	Positive crosstalk	[480,509]
A_1R-DRD_1	Class A	PD Schizophrenia Addiction	Negative crosstalk	[446,510,511,513,515–518,551,898–900]
$A_{2A}R$-DRD_2	Class A	PD Schizophrenia Addiction	Negative crosstalk	[71,448,515,519–528,901–904]
$A_{2A}R$-DRD_3	Class A	Schizophrenia	Negative crosstalk	[538]
DRD_1-H_3R	Class A	ADHD Schizophrenia Addiction	Positive crosstalk	[540–543]
DRD_2-H_3R	Class A	PD	Negative crosstalk	[544,545]
DRD_2-SST_5R	Class A	Depression	Positive crosstalk	[547–549,905]
DRD_2-NTS_1R	Class A	PD Schizophrenia	Negative crosstalk	[550–555]

DRD_2-TAA_1R	Class A	Schizophrenia	Negative crosstalk	[299,310,556–558]
DRD_2-OTR	Class A	Anxiety Autism	Positive crosstalk	[559,560,897]
DRD_2-GHS-R_{1A}	Class A	Eating disorders	Negative crosstalk	[568,906,907]
A_1R-$A_{2A}R$	Class A	Drug tolerance	Negative crosstalk	[445,546,569,571–574]
A_1R-5-HT_2AR	Class A	Schizophrenia Anxiety	Negative crosstalk	[577,578]
$A_{2A}R$-H_3R	Class A	PD	Negative crosstalk	[579,908]
MOR-DOR	Class A	Chronic pain	Positive crosstalk	[587,591–600,909,910]
MOR-KOR	Class A	Chronic pain	Positive crosstalk	[588,590,601]
MOR-$A_{2A}R$	Class A	Addiction	Negative crosstalk	[590,602–605,911–914]
MOR-GPR139	Class A	Chronic pain	Negative crosstalk	[590,609]
MOR-$V_{1B}R$	Class A	Chronic pain Morphine tolerance	Positive crosstalk	[590,610]
MOR-GAL_1R	Class A	Chronic pain Addiction	Positive crosstalk	[590,611,612]
MOR-CB_1R	Class A	Chronic pain	Negative crosstalk	[590,613,615–619]
MOR-CCKBR	Class A	Chronic pain	Negative crosstalk	[590,602]
MOR-CCR5	Class A	Chronic pain	Negative crosstalk	[622,623]

MOR-DRD$_1$	Class A	PD Addiction	Negative crosstalk	[625]
MOR-DRD$_2$	Class A	Addiction	Negative crosstalk	[626–629]
5-HT$_{1A}$R-5-HT$_{2A}$R	Class A	Depression	Negative crosstalk	[632–635]
5-HT$_{2A}$-5-HT$_{2B}$	Class A	Addiction Depression	Negative crosstalk	[637,638,641]
5-HT$_{2A}$R-5-HT$_{2C}$R	Class A	Addiction Depression	Negative crosstalk	[637,638,641,915,916]
5-HT$_{1A}$R-5-HT$_7$R	Class A	Depression Anxiety Schizophrenia Addiction	Negative crosstalk	[642,643,645,646]
5-HT$_{1A}$R-DRD$_2$	Class A	Schizophrenia	Positive crosstalk	[634,647–651]
5-HT$_{2A}$R-DRD$_2$	Class A	Schizophrenia Autism	Positive crosstalk	[551,648,649,652,897]
5-HT$_{1A}$R-GAL$_1$R	Class A	Depression	Negative crosstalk	[654,656,658,660,661]
5-HT$_{2A}$R-OTR	Class A	Anxiety Autism Depression	Negative crosstalk	[662][676,910]
5-HT$_{2C}$R-OTR	Class A	Depression	Negative crosstalk	[667]
5-HT$_{2C}$R-MT$_2$R	Class A	Depression Anxiety	Positive crosstalk	[668–673]
5-HT$_{1A}$R-MOR	Class A	Chronic pain	Positive crosstalk	[674]

CB_1R-CB_2R	Class A	AD PD	Positive crosstalk	[673,684–686]
CB_1R-DRD_1	Class A	PD	Positive crosstalk	[693–696]
CB_1R-DRD_2	Class A	PD Schizophrenia Addiction Autism	Negative crosstalk	[690,699–702,704–706,708,897,917]
CB_1R-$A_{2A}R$	Class A	Depression	Negative crosstalk	[709,710,712]
CB_1R-5-$HT_{2A}R$	Class A	Addiction Anxiety	Positive crosstalk	[717,724]
GAL_1R-GAL_2R	Class A	Depression Anxiety	Positive crosstalk	[726,727]
AT_1R-AT_2R	Class A	PD	Positive crosstalk	[729,730,918]
$mGlu_1R$-$mGlu_5R$	Class C	PD AD Schizophrenia Autism	Unknown	[35,812]
$mGlu_2R$ – $mGlu_4R$	Class C	PD AD Schizophrenia	Negative crosstalk	[810,811,919]
$GABA_{B1}R$-$GABA_{B2}R$	Class C	Nonspecific neurological diseases	Positive crosstalk	[792–797,920]
DRD_1-$mGlu_5R$	Class A and C	PD	Positive crosstalk	[817]
A_1R-$mGlu_1R$	Class A and C	Schizophrenia	Negative crosstalk	[820–822]
5-$HT_{2A}R$-$mGLU_2R$	Class A and C	Schizophrenia Autism	Negative crosstalk	[824,825,827,897,921,922]

MOR-mGlu$_5$R	Class A and C	Chronic pain Addiction	Negative crosstalk	[832,833]
A$_{2A}$R–CB$_1$R–DRD$_2$	Class A	Schizophrenia	Negative crosstalk	[519,690,707,708,712,834,842–849]
A$_{2A}$R-DRD$_2$-mGlu$_5$R	Class A and C	PD Schizophrenia Addiction Autism	Negative crosstalk	[850,851,853,897]

This chapter describes the principles behind the applied methods in this study. The chapter is divided into two sections: Pharmacological and computational methodologies

1.2. Pharmacological and computational methodologies

GPCRs are the targets of more than 40% of food and drug administration (FDA)-approved drugs; hence, they are the most intensively studied protein family, which has led to the development of a wide array of biological and computational methods to study GPCRs [35,923]. Over the years high-throughput screenings (HTS) *in vitro* and *in silico* have been applied to screen clinically relevant GPCRs, and these methods still are first-line drug discovery tools [924].

1.2.1. Pharmacological methods used to study G protein-coupled receptors

Pharmacological/biological experiments typically characterize either binding properties of a ligand bound to its target protein or measure a functional response within a biological context. Affinity, potency and/or efficacy can be determined.

The affinity describes the strength of the physical interaction between ligand and receptor, which is expressed as K_D (or K_i) value, defined as the equilibrium constant that describes the concentration of a ligand required to occupy 50% of the available target binding sites [925]. Affinity (or binding affinity) is hereby independently of the ligand's function, e.g. whether it activates or inactivates the target receptor. K_D can be determined directly from saturation type ligand-binding experiments using radioisotope- or fluorescence-labeled ligands [925]. Given a functional assay system, the potency describes the required concentration for a half-maximum response of a ligand at its target, expressed as EC_{50} (agonist effect, activating response) or IC_{50} (antagonist effect, inhibiting response) [926]. The maximum effect of an agonist/activating response in a functional assay system is described as efficacy and is expressed as the E_{max} value, which is an absolute value dependent on the assay-specific readout, for example, fluorescence intensity or percentage relative to a reference such as the endogenous agonist [927]. Such functional assays determine potency and efficacy of a ligand by measuring the response of a biological system following the stimulation of inhibition of the target GPCR. Commonly used pharmacological assays determine responses of receptor activation or blockade in cells by quantifying second messenger concentration, for example, cAMP accumulation or intracellular calcium mobilization. In addition, more recent assay systems use artificial probes that do not occur in nature, such as effector proteins or fluorescent tags, allowing 1:1 indirect measurement of the pathway activated (or inhibited) by the target GPCR.

1.2.1.1. β-arrestin recruitment assay

In this study, the β-arrestin recruitment assay was a useful tool for detecting GPCR activation after ligand stimulation. β-arrestin recruitment relies on β-arrestin biosoners, which are based on BRET technology, as well as enzyme complementation [928]. All assay systems require modification at the receptor (C- or N-terminus), such as insertion of tags, for example, enzyme fragments, luciferases, fluorescent tags, and many more [929–935].

The β-arrestin recruitment assay system PathHunter® developed by Eurofins DiscoverX® (Fremont, CA, USA, https://www.discoverx.com/arrestin, accessed on 10 July 2023, **Figure 3**) is based on enzyme fragment complementation of β-galactosidase [936]. The enzyme β-galactosidase is split in two parts, the Enzyme Acceptor (EA), which is fused to the β-arrestin protein and the ProLink (PL), which is fused to the C-terminus of receptor of interest [936,937]. EA and PL are inactive as single fragments. Both constructs, β-arrestin-EA and GPCR-PL are located on two different plasmids which are transfected to Chinese Hamster Ovary (CHO) cells (**Figure 4**). To ensure receptor expression antibiotic selection is then applied.

In the life cycle of GPCRs, the binding of a ligand leads to activation of the GPCR [938]. The receptor undergoes several conformational rearrangements, thus enabling space from the intracellular side for the trimeric G protein to bind [938]. Aside from the dissociation of the G protein into its three subunits alpha, beta and gamma, GPCRs are also able to be silenced by β-arrestin proteins [939,940]. Binding of β-arrestin leads to desensitization of the GPCRs [940].

With regards to the β-arrestin recruitment assay, this step assembles a fully active β-galactosidase. The active enzyme is then able to catalyze hydrolysis of its 1,2-dioxethane substrate, which is added to the cells together with a reaction buffer, creating a chemiluminescent signal [941]. 1,2-dioxetane substrates emit visible light upon enzyme-catalyzed decomposition and are extremely sensitive as a result of low background luminescence coupled with high-intensity light output [941]. The energy for light emission is generated upon dioxetane degradation, whereas fluorescence requires an external light source for excitation energy, which must be filtered to discriminate the fluorescent signal. In addition, the reaction buffer contained an enhancer that amplified the chemiluminescent light signal. Hence, measured chemiluminescence or activity of the β-galactosidase correlates with receptor activation.

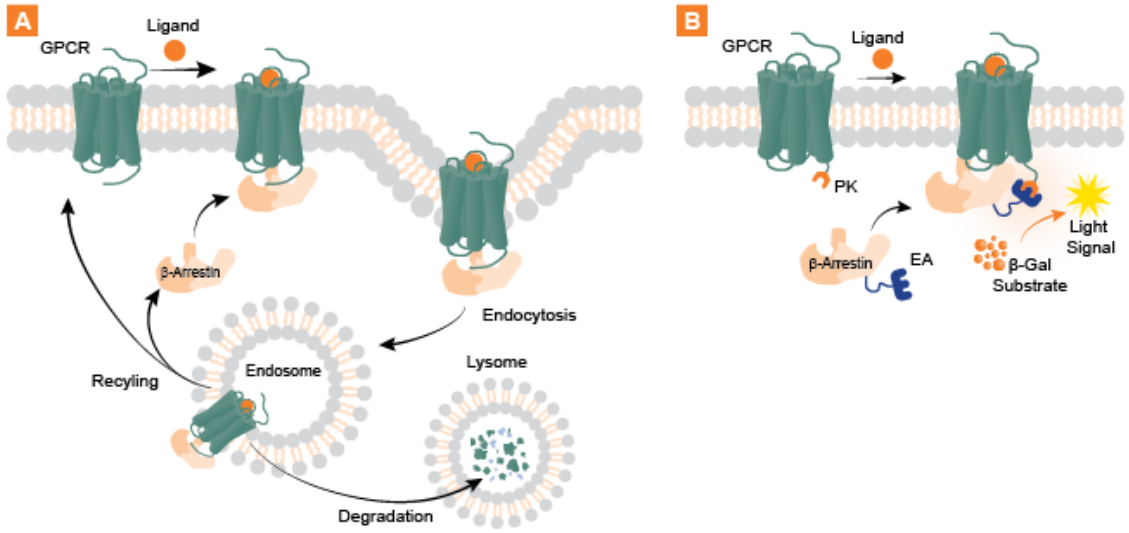

Figure 3. Assay principle of the Pathhunter β-arrestin recruitment assay by Eurofins DiscoverX®. A: Internalization of GPCRs by β-arrestin. B: Assay principle (https://www.discoverx.com/technologies-platforms/enzyme-fragment-complementation-technology/cell-based-efc-assays/protein-protein-interactions/gpcrs-b-arrestin-en, accessed August 24th, 2023).

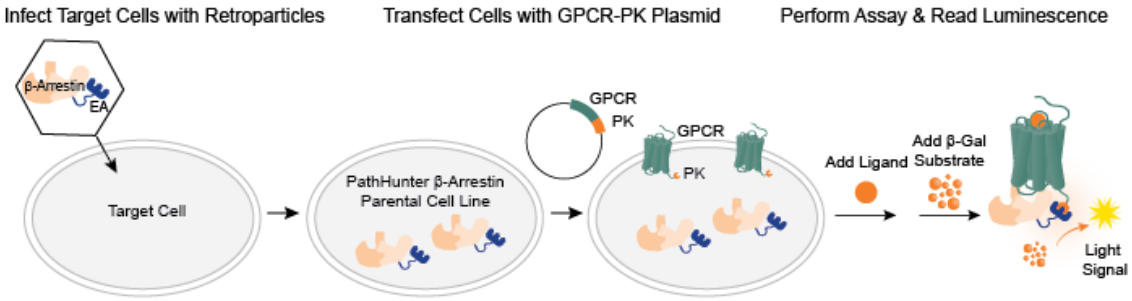

Figure 4. Creating a cell line for Pathhunter β-arrestin recruitment assay and assay principle short by Eurofins DiscoverX® (https://www.discoverx.com/technologies-platforms/enzyme-fragment-complementation-technology/cell-based-efc-assays/protein-protein-interactions/gpcrs-b-arrestin-en, accessed August, 24th, 2023).

1.2.1.2. Fluorescence Resonance Energy Transfer (FRET)

FRET has been shown to effectively detect molecular interactions between proteins at a cellular level [942]. Detecting relevant PPIs through *in vitro* and *in vivo* methods have been further developed [943].

FRET was initially discovered by the French physicist Jean Perin 1932 [944] and further developed later by the German scientist Theodor Förster in 1948 [945]. FRET is a process where an excited fluorophore molecule (donor) transfers its energy in the form of a photon non-radiatively to another fluorophore partner (acceptor) [946]. In order for this transfer to occur, donor and acceptor molecules have to be <10 nm close to each other, the emission spectrum of the donor needs to have sufficient overlap with the absorption spectrum of the acceptor and the emission and absorption dipole moment of both, donor and acceptor must not be perpendicular [942,946]. The amount of FRET

events is then expressed as FRET efficiency, which is described as the fraction of the photons transferred to the acceptor [942,946]. FRET therefore is highly sensitive to the distance between donor and acceptor dipoles and suitable for detecting PPIs, aside from also being able to detect conformational changes, intracellular ion concentrations and enzyme activity, basically all events that lead to changes in molecular proximity [947–949]. Another advantage of FRET is that it can be performed optically in live cells in a non-destructive and minimally invasive way [949]. Selecting two fluorophores are the key to the high performance of biosensors in living cells [947,950]. Several FRET-pairs have been described such as cyan fluorescent protein (CFP) and yellow fluorescent protein (YFP), green fluorescent protein (GFP) and red fluorescent protein (RFP), far red and infra-red fluorescent protein (FFP-IFP) and many more as well as multicolor pairs [947]. One of the most popular FRET pairs is CFP-YFP [950,951]. This pair has been previously described to have a strong spectral overlap for recording FRET events and provides powerful insights into kinetics and mechanisms of associations and conformational changes of GPCRs in live cells [952–954].

To date, two measurement categories have been developed to quantify PPIs in the form of FRET changes: (1) direct methods, which directly correlate changes in fluorescence intensity, such as sensitized emission methods and polarization-resolved FRET; (2) indirect methods, which involve measurements of FRET efficiency in different states, such as spectral imaging, acceptor photobleaching, and fluorescence lifetime imaging FRET [947].

In this study, we utilized two methods: the sensitized emission method and acceptor photobleaching (**Figure 5**).

With the sensitized emission method acceptor fluorescence can be detected using donor excitation (Da) [942]. This method can be carried out on a conventional wide-field confocal microscope, but recorded FRET intensities require normalization [943]. This is necessary due to secondary effects like fluorescence of the acceptor can be induced inadvertently by light intended to excite the donor or bleeding of donor emission into the acceptor emission channel [943].

For each donor and acceptor channel the changed in the intensities of the donor at the donor emission (Dd), the acceptor at the acceptor emission (Aa), and the acceptor at the donor emission (Da) are recorded and lastly the FRET signal is corrected ($FRET_{corr}$, (**Equation 3**)) [955]. Using the correction factors (CoA and CoB, (**Equation 1**), (**Equation 2**)) and the corrected FRET intensities ($FRET_{corr}$) the overall FRET efficiency (**Equation 4**) can then be determined.

$$CoA = Da\ ACCEPTOR/Aa\ ACCEPTOR \quad (\mathbf{1})$$

$$CoB = Da\ DONOR/Dd\ DONOR \quad (\mathbf{2})$$

$$FRET_{CORR} = Da\ FRET - (Dd\ FRET \times CoB) - (Aa\ FRET \times CoA) \quad (\mathbf{3})$$

FRET EFFICIENCY [%]= (FRET CORR / Dd FRET) × 100 (**4**)

The acceptor photobleaching method measures the increase in donor fluorescence after complete destruction of the acceptor fluorescence by laser-bleaching [942]. The signal of the donor fluorescence is then un-quenched by the spectral overlap of the acceptor spectrum and can therefore be detected [943]. Images are taken in donor and acceptor channels simultaneously before and after the bleaching and FRET efficiency is then calculated by subtracting the donor emission before bleaching (IB) from the donor emission after bleaching (IA) (**Equation 5**).

FRET EFFICIENCY [%] = (IA − IB) × 100/ IA (**5**)

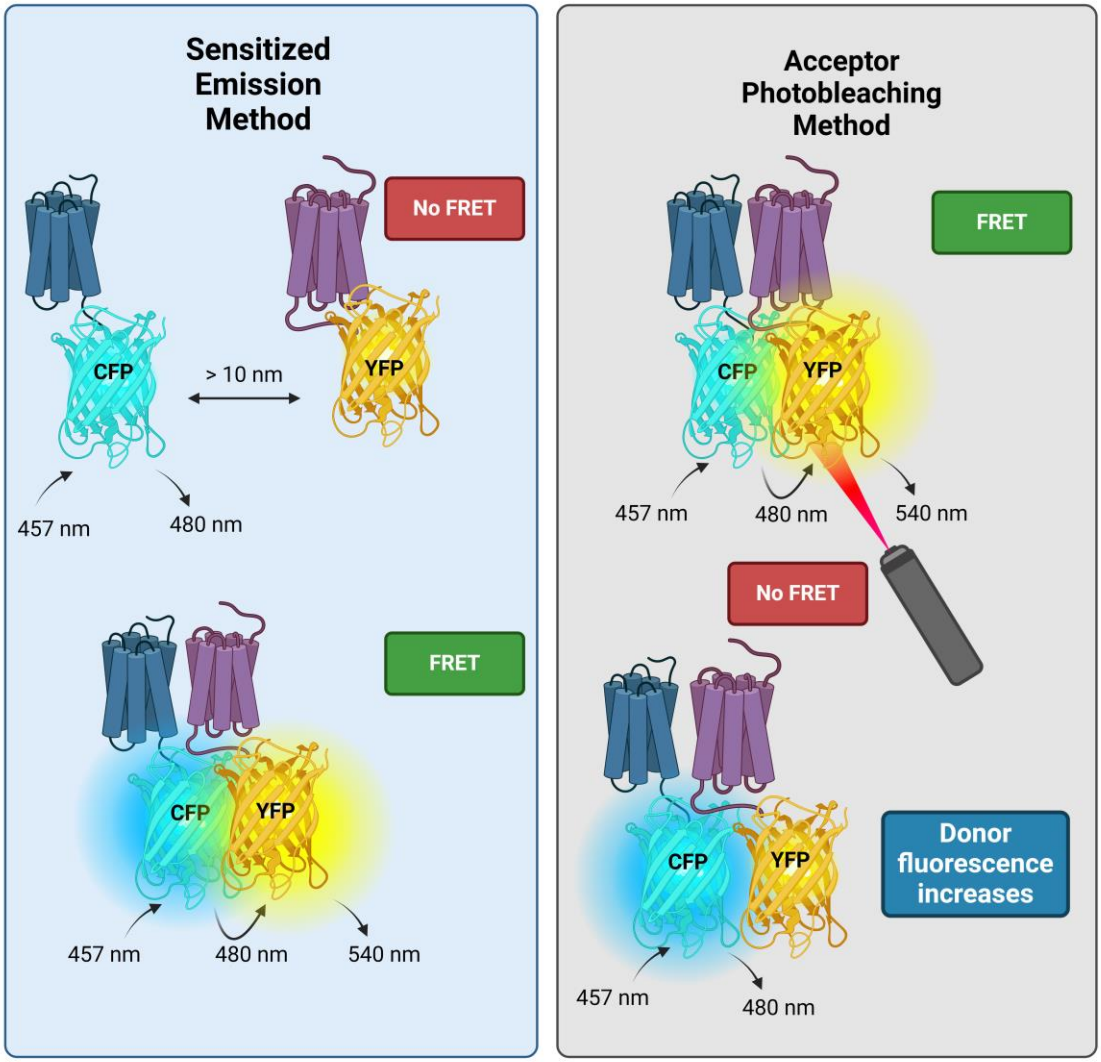

Figure 5. Principle of FRET sensitized emission method (left) and acceptor photobleaching (right).

1.2.1.3. Western Blot

Western blotting is a technique to separate and identify proteins based on their molecular weight by gel electrophoresis [956,957]. [956,957]. A given protein sample was loaded onto a gel and proteins were separated by electrophoresis. For this protein, samples were diluted in a loading buffer containing glycerol for the samples to sink to the wells of the gel and a tracking dye, which is usually bromophenol blue, in order to track the progress of the run. Furthermore, samples are usually heated before dilution with a loading buffer to denature the proteins and retain sulfide bridges [958]. The SDS-PAGE method, which is the most common form of western blotting, makes use of the detergent sodium dodecyl sulfate (SDS) that is added to the loading buffer, which strongly binds to proteins and then gains a negative charge in proportion to their molecular size [959,960]. A negative charge is required for proteins to be pulled through a polyacrylamide gel by electrophoresis (PAGE) [959]. In addition, a negative charge was maintained, even when the samples were boiled for denaturation.

The proteins are then separated by their molecular size, which is determined by the distance they can travel through the gel, where smaller proteins can travel quickly [960]. In addition, one SDS molecule can bind two amino acids when SDS is present in 0.1% of the protein sample [961]. Western blot gels consist of two different types of agarose gels: stacking and separating [958]. The stacking gel had a lower polyacrylamide concentration and was slightly acidic, allowing the sample to form thin, sharply defined bands [958]. The separating gel (lower gel) is more basic and has a higher polyacrylamide concentration; hence, the gel pores are narrower [958]. Once the proteins are loaded on the gel, the negative charge allows them to travel towards the positive electrode when a voltage is applied.

Electrophoretic transfer was applied after running the gel, where an electric field was used to elute proteins from the gels and transfer them to membranes [962,963]. To achieve this, the membrane and gel were placed together with a filter paper between the two electrodes. A high-voltage current is the driving force for the proteins to migrate from the gel to the membrane due to the negative charge of SDS.

After transfer, Ponceau S staining was used to visualize its success [963,964]. Ponceau S (also known as Acid Red 112) is a bisazo dye used for reversible staining of proteins on membranes. It was first described by Salinovich and Montelaroused in 1986 as an alternative to Coomassie Brilliant blue staining [965]. Apart from Ponceau S and Coomassie brilliant blue, there are many more dyes with different binding properties and detection limits [964]. With Ponceau S staining and a suitable protein ladder, the size of the proteins can already be determined.

However, to identify a particular protein of interest with the corresponding band size, antibody staining is usually the method of choice for western blotting. Before antibodies can be applied to proteins on the membrane, the membrane must be blocked to prevent nonspecific binding of the antibodies [958]. Usually, blocking is performed with 5% bovine serum albumin (BSA) or non-fat dried milk powder diluted in Tris-buffered saline buffer with Tween20 buffer, so the background signal is reduced [958,966]. After blocking and washing the membrane the antibody staining can be carried out. First, the

primary antibody is applied, which directly binds to its specific antigen (target epitope), f.e. against the human D_2R [967,968]. Then, the secondary antibody is applied that recognizes the primary antibody [968]. Usually secondary antibodies are conjugated with fluorescent molecules for detection. An alternative to fluorescent secondary antibodies are ones that catalyze a chemical reaction leading then to chemiluminescence. Typically it is an oxidation reaction of a substrate such as luminol, which is oxidized by enzymes like the horseradish peroxidase (HRP) [969,970]. The oxidation then produces light as a by-product [969]. The signal is captured on a film or an imager, and it is produced corresponding to the position of the target protein.

1.2.2. Computational approaches to study G protein-coupled receptors

1.2.2.1. Homology modeling

GPCRs have been previously characterized by a fraction of three-dimensional (3D) information available. For many years, structural information has only been available for rhodopsin, whose atomic resolution was solved in 2000 [971–973]. While rhodopsin was crystallized in its native state, the first ligand-bound receptor, β_2AR, was solved in 2007 (**Figure 6**) [974,975].

Quality of the template structure

Major progress in GPCR nuclear magnetic resonance-spectroscopy (NMR-spec), X-ray crystallography (X-ray) and cryo-electron microscopy (cryo-EM) has led to the resolution of many additional receptor structures, which can be viewed and downloaded from the Protein Data Bank (PDB) (www.rcsb.org) [971,976]. Initially, most structures were solved by X-ray crystallography; however, recent advances in cryo-EM have made GPCR tractable targets [976]. According to GPCRdb, from 988 deposited structures, 462 were obtained by X-ray crystallography, whereas 524 were obtained by cryo-EM (May 2023) [977,978].

In addition, the first ligand-bound structures of GPCRs are mainly in antagonist-bound or-inactive states [976]. Crystallization of the fully active states of GPCRs, usually coupled to a G protein or β-arrestin, is required [976]. However, GPCR-G protein/β-arrestin complexes are extremely flexible and have difficulties forming crystal contacts [118,976,979]. Alternative strategies for X-ray crystallography to obtain active GPCR structures include the application of conformation-specific nanobodies and C-terminal peptides of the Gα subunit or mini-G proteins [980–985]. Such structures are highly informative for studying receptor conformations but are rather difficult to obtain. In contrast, cryo-EM has been proven to be an optimal technique for resolving GPCR-G protein/β-arrestin complexes [976]. New electron microscopes with higher resolution, direct electron detectors and advanced image processing software have significantly improved this method [976,986–989]. Hence, the first GPCR structure solved using cryo-EM was published in 2017 [990].

The aim of these methods is to obtain a 3D-molecular structure from a crystal.

For **X-ray** these crystals are then exposed to an X-ray beam, which then diffracts. The resulting diffraction patterns are catched by a detector and are then processed using Fourier-Transformation. The symmetry and size of the repeating patterns and spots determines the intensity, which in turn then can be used to calculate a map of the electron density [991,992]. Various adjustments can be used to improve the quality of the electron density map until it carries sufficient information to allow the building of the molecular structure following its protein sequence. The map and structure are then combined to more accurately adopt a thermodynamically favored conformation of the resulting 3D-structure [991,992]. These crystals contain a high concentration of purified protein.
For **NMR-spec**, the protein was purified, placed in a strong magnetic field, and then probed with radio waves [993]. The local magnetic fields around the atomic nuclei change the resonance frequency, providing information on the electronic structure of the respective atom [994,995]. The resonance of electromagnetic radiation in a magnetic field is analyzed, and atoms that are bonded together give a characteristic local conformation. Together, these results provide a list of close atomic nuclei and restraints that are used to build a model of a protein that shows the location of each atom. Areas with fewer restraints correspond to flexible parts of the protein [127].

Cryo-EM, especially single-particle cryo-EM, has revolutionized the structure determination of large protein complexes [996,997]. Unlike X-ray crystallography, the protein probe does not have to be crystallized; rather, it is flash-frozen and can therefore be examined in near-native states [998]. This is a huge advantage over X-ray crystallography, where the resolution is limited by the purity of the crystal and coaxing GPCRs into a crystalline state can be very time-consuming [999]. The frozen proteins were prepared in a water-free environment and imaged several times with an electron microscope under conditions below -150°C. Computational alignment and averaging of the images led to 3D reconstruction of the protein [978,1000,1001]. Despite the ease of preparing protein samples for cryo-EM, the resolution of the structures has not been as high as that of structures obtained by X-ray crystallography, with resolutions around 3–4 Å, compared to 1.5 Å for X-ray crystallography [976,1002]. However, single-particle cryo-EM has been reported to resolve GPCR complexes reaching atomic resolutions up to 1.2 Å [997,1003,1004].

For some use cases, it might be rational to check the **B-factor** for a given protein structure. The B-factor, also known as the Debye-Waller factor, is used to describe the attenuation of X-ray or neutron scattering through thermal motion (oscillation) that occurs during protein crystallography [1005]. For proteins, this can be seen as a metric to identify the flexibility of atoms, side chains, or even whole regions, and are refined isotropically under the assumption that oscillation amplitudes are identical in all directions [1005,1006]. B-factor information can be helpful for sequence-based predictions of local protein flexibility [1007–1012]. Finally, an increasing number of structures can be determined by nuclear magnetic resonance spectroscopy [1013].
To date, only 140/800 experimentally determined structures of known human GPCRs have been published (January 2023) [1014]. Without a published structure as a starting point, the generation of homology models is required. Hence, the resolution of the template structure (Å), particularly around a potential binding pocket, is crucial for further model construction and assessment.

Constructing a homology model

Given this knowledge gap, homology modeling is an important tool for studying the targets of interest *in silico*. This methodology uses a template 3D-structure, in which the sequence of the target receptor is modeled onto its backbone coordinates [972,1015]. If the sequence similarity is sufficiently high (minimum of 20-30%), a single template structure is sufficient for target structure prediction; however, this is still prone to fail to generate accurate models [972]. The use of multiple templates has become increasingly popular for sequence identities below 50% for any template [972,1016–1020]. Furthermore, the availability of receptors co-crystallized with different ligands, as well as G proteins or β-arrestin, increases the quality of homology models. In addition, the resolution of the template structure is crucial. If the electron densities around an estimated binding pocket are not well resolved, major drawbacks can occur in structure-based drug design [976]. Amino acid sequences of the candidate templates are aligned with their target sequences, since the transmembrane regions, including HX8, are highly conserved for GPCRs, so the best possible selection can be made. In contrast, higher sequence variability is observed for the extra- and intracellular regions; hence, sequence identity does not necessarily have to be the highest in these regions [971,1021]. Before subjecting PDB files to structure-based sequence alignments, for example, by ClustalOmega (EMBL-EBI, Cambridgeshire, UK) [1022], the files should be edited, in particular, removing all components apart from the receptor structure (and ligand), since they are not relevant for homology modeling. All the records pertinent to these components were deleted. Once an alignment is performed, there exist several software and web servers that then construct the target sequence onto the 3D-coordinates of the template structures, such as Robetta and Rosetta[1023–1025], MODELLER [1026,1027], and commercial programs such as Molecular Operating Environment (MOE; Chemical Computing Group) or Yet Another Scientific Artificial Reality Application (YASARA) [1028,1029]. Apart from alphaFold [1030], other *ab initio* solutions exist where the 3D-coordinates of a template are not required anymore [1031,1032]. Especially alphaFold was a major breakthrough in structure prediction as it is an artificial intelligence system that has access to the largest protein sequence data bank. Hence, it can directly predicts the 3D coordinates of all heavy atoms for a given protein using the primary amino acid sequence and aligned sequences of homologues as inputs [1030].

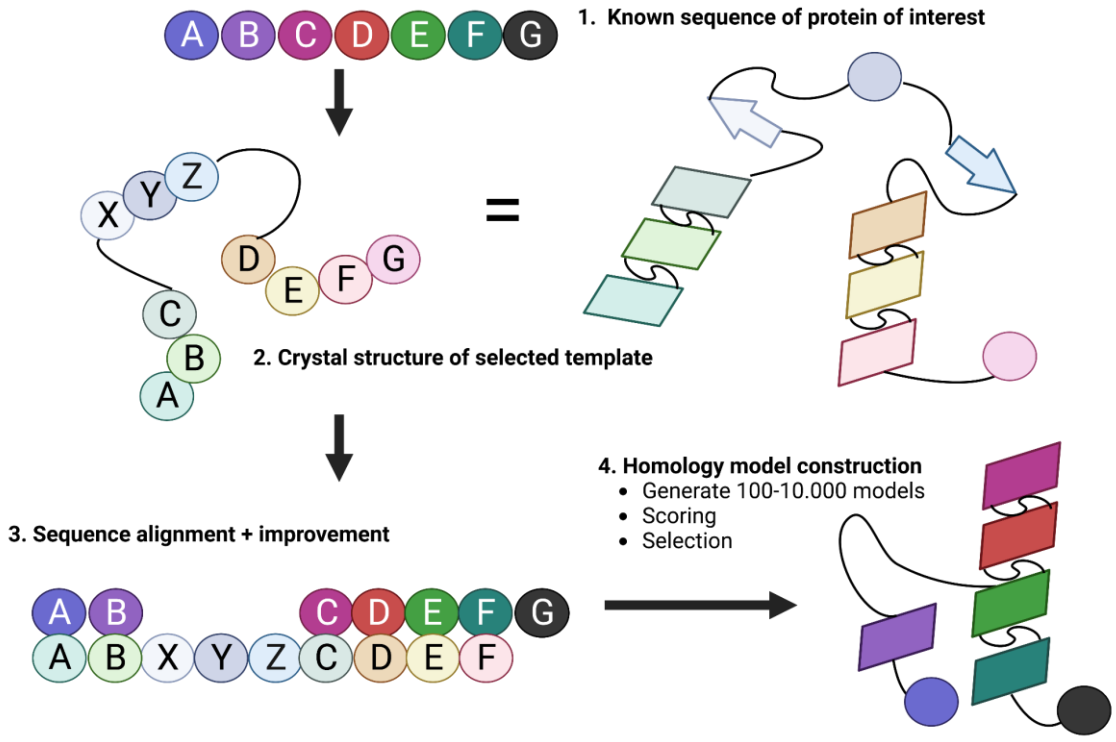

Figure 6. Workflow of creating a homology model.

Later on the AlphaFold Protein Structure Database was released (AlphaFold DB, https://alphafold.ebi.ac.uk) [1033] that is an unprecedented collection of high-accuracy protein-structure predictions powered by AlphaFold V2.0 of DeepMind, containing 360,000 predicted structures across 21 model-organism proteomes. It is reported to cover most of representative sequences from the UniRef90 data set (over 100 million) [1033].

It should also be noted that for non-conserved regions, such as loops, refinement of these regions would improve the quality of the model, where AlphaFold has already elucidated many of such regions. In addition, *de novo* modeling or omission of the loop, which is usually performed for ICL3, are viable solutions [971]. Furthermore, conserved disulfide bridges within the receptor were added during model construction. Usually, minimums of approximately 100 models are required to select the most accurate candidate.

Scoring

Having constructed several potential homology models for the target of interest, the question of how to select the most accurate candidate based on qualitative methods, such as scores, remains. Despite relying on the built-in metrics of open-source and licensed software, visual inspection is still one of the best approaches for selecting the best homology model [1034–1036]. In our experience, a combination of different metrics can provide adequate models[1037]. For instance, the combination of MODELLER's metrics [1038], ProSA-web [1039,1040] and ProQ [1041,1042] has shown to be a

reliable combination to validate homology models and has been followed in this work. MODELLER's built-in metric, Discrete Optimized Protein Energy (DOPE) [1043], and initial visual inspection help remove incorrect models before they are processed through ProSA-web and ProQ. Generally, all maps aim to map the free energy of a given protein. Because the goal is to generate a homology model with the west free energy, it is valuable to know what each metric considers as the lowest free energy achievable, so that it can then be evaluated as to the importance of the absolute value.

DOPE accounts for the finite and spherical shape of native protein states, which generally have the lowest free energy[1043,1044]. It calculates the statistical potential based on the improved reference state of the non-interacting atoms. This estimation of statistical potential is derived from the negative logarithm of the joint probability density function of a protein [1043]. This potential list is also distance-dependent on an atomistic level without recourse to statistical mechanics and the assumption of the Boltzmann distribution [1043]. Furthermore, this reference statistical potential solely depends on the size of the native structures, while it should be noted that the statistical potentials commonly used rely only on atomic distances [1043].

ProSA-web calculates the z-score with values around −4 are considered acceptable[1040]. In addition to the z-score, problematic regions were highlighted in a 3D viewer, where the output model was represented. For ProSA, Cα potentials, which are knowledge-based, have the advantage that low-resolution input can also be evaluated through a web service [1045]. Using the coordinates of the input protein, the distance-based pair potential estimates the total energy (z-score) [1046,1047]. Z-scores outside the characteristic range for native proteins are considered faulty models. This comparison of particular values is displayed in an additional plot that shows the z-scores of all experimentally solved protein structures from the PDB, where the different sources (X-ray and NMR) are color-coded [1040]. Furthermore, another plot of residue energies is output, which is calculated based on the general solvent exposure of protein residues [1048]. It should be noted that the z-score is usually considered a globular protein; therefore, for GPCRs, the z-score is not the most accurate metric [1040,1046].

ProQ analysis provides two scoring metrics, LGscore and MaxSub, and operates based on a neural network [1038,1049]. For LGscore values > 3, MaxSub values > 0.5 are typically considered as "good."
The LGscore detects the most significant non continuous segment of a model after structural superposition [1050]. Similarity is measured using the negative log of a set of structural P-values defined by Levitt and Gerstein 1998 [1050].

$$S_{str} = M(\sum 1/(1+(d_{ij}/d_0)^2) - (N_{gap}/2)) \quad (\mathbf{6})$$

According Levitt and Gerstein, a structural P value (= significance of similarity, S_{str}, **Equation 6**), where M is equal to 20, d_{ij} is the distance between residues i and j, d_0 is equal to 5 Å and N_{gap} is the number of gaps in the alignment. For calculating the entire set, the distribution for collection of structural alignments of unrelated proteins S_{str}

dependent on the alignment length was calculated [1038,1050]. From this distribution the P-values dependent on S_{str} could be determined.

MaxSub also determines the similarity of a model to its corresponding experimental structure in the range of 0 to 1 (0= completely wrong, 1= perfect model), considering Cα atoms [1049]. This range is thereby correlated with the normalization of the size of the largest "well-predicted" subset and uses a variation of a formula by Levitt and Gerstein [1049,1050]. MaxSub displays the maximum number of predicted residues that can be superimposed over an experimental structure within a given threshold [1049]. Hence, the limiting number of the residues is the factor as well as the threshold which represents the distance between residue pairs that is allowed after superposition and usually set to 3.5 Å [1049]. For more details on the algorithm, please refer to Siew et al. [1049]. In addition, ProQ allows the addition of secondary structure information generated by solutions such as PSIPRED to improve prediction accuracy [1051]. Finally, the root-mean-square distance (rmsd) between two given structures can also be used to quantify the similarity between two structures [1038].

1.2.2.2. Understanding proteins in 3D

The difference between molecular docking and simulations

Molecular docking is the computational modeling of two interacting molecules with the aim of predicting their best orientation. The goal of docking is to explore and optimize the behavior of the two molecules of interest in 3D, which can either be two proteins (PPIs) or small molecules, or ligands with their target protein, to reduce the total free energy of the system [1052,1053]. Protein-ligand docking has been particularly helpful in drug design by predicting the binding mode and affinity of drugs within the binding site of a protein (receptor) [1054]. The earliest reported docking methods were based on the lock-and-key assumption, where both entities were treated as rigid, and their affinity was directly proportional to the geometric fit between their shapes (**Figure 7A**). To assess meaningful interactions between the two molecules of interest, the maximizing attracting and minimizing repulsive forces are mathematically determined. To define the range of interactions and relations that either protein-protein or protein-ligand complexes can undergo, empirical rules based on physical principles such as van der Waals forces and hydrogen bond lengths are applied to predict the potency and type of signal (agonism and antagonism) [1055]. Finally, geometric algorithms are applied to generate a 3D representation of the binding interface, which can be used to calculate binding conformations and binding affinities. Typically, the protein conformation is treated as fixed with the defined binding site, the ligand is often treated as flexible, and the protein is assumed to be rigid. For protein–protein docking, both are treated as semi-flexible, with the backbone treated as rigid and only allowing the side chains to be flexible.

Molecular Dynamics simulations (MDs) are used to study the dynamic behavior/movement and interactions as a function of time. MDs allow the exploration of protein flexibility, conformational changes, and equilibration of the defined molecular system. All entities of the system (ligands, proteins, water, lipids, etc.) are treated as

flexible[1056]. All atoms are allowed to interact for a given fixed period of time, and the created trajectories of the atoms are determined by numerically solving Newton's laws of motion (classical mechanics) [1054,1057,1058]. Such simulations typically use a full atomistic 3D representation of the molecules, can provide detailed insight into protein dynamics and structural changes, and can be useful for interpreting experimental results[1059]. In summary, molecular docking focuses on predicting ligand-binding modes and affinities within a fixed protein structure, while molecular simulations aim to understand the dynamic behavior and interactions of proteins by simulating their motions and exploring various conformations over time (**Figure 7B**).

Since both methods involve (i.) 3D representations of proteins and molecules and require (ii) definition of molecular interactions at an atomistic level, such as potential energies and the use of mechanical force fields, we will briefly introduce these determinants before covering the entire process of molecular docking and MD simulation:

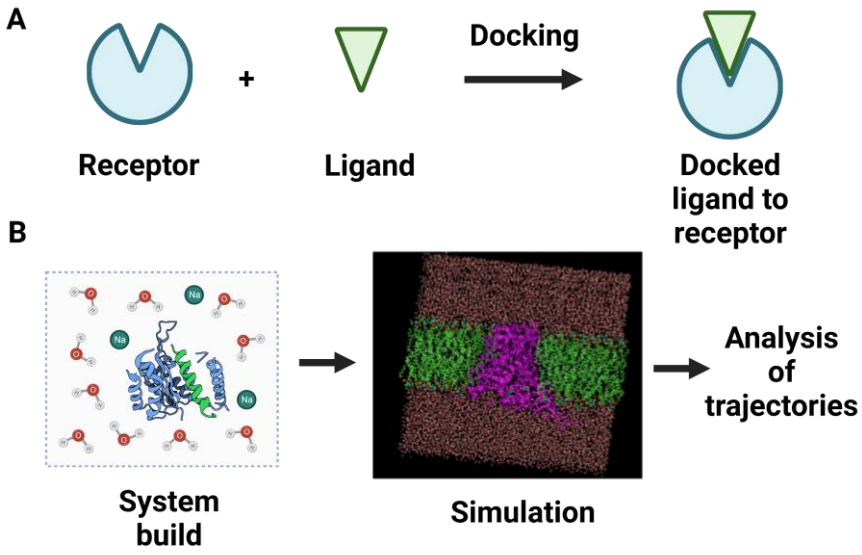

Figure 7. Basic principles of molecular docking (**A**) and molecular dynamics simulations (**B**).

Protein representation

Computationally mimicking proteins and molecules is crucial for creating realistic molecular complexes of biological protein functions, however classical all-atom representations are still limited by the algorithmic efficiency and computing power [1060–1064]. The representation of all atoms is expensive because it requires the calculation of the interactions between all atom pairs that grow rapidly (n^2) with the number of atoms. Hence, coarse-grained protein representations have been developed as a practical alternative, which is also part of the Rosetta docking search algorithm used in this study, which previously helped to understand protein folding in general [1065–1072]. Coarse-grained protein models assume various levels of a reduced representation of their chains [1066,1067,1073]. The main purpose of these models is to reduce the number of degrees of freedom [1069]. However, as we were concerned with key details of the relationship structure function, these were not used in this study.

Early computational approaches by Levitt, Warshel and Karplus aimed to design a simplified representation of a protein, where spheres (so-called “pseudo-atoms" or “beads” would represent amino acids for the structural characterization of lysozyme and later turned out to be the first coarse-grained model for a protein system (pancreatic trypsin inhibitor) [1070,1074–1076]. From these simulations, the so-called “Levinthal paradox” was formulated [1077], which describes that the protein folding process has a relatively small number of conformations. For instance, in their protein model, each residue consisted of only two pseudo-atoms: the Cα atom and the centroid of the side chain. The United pseudo-atoms were then placed at the centers of their average conformations to mimic the side chains (apart from glycine). The angle between three consecutive Cα was assumed to be constant and planar and equal to the statistical average known from familiar protein structures. Furthermore, non-bonded interactions occurred only between the side chains. Hence, torsion angles for the central pseudo-bonds between four consecutive Cα atoms were considered, which reduced the degrees of freedom per residue to 1 [1069,1076]. The Lennard-Jones potential describes the interactions between united atoms. The sampling scheme was described using simple Brownian dynamics (BD). They demonstrated with their work that the packing and pairwise interactions of side chains are the driving forces leading to specific folded structures, among other factors [1078]. Levitt, Warshel, and Karplus received the Nobel Prize in Chemistry in 2013 [1076]. Moreover, many of these principles are now well-established quantum mechanics/molecular mechanics (QM/MM) methods [1074].

Definition of molecular interactions on an atomistic level and force fields

At the atomic level, **molecular interactions** refer to the forces and interactions between individual atoms or groups of atoms within a molecule, or between different molecules. Such interactions are covalent and non-covalent, consisting of van der Waals forces, electrostatic effects, π-effects, and hydrophobic effects [1079,1080]. In the context of MD, a force field (FF) is a mathematical expression describing the energy of a system depending on the coordinates of its particles (atoms) [1081]. This allows for the calculation of the potential energy surface of the system and the calculation of forces and energies occurring between the interacting atoms with respect to their coordinates [1082]. Force fields provide a framework for calculating the potential energy and forces acting on each atom based on their interactions with neighboring atoms. The FF parameters (chosen energy functions) were derived from experimental physics, chemical data, quantum mechanical calculations, or both. Such parameters may include equilibrium bond lengths, bond angles, dihedral angles, force constants, van der Waals parameters, partial charges, and other terms that describe specific interactions, such as hydrogen bonding or metal-ligand coordination [1083,1084]. Here again, it can be distinguished between all-atom force fields, which provide parameters for every type of atom in a system, or coarse-grained potential, which omits certain chemical details, depending on the purpose [1069].

An FF typically consists of the interatomic potential energy (U) defined by a set of parameters (**Equation 7)**, where the bonded terms for interactions are covalent bonds, and the non-bonded terms are described by long-range electrostatic and van der Waals forces.

$$U = \sum_{bonded} - \sum_{non\text{-}bonded} \quad (7)$$

The bonded terms for interactions are covalent bonds, and the non-bonded terms are described by long-range electrostatic and van der Waals forces.

Covalent bonds - Intramolecular energy terms

Covalent bonds are formed when atoms share electrons to achieve a more stable electron configuration, leading to atoms holding together within a molecule [1085–1087]. Furthermore, covalent contributions carry terms for harmonic energy functions for angles, dihedral, and torsions, and do not allow bond breaking [1088]. Each factor is described by an individual energy term, which can be expressed as i.) bond energy (energy associated with the stretching, bending, or rotation of covalent bonds within a molecule), ii.) angle energy (energy associated with the bending or deformation of bond angles within a molecule); iii.) torsional energy (energy associated with the rotation around a dihedral angle (the angle between two connected bonds) within a molecule)) [1089,1090].

These intramolecular energy terms can be further extended by different descriptions, such as “improper torsional” terms, to enforce the planarity of aromatic rings or amide bonds [1083]. In addition, explicit terms for hydrogen bonds were added. For all energies described above, the harmonic energy function is usually applied, which describes the molecules as a set of atoms that are held together by simple elastic (harmonic) forces [1083]. Within the FF, the true potential is replaced by a simplified model (**Equation 8**).

$$V_{bond} = k_b * (r_{ij} - r_0)^2 \quad (8)$$

Where V_{Bond} is the potential energy associated with the bond at a given bond length r, k_b is the force constant, and r_0 is the equilibrium bond length, which is the distance at which the potential energy is minimum [1083,1091]. Therefore, the harmonic potential represents a simple oscillator. When the bond length deviates from the equilibrium value, the potential energy increases quadratically, reflecting the restoring force that pulls the atoms back toward the equilibrium position. Consequently, in a bond, the energy may oscillate between the kinetic energy of the atom mass and the potential energy stored. The angle energy is defined for each triplet of the bonded atoms (**Equation 9**).

$$V_{Angle} = k_\theta * (\theta_{ij}k - \theta_0)^2 \quad (9)$$

V_{Angle} is the potential energy associated with a given force constant k_θ with an equilibrium angle θ_0. The torsional energy was set for four sequentially bonded atoms, and the torsion angle ϕ describes the angle of rotation of the covalent bond between two atoms, n describes the periodicity and δ is the phase shift angle (**Equation 10**).

$V_{Dihed} = k\phi *(1+\cos(n-\delta))+...$ (**10**)

Non-covalent bond - Intermolecular energy terms

Noncovalent interactions are relatively weak compared to covalent bonds but are essential in determining the molecular structure and properties. These can be subdivided into van der Waals forces and electrostatic interactions. Van der Waals forces arise from temporary fluctuations in electron density, resulting in attractive forces between atoms or molecules, and do not result from chemical electronic bonds, such as ionic or covalent bonds [1092,1093]. Van der Waals interactions are formed if no other forces are present [1094]. The Lennard Jones potential is usually a suitable approach to describe the van der Waals forces as an energy term in FF [1095,1096]. The Lennard-Jones potential captures the general shape and behavior of van der Waals interactions, with the attractive term dominating at longer distances and the repulsive term becoming significant as atoms get closer to each other (**Equation 11**) [1097].

$V(r) = 4\varepsilon[(\sigma/r)^{12} - (\sigma/r)^6]$ (**11**)

V(r) represents the potential energy between the two atoms as a function of the separation distance (r). ε represents the depth of the potential energy well, which determines the strength of the van der Waals interaction, whereas σ represents the distance at which the potential energy is zero, also known as the van der Waals radius. The term (σ/r)^12 describes the attractive van der Waals forces, while (σ/r)^6 represents the repulsive forces. The parameters ε and σ are specific to each atom type and are typically obtained by fitting the potential energy surface to the experimental or quantum mechanical data.

Overall, van der Waals interactions are described as weaker than covalent (and ionic) bonds; their strength is distance dependent; they are additive and cannot be saturated; they have no directional characteristics and are independent of temperature, except for dipole-dipole interactions[1098–1102].

Molecular dipoles are described in FF with the use of partial charges described by Coulombic terms [1103–1105]. Dipole-dipole interactions: Dipole-dipole interactions arise from the electrostatic attraction between polar molecules [1106]. These interactions depend on the orientation and magnitude of the molecular dipoles and are accounted for in force fields through the assignment of partial charges and the use of Coulombic terms, which consider the charges and distances between the atoms [1106]. The Coulombic terms capture the attractive or repulsive forces between charges (**Equation 12**).

$V(r) = k*q1*q2 / r^2$ (**12**)

Where V(r) represents the electrostatic potential energy between two charged particles, q1 and q2, separated by distance r. k is a constant that depends on the units and system of measurement used in the force field. Hence, equally charged atoms repel each other, while oppositely charged atoms attract each other. Electrostatic interactions occur between charged atoms, such as ions, and hydrogen bonds [1080,1107,1108]. While ionic bonds are formed between full permanent charges, such as Na^+ (cation) and Cl^- (anion), hydrogen bonds are formed between H atoms, basically dipole–dipole attraction between a partially positive H atom and a highly electronegative, partially negative atom, such as oxygen, nitrogen, or sulfur.

Representing long-range electrostatic interactions computationally can be challenging because of the decreasing coulombic potential with increasing distance. The Ewald summation overcomes this gap by electrostatic potential into short- and long-range components and uses different techniques to compute each component [1109]. It assumes real-space (Vreal, short-range interactions within a specified cutoff distance) and reciprocal space (Vrecip, long-range interactions computed in Fourier space) contributions to accurately account for long-range electrostatic interactions (**Equation 13**) [1110,1111]. Self-energy term that corrects the self-interaction of charged particles [1112].

$V_{Ewald} = V_{real} + V_{recip} + V_{self}$ (**13**)

The Ewald summation is a starting point for molecular dynamics algorithms. To compute long-range electrostatic interactions, Particle Mesh Ewald (PME) [1113] and Smooth Particle Mesh Ewald (SPME) [1114] are techniques for defining periodic boundary conditions [1115]. SPME is one of the most popular long-range algorithms among mainstream molecular simulation packages, for example, AMBER [1116] and GROMACS [1117,1118]. PME and SPME accelerate the calculation of the long-range electrostatic potential of a system by employing a fast Fourier transform (FFT) algorithm [1119] and mesh-based representation of the potentials. The PME describes the charge distribution of the system on a three-dimensional grid, known as the mesh. The charge density on the grid is then transformed into a reciprocal space using FFT. This transformation allows for efficient calculation of the electrostatic potential in reciprocal space. Subsequently, the potential is transformed back to real space using the inverse FFT, and the short- and long-range contributions are combined [1115,1120]. SPME can be seen as an improvement over PME, where the issue of grid artifacts is eliminated owing to the introduction of a smoothing function [1121,1122]. Furthermore, π–π stacking can be a relevant noncovalent interaction [1123]. π–π stacking refers to interactions between aromatic systems, where the π orbitals of adjacent aromatic rings align and interact. This stacking interaction contributes to the stability of molecular assemblies and can be modeled using force field parameters that capture favorable aromatic-aromatic interactions [1124]. π-π stacking configurations are sandwiched, displaced, or edge-to-face [1080]. Finally, solvent effects can also be mathematically described, as they have significant effects on non-covalent interactions. Some FF

include explicit solvent models used to generate a generalized description of the solvent environment and approximate their effects.

Types of force fields

Many force fields (FF) available in the literature with different levels of complexity [1083]. FFs can be divided into physics-based, knowledge-based statistical, and structure-based FFs. The most used force fields in molecular simulations are based on classical mechanics, the so-called physics-based FF, and they make certain approximations to simplify the calculations.

i.) Physics-based FF // Molecular Mechanics FF

Physics-based FF are empirical models that approximate the potential energy of a system based on classical physics principles [1125]. They rely on mathematical functions to describe the interactions between atoms and include terms for the bonded and non-bonded interactions described above. The parameters for these types of FFs were derived from the experimental data or QM calculations. Examples of physics-based FFs include the empirical conformational energy program for peptides (ECEPP) [1126–1128], Molecular Mechanics (MM) FF [1129–1131] Chemistry at Harvard Molecular Mechanics (CHARMM) FF [1132–1135], Assisted Model Building with Energy Refinement (AMBER) FF [1136–1139], GROMOS FF [1140], and the Universal (UFF) force field[1141], which contains parameters for all the atoms in the periodic table [1125]. Many of these force fields are continuously evolving and different versions are available [1083].

ii.) Knowledge-based statistical FF

Knowledge-based statistical FF, also known as knowledge-based or empirical potential, is derived from statistical analyses (probability of a chosen observable) of known protein structures and their corresponding experimental data [1142,1143]. Such FF captures the statistical tendencies of atom-atom interactions and is developed by analyzing databases of protein structures [1144]. Examples for knowledge-based statistical FF are: DOPE [1043], CABS [1145], Rosetta [1146], just to name a few examples [1143]. In addition, more recent approaches improve the performance of these FF by combination with experimental data such as RosettaEPR [1147–1149]

iii.) Structure-based FF

Structure-based force fields are a subset of physics-based force fields that specifically derive their parameters and functional forms based on their molecular structures and electronic properties [1083,1150]. Examples include Density Functional Tight Binding (DFTB), which combines density functional theory (DFT) with the computational efficiency of MM [1151] and AM1/PM3/PM6, which are all semi-empirical quantum mechanical methods based on the neglect of diatomic overlap (NDDO) approximation [1152] or Atomic Multipole Optimized Energetics for Biomolecular Simulation (AMOEBA), which includes polarization effects, and the Reactive Force Field (ReaxFF), which is capable of describing chemical reactions [1153,1154].

For instance, Density Functional Theory (DFT), developed by Walter Kohn, is a QM method that can calculate the electronic structure of atoms (and consequently molecules) [1155]. It was originally developed in the 1970s and is currently the most widely used electronic structure method, for which Walter Kohn received the Nobel Prize in 1998 [1156]. DFT provides the possibility of calculating the total energy of a system by considering the electron density rather than the wavefunctions of individual electrons, as in the Møller–Plesset perturbation theory, which improves the performance of DFT-based MDs [1157].

Molecular docking - the process

Apart from "classical" molecular docking, for example, docking a small-molecule ligand to a target protein, protein-protein docking (PPD) has become an interesting approach to study PPIs. The PPD question can be summarized as a prediction of the complex, given the structures of the individual proteins, where additional information is available [1158]. The introduction of rigid-body docking algorithms by Vakser in the late 1980s can be considered an early principle of PPD. Using geometric and energetic estimations, searches were performed using shape complementarity [1158]. Usually, a potential binding site is required, which is not necessary for protein-protein docking. The binding site is defined as the active site of a target protein where a ligand can bind [1159]. Such forecasts, as well as the binding conformation of the target of interest, are mes-structure-based drug designs because the 3D protein structure is used as the basis for designing new drugs [1055]. Compared to this approach, ligand-based drug design relies on known binders of the target for rational drug design. Moreover, the implementation of artificial intelligence has been reported to significantly improve drug design [1160].

In general, molecular docking programs perform a search in which the conformation of the complex is evaluated recursively until the minimum energy is reached, by generating many docking poses (**searching/sampling step**) (**Figure 8**). This convergence is expressed by a scoring function, which is usually ΔG [U total in kcal/mol] and is associated with every docked pose (**scoring step**) [1161–1163]. However, proteins can be described as semiflexible oligomers that can form two or three specific shapes, depending on their amino acid sequences. These amino acids are linked via covalent peptide bonds, which always adopt a trans conformation. This in turn leads to limitations in the space and conformation available for the protein backbone. Hence, characteristic native 3D protein structures are not only determined by the conformational properties of the main chain but also by specific packing and interactions of the side chain [1069]. These determinants are considered in molecular docking, and apart from the aim to fit molecules together in their minimum energy are certain driving forces, such as electrostatic and van der Waals energies, hydrogen bonds, and interactions between amino acid side chains [1052,1069,1164,1165].

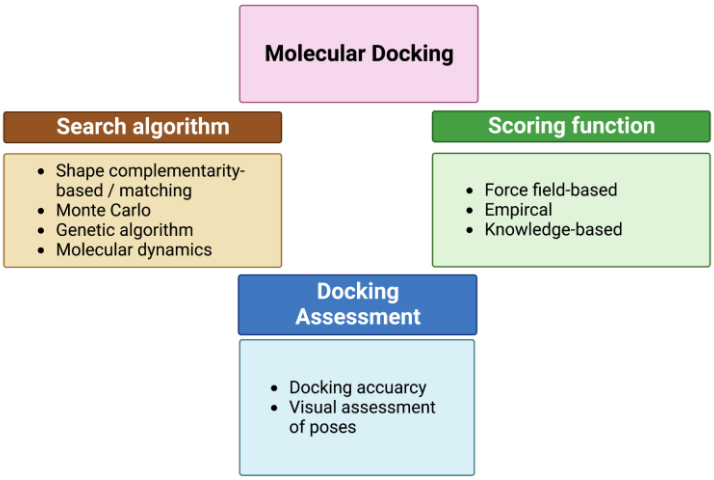

Figure 8. Workflow of molecular docking.

Search/sampling algorithms for the conformational space

The search algorithm should create an optimum number of docking poses that represent the probable experimental binding modes. Instead of a rigorous search of all possible poses between two molecules, several algorithms have been developed to reduce the computing time and reasonably access the conformational space between two molecules. The search for optimal docking poses involves exploring the conformational space of both the ligand and the protein, or two proteins for the case of PPD. Several search algorithms have been developed in recent decades to search for potential spaces, which consist of all possible orientations of the two interactants [1166]. There are two general types of docking: rigid docking, which treats only the ligand as flexible, and flexible docking (induced-fit), which also treats the binding pocket residues as flexible [1167–1169]. Depending on the type of docking, different search algorithms developed for molecular docking can be divided into exhaustive search/shape complementarity, Generic Algorithms (GAs), Monte Carlo (MC) methods, docking with molecular dynamics, and flexible docking among hybrid and machine learning methods.

Shape complementarity-based searches or matching algorithms [1170–1173] are based on molecular shape (geometric) maps, where a ligand is docked into the binding site based on shape features and chemical information, such as hydrogen bond donors and acceptors or steric surface complementarity [1174]. The ligand is represented as a pharmacophore, and new conformations are defined by the distance matrix between the pharmacophore and corresponding ligand atoms, following the idea of matching as many points as possible. An example of this is DOCK [1175]. In addition, solvent-accessible surface area (SASA) is often used to assess the structural complementarity of ligand-receptor complexes [1176,1177].

In contrast to matching based on geometry, stochastic methods such as **Monte Carlo (MC)** and **genetic algorithms (GA)**, which randomly modify ligand conformations in

order to position them best possible into an attempted binding pocket [1174], MC algorithms generate ligand poses through bond rotation, rigid-body translation, or rotation [1178]. The generated conformations were tested using different energy-based selection criteria, which were sequentially tested, saved, and further modified to generate the next conformation. These iterations proceed until the requested number of conformations is generated. Software such as AutoDock [1179] and ParDOCK [1180] make use of MC sampling. Regarding protein-protein docking, MC is used in Rosetta [1178,1181].

Genetic algorithms (GA) [1182–1184] are another form of stochastic method derived from the Darwin theory of evolution [1174]. They are commonly used to solve complex problems by mimicking the principles of evolution such as selection, reproduction, crossover, and mutation. For GAs, the ligand is described by its degrees of freedom encoded as binary strings (genes), which make up to the “chromosome” describing the pose of the ligand within the protein binding pocket [1174,1185]. Mutations and crossover calculations were performed using the docking pose described as a “chromosome.” While mutations cause random changes in the pose, crossover exchanges degrees of freedom between two docked poses [1174]. New poses that pass a given threshold are used for the next round until the desired number of poses is generated, which is called Lamarckian GA [1174,1186,1187]. GAs have been used by AutoDock [1182], GOLD [1188] or DARWIN [1189]. GAs are also useful for PPD [1190]. In addition to these general algorithms, many hybrid methods have been developed, including GLIDE [1174,1191].

Scoring functions

The scoring function consists of several mathematical methods used to predict the potential binding affinity of a docked ligand to its receptor. An energy scoring function that can rapidly and accurately describe the interaction between the protein and ligand was used. The lower the energy of a system, the more reliable the docked pose. Scoring functions are usually differentiated as FF-based, empirical, and knowledge-based (see the **types of force fields**).

Briefly, **FF-based scoring functions** calculate the binding energy as a non-covalent sum, based on the Coulombic formulation [1192–1194]. While van der Waals interactions are usually described by the Lennard-Jones potential, charge-charge interactions are described by a distance-dependent dielectric function. In addition, hydrogen bonds, solvation, and entropy contributions can be considered[1175,1195–1197]. FF-based scoring functions can be further refined and improved using linear interaction energy (LIE) and free-energy perturbation (FEP) methods [1192,1198,1199]. While LIE estimates the free energy change by considering the contributions from non-covalent contributions (such as electrostatic and van der Waals interactions) between the ligand and receptor, assuming a linear relationship between the energy and experimentally measured binding affinity [1057,1200–1202], FEP calculations are based on the free energy difference between two states by gradually transforming one state into another through a series of intermediate states [1203–1205]. This is typically achieved by applying thermodynamic integration or a related technique to obtain the

free-energy profile along the transformation pathway [1205–1207]. Both use the Zwanzig expression for free-energy perturbation [1208].

Empirical scoring functions calculate the binding energy as the sum of several energy components, including hydrogen bonding, ionic interactions, entropy, and hydrophobic effects. Each component is multiplied by a coefficient derived from regression analysis and then summed up in a final score [1209–1212].

Knowledge-based scoring functions use statistical analysis of crystal structures of receptor-protein complexes to calculate interatomic contact frequencies and/or the distance between the protein and its ligand [1213–1216]. Based on the assumption that a greater contact frequency is the more favorable docked position, these frequencies were converted into pairwise atom-type potentials, favoring preferred contacts and penalizing repulsive interactions, leading to a total score [1217–1219].

Hybrid scoring functions such as consensus scoring are also possible [1220,1221], as well as scoring functions that implement the treatment of the solvation effect by using the Poisson-Boltzmann and generalized Born assumptions to calculate the SASA [1222,1223] or HYDE, which considers desolvation and solvation terms [1224,1225]**.**

Molecular dynamics simulations - the process

Molecular dynamics (MD) simulations are used to study the behavior and dynamics of the atoms and molecules over time. It simulates the motion and interactions of atoms by numerically solving Newton's equations of motion and requires considerable computational power. Newton’s laws of motion, more precisely Brownian motion, enable us to calculate motion and quantities such as position, velocity, acceleration, and energy of atoms in a given fluid system [1226,1227]. In particular, the Langevin equation, which combines deterministic and stochastic forces to describe the motion of atoms in a fluid environment, is solved [1226,1228]. The deterministic forces arise from the potential energy gradients acting on the atoms, whereas the stochastic forces represent random fluctuations due to thermal energy, which is dependent on the temperature defined for the system. For thermal energy, the Born–Oppenheimer approximation is assumed to be valid, and the potential energy of all systems is calculated as a function of the nuclear coordinates using force fields [1229,1230]. To run an MD simulation, the initial configuration and **build of the system** must be established. This includes specifying the positions and velocities of atoms as well as assigning force field parameters that describe the interactions between atoms. As soon as the system is defined, one can proceed with **setting box size and boundary conditions**. Thus, to integrate the equations of motion and their accelerations, integration schemes such as the Verlet algorithm are used to numerically integrate these forces over small-time steps [1231,1232]. The system further evolves by defining a time propagation, where the forces on all atoms are updated based on their current positions, velocities, and force field [1233,1234]. In addition, periodic boundary conditions were applied to mimic an infinite system, ensuring that atoms that moved out of the defined simulation box re-entered the opposite site [1235,1236]. Before starting an MD, the initial atomic positions and velocities have to be set in the simulation box, which are usually randomized from a Maxwell-Boltzmann distribution at a given temperature as well as thermostats and barostats [1237–1239]. After the initial positions and velocities are set, an equilibration phase is often performed to relax the system to the desired temperature and pressure. This involves running the simulation for a certain number of steps, allowing the system to reach a stable state by adjusting particle

velocities and positions. Then, MDs can be run using predefined ensembles such as the NVE ensemble (constant number of particles, volume, and energy), NVT ensemble (constant number of particles, volume, and temperature), or NPT ensemble (constant number of particles, pressure, and temperature) [1240], which maintain the temperature and pressure of the system constant. Furthermore, time steps must be defined. Unfortunately, the time step in MDs is limited by the fastest motions, which are bond oscillations owing to their high frequency and low amplitude, which are in the femtosecond range (fs) [1241]. To overcome the timescale gap between MDs and biological processes, which usually takes up to milliseconds [1240], these bond vibrations involving hydrogen atoms are replaced by constraints [1241]. Hess developed a method to parallelize the application of these constraints, which are usually solved linearly over processor boundaries; hence, the fastest time step unit in MDs is approximately 10 fs [1240,1241]. This method, called the Parallel LINear Constraint Solver (P-LINCS), was implemented in GROMACS [1242]. However, there exist other constraints that will allow the speedup of time steps in MDs [1243]. Lastly, whenever the algorithm proceeds in a time step that contains all the information about the positions and velocities of every atom of a system, these are stored in so-called trajectories. The trajectory is obtained by repeatedly updating the positions and velocities of atoms based on the forces acting on them [1244]. Each time step continuously solved the equations of motion numerically, and the simulation calculated the positions and velocities of the atoms. The information stored in the trajectories can be analyzed and visualized in 3D using software tools to gain insight into the dynamic behavior of the simulated system.

Chapter 2: Objectives and thesis outline

This chapter describes the objectives that were tackled in this study as well a brief outline on the workflow that was followed.

In the past 15 years, molecular dynamics and the increasing availability of new functional assays have helped to study drug-receptor interactions and improve drug design. The appreciation of GPCRs as dynamic systems of varying micro-conformations, also called ensembles, has increased the understanding of GPCR signaling bias, and thus the ability to dissect multiple signals from receptors, and GPCR oligomerization.

Both events, signaling bias and oligomerization, diversify and fine-tune GPCR signaling and finally set the ground for cells to process a wide array of physiological signals. Furthermore, there has been a paradigm shift in describing responses not as monotonic signals from the receptor to the cell, but rather as versatility of interactions between proteins and ligands and proteins with proteins. From a pharmacological perspective, small-molecule drug development has shifted from copying natural ligands, such as neurotransmitters and hormones, to new scaffolds and ideas and may have opened new therapeutic targets. Dimerization/oligomerization of GPCRs induces changes in ligand coupling, receptor signaling, and trafficking in both physiological and pathological states. However, the functional implications of these interactions are not fully understood.

This study aimed to elucidate the structure and function of the G protein-coupled receptor 143 (GPR143). We hypothesized that GPR143 functions in multiple roles because of its ability to bind partner proteins that modulate its function. We proposed that one binding partner was a DR, which was already shown by co-localization experiments and that the observed L-DOPA effects are mediated by the altered pharmacology of GPR143-DRs.

The workflow encompassed a set of scientific and technological objectives.

- To mine all known GPCR-dimers relevant for neurological and neurodegenerative diseases that are mostly localized in the brain, since DRs are key players in neuronal transmission and plasticity, among others. We aimed to detect the influence of partnered protomers on each other by promoting or inhibiting each other's downstream signaling cascade.

- To collect experimental proof of GPR143 undergoing PPIs with DRs. Given the robust response of DRs in the β-arrestin recruitment assay towards dopamine, this was a suitable approach to quantify the effect of GPR143 on dopaminergic

signaling. Furthermore, fluorescence microscopy helped to localize the GPR143-DR PPI within the cell.

- To understand GPCR-dimerization from a computational point of view, D_2R-D_2R homodimers in different combinations of protomer conformations were constructed and subjected to molecular dynamics simulation to precisely determine the effect of dimerization on monomeric entities.

The remainder of this dissertation is structured as follows.

In Chapter 1, an introduction into the biological context of GPCR dimerization is given, as well as the theoretical background behind the *in vitro* and *in silico* methods.

In Chapter 2 (present chapter), the objectives of this study are described.

Chapter 3 is divided into two sections that describe the main findings of this study. The first part describes the discovery of a biologically relevant PPI between GPR143, D_2R, and D_3R. The negative allosteric effects of GPR143 on the affinity of DRs for dopamine could be determined. Furthermore, a brief overview of the GPR143 expression was provided. Additionally, the PPI between GRP143 and DRs was localized in vesicles near the cellular plasma membrane. In the second section, the computational framework for constructing a robust model to study GPCR dimers was described. Using a well-studied target, D_2R, for which X-ray crystal structures were published with different ligands, allowed to construct dimers with pairs of different conformations of the protomers. These models were then subjected to MD simulations. The results obtained from this study help to understand the specific requirements of class A GPCR dimerization.

In Chapter 4, the main contributions are summarized, and an experimental outlook is provided on future studies on this topic. Based on the findings of this thesis, the overall results were analyzed, and some ideas for improvement were proposed.

Chapter 3: Results

3.1. Evidence for Protein–Protein Interaction between Dopamine Receptors and the G Protein-Coupled Receptor 143

This chapter is an unmodified version of a research article published in the International Journal of Molecular Sciences written in co-authorship with Prashiela Manga, Erika Penner and Anke C. Schiedel. The manuscript was up-to-date at the time of submission (August 2021).

3.1.1. Introduction

GPCRs constitute the largest family of transmembrane proteins and are involved in almost all (patho)physiological processes. GPCRs can contribute directly to disease due to pathogenic mutations that modulate function or modify expression levels, but are also excellent therapeutic targets. Over 40% of all marketed drugs target GPCRs, rendering them the largest class of drug targets [25,1245].

GPCRs were previously thought to function as monomers; however, it is now widely accepted that the receptors form highly dynamic, yet specific, functional homo- and/or heterodimers or even higher-order oligomers that can increase the number of roles a single protein can play [71,72]. Formation of heteromers can modulate the GPCR activity by influencing ligand recognition sites (e.g., changing or creating orthosteric and allosteric binding sites), G protein-coupling, and switching from G protein- to β-arrestin-coupling [81]. The structural basis underlying dimerization and receptor modulation is not fully understood, and the role of dimers in pathological conditions such as asthma, cardiac failure, and neurological diseases has only been reported in recent years [71]. These interactions can thus provide novel opportunities for future drug development.

The DRs, DRD_1-DRD_5, are a family of GPCRs that regulate numerous physiological functions including vision, cognitive function, and voluntary movement. They have been associated with pathological conditions and mental disorders such as PD, schizophrenia, and nicotine addiction [179,183,1246]. DR activity can be modulated by dimerization and/or oligomerization with other DRs as well as other GPCRs such as adenosine A1 receptors, NMDA receptors, or cannabinoid 1 receptors, which can further diversify and fine-tune their function [76–79,525,1247]. For example, DRD_2 forms hetero-dimers and

high-order oligomers with adenosine 2A receptors ($A_{2A}AR$) [76,519,703] that block activation of dopaminerigc transmission by $A_{2A}AR$, as well as the modulation of MAPK responses [75,466]. DRD_3-$A_{2A}AR$-complexes display similar allosteric antagonistic receptor–receptor interactions [179,1248,1249].

We previously performed a chemical library screen to identify small molecules that modulate activity of the orphan receptor GPR143 and identified pimozide as an antagonist [1250]. Pimozide is an oral antipsychotic that is also an antagonist of DRD_2 and -D_3 [1251–1254], we therefore hypothesized that, given the overlap in areas of expression in the eyes and brain [1255,1256], GPR143 could interact with these DRs.

GPR143 is an atypical GPCR found primarily in pigment cells but is also expressed in some neurons [1257]. In pigment cells, it is localized intracellularly at endolysosomes and melanosomes (specialized organelles in which the pigment melanin is synthesized) rather than the cell membrane where most other GPCRs function [1258–1260]. GPR143 mutations result in ocular albinism type 1 (OA1) [1261], an X-linked recessive disorder that is characterized by visual anomalies including loss of stereoscopic vision due to misrouting of the optic fibers at the optic chiasm [1262,1263].

The precise role of GPR143 remains to be determined; however, modulation and translocation of other proteins may be a key feature of its function - for example, the melanocyte protein melanoma antigen recognized by T cells-1 (MART-1) has been shown to interact with GPR143, which serves as an escort/stabilizing protein [1264]. Furthermore, GPR143 is co-immunoprecipitated with tubulin, suggesting a physical interaction with the cytoskeleton [1265]. GPR143 has also been shown to physically interact with the heterotrimeric G protein $G\alpha_{i3}$ [1266][38] and fine-tune activity of the vascular $alpha_{1B}$ adrenergic receptor [1267]. Given the propensity for GPR143 to interact with other proteins and our finding that the DRD_2/-D_3 antagonist pimozide also modulates GPR143 activity, we hypothesized that GPR143 could also interact with these DRs and modulate their activity.

3.1.2. Results

3.1.2.1. Fluorescence resonance energy transfer

FRET in order to investigate GPR143-DR interactions. FRET analysis allows observation of interactions between two proteins localized within 10 nm of each other.

We first used the sensitized emission method to evaluate FRET efficiency. If proteins are in close enough proximity for energy transfer to occur, donor fluorophore excitation CFP leads to acceptor molecule emission YFP. Images of transfected cells were simultaneously acquired in all three channels (CFP, YFP, and FRET, **Figures 9 and 10).** Correction parameters (CoA and CoB) were calculated by means of single transfected COS7s (**Figure S1**) and FRET efficiency values of each pixel in a pixel-to-pixel manner. This way, a FRET efficiency distribution across the picture was obtained, color-coded in a transition from purple to red (0 to 100 %; **Figures 9 and 10**, right panels). A high FRET efficiency indicates an intense protein–protein interaction.

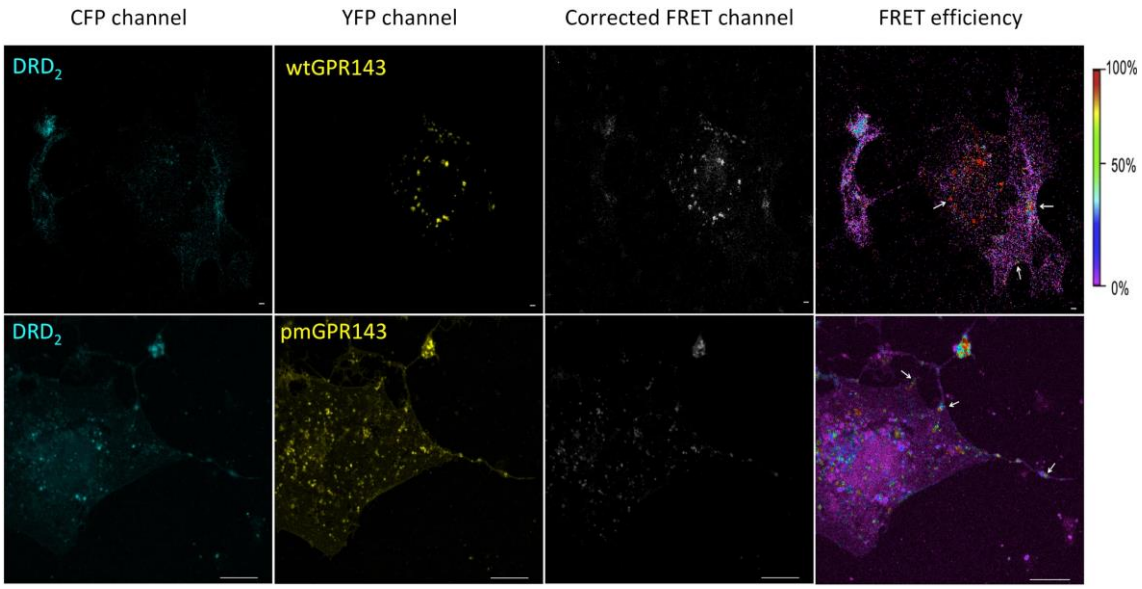

Figure 9. FRET of GPR143-YFP and DRD_2-CFP in COS7 cells. The sensitized emission method was used to detect interaction between GPR143 (YFP channel) and DRD2 (CFP channel). FRET signal, corrected by CoA and CoB parameters, and FRET efficiency (color scale on the far right) are shown. White arrows indicate regions where the FRET signal is localized. Controls are shown in **Figure S2**. Scale bar = 20 μm.

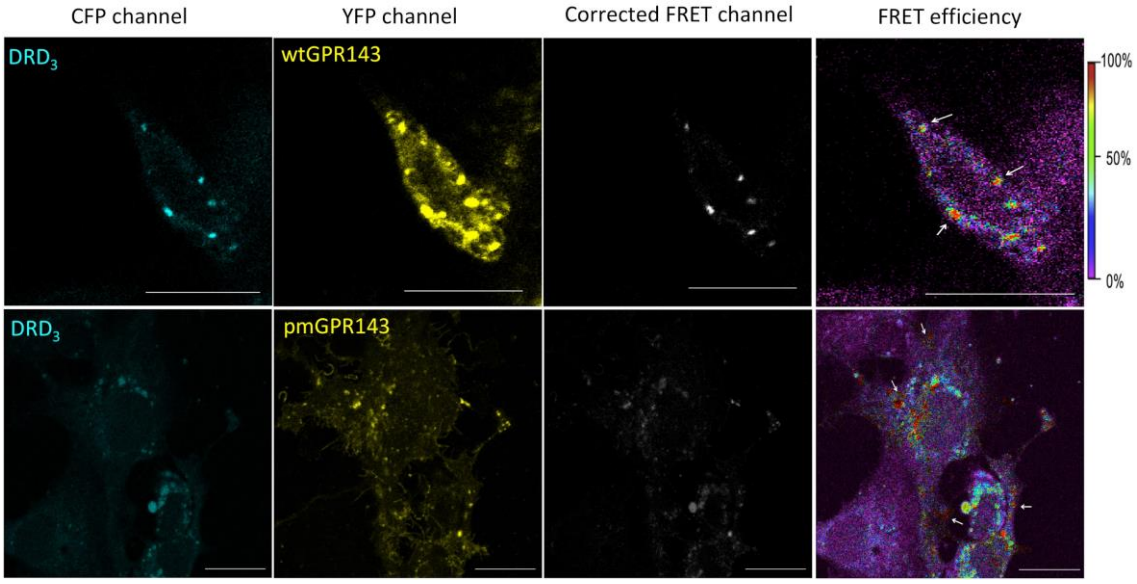

Figure 10. FRET of GPR143-YFP and DRD_3-CFP in COS7 cells. A sensitized emission method was used to detect interaction between GPR143 (YFP channel) and DRD3 (CFP channel). FRET signal, corrected by CoA and CoB parameters, and FRET efficiency (color scale on the far right) are shown. White arrows indicate regions where the FRET signal is localized. Controls are shown in **Figure S2**. Scale bar = 20 μm.

In this study, we used two GPR143 expression plasmids, one encoding wildtype GPR143 (wtGPR143) that is usually found on melanosomes of melanocytes (pigment cells) and in late endosomal/lysosomal fractions in the intracellular space in non-melanocytic cells [1245,1268–1271]. The other encodes a mutant GPR143 that is fully

functional but localizes to the plasma membrane (pmGPR143). Plasmids were generated as previously described [1245].

In the sensitized emission FRET experiments, when wtGPR143 was co-expressed with DRD_2, the FRET signal was observed in several vesicles around the perinuclear region, as well as near the plasma membrane with lower FRET efficiency (**Figure 9**, upper panels, white arrows). Similarly, when wtGPR143 was co-expressed with DRD_3, the FRET signal was exclusively found in vesicles in the intracellular space around the perinuclear region (**Figure 10**, upper panels). pmGPR143 was found to interact with DRD_2 and DRD_3 in vesicles at or near the plasma membrane and spread at intracellular locations (**Figures 9** and **10**, lower panels, white arrows). In control experiments with $A_{2A}AR$, known to bind DRs, $A_{2A}AR$-DRD_2 and $A_{2A}AR$-DRD_3 interactions (up to 100% FRET efficiency) were mostly found at the plasma membrane (**Figure S1**, panels B and C). When comparing the double transfected with the single transfected COS7 cells (**Figure S1**, panel F and G), it was evident that co-transfection caused a change in the localization of the DRs. When the DRs were expressed alone, they showed a uniform distribution across the cell, while co-expression of wtGPR143 or pmGPR143 increased intracellular localization of the DRs. In contrast, co-expression of $A_{2A}AR$ or GPR18 did not cause a similar internal restriction of DRs (**Figure S1**, panels B-E). GPR18, a cannabinoid related orphan receptor [1272], was used as negative control, since no interaction between GPR18 and DRs has been reported to date. When GPR18 was coexpressed with DRs, there was no evidence of interaction (**Figure S1**, panels D and E) and distribution within the cells did not differ from single transfected COS7 cells (**Figure S1**, panels F–I).

To further validate GPR143 and DR interactions, we used a quantitative FRET approach, the acceptor photobleaching method. During FRET, the donor fluorescence is partially quenched by the acceptor. Photobleaching the acceptor irreversibly eliminates the quenching effect and the level of donor fluorescence increases. Thus, this method was used to measure donor “dequenching” as an indicator of colocalization. Bleaching was limited to designated regions of interest (ROI, **Figure S2**). For wtGPR143 samples, intracellular regions where colocalization was observed were chosen. Images captured before and after photobleaching display fluorescence in the CFP and YFP channels (**Figure S2**). The absolute fluorescence in the ROIs was used to calculate the ratio of emission intensity after versus before photobleaching and FRET efficiency (**Figure 11**). When GPR143 and DRs were coexpressed, the intensity of CFP emission increased, indicating that the two fluorophores were in close proximity and involved in resonance energy transfer before photobleaching (**Figure 11**). The FRET efficacy of the co-transfected receptors was slightly higher for DRD_3 as compared to DRD_2. While co-expression of wtGPR143 yielded similar FRET efficacies for both DRs (24.5 ± 1.3 for DRD_2 and 29.5 ± 1.3 for DRD_3), the co-expression of pmGPR143 with DRD_3 (34.5 ± 1.2) was significantly higher compared to DRD_2 (19.2 ± 1.0). When $A_{2A}AR$ was co-expressed with DRs, FRET efficacy reached up to 30% (28.9 ± 1.0 for DRD_2 and 32.5 ± 1.8 for DRD_3), which was comparable with the control pECFP-EYFP fusion protein (29.4 ± 1.3), suggesting maximal ratio. GPR18 was used as a negative control. Fluorescence ratios in the photobleaching experiment confirmed that, for GPR18, there was almost no CFP increase in fluorescence after photobleaching, indicating that the DRs do not interact with this receptor. The FRET efficacy calculated for the control experiment (1.2 ± 1.2 for

DRD_2 and −4.8 ± 2.3 for DRD_3) was significantly different ($p < 0.0001$) from the positive controls (A_{2A}AR-DRs and fusion protein CFP-YFP, **Figure S3**). In addition, the GPR18 transfected samples did not differ in FRET efficiency from the single transfected samples ($p > 0.05$). FRET efficiency values are similar to those reported in previous studies using CFP-YFP [947,1245,1273,1274], suggesting that they can be considered reliable. Hence, we demonstrate that GPR143 and DRs directly interact with each other in several regions of the cell.

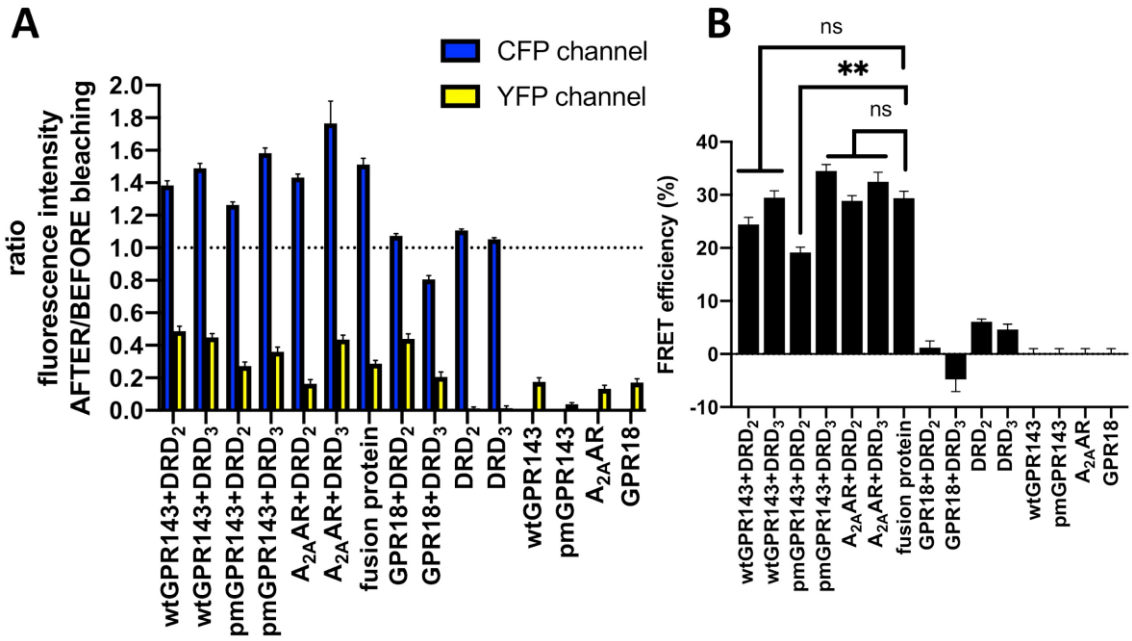

Figure 11. Quantification of acceptor photobleaching FRET. Wt or pmGPR143-YFP, A_{2A}AR-YFP or GPR18-YFP and DRs-CFP (DRD_2 or DRD_3) were co-transfected in COS7s. (A) Ratio of emission intensity after:before bleaching was determined. Controls = single transfected COS7s, DRs-CFP + GPR18-YFP, and CFP-YFP fusion protein; (B) FRET efficiency was quantified for co-transfected COS7s. Controls = Single transfected cells, DRs-CFP + GPR18-YFP, and CFP-YFP fusion protein. Data represent means ± SEM of three independent experiments; on average, 92 ± 9 ROIs were analyzed per sample. Significant differences between controls (single transfected and +GPR18 samples) and treatment samples including the positive control CFP-YFP fusion protein were observed. Wt and pmGPR143 and A_{2A}AR-transfected samples did not differ from the CFP-YFP fusion-protein, except for pmGPR143+DRD_2. Values refer to limited regions (see Figures S3 and S4). * = $p < 0.0001$, ns = not significant.

3.1.2.2. GPR143 Influences Dopaminergic Signaling in the β-arrestin Recruitment Assay

Having determined that GPR143 and DRs, as well as A_{2A}AR and DRs, also colocalize in CHO cells (**Figure S4**, panels A and B), we performed a β-arrestin recruitment assay (PathHunter®, DiscoverX, Fremont, CA, USA) to determine if dimerization with GPR143 affects functionality of the DRs. This assay is based on enzyme fragment complementation of β-galactosidase. When a ligand binds and activates the GPCR, β-arrestin-2 is recruited, thereby complementing the enzyme and rendering it active. The active β-galactosidase now can hydrolyze a substrate generating chemiluminescence, which can be quantitated as a correlate of receptor activation. Dopamine, the endogenous DR ligand chosen for the experiments, was used at 10 μM. A_{2A}AR-DRD_2-complex formation also modulates DRD_2 ligand binding affinity and G-protein coupling [525] and A_{2A}AR was therefore a suitable positive control. GPR18 was used as a

negative control, as this receptor did not colocalize in FRET studies. Having established a functional system, we were able to determine a physiologically relevant functional interaction between GPR143 and DRs. Co-expression of either wt or pmGPR143 resulted in significant inhibition of the DR response towards dopamine (Figure 12, p = 0.0113 for wtGPR143+DRD_2, $p < 0.0001$ for wtGPR143+DRD_3, p = 0.0052 for pmGPR143+DRD_2 and $p < 0.0001$ for pmGPR143+DRD_3) compared to co- expression of A_{2A}AR-DR which significantly inhibited the DRs response to dopamine at any concentration (up to 90%, **Figure 12**), in concordance with the antagonistic allosteric effect of the A_{2A}AR on DRD_2 and DRD_3 [538,703,1249,1275,1276]. Lastly, GPR18 did not have an effect on the DRs response to dopamine, as it was not different from the DR only controls.

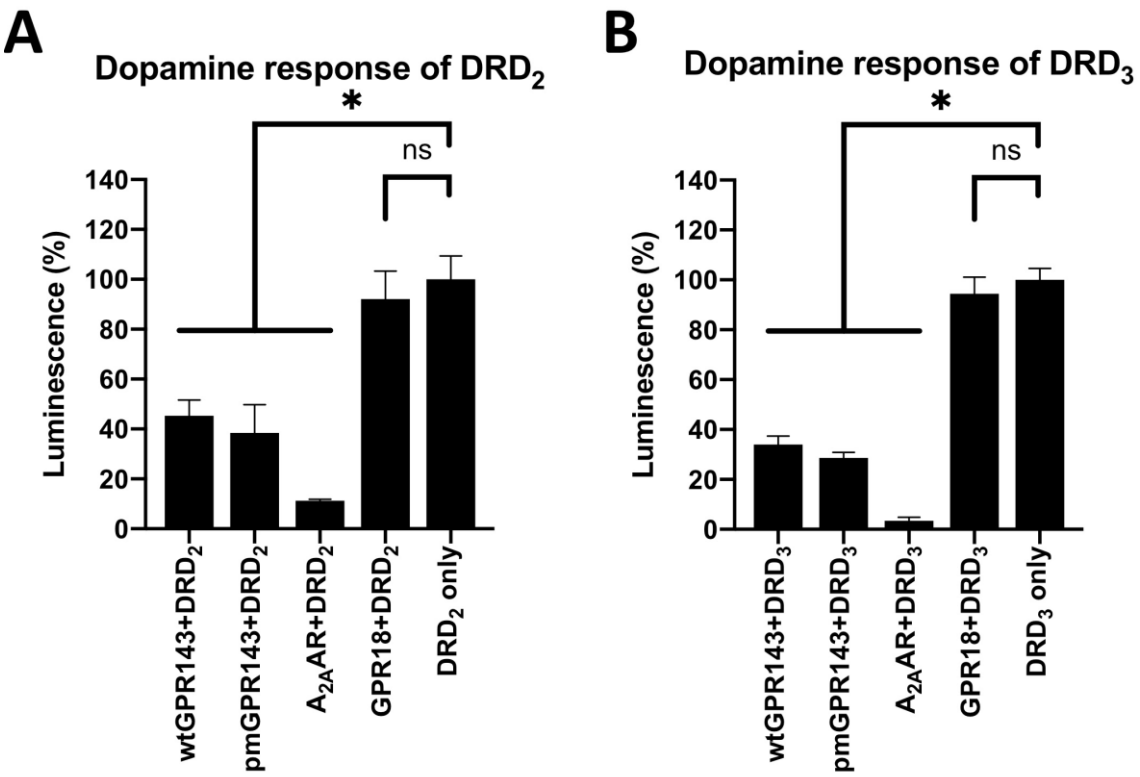

Figure 12. Dopamine response in CHO β-arrestin cells expressing DRD_2 and DRD_3 co-transfected with a second GPCR. β-arrestin assays were performed on dopamine-treated CHO cells expressing DRD_2 (A) or DRD_3 (B), co-transfected with a second GPCR. The data were baseline corrected and correspond to 2–3 independent experiments performed in duplicates or triplicates. (A) Significant differences were observed between the DRD_2 alone and the other dimer pairs (vs. wtGPR143+DRD_2 p = 0.0113; vs. pmGPR143+DRD_2 p = 0.0052 and vs. A_{2A}AR+DRD_2 p = 0.0052), except for GPR18+DRD_2 where no significant difference was observed (p = 0.8082). (B) Significant differences were also observed between DRD_3 alone and the other dimer pairs (* = $p < 0.0001$ for all), except for GPR18+DRD_3 where no significant difference (ns = not significant) was observed (p = 0.1192).

Next, we performed β-arrestin assays with DRD_2 or -D_3 expressing cells co-expressing different amounts of GPR143 receptors (**Figure 13**) in order to show that changes in dopamine activation of DR's correlated with the presence of GPR143 (or $A_{2A}AR$). Cells stably transfected with DRs were transiently co-transfected with decreasing amounts of GPR143 or $A_{2A}AR$ plasmid (8, 4, 2, 0.2, 0.02 µg, for Western blot analysis confirmation, see **Figure S5**). The luminescence signal, corresponding to the DR activation by dopamine, was decreased with increasing amounts of co-transfected receptors. This was also the case for $A_{2A}AR$, as expected [1249]. We did not observe differences in the DR's response towards dopamine for GPR18.

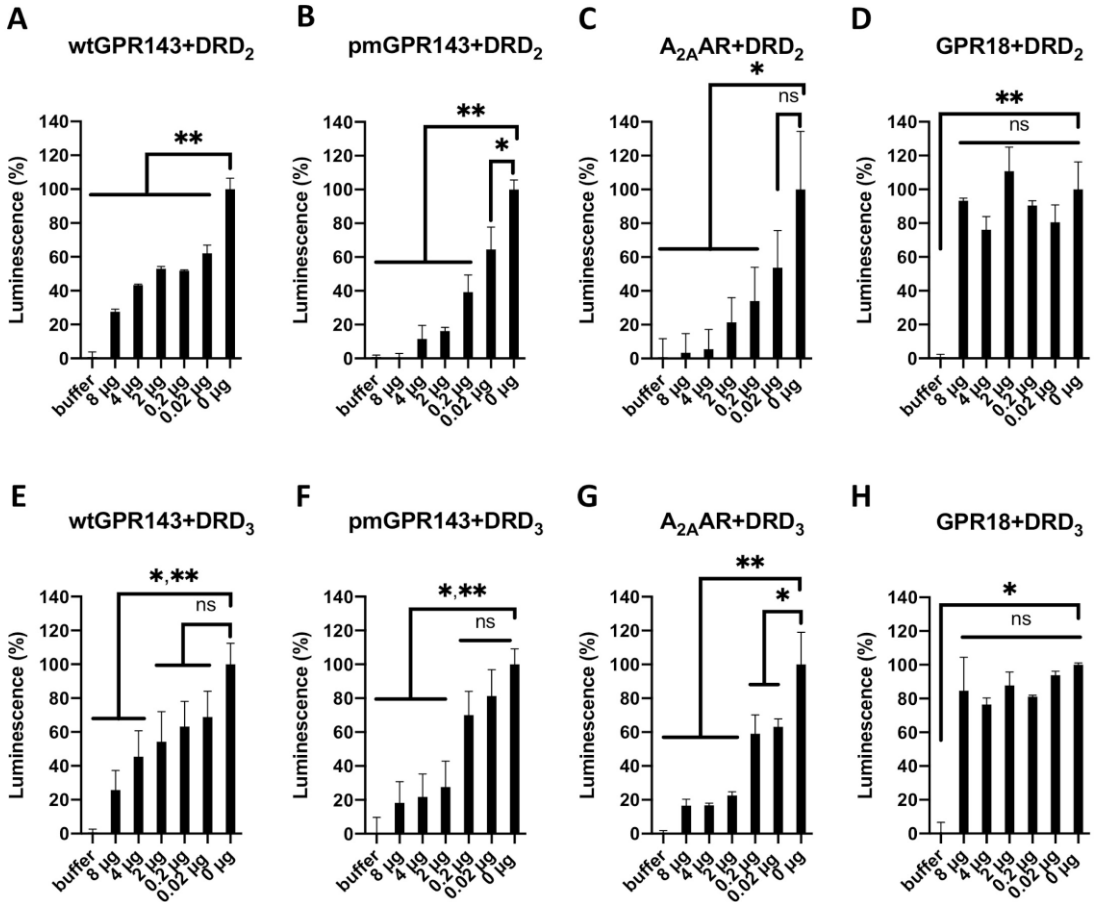

Figure 13. Dopamine response of CHO β-arrestin DRD_2 and DRD_3 cells co-transfected with different concentrations of wtGPR143-, pmGPR143-, $A_{2A}AR$- and GPR18-YFP in the β-arrestin recruitment assay. CHO β-arrestin DRD_2 and DRD_3 cells were transfected with different amounts of plasmids containing receptor cDNA (8, 4, 2, 0.2, and 0.02 µg) and treated with 10 µM dopamine (or buffer). Data were normalized to buffer (0%), and DRs only (0 µg, 100%) and correspond to mean ± SEM of two to three independent experiments performed in triplicates or quadruplicates. (A) Coexpression of wtGPR143 had a significant effect on DRD_2 at all concentrations ($p < 0.0001$). (B) Coexpression of pmGPR143 had a significant effect overall on DRD_2 activity ($p < 0.0127$). The 0 µg vs. 0.02 µg sample differed less ($p = 0.003$), while the other concentrations differed more significantly ($p < 0.0001$ for 0 µg vs. 0.2–8 µg). (C) Coexpression of $A_{2A}AR$ did not have a significant effect on DRD_2 for 0 µg vs. 0.02 µg ($p = 0.1037$), while significant differences were observed for the other concentrations (0.2 µg $p = 0.0445$; vs. 2 µg $p = 0.0222$; vs. 4 µg $p = 0.0066$; vs. 8 µg $p = 0.0066$). (D) Coexpression of GPR18 had no significant effect on DRD_2 ($p > 0.05$ for all). (E) Coexpression of wtGPR143 had a significant effect on DRD_3 at concentrations of 4 µg and 8 µg ($p = 0.0301$, $p = 0.0024$). (F) Coexpression of pmGPR143 had a significant effect on DRD_3 overall ($p < 0.0001$). Post-hoc comparisons indicated significant differences in activity for concentrations greater than 2 µg (vs. 2 µg $p = 0.012$; vs. 4 µg $p = 0.0006$, vs. 8 µg $p = 0.0004$). (G) Coexpression of $A_{2A}AR$ had a significant effect on DRD_3. Post-hoc comparisons indicated that the transfection of 0.02 µg and 0.2 µg significantly differed from the 0 µg sample ($p = 0.071$; $p = 0.0066$, respectively), while higher concentrations had a greater effect (vs. 2–8 µg $p < 0.0001$ for all). (H) Coexpression of GPR18 had no significant effect on DRD_3 ($p > 0.05$ for all, except for buffer). * = $p \leq 0.05$; ** = $p \leq 0.01$. ns = not significant.

3.1.3. Discussion

DRs regulate numerous physiological functions and have been linked to numer- ous pathological conditions [179,183]. DRs have been shown to be very promiscuous and complex with many other GPCRs in order to carry out these multiple functions with specificity [79,179,510,690,703,850,1248,1277,1278]. Among them, the A_{2A}AR-DRD_2-complex is the most studied heteromer, as it appears to be highly relevant for schizophrenia and Parkinson's disease [71,179,530].

We previously demonstrated that pimozide, a DRD_2 and DRD_3 antagonist [1252–1254,1279], also modulates activity of the orphan receptor GPR143 [1250]. We therefore hypothesized that GPR143 and DRs may interact with each other in ocular and brain tissues [1255,1256]. Our hypothesis was supported by a number of studies that observed protein–protein interactions between GPR143 and other proteins, which similar to DRs, facilitate multiple functions. GRP143 binds MART-1 [1264], tyrosinase (a key enzyme required for melanin synthesis) [1245] and $G\alpha_{i3}$ [1266], which may underlie its regulation of melanosome differentiation and maturation. Furthermore, melanocytes express $DRs_{1–5}$ [1280] and expression of DRs and GRP143 overlap in various areas of the brain [1256].

Various roles have been proposed for GPR143; however, a precise function remains to be defined. Lack of GPR143 function results in formation of abnormal melanosomes [1281]. Rather than small distinct organelles, macromelanosomes form, thus GPR143 appears to function as a "sensor" of melanosomal maturation to prevent formation of macro-organelles [1258]. GPR143 function has also been shown to modulate the number of early- stage melanosomes [1282] and form the trafficking fork separating lysosome and early melanosome bound proteins [1283]. GPR143 may also control intracellular melanosome transport by regulating microtubule-mediated motility through interaction with tubulin [1265]. Recent studies have shown that GPCRs can bind ligands on both membrane faces [1284], which may underlie the interaction with tubulin. GPR143 may also regulate transcription of several melanosomal genes through modulation of the microphthalmia-associated tran- scription factor (MITF), thus forming a feedback loop being both a regulator and target of MITF [1285,1286]. In addition to its role in pigment cells, GPR143 has also been shown to mediate depressor response in the brain stem solitary nucleus [1257], is expressed in several regions of the central nervous system such as the hippocampus [1256], and, most recently, GPR143 was shown to be associated with nicotine addiction [1287]. GPR143, like DRs, has multiple functions, numerous binding partners, and functions in various areas of the brain.

In this study, we investigated the influence of GPR143 on DRD_2 and DRD_3. FRET studies demonstrated that GPR143 and DRs interact, while β-arrestin recruitment assays showed that GPR143 can reduce DR activity by at least 50%. The reduction in activity may be due to reduced DR levels at the plasma membrane as we observed an increase in intracellular DRs colocalized with GPR143; alternatively, GPR143 may modulate DR affinity for dopamine or a combination of the two effects.

The site of DR-GPR143 interaction appears to be determined by the location of GPR143, since we observed the difference depending on the GPR143 plasmid used for transfection. In pigment cells, wtGPR143 localizes intracellularly [1268]. In non-pigment

cells, such as COS cells or yeast (*Saccharomyces cerevisiae*), wtGPR143 is found in late endosomal/lysosomal fractions in the intracellular space or in the prevacuolar compartment, which are both functionally equivalent to melanosomes/late endosomes [1245,1269–1271]. pmGPR143 sorts to the plasma membrane [1245,1250,1288]. When wtGPR143 was co-transfected, DR-complexes were found exclusively in vesicles in the intracellular space and more often in the perinuclear region, while pmGPR143-DR-complexes were also found in vesicles in the intracellular space, but some appeared near the plasma membrane. It should, however, be noted that some studies reported that GPR143 protein can be found at the cell surface in human retinal pigment epithelial cells in situ but only 4% of total GPR143 protein [1289], thus some interactions may take place at the plasma membrane. In addition, overexpression of GPR143 can cause accumulation at the cell surface [1268,1271]; however, our experiments were optimized such that we did not observe any accumulation at the plasma membrane [1245,1250].

The concept of orphan receptors modulating non-orphan receptors is not novel— for example, GPR50 modulates melatonin receptors MT1 and MT2 [1290,1291] and GPR143 itself has been shown to modulate the activity of the $alpha_{1B}$ adrenergic receptor [1267]. Consequently, GPR143 may play a similar role in modulating DR function.

The results of the β-arrestin assays demonstrated a significant reduction (at least 50%) in the DR response to activation with dopamine when GPR143 was co-expressed. The effect was less pronounced than the effect A_{2A}AR had on the DRs (reduction of DR activity up to 90%), which is in concordance with previous studies that demonstrated that active A_{2A}AR has a negative allosteric effect on dopaminergic signaling [76,1249].

Although GPR143 is expressed primarily in pigment cells, several studies have suggested a link between the pigmentary system and dopaminergic signaling. For example, tyrosinase activity (which produces L-DOPA, a dopamine precursor, for pigment biosynthesis) and GPR143 expression are necessary for precise development of the optic tract [1292], which may require an L-DOPA concentration gradient for correct nerve projection [70]. We have shown that GPR143 binds tyrosinase [1250], which may allow for direct regulation of L-DOPA production and pigment synthesis. GPR143 may thus play a role in regulating both the production of L-DOPA by tyrosinase and dopamine-mediated signaling through DRs.

A potential model for DR-GPR143 interaction may involve dimer formation which occurs in late endosomes/multivesicular bodies, since these organelles are important for transport and sorting of proteins coming from the Golgi apparatus on their way to organelles such as lysosomes and melanosomes as well as for internalized receptors on their way to degradation or recycling [1293]. It is also possible that the GPR143-DR interaction occurs during the transport of DRs to the plasma membrane. This interaction may, for example, delay DR recycling to the plasma membrane. While GPCR activity at the plasma membrane has been well characterized, recent studies have demonstrated a key role for intracellular activity of several GPCRs [1294]; furthermore, this activity can be therapeutically targeted [1295].

In conclusion, we have shown that GPR143 interacts with DRD_2 and DRD_3 and negatively modulates DR activity in response to dopamine. Furthermore, we have shown that GPR143-DR-complexes are primarily formed in vesicles in the intracellular space, even when a plasma membrane-localizing GPR143 variant, pmGPR143, was co-

expressed. Whether GPR143 modulates DR activity by promoting its localization away from the plasma membrane and/or through allosteric modulation remains to be determined, as does the question of whether this mechanism is shared by melanocytes, the retinal pigment epithelium and other GPR143 expressing cells.

3.1.4. Materials and Methods

3.1.4.1. Plasmids

The cDNA sequences of the human DRD2short and DRD3 genes were inserted into pE-CFP-N1 and pCMV-ARMS2-Prolink2 (DiscoverX, Fremont, CA, USA) vectors using NheI and HindIII restriction enzymes. For insertion into pCMV-ARMS2-Prolink2, an additional amino acid sequence (TC) was added to the 3′-end of the coding sequence. To generate pE- YFP-N1-wtGPR143, pE-YFP-N1-pmGPR143 and pE-YFP-N1-ADORA2A cDNA sequences of the human wtGPR143, pmGPR143 and ADORA2A were inserted into pE-YFP-N1 vector using KpnI and AgeI restriction enzymes as we previously described [1245]. We removed the stop codon, so that the C terminal tag was in frame. pE-YFP-N1-GPR18 was kindly provided by the Mueller Lab (University of Bonn, Dept. Pharmaceutical and Medicinal Chemistry). The fusion protein pECFP-EYFP vector (referred to as CFP-YFP hereafter) was cloned as previously described ([1245], Chapter 7.1.). CFP-YFP was used as internal control for statistical analysis. All plasmids were verified by sequencing (Eurofins Genomics Germany, Ebersberg, Germany). GPR143 is typically restricted to endosomal compartments in the intracellular space. It has been previously reported that the addition of a GFP tag at the C terminus does not affect the localization of GPR143 [1258,1260,1270,1271,1288]. Therefore, the YFP protein was also fused to the C-terminus.

3.1.4.2. Cell culture and Transfection

Chinese Hamster Ovary (CHO) β-arrestin cells were engineered by DiscoverX (Fremont, CA, USA) to express the β-galactosidase EA fragment fused to β-arrestin. CHO β-arrestin cells were cultured in a humidified incubator with 5% CO_2 at 37°C in Gibco F12 (Ham) (1×) medium supplemented with 10% FCS, 5 U/mL penicillin, 5 mg/mL streptomycin, 300 µg/mL hygromycin. β-arrestin CHO cells were transfected with DRD_2 and DRD_3 expression plasmids using LipofectamineTM2000 (Thermo Fischer Scientific, Schwerte, Germany) according to the manufacturer's recommendations and stable lines generated by antibiotic selection with G418. Cells were then maintained in 800 µg/mL G418 for maintenance of transfected cells. CHO β-arrestin-DRD_2 and -DRD_3 cells were then transiently transfected with expression plasmids for wtGPR143, pmGPR143, and A_{2A}AR or GPR18. COS7 cells were cultured in Dulbeccos's modified eagle medium (DMEM) supplemented with 10 % fetal calf serum, 5 U/mL penicillin, and 5 mg/mL streptomycin at 37°C with 10% CO_2. Transient transfections were performed for microscopy experiments using Lipofectamine™ 2000 (Thermo Fischer Scientific, Schwerte, Germany) according to the manufacturer's recommendations.

3.1.4.3. β-arrestin Assay

The β-arrestin recruitment assay system PathHunter®developed by DiscoverX (Fremont, CA, USA, https://www.discoverx.com/arrestin, accessed on 30 July 2021) detects GPCR activation following ligand stimulation. The assay is based on enzyme fragment complementation of β-galactosidase. The assay is performed using a cell line expressing an Enzyme Acceptor (EA) which is fused to the β-arrestin. The second part of the enzyme (ProLink/ PL) is fused to the C terminus of the GPCR of interest. EA and PL are inactive as single fragments. When a ligand binds and activates the GPCR of interest, the β-arrestin-2 protein is recruited to the GPCR since it is involved in receptor desensitizing and recycling. The recruitment of the β-arrestin leads to the complementation of the β-galactosidase. The active enzyme can catalyze hydrolysis and generate chemiluminescence when an appropriate substrate is proved. Thus, measured chemiluminescence (or β-galactosidase activity) correlates with receptor activation. In this study, the recruitment assay was performed using engineered CHO cell lines stably expressing the β-arrestin protein linked to the EA fragment. The cell lines were transfected with the GPCR cDNA of interest fused to the ProLink-tag.

At 48 h post-transfection, co-transfected CHO β-arrestin DRD_2 and DRD_3 cells were seeded in 96 well-plates (NunclonTM F96 MicroWell™, Thermo Fischer Scientific, Scwerte, Germany). On the day of the assay, the medium was changed for 90 µl of F12 with 100 U/mL penicillin G, 100 µg/mL streptomycin, and the cells were incubated for at least 2 h at 37°C with 5% CO_2. Then, 10 µl of dimethyl sulfoxide (DMSO)-diluted dopamine was added. Unsupplemented F12 medium was used as negative control. The final DMSO concentration per well was 1%. After 90 min, the PathHunter®detection reagent (DiscoverX, Fremont, CA, USA) was added to the cell plate (50 µL/well) and incubated 1 h at room temperature in the dark, and finally chemiluminescence was detected by using the MikroWin2000 software and a multimode microplate reader (Mithras LB 940, Berthold Technologies, Bad Wildbad, Germany).

3.1.4.4. Immunostaining

At 48 h post-transfection, the same co-transfected CHO β-arrestin DRD_2 and DRD_3 cells used in the β-arrestin recruitment assay were seeded on sterile coverslips in a 12 well-plate (Sarstedt, Nümbrecht, Germany) and cultured overnight. The next day (in parallel with the β-arrestin assay), the CHO cells were fixed with 4% paraformaldehyde (pre-heated at 37°C) for 20 min at room temperature. The cells were then washed with phosphate-buffered saline (1xPBS, pH 7.4) and blocked for 15 min with 1% bovine serum albumin (BSA)/1xPBS solution. Cells were incubated in the dark for 60 min with the primary antibody and then 30 min with the secondary antibody, both diluted in 1% BSA/1xPBS. The primary antibody was diluted 1:1000 and the secondary antibody 1:500). 1xPBS was used to wash cells between and after antibody incubations. In addition, the nuclei of the cells were stained with DAPI (1 mg/µl diluted 1:1000 in 1% BSA/1xPBS) for 5 min in the dark. Finally, coverslips were mounted using FluoromountTM Aqueous Mounting medium (Sigma-Aldrich, Merck KGaA, Darmstadt, Germany) and stored in the dark at 4°C. The mouse monoclonal anti-PK/PL antibody (DiscoverX, Fremont, CA, USA) was used as the primary antibody and donkey anti-

mouse-AlexaFluor594 (Jackson Immuno Research, Hamburg, Germany) as the secondary antibody to stain the Prolink tag on DRD_2 and DRD_3. Cotransfected receptors (wtGPR143, pmGPR143, and $A_{2A}AR$) were tagged with a YFP-fluorophore-tag in order to reduce the spectral overlap of the fluorophores. A Nikon A1 Spectral confocal microscope operating with an argon laser (Pharmaceutical Institute, University of Bonn, Bonn, Germany) and the NIS Element Advanced Research software 4.0 were used for image acquisition and analysis. Each transfection and staining was repeated two to three times and at least ten squares (60× objective) containing 3–15 cells each were imaged for each sample. The cells that are most representative of the majority of each condition are shown.

3.1.4.5. Fluorescence Resonance Energy Transfer

COS7 cells were seeded on sterile coverslips in 12 well-plates at 80–90% confluence and transfected with DRD_2- and DRD_3-CFP alone or in combination with YFP-tagged wtGPR143, pmGPR143 or $A_{2A}AR$. After 48 h, cells were fixed with 4% paraformaldehyde (pre-heated at 37°C) for 20 min at room temperature. The cells were then washed with phosphate-buffered saline (1xPBS, pH 7.4) and blocked for 15 min with 0.1% BSA/1xPBS solution. For the sensitized emission method, cells were mounted on slides using FluoromountTM Aqueous Mounting medium (Sigma-Aldrich), while, for the photobleaching method, Mowiol 4–88 medium (Roth, Karlsruhe, Germany) was utilized as mounting medium. A Nikon A1 Spectral confocal microscope operating with an argon laser (Pharmaceutical Institute, University of Bonn, Bonn, Germany) and the NIS Element Advanced Research software 4.0 were used for image acquisition and analysis. Cells were examined with a 60× oil immersion objective. Each transfection and staining was repeated two to three times. The cell that was most representative of the majority of each condition was shown.

For the sensitized emission method, different optical configurations were set up: “Dd channel” for excitation and emission of the donor chromophore (ECFP, excitation filter: 457 nm, emission filter: 482/35 nm), “Aa channel” for excitation and emission of the accep- tor chromophore (EYFP, excitation filter: 514 nm, emission filter: 540/30 nm) and “FRET channel” for the excitation of the donor and emission of the acceptor chromophore (excita- tion filter: 457 nm, emission filter: 540/30 nm). For each image, parameters (high voltage, offset, and laser intensity) were adjusted in order to limit the spectral bleed through and to avoid the pixel over-saturation. The laser intensity was equalized in both FRET and donor channel, while the high voltage was equalized in both FRET and acceptor channel. The FRET calibration was performed with single transfected cells expressing DRD_2-CFP, DRD_3- CFP, $A_{2A}AR$ -YFP, wtGPR143-YFP, pmGPR143-YFP, or GPR18-YFP. Correction parameters (CoA and CoB) were calculated by the software using the following formulas:

$$CoA = Da\ ACCEPTOR/Aa\ ACCEPTOR \quad (1)$$

$$CoB = Da\ DONOR/Dd\ DONOR \quad (2)$$

where Aa corresponds to the channel where the excitation and the emission of acceptor is measured, Dd corresponds to the channel of excitation and emission of the donor, and Da corresponds to the channel of the excitation of the donor and emission of the acceptor.

Xx DONOR/ACCEPTOR coefficients are average intensities of the donor/acceptor-only images. The corrected FRET signal and the FRET efficiency were calculated for each image using the following formulas:

$FRET_{CORR}$= Da FRET − (Dd FRET x CoB) − (Aa FRET × CoA) (3)

FRET EFFICIENCY [%]= (FRET CORR / Dd FRET) × 100 (4)

where Xx FRET members are average intensities of assigned FRET image components. For the acceptor photobleaching method, images were captured before and after the photobleaching of acceptor molecules in a specific region of the cell (ROIs). If any interactions leading to energy transfer were present, photobleaching of the acceptor wil lead to an increase of donor fluorescence, as it is no longer quenched by the acceptor. Acceptor photobleaching was performed with a high-intensity laser pulse at 514 nm. Images in the Aa and Dd channels were captured simultaneously before and after the photobleaching. FRET efficiency was calculated using the following formula:

FRET EFFICIENCY [%] = (IA − IB) × 100/ IA (5)

where IA is the CFP intensity emission after bleaching, and IB is the CFP intensity emission before bleaching.

3.1.4.5. Western Blot

At 48 h post-transfection, co-transfected CHO β-arrestin DRD_2 and DRD_3 expressing cells were scrapped off the plates, washed with PBS, and lysed on ice using an ultra-sound sonicator. The protein concentration was determined using a Bradford reagent. In addition, 30 µg of sample protein was mixed with loading buffer containing 2% SDS and warmed at 37°C for 30 min. Then, proteins were separated on 10% SDS-PAGE gel and then transferred to a nitrocellulose membrane (PROTRAN—Nitrocellulose Transfer Membrane—Whatman, Sigma, Taufkirchen, Germany). The Mark12™ Unstained Standard and PageRuler™ Prestained Protein Ladder were used as protein markers. The membrane was blocked 1 h in a 5% powdered milk/PBS-Tween solution. Afterwards, the membrane was incubated with the primary antibody overnight at 4°C or 1 h at RT, washed 1 h with PBS-Tween, incubated with secondary antibody and washed again. The detection was performed with ECL kit (GE Healthcare, Amersham, Arlington, IL, USA—Dassel, Germany) according to the manufacturer's instructions. The following antibodies were used: mouse monoclonal anti-GFP (Biolegend, San Diego, CA, USA) and anti-mouse-HRP (Jackson Immuno Research, Hamburg, Germany).

3.1.4.6. Data Analysis

Data were analyzed using Prism 8.0 (GraphPad Software Inc., San Diego, CA, USA). NIS Element Advanced Research software 4.0 was used for microscopy image acquisition and analysis.

3.1.4.7. Statistical Analysis

Ordinary one-way ANOVA and the Holm–Sidak test for post-hoc comparisons were used for statistical analysis of the data.

3.1.4.8. Supplementary Materials

The following are available online at https://www.mdpi.com/article/10.3390/ijms22158328/s1, Figure S1: Control images of sensitized emission FRET; Figure S2: Acceptor photobleaching FRET in COS7 cells; Figure S3: Control images of FRET acceptor photobleaching.; Figure S4: Colocalization of GPR143 and DRs by immunofluorescence in CHO cells; Figure S5: Western blot analysis shown as an example for wtGPR143+DRD_3. The figures can also be found in Chapter 7.1.

3.2. The world of GPCR dimers - mapping dopamine receptor D2 homodimers in different activation states and configuration arrangements

This chapter is an unmodified version of the research article published the Computational and Structural Biotechnology written in co-authorship with Pedro R. Magalhães, Carlos A.V. Barreto, Rita Melo, Anke C. Schiedel, Miguel Machuqueiro, and Irina S. Moreira (September 2023).

3.2.1. Introduction

The G protein-coupled receptor (GPCR) family, the largest class of membrane receptors, targets more than 40% of the marketed pharmaceuticals [1296]. Moreover, GPCRs mediate almost all (patho)physiological responses in humans [30,31]. Over the past few decades, it has been widely accepted that GPCRs increase their signaling repertoire by forming homo- or heterodimers or even higher-order oligomers [1297,1298]. The physiological consequences of GPCR dimerization have been reported to modulate downstream signaling, trafficking, and regulation as well as the negative and positive cooperativity of ligand binding [71,79,80]. Dimerization can influence ligand recognition by modulating orthosteric and allosteric binding sites. It can also influence G protein-coupling and selectivity and may cause switching from G protein- to β-Arrestin-coupling [81]. Moreover, dimerization may lead to the formation of novel allosteric sites, which can result in different pharmacological properties [81].

Several GPCR dimers have been implicated in numerous pathological conditions, [71,1299] including asthma, cardiac failure, preeclampsia, schizophrenia, and Parkinson's disease (PD), [71,1299,1300] which have drawn special interest in elucidating the mechanism of dimerization and oligomerization, as well as the development of drugs that are capable of targeting both monomers within the dimers, known as bivalent ligands [71,79,876,877,1297].

In general, for class A receptors, transmembrane helices (TM) 1, 4, and 5 possess the largest membrane-accessible areas and hence were reported to be of most relevance for dimerization [1301]. It was reported that the common orientations in class A dimers derived from crystal structures are head-to-head TM1/2 and TM4/5 [1301]. Since most crystallographic structures miss the N- and C-termini and the long intracellular loop (ICL) 3, these parts of the receptors and their possible roles cannot be clearly

evaluated [1302]. Before computational approaches became feasible to study GPCR dimers, in vitro studies first showed their existence. For instance, early studies of Guo et al. (2003, 2005, 2008) used cysteine-crosslinking experiments and mutagenesis studies with substituted cysteine residues [472,1303,1304]. Using cysteines in order to determine interaction contacts between proteins is advantageous for GPCRs as cysteines are conserved in most rhodopsin-like GPCRs among others [1305]. Cysteine contains a highly reactive thiol group and a disulfide bond can be formed between two that are in close vicinity under oxidizing conditions, which can only be reversed by reducing agents [1306]. Furthermore, fluorescence/bioluminescence resonance energy transfer (FRET, BRET) and time-resolved FRET strategies as well as co-immunoprecipitation (Co-IP) have become increasingly successful in determining GPCR interfaces among other methods [79,1307,1308].

While classical biochemical methods such as Co-IP, rarely determine the existence of such dimers and often require the availability of highly selective antibodies, RET methods are able to monitor their active movement [79]. For example, a study by Wouters et al. used complementation-based NanoLuciferase® Binary Technology (NanoBiT® assay) to investigate the effect of antagonists on the formation of D2R-homodimers (D_{2long}), with a focus on the TM5-TM6-TM5-TM6 interface [77]. Another more recent study by Cheng et al. described a combinatorial approach using experimental and computational methods to characterize the interface of Apelin receptor (APJ)/Nociceptin receptor 1 (ORL1) and APJ/Vasopressin receptor 2 (V2R) dimers [1308]. Chen and co-workers used a TM peptide containing a human immunodeficiency virus trans-acting transcriptional activator (HIV-TAT) protein transduction motif, together with matrix-assisted laser desorption tandem time-of-flight mass spectrometry (MADLITOF-MS) and BRET to demonstrate the switches of the dimers from active to inactive states [1308]. They reported that transitions would range from a TM1/TM2 interface in the inactive state to an active TM5 interface [1308]. From the experimental information obtained they constructed atomic resolution models.

Despite the fact that various strategies have been developed to study GPCR dimers and explore their functional significance, many questions still remain unsolved. While some experimental methods do not deliver results that are robust enough, computational calculations are laborious and time-consuming. Hence, we focused our work on a well-studied example of D_2R-homodimer, which was first described by Ng et al. in 1996 and was considered pathologically relevant [468].

The five dopamine receptors (D_1R-D_5R) mediate the essential functions of dopamine and are highly promiscuous, forming homo- and heterodimers, as well as higher-order complexes that play a role in several neurological or neurodegenerative diseases [79,179,876,1297,1309–1312]. By binding to different types of G proteins, the secondary messenger cAMP is either stimulated or inhibited by dopamine receptors. D_1R and D_5R are coupled to $G\alpha_s$ and $G\alpha_{olf}$ and are therefore classified as D1-like receptors, whereas D_2R-D_4R is coupled to $G\alpha_{i/o}$ and belongs to the D2-like receptors [179,180,1313]. In addition, D_2R exists as two isoforms, D_{2long} and D_{2short}, generated by alternative splicing [1314]. Dimerization phenomena with their family members have been documented for all five receptors (D_1R-D_3R [464], D_1R-D_2R [465], D_2R-D_3R [471], D_3R-D_3R [469], D_2R-D_5R [470], D_4R-D_4R [467]; additional combinations are reviewed in Schiedel et al. [77,79,466]). Increased formation of the D_2R homodimer has been correlated with

schizophrenia, chronic social defeat stress, and a sensitized state after exposure to amphetamine, which can cause psychosis [77,1315,1316].

Although DR dimers have been analyzed in vivo and in vitro, and the targetability of the dimers has been shown experimentally, the structural details have not yet been fully understood. The crystal structure of GPCRs is a useful and indispensable tool for drug design [1317]. However, in silico studies of GPCR dimers are scarce [76,1318,1319] with the dimer interface and their monomer conformational states being unexplored for most known GPCR dimers.

Several studies by Guo et al. proposed a symmetrical interface of the D2R homodimer involving TM4 [472,1303,1304]. This hypothesis was further supported by the existence of an interface between TM4 and TM5 in the inactive inverse agonist-bound state, whereas in the active state, TM4-TM4 was shown to form the interface [472]. In addition, a different study by Guo et al. identified a second symmetrical interface of TM1 that is relevant for higher-order oligomerization and does not seem to undergo major conformational changes upon ligand binding [1304]. The authors showed that neither agonists (quinpirole and bromocriptine) nor antagonists (sulpiride and butaclamol) affected dimer formation and concluded that D_2R exists as a constitutive dimer [1303]. Similar conclusions were drawn in a study by Armstrong and Strange, where they showed in radioligand binding studies using CHO cells that the D_2R homodimer has two identical and functional ligand-binding sites [1320]. Moreover, receptor crosslinking, as observed by Guo et al., does not impair the inhibition of adenylate cyclase by dopamine [472,1303,1304]. Guo and coworkers concluded from their results that each of the D_2R dimer subunits is, therefore, able to bind to a Gi protein [1303]. Using the same experimental approach, a similar pattern was found for the metabotropic glutamate 2 receptor ($mGlu_2R$) [1321]. Both D_2R and $mGlu_2R$ homodimers share similar inactive interfaces via TM4-TM5, while the active interface occurs via TM4 in D_2R and via TM6 in $mGlu_2R$ [1301]. Lee et al. studied the role of highly conserved cysteine residues in extracellular loops (ECL) 1 and 2 in D_2R oligomerization [1305]. These cysteine residues are conserved in most rhodopsin-like GPCRs [1305]. Cys→Ala mutations in the extracellular loops were not significantly different between the mutant and wild-type D_2R. They also identified TM4 as the site of interaction in D_2R dimerization, which supports the proposal of a symmetrical TM4-TM4 interface. Similar to the full-length receptor, D_2R truncation mutants incorporating TM4 and TM5 (e.g., D2TM4-ICL3) or consisting of TM1-TM4 (D2AT-TM4) were able to form dimers. Truncated mutants lacking TM4 were identified only as monomers. To confirm this hypothesis, disruption of the helical structure of TM4 by the introduction of a proline residue in the truncation mutant, composed only of TM4 and TM5 domains, prevented the formation of dimers. This is important evidence but does not exclude the possible role of TM5 in the dimerization process [1305]. Marsago et al. showed another possible homodimer interface involving TM1 and TM2, along with HX8 [1322]. In addition to these interfaces, it has been widely described that D_2R can form heteromers through a TM4–TM5–TM4–TM5 interface with other class A GPCRs such as A2AR and angiotensin 1 receptors (AT1R) [77]. However, such interfaces between homo- and heterodimers for the same GPCRs could be different [77]. More information on dimerization can be found in the Supplementary Information.

To date, the most biologically relevant interface for D_2R homodimers remains unknown. It is also possible that the interface depends on the specific conformation (active or

inactive) of the protomers. According to Cordomi et al., the activation of a single monomer implies a symmetry change in the established interface [1301]. This was shown by Guo et al., where, upon ligand binding, the D_2R homodimer interface moved from the inactive TM4-TM5-TM4-TM5 toward an active TM4-TM4 interface [472]. Understanding the mechanism of action of D_2R homodimer formation, as well as the interactions formed upon dimerization, is of great importance and may offer new insights into the pathophysiology of dopamine-related diseases.

Therefore, we address the following key questions regarding the interface composition using a well-studied example: (i) What are the possible D_2R homodimer configurations and their dependence on the monomer activation status, (ii) are these physiologically stable, (iii) which interfacial amino acids and which main interactions are relevant in the process, and (iv) what are the structural and dynamic consequences of dimer formation in the macro- and microswitches? We used published structures of D_2R in different conformational states: inactive (PDB-id:6CM4 [1323]) and active (PDB-id:6VMS [1324]). We successfully built several dimer models, studied them using molecular dynamics (MD) simulations, and performed a thorough structural analysis of the data.

3.2.2. Results

3.2.2.1. Model generation and analysis

The application of typical protein-protein docking procedures to GPCR dimers is not straightforward [1325,1326]. A previously published protocol has been successfully applied to model a D_2R homodimer in an inactive conformation [1302,1310], among other studies on different GPCRs [1327,1328]. Therefore, we extended its application to other possible configurations of D_2R homodimers in various activation states. After selecting the most suitable models for the MD simulations, they were checked for overall structural equilibration over time. Next, the interface and relevant residues were identified and compared with the initial prediction before structural relaxation was obtained using MD simulations. Important macro- and microswitches for class A GPCR activation were analyzed and compared among dimer configurations to observe any conformational changes in the monomers when complexed as dimers (protomers). The significant interfacial elements were assessed and compared.

3.2.2.2. Contributing transmembrane helices

Upon generation of dimer models, it was shown that different combinations of TMs were involved in the establishment of the interface (**Table 2, Figure S6**). To determine the biological relevance of our different D_2R decoy configurations, they were subjected to the PRODIGY-CRYSTAL and PRODIGY-PROTEIN algorithms (**Table S2**). Using consensus scoring, we selected two **ac-ac** dimers as equally possible: one with a proposed TM4-TM5-TM4-TM5 interface and a second (B) with a proposed TM4-TM5-TM7-TM1 interface (**Table 1, Figure S6**).

Table 2. Proposed interfaces of D_2R homodimer configurations based on consensus scoring (Figure S6).

	Dimer configuration	Proposed interface	Template used
1	in-in	TM4-TM5-TM4-TM5	6CM4-6CM4
2	ac-ac-B	TM4-TM5-TM7-TM1	6VMS-6VMS-B
3	ac-ac	TM4-TM5-TM4-TM5	6VMS-6VMS
4	ar-ar	TM4-TM5-TM4-TM5	6U1N-6U1N
5	ac-in	TM1-TM2-TM4-TM5	6VMS-6CM4
6	in-ar	TM3-TM4-TM4-TM5	6CM4-6U1N
7	ac-ar	TM4-TM5-TM4-TM5	6VMS-6U1N

The TM4-TM5-TM4-TM5 interface was the most prominent among the dimers. Other possible interfaces were determined for the **ac-ac-B**, **ac-in,** and **in-ar** dimers. For D_2R, only **in-in**, **ac-ac** and **ac-in** D_2R homodimers have been experimentally detected thus far, but all relevant combinations are nevertheless theoretically possible [87,439,472].

3.2.2.3. Predicted interface in models

We identified interfacial amino acids in the static model structures using both PRODIGY algorithms (**Table S2**) [1329–1331]. We found that the number of residues varied between 21 and 35 and that the composition of interfacial amino acids was slightly different among the different D_2R homodimer configurations. Although the total number of interfacial amino acids differed between dimer configurations, they were similar for the pairs of monomers complexed together (**Table S2**). In addition, we identified amino acids present in two or more dimers, marked in bold in **Table S2**, while the others were unique (frequency = 1), marked in italics in **Table S2**. Subsets of frequently appearing amino acids were found in configurations with a symmetric interface (TM4-TM5-TM4-TM5). No unique residues were found for one protomer in the **in-in**, **ar-ar**, or **ac-protomer** of the **ac-ar** configuration. We also analyzed the frequency of common residues across all dimer configurations (**Table S3**). These 98 residues were sorted into three categories: very frequent (8-12x), moderate (3-7x), and rare (1-2x). Nineteen frequent residues were found: 110Met (ICL2), 160Ala (ECL2), $Tyr^{3.48}$, $Tyr^{3.51}$, $Thr^{3.52}$, $Ala^{3.55}$, $Arg^{4.40}$, $Arg^{4.41}$, $Val^{4.44}$, $Ile^{4.48}$, $Leu^{4.52}$, $Thr^{4.55}$, $Pro^{4.59}$, $Tyr^{5.41}$, $Val^{5.45}$, $Val^{5.49}$, $Ile^{5.52}$, $Val^{5.53}$, and $Leu^{5.56}$. More detailed analyses of the various interfaces are provided in the Supplemental material (Chapter 7).

3.2.2.4. Analysis of the simulated systems

After analyzing the final models, they were subjected to MD simulations. We first ensured that the systems were stable during simulation, that is, no disruption of the dimer occurred, and that the binding interfaces achieved equilibrium before further analysis.

This was not the case for **ac-ac-B**, which was disrupted upon initialization and was therefore excluded from further analysis (**Figure S7**).

3.2.2.5. Equilibration and stability of the systems

We evaluated the equilibration of the system by calculating the distance over time between a subset of residues located roughly at the center of each TM and the average position of the membrane P atoms. Two residues were selected per TM (1.44, 1.45, 2.52, 2.53, 3.37, 3.38, 4.51, 4.52, 5.49, 5.50, 6.44, 6.45, 7.49, and 7.50), and their distance to the membrane center along the z-coordinate was calculated (**Figure S7**). Based on these results, an equilibration period of 200 ns was determined to be appropriate (black area in **Figure S7**). RMSD calculations were used to determine the stability and relative orientation of the TMs, loops, and important structural motifs of the D_2R homodimer and were compared with those of the monomers (**Figure S8**). RMSD calculations were therefore performed for the individual monomers (in M), for each protomer within the dimer (in D), and for the entire dimer itself (Dim), and averaged among replicates. Overall, the systems were stable over time, with no major movements or disruptions of TMs. Analysis of microswitches and key domains showed that dimers had higher RMSD values than monomers, likely due to conformational rearrangement upon complex formation. A more widespread distribution was also observed for dimers, particularly at the DRY, CWxP, NPxxY, PIF, arginine cage domains, serine residues, and toggle switch, likely because of the same conformational rearrangement. We also monitored certain macro- and microswitches over time, including the relative orientation of the dimers (**Figure S9**), the interface area (**Figure S10**), the distance between TM3-TM6 (**Figure S14**) and TM3-TM7 (**Figure S15**), the angle between the centroids of the benzene ring of residues 5.51Phe, 6.44Phe, and 6.45Ile (**Figure S23**), the opening of the hydrophobic lock (**Figure S25**), both angles χ_1 and χ_2 of $Tyr^{7.53}$ (**Figures S26** and **S27**), and the sizes of the G protein and β-arrestin binding sites (**Figures S33** and **S34**). For most time-series captures, no major changes were observed, indicating that an equilibration time of 200 ns was sufficient for the systems to reach convergence.

3.2.2.6. The D_2R homodimer interface

Relative orientation of the dimers

We determined the relative orientation of the receptors in the dimeric state by calculating the relative rotational angles of the two receptors (**Figure S9**). The two-dimensional plots indicated that the symmetrical **in-in** dimer was highly stable across the MD simulations, suggesting a nonflexible dimer interface. Except the **ac-ac** configuration, all others populated two similar conformation states. The **ac-ac** configuration showed higher plasticity and could be mapped to three different dimer configurations.

Key residues and interface area

We calculated the interface area values of the various dimer configurations (**Figures 14 and S10**) and found that these values were consistent across replicates over time. In terms of the size of the homodimer interface, the smallest area was observed in the **ar-ar** configuration, whereas the largest area was observed in the **in-ar** configuration. Furthermore, configurations with the same interface type (e.g., TM4-TM5-TM4-TM5)

varied in size, with **ar-ar** configurations having the smallest interfacial area and **in-in** configurations having the largest interfacial area.

To consider the dynamical behavior of the systems and to determine which residues formed the so-called "decoy original interface" of the dimer, we calculated the ΔSASA of each residue at the start of the simulation, where ΔSASA = $SASA_m$ - $SASA_d$, where $SASA_m$ and $SASA_d$ are the SASA values in the monomeric and dimeric forms, respectively. The rationale was that residues with a ΔSASA of 0 had the same exposure in both the dimeric and monomeric forms and, as such, were not part of the initial interface. In addition to the requirement of a ΔSASA >0, we employed another set of criteria to further narrow down this list: residues should have a ΔSASA higher than 0.05 nm^2 in at least 2 out of the 3 replicates. We then calculated ΔSASA over time for each residue on this list, and for each residue, we performed normalization by dividing by $SASA_{max}$, defined as the maximum SASA value for that residue type (i.e., when fully

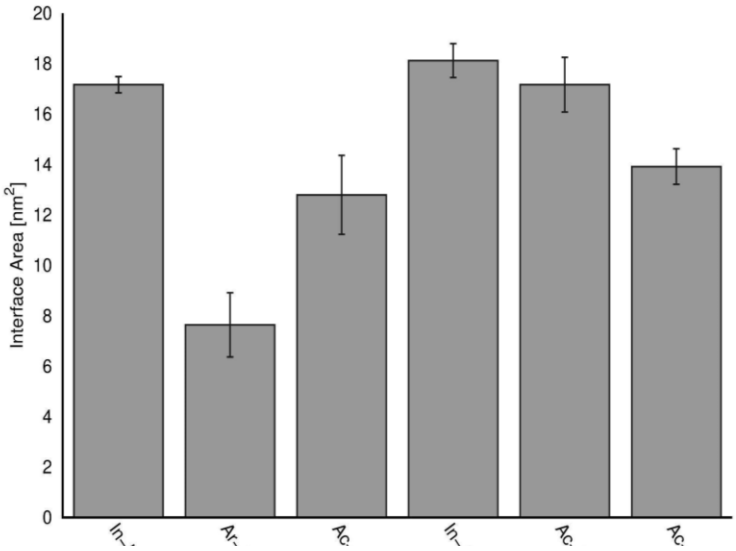

Figure 14. Interface area of each D_2R homodimer system. The interface area was calculated for each system, and replicates are summarized as the mean ± standard error of the mean (SEM).

exposed). Only residues with a normalized ΔSASA >10% were considered to belong to the initial interface (**Figure S11, Table S4**).

We observed that most of the residues of the original interface remained there for more than 50% of the simulation time, but there were exceptions (detailed analysis can be found in **Figure S11** and **Table S4**). In addition, we also found that a significant number of residues located in the loops contributed to the interface, especially residues from ICL2 (110Met, 111Pro, 112Met, 113Leu, 114Tyr, 115Asn,

116Thr, 117Arg, 118Tyr, 119Ser, 120Ser, 121Lys) and ECL2 (144Phe, 145Gly, 146Leu, 147Asn, 148Asn, 158Asn, 159Pro, 160Ala). In addition, we determined that TM7 and ICL3 do not contribute to the interface of any configuration. For **in-protomer-2** of the **in-in** dimer and the **in-protomer** of the **in-ar**, but not for **ac-in**, two residues from TM6 ($Ile^{6.56}$, $Ile^{6.59}$) were part of the interface, which was unexpected because TM6 was not part of the initially predicted interface. In addition, **ar-protomer-2** of the **ar-ar**

configuration and the **in-protomer** of the **in-ar** configuration possessed 248His (ECL3) as part of their interface. Furthermore, for the two hetero-configuration dimers, **ac-in** and **in-ar**, residues from TM1, ICL1 and TM2 (Val$^{1.51}$, Cys$^{1.54}$, Met$^{1.55}$, Ser$^{1.58}$, Arg$^{1.59}$, 35Lys, 38Gln, Tyr$^{2.41}$, Val$^{2.48}$, Leu$^{2.52}$, Thr$^{2.55}$, Leu$^{2.56}$) contributed to their interface. While the **ac-in** configuration was formed by TM1-TM2 of the **ac-protomer**, the **in-ar** configuration was formed by TM4-TM5 of the **ar-protomer**. A unique feature was also observed in the **ar-protomer** of the **in-ar** configuration, which contained one ECL1 residue (75Ser) and two HX8 residues (Ile$^{8.53}$ and Cys$^{8.56}$) at the interface.

We compared the "decoy original interface" to the prediction made with the PRODIGY/static structure using homodimers before they underwent MD simulations (**Table S5**) [1326–1328]. While most residues were accurately predicted, there were some changes in the interface residue list, indicating some conformational rearrangement. It is worth noting that all relevant residues from the Guo et al. studies were present among the dimer configurations (**Figure 15**) [472,1312,1313].

Predicted static interface vs. dynamical interface

After comparing the PRODIGY/static structure and the SASA/dynamical interfaces and sorting all residues according to their frequency (**Table S2-S6**), we identified the following highly frequent residues in the D_2R homodimer: 160Ala (ECL2), Arg$^{4.40}$, Val$^{4.44}$, Ile$^{4.48}$, Val$^{4.51}$, Leu$^{4.52}$, Thr$^{4.55}$, Pro$^{4.59}$, Tyr$^{5.41}$, Val$^{5.45}$, Val$^{5.49}$, and Val$^{5.53}$. Interestingly, we also observed that partnered protomers with different TMs, such as the **ac-protomer** of the **ac-in** configuration, which uses TM1 and TM2 as part of the interface, also included Arg$^{4.40}$ and Val$^{4.51}$ among the prevalent residues. Similarly, the **in-protomer** of the **in-ar** configuration, which uses TM3 and TM4 as part of the interface, also contains residues from TM5 (Val$^{5.40}$, Tyr$^{5.41}$, Ile$^{5.44}$, Val$^{5.45}$, Val$^{5.49}$, Ile$^{5.52}$, Val$^{5.53}$, Leu$^{5.56}$, Lys$^{5.60}$, Arg$^{5.67}$) and TM6 (Arg$^{6.67}$, Ile$^{6.56}$, Ile$^{6.59}$).

In addition to the highly prevalent residues, certain regions of the receptor also contribute to the size of the interface in the dimer with the TM4-TM5-TM4-TM5 interface, such as TM3, ECL2, and ICL2. For example, many residues from TM3 and the loops contributed to the interface in the **in-in** symmetric dimer, while this was not the case for the **ac-ac** and **ar-ar** dimers. Almost no residues from the loops contributed to the interface in the **ar-ar** homodimer. In contrast, various residues from the loops were important for binding in the **ac-ac** dimer, but only one residue from TM3 (Ala$^{3.55}$) was part of the interface.

Similarly, only Ile$^{3.48}$ and Thr$^{3.52}$ were part of the TM4-TM5-TM4-TM5 interface in the **ac-ar configuration.**

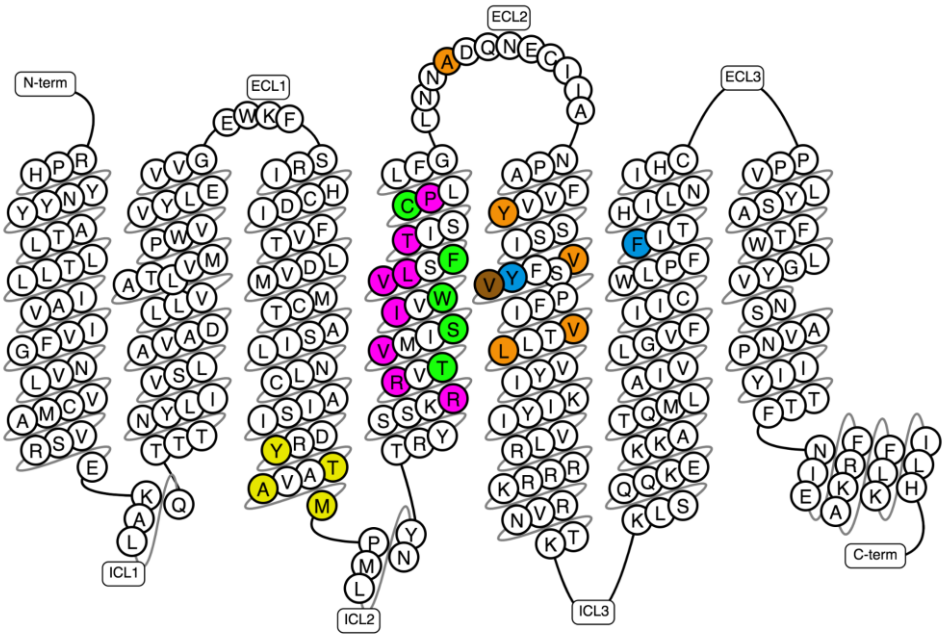

Figure 15. Snake plot of D_2R showing relevant residues from the literature and this study. Residues known from literature from studies of Guo and co-workers for the active conformation (green) and from Wouters and co-workers (blue) which considered TM5 and TM6 as determinants of the interface. In this study, PRODIGY-predicted frequent residues are colored yellow, and SASA-determined frequent residues are shown in brown. Common residues between the PRODIGY and SASA analyses are colored orange. The residues predicted in our study by PRODIGY and SASA are shown in pink by Guo et al.

For dimers with a nonsymmetric interface, such as **ac-in** (TM1-TM2-TM4-TM5), we again found that residues from other regions, such as TM3 and ICL1, contributed to the interface. Interestingly, for the **in-ar** (TM3-TM4-TM4-TM5) configuration, some residues from TM5 and TM6 were part of the interface on the **in-protomer** side (TM3 and TM4), while residues from TM1, ICL1, TM2, TM3, and HX8 contributed from the **ar-protomer** side (TM4-TM5). This finding is consistent with the large interfacial area of the **in-ar** configuration (**Figure 14**). The same observation was also made for the **ac-in** interface (**Figure 14**).

Apart from the size of the interface area and, consequently, the number of interfacial residues, we also wanted to determine the types of residues that are preferentially conserved in these interfaces. As expected, most of the 12 conserved/highly frequent residues were nonpolar, including 5 valine residues. Asp and Glu were the only amino acid residues that were not found at any of the interfaces.

Interaction type established for the different interfaces

The type of pairwise interaction was determined and averaged among replicates (**Figure S12**). Each system displayed a unique pattern, and interestingly, they were not solely found between the TMs of partnered receptors (a detailed analysis can be found in **Figure S12**).

Overall, the results showed that the conformational status of the monomers contributed to the interaction patterns when considering dimer configurations with the same

interface. For example, in the **in-in** configuration, interactions involving TM5 were not present even though TM5 was part of the interface. TM4 was relevant for forming H-bonds and π-cation interactions with ICL2 as well as H-bonds and salt bridges with TM3. The subset of interfacial residues on TM3 comprises Ile$^{3.48}$, Tyr$^{3.51}$, Thr$^{3.52}$, and Ala$^{3.55}$. ICL2, ECL2, and ECL3 were the domains mainly involved in the formation of π-stacking, T-stacking, and some H-bond and π-cation interactions. Moreover, residues on ECL3 have not been previously identified as part of the interface. ICL2 consisted of only a few residues, 110Met, 111Pro, and 120Ser, whereas the ECL2 interfacial residues were 146Leu, 147Asn, 159Pro, and 160Ala. Ile$^{6.59}$ was the only relevant residue identified in TM6.

When comparing these findings to other configurations with the same interface, we found that for **ar-ar** and **ac-ac**, where the protomers possess the same conformation, no salt bridges were present. However, conserved salt bridges between TM4 and TM3 were found for the **ac-ar** configuration, similar to our observation for the **in-in** configuration. In the **ar-ar** configuration, TM4 and TM5 are involved in the formation of H-bonds. Although this configuration has the smallest interface (**Figure 14**) with only 12 residues, it appears to be crucial for many of the interactions.

For instance, the TM5 residues, comprising Phe$^{5.38}$, Tyr$^{5.41}$, and Val$^{5.45}$ from protomers 1 and Val$^{5.40}$, Ile$^{5.44}$, Tyr$^{5.48}$, Val$^{5.49}$, Ile$^{5.52}$, Leu$^{5.56}$, Lys$^{5.60}$ from protomer 2. Only π-cation interactions were formed by residues from TM4, ECL2 and ECL3. In contrast to the **ar-ar** and **in-in** configurations, the **ac-ac** configuration behaved differently. H-bond interactions were mainly formed by TM3, TM4 and TM5, while π- and T-stacking interactions were again mostly formed by TM5. However, for this configuration, the loops appeared to be less involved in establishing meaningful interactions. This was also true for the **ac-ar** configuration. We also concluded that TM3 was highly involved in other types of interactions, such as H-bonds and π-cation interactions, which is quite interesting, as only Ile$^{3.48}$ and Thr$^{3.52}$ were previously considered part of the interface. When looking at the major structures involving mixed conformational dimers, such as **in-ar** and **ac-in**, a larger subset of salt bridges was found compared to the other homo-conformational configurations. For the **in-ar** configuration, ICL1 residues 35Lys and 38Gln were also involved in the observed interactions. Interestingly, π-cation interactions were also formed by residues from HX8, namely Ile$^{8.53}$ and Cys$^{8.56}$. For the **ac-in** configuration, HX8 also contributed to H-bond and π-cation interactions. In this configuration, residues from the relevant TMs interact with each other or with residues from the loops, particularly ICL2 (117Arg, 118Tyr, 121Lys) and ECL2 (144Phe, 145Gly, 147Asn, 160Ala).

3.2.2.7. Macro- and microswitches upon dimerization

The effects of activation on different macro- and microswitches are reviewed in the Supplementary Information. In this study, we investigated these effects in the context of dimerization.

Outward movement of TM6, inward movement of TM7, and disruption of the ionic lock

A description of the GPCR activation mechanism and main effects can be found in the Supplementary Information (**Figure S13**). First, we compared the distance between the Cα atoms of residues 3.50-6.34 (TM3-TM6) and 3.50-7.53 (TM3-TM7) (**Figure S14 and S15**). $Arg^{3.50}$ is part of the ionic lock and is known to form a salt bridge with $Glu^{6.30}$, which stabilizes the inactive state [1332–1334]. The ionic lock is disrupted upon activation, leading to the outward movement of TM6, for which 6.34 was chosen as the representative part of the key DRY motif [1335]. In addition, $Tyr^{7.53}$, also part of the NPxxY motif, is a highly conserved tyrosine that undergoes conformational transitions depending on the activation state of the receptor [107,1332]. According to Zhou et al., $Tyr^{7.53}$ also experiences several rewiring events with a shortening of its distance to TM3 [97]. As expected, we obtained a shorter TM3-TM6 distance and a higher TM3-TM7 for the **in-monomer** conformation, whereas these values were higher for the **ar-** and **ac-monomers** and dimers containing them. For the various dimer configurations, we observed that the TM3-TM6 distances were (i) even lower for **in-in**, (ii.) lower for one protomer on the **ar-ar** dimer, (iii.) constant for the **ar-protomer** in **the in-ar** and **ac-ar;** (iv.) higher for the **ac-protomer** in the **ac-ar** dimer, and (v.) lower for the **ac-protomer** in the **ac-in** dimer configuration.

Second, the distances between the Cα atoms of residues 3.50 and 6.34 (TM3-TM6) and between 5.46 and 7.41 (TM5-TM7) were measured to observe the overall concerted movement of the TMs (**Figure S16, S17**). The role these residues play in activation is further explained in the Supplementary Information. As for TM3-TM7 (3.50-7.53), the distance between TM5-TM7 (5.46-7.41) should also be short when the receptor is activated. For the distance between TM5 and TM7, we expected distances similar to those observed for TM3-TM7. When comparing these two measurements for the individual monomers, we found that the distance between TM3-TM6 was shorter (between 0.5-1.0 nm) for the in-monomer, while the distance between TM5-TM7 was larger (between 1.6-2.0 nm). For the ar-monomer, the distance between TM3-TM6 was consistent at approximately 1-1.5 nm, while a high dispersion was found for the TM5-TM7 distance ranging from 1.4-2.4 nm over time. However, the distance between TM5-TM7 was much larger than that between TM3-TM7. The opposite was true for the ac-monomer configuration. The distance between TM5 and TM7 was consistently between 1.6 and 2 nm over time, which was larger than the distance between TM3 and TM7. In contrast, the distance between TM3 and TM6 showed considerable variability over time, ranging from 0.7-1.7 nm.

As a third metric, we analyzed the distance between the Cα atoms of residues 3.50 and 6.34 and between 5.58 and 7.53 (**Figure S18, S19**). While the distance between 3.50 and 6.34 is an indicator of outward movement of TM6, the distance between the two conserved tyrosine residues Tyr5.58 and Tyr7.53 represents an important microswitch in class A GPCR activation [1336]. Residues from TM5 that interact with the ligand, such as 5.46, cause rearrangements in the NPxxY motif in form of a twist, which reorients Tyr7.53 towards Tyr5.58, forming a water-mediated interaction known as the Y-Y interaction [1336,1337]. Together with the displacement of TM6, captured by the distance between 3.50 and 6.34, the formation of the G protein binding site was established [1336]. Therefore, we expected that the fully active conformation of the monomers would result in a short distance between the two tyrosines (Y-Y interaction). Conversely, we expected inactive conformers to exhibit longer distances between the

two tyrosine residues. Our observations for the monomers (**Figure S18**) support these expectations. The **in-monomer** showed a short distance between TM3-TM6 and a large distance between Y and Y-Y. The **ar-monomer** had a larger distance between TM3-TM6 but a visibly shorter distance between Y-Y. For the **ac-monomer**, at some time points, the distances were even shifted towards a more active conformation compared to those measured for the **ar-monomer**. When comparing the monomer and dimer configurations, it could be shown that some conformational changes occurred within the dimers (**Figure S19**). While most of the protomers displayed similar properties to their uncomplexed monomers, the **ac-protomer** of the **ac-ar** configuration was found to be fully active than the monomer only, while this was not the case for its partnered **ar-protomer.** However, the **ac-protomer** in the **ac-in** dimer was clearly shifted towards a more inactive conformation, displaying a short distance between TM3-TM6 and a larger distance between Y-Y. We also monitored the comparison of the distances between the Cα atoms of residues 5.46-7.41 (TM5 bulge) and the ΔRMSD of two residues of the PIF motif ($Ile^{3.40}$ and $Phe^{6.44}$) (**Figure 16, S20**). According to Fleetwood et al., the formation of a bulge on TM5 by residues 5.46 and 7.41 influences the intracellular distance between residues 3.40 and 6.44, which are part of the PIF motif (connector motif) [1336]. These residues are also known to be in contact with highly conserved Asp2.50 and NPxxY through a network of water molecules [1336]. When analysing the results for the free monomers (**Figure S15**), it is clear that the **in-monomer** had the distance of the TM5 bulge varied between 1.60–2.00 nm, while the ΔRMSD of the connector ranged between -0.15 and -0.10 nm. In contrast to the **in-monomer**, the ΔRMSD of the connector of the **ac-** and **ar-monomer** was between 0.00 and 0.15 nm. In addition, the distance between the residues of the TM5 buffer showed a more dispersed distribution (range 1.40–2.20 nm) for the **ar-monomer** and was more concentrated (approximately 1.50–1.90 nm) for the **ac-monomer**. These findings are in agreement with those reported by Fleetwood et al. (Figure 4 of Fleetwood et al., panels d-f, [1335]) and put the **ar**-**monomer** in an intermediate activation state compared with the fully activated **ac**-**monomer**. In the **in-in** dimer configuration (**Figure 16**), there is a decrease in the ΔRMSD towards -0.20 nm and a different behavior of the two protomers, with one accessing more inactive-like conformations. In the **in-ar** and **in-ac** dimers, we also observed a high stability of the **in-protomer** in its inactive state. Both inactive and active conformations of the TM5 bulge were populated in the **ar-ar** dimer, reaching even higher values for the **ar-protomer** in the **in-ar** dimer. In contrast, the **ar-protomer** in the **ac-ar** dimer populated only the active-like states. The **ac-protomer** is very stable in an active conformation in the **ac-ac**, **ac-ar**, and **ac-in** dimers.

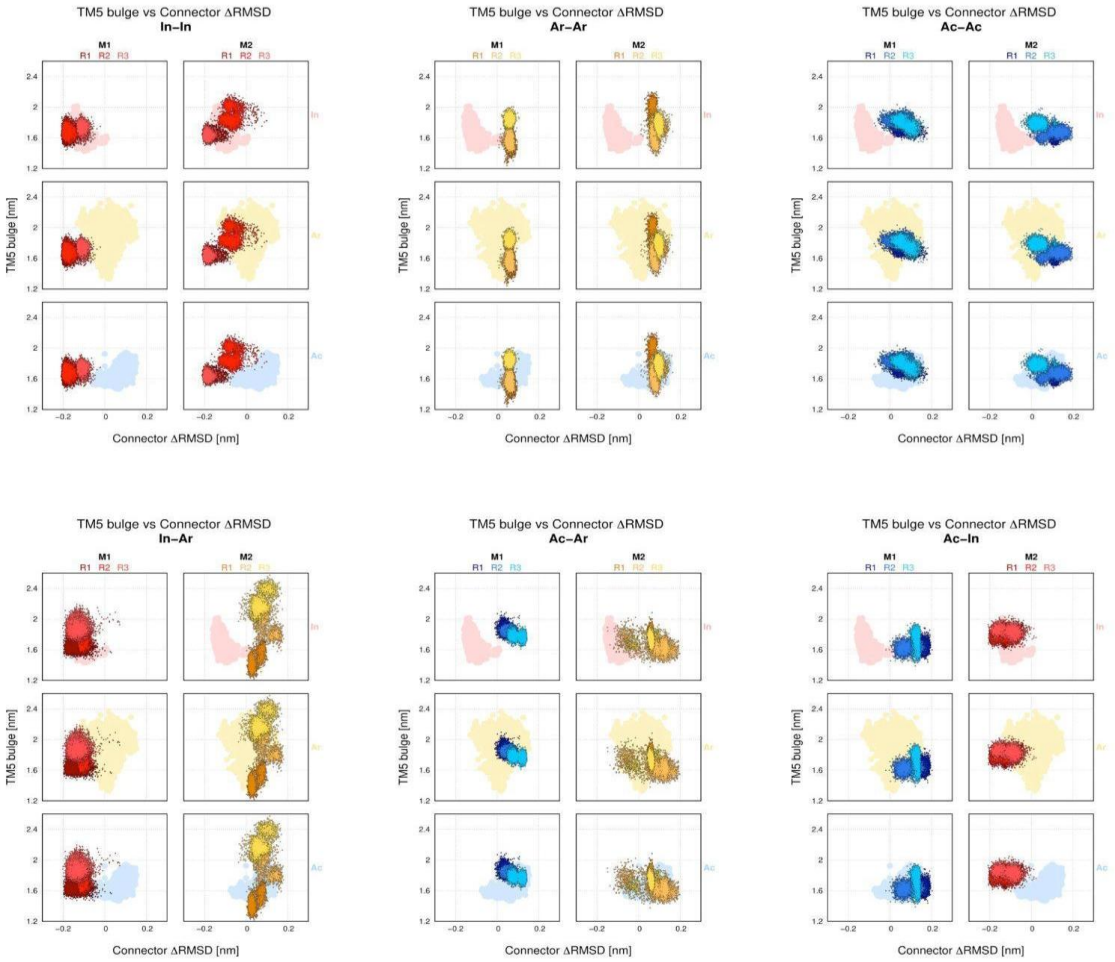

Figure 16. Comparison of TM5 bulge movement and RMSD of residues I.340 and F.644 (connectors) for the D_2R homodimer configurations. Comparison of Cα-distance between 5.46 and 7.41 and the RMSD of residues $Ile^{3.40}$ and $Phe^{6.44}$, which were measured for all protomers and replicates over time. For easier comparison, the distances of the individual monomers in the three activation states (in, ar, and ac) are shown as light-colored clouds in the background in three different lines. Conformations are color-coded as inactive-red, arrestin-yellow, active – blue.

Lu et al. tracked the angle between the centroids of the benzene ring of three phenylalanines (5.51, 6.44, and 6.45) over time. We replicated this analysis in our current study (**Figure S23**) [1339]. Upon activation, residues 6.44 and 6.45 moved towards residue 5.51, which then promoted an outward movement of TM6. Furthermore, all residues near the aromatic microdomain, where the rotamer toggle switch takes place, also moved forward [182,1339,1340]. For the uncomplexed monomers, the **in-monomer** was constant at 50–60°, while the **ar-monomer** was found at 70–90°, and the **ac-monomer** was found between 60 and 80°.

Upon closer examination of the properties of TM6, we observed that the conformational states of the individual monomers did not change significantly during simulation. However, the configurations of most dimers changed, with the exception of **in-conformers**. The **ac-protomer** in the **ac-in** configuration adopted the properties of an inactive conformer. In the **ac-ac**, **ar-ar**, and **ac-ar** configurations, one protomer appeared to be more active than the other, indicating that it may shift between a fully active

conformation and an intermediate state, which has several properties similar to the arrestin-bound conformation. This can also explain the differences between the protomers of the **ar-ar** configuration.

The collapse of the sodium pocket

Numerous studies have shown that ligand binding and activation of class A GPCRs lead to changes around the CWxP, TM5, and PIF motifs, resulting in the collapse of the sodium pocket around the conserved aspartic acid 2.50. This process involves dehydration, displacement of the sodium ion, and protonation of $Asp^{2.50}$, ultimately leading to a rewiring of the NPxxY motif [130,133,134,1336,1341]. The allosteric Na^+ ion forms strong interactions with residues $Asp^{2.50}$ and $Ser^{3.39}$ and several water molecules, all stabilizing the inactive state of GPCRs [1336,1342–1344]. Upon activation, the ionic lock is disrupted, and the sodium pocket around $Asp^{2.50}$ collapses and releases the sodium towards the intracellular space [134]. In our study, we also monitored changes in these two regions by calculating the distance between the Cα atom of $Asp^{2.50}$ and the

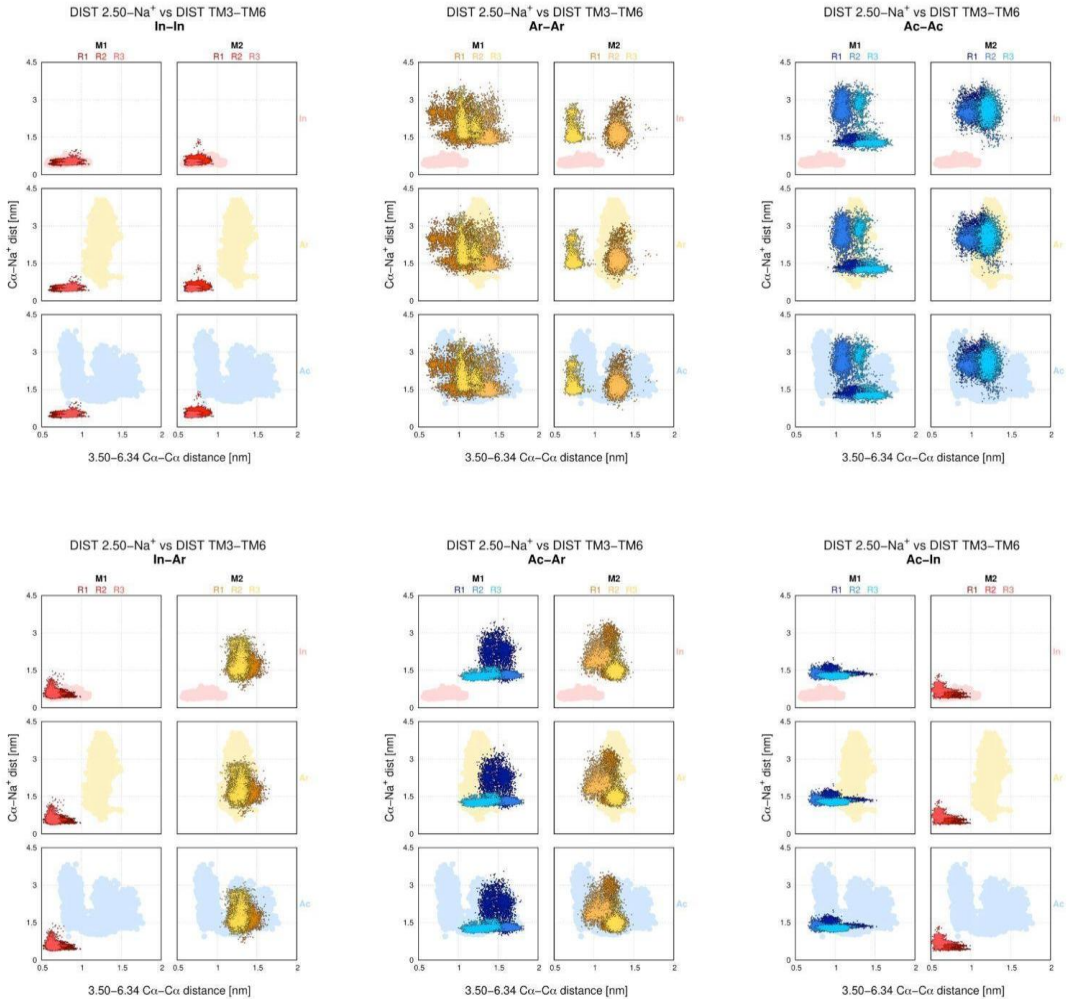

Figure 17. Comparison of disruption of the ionic lock represented as a distance between 3.50 and 6.34, and the distance between $Asp^{2.50}$ and its closest sodium for the D_2R homodimer configurations. Comparison of the Cα-distance between 3.50 and 6.34 and the distance between the Cα atom of the conserved residue $Asp^{2.50}$ and sodium (Na+), which were measured for all protomers and replicates over time. For easier comparison, the distances of the individual monomers in the three activation states (in, ar, and ac) are shown as light-colored clouds in the background in three different lines. Conformations are color-coded as inactive-red, arrestin-yellow, and active-blue.

closest sodium atom and compared this to the distance between the Cα atoms of residues $Arg^{3.50}$ and $Thr^{6.34}$, the ionic lock (**Figure 17, S24**). When looking at the individual monomers, the **in-monomer** appeared to have a short distance towards sodium, whereas in the **ac-** and **ar-monomers,** sodium was located more than 1.5 nm away from $Asp^{2.50}$ (**Figure S24).** The distance between $Arg^{3.50}$ and $Thr^{6.34}$ was less than 1.0 nm for the **in-monomer**, indicating that the ionic lock had not yet been disrupted. Distances above 1.0 nm were considered indicators of activated conformations, which was the case for **ac-** and **ar-monomers** (1.0-1.5 nm). When comparing these results with the dimer configurations (**Figure 17**), we see that all the **in-protomer**, **ac-ac**, **ar-ar**, and **in-ar** configurations have metrics similar to their individual uncomplexed forms. In the **ac-ar** configuration, the ionic lock residues of the **ac-protomer** were more widely separated than those of the uncomplexed monomers, and the same was true for the **ar-protomer.** In the **ac-in** dimer, the **ac-protomer** had properties of an inactive receptor, with approximately 1.5 nm and a closed ionic lock (0.5-1.5 nm). Another indicator of disruption of the sodium pocket is the number of water molecules in its vicinity. Therefore, we calculated the number of water molecules within a 0.8 nm radius around $Asp^{2.50}$ (**Figure 18**).

We found that the number of water molecules was consistently higher (~30) in the **in-conformer** than in the **ac-** and **ar-conformers** (~10). Interestingly, a clear distribution between the conformers was observed for the individual monomers. A comparison of these findings with the dimer configurations showed that the number of water molecules

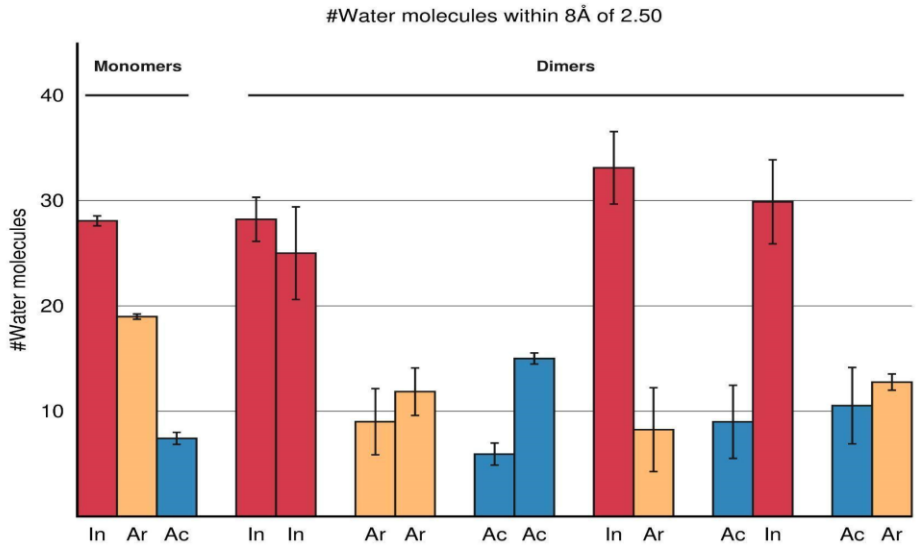

Figure 18. The number of water molecules within 8 Å of $Asp^{2.50}$ for the D_2R homodimer configurations. The number of water molecules within 8 Å of the conserved residue $Asp^{2.50}$ for the complete simulation time are represented as mean ± SEM. Conformations are color-coded: inactive - red, arrestin - yellow, active - blue

in the **in-in** configuration was similar to that of the individual monomers. Interestingly, the average number of water molecules differed between the two protomers within the **ac-ac** dimers. In this configuration, protomer 2 contains approximately twice as many water molecules as protomer 1. Furthermore, in the **ar-ar** configuration, the number of

water molecules is significantly reduced by 50% upon dimerization. For the **in-conformation,** we found that they remained inactive regardless of the partnered monomer, whereas the **ac-** and **ar-conformations** behaved very similarly to the active conformers (**Figure 18**).

Hydrophobic lock

After GPCR activation, the breaking of the hydrophobic lock comprising the hydrophobic residues at positions 3.43Leu$^{3.43}$, Val$^{6.40}$, and Leu$^{6.41}$ is another important microswitch event that loosens the connection between TM3 and TM6 [97,1339]. It also promotes the breaking of the ionic lock between Arg$^{3.50}$ and Glu$^{6.30}$, which finally releases TM6 outwards [97,126,1339]. To observe the status of the hydrophobic lock, we measured the area of the angle composed of the Cγ atom of Lys$^{3.43}$, the Cβ atom of Val$^{6.41}$, and the Cβ atom of Ile$^{6.40}$ over time, as described by Lu et al. (**Figure S25**) [1339]. The authors suggested that an area of approximately 15 Å^2 represents an inactive state, 10-20 Å^2 indicated an intermediate state, and everything above 20 Å^2 represents an active state of a GPCR [1339]. We only found breaking of the hydrophobic lock upon activation in the **ac-conformers**, while all **in-protomers** behaved like inactive conformers, regardless of their partners.

Microswitch: Transition of dihedral angles χ_1 and χ_2 tyrosine 7.53

Upon class A GPCR activation, the highly conserved tyrosine 7.53 undergoes conformational transitions between its dihedral angles χ_1 and χ_2 according to Yuan and coworkers [107]. Following the angles over time (**Figure S26**, **S27**), we observed major differences between the different conformational states of the individual monomers and the dimer configurations. The χ_2 angle displayed several, large conformational shifts, foremost for **ac-** and **ar-conformers** at any combination undergoing large movements, while **in-conformers** were more restricted. When comparing the dihedral angles χ_1 and χ_2 (**Figure S28 and S29**), it became clear that some of the configurations showed more variation than others. The smaller variation in χ_1 can be explained by the large rotations at this angle, which lead to steric clashes with the protein backbone. We also observed a lower rotation in Tyr$^{7.53}$ for **in-conformers**, while rotations of χ_2 in **ar-** and **ac-conformers** indicated that these conformations switch from active to inactive conformations. Moreover, the **ac-protomers** in the mixed configurations showed more constricted variation than that in the uncomplexed form, which can be explained by less space to unfold into a fully active conformation when complexed.

Transitions in the NPxxY motif

According to Leioatts et al. [1332] and Dror et al. [1345], the deactivation of class A GPCRs consists of a two-step process, where the NPxxY motif undergoes transitions towards an inactive conformation first, followed by ionic lock closing as TM6 moves inward to the helical bundle. Hence, the RMSD of NPxxY and the distance between the Cα-atoms of residues of the ionic lock Arg$^{3.50}$ and Glu$^{6.30}$ should give us the possibility to map this process [1332]. When we calculated these structural properties for the different D_2R homodimer configurations, we observed that specific values could be determined for individual monomers based on their conformation (**Figure 6, S25**). For the **in-**

monomer, the distributions of both the RMSD of NPxxY and the distance of the ionic lock were relatively small and concentrated, indicating that the ionic lock was closed in the inactive conformation,, and no significant transitions occurred in the NPxxY motif. (**Figure S30**). For the **ar-monomer,** the RMSD of NPxxY varied more than the ionic-lock distance. For the **ac-monomer**, the RMSD of the NPxxY motif was more diverse, and the distance of the ionic lock was increased. In the dimer configurations, the protomers remained inactive in the inactive conformations, whereas differences between monomers and complexes were observed for the **ac-** and **ar-conformers** (**Figure 19**). It is worth noting that the **ar-protomers** adopt inactive-like conformations in the **in-ar**

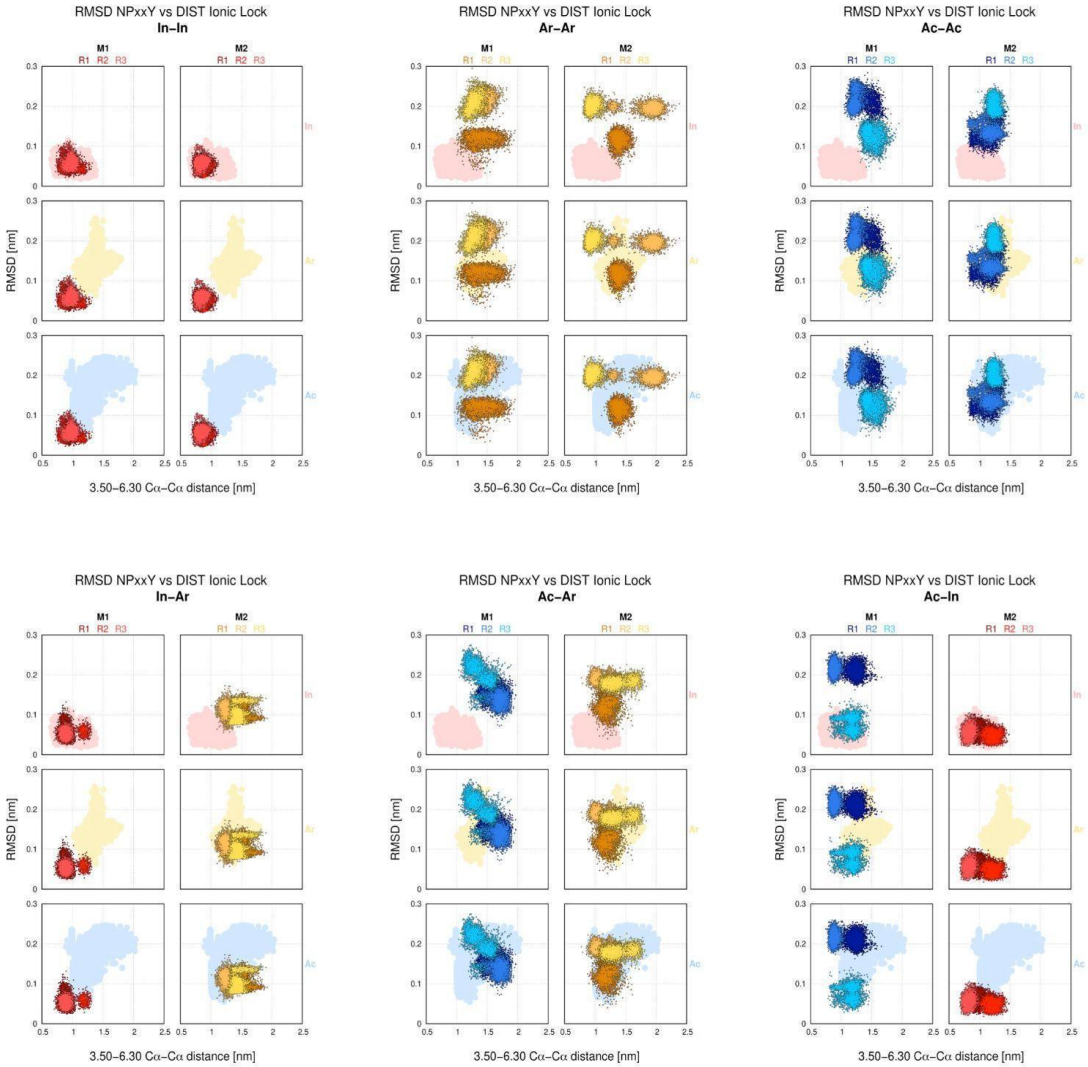

Figure 19. Comparison of the RMSD of NPxxY and the distance between Cα-atoms of residues of ionic lock 3.50 and 6.30. Comparison of the RMSD of NPxxY and the distance between Cα-atoms of residues of ionic lock 3.50 and 6.30, for which RMSD and distances [nm] of the uncomplexed monomers are shown as light-colored clouds in the background. Conformations are color-coded: inactive - red, arrestin - yellow, active - blue.

dimer, and the **ac-protomers** are distributed over both According to Leioatts et al. [1332] and Dror et al. [1345], the deactivation of class A GPCRs consists of a two-step process, where the NPxxY motif undergoes transitions towards an inactive conformation first, followed by ionic lock closing as TM6 moves inward to the helical bundle. Hence,

the RMSD of NPxxY and the distance between the Cα-atoms of residues of the ionic lock $Arg^{3.50}$ and $Glu^{6.30}$ should give us the possibility to map this process [1332] (**Figure 19**). When we calculated these structural properties for the different D_2R homodimer configurations, we observed that specific values could be determined for individual monomers based on their conformation (**Figure 19, S30**). For the **in-monomer**, the distributions of both the RMSD of NPxxY and the distance of the ionic lock were relatively small and concentrated, indicating that the ionic lock was closed in the inactive conformation, and no significant transitions occurred in the NPxxY motif. (**Figure S30)**. For the **ar-monomer,** the RMSD of NPxxY varied more than the ionic-lock distance. For the **ac-monomer**, the RMSD of the NPxxY motif was more diverse, and the distance of the ionic lock was increased. In the dimer configurations, the protomers remained inactive in the inactive conformations, whereas differences between monomers and complexes were observed for the **ac-** and **ar-conformers** (**Figure 19**). It is worth noting that the **ar-protomers** adopt inactive-like conformations in the **in-ar** dimer, and the **ac-protomers** are distributed over both active and inactive-like populations in the **ac-in** dimer.

We analyzed changes in the NPxxY motif by comparing ΔSASA with the RMSD of this motif (**Figures S26** and **S27**). When examining the individual monomers, we found that for the **in-monomer**, the RMSD was between 0.0 and 0.1 nm, and the ΔSASA was between 9% and 18%, while the RMSD was increased to 0.1-0.2 nm for the **ar-monomer** and the ΔSASA did not change significantly. For the **ac-monomer**, the RMSD increased above 0.2 nm, and the ΔSASA was spread between 9% and 20%. In the dimer configurations, the **in-conformers** always displayed the same values, regardless of the partner, whereas more variation was observed for the other conformers (**Figure S27**). Analysis of the NPxxY motif in the monomer and dimer configurations confirmed the results obtained for other motifs. The **in-conformer** is always inactive, whereas the **ar-ar**, **ac-ac**, and **ac-ar** configurations display properties similar to those of the activated receptors.

3.2.2.7. Sizes of G protein- and β-arrestin-binding areas

The sizes of the binding sites for the G protein and β-arrestin were determined using SASA values of relevant residues, which were then normalized to the $SASA_{max}$ values determined earlier for each type of amino acid. The sizes (expressed as a percentage) were calculated over time (**Figures 33** and **S34**), and then averaged and compared within the different dimer configurations (**Figure 20**). According to Yuan et al., small binding areas suggest an inactive state of the receptor, as there is no space available for the binding of a G protein or β-arrestin [107]. We observed the smallest areas of the binding sites for the inactive protomers (**Figure 20**). The largest values were determined for the **ar-ar** and **ac-ac** dimer configurations. Additionally, the ratios between the protomers were consistent for both the G protein- and β-arrestin-binding sites.

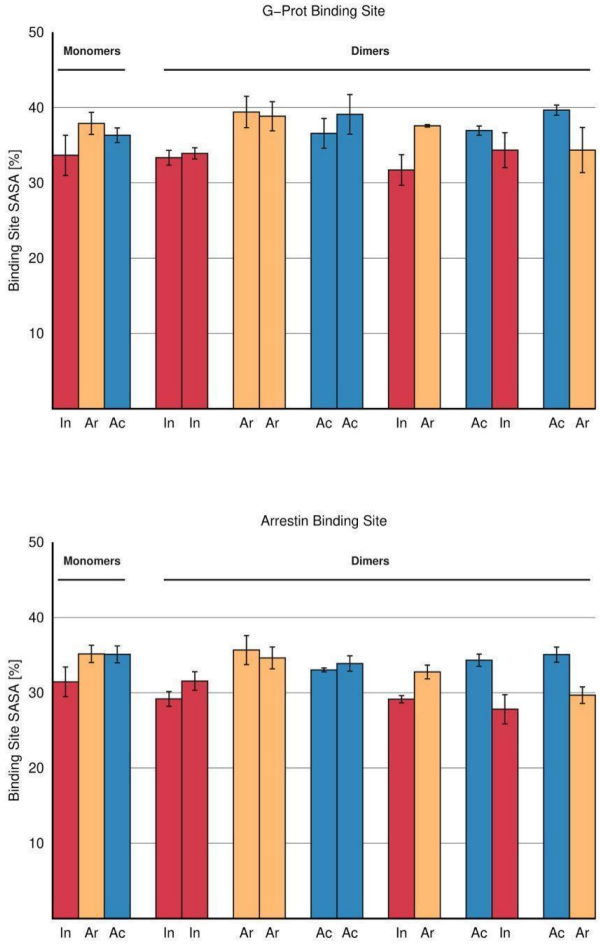

Figure 20. Size of binding sites for the G-protein and β-arrestin. The sizes of G protein and β-arrestin binding sites [%] were determined using SASA values of binding sites resides retrieved from Preto et al. (2020). This were then normalised to the SASAmax values determined for each type of amino acid. The volumes are shown as mean ± SEM. Conformations are colour-coded: inactive - red, arrestin - yellow, active - blue.

3.2.3. Discussion

3.2.3.1. Dimer configurations are stable

The goal of our study was to design a straightforward protocol for building GPCR homodimers, identifying their most stable interfaces, and complementing previous studies on other GPCR dimers, including those of Kaczor et. al [1310,1327,1328]. We used the D2R homodimer as a case study since the TMs involved in its interface were previously experimentally identified.

Our results show that different dimer configurations can form stable TM4-TM5-TM4-TM5 interfaces, regardless whether the partnered protomers are active or inactive. This is in line with experimental studies showing that the dimers seem to be pre assembled independent of ligands and therefore also independent of the conformation of partnered protomers.

However, we found that the inactive conformation was maintained in all combinations, whereas the **ac-** and **ar**-conformations were either active or desensitized (activated state). We observed variations in some metrics for **ac-** and **ar**-conformers, particularly in terms of helix movement. The ac-ac combination was found to be active while the individual monomers were rather found in an intermediate conformation, between inactive and active. This indicates that the active protomers stabilize each other's active conformations. Most notably, we observed that an active protomer adopts properties of the inactive conformation when paired with an inactive protomer, particularly in terms of helix movement, transitions in the NPxxY motif, and the position of the ionic lock. The latter was only observed for the **in-ac** dimer. Additionally, we found that this ionic lock was broken for **ac conformers** in all combinations, even when paired with an inactive protomer. The addition of G proteins may change this behavior. We verified that the dimers with the TM4-TM5-TM4-TM5 proposed interface followed the same behavior as previously described for a similar configuration in the serotonin$_{1A}$ receptor [1346,1347].
The **in-conforme**r was always inactive, whereas the **ar-ar**, **ac-ac**, and **ac-ar** configurations displayed properties similar to those of the activated receptors. Analyses of the macro- and microswitches revealed that the inactive configuration was unperturbed by its partnered protomer, whereas in the **ac-in** dimer, the active protomer adopted the properties of an inactive receptor. In some cases, the arrestin configuration displayed properties of an active receptor in the absence of an agonist, suggesting that a switch to another meta-state within the dimerization process was observed. In summary, the relevant residues found in our study are in agreement with experimental data, thus, validating our computational protocol. This method can easily be adapted to heterodimers and may also be extended by adding additional proteins such as G proteins or β-arrestins.

3.2.3.2. The central role of transmembrane domains 4 and 5 in dimer formation

TM1, TM4, and TM5 bear the largest membrane-accessible areas, which indicates their importance in the establishment of protein-protein interactions [1301]. Several studies have revealed the importance of TM4 and TM5 in homo- and heterodimer formation [825,1305,1318,1346,1348–1354]. However, many other interface points have been identified, including TM5-TM6-TM5-TM6 [77,1355], TM1, TM2, HX8, and ECL1 [876,1247,1310,1351,1354,1356]. Here, we observed that the involvement of TMs changed depending on the combination of conformers. A symmetric interface of TM4-TM5-TM4-TM5 was determined for most configurations, except for two very different arrangements: **ac-in** (TM1-TM2-TM4-TM5) and **in-ar** (TM3-TM4-TM4-TM5). This is consistent with the "rolling dimer" interface model proposed by Dijkman et al., which suggests that GPCRs can exploit multiple interaction interfaces that can coexist and interconvert [1357]. In the **ac-in** and **in-ar** dimers, the interaction between GPCRs led to the establishment of asymmetrical and larger interfaces in comparison to the **ac-ac** configurations and were therefore, closer in size to the **in-in** dimer.
Overall, our findings are in agreement with earlier experimental studies by Guo et al., which reported that TM4-TM5 is the most likely physiological interface of the D_2R homodimer [472,1303,1318]. However, other studies have supported these alternative possibilities. Marsago et al. showed that the D_3R homodimer has two potential interfaces:

one involving residues from TM1, TM2, and HX8, and the other involving TM4 and TM5 [1298,1322]. TM3 has also been found at the interface of the $A_{2A}R$-D_2R heterodimer [76]. TM6 is unlikely to play a significant role in complex formation, as it would likely cause steric clashes between the protomers upon activation due to its outward movement [1357–1359].

3.2.3.3. Transmembrane domain and loop involvement in dimer formation

The interfacial characterization of all configurations in this study highlights the important role of the TM regions and loops in driving complex formation. This finding is in agreement with those reported by Simpson et al. [1319], Pulido et al. [1360], and Filizola et al. [1352], pinpointing ICL2 and ECL2 as particularly relevant, which has also been observed in other studies [1361]. ICL3 also forms relevant interactions, particularly at the C-terminal regions. However, it is difficult to fully assess their involvement because these loops are very large and flexible, and cannot be well-captured by experimental techniques or well-modeled by computational methods. Consequently, the analysis of the ensemble of conformations involving these loops remains elusive. We identified a subset of highly conserved residues that were relevant for all dimer configurations determined in a static structure (PRODIGY) and we considered the dynamic behavior of the dimers (SASA) during the simulation:160ALA (ECL2), $Arg^{4.40}$, $Val^{4.44}$, $Ile^{4.48}$, $Val^{4.51}$, $Leu^{4.52}$, $Thr^{4.55}$, $Pro^{4.59}$, $Tyr^{5.41}$, $Val^{5.45}$, $Val^{5.49}$, and $Val^{5.53}$. Comparing these findings with those of Guo et al., some differences and similarities were observed [472,1303,1304]. For example, $Arg^{4.40}$, $Val^{4.44}$, $Ile^{4.48}$, $Val^{4.51}$, $Thr^{4.55}$, and $Pro^{4.59}$ residues were involved in both studies. Guo and coworkers [472,1303,1304] stated that residues $Trp^{4.50}$, $Phe^{4.54}$, $Cys^{4.58}$, and $Arg^{4.43}$ were relevant to mediate the crosstalk between the protomers in an active conformation. Herein, we observed their participation only in **the ac-** and **ar-conformers**. Guo et al. reported different amino acid combinations for TM4-TM5 (inactive dimer configuration) and TM4-TM4 (active dimer configuration) [472]. It has also been reported that the replacement of $Cys^{4.58}$ leads to the elimination of receptor crosstalk and that this amino acid is relevant for the active TM4-TM4 conformation of the D_2R homodimer. In our study, $Cys^{4.58}$ was present in both protomers of the **ac-ac** configuration with the TM4-TM5-TM4-TM5 interface and in both protomers of the **ac-ar** dimer (**Table S2**). Guo et al. also identified other residues relevant for an additional interface involving TM1 ($Pro^{1.30}$, $Tyr^{1.34}$, $Tyr^{1.35}$, $Leu^{1.38}$, $Leu^{1.41}$, $Asn^{1.50}$, $Arg^{1.59}$, and $Phe^{7.65}$) [1304]. Residues $Tyr^{1.34}$, $Tyr^{1.35}$, and $Arg^{1.59}$ were also relevant for our dimer configurations. Residue $Arg^{1.59}$ could be identified on the **ac-protomer** of **ac-in** and on the **ar-protomer** of **in-ar** [1304]. Lastly, Wouters et al. suggested the formation of a TM5-TM6-TM5-TM6 interface and that $Tyr^{5.48}$ and $Phe^{6.52}$ are important for dimerization [77]. While $Phe^{6.52}$ was not found at any D_2R homodimer, $Tyr^{5.48}$ was found twice on the **in-in** dimer, once on the **ac-ac**, once on the **ar-ar**, on the **in-protomer** of the **ac-in,** and of the **in-ar** configuration.

The highly prevalent residues identified in our study (mostly from TM4 and TM5) were nonpolar and, therefore, complementary to establishing stable interfaces. These types of residues are expected, considering the nature of TMs, as exposing charged or polar residues to the lipid bilayer could lead to transient dimerization [1318,1362]. It has previously been shown that at least two adjacent arginine, glutamic acid, aspartic acid, or phosphorylated amino acid residues are sufficient to induce stable noncovalent

complexes in heterodimers [1353,1363,1364]. From our set of highly preserved residues, $Arg^{4.40}$, $Thr^{4.55}$, and $Tyr^{5.41}$ were the most capable of establishing electrostatic interactions.

Our results indicate the involvement of ICL2, ECL2, ECL3, and TM3 in stabilizing interactions. This is also in line with a study on opioid receptor homodimers, showing that residues from loops TM3 and TM2 stabilize the TM4/TM5 interface [1365]. In the same study, the authors described a specific subset of conserved residues (4.39, 4.43, 4.47, 4.50, 4.51, 4.54, and 4.62), similar to our identified prevalent residues in the case of the dopamine receptor [1365]. In another study investigating the D_1R-D_2R heterodimer, it was found that mutations to valine, proline, and serine residues altered the dimerization propensity of D_1R and D_2R [1366]. The authors also stated that valine and proline residues would promote the formation of the D_2R homodimer interface [1366]. Interestingly, Johnston et al. also identified two important valine residues, whereas we found five across all configurations [1365].

H-bonds were predominant, involving several residues from the TMs and loops, particularly in the **in-in**, **ac-ac**, **ac-in**, and **in-ar** dimer configurations. In contrast to these types of interfaces, most interactions were found between TMs for the **ar-ar** configuration, especially involving TM5. In a comprehensive study involving the $A_{2A}R$-D_2R heterodimer, it was also shown that TM5 was responsible for interactions between the two protomers, thus promoting the negative allosteric effect of the adenosine receptor on dopaminergic signaling [76,1367]. However, most interactions, such as π-cation, π-stacking, T-stacking, or even salt bridges, are formed between loops or between a loop and TM. Hence, loops can be the main drivers of interface formation and provide extra affinity to stabilize the final dimers. Similarly, O'Dowd et al. found a pair of adjacent glutamic acids (at the C-terminus of D_1R) and a pair of adjacent arginines (from ICL3 of D_2R) in the D_1R-D_2R heterodimer interface, forming stable electrostatic interactions [448,485].

3.2.3.4. The conformational status of individual protomers affects the macro- and microswitches

Macro- and microswitches of class A GPCRs are known to be involved in conformational rearrangements upon ligand binding to promote the outward movement of TM6 and its activation by enabling the necessary space for binding of a G protein (**Figure S13**) [97,485]. Our results indicated that the conformational status of the protomers remained consistent over time and that the movements of the relevant TMs (TM3, TM5, TM6, and TM7) are in agreement with what is known about the mechanism of class A GPCR activation.

However, two motifs remained active for **ac-conformers** in all combinations: (i) the distance between the TM5 bulge and the ΔRMSD of the connector motif and (ii) the sodium-binding pockets. This can be attributed to the large volume occupied by the bound bromocriptine ligand in the orthosteric binding pocket, which leads to the partial activation of some motifs, such as CWxP and the sodium-binding pocket. These rearrangements did not extend throughout the entire receptor to the ionic lock, NPxxY, or other motifs because of the presence of the protomer in an inactive conformation. This would be seen as negative allosteric crosstalk, which has been reported for many heterodimers involving DRs [1297]. In contrast, the **ar-conformer** within the **ac-ar** dimer

appeared to possess a collapsed sodium pocket, although no ligand was bound to this conformer.

In contrast, the **ar-protomer** within the **in-ar** configuration displayed the same properties as its individual monomer, namely the properties of an active receptor, which seemed not to be influenced by its inactive protomer. **Ac-ac, ar-ar** and **ac-ar** dimers displayed larger variations after simulation, remaining, however, in an active form. Interestingly, we found that one protomer in the **ar-ar** configuration displayed asymmetric properties of active receptors. Their outward movement of TM6 was not as pronounced as that of the **ar-conformers**. In fact, one protomer of the **ar-ar** dimer transitioned to an active conformation when comparing the distance of the ionic lock and Y-Y motif, and showed that the **ar-protomers** in the **ar-ar** dimer behaved differently, pointing to two distinctive active-like states. We also observed slight differences between the homo-conformation and mixed conformation. The **ac-ac** configuration displayed the properties of activated protomers, but it was difficult to assign the conformational status of the **ac-ar** dimer. For some structural properties, the **ar-protomer** adopted values of an active conformation, whereas the **ac-protomer** appeared to be less active in the **ac-ar** configuration.

According to Caniceiro et al., most studies reported positive crosstalk for DR-DR dimers, and in some cases, this resulted in a hyperdopaminergic response, which other authors have linked to schizophrenia or the use of amphetamines [448,1297,1368]. Such an effect would be represented by configurations **ac-ac**, **ar-ar,** and **ac-ar**, where at least one bromocriptine was bound to the dimer. This is also in line with the results of Guo et al., who stated that ligand binding to one of the protomers would be enough to bind a G protein and cause conformational arrangements within the ligand-free protomer towards an active-like state [815,1304,1369]. For instance, a study with D_1R-D_3R heterodimers showed that coactivation of both receptors leads to a negative interaction at the level of adenylate cyclase, recruitment of β-arrestin-1, and selective activation of MAPK signaling mediated by a G protein-independent mechanism [490,491,1367]. Likewise, it has been reported that the D_2R-D_3R heterodimer could suppress forskolin-induced activation of adenylate cyclase at very high levels without the need for ligands [471,500,501]. One possible explanation for this is that, in the **ac-in** configuration, the **ac-protomer** adopts the conformation of an inactive receptor. The asymmetrical TM4-TM5-TM4-TM5 interface was not found for this dimer, which may prevent both protomers from reaching active-like conformations, as the **ac-protomer** does not contribute to TM4 at the interface.

This also supports the idea that in the **in-ar** configuration, where the **in-protomer** contributes TM3 and TM4 to the interface and the **ar-conformer** contributes TM4 and TM5, the correct conformations can be achieved, and both protomers are in an inactive or activated/intermediate state due to the absence of a ligand. Additionally, the results for the hydrophobic lock showed that the **ac-ar** configuration had the most active-like values for both protomers, suggesting that one **ac-monomer** alone may not be fully activated in the absence of a G protein. As only one protomer in the mixed conformations had a smaller binding site for the G protein, it could be assumed that it would be possible to bind only one G protein. Nevertheless, because the **ac-ac** and **ar-ar** dimers have similar binding site sizes for both protomers, this hypothesis does not seem to hold. In fact, the composition of the dimer interface and the presence of an agonist may affect

the size of the G protein binding area (and β-arrestin), supporting the 'rolling dimer' interface model proposed by Dijkman et al.[1357].

3.2.3.5. Key residues and pathogenic relevance

According to a study by Caniceiro et al., mutations of certain residues can have pathological consequences for DRs [1370]. For example, the presence of $Arg^{1.59}$, $Thr^{3.52}$, $Arg^{4.40}$, $Arg^{4.41}$, and $Val^{5.49}$ have been found in different dimer configurations. Guo et al. [1304] as well as other authors [1346,1371] reported that $Arg^{4.40}$, $Arg^{4.41}$, and $Arg^{1.59}$ were key residues, which led to changes in the secondary structure of the helix when mutated [1372]. In addition, $Arg^{4.40}$ was identified as a key residue in another study involving the 5-hydroxytryptamine 1A receptor and orexin receptor 1 heterodimer, changing its interface from TM4-TM5 in the basal state to TM6 in the active conformation [1371]. Zhang and coworkers also showed that mutations of $Arg^{4.40}$ can affect G protein binding [1371]. The ability of arginine residues to better accommodate hydrophobic mismatches at TM4 of GPCRs may explain why the mutation of $Arg^{4.40}$ can affect G protein binding [1373,1374]. Residues at positions 3.52 and $Arg^{4.41}$ have been found to be important for the formation of the TM4-TM5 interface for serotonin receptors [1346]. $Arg^{4.40}$ and $Arg^{4.41}$ can interact with the corresponding amino acids in the opposite protomer. $Arg^{1.59}$ has been reported to be relevant for G protein binding, particularly in the interaction between $G\alpha_s$ and $G\alpha_{i1}$ for the β_1-adrenoceptor [1375]. According to Wang et al., residues at position 3.52, $Thr^{3.52}$ for D_2R, would only be relevant for G protein binding if they were hydrophobic [1376,1377]. Overall, residues on TM4, such as $Arg^{4.40}$ and $Arg^{4.41,}$ are important for homo- and heterodimers comprising the TM4-TM5 interface and can be pathogenic when mutated. In addition, mutations in the residues at positions 1.59 and 3.52 may affect G protein binding.
Understanding GPCR homo- and heterodimers is of key relevance for the development of new biased drugs [1378] because these dimers can display unique allosteric properties, and the interface can be targeted with agents that either stabilize or disrupt the dimerization process.

3.2.4. Conclusion

The goal of our work was to develop a workflow for identifying GPCR homo- and heterodimer interfaces and to validate them with available experimental data. As proof of concept, we chose the D_2R-homodimer as it is a well-studied GPCR.
We found that the protomer interaction types were very specific to the type of dimer configuration and the formed interfaces and that they were stable over time, suggesting a conserved pattern. Most interactions were formed by loops (especially ICL2 and ECL2) rather than TMs, since loops have a higher electrostatic character, whereas TMs were mostly composed of nonpolar amino acids at favorable positions in the lipid bilayer. Highly conserved residues in TM4 and TM5 were rarely involved in forming interactions, and a large interface area correlated with the establishment of stabilizing interactions by TM residues. Our models are in good agreement with those reported in the literature, including in identifying the roles of important residues and TMs. For example, TM4 and TM5 were found to be critical for dimer formation, regardless of the conformational status of the protomers, which is consistent with experimental findings.

Using different conformations of one receptor, we gained insights into the dynamic nature of the D_2R homodimer by mapping and comparing known macro- and microswitches of class A GPCR activation. We found that the proposed dimer interfaces are physiologically stable and that different homodimer configurations and interfaces are possible, which are highly dynamic and possess fully or partially adapting features of activation/inactivation. Key conformational changes relevant to dimer function and signaling were also observed. We also identified a subset of mostly nonpolar key residues present in all dimer configurations located on TM4 and TM5 and observed that loops and neighboring TMs significantly contribute to dimer formation. It should also be noted that large conformational transitions in GPCRs require large-scale MD simulations, since such processes usually occur in the µs timescale [1379–1381].
This protocol can be easily applied to identify the interface of any type of GPCR homo- or heterodimer and will be a useful tool for understanding the molecular and structural properties of other dimers. Furthermore, it can be extended by adding ligands, G proteins, and β-arrestins, and will be useful for the development of dimer-targeting pharmaceuticals targeting different pathological conditions.

3.2.5. Material and Methods

3.2.5.1. Homology modeling

The receptors were modeled using the MODELLER package [1026] as previously described [1382]. As stated in Preto et al. an Ala_n linker was added to connect TM5 and TM6, which were modeled with an extended helical segment (beyond the membrane) up to the linker, making the intracellular extension of these helices similar to that observed in the crystal structure of the β_2-adrenergic receptor (β_2AR)-Gs complex (PDB-id: 3SN6 [118]) and therefore corresponds to the D_{2short} isoform [1382]. D_2R was modeled in three different conformations. The D_2R inactive (**in**) was based on the structure of the D_2R bound to risperidone (PDB-id: 6CM4 [1323]), whereas the D_2R active (**ac**) (G protein-bound) was based on the D_2R-G protein complex (PDB-id: 6VMS [1324]). The D_2R β-arrestin-bound conformation (**ar**) was modeled using the M2 muscarinic acetylcholine receptor (M_2R)-β-arrestin-complex (PDB-id: 6U1N [1383]) as a template.

3.2.5.2. Dimer assembly protocol

The Kaczor et al. [1302,1310] pipeline was used to construct the D_2R homodimers. The protocol was applied for each configuration of the D_2R homodimer: inactive-inactive (6CM4-6CM4/**in-in**), two configurations of the active-active (6VMS-6VMS/**ac-ac** and 6VMS-6VMS-B/**ac-ac-B**, as a result of consensus scoring), arrestin-arrestin (6U1N-6U1N/**ar-ar**), active-inactive (6VMS-6CM4/**ac-in**), inactive-arrestin (6CM4-6U1N/**in-ar**) and active-arrestin (6VMS-6U1N/**ac-ar**).

3.2.5.4. Initial set of dimers

The initial set of possible dimer interfaces (composed of 144 conformational arrangements) was obtained by rotating one monomer around the other in steps of 30

degrees. This task was performed using the Visual Molecular Dynamics (VMD) tcl script [1384] provided by Kaczor et al. [1302,1310].

3.2.5.5. Protein-protein docking in Rosetta

Protein-protein docking using Rosetta [1385] was applied to obtain 10 models per interface, resulting in a total of 1440 models. The docking was run in "*refine only*" mode to generate dimers compatible with membrane integration (as suggested by Kaczor et al.) [1302,1310]. Additionally, all 1440 models were analyzed using the *InterfaceAnalyzer* implemented by Rosetta [1385]**.**

3.2.5.6. Scoring parameters and scoring procedure

In our study, we used scoring parameters similar to the default ones, as they were previously considered capable of reproducing the interfaces from X-ray structure dimers [1302]. We used the Rosetta interface score (I_sc), the solvent-accessible area buried at the interface (dSASA, like interface area), the free energy of binding (dG_ separated), the energy of hydrogen bond interactions (hbond_E_fraction), and the number of residues at the interface (nres_int). All scores were provided by *InterfaceAnalyzer [1385]*, except for the Rosetta Interface score (I_sc), which is a direct output of the protein-protein docking procedure [1385]. The number of residues at the interface (nres_int) was additionally chosen, assuming that a relevant interface would have a higher number of stabilizing interactions and that the different combinations of conformations would likely involve a varying number of residues.

Two methods of consensus scoring were used, as previously described [1310]: (i) average scores of the 100 best-scored dimers concerning each interface and (ii) frequencies of the interfaces among the 100 best-scoring dimers. Before consensus scoring, values were normalized between 0 and 1. These two scoring methods were chosen to avoid bias when using only one, and the top-scoring model would be found with both methods. Similar to Kaczor et al. [1302], we set the most favorable value of a given scoring factor in the normalization process to 1 and subsequently adjusted the other values. For dG_separated and hbond_E_fraction, negative values were considered favorable, whereas, for dSASA and nres_int, positive values were considered favorable. For I_sc, Rosetta documentation considers values from -5 to -10 as a good interface score (https://www.rosettacommons.org/docs/latest/application_documentation/docking/docking protocol). To obtain the most favorable value for performing subsequent scoring, the mean of all 1440 models with an I_sc within this range was calculated upon normalization. Scores closest to 1 (range, 1.2, and 0.9) were selected for further evaluation.

The best interface for each configuration of the D_2R homodimer was chosen based on the ranking of each parameter (the top three were considered). After determining the interface, all models (of the pool of 1440 models) possessing this interface were ranked again. The top three models were considered for the selection of the final model. These were submitted for a quality evaluation.

3.2.5.7. Quality evaluation of the final dimers

The chosen representative model for each configuration of the D_2R homodimer was analyzed using PRODIGY-CRYSTAL, a machine-learning algorithm trained to distinguish between biologically relevant complexes and crystallization artifacts [1329–1331]. PRODIGY [1331,1386,1387] was used to estimate the binding affinity, dissociation constant, and listing of interfacial residues. Finally, the predicted residues of PRODIGY-CRYSTAL and PRODIGY-PROTEIN were compared to define the dimer interfaces of the selected models. Selected dimers were inserted into a lipid bilayer system and subjected to MD simulations. To easily locate relevant residues and important motifs and to compare them to other GPCRs, residues were annotated using Ballesteros and Weinstein nomenclature [96]. According to this nomenclature, the first digit identifies the TM helix, and the second digit identifies the residue position in relation to the most conserved residues on each helix (assigned index number X.50). Subsequently, the number decreases towards the N-terminus and increases towards the C-terminus [70,96].

3.2.5.8. Molecular dynamics simulations

Membrane orientation
Protein orientation in the membrane was obtained using the OPM-PPM-server for every modeled dimer structure (https://opm.phar.umich.edu/ppm_server) [1388].

System building
The dimer structures (as well as the monomers to be used as controls) were inserted into a lipid bilayer membrane in a cubic simulation box hydrated with TIP3 waters and 0.15 M NaCl using CHARMM-GUI Membrane Builder (http://www.charmm-gui.org) [1389–1392]. Termini ACE (or ACP in the case of D_2R **ac-monomer**)/CT1 were used as caps at the N- and C-termini. Disulfide bonds were established between residues 79/154 and 249/251 in the **in-monomer** and **ar-monomer** structures, respectively. Since the template structure of the **ac-monomer** (6VMS) was found to be three amino acids shorter at the N-terminus, their disulfide bonds involved residues 76/151 and 246/248. Palmitoylation of the last Cys residue (Cys293 for **in-monomer**, **ar-monomer**, or Cys290 for **ac-monomer**) was performed. The protonation state of the important Asp at position 2.50 was defined as follows: for the D_2R **in-monomer,** it was charged (not protonated), whereas, for the D_2R **ar-monomer** (residue 52) and **ac-monomer** (residue 49), it was set to neutral (protonated), as upon class A GPCR activation, protonation of $Asp^{2.50}$ takes place due to dehydration and displacement of the $Asp^{2.50}$-bound sodium ion [130,133,134,1336,1341]. Owing to the importance of water molecules for GPCR activation, [1341] we also added pore water using protein geometry. A heterogeneous lipid bilayer was built around the dimer structures with POPC and cholesterol (CHL1) (ratio 9:1), with 240 lipids in each leaflet (for the monomers, a total of 100 lipids per leaflet was chosen). The size of the x/y plane is based on the number of lipid components. The box was rectangular, and its hydration number was set to 100 (100 water molecules per lipid). The D_2R **ac-monomer** (single and part of the dimer) also contains the co-crystallized ligand bromocriptine in the same orientation as in the 6VMS crystal structure

(PDB-id:6VMS [1324]). Consequently, the **ac-ac** dimer possesses two ligands, one per receptor. The ligand itself was parameterized using the CHARMM-GUI ligand reader and modeller [1393] and added to the system while building CHARMM-GUI. CHARMM36m was selected as the force field [1390]. The remaining options were set to default.

Molecular dynamics parameters

MD simulations were performed using GROMACS 2019.4 and the CHARMM36m force field [1242,1390,1394,1395]. The systems were simulated using the NPT (isothermal-isobaric) ensemble. To achieve and maintain the desired temperature (310 K), a v-rescale thermostat was used, with a coupling constant of 0.1 ps [1396]. Pressure coupling was performed using a semi-isotropic Parrinello-Rahman barostat at 1 bar with a compressibility of 4.5×10^{-5} bar^{-1} and a coupling constant of 1.0 ps [1397,1398]. Electrostatic interactions were computed with the particle-mesh Ewald (PME) method with a Fourier grid of 0.12 nm and a cut-off of 1.2 nm for direct contributions [1113,1114]. Lennard-Jones interactions were computed using a non-bonded neighbor pair list with a cut-off of 1.2 nm, enabling the use of the Verlet scheme [1399]. Solute bonds were constrained using the Parallel LINear Constraint Solver, P-LINCS [1241]. The steepest descent algorithm was used to minimize the initial energy of the system through a 50,000-step run [1400]. The systems were then initialized for 25 ns: five runs of 5 ns each with successively lower constraints for lipid heavy atoms and protein carbon alpha (1.000, 500, 100, 10, and 0 kJ nm^{-2} mol^{-1}). Three replicates (500 ns long) were performed for each dimer configuration and monomer, and the initial 200 ns were discarded to ensure a good system equilibration.

3.2.5.9. Analysis

Plots were generated using GraphPad Prism (GraphPad Prism Version 8.1.0, GraphPad Software, San Diego, California USA, www.graphpad.com) and Gnuplot (Gnuplot Version 5.2, Williams, T., and Kelley, C., www.gnuplot.info). Residue-residue interactions were determined using GetContacts (https://getcontacts.github.io/interactions.html), and flare plots were created using gpcrviz.github.io/flareplot/?p=create. All remaining calculations were performed using in-house scripting.

We focused our analyses on the transmembrane helices, loops, and structural motifs, including DRY ($Asp^{3.49}$, $Arg^{3.50}$, and $Tyr^{3.51}$), CWxP ($Cys^{6.47}$, $Trp^{6.48}$, $Leu^{6.49}$, and $Pro^{6.50}$), ionic lock ($Arg^{3.50}$ and $Glu^{6.30}$), NPxxY ($Asn^{7.49}$, $Pro^{7.50}$, $Ile^{7.51}$, $Ile^{7.52}$, and $Tyr^{7.53}$), PIF ($Pro^{5.50}$, $Ile^{3.40}$ and $Phe^{6.44}$), arginine cage ($Ile^{3.46}$ and $Leu^{6.37}$), serine microdomain ($Ser^{5.42}$, $Ser^{5.43}$,and $Ser^{5.46}$), and rotamer toggle switch ($Trp^{6.48}$, $Phe^{6.51}$, $Phe^{6.52}$, and $His^{6.55}$), which were previously described as important determinants of the GPCR activation mechanism[70,97,182]. The following calculations were performed: (i.) the distance over time between a subset of residues located roughly at the center of each TM and the average position of the membrane using its phosphorus atoms as references; (ii.) the root-mean-square-deviation (RMSD) of the TM and the other mentioned domains; (iii.) the relative dimer orientation by calculating two pseudo-dihedral angles along the MD simulations: θ1 consisting of residues $Phe^{1.48}$, $Ser^{4.53}$, $Ile^{4.56}$ from protomer 1 and $Ile^{4.56}$ from protomer 2; and θ2, consisting of residues $Phe^{1.48}$, $Ser^{4.53}$, $Ile^{4.56}$ from protomer 2 and $Ile^{4.56}$ from protomer 1; (iv.) the solvent-accessible

surface area (SASA); (v.) the number of intermolecular H- bonds, salt bridges, π-cation, π-stacking and T-stacking interactions using GetContacts; (vii.) pairwise distances between Cα-Cα of interfacial residues; (viii.) TM5 bulge as the distance between the heavy atoms of $Ser^{5.46}$ and $Leu^{7.41}$; (ix.) ΔRMSD as the difference between the average RMSD of $Ile^{3.40}$ and $Phe^{6.44}$ heavy atoms and the inactive and active structures 2RH1 [974] and 3P0G [980], respectively; (x.) angles between the centroids of the benzene ring of three phenylalanines $Phe^{5.51}$, $Phe^{6.44}$ and $Phe^{6.45}$ over time; (xi.) distance between the Cα atom of $Asp^{2.50}$ and the closest sodium atom; (xii.) number of water molecules within an 8 Å distance cut-off of $Asp^{2.50}$; (xiii.) the angles between the Cγ atom of $Lys^{3.43}$, the Cβ atom of $Val^{6.41}$, and the Cβ atom of $Ile^{6.40}$; (xiv.) RMSD of the NPxxY domain and the distance between Cα atoms of residues of the ionic lock, $Arg^{3.50}$ and $Glu^{6.30}$; (xv.) size of the binding sites for G protein and β-arrestin using the SASA values of relevant residues and normalized to the $SASA_{max}$ values determined earlier for each type of amino acid.

3.2.5.10. Data availability

Flare plots were published in Zenodo (10.5281/zenodo.7515851)**.** Additional information can be found in Chapter 7.2., containing the tables (S1-S5) and 29 figures, which present the following information: S6 - Results of the consensus scoring for the D_2R-homodimer configurations; S7 - Distance of the phospholipids of the lipid bilayer and a geometric membrane center as measure for equilibration of the D_2R homodimer configurations; S8 - Root-mean-square-deviations calculated for backbone, transmembrane helices, loops and structural motifs such as DRY, CWxP, ionic lock, NPxxY, PIF, arginine cage, serine microdomain, rotamer toggle switch of the D_2R homodimer configurations and monomers, which were followed over time; S9 - Orientation of the D_2R homodimer configurations followed over time by measuring the angles θ1 and θ2; S10- Interface area over time; S11 - Decoy original interface residues of the D_2R homodimer configurations; S12 - Types of interaction of the original interface; S13 - General activation mechanism of class A GPCRs; S14 - Distance between TM3 and TM6 over time; S15 - Distance between TM3 and TM7 over time; S16 - Distance between TM3 and TM6 vs. the distance TM3 and TM7 for the monomers; S17 - Distance between TM3 and TM6 vs. the distance TM3 and TM7 for the D_2R homodimer configurations; S18 - Distance between TM3 and TM6 vs. the distance between TM5 and TM7 (YY motif) for the monomers; S19 - Distance between TM3 and TM6 vs. the distance between TM5 and TM7 (YY motif) for the D_2R homodimer configurations; S20 - Comparison of Cα-atom distances between TM5-TM7 (5.58-7.41) and the dRMSD of a connector module, consisting of residues 3.40 (F of PIF motif) and 6.44 (I of PIF motif) for the monomers; S21 - Distance TM5-TM7 vs. angle of Cα atoms of 6.34-6.47-2.41 for the monomers; S22- Comparison of the angle between residues 6.34-6.47-2.41 and the distance between the Cα-atoms of residues 5.55 and 7.46 for the D_2R homodimer configurations; S23 - Angle of benzene centroids of residues Phe5.51, Phe6.44 and Ile6.45 followed over time; S24 - Comparison of Cα-atom distances between 3.50 and 6.34 (TM3-TM6) representing the ionic lock and between Asp2.50 and the closest sodium atom for the monomers; S25 - Opening of the hydrophobic lock measured as the area of the angle composed by the Cγ atom of residue 3.43, the Cβ of residue 6.41 and 6.40 and followed over time; S26 - Angle χ1 of the conserved tyrosine 7.53 followed over time; S27 - Angle

χ2 of the conserved tyrosine 7.53 followed over time; S28 - Comparison of the dihedral angles χ1 and χ2 of Tyr7.53 for the monomers; S29 - Comparison of the dihedral angles χ1 and χ2 of Tyr7.53 for the D_2R homodimer configurations; S30 - Comparison of the distance between residues of the ionic lock and the RMSD of the NPxxY motif for the monomers; S31 - Comparison of the NPxxY motif using RMSD and dSASA for the monomers; S32 - Comparison of RMSD and dSASA of the NPxxY motif of the D_2R homodimer configurations; S33 - Sizes of binding site the for the G protein over time; S34 - Sizes of binding site the for β-arrestin over time.

Chapter 4: Conclusions and future work

This chapter summarizes the main findings of this study and evaluates the relevance for the scientific community. In addition, an outlook is given how the study could be continued in the future. Furthermore, a publication list is enclosed with all papers published during the PhD period.

4.1. Main contributions

PPIs play a crucial role in cellular signaling and are fundamental to the functioning of various biological processes[88,437,1398]. Among the diverse range of proteins in the human body, GPCRs are of great importance and are the highest targeted protein class for pharmaceuticals, with over 30% of FDA-approved drugs being the primary targets for drug discovery and design[35,1296]. In this study, we investigated the PPIs between known and orphan GPCRs.

Although monomeric GPCR downstream signaling is already complex, since GPCRs mediate almost all physiological functions, the concept of PPIs between GPCRs upon dimerization and oligomerization adds another level of complexity to be elucidated[78,88]. Hence, understanding the interactions between GPCRs and other proteins sheds light on their activation, regulation, and altered downstream signaling cascades. Additionally, by identifying non-GPCR proteins that interact with GPCRs, new molecular mechanisms can be identified. Consequently, PPIs involving GPCRs have immense implications in drug discovery and development.
Putting PPIs in a larger context has broader implications for systems biology and network pharmacology because they are considered integral components of biological networks [1399,1400]. Over the years rather a system-level understanding of biological processes has emerged for which PPIs are crucial nodes within such a network/system. Furthermore, this knowledge guides network pharmacology approaches in which drugs are designed to modulate multiple targets within a network to achieve multiple therapeutic effects.
GPCRs are interactive systems which closely associate with other proteins and molecules within the cell and extracellular space. Furthermore, the allosteric interactions of ligands towards their GPCRs also transferred onto interactions between GPCRs and partnered proteins.

We investigated the allosteric effect within the GPCR-dimers using pharmacological and computational methods.

Part 1:
We discovered a new GPCR-dimer between D_2R and D_3R with GPR143, an orphan receptor, with an undefined physiological role. Hence, this finding is an important

advancement in our understanding of the potential role of GPR143, which is still an orphan receptor. GPR143 is primarily related to pigmentation of skin, hair, and other tissues[1245]. Genetic mutations in the GPR143 gene, resulting in impaired function of the receptor, trigger X-linked OA1, leading to altered melanosome development and melanin distribution in melanocytes. This disruption affects the normal development and function of the retina, resulting in reduced visual acuity, nystagmus (involuntary eye movements), and light sensitivity[1258,1265,1270,1401]. It is known that GPR143 is able to interact with other proteins[1402] such as melanoma antigen recognized by T-cells (MART-1)[1264], tyrosinase[1245], tubulin[1265], master regulator of melanocyte differentiation (MITF) and premelanosome protein (PMEL)[1285], among many more. GPR143 has already been reported to interact with a GPCR. For instance, Masukawa et al. determined that α1b-adrenoceptor and GPR143 can form functional heteromers that modulate noradrenaline-mediated regulation of blood pressure[1267,1403].
In our study, the two DRs and GPR143 were shown to physiologically interact with each other, with GPR143 negatively modulating the DR activity in response to dopamine. The discovery of a new GPCR dimer involving D_2R and D_3R and GPR143 represents an important advancement in our understanding of these receptors and their interactions.
We took advantage of pharmacological assays, in this case the β-arrestin recruitment assay, which enabled us to monitor GPR143-DR interactions in functional cell systems, and showed that GPR143 significantly reduced the affinity of DR for its endogenous ligand dopamine (by 57% for D_2R and 67% for D_3R) at an amplitude similar to that of the D_2R-A_{2A}AR-dimer[75,519]. Furthermore, we showed that GPR143-DR-complexes were mostly located in vesicles in the intracellular space, even when DRs were complexed with the plasma membrane-localized GPR143 variant, pmGPR143, using confocal microscopy and two FRET methods. Overall, the combination of pharmacological assays and fluorescence microscopy provides a comprehensive approach for studying GPR143-DR interactions and their functional consequences. This research has shed light on a previously unknown dimerization between these receptors, revealed the negative modulatory role of GPR143 in DR activity, and provided valuable insights into the subcellular localization and functional consequences of GPR143-DR complexes.

Part 2:
In the second part of this work, we gained insight into the structural basis of GPCR dimerization from a computational perspective using the D_2R-homodimer. We developed a computational framework to generate dimer models with different combinations of protomer conformations: active, inactive, and β-arrestin-bound. The aim was to understand the interfaces and molecular details of these dimeric structures and to investigate the impact of different monomer activation states on the overall quaternary structure and dynamics.
We discovered that TM4 and TM5 are frequently found at the dimer interface of the D_2R-homodimer. These regions contain a subset of key residues, mostly nonpolar, which play a significant role in mediating the dimerization process. This observation suggests that TM4 and TM5 are critical for stabilizing the D_2R-homodimer, which is supported by experimental findings[472,1312,1313]. In addition, this interface combination can be superimposed on other GPCR dimers and has already been described for other cases; however, TM1, TM2, TM4 and TM5, are often involved in forming the dimer interface in GPCR dimers[1316,1343,1345]. Apart from TM4 and TM5, we also found that TM2 and

TM3 in certain combinations within the dimers can also be relevant for the interface. Hence, we conclude from these results that variations exist not only between receptor subtypes and combinations, but also between the conformational combinations of partnered protomers. This might also have functional implications, such as ligand binding and residues relevant for stabilizing the dimer interface; hence, we also determined the key residues that we propose to be crucial for the TM4-TM5 interface. Furthermore, we demonstrated that for certain combinations, the conformational status of one protomer within the dimer could influence the behavior of its partner protomer, which underlines the dynamic nature of the GPCR dimers. We showed that one protomer can adopt the conformational properties of its partner. Such conformational mimicry indicates that the rotation or tilting of TMs or repositioning of extracellular loops can impact the stability and geometry of the dimer interface. This can affect the strength and specificity of the dimeric interaction, leading to changes in the signaling properties or ligand-binding affinity of the partner protomer. We showed that such a flow of information through the interface existed for specific combinations, such as for the active-inactive dimer, where the active protomer adopted an inactive conformation, although a ligand was bound to its binding pocket.

Overall, this approach contributes to our understanding of the molecular mechanisms underlying GPCR dimerization and its functional consequences. This provides a foundation for further investigations into the complex nature of GPCR interactions and their roles in cellular signaling pathways. The conformational changes and interactions described within DRD_2-homodimers can also be extrapolated to modulate the ligand-binding affinity, signaling efficacy, and desensitization kinetics of the receptors. Finally, the computational framework developed in this study can be adapted to study other GPCR dimers, including heterodimers, and potentially extended to include additional proteins, such as G proteins or β-arrestins, which are known to interact with GPCRs.

4.2. Future Work

Investigation of PPIs between known and orphan GPCRs is of immense importance in various areas of biological research. Understanding these interactions contributes to the further functional characterization of GPCRs, aids in drug discovery and development, provides information for receptor deorphanization, unravels possible new signal transduction networks, and advances the field of systems biology. The investigation of these interactions opens new avenues for understanding the complexity of cellular processes and holds significant potential for the development of novel therapeutic interventions in the future.

The findings of this study suggest that GPR143 may modulate DR activity through two potential mechanisms: by sequestering the receptors away from the plasma membrane and/or by allosterically modulating the binding pocket of the DRs, resulting in a lower affinity for dopamine binding. The precise mechanism remains to be determined through further experimental investigation. Experimental approaches, such as co-immunoprecipitation, proximity ligation assays, and live-cell imaging techniques, should be employed to examine the physical interaction between GPR143 and the DRs, as well as to further elucidate their cellular localization patterns in other cell types, such as the retinal pigment epithelium and other GPR143-expressing cells, to determine if the

interaction is robust. Additionally, mutagenesis studies and functional assays can be performed to identify key residues or domains involved in the interaction and determine their impact on DR activity.

By elucidating the precise mechanisms by which GPR143 influences DR activity, we can gain a more comprehensive understanding of the complex interplay between these receptors and potentially identify novel therapeutic targets for conditions involving dysregulated dopamine signaling.

The experimental validation of the D_2R-homodimer will be relevant for future studies. For instance, the conformational changes and interactions described within D_2R homodimers can be expanded to modulate the ligand-binding affinity, signaling efficacy, and desensitization kinetics of the receptors, which helps to further investigate the functional consequences of dimerization. Experimental validation can be achieved using techniques, such as site-directed mutagenesis, cell-based pharmacological assays, and structural determination methods, such as X-ray crystallography or cryo-EM. Experimental verification of the predicted dimer interfaces and their key residues would provide further insight into the molecular and structural basis of GPCR dimerization. Understanding how dimerization influences ligand-binding affinity, signaling pathways, and cellular responses would have implications for drug discovery and therapeutic interventions targeting GPCRs.

In addition, the computational framework developed in this study can be extended to investigate the dimerization of GPCRs with different subtypes (heterodimers). By applying the same approach to heterodimers, this study provides a deeper understanding of the molecular mechanisms underlying the dimerization of different GPCR subtypes and explores the implications for signaling and functional outcomes. In addition, the potential extension of the computational framework to include additional proteins such as G proteins or β-arrestins would be helpful. Investigating the interactions and conformational dynamics of GPCRs with these downstream effectors in the context of dimerization would enhance our understanding of intricate signaling networks.

Finally, the integration of experimental and computational approaches to constantly improve models will be a comprehensive and integrated approach for studying GPCR dimerization in general. This iterative interplay between the computational and experimental methods can further refine the models and enhance our understanding of GPCR dimers.

4.3. Publications

- **Bueschbell B**, Manga P, Penner E, Schiedel AC. Evidence for Protein-Protein Interaction between Dopamine Receptors and the G Protein-Coupled Receptor 143. Int J Mol Sci. **2021** Aug 3;22(15):8328. doi: 10.3390/ijms22158328. PMID: 34361094; PMCID: PMC8348196.

- Preto AJ, Marques-Pereira C, Baptista SJ, **Bueschbell B**, Carlos Barreto CAV, Gaspar AT, Pinheiro I, Pereira, Pires M, Ramalhão D, Silvério D, Rosário-Ferreira N, Melo R, Mourão J, Moreira IS. 2.08 - Targeting GPCRs Via Multi-Platform Arrays and AI, Editor(s): Terry Kenakin, Comprehensive Pharmacology,

Elsevier, **2022**, Pages 135-162, ISBN 9780128208762, https://doi.org/10.1016/B978-0-12-820472-6.00048-7.

- Caniceiro AB, **Bueschbell B**, Schiedel AC, Moreira IS. Class A and C GPCR Dimers in Neurodegenerative Diseases. Curr Neuropharmacol. **2022**;20(11):2081-2141. doi: 10.2174/1570159X20666220327221830. PMID: 35339177; PMCID: PMC9886835.

- **Bueschbell B**, Caniceiro AB, Suzano PMS, Machuqueiro M, Rosário-Ferreira N, Moreira IS. Network biology and artificial intelligence drive the understanding of the multidrug resistance phenotype in cancer. Drug Resist Updat. **2022** Jan;60:100811. doi: 10.1016/j.drup.2022.100811. Epub 2022 Jan 28. PMID: 35121338.

- Caniceiro AB, **Bueschbell B**, Barreto CAV, Preto AJ, Moreira IS. MUG: A mutation overview of GPCR subfamily A17 receptors. Comput Struct Biotechnol J. **2022** Dec 21;21:586-600. doi: 10.1016/j.csbj.2022.12.031. PMID: 36659920; PMCID: PMC9822836.

5. Bibliography

1. Azam S, Haque ME, Jakaria M, Jo S-H, Kim I-S, Choi D-K. G-Protein-Coupled Receptors in CNS: A Potential Therapeutic Target for Intervention in Neurodegenerative Disorders and Associated Cognitive Deficits. Cells. 2020;9. doi:10.3390/cells9020506

2. Przedborski S, Vila M, Jackson-Lewis V. Neurodegeneration: what is it and where are we? J Clin Invest. 2003;111: 3–10. doi:10.1172/JCI17522

3. Jakaria M, Azam S, Cho D-Y, Haque ME, Kim I-S, Choi D-K. The Methanol Extract of Allium cepa L. Protects Inflammatory Markers in LPS-Induced BV-2 Microglial Cells and Upregulates the Antiapoptotic Gene and Antioxidant Enzymes in N27-A Cells. Antioxidants. 2019. p. 348. doi:10.3390/antiox8090348

4. Jakaria, Jakaria, Azam, Jo, Kim, Dash, et al. Potential Therapeutic Targets of Quercetin and Its Derivatives: Its Role in the Therapy of Cognitive Impairment. Journal of Clinical Medicine. 2019. p. 1789. doi:10.3390/jcm8111789

5. Huang Y, Todd N, Thathiah A. The role of GPCRs in neurodegenerative diseases: avenues for therapeutic intervention. Curr Opin Pharmacol. 2017;32: 96–110. doi:10.1016/j.coph.2017.02.001

6. Arlt S. Non-Alzheimer's disease-related memory impairment and dementia. Dialogues Clin Neurosci. 2013;15: 465–473. doi:10.31887/DCNS.2013.15.4/sarlt

7. Bertram L, Tanzi RE. The genetic epidemiology of neurodegenerative disease. J Clin Invest. 2005;115: 1449–1457. doi:10.1172/JCI24761

8. Lemos A, Melo R, Preto AJ, Almeida JG, Moreira IS, Dias Soeiro Cordeiro MN. In Silico Studies Targeting G-protein Coupled Receptors for Drug Research Against Parkinson's Disease. Curr Neuropharmacol. 2018;16: 786–848. doi:10.2174/1570159X16666180308161642

9. Serrano-Pozo A, Frosch MP, Masliah E, Hyman BT. Neuropathological alterations in Alzheimer disease. Cold Spring Harb Perspect Med. 2011;1: a006189. doi:10.1101/cshperspect.a006189

10. Lopez OL. The growing burden of Alzheimer's disease. Am J Manag Care. 2011;17 Suppl 13: S339–45. Available: https://www.ncbi.nlm.nih.gov/pubmed/22214391

11. Dickerson BC, Bakkour A, Salat DH, Feczko E, Pacheco J, Greve DN, et al. The cortical signature of Alzheimer's disease: regionally specific cortical thinning relates to symptom severity in very mild to mild AD dementia and is detectable in asymptomatic amyloid-positive individuals. Cereb Cortex. 2009;19: 497–510.

doi:10.1093/cercor/bhn113

12. Kalia LV, Lang AE. Parkinson's disease. Lancet. 2015;386: 896–912. doi:10.1016/S0140-6736(14)61393-3

13. Yassi N, Desmond PM, Masters CL. Magnetic Resonance Imaging of Vascular Contributions to Cognitive Impairment and Dementia. J Mol Neurosci. 2016;60: 349–353. doi:10.1007/s12031-016-0799-3

14. Kalaria RN. Neuropathological diagnosis of vascular cognitive impairment and vascular dementia with implications for Alzheimer's disease. Acta Neuropathol. 2016;131: 659–685. doi:10.1007/s00401-016-1571-z

15. Warren JD, Rohrer JD, Rossor MN. Clinical review. Frontotemporal dementia. BMJ. 2013;347: f4827. doi:10.1136/bmj.f4827

16. Jicha GA, Nelson PT. Management of frontotemporal dementia: targeting symptom management in such a heterogeneous disease requires a wide range of therapeutic options. Neurodegener Dis Manag. 2011;1: 141–156. doi:10.2217/nmt.11.9

17. Ross CA, Aylward EH, Wild EJ, Langbehn DR, Long JD, Warner JH, et al. Huntington disease: natural history, biomarkers and prospects for therapeutics. Nat Rev Neurol. 2014;10: 204–216. doi:10.1038/nrneurol.2014.24

18. Andrew SE, Goldberg YP, Kremer B, Telenius H, Theilmann J, Adam S, et al. The relationship between trinucleotide (CAG) repeat length and clinical features of Huntington's disease. Nat Genet. 1993;4: 398–403. doi:10.1038/ng0893-398

19. Gutekunst CA, Li SH, Yi H, Mulroy JS, Kuemmerle S, Jones R, et al. Nuclear and neuropil aggregates in Huntington's disease: relationship to neuropathology. J Neurosci. 1999;19: 2522–2534. doi:10.1523/JNEUROSCI.19-07-02522.1999

20. Hinz FI, Geschwind DH. Molecular Genetics of Neurodegenerative Dementias. Cold Spring Harb Perspect Biol. 2017;9. doi:10.1101/cshperspect.a023705

21. Dickson DW, Ahmed Z, Algom AA, Tsuboi Y, Josephs KA. Neuropathology of variants of progressive supranuclear palsy. Curr Opin Neurol. 2010;23: 394–400. doi:10.1097/WCO.0b013e32833be924

22. Braak H, Thal DR, Ghebremedhin E, Del Tredici K. Stages of the pathologic process in Alzheimer disease: age categories from 1 to 100 years. J Neuropathol Exp Neurol. 2011;70: 960–969. doi:10.1097/NEN.0b013e318232a379

23. Dugger BN, Hentz JG, Adler CH, Sabbagh MN, Shill HA, Jacobson S, et al. Clinicopathological outcomes of prospectively followed normal elderly brain bank volunteers. J Neuropathol Exp Neurol. 2014;73: 244–252. doi:10.1097/NEN.0000000000000046

24. Dugger BN, Dickson DW. Pathology of Neurodegenerative Diseases. Cold Spring

Harb Perspect Biol. 2017;9. doi:10.1101/cshperspect.a028035

25. Jabeen A, Ranganathan S. Applications of machine learning in GPCR bioactive ligand discovery. Curr Opin Struct Biol. 2019;55: 66–76. doi:10.1016/j.sbi.2019.03.022

26. Saikia S, Bordoloi M, Sarmah R. Established and In-trial GPCR Families in Clinical Trials: A Review for Target Selection. Curr Drug Targets. 2019;20: 522–539. doi:10.2174/1389450120666181105152439

27. Sensoy O, Almeida JG, Shabbir J, Moreira IS, Morra G. Computational studies of G protein-coupled receptor complexes: Structure and dynamics. Methods Cell Biol. 2017;142: 205–245. doi:10.1016/bs.mcb.2017.07.011

28. Guerram M, Zhang L-Y, Jiang Z-Z. G-protein coupled receptors as therapeutic targets for neurodegenerative and cerebrovascular diseases. Neurochem Int. 2016;101: 1–14. doi:10.1016/j.neuint.2016.09.005

29. Heng BC, Aubel D, Fussenegger M. An overview of the diverse roles of G-protein coupled receptors (GPCRs) in the pathophysiology of various human diseases. Biotechnol Adv. 2013;31: 1676–1694. doi:10.1016/j.biotechadv.2013.08.017

30. Rosenbaum DM, Rasmussen SGF, Kobilka BK. The structure and function of G-protein-coupled receptors. Nature. 2009;459: 356–363. doi:10.1038/nature08144

31. Fredriksson R, Lagerström MC, Lundin L-G, Schiöth HB. The G-protein-coupled receptors in the human genome form five main families. Phylogenetic analysis, paralogon groups, and fingerprints. Mol Pharmacol. 2003;63: 1256–1272. doi:10.1124/mol.63.6.1256

32. Jabeen A, Vijayram R, Ranganathan S. BIO-GATS: A Tool for Automated GPCR Template Selection Through a Biophysical Approach for Homology Modeling. Front Mol Biosci. 2021;8: 617176. doi:10.3389/fmolb.2021.617176

33. Miyagi H, Asada H, Suzuki M, Takahashi Y, Yasunaga M, Suno C, et al. The discovery of a new antibody for BRIL-fused GPCR structure determination. Sci Rep. 2020;10: 11669. doi:10.1038/s41598-020-68355-x

34. Zhang Y, DeVries ME, Skolnick J. Structure Modeling of All Identified G Protein–Coupled Receptors in the Human Genome. PLoS Comput Biol. 2006;2: e13. doi:10.1371/journal.pcbi.0020013

35. Hauser AS, Attwood MM, Rask-Andersen M, Schiöth HB, Gloriam DE. Trends in GPCR drug discovery: new agents, targets and indications. Nat Rev Drug Discov. 2017;16: 829–842. doi:10.1038/nrd.2017.178

36. Huang Y, Thathiah A. Regulation of neuronal communication by G protein-coupled receptors. FEBS Lett. 2015;589: 1607–1619. doi:10.1016/j.febslet.2015.05.007

37. Betke KM, Wells CA, Hamm HE. GPCR mediated regulation of synaptic

transmission. Prog Neurobiol. 2012;96: 304–321. doi:10.1016/j.pneurobio.2012.01.009

38. Snyder SH, Innis RB. Peptide neurotransmitters. Annu Rev Biochem. 1979;48: 755–782. doi:10.1146/annurev.bi.48.070179.003543

39. Lodish H, Berk A, Zipursky SL, Matsudaira P. Neurotransmitters, synapses, and impulse transmission. Mol Cell Biol Res Commun.

40. Hall RA. Beta-adrenergic receptors and their interacting proteins. Semin Cell Dev Biol. 2004;15: 281–288. doi:10.1016/j.semcdb.2003.12.017

41. Pytliak M, Vargová V, Mechírová V, Felšöci M. Serotonin receptors - from molecular biology to clinical applications. Physiol Res. 2011;60: 15–25. doi:10.33549/physiolres.931903

42. Hoyer D, Bartfai T. Neuropeptides and neuropeptide receptors: drug targets, and peptide and non-peptide ligands: a tribute to Prof. Dieter Seebach. Chem Biodivers. 2012;9: 2367–2387. doi:10.1002/cbdv.201200288

43. Kruse AC, Kobilka BK, Gautam D, Sexton PM, Christopoulos A, Wess J. Muscarinic acetylcholine receptors: novel opportunities for drug development. Nat Rev Drug Discov. 2014;13: 549–560. doi:10.1038/nrd4295

44. Vaidya A, Jain S, Jain AK, Agrawal A, Kashaw SK, Jain SK, et al. Metabotropic glutamate receptors: a review on prospectives and therapeutic aspects. Mini Rev Med Chem. 2013;13: 1967–1981. doi:10.2174/1389557511313130010

45. Beaulieu J-M, Gainetdinov RR. The physiology, signaling, and pharmacology of dopamine receptors. Pharmacol Rev. 2011;63: 182–217. doi:10.1124/pr.110.002642

46. Emerson GM. Emerson studies on growth hormone effects in the Norway rat. Ala J Med Sci. 1973;10: 410–416. Available: https://www.ncbi.nlm.nih.gov/pubmed/4791010

47. Marston OJ, Garfield AS, Heisler LK. Role of central serotonin and melanocortin systems in the control of energy balance. Eur J Pharmacol. 2011;660: 70–79. doi:10.1016/j.ejphar.2010.12.024

48. Ikemoto S. Brain reward circuitry beyond the mesolimbic dopamine system: a neurobiological theory. Neurosci Biobehav Rev. 2010;35: 129–150. doi:10.1016/j.neubiorev.2010.02.001

49. Rinaman L. Hindbrain noradrenergic A2 neurons: diverse roles in autonomic, endocrine, cognitive, and behavioral functions. Am J Physiol Regul Integr Comp Physiol. 2011;300: R222–35. doi:10.1152/ajpregu.00556.2010

50. Iwańczuk W, Guźniczak P. Neurophysiological foundations of sleep, arousal, awareness and consciousness phenomena. Part 1. Anaesthesiol Intensive Ther.

2015;47: 162–167. doi:10.5603/AIT.2015.0015

51. Trofimova I, Robbins TW. Temperament and arousal systems: A new synthesis of differential psychology and functional neurochemistry. Neurosci Biobehav Rev. 2016;64: 382–402. doi:10.1016/j.neubiorev.2016.03.008

52. Bittigau P, Ikonomidou C. Glutamate in neurologic diseases. J Child Neurol. 1997;12: 471–485. doi:10.1177/088307389701200802

53. Werner F-M, Coveñas R. Classical neurotransmitters and neuropeptides involved in major depression: a review. Int J Neurosci. 2010;120: 455–470. doi:10.3109/00207454.2010.483651

54. Mehta TR, Monegro A, Nene Y, Fayyaz M, Bollu PC. Neurobiology of ADHD: A Review. Current Developmental Disorders Reports. 2019;6: 235–240. doi:10.1007/s40474-019-00182-w

55. Meister B. Neurotransmitters in key neurons of the hypothalamus that regulate feeding behavior and body weight. Physiol Behav. 2007;92: 263–271. doi:10.1016/j.physbeh.2007.05.021

56. Li Y, Wang X, Ge S-N, Wang X-L. Alterations in Neurotransmitters Targeted Metabolomics from the Key Nuclei of Brain Reward Circuits in Cocaine-Induced Behavioral Sensitization for Self-Administering Rats. 2022. doi:10.2139/ssrn.4037936

57. Palkovits M. [The brain and the pain: neurotransmitters and neuronal pathways of pain perception and response]. Orv Hetil. 2000;141: 2231–2239. Available: https://www.ncbi.nlm.nih.gov/pubmed/11184247

58. Shetty DN, Pathak SS. Correlation between plasma neurotransmitters and memory loss in pregnancy. J Reprod Med. 2002;47: 494–496. Available: https://www.ncbi.nlm.nih.gov/pubmed/12092020

59. Dobryakova E, Genova HM, DeLuca J, Wylie GR. The dopamine imbalance hypothesis of fatigue in multiple sclerosis and other neurological disorders. Front Neurol. 2015;6: 52. doi:10.3389/fneur.2015.00052

60. Fernandez MV, Kim JH, Budde JP, Black K, Medvedeva A, Saef B, et al. Analysis of neurodegenerative Mendelian genes in clinically diagnosed Alzheimer Disease. PLoS Genet. 2017;13: e1007045. Available: https://journals.plos.org/plosgenetics/article?id=10.1371/journal.pgen.1007045

61. Schiöth HB, Fredriksson R. The GRAFS classification system of G-protein coupled receptors in comparative perspective. Gen Comp Endocrinol. 2005;142: 94–101. doi:10.1016/j.ygcen.2004.12.018

62. Alexander SPH, Kelly E, Mathie A, Peters JA, Veale EL, Armstrong JF, et al. THE CONCISE GUIDE TO PHARMACOLOGY 2019/20: Introduction and Other Protein Targets. Br J Pharmacol. 2019;176 Suppl 1: S1–S20. doi:10.1111/bph.14747

63. Alexander SPH, Christopoulos A, Davenport AP, Kelly E, Mathie A, Peters JA, et al. THE CONCISE GUIDE TO PHARMACOLOGY 2019/20: G protein-coupled receptors. Br J Pharmacol. 2019;176 Suppl 1: S21–S141. doi:10.1111/bph.14748

64. Hu G-M, Mai T-L, Chen C-M. Visualizing the GPCR Network: Classification and Evolution. Sci Rep. 2017;7: 15495. doi:10.1038/s41598-017-15707-9

65. Attwood TK, Findlay JB. Fingerprinting G-protein-coupled receptors. Protein Eng. 1994;7: 195–203. doi:10.1093/protein/7.2.195

66. Kolakowski LF Jr. GCRDb: a G-protein-coupled receptor database. Receptors Channels. 1994;2: 1–7. Available: https://www.ncbi.nlm.nih.gov/pubmed/8081729

67. Lee Y, Basith S, Choi S. Recent Advances in Structure-Based Drug Design Targeting Class A G Protein-Coupled Receptors Utilizing Crystal Structures and Computational Simulations. J Med Chem. 2018;61: 1–46. doi:10.1021/acs.jmedchem.6b01453

68. Basith S, Cui M, Macalino SJY, Park J, Clavio NAB, Kang S, et al. Exploring G Protein-Coupled Receptors (GPCRs) Ligand Space via Cheminformatics Approaches: Impact on Rational Drug Design. Front Pharmacol. 2018;9: 128. doi:10.3389/fphar.2018.00128

69. Zöllner C, Stein C. Opioids. Handb Exp Pharmacol. 2007; 31–63. doi:10.1007/978-3-540-33823-9_2

70. Moreira IS. Structural features of the G-protein/GPCR interactions. Biochim Biophys Acta. 2014;1840: 16–33. doi:10.1016/j.bbagen.2013.08.027

71. Somvanshi RK, Kumar U. Pathophysiology of GPCR Homo- and Heterodimerization: Special Emphasis on Somatostatin Receptors. Pharmaceuticals . 2012;5: 417–446. doi:10.3390/ph5050417

72. Ferré S, Casadó V, Devi LA, Filizola M, Jockers R, Lohse MJ, et al. G protein-coupled receptor oligomerization revisited: functional and pharmacological perspectives. Pharmacol Rev. 2014;66: 413–434. doi:10.1124/pr.113.008052

73. Mondal S, Khelashvili G, Johner N, Weinstein H. How the Dynamic Properties and Functional Mechanisms of GPCRs Are Modulated by Their Coupling to the Membrane Environment. In: Filizola M, editor. G Protein-Coupled Receptors - Modeling and Simulation. Dordrecht: Springer Netherlands; 2014. pp. 55–74. doi:10.1007/978-94-007-7423-0_4

74. Filizola M, Weinstein H. The study of G-protein coupled receptor oligomerization with computational modeling and bioinformatics. FEBS J. 2005;272: 2926–2938. doi:10.1111/j.1742-4658.2005.04730.x

75. Borroto-Escuela DO, Fuxe K. Oligomeric Receptor Complexes and Their Allosteric Receptor-Receptor Interactions in the Plasma Membrane Represent a New Biological Principle for Integration of Signals in the CNS. Front Mol Neurosci.

2019;12: 230. doi:10.3389/fnmol.2019.00230

76. Borroto-Escuela DO, Rodriguez D, Romero-Fernandez W, Kapla J, Jaiteh M, Ranganathan A, et al. Mapping the Interface of a GPCR Dimer: A Structural Model of the A2A Adenosine and D2 Dopamine Receptor Heteromer. Front Pharmacol. 2018;9: 829. doi:10.3389/fphar.2018.00829

77. Wouters E, Marín AR, Dalton JAR, Giraldo J, Stove C. Distinct Dopamine D_2 Receptor Antagonists Differentially Impact D_2 Receptor Oligomerization. Int J Mol Sci. 2019;20. doi:10.3390/ijms20071686

78. Farran B. An update on the physiological and therapeutic relevance of GPCR oligomers. Pharmacol Res. 2017;117: 303–327. doi:10.1016/j.phrs.2017.01.008

79. Schiedel AC, Kose M, Barreto C, Bueschbell B, Morra G, Sensoy O, et al. Prediction and Targeting of Interaction Interfaces in G-protein Coupled Receptor Oligomers. Curr Top Med Chem. 2018;18: 714–746. doi:10.2174/1568026618666180604082610

80. Guo H, An S, Ward R, Yang Y, Liu Y, Guo X-X, et al. Methods used to study the oligomeric structure of G-protein-coupled receptors. Biosci Rep. 2017;37. doi:10.1042/BSR20160547

81. Fuxe K, Borroto-Escuela DO, Marcellino D, Romero-Fernandez W, Frankowska M, Guidolin D, et al. GPCR heteromers and their allosteric receptor-receptor interactions. Curr Med Chem. 2012;19: 356–363. doi:10.2174/092986712803414259

82. Yang J, Gong Z, Lu Y-B, Xu C-J, Wei T-F, Yang M-S, et al. FLIM-FRET-Based Structural Characterization of a Class-A GPCR Dimer in the Cell Membrane. J Mol Biol. 2020;432: 4596–4611. doi:10.1016/j.jmb.2020.06.009

83. Townsend-Nicholson A, Altwaijry N, Potterton A, Morao I, Heifetz A. Computational prediction of GPCR oligomerization. Curr Opin Struct Biol. 2019;55: 178–184. doi:10.1016/j.sbi.2019.04.005

84. Pin J-P, Bettler B. Organization and functions of mGlu and GABAB receptor complexes. Nature. 2016;540: 60–68. doi:10.1038/nature20566

85. Møller TC, Moreno-Delgado D, Pin J-P, Kniazeff J. Class C G protein-coupled receptors: reviving old couples with new partners. Biophys Rep. 2017;3: 57–63. doi:10.1007/s41048-017-0036-9

86. Möller J, Isbilir A, Sungkaworn T, Osberg B, Karathanasis C, Sunkara V, et al. Single-molecule analysis reveals agonist-specific dimer formation of μ-opioid receptors. Nat Chem Biol. 2020;16: 946–954. doi:10.1038/s41589-020-0566-1

87. Kasai RS, Ito SV, Awane RM, Fujiwara TK, Kusumi A. The Class-A GPCR Dopamine D2 Receptor Forms Transient Dimers Stabilized by Agonists: Detection

by Single-Molecule Tracking. Cell Biochem Biophys. 2018;76: 29–37. doi:10.1007/s12013-017-0829-y

88. Lazim R, Suh D, Lee JW, Vu TNL, Yoon S, Choi S. Structural Characterization of Receptor-Receptor Interactions in the Allosteric Modulation of G Protein-Coupled Receptor (GPCR) Dimers. Int J Mol Sci. 2021;22. doi:10.3390/ijms22063241

89. Zoli M, Agnati LF, Hedlund PB, Li XM, Ferré S, Fuxe K. Receptor-receptor interactions as an integrative mechanism in nerve cells. Mol Neurobiol. 1993;7: 293–334. doi:10.1007/BF02769180

90. Ferré S, Baler R, Bouvier M, Caron MG, Devi LA, Durroux T, et al. Building a new conceptual framework for receptor heteromers. Nat Chem Biol. 2009;5: 131–134. doi:10.1038/nchembio0309-131

91. Tuteja N. Signaling through G protein coupled receptors. Plant Signal Behav. 2009;4: 942–947. doi:10.4161/psb.4.10.9530

92. Moreira IS, Shi L, Freyberg Z, Ericksen SS, Weinstein H, Javitch JA. Structural Basis of Dopamine Receptor Activation. The Dopamine Receptors. 2010. pp. 47–73. doi:10.1007/978-1-60327-333-6_3

93. Vauquelin G, Van Liefde I. G protein-coupled receptors: a count of 1001 conformations. Fundam Clin Pharmacol. 2005;19: 45–56. doi:10.1111/j.1472-8206.2005.00319.x

94. Latek D, Pasznik P, Carlomagno T, Filipek S. Towards improved quality of GPCR models by usage of multiple templates and profile-profile comparison. PLoS One. 2013;8: e56742. doi:10.1371/journal.pone.0056742

95. Isberg V, de Graaf C, Bortolato A, Cherezov V, Katritch V, Marshall FH, et al. Generic GPCR residue numbers - aligning topology maps while minding the gaps. Trends Pharmacol Sci. 2015;36: 22–31. doi:10.1016/j.tips.2014.11.001

96. Ballesteros JA, Weinstein H. [19] Integrated methods for the construction of three-dimensional models and computational probing of structure-function relations in G protein-coupled receptors. In: Sealfon SC, editor. Methods in Neurosciences. Academic Press; 1995. pp. 366–428. doi:10.1016/S1043-9471(05)80049-7

97. Zhou Q, Yang D, Wu M, Guo Y, Guo W, Zhong L, et al. Common activation mechanism of class A GPCRs. Elife. 2019;8. doi:10.7554/eLife.50279

98. Ballesteros J, Kitanovic S, Guarnieri F, Davies P, Fromme BJ, Konvicka K, et al. Functional microdomains in G-protein-coupled receptors. The conserved arginine-cage motif in the gonadotropin-releasing hormone receptor. J Biol Chem. 1998;273: 10445–10453. doi:10.1074/jbc.273.17.10445

99. Schneider EH, Schnell D, Strasser A, Dove S, Seifert R. Impact of the DRY motif and the missing “ionic lock” on constitutive activity and G-protein coupling of the human histamine H4 receptor. J Pharmacol Exp Ther. 2010;333: 382–392.

doi:10.1124/jpet.109.163220

100. Ballesteros JA, Jensen AD, Liapakis G, Rasmussen SG, Shi L, Gether U, et al. Activation of the beta 2-adrenergic receptor involves disruption of an ionic lock between the cytoplasmic ends of transmembrane segments 3 and 6. J Biol Chem. 2001;276: 29171–29177. doi:10.1074/jbc.M103747200

101. Schönegge A-M, Gallion J, Picard L-P, Wilkins AD, Le Gouill C, Audet M, et al. Evolutionary action and structural basis of the allosteric switch controlling β2AR functional selectivity. Nat Commun. 2017;8: 2169. doi:10.1038/s41467-017-02257-x

102. Alhadeff R, Vorobyov I, Yoon HW, Warshel A. Exploring the free-energy landscape of GPCR activation. Proc Natl Acad Sci U S A. 2018;115: 10327–10332. doi:10.1073/pnas.1810316115

103. Jacobson KA, Costanzi S, Paoletta S. Computational studies to predict or explain G protein coupled receptor polypharmacology. Trends Pharmacol Sci. 2014;35: 658–663. doi:10.1016/j.tips.2014.10.009

104. Feng X, Ambia J, Chen K-YM, Young M, Barth P. Computational design of ligand-binding membrane receptors with high selectivity. Nat Chem Biol. 2017;13: 715–723. doi:10.1038/nchembio.2371

105. Roth BL, Irwin JJ, Shoichet BK. Discovery of new GPCR ligands to illuminate new biology. Nat Chem Biol. 2017;13: 1143–1151. doi:10.1038/nchembio.2490

106. Shihoya W, Nishizawa T, Yamashita K, Inoue A, Hirata K, Kadji FMN, et al. X-ray structures of endothelin ETB receptor bound to clinical antagonist bosentan and its analog. Nat Struct Mol Biol. 2017;24: 758–764. doi:10.1038/nsmb.3450

107. Yuan S, Filipek S, Palczewski K, Vogel H. Activation of G-protein-coupled receptors correlates with the formation of a continuous internal water pathway. Nat Commun. 2014;5: 4733. doi:10.1038/ncomms5733

108. Filizola M, Weinstein H. Structural models for dimerization of G-protein coupled receptors: the opioid receptor homodimers. Biopolymers. 2002;66: 317–325. doi:10.1002/bip.10311

109. Weinstein H. Hallucinogen actions on 5-HT receptors reveal distinct mechanisms of activation and signaling by G protein-coupled receptors. AAPS J. 2006;7: E871–84. doi:10.1208/aapsj070485

110. Visiers I, Ballesteros JA, Weinstein H. Three-dimensional representations of G protein-coupled receptor structures and mechanisms. Methods Enzymol. 2002;343: 329–371. doi:10.1016/s0076-6879(02)43145-x

111. Fritze O, Filipek S, Kuksa V, Palczewski K, Hofmann KP, Ernst OP. Role of the conserved NPxxY(x)5,6F motif in the rhodopsin ground state and during activation. Proc Natl Acad Sci U S A. 2003;100: 2290–2295. doi:10.1073/pnas.0435715100

112. Trzaskowski B, Latek D, Yuan S, Ghoshdastider U, Debinski A, Filipek S. Action of molecular switches in GPCRs--theoretical and experimental studies. Curr Med Chem. 2012;19: 1090–1109. doi:10.2174/092986712799320556

113. Chen S, Lu M, Liu D, Yang L, Yi C, Ma L, et al. Human substance P receptor binding mode of the antagonist drug aprepitant by NMR and crystallography. Nat Commun. 2019;10: 638. doi:10.1038/s41467-019-08568-5

114. Venkatakrishnan AJ, Deupi X, Lebon G, Heydenreich FM, Flock T, Miljus T, et al. Diverse activation pathways in class A GPCRs converge near the G-protein-coupling region. Nature. 2016;536: 484–487. doi:10.1038/nature19107

115. Angel TE, Chance MR, Palczewski K. Conserved waters mediate structural and functional activation of family A (rhodopsin-like) G protein-coupled receptors. Proc Natl Acad Sci U S A. 2009;106: 8555–8560. doi:10.1073/pnas.0903545106

116. Prioleau C, Visiers I, Ebersole BJ, Weinstein H, Sealfon SC. Conserved helix 7 tyrosine acts as a multistate conformational switch in the 5HT2C receptor. Identification of a novel “locked-on” phenotype and double revertant mutations. J Biol Chem. 2002;277: 36577–36584. doi:10.1074/jbc.M206223200

117. Angel TE, Gupta S, Jastrzebska B, Palczewski K, Chance MR. Structural waters define a functional channel mediating activation of the GPCR, rhodopsin. Proc Natl Acad Sci U S A. 2009;106: 14367–14372. doi:10.1073/pnas.0901074106

118. Rasmussen SGF, DeVree BT, Zou Y, Kruse AC, Chung KY, Kobilka TS, et al. Crystal structure of the β2 adrenergic receptor-Gs protein complex. Nature. 2011;477: 549–555. doi:10.1038/nature10361

119. Filipek S. Molecular switches in GPCRs. Curr Opin Struct Biol. 2019;55: 114–120. doi:10.1016/j.sbi.2019.03.017

120. Wescott MP, Kufareva I, Paes C, Goodman JR, Thaker Y, Puffer BA, et al. Signal transmission through the CXC chemokine receptor 4 (CXCR4) transmembrane helices. Proc Natl Acad Sci U S A. 2016;113: 9928–9933. doi:10.1073/pnas.1601278113

121. Nygaard R, Frimurer TM, Holst B, Rosenkilde MM, Schwartz TW. Ligand binding and micro-switches in 7TM receptor structures. Trends Pharmacol Sci. 2009;30: 249–259. doi:10.1016/j.tips.2009.02.006

122. Hofmann KP, Scheerer P, Hildebrand PW, Choe H-W, Park JH, Heck M, et al. A G protein-coupled receptor at work: the rhodopsin model. Trends in Biochemical Sciences. 2009. pp. 540–552. doi:10.1016/j.tibs.2009.07.005

123. Kaiser A, Hempel C, Wanka L, Schubert M, Hamm HE, Beck-Sickinger AG. G protein preassembly rescues efficacy of W6. 48 toggle mutations in neuropeptide Y2 receptor. Mol Pharmacol. 2018;93: 387–401. Available:

https://molpharm.aspetjournals.org/content/93/4/387.abstract

124. Holst B, Nygaard R, Valentin-Hansen L, Bach A, Engelstoft MS, Petersen PS, et al. A Conserved Aromatic Lock for the Tryptophan Rotameric Switch in TM-VI of Seven-transmembrane Receptors. Journal of Biological Chemistry. 2010. pp. 3973–3985. doi:10.1074/jbc.m109.064725

125. Zhang XC, Zhou Y, Cao C. Proton transfer during class-A GPCR activation: do the CWxP motif and the membrane potential act in concert? Biophysics Reports. 2018;4: 115–122. doi:10.1007/s41048-018-0056-0

126. Tehan BG, Bortolato A, Blaney FE, Weir MP, Mason JS. Unifying family A GPCR theories of activation. Pharmacol Ther. 2014;143: 51–60. doi:10.1016/j.pharmthera.2014.02.004

127. Eddy MT, Lee M-Y, Gao Z-G, White KL, Didenko T, Horst R, et al. Allosteric Coupling of Drug Binding and Intracellular Signaling in the A2A Adenosine Receptor. Cell. 2018;172: 68–80.e12. doi:10.1016/j.cell.2017.12.004

128. Ishchenko A, Wacker D, Kapoor M, Zhang A, Han GW, Basu S, et al. Structural insights into the extracellular recognition of the human serotonin 2B receptor by an antibody. Proc Natl Acad Sci U S A. 2017;114: 8223–8228. doi:10.1073/pnas.1700891114

129. Kato HE, Zhang Y, Hu H, Suomivuori C-M, Kadji FMN, Aoki J, et al. Conformational transitions of a neurotensin receptor 1-Gi1 complex. Nature. 2019;572: 80–85. doi:10.1038/s41586-019-1337-6

130. Liu W, Chun E, Thompson AA, Chubukov P, Xu F, Katritch V, et al. Structural basis for allosteric regulation of GPCRs by sodium ions. Science. 2012;337: 232–236. doi:10.1126/science.1219218

131. Yuan S, Vogel H, Filipek S. The role of water and sodium ions in the activation of the μ-opioid receptor. Angew Chem Int Ed Engl. 2013;52: 10112–10115. doi:10.1002/anie.201302244

132. Fenalti G, Giguere PM, Katritch V, Huang X-P, Thompson AA, Cherezov V, et al. Molecular control of δ-opioid receptor signalling. Nature. 2014;506: 191–196. doi:10.1038/nature12944

133. Vickery ON, Carvalheda CA, Zaidi SA, Pisliakov AV, Katritch V, Zachariae U. Intracellular Transfer of Na+ in an Active-State G-Protein-Coupled Receptor. Structure. 2018;26: 171–180.e2. doi:10.1016/j.str.2017.11.013

134. Katritch V, Fenalti G, Abola EE, Roth BL, Cherezov V, Stevens RC. Allosteric sodium in class A GPCR signaling. Trends in Biochemical Sciences. 2014. pp. 233–244. doi:10.1016/j.tibs.2014.03.002

135. White KL, Eddy MT, Gao Z-G, Han GW, Lian T, Deary A, et al. Structural Connection between Activation Microswitch and Allosteric Sodium Site in GPCR

Signaling. Structure. 2018;26: 259–269.e5. doi:10.1016/j.str.2017.12.013

136. Ye L, Neale C, Sljoka A, Lyda B, Pichugin D, Tsuchimura N, et al. Mechanistic insights into allosteric regulation of the A2A adenosine G protein-coupled receptor by physiological cations. Nat Commun. 2018;9: 1372. doi:10.1038/s41467-018-03314-9

137. Yuan S, Filipek S, Vogel H. A Gating Mechanism of the Serotonin 5-HT3 Receptor. Structure. 2016;24: 816–825. doi:10.1016/j.str.2016.03.019

138. Venkatakrishnan AJ, Ma AK, Fonseca R, Latorraca NR, Kelly B, Betz RM, et al. Diverse GPCRs exhibit conserved water networks for stabilization and activation. Proc Natl Acad Sci U S A. 2019;116: 3288–3293. doi:10.1073/pnas.1809251116

139. Kaneez FS. Serotonin: A Chemical Messenger Between All Types of Living Cells. BoD – Books on Demand; 2017. Available: https://play.google.com/store/books/details?id=E8WPDwAAQBAJ

140. Dorszewska J, Prendecki M, Oczkowska A, Rozycka A, Lianeri M, Kozubski W. Polymorphism of the COMT, MAO, DAT, NET and 5-HTT Genes, and Biogenic Amines in Parkinson's Disease. Curr Genomics. 2013;14: 518–533. doi:10.2174/1389202914666131210210241

141. Mohammad-Zadeh LF, Moses L, Gwaltney-Brant SM. Serotonin: a review. J Vet Pharmacol Ther. 2008;31: 187–199. doi:10.1111/j.1365-2885.2008.00944.x

142. Hannon J, Hoyer D. Molecular biology of 5-HT receptors. Behav Brain Res. 2008;195: 198–213. doi:10.1016/j.bbr.2008.03.020

143. Armstrong JF, Faccenda E, Harding SD, Pawson AJ, Southan C, Sharman JL, et al. The IUPHAR/BPS Guide to PHARMACOLOGY in 2020: extending immunopharmacology content and introducing the IUPHAR/MMV Guide to MALARIA PHARMACOLOGY. Nucleic Acids Res. 2020;48: D1006–D1021. doi:10.1093/nar/gkz951

144. Xu P, Huang S, Zhang H, Mao C, Zhou XE, Cheng X, et al. Structural insights into the lipid and ligand regulation of serotonin receptors. Nature. 2021;592: 469–473. doi:10.1038/s41586-021-03376-8

145. Kowalska M, Prendecki M, Kozubski W, Lianeri M, Dorszewska J. Molecular factors in migraine. Oncotarget. 2016;7: 50708–50718. doi:10.18632/oncotarget.9367

146. Theodore WH. Does Serotonin Play a Role in Epilepsy? Epilepsy Curr. 2003;3: 173–177. doi:10.1046/j.1535-7597.2003.03508.x

147. Hercigonja Novkovic V, Rudan V, Pivac N, Nedic G, Muck-Seler D. Platelet serotonin concentration in children with attention-deficit/hyperactivity disorder. Neuropsychobiology. 2009;59: 17–22. doi:10.1159/000202825

148. Whitney MS, Shemery AM, Yaw AM, Donovan LJ, Glass JD, Deneris ES. Adult Brain Serotonin Deficiency Causes Hyperactivity, Circadian Disruption, and Elimination of Siestas. J Neurosci. 2016;36: 9828–9842. doi:10.1523/JNEUROSCI.1469-16.2016

149. Sandyk R. Serotonergic mechanisms in amyotrophic lateral sclerosis. Int J Neurosci. 2006;116: 775–826. doi:10.1080/00207450600754087

150. Kendall DA, Yudowski GA. Cannabinoid Receptors in the Central Nervous System: Their Signaling and Roles in Disease. Front Cell Neurosci. 2016;10: 294. doi:10.3389/fncel.2016.00294

151. Aizpurua-Olaizola O, Elezgarai I, Rico-Barrio I, Zarandona I, Etxebarria N, Usobiaga A. Targeting the endocannabinoid system: future therapeutic strategies. Drug Discov Today. 2017;22: 105–110. doi:10.1016/j.drudis.2016.08.005

152. Pryce G, Ahmed Z, Hankey DJR, Jackson SJ, Croxford JL, Pocock JM, et al. Cannabinoids inhibit neurodegeneration in models of multiple sclerosis. Brain. 2003;126: 2191–2202. doi:10.1093/brain/awg224

153. Klein TW. Cannabinoid-based drugs as anti-inflammatory therapeutics. Nat Rev Immunol. 2005;5: 400–411. doi:10.1038/nri1602

154. Campbell VA, Gowran A. Alzheimer's disease; taking the edge off with cannabinoids? Br J Pharmacol. 2007;152: 655–662. doi:10.1038/sj.bjp.0707446

155. Bilkei-Gorzo A. The endocannabinoid system in normal and pathological brain ageing. Philos Trans R Soc Lond B Biol Sci. 2012;367: 3326–3341. doi:10.1098/rstb.2011.0388

156. Scotter EL, Abood ME, Glass M. The endocannabinoid system as a target for the treatment of neurodegenerative disease. Br J Pharmacol. 2010;160: 480–498. doi:10.1111/j.1476-5381.2010.00735.x

157. Fernández-Ruiz J, Moreno-Martet M, Rodríguez-Cueto C, Palomo-Garo C, Gómez-Cañas M, Valdeolivas S, et al. Prospects for cannabinoid therapies in basal ganglia disorders. Br J Pharmacol. 2011;163: 1365–1378. doi:10.1111/j.1476-5381.2011.01365.x

158. Marsicano G, Kuner R. Anatomical Distribution of Receptors, Ligands and Enzymes in the Brain and in the Spinal Cord: Circuitries and Neurochemistry. In: Köfalvi A, editor. Cannabinoids and the Brain. Boston, MA: Springer US; 2008. pp. 161–201. doi:10.1007/978-0-387-74349-3_10

159. Jordan CJ, Xi Z-X. Progress in brain cannabinoid CB2 receptor research: From genes to behavior. Neurosci Biobehav Rev. 2019;98: 208–220. doi:10.1016/j.neubiorev.2018.12.026

160. Mackie K. Cannabinoid receptors: where they are and what they do. J Neuroendocrinol. 2008;20 Suppl 1: 10–14. doi:10.1111/j.1365-2826.2008.01671.x

161. Bosier B, Muccioli GG, Hermans E, Lambert DM. Functionally selective cannabinoid receptor signalling: therapeutic implications and opportunities. Biochem Pharmacol. 2010;80: 1–12. doi:10.1016/j.bcp.2010.02.013

162. Nogueras-Ortiz C, Yudowski GA. The Multiple Waves of Cannabinoid 1 Receptor Signaling. Mol Pharmacol. 2016;90: 620–626. doi:10.1124/mol.116.104539

163. Di Marzo V, Stella N, Zimmer A. Endocannabinoid signalling and the deteriorating brain. Nat Rev Neurosci. 2015;16: 30–42. doi:10.1038/nrn3876

164. Palazuelos J, Aguado T, Pazos MR, Julien B, Carrasco C, Resel E, et al. Microglial CB2 cannabinoid receptors are neuroprotective in Huntington's disease excitotoxicity. Brain. 2009;132: 3152–3164. doi:10.1093/brain/awp239

165. Yeh FL, Wang Y, Tom I, Gonzalez LC, Sheng M. TREM2 Binds to Apolipoproteins, Including APOE and CLU/APOJ, and Thereby Facilitates Uptake of Amyloid-Beta by Microglia. Neuron. 2016;91: 328–340. doi:10.1016/j.neuron.2016.06.015

166. Sagredo O, García-Arencibia M, de Lago E, Finetti S, Decio A, Fernández-Ruiz J. Cannabinoids and neuroprotection in basal ganglia disorders. Mol Neurobiol. 2007;36: 82–91. doi:10.1007/s12035-007-0004-3

167. Ramírez BG, Blázquez C, Gómez del Pulgar T, Guzmán M, de Ceballos ML. Prevention of Alzheimer's disease pathology by cannabinoids: neuroprotection mediated by blockade of microglial activation. J Neurosci. 2005;25: 1904–1913. doi:10.1523/JNEUROSCI.4540-04.2005

168. Dockray GJ. Cholecystokinins in rat cerebral cortex: identification, purification and characterization by immunochemical methods. Brain Res. 1980;188: 155–165. doi:10.1016/0006-8993(80)90564-8

169. Innis RB, Snyder SH. Distinct cholecystokinin receptors in brain and pancreas. Proc Natl Acad Sci U S A. 1980;77: 6917–6921. doi:10.1073/pnas.77.11.6917

170. Bradwejn J, Koszycki D, Meterissian G. Cholecystokinin-tetrapeptide induces panic attacks in patients with panic disorder. Can J Psychiatry. 1990;35: 83–85. doi:10.1177/070674379003500115

171. Ballaz S. The unappreciated roles of the cholecystokinin receptor CCK(1) in brain functioning. Rev Neurosci. 2017;28: 573–585. doi:10.1515/revneuro-2016-0088

172. Beglinger C, Degen L, Matzinger D, D'Amato M, Drewe J. Loxiglumide, a CCK-A receptor antagonist, stimulates calorie intake and hunger feelings in humans. Am J Physiol Regul Integr Comp Physiol. 2001;280: R1149–54. doi:10.1152/ajpregu.2001.280.4.R1149

173. Dockray GJ. Cholecystokinin. Curr Opin Endocrinol Diabetes Obes. 2012;19:

8–12. doi:10.1097/MED.0b013e32834eb77d

174. Beglinger C. Overview. Cholecystokinin and eating. Curr Opin Investig Drugs. 2002;3: 587–588. Available: https://www.ncbi.nlm.nih.gov/pubmed/12090729

175. Choi JG, Jeong M, Joo BR, Ahn J-H, Woo J-H, Kim D-H, et al. Reduced Levels of Intestinal Neuropeptides and Neurotrophins in Neurotoxin-Induced Parkinson Disease Mouse Models. J Neuropathol Exp Neurol. 2021;80: 15–20. doi:10.1093/jnen/nlaa113

176. Fasano A, Visanji NP, Liu LWC, Lang AE, Pfeiffer RF. Gastrointestinal dysfunction in Parkinson's disease. Lancet Neurol. 2015;14: 625–639. doi:10.1016/S1474-4422(15)00007-1

177. Everitt BJ, Meister B, Hökfelt T, Melander T, Terenius L, Rökaeus A, et al. The hypothalamic arcuate nucleus-median eminence complex: immunohistochemistry of transmitters, peptides and DARPP-32 with special reference to coexistence in dopamine neurons. Brain Res. 1986;396: 97–155. doi:10.1016/s0006-8993(86)80192-5

178. Hökfelt T, Skirboll L, Rehfeld JF, Goldstein M, Markey K, Dann O. A subpopulation of mesencephalic dopamine neurons projecting to limbic areas contains a cholecystokinin-like peptide: evidence from immunohistochemistry combined with retrograde tracing. Neuroscience. 1980;5: 2093–2124. doi:10.1016/0306-4522(80)90127-x

179. Beaulieu J-M, Espinoza S, Gainetdinov RR. Dopamine receptors - IUPHAR Review 13. Br J Pharmacol. 2015;172: 1–23. doi:10.1111/bph.12906

180. Kebabian JW. Multiple classes of dopamine receptors in mammalian central nervous system: the involvement of dopamine-sensitive adenylyl cyclase. Life Sci. 1978;23: 479–483. doi:10.1016/0024-3205(78)90157-1

181. Spano PF, Govoni S, Trabucchi M. Studies on the pharmacological properties of dopamine receptors in various areas of the central nervous system. Adv Biochem Psychopharmacol. 1978;19: 155–165. Available: https://www.ncbi.nlm.nih.gov/pubmed/358777

182. Bueschbell B, Barreto CAV, Preto AJ, Schiedel AC, Moreira IS. A Complete Assessment of Dopamine Receptor- Ligand Interactions through Computational Methods. Molecules. 2019;24. doi:10.3390/molecules24071196

183. Cokan KB, Mavri M, Rutland CS, Glišić S, Senćanski M, Vrecl M, et al. Critical Impact of Different Conserved Endoplasmic Retention Motifs and Dopamine Receptor Interacting Proteins (DRIPs) on Intracellular Localization and Trafficking of the D2 Dopamine Receptor (D2-R) Isoforms. Biomolecules. 2020. p. 1355. doi:10.3390/biom10101355

184. Mitsukawa K, Lu X, Bartfai T. Galanin, galanin receptors and drug targets. Cell

Mol Life Sci. 2008;65: 1796–1805. doi:10.1007/s00018-008-8153-8

185. Tatemoto K, Rökaeus A, Jörnvall H, McDonald TJ, Mutt V. Galanin - a novel biologically active peptide from porcine intestine. FEBS Lett. 1983;164: 124–128. doi:10.1016/0014-5793(83)80033-7

186. Ottlecz A, Samson WK, McCann SM. Galanin: evidence for a hypothalamic site of action to release growth hormone. Peptides. 1986;7: 51–53. doi:10.1016/0196-9781(86)90060-4

187. Lu X, Sharkey L, Bartfai T. The brain galanin receptors: targets for novel antidepressant drugs. CNS Neurol Disord Drug Targets. 2007;6: 183–192. doi:10.2174/187152707780619335

188. Hua X-Y, Salgado KF, Gu G, Fitzsimmons B, Kondo I, Bartfai T, et al. Mechanisms of antinociception of spinal galanin: how does galanin inhibit spinal sensitization? Neuropeptides. 2005;39: 211–216. doi:10.1016/j.npep.2004.12.024

189. Nordström O, Melander T, Hökfelt T, Bartfai T, Goldstein M. Evidence for an inhibitory effect of the peptide galanin on dopamine release from the rat median eminence. Neurosci Lett. 1987;73: 21–26. doi:10.1016/0304-3940(87)90024-3

190. Liu H-X, Hökfelt T. The participation of galanin in pain processing at the spinal level. Trends Pharmacol Sci. 2002;23: 468–474. doi:10.1016/s0165-6147(02)02074-6

191. Wrenn CC, Crawley JN. Pharmacological evidence supporting a role for galanin in cognition and affect. Prog Neuropsychopharmacol Biol Psychiatry. 2001;25: 283–299. doi:10.1016/s0278-5846(00)00156-1

192. Hökfelt T, Wiesenfeld-Hallin Z, Villar M, Melander T. Increase of galanin-like immunoreactivity in rat dorsal root ganglion cells after peripheral axotomy. Neurosci Lett. 1987;83: 217–220. doi:10.1016/0304-3940(87)90088-7

193. Elliott-Hunt CR, Marsh B, Bacon A, Pope R, Vanderplank P, Wynick D. Galanin acts as a neuroprotective factor to the hippocampus. Proc Natl Acad Sci U S A. 2004;101: 5105–5110. doi:10.1073/pnas.0304823101

194. Counts SE, Perez SE, Ginsberg SD, De Lacalle S, Mufson EJ. Galanin in Alzheimer disease. Mol Interv. 2003;3: 137–156. doi:10.1124/mi.3.3.137

195. Mazarati A, Lu X, Kilk K, Langel U, Wasterlain C, Bartfai T. Galanin type 2 receptors regulate neuronal survival, susceptibility to seizures and seizure-induced neurogenesis in the dentate gyrus. Eur J Neurosci. 2004;19: 3235–3244. doi:10.1111/j.0953-816X.2004.03449.x

196. Hökfelt T, Bartfai T, Bloom F. Neuropeptides: opportunities for drug discovery. Lancet Neurol. 2003;2: 463–472. doi:10.1016/s1474-4422(03)00482-4

197. Mazarati AM. Galanin and galanin receptors in epilepsy. Neuropeptides.

2004;38: 331–343. doi:10.1016/j.npep.2004.07.006

198. Wiesenfeld-Hallin Z, Xu X-J, Crawley JN, Hökfelt T. Galanin and spinal nociceptive mechanisms: recent results from transgenic and knock-out models. Neuropeptides. 2005;39: 207–210. doi:10.1016/j.npep.2004.12.017

199. Wang P, Li H, Barde S, Zhang M-D, Sun J, Wang T, et al. Depression-like behavior in rat: Involvement of galanin receptor subtype 1 in the ventral periaqueductal gray. Proc Natl Acad Sci U S A. 2016;113: E4726–35. doi:10.1073/pnas.1609198113

200. Lundström L, Elmquist A, Bartfai T, Langel U. Galanin and its receptors in neurological disorders. Neuromolecular Med. 2005;7: 157–180. doi:10.1385/NMM:7:1-2:157

201. Panula P, Chazot PL, Cowart M, Gutzmer R, Leurs R, Liu WLS, et al. International Union of Basic and Clinical Pharmacology. XCVIII. Histamine Receptors. Pharmacol Rev. 2015;67: 601–655. doi:10.1124/pr.114.010249

202. Nieto-Alamilla G, Márquez-Gómez R, García-Gálvez A-M, Morales-Figueroa G-E, Arias-Montaño J-A. The Histamine H3 Receptor: Structure, Pharmacology, and Function. Mol Pharmacol. 2016;90: 649–673. doi:10.1124/mol.116.104752

203. Keppel Hesselink JM. The terms “autacoid”, “hormone” and “chalone” and how they have shifted with time. Auton Autacoid Pharmacol. 2015;35: 51–58. doi:10.1111/aap.12037

204. Wouters MM, Vicario M, Santos J. The role of mast cells in functional GI disorders. Gut. 2016;65: 155–168. doi:10.1136/gutjnl-2015-309151

205. Blandina P, Munari L, Provensi G, Passani MB. Histamine neurons in the tuberomamillary nucleus: a whole center or distinct subpopulations? Front Syst Neurosci. 2012;6: 33. doi:10.3389/fnsys.2012.00033

206. Stromberga Z, Chess-Williams R, Moro C. Histamine modulation of urinary bladder urothelium, lamina propria and detrusor contractile activity via H1 and H2 receptors. Sci Rep. 2019;9: 3899. doi:10.1038/s41598-019-40384-1

207. Passani MB, Panula P, Lin J-S. Histamine in the brain. Front Syst Neurosci. 2014;8: 64. doi:10.3389/fnsys.2014.00064

208. Bond RA, Ijzerman AP. Recent developments in constitutive receptor activity and inverse agonism, and their potential for GPCR drug discovery. Trends Pharmacol Sci. 2006;27: 92–96. doi:10.1016/j.tips.2005.12.007

209. Baronio D, Gonchoroski T, Castro K, Zanatta G, Gottfried C, Riesgo R. Histaminergic system in brain disorders: lessons from the translational approach and future perspectives. Ann Gen Psychiatry. 2014;13: 34. doi:10.1186/s12991-014-0034-y

210. Jadidi-Niaragh F, Mirshafiey A. Histamine and histamine receptors in pathogenesis and treatment of multiple sclerosis. Neuropharmacology. 2010;59: 180–189. doi:10.1016/j.neuropharm.2010.05.005

211. Naddafi F, Mirshafiey A. The Neglected Role of Histamine in Alzheimer's Disease. American Journal of Alzheimer's Disease & Other Dementiasr. 2013. pp. 327–336. doi:10.1177/1533317513488925

212. Ito C. The role of the central histaminergic system on schizophrenia. Drug News Perspect. 2004;17: 383–387. doi:10.1358/dnp.2004.17.6.829029

213. Mahmood D. Histamine H3 receptors and its antagonism as a novel mechanism for antipsychotic effect: a current preclinical & clinical perspective. Int J Health Sci . 2016;10: 564–575. doi:10.1016/j.biopsych.2015.08.026

214. Liu Q, Fan W, He H, Huang F. The role of peripheral opioid receptors in orofacial pain. Oral Dis. 2021;27: 1106–1114. doi:10.1111/odi.13435

215. Wiffen PJ, Wee B, Derry S, Bell RF, Moore RA. Opioids for cancer pain - an overview of Cochrane reviews. Cochrane Database Syst Rev. 2017;7: CD012592. doi:10.1002/14651858.CD012592.pub2

216. Barber A. Mu- and kappa-opioid receptor agonists produce peripheral inhibition of neurogenic plasma extravasation in rat skin. Eur J Pharmacol. 1993;236: 113–120. doi:10.1016/0014-2999(93)90233-8

217. Earl JR, Grootveld MC, Blake DR, Morris CJ. Effect of mu, delta and kappa opioid receptor agonists on a reactive oxygen species mediated model of skin inflammation. Skin Pharmacol. 1996;9: 250–258. doi:10.1159/000211422

218. Stein C, Machelska H. Modulation of peripheral sensory neurons by the immune system: implications for pain therapy. Pharmacol Rev. 2011;63: 860–881. doi:10.1124/pr.110.003145

219. Corbett AD, Henderson G, McKnight AT, Paterson SJ. 75 years of opioid research: the exciting but vain quest for the Holy Grail. Br J Pharmacol. 2006;147 Suppl 1: S153–62. doi:10.1038/sj.bjp.0706435

220. Israel Y, Kandov Y, Khaimova E, Kest A, Lewis SR, Pasternak GW, et al. NPY-induced feeding: pharmacological characterization using selective opioid antagonists and antisense probes in rats. Peptides. 2005;26: 1167–1175. doi:10.1016/j.peptides.2005.01.017

221. Cai Z, Ratka A. Opioid system and Alzheimer's disease. Neuromolecular Med. 2012;14: 91–111. doi:10.1007/s12017-012-8180-3

222. Nissen JB, Kragballe K. Enkephalins modulate differentiation of normal human keratinocytes in vitro. Exp Dermatol. 1997;6: 222–229. doi:10.1111/j.1600-0625.1997.tb00166.x

223. Hadjiconstantinou M, Neff NH. Nicotine and endogenous opioids: neurochemical and pharmacological evidence. Neuropharmacology. 2011;60: 1209–1220. doi:10.1016/j.neuropharm.2010.11.010

224. Jeftinija S. Enkephalins modulate excitatory synaptic transmission in the superficial dorsal horn by acting at mu-opioid receptor sites. Brain Res. 1988;460: 260–268. doi:10.1016/0006-8993(88)90371-x

225. Kong H, Raynor K, Yano H, Takeda J, Bell GI, Reisine T. Agonists and antagonists bind to different domains of the cloned kappa opioid receptor. Proc Natl Acad Sci U S A. 1994;91: 8042–8046. doi:10.1073/pnas.91.17.8042

226. Maggi R, Pimpinelli F, Martini L, Piva F. Inhibition of luteinizing hormone-releasing hormone secretion by delta-opioid agonists in GT1-1 neuronal cells. Endocrinology. 1995;136: 5177–5181. doi:10.1210/endo.136.11.7588256

227. Meucci E, Delay-Goyet P, Roques BP, Zajac JM. Binding in vivo of selective mu and delta opioid receptor agonists: opioid receptor occupancy by endogenous enkephalins. Eur J Pharmacol. 1989;171: 167–178. doi:10.1016/0014-2999(89)90105-2

228. Stein C. Opioid Receptors. Annu Rev Med. 2016;67: 433–451. doi:10.1146/annurev-med-062613-093100

229. Alfaras-Melainis K, Gomes I, Rozenfeld R, Zachariou V, Devi L. Modulation of opioid receptor function by protein-protein interactions. Front Biosci . 2009;14: 3594–3607. doi:10.2741/3474

230. Simonds WF. The molecular basis of opioid receptor function. Endocr Rev. 1988;9: 200–212. doi:10.1210/edrv-9-2-200

231. Barreto CAV, Baptista SJ, Preto AJ, Silvério D, Melo R, Moreira IS. Decoding Partner Specificity of Opioid Receptor Family. Front Mol Biosci. 2021;8: 715215. doi:10.3389/fmolb.2021.715215

232. Chu Sin Chung P, Kieffer BL. Delta opioid receptors in brain function and diseases. Pharmacol Ther. 2013;140: 112–120. doi:10.1016/j.pharmthera.2013.06.003

233. Stein C. Opioids, sensory systems and chronic pain. Eur J Pharmacol. 2013;716: 179–187. doi:10.1016/j.ejphar.2013.01.076

234. Rittner HL, Brack A, Stein C. Pain and the immune system. Br J Anaesth. 2008;101: 40–44. doi:10.1093/bja/aen078

235. Epelbaum J, Dournaud P, Fodor M, Viollet C. The neurobiology of somatostatin. Crit Rev Neurobiol. 1994;8: 25–44. Available: https://www.ncbi.nlm.nih.gov/pubmed/7907281

236. Patel YC. Somatostatin and its receptor family. Front Neuroendocrinol. 1999;20:

157–198. doi:10.1006/frne.1999.0183

237. Reichlin S. Somatostatin. N Engl J Med. 1983;309: 1495–1501. doi:10.1056/NEJM198312153092406

238. Ramírez JL, Mouchantaf R, Kumar U, Otero Corchon V, Rubinstein M, Low MJ, et al. Brain somatostatin receptors are up-regulated in somatostatin-deficient mice. Mol Endocrinol. 2002;16: 1951–1963. doi:10.1210/me.2002-0068

239. Reisine T, Bell GI. Molecular biology of somatostatin receptors. Endocr Rev. 1995;16: 427–442. doi:10.1210/edrv-16-4-427

240. Hukovic N, Rocheville M, Kumar U, Sasi R, Khare S, Patel YC. Agonist-dependent up-regulation of human somatostatin receptor type 1 requires molecular signals in the cytoplasmic C-tail. J Biol Chem. 1999;274: 24550–24558. doi:10.1074/jbc.274.35.24550

241. Hukovic N, Panetta R, Kumar U, Patel YC. Agonist-dependent regulation of cloned human somatostatin receptor types 1-5 (hSSTR1-5): subtype selective internalization or upregulation. Endocrinology. 1996;137: 4046–4049. doi:10.1210/endo.137.9.8756582

242. Song Y-H, Yoon J, Lee S-H. The role of neuropeptide somatostatin in the brain and its application in treating neurological disorders. Exp Mol Med. 2021;53: 328–338. doi:10.1038/s12276-021-00580-4

243. Francis BH, Baskin DG, Saunders DR, Ensinck JW. Distribution of somatostatin-14 and somatostatin-28 gastrointestinal-pancreatic cells of rats and humans. Gastroenterology. 1990;99: 1283–1291. doi:10.1016/0016-5085(90)91151-u

244. Liguz-Lecznar M, Urban-Ciecko J, Kossut M. Somatostatin and Somatostatin-Containing Neurons in Shaping Neuronal Activity and Plasticity. Front Neural Circuits. 2016;10: 48. doi:10.3389/fncir.2016.00048

245. Baraban SC, Tallent MK. Interneuron Diversity series: Interneuronal neuropeptides – endogenous regulators of neuronal excitability. Trends in Neurosciences. 2004. pp. 135–142. doi:10.1016/j.tins.2004.01.008

246. Bichet D, Bouvier M, Chini B, Gimpl G, Guillon G, Kimura T, et al. Vasopressin and oxytocin receptors (version 2019.4) in the IUPHAR/BPS Guide to Pharmacology Database. IUPHAR/BPS Guide to Pharmacology CITE. 2019. doi:10.2218/gtopdb/f66/2019.4

247. Holmes CL, Landry DW, Granton JT. Critical Care. 2003. p. 427. doi:10.1186/cc2337

248. Fineberg SK, Ross DA. Oxytocin and the Social Brain. Biol Psychiatry. 2017;81: e19–e21. doi:10.1016/j.biopsych.2016.11.004

249. Lee H-J, Macbeth AH, Pagani JH, Young WS 3rd. Oxytocin: the great facilitator of life. Prog Neurobiol. 2009;88: 127–151. doi:10.1016/j.pneurobio.2009.04.001

250. Yang H-P, Wang L, Han L, Wang SC. Nonsocial functions of hypothalamic oxytocin. ISRN Neurosci. 2013;2013: 179272. doi:10.1155/2013/179272

251. Rousseau-Merck MF, René P, Derré J, Bienvenu T, Berger R, de Keyzer Y. Chromosomal localization of the human V3 pituitary vasopressin receptor gene (AVPR3) to 1q32. Genomics. 1995;30: 405–406. Available: https://www.ncbi.nlm.nih.gov/pubmed/8586456

252. Thibonnier M, Preston JA, Dulin N, Wilkins PL, Berti-Mattera LN, Mattera R. The human V3 pituitary vasopressin receptor: ligand binding profile and density-dependent signaling pathways. Endocrinology. 1997;138: 4109–4122. doi:10.1210/endo.138.10.5432

253. Thibonnier M, Conarty DM, Preston JA, Wilkins PL, Berti-Mattera LN, Mattera R. Molecular pharmacology of human vasopressin receptors. Adv Exp Med Biol. 1998;449: 251–276. doi:10.1007/978-1-4615-4871-3_34

254. Koshimizu T-A, Nasa Y, Tanoue A, Oikawa R, Kawahara Y, Kiyono Y, et al. V1a vasopressin receptors maintain normal blood pressure by regulating circulating blood volume and baroreflex sensitivity. Proc Natl Acad Sci U S A. 2006;103: 7807–7812. doi:10.1073/pnas.0600875103

255. Aoyagi T, Birumachi J-I, Hiroyama M, Fujiwara Y, Sanbe A, Yamauchi J, et al. Alteration of glucose homeostasis in V1a vasopressin receptor-deficient mice. Endocrinology. 2007;148: 2075–2084. doi:10.1210/en.2006-1315

256. Birumachi J-I, Hiroyama M, Fujiwara Y, Aoyagi T, Sanbe A, Tanoue A. Impaired arginine-vasopressin-induced aldosterone release from adrenal gland cells in mice lacking the vasopressin V1A receptor. Eur J Pharmacol. 2007;566: 226–230. doi:10.1016/j.ejphar.2007.03.022

257. Briley EM, Lolait SJ, Axelrod J, Felder CC. The cloned vasopressin V1a receptor stimulates phospholipase A2, phospholipase C, and phospholipase D through activation of receptor-operated calcium channels. Neuropeptides. 1994;27: 63–74. doi:10.1016/0143-4179(94)90017-5

258. Chandrashekhar Y, Prahash AJ, Sen S, Gupta S, Roy S, Anand IS. The role of arginine vasopressin and its receptors in the normal and failing rat heart. J Mol Cell Cardiol. 2003;35: 495–504. doi:10.1016/s0022-2828(03)00053-1

259. Yirmiya N, Rosenberg C, Levi S, Salomon S, Shulman C, Nemanov L, et al. Association between the arginine vasopressin 1a receptor (AVPR1a) gene and autism in a family-based study: mediation by socialization skills. Mol Psychiatry. 2006;11: 488–494. doi:10.1038/sj.mp.4001812

260. Young LJ, Nilsen R, Waymire KG, MacGregor GR, Insel TR. Increased

affiliative response to vasopressin in mice expressing the V1a receptor from a monogamous vole. Nature. 1999;400: 766–768. doi:10.1038/23475

261. Bielsky IF, Hu S-B, Szegda KL, Westphal H, Young LJ. Profound impairment in social recognition and reduction in anxiety-like behavior in vasopressin V1a receptor knockout mice. Neuropsychopharmacology. 2004;29: 483–493. doi:10.1038/sj.npp.1300360

262. Lim MM, Wang Z, Olazábal DE, Ren X, Terwilliger EF, Young LJ. Enhanced partner preference in a promiscuous species by manipulating the expression of a single gene. Nature. 2004;429: 754–757. doi:10.1038/nature02539

263. Gaillard RC, Schoenenberg P, Favrod-Coune CA, Muller AF, Marie J, Bockaert J, et al. Properties of rat anterior pituitary vasopressin receptors: relation to adenylate cyclase and the effect of corticotropin-releasing factor. Proc Natl Acad Sci U S A. 1984;81: 2907–2911. doi:10.1073/pnas.81.9.2907

264. Lolait SJ, O'Carroll AM, Mahan LC, Felder CC, Button DC, Young WS 3rd, et al. Extrapituitary expression of the rat V1b vasopressin receptor gene. Proc Natl Acad Sci U S A. 1995;92: 6783–6787. doi:10.1073/pnas.92.15.6783

265. Lolait SJ, Stewart LQ, Jessop DS, Young WS 3rd, O'Carroll A-M. The hypothalamic-pituitary-adrenal axis response to stress in mice lacking functional vasopressin V1b receptors. Endocrinology. 2007;148: 849–856. doi:10.1210/en.2006-1309

266. René P, Lenne F, Ventura MA, Bertagna X, de Keyzer Y. Nucleotide sequence and structural organization of the human vasopressin pituitary receptor (V3) gene. Gene. 2000;241: 57–64. doi:10.1016/s0378-1119(99)00468-0

267. Griebel G, Simiand J, Serradeil-Le Gal C, Wagnon J, Pascal M, Scatton B, et al. Anxiolytic- and antidepressant-like effects of the non-peptide vasopressin V1b receptor antagonist, SSR149415, suggest an innovative approach for the treatment of stress-related disorders. Proc Natl Acad Sci U S A. 2002;99: 6370–6375. doi:10.1073/pnas.092012099

268. Nikkheslat N, McLaughlin AP, Hastings C, Zajkowska Z, Nettis MA, Mariani N, et al. Childhood trauma, HPA axis activity and antidepressant response in patients with depression. Brain Behav Immun. 2020;87: 229–237. doi:10.1016/j.bbi.2019.11.024

269. Rosenblat JD, McIntyre RS, Alves GS, Fountoulakis KN, Carvalho AF. Beyond Monoamines-Novel Targets for Treatment-Resistant Depression: A Comprehensive Review. Curr Neuropharmacol. 2015;13: 636–655. doi:10.2174/1570159x13666150630175044

270. Juruena MF, Pariante CM, Papadopoulos AS, Poon L, Lightman S, Cleare AJ. Prednisolone suppression test in depression: prospective study of the role of HPA axis dysfunction in treatment resistance. Br J Psychiatry. 2009;194: 342–349.

doi:10.1192/bjp.bp.108.050278

271. Stetler C, Miller GE. Depression and hypothalamic-pituitary-adrenal activation: a quantitative summary of four decades of research. Psychosom Med. 2011;73: 114–126. doi:10.1097/PSY.0b013e31820ad12b

272. Dinan TG, Scott LV. Anatomy of melancholia: focus on hypothalamic-pituitary-adrenal axis overactivity and the role of vasopressin. J Anat. 2005;207: 259–264. doi:10.1111/j.1469-7580.2005.00443.x

273. Meynen G, Unmehopa UA, van Heerikhuize JJ, Hofman MA, Swaab DF, Hoogendijk WJG. Increased arginine vasopressin mRNA expression in the human hypothalamus in depression: A preliminary report. Biol Psychiatry. 2006;60: 892–895. doi:10.1016/j.biopsych.2005.12.010

274. Zhou JN, Riemersma RF, Unmehopa UA, Hoogendijk WJ, van Heerikhuize JJ, Hofman MA, et al. Alterations in arginine vasopressin neurons in the suprachiasmatic nucleus in depression. Arch Gen Psychiatry. 2001;58: 655–662. doi:10.1001/archpsyc.58.7.655

275. van Londen L, Goekoop JG, van Kempen GM, Frankhuijzen-Sierevogel AC, Wiegant VM, van der Velde EA, et al. Plasma levels of arginine vasopressin elevated in patients with major depression. Neuropsychopharmacology. 1997;17: 284–292. doi:10.1016/S0893-133X(97)00054-7

276. Purba JS, Hoogendijk WJ, Hofman MA, Swaab DF. Increased number of vasopressin- and oxytocin-expressing neurons in the paraventricular nucleus of the hypothalamus in depression. Arch Gen Psychiatry. 1996;53: 137–143. doi:10.1001/archpsyc.1996.01830020055007

277. Chaki S. Vasopressin V1B Receptor Antagonists as Potential Antidepressants. Int J Neuropsychopharmacol. 2021;24: 450–463. doi:10.1093/ijnp/pyab013

278. Ala Y, Morin D, Mouillac B, Sabatier N, Vargas R, Cotte N, et al. Functional studies of twelve mutant V2 vasopressin receptors related to nephrogenic diabetes insipidus: molecular basis of a mild clinical phenotype. J Am Soc Nephrol. 1998;9: 1861–1872. doi:10.1681/ASN.V9101861

279. Sato K, Fukuno H, Taniguchi T, Sawada S, Fukui T, Kinoshita M. A novel mutation in the vasopressin V2 receptor gene in a woman with congenital nephrogenic diabetes insipidus. Intern Med. 1999;38: 808–812. doi:10.2169/internalmedicine.38.808

280. Schöneberg T, Kostenis E, Liu J, Gudermann T, Wess J. Molecular aspects of vasopressin receptor function. Adv Exp Med Biol. 1998;449: 347–358. doi:10.1007/978-1-4615-4871-3_44

281. Weig HJ, Laugwitz KL, Moretti A, Kronsbein K, Städele C, Brüning S, et al. Enhanced cardiac contractility after gene transfer of V2 vasopressin receptors In

vivo by ultrasound-guided injection or transcoronary delivery. Circulation. 2000;101: 1578–1585. doi:10.1161/01.cir.101.13.1578

282. Akerlund M, Bossmar T, Brouard R, Kostrzewska A, Laudanski T, Lemancewicz A, et al. Receptor binding of oxytocin and vasopressin antagonists and inhibitory effects on isolated myometrium from preterm and term pregnant women. Br J Obstet Gynaecol. 1999;106: 1047–1053. doi:10.1111/j.1471-0528.1999.tb08112.x

283. Juul KV, Bichet DG, Nielsen S, Nørgaard JP. The physiological and pathophysiological functions of renal and extrarenal vasopressin V2 receptors. Am J Physiol Renal Physiol. 2014;306: F931–40. doi:10.1152/ajprenal.00604.2013

284. Yayla MA, Arda B, Çağlar Ö, Erbaş O. Peptide Hormones and Neurodegenerative Diseases. JEBMS. 2021;2: 062–075. doi:10.5606/jebms.2021.75639

285. Buisman-Pijlman FTA, Sumracki NM, Gordon JJ, Hull PR, Carter CS, Tops M. Individual differences underlying susceptibility to addiction: Role for the endogenous oxytocin system. Pharmacol Biochem Behav. 2014;119: 22–38. doi:10.1016/j.pbb.2013.09.005

286. Viviani D, Stoop R. Opposite effects of oxytocin and vasopressin on the emotional expression of the fear response. Prog Brain Res. 2008;170: 207–218. doi:10.1016/S0079-6123(08)00418-4

287. Kirsch P, Esslinger C, Chen Q, Mier D, Lis S, Siddhanti S, et al. Oxytocin modulates neural circuitry for social cognition and fear in humans. J Neurosci. 2005;25: 11489–11493. doi:10.1523/JNEUROSCI.3984-05.2005

288. Petersson M, Lundeberg T, Sohlström A, Wiberg U, Uvnäs-Moberg K. Oxytocin increases the survival of musculocutaneous flaps. Naunyn Schmiedebergs Arch Pharmacol. 1998;357: 701–704. doi:10.1007/pl00005227

289. Grewen KM, Light KC, Mechlin B, Girdler SS. Ethnicity is associated with alterations in oxytocin relationships to pain sensitivity in women. Ethn Health. 2008;13: 219–241. doi:10.1080/13557850701837310

290. Neumann ID, Landgraf R. Balance of brain oxytocin and vasopressin: implications for anxiety, depression, and social behaviors. Trends Neurosci. 2012;35: 649–659. doi:10.1016/j.tins.2012.08.004

291. McQuaid RJ, McInnis OA, Abizaid A, Anisman H. Making room for oxytocin in understanding depression. Neurosci Biobehav Rev. 2014;45: 305–322. doi:10.1016/j.neubiorev.2014.07.005

292. Wulsin AC, Herman JP, Solomon MB. Mifepristone decreases depression-like behavior and modulates neuroendocrine and central hypothalamic-pituitary-adrenocortical axis responsiveness to stress. Psychoneuroendocrinology. 2010;35: 1100–1112. doi:10.1016/j.psyneuen.2010.01.011

293. Bey K, Campos-Martin R, Klawohn J, Reuter B, Grützmann R, Riesel A, et al. Hypermethylation of the oxytocin receptor gene (OXTR) in obsessive-compulsive disorder: further evidence for a biomarker of disease and treatment response. Epigenetics. 2022;17: 642–652. doi:10.1080/15592294.2021.1943864

294. Gabery S, Ahmed RM, Caga J, Kiernan MC, Halliday GM, Petersén Å. Loss of the metabolism and sleep regulating neuronal populations expressing orexin and oxytocin in the hypothalamus in amyotrophic lateral sclerosis. Neuropathol Appl Neurobiol. 2021;47: 979–989. doi:10.1111/nan.12709

295. Borowsky B, Adham N, Jones KA, Raddatz R, Artymyshyn R, Ogozalek KL, et al. Trace amines: identification of a family of mammalian G protein-coupled receptors. Proc Natl Acad Sci U S A. 2001;98: 8966–8971. doi:10.1073/pnas.151105198

296. Kennedy JL, Olson SB, Magenis RE, Amara SG. Amphetamine, 3, 4-methylenedioxymethamphetamine, lysergic acid diethylamide, and metabolites of the catecholamine neurotransmitters are agonists of a rat trace …. Molecular. 2001. Available: https://molpharm.aspetjournals.org/content/60/6/1181.short?casa_token=2LQ00oulm1cAAAAA:8HeAcZb6KQFW5LH4Jlds8opBseCxwUMFsrN0NMY-DQ8JyDPMbijQnc1JTOJjRfYNFtCufdkGa-4

297. Eyun S-I, Moriyama H, Hoffmann FG, Moriyama EN. Molecular Evolution and Functional Divergence of Trace Amine-Associated Receptors. PLoS One. 2016;11: e0151023. doi:10.1371/journal.pone.0151023

298. Lindemann L, Ebeling M, Kratochwil NA, Bunzow JR, Grandy DK, Hoener MC. Trace amine-associated receptors form structurally and functionally distinct subfamilies of novel G protein-coupled receptors. Genomics. 2005;85: 372–385. doi:10.1016/j.ygeno.2004.11.010

299. Revel FG, Moreau JL, Pouzet B, Mory R, Bradaia A, Buchy D, et al. A new perspective for schizophrenia: TAAR1 agonists reveal antipsychotic-and antidepressant-like activity, improve cognition and control body weight. Mol Psychiatry. 2013;18: 543–556. Available: https://idp.nature.com/authorize/casa?redirect_uri=https://www.nature.com/articles/mp201257&casa_token=vmkW7-hEtkwAAAAA:ebPoIeb-y04tKai9HTDtQWknh4X04ZCllR-IgLBcdIw4AIa6_bo27oVlbjfNS6KvfyXq2zVjlI-sQ5mu

300. Pei Y, Asif-Malik A, Canales JJ. Trace Amines and the Trace Amine-Associated Receptor 1: Pharmacology, Neurochemistry, and Clinical Implications. Front Neurosci. 2016;10: 148. doi:10.3389/fnins.2016.00148

301. Raab S, Wang H, Uhles S, Cole N, Alvarez-Sanchez R, Künnecke B, et al. Incretin-like effects of small molecule trace amine-associated receptor 1 agonists. Mol Metab. 2016;5: 47–56. doi:10.1016/j.molmet.2015.09.015

302. Bunzow JR, Sonders MS, Arttamangkul S, Harrison LM, Zhang G, Quigley DI, et al. Amphetamine, 3,4-methylenedioxymethamphetamine, lysergic acid diethylamide, and metabolites of the catecholamine neurotransmitters are agonists of a rat trace amine receptor. Mol Pharmacol. 2001;60: 1181–1188. doi:10.1124/mol.60.6.1181

303. Zucchi R, Chiellini G, Scanlan TS, Grandy DK. Trace amine-associated receptors and their ligands. Br J Pharmacol. 2006;149: 967–978. doi:10.1038/sj.bjp.0706948

304. Gainetdinov RR, Hoener MC, Berry MD. Trace Amines and Their Receptors. Pharmacol Rev. 2018;70: 549–620. doi:10.1124/pr.117.015305

305. Boulton AA. Phenylethylaminergic modulation of catecholaminergic neurotransmission. Prog Neuropsychopharmacol Biol Psychiatry. 1991;15: 139–156. doi:10.1016/0278-5846(91)90076-d

306. Rutigliano G, Accorroni A, Zucchi R. The Case for TAAR1 as a Modulator of Central Nervous System Function. Front Pharmacol. 2017;8: 987. doi:10.3389/fphar.2017.00987

307. Jones RS. Noradrenaline-octopamine interactions on cortical neurones in the rat. Eur J Pharmacol. 1982;77: 159–162. doi:10.1016/0014-2999(82)90012-7

308. Espinoza S, Ghisi V, Emanuele M, Leo D, Sukhanov I, Sotnikova TD, et al. Postsynaptic D2 dopamine receptor supersensitivity in the striatum of mice lacking TAAR1. Neuropharmacology. 2015;93: 308–313. doi:10.1016/j.neuropharm.2015.02.010

309. Harmeier A, Obermueller S, Meyer CA, Revel FG, Buchy D, Chaboz S, et al. Trace amine-associated receptor 1 activation silences GSK3β signaling of TAAR1 and D2R heteromers. Eur Neuropsychopharmacol. 2015;25: 2049–2061. doi:10.1016/j.euroneuro.2015.08.011

310. Bradaia A, Trube G, Stalder H, Norcross RD, Ozmen L, Wettstein JG, et al. The selective antagonist EPPTB reveals TAAR1-mediated regulatory mechanisms in dopaminergic neurons of the mesolimbic system. Proc Natl Acad Sci U S A. 2009;106: 20081–20086. doi:10.1073/pnas.0906522106

311. Revel FG, Moreau J-L, Gainetdinov RR, Bradaia A, Sotnikova TD, Mory R, et al. TAAR1 activation modulates monoaminergic neurotransmission, preventing hyperdopaminergic and hypoglutamatergic activity. Proc Natl Acad Sci U S A. 2011;108: 8485–8490. doi:10.1073/pnas.1103029108

312. Liberles SD, Buck LB. A second class of chemosensory receptors in the olfactory epithelium. Nature. 2006;442: 645–650. doi:10.1038/nature05066

313. Wallrabenstein I, Kuklan J, Weber L, Zborala S, Werner M, Altmüller J, et al. Human trace amine-associated receptor TAAR5 can be activated by

trimethylamine. PLoS One. 2013;8: e54950. doi:10.1371/journal.pone.0054950

314. Dinter J, Mühlhaus J, Wienchol CL, Yi C-X, Nürnberg D, Morin S, et al. Inverse agonistic action of 3-iodothyronamine at the human trace amine-associated receptor 5. PLoS One. 2015;10: e0117774. doi:10.1371/journal.pone.0117774

315. Mühlhaus J, Dinter J, Nürnberg D, Rehders M, Depke M, Golchert J, et al. Analysis of human TAAR8 and murine Taar8b mediated signaling pathways and expression profile. Int J Mol Sci. 2014;15: 20638–20655. doi:10.3390/ijms151120638

316. Mazella J, Sarret P, Vincent J-P. Neurotensin receptors (version 2019.4) in the IUPHAR/BPS Guide to Pharmacology Database. IUPHAR BPS Guide Pharm CITE. 2019;2019. doi:10.2218/gtopdb/f47/2019.4

317. Vita N, Laurent P, Lefort S, Chalon P, Dumont X, Kaghad M, et al. Cloning and expression of a complementary DNA encoding a high affinity human neurotensin receptor. FEBS Lett. 1993;317: 139–142. doi:10.1016/0014-5793(93)81509-x

318. Zhang X, Xu ZQ, Bao L, Dagerlind A, Hökfelt T. Complementary distribution of receptors for neurotensin and NPY in small neurons in rat lumbar DRGs and regulation of the receptors and peptides after peripheral axotomy. J Neurosci. 1995;15: 2733–2747. doi:10.1523/JNEUROSCI.15-04-02733.1995

319. Elde R, Schalling M, Ceccatelli S, Nakanishi S, Hökfelt T. Localization of neuropeptide receptor mRNA in rat brain: initial observations using probes for neurotensin and substance P receptors. Neurosci Lett. 1990;120: 134–138. doi:10.1016/0304-3940(90)90187-e

320. Chalon P, Vita N, Kaghad M, Guillemot M, Bonnin J, Delpech B, et al. Molecular cloning of a levocabastine-sensitive neurotensin binding site. FEBS Lett. 1996;386: 91–94. doi:10.1016/0014-5793(96)00397-3

321. Mazella J, Botto JM, Guillemare E, Coppola T, Sarret P, Vincent JP. Structure, functional expression, and cerebral localization of the levocabastine-sensitive neurotensin/neuromedin N receptor from mouse brain. J Neurosci. 1996;16: 5613–5620. doi:10.1523/JNEUROSCI.16-18-05613.1996

322. Vita N, Oury-Donat F, Chalon P, Guillemot M, Kaghad M, Bachy A, et al. Neurotensin is an antagonist of the human neurotensin NT2 receptor expressed in Chinese hamster ovary cells. Eur J Pharmacol. 1998;360: 265–272. doi:10.1016/s0014-2999(98)00678-5

323. Sarret P, Beaudet A, Vincent JP, Mazella J. Regional and cellular distribution of low affinity neurotensin receptor mRNA in adult and developing mouse brain. J Comp Neurol. 1998;394: 344–356. Available: https://www.ncbi.nlm.nih.gov/pubmed/9579398

324. Walker N, Lepee-Lorgeoux I, Fournier J, Betancur C, Rostene W, Ferrara P, et

al. Tissue distribution and cellular localization of the levocabastine-sensitive neurotensin receptor mRNA in adult rat brain. Brain Res Mol Brain Res. 1998;57: 193–200. doi:10.1016/s0169-328x(98)00074-6

325. Amar S, Kitabgi P, Vincent JP. Activation of phosphatidylinositol turnover by neurotensin receptors in the human colonic adenocarcinoma cell line HT29. FEBS Lett. 1986;201: 31–36. doi:10.1016/0014-5793(86)80565-8

326. Amar S, Kitabgi P, Vincent JP. Stimulation of inositol phosphate production by neurotensin in neuroblastoma N1E115 cells: implication of GTP-binding proteins and relationship with the cyclic GMP response. J Neurochem. 1987;49: 999–1006. doi:10.1111/j.1471-4159.1987.tb09986.x

327. Gailly P, Najimi M, Hermans E. Evidence for the dual coupling of the rat neurotensin receptor with pertussis toxin-sensitive and insensitive G-proteins. FEBS Lett. 2000;483: 109–113. doi:10.1016/s0014-5793(00)02095-0

328. Amar S, Mazella J, Checler F, Kitabgi P, Vincent JP. Regulation of cyclic GMP levels by neurotensin in neuroblastoma clone N1E115. Biochem Biophys Res Commun. 1985;129: 117–125. doi:10.1016/0006-291x(85)91411-1

329. Bozou J-C, Amar S, Vincent J-P, Kitabgi P. Neurotensin-mediated inhibition of cyclic AMP formation in neuroblastoma NIE115 cells: involvement of the inhibitory GTP-binding component of adenylate cyclase. Mol Pharmacol. 1986;29: 489–496. Available: https://citeseerx.ist.psu.edu/document?repid=rep1&type=pdf&doi=85d2cf5127bc41973c76bf2da6ac0bc2db8b403c

330. Clineschmidt BV, McGuffin JC. Neurotensin administered intracisternally inhibits responsiveness of mice to noxious stimuli. Eur J Pharmacol. 1977;46: 395–396. doi:10.1016/0014-2999(77)90236-9

331. Furuta S, Kisara K, Sakurada S, Sakurada T, Sasaki Y, Suzuki K. Structure-antinociceptive activity studies with neurotensin. Br J Pharmacol. 1984;83: 43–48. doi:10.1111/j.1476-5381.1984.tb10117.x

332. Kleczkowska P, Lipkowski AW. Neurotensin and neurotensin receptors: characteristic, structure-activity relationship and pain modulation--a review. Eur J Pharmacol. 2013;716: 54–60. doi:10.1016/j.ejphar.2013.03.004

333. Karnik SS, Unal H, Kemp JR, Tirupula KC, Eguchi S, Vanderheyden PML, et al. International Union of Basic and Clinical Pharmacology. XCIX. Angiotensin Receptors: Interpreters of Pathophysiological Angiotensinergic Stimuli [corrected]. Pharmacol Rev. 2015;67: 754–819. doi:10.1124/pr.114.010454

334. de Gasparo M, Catt KJ, Inagami T, Wright JW, Unger T. International union of pharmacology. XXIII. The angiotensin II receptors. Pharmacol Rev. 2000;52: 415–472. Available: https://www.ncbi.nlm.nih.gov/pubmed/10977869

335. Alexander W, Bernstein KE, Catt KJ, De Gasparo M, Singh KD, Eguchi S, et al. Angiotensin receptors (version 2019.4) in the IUPHAR/BPS Guide to Pharmacology Database. IUPHAR/BPS Guide to Pharmacology CITE. 2019. doi:10.2218/gtopdb/f6/2019.4

336. Verma K, Pant M, Paliwal S, Dwivedi J, Sharma S. An Insight on Multicentric Signaling of Angiotensin II in Cardiovascular system: A Recent Update. Front Pharmacol. 2021;12: 734917. doi:10.3389/fphar.2021.734917

337. Adamcova M, Kawano I, Simko F. The Impact of microRNAs in Renin-Angiotensin-System-Induced Cardiac Remodelling. Int J Mol Sci. 2021;22. doi:10.3390/ijms22094762

338. Matsubara H. Pathophysiological role of angiotensin II type 2 receptor in cardiovascular and renal diseases. Circ Res. 1998;83: 1182–1191. doi:10.1161/01.res.83.12.1182

339. Kawai T, Forrester SJ, O'Brien S, Baggett A, Rizzo V, Eguchi S. AT1 receptor signaling pathways in the cardiovascular system. Pharmacol Res. 2017;125: 4–13. doi:10.1016/j.phrs.2017.05.008

340. Allen AM, MacGregor DP, McKinley MJ, Mendelsohn FA. Angiotensin II receptors in the human brain. Regul Pept. 1999;79: 1–7. doi:10.1016/s0167-0115(98)00138-4

341. Li Y, Li X-H, Yuan H. Angiotensin II type-2 receptor-specific effects on the cardiovascular system. Cardiovasc Diagn Ther. 2012;2: 56–62. doi:10.3978/j.issn.2223-3652.2012.02.02

342. Higuchi S, Ohtsu H, Suzuki H, Shirai H, Frank GD, Eguchi S. Angiotensin II signal transduction through the AT1 receptor: novel insights into mechanisms and pathophysiology. Clin Sci . 2007;112: 417–428. doi:10.1042/CS20060342

343. Catt KJ, Mendelsohn FA, Millan MA, Aguilera G. The role of angiotensin II receptors in vascular regulation. J Cardiovasc Pharmacol. 1984;6 Suppl 4: S575–86. doi:10.1097/00005344-198406004-00004

344. Hurt RC, Garrett JC, Keifer OP Jr, Linares A, Couling L, Speth RC, et al. Angiotensin type 1a receptors on corticotropin-releasing factor neurons contribute to the expression of conditioned fear. Genes Brain Behav. 2015;14: 526–533. doi:10.1111/gbb.12235

345. Marvar PJ, Goodman J, Fuchs S, Choi DC, Banerjee S, Ressler KJ. Angiotensin type 1 receptor inhibition enhances the extinction of fear memory. Biol Psychiatry. 2014;75: 864–872. doi:10.1016/j.biopsych.2013.08.024

346. Nazzaro P, Manzari M, Merlo M, Triggiani R, Scarano A, Ciancio L, et al. Distinct and combined vascular effects of ACE blockade and HMG-CoA reductase inhibition in hypertensive subjects. Hypertension. 1999;33: 719–725.

doi:10.1161/01.hyp.33.2.719

347. Nakajima M, Hutchinson HG, Fujinaga M, Hayashida W, Morishita R, Zhang L, et al. The angiotensin II type 2 (AT2) receptor antagonizes the growth effects of the AT1 receptor: gain-of-function study using gene transfer. Proc Natl Acad Sci U S A. 1995;92: 10663–10667. doi:10.1073/pnas.92.23.10663

348. Millatt LJ, Abdel-Rahman EM, Siragy HM. Angiotensin II and nitric oxide: a question of balance. Regul Pept. 1999;81: 1–10. doi:10.1016/s0167-0115(99)00027-0

349. Griendling KK, Lassègue B, Alexander RW. Angiotensin receptors and their therapeutic implications. Annu Rev Pharmacol Toxicol. 1996;36: 281–306. doi:10.1146/annurev.pa.36.040196.001433

350. De Gasparo M, Bottari S, Levens NR. Characteristics of angiotensin II receptors and their role in cell and organ physiology. Laragh JH and BM Brenner New York: Raven.

351. Horiuchi M, Akishita M, Dzau VJ. Recent progress in angiotensin II type 2 receptor research in the cardiovascular system. Hypertension. 1999;33: 613–621. doi:10.1161/01.hyp.33.2.613

352. de Gasparo M, Siragy HM. The AT2 receptor: fact, fancy and fantasy. Regul Pept. 1999;81: 11–24. doi:10.1016/s0167-0115(99)00023-3

353. D'Amore A, Black MJ, Thomas WG. The angiotensin II type 2 receptor causes constitutive growth of cardiomyocytes and does not antagonize angiotensin II type 1 receptor-mediated hypertrophy. Hypertension. 2005;46: 1347–1354. doi:10.1161/01.HYP.0000193504.51489.cf

354. Gold S, Haran I, Attias J, Shapira I, Shahar A. Biochemical and cardiovascular measures in subjects with noise-induced hearing loss. J Occup Med. 1989;31: 933–937. doi:10.1097/00043764-198911000-00018

355. Padia SH, Kemp BA, Howell NL, Fournie-Zaluski M-C, Roques BP, Carey RM. Conversion of renal angiotensin II to angiotensin III is critical for AT2 receptor-mediated natriuresis in rats. Hypertension. 2008;51: 460–465. doi:10.1161/HYPERTENSIONAHA.107.103242

356. Kemp BA, Bell JF, Rottkamp DM, Howell NL, Shao W, Navar LG, et al. Intrarenal angiotensin III is the predominant agonist for proximal tubule angiotensin type 2 receptors. Hypertension. 2012;60: 387–395. doi:10.1161/HYPERTENSIONAHA.112.191403

357. Barber MN, Sampey DB, Widdop RE. AT(2) receptor stimulation enhances antihypertensive effect of AT(1) receptor antagonist in hypertensive rats. Hypertension. 1999;34: 1112–1116. doi:10.1161/01.hyp.34.5.1112

358. Buisson B, Laflamme L, Bottari SP, de Gasparo M, Gallo-Payet N, Payet MD. A

G protein is involved in the angiotensin AT2 receptor inhibition of the T-type calcium current in non-differentiated NG108-15 cells. J Biol Chem. 1995;270: 1670–1674. doi:10.1074/jbc.270.4.1670

359. Stroth U, Blume A, Mielke K, Unger T. Angiotensin AT(2) receptor stimulates ERK1 and ERK2 in quiescent but inhibits ERK in NGF-stimulated PC12W cells. Brain Res Mol Brain Res. 2000;78: 175–180. doi:10.1016/s0169-328x(00)00093-0

360. Tsutsumi Y, Matsubara H, Masaki H, Kurihara H, Murasawa S, Takai S, et al. Angiotensin II type 2 receptor overexpression activates the vascular kinin system and causes vasodilation. J Clin Invest. 1999;104: 925–935. doi:10.1172/JCI7886

361. Wu L, Iwai M, Nakagami H, Chen R, Suzuki J, Akishita M, et al. Effect of angiotensin II type 1 receptor blockade on cardiac remodeling in angiotensin II type 2 receptor null mice. Arterioscler Thromb Vasc Biol. 2002;22: 49–54. doi:10.1161/hq0102.102277

362. Wu L, Iwai M, Nakagami H, Li Z, Chen R, Suzuki J, et al. Roles of angiotensin II type 2 receptor stimulation associated with selective angiotensin II type 1 receptor blockade with valsartan in the improvement of inflammation-induced vascular injury. Circulation. 2001;104: 2716–2721. doi:10.1161/hc4601.099404

363. Yamada T, Horiuchi M, Dzau VJ. Angiotensin II type 2 receptor mediates programmed cell death. Proc Natl Acad Sci U S A. 1996;93: 156–160. doi:10.1073/pnas.93.1.156

364. Zimpelmann J, Burns KD. Angiotensin II AT(2) receptors inhibit growth responses in proximal tubule cells. Am J Physiol Renal Physiol. 2001;281: F300–8. doi:10.1152/ajprenal.2001.281.2.F300

365. Hansen JL, Servant G, Baranski TJ, Fujita T, Iiri T, Sheikh SP. Functional reconstitution of the angiotensin II type 2 receptor and G(i) activation. Circ Res. 2000;87: 753–759. doi:10.1161/01.res.87.9.753

366. Zhang J, Pratt RE. The AT2 receptor selectively associates with Gialpha2 and Gialpha3 in the rat fetus. J Biol Chem. 1996;271: 15026–15033. Available: https://www.ncbi.nlm.nih.gov/pubmed/8663053

367. Cui T, Nakagami H, Iwai M, Takeda Y, Shiuchi T, Daviet L, et al. Pivotal role of tyrosine phosphatase SHP-1 in AT2 receptor-mediated apoptosis in rat fetal vascular smooth muscle cell. Cardiovasc Res. 2001;49: 863–871. doi:10.1016/s0008-6363(00)00299-6

368. Dimitropoulou C, White RE, Fuchs L, Zhang H, Catravas JD, Carrier GO. Angiotensin II Relaxes Microvessels Via the AT2 Receptor and Ca2+-Activated K+ (BKCa) Channels. Hypertension. 2001;37: 301–307. doi:10.1161/01.HYP.37.2.301

369. Fischer TA, Singh K, O'Hara DS, Kaye DM, Kelly RA. Role of $AT_1$and AT_2receptors in regulation of MAPKs and MKP-1 by ANG II in adult cardiac

myocytes. Am J Physiol Heart Circ Physiol. 1998;275: H906–H916. doi:10.1152/ajpheart.1998.275.3.h906

370. Gohlke P, Pees C, Unger T. AT2 receptor stimulation increases aortic cyclic GMP in SHRSP by a kinin-dependent mechanism. Hypertension. 1998;31: 349–355. doi:10.1161/01.hyp.31.1.349

371. Fischer TA, Singh K, O'Hara DS, Kaye DM, Kelly RA. Role of AT1 and AT2 receptors in regulation of MAPKs and MKP-1 by ANG II in adult cardiac myocytes. Am J Physiol. 1998;275: H906–16. doi:10.1152/ajpheart.1998.275.3.H906

372. Kang J, Richards EM, Posner P, Sumners C. Modulation of the delayed rectifier K+ current in neurons by an angiotensin II type 2 receptor fragment. Am J Physiol. 1995;268: C278–82. doi:10.1152/ajpcell.1995.268.1.C278

373. Rueckschloss U, Quinn MT, Holtz J, Morawietz H. Dose-dependent regulation of NAD(P)H oxidase expression by angiotensin II in human endothelial cells: protective effect of angiotensin II type 1 receptor blockade in patients with coronary artery disease. Arterioscler Thromb Vasc Biol. 2002;22: 1845–1851. doi:10.1161/01.atv.0000035392.38687.65

374. Silvestre J-S, Tamarat R, Senbonmatsu T, Icchiki T, Ebrahimian T, Iglarz M, et al. Antiangiogenic effect of angiotensin II type 2 receptor in ischemia-induced angiogenesis in mice hindlimb. Circ Res. 2002;90: 1072–1079. doi:10.1161/01.res.0000019892.41157.24

375. Sohn HY, Raff U, Hoffmann A, Gloe T, Heermeier K, Galle J, et al. Differential role of angiotensin II receptor subtypes on endothelial superoxide formation. Br J Pharmacol. 2000;131: 667–672. doi:10.1038/sj.bjp.0703566

376. Touyz RM, Berry C. Recent advances in angiotensin II signaling. Braz J Med Biol Res. 2002;35: 1001–1015. doi:10.1590/s0100-879x2002000900001

377. Inagami T, Iwai N, Sasaki K, Guo DF, Furuta H, Yamano Y, et al. Angiotensin II receptors: cloning and regulation. Arzneimittelforschung. 1993;43: 226–228. Available: https://www.ncbi.nlm.nih.gov/pubmed/8498969

378. Albiston AL, Mustafa T, McDowall SG, Mendelsohn FAO, Lee J, Chai SY. AT4 receptor is insulin-regulated membrane aminopeptidase: potential mechanisms of memory enhancement. Trends Endocrinol Metab. 2003;14: 72–77. doi:10.1016/s1043-2760(02)00037-1

379. Chaki S, Inagami T. A newly found angiotensin II receptor subtype mediates cyclic GMP formation in differentiated Neuro-2A cells. Eur J Pharmacol. 1992;225: 355–356. doi:10.1016/0922-4106(92)90111-8

380. Hallberg M. Targeting the insulin-regulated aminopeptidase/AT4 receptor for cognitive disorders. Drug News Perspect. 2009;22: 133–139. doi:10.1358/dnp.2009.22.3.1325032

381. Harding JW, Cook VI, Miller-Wing AV, Hanesworth JM, Sardinia MF, Hall KL, et al. Identification of an AII(3-8) [AIV] binding site in guinea pig hippocampus. Brain Res. 1992;583: 340–343. doi:10.1016/s0006-8993(10)80047-2

382. Benoist CC, Wright JW, Zhu M, Appleyard SM, Wayman GA, Harding JW. Facilitation of hippocampal synaptogenesis and spatial memory by C-terminal truncated Nle1-angiotensin IV analogs. J Pharmacol Exp Ther. 2011;339: 35–44. doi:10.1124/jpet.111.182220

383. Wright JW, Harding JW. Brain renin-angiotensin--a new look at an old system. Prog Neurobiol. 2011;95: 49–67. doi:10.1016/j.pneurobio.2011.07.001

384. Beyer CE, Dwyer JM, Platt BJ, Neal S, Luo B, Ling H-P, et al. Angiotensin IV elevates oxytocin levels in the rat amygdala and produces anxiolytic-like activity through subsequent oxytocin receptor activation. Psychopharmacology . 2010;209: 303–311. doi:10.1007/s00213-010-1791-1

385. Davis CJ, Kramár EA, De A, Meighan PC, Simasko SM, Wright JW, et al. AT4 receptor activation increases intracellular calcium influx and induces a non-N-methyl-D-aspartate dependent form of long-term potentiation. Neuroscience. 2006;137: 1369–1379. doi:10.1016/j.neuroscience.2005.10.051

386. Chai SY, Fernando R, Peck G, Ye S-Y, Mendelsohn FAO, Jenkins TA, et al. The angiotensin IV/AT4 receptor. Cell Mol Life Sci. 2004;61: 2728–2737. doi:10.1007/s00018-004-4246-1

387. Laviano A, Molfino A, Rianda S, Fanelli FR. The Growth Hormone Secretagogue Receptor (Ghs-R). Current Pharmaceutical Design. 2012. pp. 4749–4754. doi:10.2174/138161212803216906

388. Soares J-B, Roncon-Albuquerque R Jr, Leite-Moreira A. Ghrelin and ghrelin receptor inhibitors: agents in the treatment of obesity. Expert Opin Ther Targets. 2008;12: 1177–1189. doi:10.1517/14728222.12.9.1177

389. Pusztai P, Sarman B, Ruzicska E, Toke J, Racz K, Somogyi A, et al. Ghrelin: a new peptide regulating the neurohormonal system, energy homeostasis and glucose metabolism. Diabetes Metab Res Rev. 2008;24: 343–352. doi:10.1002/dmrr.830

390. Guan XM, Yu H, Palyha OC, McKee KK, Feighner SD, Sirinathsinghji DJ, et al. Distribution of mRNA encoding the growth hormone secretagogue receptor in brain and peripheral tissues. Brain Res Mol Brain Res. 1997;48: 23–29. doi:10.1016/s0169-328x(97)00071-5

391. Schellekens H, Dinan TG, Cryan JF. Lean mean fat reducing “ghrelin” machine: hypothalamic ghrelin and ghrelin receptors as therapeutic targets in obesity. Neuropharmacology. 2010;58: 2–16. doi:10.1016/j.neuropharm.2009.06.024

392. Gnanapavan S, Kola B, Bustin SA, Morris DG, McGee P, Fairclough P, et al.

The tissue distribution of the mRNA of ghrelin and subtypes of its receptor, GHS-R, in humans. J Clin Endocrinol Metab. 2002;87: 2988. doi:10.1210/jcem.87.6.8739

393. Gómez R, Lago F, Gómez-Reino JJ, Gualillo O. Novel factors as therapeutic targets to treat diabetes. Focus on leptin and ghrelin. Expert Opin Ther Targets. 2009;13: 583–591. doi:10.1517/14728220902914834

394. Broglio F, Gianotti L, Destefanis S, Fassino S, Abbate Daga G, Mondelli V, et al. The endocrine response to acute ghrelin administration is blunted in patients with anorexia nervosa, a ghrelin hypersecretory state. Clin Endocrinol . 2004;60: 592–599. doi:10.1111/j.1365-2265.2004.02011.x

395. Müller TD, Tschöp MH, Jarick I, Ehrlich S, Scherag S, Herpertz-Dahlmann B, et al. Genetic variation of the ghrelin activator gene ghrelin O-acyltransferase (GOAT) is associated with anorexia nervosa. J Psychiatr Res. 2011;45: 706–711. doi:10.1016/j.jpsychires.2010.10.001

396. Laviano A, Meguid MM, Inui A, Muscaritoli M, Rossi-Fanelli F. Therapy insight: Cancer anorexia-cachexia syndrome--when all you can eat is yourself. Nat Clin Pract Oncol. 2005;2: 158–165. doi:10.1038/ncponc0112

397. Ma X, Lin L, Qin G, Lu X, Fiorotto M, Dixit VD, et al. Ablations of ghrelin and ghrelin receptor exhibit differential metabolic phenotypes and thermogenic capacity during aging. PLoS One. 2011;6: e16391. doi:10.1371/journal.pone.0016391

398. Nagaya N, Kangawa K. Ghrelin, a novel growth hormone-releasing peptide, in the treatment of chronic heart failure. Regul Pept. 2003;114: 71–77. doi:10.1016/s0167-0115(03)00117-4

399. Gjesing AP, Larsen LH, Torekov SS, Hainerová IA, Kapur R, Johansen A, et al. Family and population-based studies of variation within the ghrelin receptor locus in relation to measures of obesity. PLoS One. 2010;5: e10084. doi:10.1371/journal.pone.0010084

400. Kamegai J, Tamura H, Shimizu T, Ishii S, Sugihara H, Oikawa S. Insulin-like growth factor-I down-regulates ghrelin receptor (growth hormone secretagogue receptor) expression in the rat pituitary. Regul Pept. 2005;127: 203–206. doi:10.1016/j.regpep.2004.12.001

401. Yada T, Dezaki K, Sone H, Koizumi M, Damdindorj B, Nakata M, et al. Ghrelin regulates insulin release and glycemia: physiological role and therapeutic potential. Curr Diabetes Rev. 2008;4: 18–23. doi:10.2174/157339908783502352

402. Dezaki K, Sone H, Yada T. Ghrelin is a physiological regulator of insulin release in pancreatic islets and glucose homeostasis. Pharmacol Ther. 2008;118: 239–249. doi:10.1016/j.pharmthera.2008.02.008

403. Zlotos DP, Jockers R, Cecon E, Rivara S, Witt-Enderby PA. MT1 and MT2 melatonin receptors: ligands, models, oligomers, and therapeutic potential. J Med Chem. 2014;57: 3161–3185. doi:10.1021/jm401343c

404. Reppert SM, Weaver DR, Ebisawa T. Cloning and characterization of a mammalian melatonin receptor that mediates reproductive and circadian responses. Neuron. 1994;13: 1177–1185. doi:10.1016/0896-6273(94)90055-8

405. Dubocovich ML, Delagrange P, Krause DN, Sugden D, Cardinali DP, Olcese J. International Union of Basic and Clinical Pharmacology. LXXV. Nomenclature, classification, and pharmacology of G protein-coupled melatonin receptors. Pharmacol Rev. 2010;62: 343–380. doi:10.1124/pr.110.002832

406. Cardinali DP, Delagrange P, Dubocovich ML, Jockers R, Krause DN, Markus RP, et al. Melatonin receptors (version 2019.4) in the IUPHAR/BPS Guide to Pharmacology Database. IUPHAR/BPS Guide to Pharmacology CITE. 2019. doi:10.2218/gtopdb/f39/2019.4

407. Emet M, Ozcan H, Ozel L, Yayla M, Halici Z, Hacimuftuoglu A. A Review of Melatonin, Its Receptors and Drugs. Eurasian J Med. 2016;48: 135–141. doi:10.5152/eurasianjmed.2015.0267

408. Boutin JA, Ferry G. Is There Sufficient Evidence that the Melatonin Binding Site MT3 Is Quinone Reductase 2? J Pharmacol Exp Ther. 2019;368: 59–65. doi:10.1124/jpet.118.253260

409. Nosjean O, Ferro M, Coge F, Beauverger P, Henlin JM, Lefoulon F, et al. Identification of the melatonin-binding site MT3 as the quinone reductase 2. J Biol Chem. 2000;275: 31311–31317. doi:10.1074/jbc.M005141200

410. Tosini G, Owino S, Guillaume J-L, Jockers R. Understanding melatonin receptor pharmacology: latest insights from mouse models, and their relevance to human disease. Bioessays. 2014;36: 778–787. doi:10.1002/bies.201400017

411. Markus RP, Cecon E, Pires-Lapa MA. Immune-pineal axis: nuclear factor κB (NF-kB) mediates the shift in the melatonin source from pinealocytes to immune competent cells. Int J Mol Sci. 2013;14: 10979–10997. doi:10.3390/ijms140610979

412. Jockers R, Maurice P, Boutin JA, Delagrange P. Melatonin receptors, heterodimerization, signal transduction and binding sites: what's new? Br J Pharmacol. 2008;154: 1182–1195. doi:10.1038/bjp.2008.184

413. Doghramji K. Melatonin and its receptors: a new class of sleep-promoting agents. J Clin Sleep Med. 2007;3: S17–23. Available: https://www.ncbi.nlm.nih.gov/pubmed/17824497

414. Harkness EM, Thorburn DN. Hemifacial microsomia label questioned. The Angle orthodontist. 1990. pp. 5–6. doi:10.1043/0003-

3219(1990)060<0005:HMLQ>2.0.CO;2

415. Dubocovich ML. Melatonin receptors: role on sleep and circadian rhythm regulation. Sleep Med. 2007;8 Suppl 3: 34–42. doi:10.1016/j.sleep.2007.10.007

416. Lépinay J, Taragnat C, Dubois J-P, Chesneau D, Jockers R, Delagrange P, et al. Negative regulation of melatonin secretion by melatonin receptors in ovine pinealocytes. PLOS ONE. 2021. p. e0255249. doi:10.1371/journal.pone.0255249

417. Jockers R, Delagrange P, Dubocovich ML, Markus RP, Renault N, Tosini G, et al. Update on melatonin receptors: IUPHAR Review 20. Br J Pharmacol. 2016;173: 2702–2725. doi:10.1111/bph.13536

418. Reppert SM, Godson C, Mahle CD, Weaver DR, Slaugenhaupt SA, Gusella JF. Molecular characterization of a second melatonin receptor expressed in human retina and brain: the Mel1b melatonin receptor. Proc Natl Acad Sci U S A. 1995;92: 8734–8738. doi:10.1073/pnas.92.19.8734

419. Besharse JC, Dunis DA. Methoxyindoles and photoreceptor metabolism: activation of rod shedding. Science. 1983;219: 1341–1343. doi:10.1126/science.6828862

420. Sharan K, Lewis K, Furukawa T, Yadav VK. Regulation of bone mass through pineal-derived melatonin-MT2 receptor pathway. J Pineal Res. 2017;63. doi:10.1111/jpi.12423

421. Rui T, Wang H, Li Q, Cheng Y, Gao Y, Fang X, et al. Deletion of ferritin H in neurons counteracts the protective effect of melatonin against traumatic brain injury-induced ferroptosis. J Pineal Res. 2021;70: e12704. doi:10.1111/jpi.12704

422. Noseda ACD, Rodrigues LS, Targa ADS, Ilkiw JL, Fagotti J, Dos Santos PD, et al. MT2 melatonin receptors expressed in the olfactory bulb modulate depressive-like behavior and olfaction in the 6-OHDA model of Parkinson's disease. Eur J Pharmacol. 2021;891: 173722. doi:10.1016/j.ejphar.2020.173722

423. Ayoub MA, Couturier C, Lucas-Meunier E, Angers S, Fossier P, Bouvier M, et al. Monitoring of ligand-independent dimerization and ligand-induced conformational changes of melatonin receptors in living cells by bioluminescence resonance energy transfer. J Biol Chem. 2002;277: 21522–21528. doi:10.1074/jbc.M200729200

424. Ayoub MA, Levoye A, Delagrange P, Jockers R. Preferential formation of MT1/MT2 melatonin receptor heterodimers with distinct ligand interaction properties compared with MT2 homodimers. Mol Pharmacol. 2004;66: 312–321. doi:10.1124/mol.104.000398

425. Baba K, Benleulmi-Chaachoua A, Journé A-S, Kamal M, Guillaume J-L, Dussaud S, et al. Heteromeric MT1/MT2 melatonin receptors modulate photoreceptor function. Sci Signal. 2013;6: ra89. doi:10.1126/scisignal.2004302

426. Takeda S, Kadowaki S, Haga T, Takaesu H, Mitaku S. Identification of G protein-coupled receptor genes from the human genome sequence. FEBS Lett. 2002;520: 97–101. doi:10.1016/s0014-5793(02)02775-8

427. Alexander SP, Christopoulos A, Davenport AP, Kelly E, Marrion NV, Peters JA, et al. THE CONCISE GUIDE TO PHARMACOLOGY 2017/18: G protein-coupled receptors. Br J Pharmacol. 2017;174 Suppl 1: S17–S129. doi:10.1111/bph.13878

428. Davenport AP, Alexander SPH, Sharman JL, Pawson AJ, Benson HE, Monaghan AE, et al. International Union of Basic and Clinical Pharmacology. LXXXVIII. G protein-coupled receptor list: recommendations for new pairings with cognate ligands. Pharmacol Rev. 2013;65: 967–986. doi:10.1124/pr.112.007179

429. Gloriam DEI, Schiöth HB, Fredriksson R. Nine new human Rhodopsin family G-protein coupled receptors: identification, sequence characterisation and evolutionary relationship. Biochim Biophys Acta. 2005;1722: 235–246. doi:10.1016/j.bbagen.2004.12.001

430. Vedel L, Nøhr AC, Gloriam DE, Bräuner-Osborne H. Pharmacology and function of the orphan GPR139 G protein-coupled receptor. Basic Clin Pharmacol Toxicol. 2020;126 Suppl 6: 35–46. doi:10.1111/bcpt.13263

431. Kononoff J, Kallupi M, Kimbrough A, Conlisk D, de Guglielmo G, George O. Systemic and Intra-Habenular Activation of the Orphan G Protein-Coupled Receptor GPR139 Decreases Compulsive-Like Alcohol Drinking and Hyperalgesia in Alcohol-Dependent Rats. eNeuro. 2018;5. doi:10.1523/ENEURO.0153-18.2018

432. Hitchcock S, Lam B, Monenschein H, Reichard H. 4-OXO-3,4-DIHYDRO-1,2,3-BENZOTRIAZINES AS MODULATORS OF GPR139. World Patent. 2016081736, 2016. Available: https://patentscope.wipo.int/search/en/detail.jsf?docId=WO2016081736

433. Ebejer JL, Duffy DL, van der Werf J, Wright MJ, Montgomery G, Gillespie NA, et al. Genome-wide association study of inattention and hyperactivity-impulsivity measured as quantitative traits. Twin Res Hum Genet. 2013;16: 560–574. doi:10.1017/thg.2013.12

434. Castellani CA, Awamleh Z, Melka MG, O'Reilly RL, Singh SM. Copy number variation distribution in six monozygotic twin pairs discordant for schizophrenia. Twin Res Hum Genet. 2014;17: 108–120. doi:10.1017/thg.2014.6

435. Al Hafid N, Christodoulou J. Phenylketonuria: a review of current and future treatments. Transl Pediatr. 2015;4: 304–317. doi:10.3978/j.issn.2224-4336.2015.10.07

436. Salim K, Fenton T, Bacha J, Urien-Rodriguez H, Bonnert T, Skynner HA, et al. Oligomerization of G-protein-coupled receptors shown by selective co-immunoprecipitation. J Biol Chem. 2002;277: 15482–15485. doi:10.1074/jbc.M201539200

437. Derouiche L, Massotte D. G protein-coupled receptor heteromers are key players in substance use disorder. Neurosci Biobehav Rev. 2019;106: 73–90. doi:10.1016/j.neubiorev.2018.09.026

438. Pellissier LP, Barthet G, Gaven F, Cassier E, Trinquet E, Pin J-P, et al. G protein activation by serotonin type 4 receptor dimers: evidence that turning on two protomers is more efficient. J Biol Chem. 2011;286: 9985–9997. doi:10.1074/jbc.M110.201939

439. Han Y, Moreira IS, Urizar E, Weinstein H, Javitch JA. Allosteric communication between protomers of dopamine class A GPCR dimers modulates activation. Nat Chem Biol. 2009;5: 688–695. doi:10.1038/nchembio.199

440. Maggio R, Rocchi C, Scarselli M. Experimental strategies for studying G protein-coupled receptor homo- and heteromerization with radioligand binding and signal transduction methods. Methods Enzymol. 2013;521: 295–310. doi:10.1016/B978-0-12-391862-8.00016-8

441. Borroto-Escuela DO, Hagman B, Woolfenden M, Pinton L, Jiménez-Beristain A, Oflijan J, et al. In Situ Proximity Ligation Assay to Study and Understand the Distribution and Balance of GPCR Homo- and Heteroreceptor Complexes in the Brain. In: Luján R, Ciruela F, editors. Receptor and Ion Channel Detection in the Brain: Methods and Protocols. New York, NY: Springer New York; 2016. pp. 109–124. doi:10.1007/978-1-4939-3064-7_9

442. Vischer HF, Castro M, Pin J-P. G Protein-Coupled Receptor Multimers: A Question Still Open Despite the Use of Novel Approaches. Mol Pharmacol. 2015;88: 561–571. doi:10.1124/mol.115.099440

443. Franco R. G-protein-coupled receptor heteromers or how neurons can display differently flavoured patterns in response to the same neurotransmitter. British Journal of Pharmacology. 2009. pp. 23–31. doi:10.1111/j.1476-5381.2009.00181.x

444. Franco R, Martínez-Pinilla E, Lanciego JL, Navarro G. Basic Pharmacological and Structural Evidence for Class A G-Protein-Coupled Receptor Heteromerization. Frontiers in Pharmacology. 2016. doi:10.3389/fphar.2016.00076

445. Ciruela F, Casadó V, Rodrigues RJ, Luján R, Burgueño J, Canals M, et al. Presynaptic control of striatal glutamatergic neurotransmission by adenosine A1-A2A receptor heteromers. J Neurosci. 2006;26: 2080–2087. doi:10.1523/JNEUROSCI.3574-05.2006

446. Ferré S, Ciruela F, Quiroz C, Luján R, Popoli P, Cunha RA, et al. Adenosine receptor heteromers and their integrative role in striatal function. ScientificWorldJournal. 2007;7: 74–85. doi:10.1100/tsw.2007.211

447. Cristóvão-Ferreira S, Navarro G, Brugarolas M, Pérez-Capote K, Vaz SH, Fattorini G, et al. A1R-A2AR heteromers coupled to Gs and G i/0 proteins modulate GABA transport into astrocytes. Purinergic Signal. 2013;9: 433–449.

doi:10.1007/s11302-013-9364-5

448. George SR, Kern A, Smith RG, Franco R. Dopamine receptor heteromeric complexes and their emerging functions. Prog Brain Res. 2014;211: 183–200. doi:10.1016/B978-0-444-63425-2.00008-8

449. Hasbi A, Fan T, Alijaniaram M, Nguyen T, Perreault ML, O'Dowd BF, et al. Calcium signaling cascade links dopamine D1-D2 receptor heteromer to striatal BDNF production and neuronal growth. Proc Natl Acad Sci U S A. 2009;106: 21377–21382. doi:10.1073/pnas.0903676106

450. So CH, Verma V, O'Dowd BF, George SR. Desensitization of the dopamine D1 and D2 receptor hetero-oligomer mediated calcium signal by agonist occupancy of either receptor. Mol Pharmacol. 2007;72: 450–462. doi:10.1124/mol.107.034884

451. Rashid AJ, So CH, Kong MMC, Furtak T, El-Ghundi M, Cheng R, et al. D1-D2 dopamine receptor heterooligomers with unique pharmacology are coupled to rapid activation of Gq/11 in the striatum. Proc Natl Acad Sci U S A. 2007;104: 654–659. doi:10.1073/pnas.0604049104

452. Portoghese PS, Lunzer MM. Identity of the putative delta1-opioid receptor as a delta-kappa heteromer in the mouse spinal cord. Eur J Pharmacol. 2003;467: 233–234. doi:10.1016/s0014-2999(03)01599-1

453. Gomes I, Jordan BA, Gupta A, Trapaidze N, Nagy V, Devi LA. Heterodimerization of mu and delta opioid receptors: A role in opiate synergy. J Neurosci. 2000;20: RC110. doi:10.1523/JNEUROSCI.20-22-j0007.2000

454. Gupta A, Mulder J, Gomes I, Rozenfeld R, Bushlin I, Ong E, et al. Increased abundance of opioid receptor heteromers after chronic morphine administration. Sci Signal. 2010;3: ra54. doi:10.1126/scisignal.2000807

455. Yekkirala AS, Kalyuzhny AE, Portoghese PS. Standard opioid agonists activate heteromeric opioid receptors: evidence for morphine and [d-Ala(2)-MePhe(4)-Glyol(5)]enkephalin as selective μ-δ agonists. ACS Chem Neurosci. 2010;1: 146–154. doi:10.1021/cn9000236

456. van Rijn RM, Whistler JL, Waldhoer M. Opioid-receptor-heteromer-specific trafficking and pharmacology. Curr Opin Pharmacol. 2010;10: 73–79. doi:10.1016/j.coph.2009.09.007

457. Waldhoer M, Fong J, Jones RM, Lunzer MM, Sharma SK, Kostenis E, et al. A heterodimer-selective agonist shows in vivo relevance of G protein-coupled receptor dimers. Proc Natl Acad Sci U S A. 2005;102: 9050–9055. doi:10.1073/pnas.0501112102

458. Daniels DJ, Kulkarni A, Xie Z, Bhushan RG, Portoghese PS. A bivalent ligand (KDAN-18) containing delta-antagonist and kappa-agonist pharmacophores bridges delta2 and kappa1 opioid receptor phenotypes. J Med Chem. 2005;48:

1713–1716. doi:10.1021/jm034234f

459. Bhushan RG, Sharma SK, Xie Z, Daniels DJ, Portoghese PS. A bivalent ligand (KDN-21) reveals spinal delta and kappa opioid receptors are organized as heterodimers that give rise to delta(1) and kappa(2) phenotypes. Selective targeting of delta-kappa heterodimers. J Med Chem. 2004;47: 2969–2972. doi:10.1021/jm0342358

460. Fuxe K, Härfstrand A, Agnati LF, Kalia M, Fredholm B, Svensson T, et al. Central catecholamine-neuropeptide Y interactions at the pre- and postsynaptic level in cardiovascular centers. J Cardiovasc Pharmacol. 1987;10 Suppl 12: S1–13. Available: https://www.ncbi.nlm.nih.gov/pubmed/2455156

461. Fuxe K, Agnati LF. Receptor-receptor interactions in the central nervous system. A new integrative mechanism in synapses. Med Res Rev. 1985;5: 441–482. doi:10.1002/med.2610050404

462. Fuxe K, Agnati LF, Benfenati F, Celani M, Zini I, Zoli M, et al. Evidence for the existence of receptor--receptor interactions in the central nervous system. Studies on the regulation of monoamine receptors by neuropeptides. J Neural Transm Suppl. 1983;18: 165–179. Available: https://www.ncbi.nlm.nih.gov/pubmed/6192208

463. Borroto-Escuela DO, Van Craenenbroeck K, Romero-Fernandez W, Guidolin D, Woods AS, Rivera A, et al. Dopamine D2 and D4 receptor heteromerization and its allosteric receptor-receptor interactions. Biochem Biophys Res Commun. 2011;404: 928–934. doi:10.1016/j.bbrc.2010.12.083

464. Fiorentini C, Busi C, Spano P, Missale C. Dimerization of dopamine D1 and D3 receptors in the regulation of striatal function. Curr Opin Pharmacol. 2010;10: 87–92. doi:10.1016/j.coph.2009.09.008

465. Błasiak E, Łukasiewicz S, Szafran-Pilch K, Dziedzicka-Wasylewska M. Genetic variants of dopamine D2 receptor impact heterodimerization with dopamine D1 receptor. Pharmacol Rep. 2017;69: 235–241. doi:10.1016/j.pharep.2016.10.016

466. Martel JC, Gatti McArthur S. Dopamine Receptor Subtypes, Physiology and Pharmacology: New Ligands and Concepts in Schizophrenia. Front Pharmacol. 2020;11: 1003. doi:10.3389/fphar.2020.01003

467. Van Craenenbroeck K, Borroto-Escuela DO, Skieterska K, Duchou J, Romero-Fernandez W, Fuxe K. Role of dimerization in dopamine D(4) receptor biogenesis. Curr Protein Pept Sci. 2014;15: 659–665. doi:10.2174/1389203715666140901110256

468. Ng GY, O'Dowd BF, Lee SP, Chung HT, Brann MR, Seeman P, et al. Dopamine D2 receptor dimers and receptor-blocking peptides. Biochem Biophys Res Commun. 1996;227: 200–204. doi:10.1006/bbrc.1996.1489

469. Karpa KD, Lin R, Kabbani N, Levenson R. The dopamine D3 receptor interacts with itself and the truncated D3 splice variant d3nf: D3-D3nf interaction causes mislocalization of D3 receptors. Mol Pharmacol. 2000;58: 677–683. doi:10.1124/mol.58.4.677

470. O'Dowd BF, Nguyen T, Ji X, George SR. D5 dopamine receptor carboxyl tail involved in D5-D2 heteromer formation. Biochem Biophys Res Commun. 2013;431: 586–589. doi:10.1016/j.bbrc.2012.12.139

471. Scarselli M, Novi F, Schallmach E, Lin R, Baragli A, Colzi A, et al. D2/D3 dopamine receptor heterodimers exhibit unique functional properties. J Biol Chem. 2001;276: 30308–30314. doi:10.1074/jbc.M102297200

472. Guo W, Shi L, Filizola M, Weinstein H, Javitch JA. Crosstalk in G protein-coupled receptors: changes at the transmembrane homodimer interface determine activation. Proc Natl Acad Sci U S A. 2005;102: 17495–17500. doi:10.1073/pnas.0508950102

473. Perreault ML, Hasbi A, Alijaniaram M, Fan T, Varghese G, Fletcher PJ, et al. The dopamine D1-D2 receptor heteromer localizes in dynorphin/enkephalin neurons: increased high affinity state following amphetamine and in schizophrenia. J Biol Chem. 2010;285: 36625–36634. doi:10.1074/jbc.M110.159954

474. Lee SP, So CH, Rashid AJ, Varghese G, Cheng R, Lança AJ, et al. Dopamine D1 and D2 receptor Co-activation generates a novel phospholipase C-mediated calcium signal. J Biol Chem. 2004;279: 35671–35678. doi:10.1074/jbc.M401923200

475. Urizar E, Yano H, Kolster R, Galés C, Lambert N, Javitch JA. CODA-RET reveals functional selectivity as a result of GPCR heteromerization. Nat Chem Biol. 2011;7: 624–630. doi:10.1038/nchembio.623

476. Perreault ML, Hasbi A, Shen MYF, Fan T, Navarro G, Fletcher PJ, et al. Disruption of a dopamine receptor complex amplifies the actions of cocaine. Eur Neuropsychopharmacol. 2016;26: 1366–1377. doi:10.1016/j.euroneuro.2016.07.008

477. Rico AJ, Dopeso-Reyes IG, Martínez-Pinilla E, Sucunza D, Pignataro D, Roda E, et al. Neurochemical evidence supporting dopamine D1-D2 receptor heteromers in the striatum of the long-tailed macaque: changes following dopaminergic manipulation. Brain Struct Funct. 2017;222: 1767–1784. doi:10.1007/s00429-016-1306-x

478. Hasbi A, Madras BK, Bergman J, Kohut S, Lin Z, Withey SL, et al. Δ-Tetrahydrocannabinol Increases Dopamine D1-D2 Receptor Heteromer and Elicits Phenotypic Reprogramming in Adult Primate Striatal Neurons. iScience. 2020;23: 100794. doi:10.1016/j.isci.2019.100794

479. Hasbi A, Sivasubramanian M, Milenkovic M, Komarek K, Madras BK, George

SR. Dopamine D1-D2 receptor heteromer expression in key brain regions of rat and higher species: Upregulation in rat striatum after cocaine administration. Neurobiol Dis. 2020;143: 105017. doi:10.1016/j.nbd.2020.105017

480. So CH, Verma V, Alijaniaram M, Cheng R, Rashid AJ, O'Dowd BF, et al. Calcium signaling by dopamine D5 receptor and D5-D2 receptor hetero-oligomers occurs by a mechanism distinct from that for dopamine D1-D2 receptor hetero-oligomers. Mol Pharmacol. 2009;75: 843–854. doi:10.1124/mol.108.051805

481. Ng J, Rashid AJ, So CH, O'Dowd BF, George SR. Activation of calcium/calmodulin-dependent protein kinase IIalpha in the striatum by the heteromeric D1-D2 dopamine receptor complex. Neuroscience. 2010;165: 535–541. doi:10.1016/j.neuroscience.2009.10.017

482. Nestler EJ, Carlezon WA Jr. The mesolimbic dopamine reward circuit in depression. Biol Psychiatry. 2006;59: 1151–1159. doi:10.1016/j.biopsych.2005.09.018

483. Tye KM, Mirzabekov JJ, Warden MR, Ferenczi EA, Tsai H-C, Finkelstein J, et al. Dopamine neurons modulate neural encoding and expression of depression-related behaviour. Nature. 2013;493: 537–541. doi:10.1038/nature11740

484. Seeman P, Van Tol HH. Dopamine receptor pharmacology. Trends Pharmacol Sci. 1994;15: 264–270. doi:10.1016/0165-6147(94)90323-9

485. O'Dowd BF, Ji X, Nguyen T, George SR. Two amino acids in each of D1 and D2 dopamine receptor cytoplasmic regions are involved in D1–D2 heteromer formation. Biochem Biophys Res Commun. 2012;417: 23–28. doi:10.1016/j.bbrc.2011.11.027

486. Lane H-Y, Lee C-C, Chang Y-C, Lu C-T, Huang C-H, Chang W-H. Effects of dopamine D2 receptor Ser311Cys polymorphism and clinical factors on risperidone efficacy for positive and negative symptoms and social function. Int J Neuropsychopharmacol. 2004;7: 461–470. doi:10.1017/S1461145704004389

487. Hasbi A, Perreault ML, Shen MYF, Fan T, Nguyen T, Alijaniaram M, et al. Activation of Dopamine D1-D2 Receptor Complex Attenuates Cocaine Reward and Reinstatement of Cocaine-Seeking through Inhibition of DARPP-32, ERK, and ΔFosB. Front Pharmacol. 2017;8: 924. doi:10.3389/fphar.2017.00924

488. Pei L, Li S, Wang M, Diwan M, Anisman H, Fletcher PJ, et al. Uncoupling the dopamine D1-D2 receptor complex exerts antidepressant-like effects. Nat Med. 2010;16: 1393–1395. doi:10.1038/nm.2263

489. Hasbi A, Perreault ML, Shen MYF, Zhang L, To R, Fan T, et al. A peptide targeting an interaction interface disrupts the dopamine D1-D2 receptor heteromer to block signaling and function in vitro and in vivo: effective selective antagonism. FASEB J. 2014;28: 4806–4820. doi:10.1096/fj.14-254037

490. Guitart X, Navarro G, Moreno E, Yano H, Cai N-S, Sánchez-Soto M, et al. Functional selectivity of allosteric interactions within G protein-coupled receptor oligomers: the dopamine D1-D3 receptor heterotetramer. Mol Pharmacol. 2014;86: 417–429. doi:10.1124/mol.114.093096

491. Guitart X, Moreno E, Rea W, Sánchez-Soto M, Cai N-S, Quiroz C, et al. Biased G Protein-Independent Signaling of Dopamine D1-D3 Receptor Heteromers in the Nucleus Accumbens. Mol Neurobiol. 2019;56: 6756–6769. doi:10.1007/s12035-019-1564-8

492. Fiorentini C, Busi C, Gorruso E, Gotti C, Spano P, Missale C. Reciprocal regulation of dopamine D1 and D3 receptor function and trafficking by heterodimerization. Mol Pharmacol. 2008;74: 59–69. doi:10.1124/mol.107.043885

493. Marcellino D, Ferré S, Casadó V, Cortés A, Le Foll B, Mazzola C, et al. Identification of dopamine D1-D3 receptor heteromers. Indications for a role of synergistic D1-D3 receptor interactions in the striatum. J Biol Chem. 2008;283: 26016–26025. doi:10.1074/jbc.M710349200

494. Farré D, Muñoz A, Moreno E, Reyes-Resina I, Canet-Pons J, Dopeso-Reyes IG, et al. Stronger Dopamine D1 Receptor-Mediated Neurotransmission in Dyskinesia. Mol Neurobiol. 2015;52: 1408–1420. doi:10.1007/s12035-014-8936-x

495. Lanza K, Meadows SM, Chambers NE, Nuss E, Deak MM, Ferré S, et al. Behavioral and cellular dopamine D1 and D3 receptor-mediated synergy: Implications for L-DOPA-induced dyskinesia. Neuropharmacology. 2018;138: 304–314. doi:10.1016/j.neuropharm.2018.06.024

496. Solís O, Garcia-Montes JR, González-Granillo A, Xu M, Moratalla R. Dopamine D3 Receptor Modulates l-DOPA-Induced Dyskinesia by Targeting D1 Receptor-Mediated Striatal Signaling. Cereb Cortex. 2017;27: 435–446. doi:10.1093/cercor/bhv231

497. Cote SR, Chitravanshi VC, Bleickardt C, Sapru HN, Kuzhikandathil EV. Overexpression of the dopamine D3 receptor in the rat dorsal striatum induces dyskinetic behaviors. Behav Brain Res. 2014;263: 46–50. doi:10.1016/j.bbr.2014.01.011

498. Surmeier DJ, Song WJ, Yan Z. Coordinated expression of dopamine receptors in neostriatal medium spiny neurons. J Neurosci. 1996;16: 6579–6591. doi:10.1523/JNEUROSCI.16-20-06579.1996

499. Joyce JN. Dopamine D3 receptor as a therapeutic target for antipsychotic and antiparkinsonian drugs. Pharmacol Ther. 2001;90: 231–259. doi:10.1016/s0163-7258(01)00139-5

500. Maggio R, Millan MJ. Dopamine D2–D3 receptor heteromers: pharmacological properties and therapeutic significance. Curr Opin Pharmacol. 2010;10: 100–107. doi:10.1016/j.coph.2009.10.001

501. Maggio R, Scarselli M, Novi F, Millan MJ, Corsini GU. Potent activation of dopamine D3/D2 heterodimers by the antiparkinsonian agents, S32504, pramipexole and ropinirole. J Neurochem. 2003;87: 631–641. doi:10.1046/j.1471-4159.2003.02038.x

502. Novi F, Millan MJ, Corsini GU, Maggio R. Partial agonist actions of aripiprazole and the candidate antipsychotics S33592, bifeprunox, N-desmethylclozapine and preclamol at dopamine D(2L) receptors are modified by co-transfection of D(3) receptors: potential role of heterodimer formation. J Neurochem. 2007;102: 1410–1424. doi:10.1111/j.1471-4159.2007.04660.x

503. Maggio R, Scarselli M, Capannolo M, Millan MJ. Novel dimensions of D3 receptor function: Focus on heterodimerisation, transactivation and allosteric modulation. Eur Neuropsychopharmacol. 2015;25: 1470–1479. doi:10.1016/j.euroneuro.2014.09.016

504. Missale C, Nash SR, Robinson SW, Jaber M, Caron MG. Dopamine receptors: from structure to function. Physiol Rev. 1998;78: 189–225. doi:10.1152/physrev.1998.78.1.189

505. Rondou P, Haegeman G, Van Craenenbroeck K. The dopamine D4 receptor: biochemical and signalling properties. Cell Mol Life Sci. 2010;67: 1971–1986. doi:10.1007/s00018-010-0293-y

506. Van Tol HH, Bunzow JR, Guan HC, Sunahara RK, Seeman P, Niznik HB, et al. Cloning of the gene for a human dopamine D4 receptor with high affinity for the antipsychotic clozapine. Nature. 1991;350: 610–614. doi:10.1038/350610a0

507. González S, Rangel-Barajas C, Peper M, Lorenzo R, Moreno E, Ciruela F, et al. Dopamine D4 receptor, but not the ADHD-associated D4.7 variant, forms functional heteromers with the dopamine D2S receptor in the brain. Mol Psychiatry. 2012;17: 650–662. doi:10.1038/mp.2011.93

508. Fuxe K, Guidolin D, Agnati LF, Borroto-Escuela DO. Dopamine heteroreceptor complexes as therapeutic targets in Parkinson’s disease. Expert Opin Ther Targets. 2015;19: 377–398. doi:10.1517/14728222.2014.981529

509. Centonze D, Grande C, Usiello A, Gubellini P, Erbs E, Martin AB, et al. Receptor subtypes involved in the presynaptic and postsynaptic actions of dopamine on striatal interneurons. J Neurosci. 2003;23: 6245–6254. doi:10.1523/JNEUROSCI.23-15-06245.2003

510. Ginés S, Hillion J, Torvinen M, Le Crom S, Casadó V, Canela EI, et al. Dopamine D1 and adenosine A1 receptors form functionally interacting heteromeric complexes. Proc Natl Acad Sci U S A. 2000;97: 8606–8611. doi:10.1073/pnas.150241097

511. Franco R, Lluis C, Canela EI, Mallol J, Agnati L, Casadó V, et al. Receptor-receptor interactions involving adenosine A1 or dopamine D1 receptors and

accessory proteins. J Neural Transm. 2007;114: 93–104. doi:10.1007/s00702-006-0566-7

512. Caillé I, Dumartin B, Bloch B. Ultrastructural localization of D1 dopamine receptor immunoreactivity in rat striatonigral neurons and its relation with dopaminergic innervation. Brain Res. 1996;730: 17–31. doi:10.1016/0006-8993(96)00424-6

513. Rivkees SA, Price SL, Zhou FC. Immunohistochemical detection of A1 adenosine receptors in rat brain with emphasis on localization in the hippocampal formation, cerebral cortex, cerebellum, and basal ganglia. Brain Res. 1995;677: 193–203. doi:10.1016/0006-8993(95)00062-u

514. Ferré S, Popoli P, Giménez-Llort L, Finnman UB, Martínez E, Scotti de Carolis A, et al. Postsynaptic antagonistic interaction between adenosine A1 and dopamine D1 receptors. Neuroreport. 1994;6: 73–76. doi:10.1097/00001756-199412300-00020

515. Ferré S, Fredholm BB, Morelli M, Popoli P, Fuxe K. Adenosine-dopamine receptor-receptor interactions as an integrative mechanism in the basal ganglia. Trends Neurosci. 1997;20: 482–487. doi:10.1016/s0166-2236(97)01096-5

516. Ferré S, Torvinen M, Antoniou K, Irenius E, Civelli O, Arenas E, et al. Adenosine A1 receptor-mediated modulation of dopamine D1 receptors in stably cotransfected fibroblast cells. J Biol Chem. 1998;273: 4718–4724. doi:10.1074/jbc.273.8.4718

517. Toda S, Alguacil LF, Kalivas PW. Repeated cocaine administration changes the function and subcellular distribution of adenosine A1 receptor in the rat nucleus accumbens. J Neurochem. 2003;87: 1478–1484. doi:10.1046/j.1471-4159.2003.02121.x

518. Rivera-Oliver M, Moreno E, Álvarez-Bagnarol Y, Ayala-Santiago C, Cruz-Reyes N, Molina-Castro GC, et al. Adenosine A1-Dopamine D1 Receptor Heteromers Control the Excitability of the Spinal Motoneuron. Mol Neurobiol. 2019;56: 797–811. doi:10.1007/s12035-018-1120-y

519. Canals M, Marcellino D, Fanelli F, Ciruela F, de Benedetti P, Goldberg SR, et al. Adenosine A2A-dopamine D2 receptor-receptor heteromerization: qualitative and quantitative assessment by fluorescence and bioluminescence energy transfer. J Biol Chem. 2003;278: 46741–46749. doi:10.1074/jbc.M306451200

520. Hillion J, Canals M, Torvinen M, Casado V, Scott R, Terasmaa A, et al. Coaggregation, cointernalization, and codesensitization of adenosine A2A receptors and dopamine D2 receptors. J Biol Chem. 2002;277: 18091–18097. doi:10.1074/jbc.M107731200

521. Fuxe K, Agnati LF, Jacobsen K, Hillion J, Canals M, Torvinen M, et al. Receptor heteromerization in adenosine A2A receptor signaling: relevance for striatal

function and Parkinson's disease. Neurology. 2003;61: S19–23. doi:10.1212/01.wnl.0000095206.44418.5c

522. Kamiya T, Saitoh O, Yoshioka K, Nakata H. Oligomerization of adenosine A2A and dopamine D2 receptors in living cells. Biochem Biophys Res Commun. 2003;306: 544–549. doi:10.1016/s0006-291x(03)00991-4

523. Trifilieff P, Rives M-L, Urizar E, Piskorowski RA, Vishwasrao HD, Castrillon J, et al. Detection of antigen interactions ex vivo by proximity ligation assay: endogenous dopamine D2-adenosine A2A receptor complexes in the striatum. Biotechniques. 2011;51: 111–118. doi:10.2144/000113719

524. Borroto-Escuela DO, Romero-Fernandez W, Garriga P, Ciruela F, Narvaez M, Tarakanov AO, et al. G protein-coupled receptor heterodimerization in the brain. Methods Enzymol. 2013;521: 281–294. doi:10.1016/B978-0-12-391862-8.00015-6

525. Fuxe K, Marcellino D, Genedani S, Agnati L. Adenosine A(2A) receptors, dopamine D(2) receptors and their interactions in Parkinson's disease. Mov Disord. 2007;22: 1990–2017. doi:10.1002/mds.21440

526. Ferre S, von Euler G, Johansson B, Fredholm BB, Fuxe K. Stimulation of high-affinity adenosine A2 receptors decreases the affinity of dopamine D2 receptors in rat striatal membranes. Proc Natl Acad Sci U S A. 1991;88: 7238–7241. doi:10.1073/pnas.88.16.7238

527. Ferré S, Fuxe K. Dopamine denervation leads to an increase in the intramembrane interaction between adenosine A2 and dopamine D2 receptors in the neostriatum. Brain Res. 1992;594: 124–130. doi:10.1016/0006-8993(92)91036-e

528. Ferré S, Quiroz C, Woods AS, Cunha R, Popoli P, Ciruela F, et al. An update on adenosine A2A-dopamine D2 receptor interactions: implications for the function of G protein-coupled receptors. Curr Pharm Des. 2008;14: 1468–1474. doi:10.2174/138161208784480108

529. Ballesteros-Yáñez I, Castillo CA, Merighi S, Gessi S. The Role of Adenosine Receptors in Psychostimulant Addiction. Front Pharmacol. 2017;8: 985. doi:10.3389/fphar.2017.00985

530. Dalrymple MB, Pfleger KDG, Eidne KA. G protein-coupled receptor dimers: functional consequences, disease states and drug targets. Pharmacol Ther. 2008;118: 359–371. doi:10.1016/j.pharmthera.2008.03.004

531. Rosin DL, Hettinger BD, Lee A, Linden J. Anatomy of adenosine A2A receptors in brain: morphological substrates for integration of striatal function. Neurology. 2003;61: S12–8. doi:10.1212/01.wnl.0000095205.33940.99

532. Fuxe K, Ferré S, Genedani S, Franco R, Agnati LF. Adenosine receptor-dopamine receptor interactions in the basal ganglia and their relevance for brain

function. Physiol Behav. 2007;92: 210–217. doi:10.1016/j.physbeh.2007.05.034

533. Gluck MR, Santana LA, Granson H, Yahr MD. Novel dopamine releasing response of an anti-convulsant agent with possible anti-Parkinson's activity. J Neural Transm. 2004;111: 713–724. doi:10.1007/s00702-004-0107-1

534. Schiffmann SN, Fisone G, Moresco R, Cunha RA, Ferré S. Adenosine A2A receptors and basal ganglia physiology. Prog Neurobiol. 2007;83: 277–292. doi:10.1016/j.pneurobio.2007.05.001

535. Shen H-Y, Coelho JE, Ohtsuka N, Canas PM, Day Y-J, Huang Q-Y, et al. A critical role of the adenosine A2A receptor in extrastriatal neurons in modulating psychomotor activity as revealed by opposite phenotypes of striatum and forebrain A2A receptor knock-outs. J Neurosci. 2008;28: 2970–2975. doi:10.1523/JNEUROSCI.5255-07.2008

536. Kim DS, Palmiter RD. Adenosine receptor blockade reverses hypophagia and enhances locomotor activity of dopamine-deficient mice. Proc Natl Acad Sci U S A. 2003;100: 1346–1351. doi:10.1073/pnas.252753799

537. Chase TN, Bibbiani F, Bara-Jimenez W, Dimitrova T, Oh-Lee JD. Translating A2A antagonist KW6002 from animal models to parkinsonian patients. Neurology. 2003;61: S107–11. doi:10.1212/01.wnl.0000095223.08711.48

538. Torvinen M, Marcellino D, Canals M, Agnati LF, Lluis C, Franco R, et al. Adenosine A2A receptor and dopamine D3 receptor interactions: evidence of functional A2A/D3 heteromeric complexes. Mol Pharmacol. 2005;67: 400–407. doi:10.1124/mol.104.003376

539. Takagi H, Morishima Y, Matsuyama T, Hayashi H, Watanabe T, Wada H. Histaminergic axons in the neostriatum and cerebral cortex of the rat: a correlated light and electron microscopic immunocytochemical study using histidine decarboxylase as a marker. Brain Res. 1986;364: 114–123. doi:10.1016/0006-8993(86)90992-3

540. Ferrada C, Moreno E, Casadó V, Bongers G, Cortés A, Mallol J, et al. Marked changes in signal transduction upon heteromerization of dopamine D1 and histamine H3 receptors. Br J Pharmacol. 2009;157: 64–75. doi:10.1111/j.1476-5381.2009.00152.x

541. Moreno E, Hoffmann H, Gonzalez-Sepúlveda M, Navarro G, Casadó V, Cortés A, et al. Dopamine D1-histamine H3 receptor heteromers provide a selective link to MAPK signaling in GABAergic neurons of the direct striatal pathway. J Biol Chem. 2011;286: 5846–5854. doi:10.1074/jbc.M110.161489

542. Moreno E, Moreno-Delgado D, Navarro G, Hoffmann HM, Fuentes S, Rosell-Vilar S, et al. Cocaine disrupts histamine H3 receptor modulation of dopamine D1 receptor signaling: σ1-D1-H3 receptor complexes as key targets for reducing cocaine's effects. J Neurosci. 2014;34: 3545–3558.

doi:10.1523/JNEUROSCI.4147-13.2014

543. Kononoff Vanhanen J, Nuutinen S, Tuominen M, Panula P. Histamine H3 Receptor Regulates Sensorimotor Gating and Dopaminergic Signaling in the Striatum. J Pharmacol Exp Ther. 2016;357: 264–272. doi:10.1124/jpet.115.230771

544. Ferrada C, Ferré S, Casadó V, Cortés A, Justinova Z, Barnes C, et al. Interactions between histamine H3 and dopamine D2 receptors and the implications for striatal function. Neuropharmacology. 2008;55: 190–197. doi:10.1016/j.neuropharm.2008.05.008

545. Pillot C, Heron A, Cochois V, Tardivel-Lacombe J, Ligneau X, Schwartz J-C, et al. A detailed mapping of the histamine H(3) receptor and its gene transcripts in rat brain. Neuroscience. 2002;114: 173–193. doi:10.1016/s0306-4522(02)00135-5

546. Ferré S, Ciruela F, Woods AS, Lluis C, Franco R. Functional relevance of neurotransmitter receptor heteromers in the central nervous system. Trends Neurosci. 2007;30: 440–446. doi:10.1016/j.tins.2007.07.001

547. Szafran K, Lukasiewicz S, Faron-Górecka A, Kolasa M, Kuśmider M, Solich J, et al. Antidepressant drugs promote the heterodimerization of the dopamine D2 and somatostatin Sst5 receptors--fluorescence in vitro studies. Pharmacol Rep. 2012;64: 1253–1258. doi:10.1016/s1734-1140(12)70921-0

548. Szafran-Pilch K, Faron-Górecka A, Kolasa M, Żurawek D, Szlachta M, Solich J, et al. Antidepressants promote formation of heterocomplexes of dopamine D2 and somatostatin subtype 5 receptors in the mouse striatum. Brain Res Bull. 2017;135: 92–97. doi:10.1016/j.brainresbull.2017.10.003

549. Faron-Górecka A, Kuśmider M, Solich J, Kolasa M, Szafran K, Zurawek D, et al. Involvement of prolactin and somatostatin in depression and the mechanism of action of antidepressant drugs. Pharmacol Rep. 2013;65: 1640–1646. doi:10.1016/s1734-1140(13)71525-1

550. Borroto-Escuela DO, Ravani A, Tarakanov AO, Brito I, Narvaez M, Romero-Fernandez W, et al. Dopamine D2 receptor signaling dynamics of dopamine D2-neurotensin 1 receptor heteromers. Biochem Biophys Res Commun. 2013;435: 140–146. doi:10.1016/j.bbrc.2013.04.058

551. Plach M, Schäfer T, Borroto-Escuela DO, Weikert D, Gmeiner P, Fuxe K, et al. Differential allosteric modulation within dopamine D2R - neurotensin NTS1R and D2R - serotonin 5-HT2AR receptor complexes gives bias to intracellular calcium signalling. Sci Rep. 2019;9: 16312. doi:10.1038/s41598-019-52540-8

552. Ferraro L, Tomasini MC, Mazza R, Fuxe K, Fournier J, Tanganelli S, et al. Neurotensin receptors as modulators of glutamatergic transmission. Brain Res Rev. 2008;58: 365–373. doi:10.1016/j.brainresrev.2007.11.001

553. Koschatzky S, Tschammer N, Gmeiner P. Cross-receptor interactions between

dopamine D2L and neurotensin NTS1 receptors modulate binding affinities of dopaminergics. ACS Chem Neurosci. 2011;2: 308–316. doi:10.1021/cn200020y

554. Antonelli T, Tomasini MC, Fuxe K, Agnati LF, Tanganelli S, Ferraro L. Receptor-receptor interactions as studied with microdialysis. Focus on NTR/D2 interactions in the basal ganglia. J Neural Transm. 2007;114: 105–113. doi:10.1007/s00702-006-0558-7

555. Tanganelli S, Antonelli T, Tomasini MC, Beggiato S, Fuxe K, Ferraro L. Relevance of dopamine D(2)/neurotensin NTS1 and NMDA/neurotensin NTS1 receptor interaction in psychiatric and neurodegenerative disorders. Curr Med Chem. 2012;19: 304–316. doi:10.2174/092986712803414268

556. Espinoza S, Salahpour A, Masri B, Sotnikova TD, Messa M, Barak LS, et al. Functional interaction between trace amine-associated receptor 1 and dopamine D2 receptor. Mol Pharmacol. 2011;80: 416–425. doi:10.1124/mol.111.073304

557. Espinoza S, Masri B, Salahpour A, Gainetdinov RR. BRET approaches to characterize dopamine and TAAR1 receptor pharmacology and signaling. Methods Mol Biol. 2013;964: 107–122. doi:10.1007/978-1-62703-251-3_8

558. Lindemann L, Meyer CA, Jeanneau K, Bradaia A, Ozmen L, Bluethmann H, et al. Trace amine-associated receptor 1 modulates dopaminergic activity. J Pharmacol Exp Ther. 2008;324: 948–956. doi:10.1124/jpet.107.132647

559. Romero-Fernandez W, Borroto-Escuela DO, Agnati LF, Fuxe K. Evidence for the existence of dopamine D2-oxytocin receptor heteromers in the ventral and dorsal striatum with facilitatory receptor-receptor interactions. Mol Psychiatry. 2013;18: 849–850. doi:10.1038/mp.2012.103

560. de la Mora MP, Pérez-Carrera D, Crespo-Ramírez M, Tarakanov A, Fuxe K, Borroto-Escuela DO. Signaling in dopamine D2 receptor-oxytocin receptor heterocomplexes and its relevance for the anxiolytic effects of dopamine and oxytocin interactions in the amygdala of the rat. Biochim Biophys Acta. 2016;1862: 2075–2085. doi:10.1016/j.bbadis.2016.07.004

561. Pradhan G, Samson SL, Sun Y. Ghrelin: much more than a hunger hormone. Curr Opin Clin Nutr Metab Care. 2013;16: 619–624. doi:10.1097/MCO.0b013e328365b9be

562. Davenport AP, Bonner TI, Foord SM, Harmar AJ, Neubig RR, Pin J-P, et al. International Union of Pharmacology. LVI. Ghrelin receptor nomenclature, distribution, and function. Pharmacol Rev. 2005;57: 541–546. doi:10.1124/pr.57.4.1

563. GHSR growth hormone secretagogue receptor [Homo sapiens (human)] - Gene - NCBI. [cited 17 Mar 2023]. Available: https://www.ncbi.nlm.nih.gov/gene?Db=gene&Cmd=DetailsSearch&Term=2693

564. Smith RG, Van der Ploeg LH, Howard AD, Feighner SD, Cheng K, Hickey GJ, et al. Peptidomimetic regulation of growth hormone secretion. Endocr Rev. 1997;18: 621–645. doi:10.1210/edrv.18.5.0316

565. Adriaenssens AE, Svendsen B, Lam BYH, Yeo GSH, Holst JJ, Reimann F, et al. Transcriptomic profiling of pancreatic alpha, beta and delta cell populations identifies delta cells as a principal target for ghrelin in mouse islets. Diabetologia. 2016;59: 2156–2165. doi:10.1007/s00125-016-4033-1

566. Meguid MM, Fetissov SO, Varma M, Sato T, Zhang L, Laviano A, et al. Hypothalamic dopamine and serotonin in the regulation of food intake. Nutrition. 2000;16: 843–857. doi:10.1016/s0899-9007(00)00449-4

567. Vucetic Z, Reyes TM. Central dopaminergic circuitry controlling food intake and reward: implications for the regulation of obesity. Wiley Interdiscip Rev Syst Biol Med. 2010;2: 577–593. doi:10.1002/wsbm.77

568. Kern A, Albarran-Zeckler R, Walsh HE, Smith RG. Apo-ghrelin receptor forms heteromers with DRD2 in hypothalamic neurons and is essential for anorexigenic effects of DRD2 agonism. Neuron. 2012;73: 317–332. doi:10.1016/j.neuron.2011.10.038

569. Franco R, Cordomí A, Llinas Del Torrent C, Lillo A, Serrano-Marín J, Navarro G, et al. Structure and function of adenosine receptor heteromers. Cell Mol Life Sci. 2021;78: 3957–3968. doi:10.1007/s00018-021-03761-6

570. Gao Z-G, Jacobson KA. Emerging adenosine receptor agonists. Expert Opin Emerg Drugs. 2007;12: 479–492. doi:10.1517/14728214.12.3.479

571. Fredholm BB, Irenius E, Kull B, Schulte G. Comparison of the potency of adenosine as an agonist at human adenosine receptors expressed in Chinese hamster ovary cells. Biochem Pharmacol. 2001;61: 443–448. doi:10.1016/s0006-2952(00)00570-0

572. Navarro G, Cordomí A, Brugarolas M, Moreno E, Aguinaga D, Pérez-Benito L, et al. Cross-communication between Gi and Gs in a G-protein-coupled receptor heterotetramer guided by a receptor C-terminal domain. BMC Biol. 2018;16: 24. doi:10.1186/s12915-018-0491-x

573. Borroto-Escuela DO, Fuxe K. Adenosine heteroreceptor complexes in the basal ganglia are implicated in Parkinson’s disease and its treatment. J Neural Transm. 2019;126: 455–471. doi:10.1007/s00702-019-01969-2

574. Ferre S, Ciruela F, Borycz J, Solinas M, Quarta D, Antoniou K, et al. Adenosine A1-A2A receptor heteromers: new targets for caffeine in the brain. Front Biosci. 2008;13: 2391–2399. doi:10.2741/2852

575. Aghajanian GK, Marek GJ. Serotonin induces excitatory postsynaptic potentials in apical dendrites of neocortical pyramidal cells. Neuropharmacology. 1997;36:

589–599. doi:10.1016/s0028-3908(97)00051-8

576. Aghajanian GK, Marek GJ. Serotonin–Glutamate Interactions: A New Target for Antipsychotic Drugs. Neuropsychopharmacology. 1999;21: S122–S133. doi:10.1016/S0893-133X(99)00106-2

577. Stutzmann GE, Marek GJ, Aghajanian GK. Adenosine preferentially suppresses serotonin2A receptor-enhanced excitatory postsynaptic currents in layer V neurons of the rat medial prefrontal cortex. Neuroscience. 2001;105: 55–69. doi:10.1016/s0306-4522(01)00170-1

578. Marek GJ. Activation of adenosine(1) (A(1)) receptors suppresses head shakes induced by a serotonergic hallucinogen in rats. Neuropharmacology. 2009;56: 1082–1087. doi:10.1016/j.neuropharm.2009.03.005

579. Márquez-Gómez R, Robins MT, Gutiérrez-Rodelo C, Arias J-M, Olivares-Reyes J-A, van Rijn RM, et al. Functional histamine H3 and adenosine A2A receptor heteromers in recombinant cells and rat striatum. Pharmacol Res. 2018;129: 515–525. doi:10.1016/j.phrs.2017.11.036

580. Ballantyne JC, Mao J. Opioid therapy for chronic pain. N Engl J Med. 2003;349: 1943–1953. doi:10.1056/NEJMra025411

581. Skolnick P. The Opioid Epidemic: Crisis and Solutions. Annu Rev Pharmacol Toxicol. 2018;58: 143–159. doi:10.1146/annurev-pharmtox-010617-052534

582. Dart RC, Surratt HL, Cicero TJ, Parrino MW, Severtson SG, Bucher-Bartelson B, et al. Trends in opioid analgesic abuse and mortality in the United States. N Engl J Med. 2015;372: 241–248. doi:10.1056/NEJMsa1406143

583. Machelska H, Celik MÖ. Advances in Achieving Opioid Analgesia Without Side Effects. Front Pharmacol. 2018;9: 1388. doi:10.3389/fphar.2018.01388

584. Li-Wei C, Can G, De-He Z, Qiang W, Xue-Jun X, Jie C, et al. Homodimerization of human mu-opioid receptor overexpressed in Sf9 insect cells. Protein Pept Lett. 2002;9: 145–152. doi:10.2174/0929866023408850

585. Yekkirala AS, Banks ML, Lunzer MM, Negus SS, Rice KC, Portoghese PS. Clinically employed opioid analgesics produce antinociception via μ-δ opioid receptor heteromers in Rhesus monkeys. ACS Chem Neurosci. 2012;3: 720–727. doi:10.1021/cn300049m

586. Costantino CM, Gomes I, Stockton SD, Lim MP, Devi LA. Opioid receptor heteromers in analgesia. Expert Rev Mol Med. 2012;14: e9. doi:10.1017/erm.2012.5

587. Gomes I, Gupta A, Filipovska J, Szeto HH, Pintar JE, Devi LA. A role for heterodimerization of mu and delta opiate receptors in enhancing morphine analgesia. Proc Natl Acad Sci U S A. 2004;101: 5135–5139. doi:10.1073/pnas.0307601101

588. Chakrabarti S, Liu N-J, Gintzler AR. Formation of mu-/kappa-opioid receptor heterodimer is sex-dependent and mediates female-specific opioid analgesia. Proc Natl Acad Sci U S A. 2010;107: 20115–20119. doi:10.1073/pnas.1009923107

589. Jordan BA, Devi LA. G-protein-coupled receptor heterodimerization modulates receptor function. Nature. 1999;399: 697–700. doi:10.1038/21441

590. Zhang L, Zhang J-T, Hang L, Liu T. Mu Opioid Receptor Heterodimers Emerge as Novel Therapeutic Targets: Recent Progress and Future Perspective. Front Pharmacol. 2020;11: 1078. doi:10.3389/fphar.2020.01078

591. Olson KM, Keresztes A, Tashiro JK, Daconta LV, Hruby VJ, Streicher JM. Synthesis and Evaluation of a Novel Bivalent Selective Antagonist for the Mu-Delta Opioid Receptor Heterodimer that Reduces Morphine Withdrawal in Mice. J Med Chem. 2018;61: 6075–6086. doi:10.1021/acs.jmedchem.8b00403

592. Rozenfeld R, Devi LA. Receptor heterodimerization leads to a switch in signaling: beta-arrestin2-mediated ERK activation by mu-delta opioid receptor heterodimers. FASEB J. 2007;21: 2455–2465. doi:10.1096/fj.06-7793com

593. Metcalf MD, Yekkirala AS, Powers MD, Kitto KF, Fairbanks CA, Wilcox GL, et al. The δ opioid receptor agonist SNC80 selectively activates heteromeric μ-δ opioid receptors. ACS Chem Neurosci. 2012;3: 505–509. doi:10.1021/cn3000394

594. Gomes I, Fujita W, Gupta A, Saldanha SA, Negri A, Pinello CE, et al. Identification of a μ-δ opioid receptor heteromer-biased agonist with antinociceptive activity. Proc Natl Acad Sci U S A. 2013;110: 12072–12077. doi:10.1073/pnas.1222044110

595. Milan-Lobo L, Whistler JL. Heteromerization of the μ- and δ-opioid receptors produces ligand-biased antagonism and alters μ-receptor trafficking. J Pharmacol Exp Ther. 2011;337: 868–875. doi:10.1124/jpet.111.179093

596. Hasbi A, Nguyen T, Fan T, Cheng R, Rashid A, Alijaniaram M, et al. Trafficking of preassembled opioid mu-delta heterooligomer-Gz signaling complexes to the plasma membrane: coregulation by agonists. Biochemistry. 2007;46: 12997–13009. doi:10.1021/bi701436w

597. Décaillot FM, Rozenfeld R, Gupta A, Devi LA. Cell surface targeting of mu-delta opioid receptor heterodimers by RTP4. Proc Natl Acad Sci U S A. 2008;105: 16045–16050. doi:10.1073/pnas.0804106105

598. He S-Q, Zhang Z-N, Guan J-S, Liu H-R, Zhao B, Wang H-B, et al. Facilitation of μ-opioid receptor activity by preventing δ-opioid receptor-mediated codegradation. Neuron. 2011;69: 120–131. doi:10.1016/j.neuron.2010.12.001

599. Erbs E, Faget L, Scherrer G, Matifas A, Filliol D, Vonesch J-L, et al. A mu-delta opioid receptor brain atlas reveals neuronal co-occurrence in subcortical networks. Brain Struct Funct. 2015;220: 677–702. doi:10.1007/s00429-014-0717-9

600. Wang D, Tawfik VL, Corder G, Low SA, François A, Basbaum AI, et al. Functional Divergence of Delta and Mu Opioid Receptor Organization in CNS Pain Circuits. Neuron. 2018;98: 90–108.e5. doi:10.1016/j.neuron.2018.03.002

601. Liu N-J, Chakrabarti S, Schnell S, Wessendorf M, Gintzler AR. Spinal synthesis of estrogen and concomitant signaling by membrane estrogen receptors regulate spinal κ- and μ-opioid receptor heterodimerization and female-specific spinal morphine antinociception. J Neurosci. 2011;31: 11836–11845. doi:10.1523/JNEUROSCI.1901-11.2011

602. Yang Y, Li Q, He Q-H, Han J-S, Su L, Wan Y. Heteromerization of μ-opioid receptor and cholecystokinin B receptor through the third transmembrane domain of the μ-opioid receptor contributes to the anti-opioid effects of cholecystokinin octapeptide. Exp Mol Med. 2018;50: 1–16. doi:10.1038/s12276-018-0090-5

603. Vilardaga J-P, Nikolaev VO, Lorenz K, Ferrandon S, Zhuang Z, Lohse MJ. Conformational cross-talk between alpha2A-adrenergic and mu-opioid receptors controls cell signaling. Nat Chem Biol. 2008;4: 126–131. doi:10.1038/nchembio.64

604. Stone LS, MacMillan LB, Kitto KF, Limbird LE, Wilcox GL. The alpha2a adrenergic receptor subtype mediates spinal analgesia evoked by alpha2 agonists and is necessary for spinal adrenergic-opioid synergy. J Neurosci. 1997;17: 7157–7165. doi:10.1523/JNEUROSCI.17-18-07157.1997

605. Bourgoin S, Pohl M, Mauborgne A, Benoliel JJ, Collin E, Hamon M, et al. Monoaminergic control of the release of calcitonin gene-related peptide- and substance P-like materials from rat spinal cord slices. Neuropharmacology. 1993;32: 633–640. doi:10.1016/0028-3908(93)90076-f

606. Kamisaki Y, Hamada T, Maeda K, Ishimura M, Itoh T. Presynaptic alpha 2 adrenoceptors inhibit glutamate release from rat spinal cord synaptosomes. J Neurochem. 1993;60: 522–526. doi:10.1111/j.1471-4159.1993.tb03180.x

607. Jordan B, Devi LA. Molecular mechanisms of opioid receptor signal transduction. Br J Anaesth. 1998;81: 12–19. doi:10.1093/bja/81.1.12

608. Richman JG, Regan JW. Alpha 2-adrenergic receptors increase cell migration and decrease F-actin labeling in rat aortic smooth muscle cells. Am J Physiol. 1998;274: C654–62. doi:10.1152/ajpcell.1998.274.3.C654

609. Wang D, Stoveken HM, Zucca S, Dao M, Orlandi C, Song C, et al. Genetic behavioral screen identifies an orphan anti-opioid system. Science. 2019;365: 1267–1273. doi:10.1126/science.aau2078

610. Koshimizu T-A, Honda K, Nagaoka-Uozumi S, Ichimura A, Kimura I, Nakaya M, et al. Complex formation between the vasopressin 1b receptor, β-arrestin-2, and the μ-opioid receptor underlies morphine tolerance. Nat Neurosci. 2018;21: 820–833. doi:10.1038/s41593-018-0144-y

611. Moreno E, Quiroz C, Rea W, Cai N-S, Mallol J, Cortés A, et al. Functional μ-Opioid-Galanin Receptor Heteromers in the Ventral Tegmental Area. J Neurosci. 2017;37: 1176–1186. doi:10.1523/JNEUROSCI.2442-16.2016

612. Cai N-S, Quiroz C, Bonaventura J, Bonifazi A, Cole TO, Purks J, et al. Opioid-galanin receptor heteromers mediate the dopaminergic effects of opioids. J Clin Invest. 2019;129: 2730–2744. doi:10.1172/JCI126912

613. Salio C, Fischer J, Franzoni MF, Mackie K, Kaneko T, Conrath M. CB1-cannabinoid and mu-opioid receptor co-localization on postsynaptic target in the rat dorsal horn. Neuroreport. 2001;12: 3689–3692. doi:10.1097/00001756-200112040-00017

614. Raehal KM, Bohn LM. β-arrestins: regulatory role and therapeutic potential in opioid and cannabinoid receptor-mediated analgesia. Handb Exp Pharmacol. 2014;219: 427–443. doi:10.1007/978-3-642-41199-1_22

615. Bouchet CA, Ingram SL. Cannabinoids in the descending pain modulatory circuit: Role in inflammation. Pharmacol Ther. 2020;209: 107495. doi:10.1016/j.pharmthera.2020.107495

616. Christie MJ. Opioid and cannabinoid receptors: friends with benefits or just close friends? British journal of pharmacology. 2006. pp. 385–386. doi:10.1038/sj.bjp.0706756

617. Manduca A, Lassalle O, Sepers M, Campolongo P, Cuomo V, Marsicano G, et al. Interacting Cannabinoid and Opioid Receptors in the Nucleus Accumbens Core Control Adolescent Social Play. Front Behav Neurosci. 2016;10: 211. doi:10.3389/fnbeh.2016.00211

618. Manduca A, Morena M, Campolongo P, Servadio M, Palmery M, Trabace L, et al. Distinct roles of the endocannabinoids anandamide and 2-arachidonoylglycerol in social behavior and emotionality at different developmental ages in rats. Eur Neuropsychopharmacol. 2015;25: 1362–1374. doi:10.1016/j.euroneuro.2015.04.005

619. Wei D, Lee D, Li D, Daglian J, Jung K-M, Piomelli D. A role for the endocannabinoid 2-arachidonoyl-sn-glycerol for social and high-fat food reward in male mice. Psychopharmacology . 2016;233: 1911–1919. doi:10.1007/s00213-016-4222-0

620. Pu SF, Zhuang HX, Han JS. Cholecystokinin octapeptide (CCK-8) antagonizes morphine analgesia in nucleus accumbens of the rat via the CCK-B receptor. Brain Res. 1994;657: 159–164. doi:10.1016/0006-8993(94)90963-6

621. Dourish CT, O'Neill MF, Coughlan J, Kitchener SJ, Hawley D, Iversen SD. The selective CCK-B receptor antagonist L-365,260 enhances morphine analgesia and prevents morphine tolerance in the rat. Eur J Pharmacol. 1990;176: 35–44. doi:10.1016/0014-2999(90)90129-t

622. Suzuki S, Chuang LF, Yau P, Doi RH, Chuang RY. Interactions of opioid and chemokine receptors: oligomerization of mu, kappa, and delta with CCR5 on immune cells. Exp Cell Res. 2002;280: 192–200. doi:10.1006/excr.2002.5638

623. Szabo I, Chen X-H, Xin L, Adler MW, Howard OMZ, Oppenheim JJ, et al. Heterologous desensitization of opioid receptors by chemokines inhibits chemotaxis and enhances the perception of pain. Proc Natl Acad Sci U S A. 2002;99: 10276–10281. doi:10.1073/pnas.102327699

624. Juhasz JR, Hasbi A, Rashid AJ, So CH, George SR, O'Dowd BF. Mu-opioid receptor heterooligomer formation with the dopamine D1 receptor as directly visualized in living cells. Eur J Pharmacol. 2008;581: 235–243. doi:10.1016/j.ejphar.2007.11.060

625. Tao Y-M, Yu C, Wang W-S, Hou Y-Y, Xu X-J, Chi Z-Q, et al. Heteromers of μ opioid and dopamine D1 receptors modulate opioid-induced locomotor sensitization in a dopamine-independent manner. Br J Pharmacol. 2017;174: 2842–2861. doi:10.1111/bph.13908

626. Dai W-L, Xiong F, Yan B, Cao Z-Y, Liu W-T, Liu J-H, et al. Blockade of neuronal dopamine D2 receptor attenuates morphine tolerance in mice spinal cord. Sci Rep. 2016;6: 38746. doi:10.1038/srep38746

627. Vasudevan L, Borroto-Escuela DO, Huysentruyt J, Fuxe K, Saini DK, Stove C. Heterodimerization of Mu Opioid Receptor Protomer with Dopamine D2 Receptor Modulates Agonist-Induced Internalization of Mu Opioid Receptor. Biomolecules. 2019;9. doi:10.3390/biom9080368

628. Grecksch G, Just S, Pierstorff C, Imhof A-K, Glück L, Doll C, et al. Analgesic tolerance to high-efficacy agonists but not to morphine is diminished in phosphorylation-deficient S375A μ-opioid receptor knock-in mice. J Neurosci. 2011;31: 13890–13896. doi:10.1523/JNEUROSCI.2304-11.2011

629. McPherson J, Rivero G, Baptist M, Llorente J, Al-Sabah S, Krasel C, et al. μ-opioid receptors: correlation of agonist efficacy for signalling with ability to activate internalization. Mol Pharmacol. 2010;78: 756–766. doi:10.1124/mol.110.066613

630. Whistler JL, von Zastrow M. Morphine-activated opioid receptors elude desensitization by beta-arrestin. Proc Natl Acad Sci U S A. 1998;95: 9914–9919. doi:10.1073/pnas.95.17.9914

631. Bohn LM, Gainetdinov RR, Caron MG. G protein-coupled receptor kinase/beta-arrestin systems and drugs of abuse: psychostimulant and opiate studies in knockout mice. Neuromolecular Med. 2004;5: 41–50. doi:10.1385/NMM:5:1:041

632. Artigas F. Serotonin receptors involved in antidepressant effects. Pharmacol Ther. 2013;137: 119–131. doi:10.1016/j.pharmthera.2012.09.006

633. Borroto-Escuela DO, Li X, Tarakanov AO, Savelli D, Narváez M, Shumilov K, et

al. Existence of Brain 5-HT1A-5-HT2A Isoreceptor Complexes with Antagonistic Allosteric Receptor-Receptor Interactions Regulating 5-HT1A Receptor Recognition. ACS Omega. 2017;2: 4779–4789. doi:10.1021/acsomega.7b00629

634. Szlachta M, Kuśmider M, Pabian P, Solich J, Kolasa M, Żurawek D, et al. Repeated Clozapine Increases the Level of Serotonin 5-HT1AR Heterodimerization with 5-HT2A or Dopamine D2 Receptors in the Mouse Cortex. Front Mol Neurosci. 2018;11: 40. doi:10.3389/fnmol.2018.00040

635. Celada P, Bortolozzi A, Artigas F. Serotonin 5-HT1A receptors as targets for agents to treat psychiatric disorders: rationale and current status of research. CNS Drugs. 2013;27: 703–716. doi:10.1007/s40263-013-0071-0

636. Millan MJ, Marin P, Bockaert J, Mannoury la Cour C. Signaling at G-protein-coupled serotonin receptors: recent advances and future research directions. Trends Pharmacol Sci. 2008;29: 454–464. doi:10.1016/j.tips.2008.06.007

637. Carr DB, Cooper DC, Ulrich SL, Spruston N, Surmeier DJ. Serotonin receptor activation inhibits sodium current and dendritic excitability in prefrontal cortex via a protein kinase C-dependent mechanism. J Neurosci. 2002;22: 6846–6855. doi:10.1523/JNEUROSCI.22-16-06846.2002

638. Anastasio NC, Stutz SJ, Fink LHL, Swinford-Jackson SE, Sears RM, DiLeone RJ, et al. Serotonin (5-HT) 5-HT2A Receptor (5-HT2AR):5-HT2CR Imbalance in Medial Prefrontal Cortex Associates with Motor Impulsivity. ACS Chem Neurosci. 2015;6: 1248–1258. doi:10.1021/acschemneuro.5b00094

639. Bubar MJ, Stutz SJ, Cunningham KA. 5-HT(2C) receptors localize to dopamine and GABA neurons in the rat mesoaccumbens pathway. PLoS One. 2011;6: e20508. doi:10.1371/journal.pone.0020508

640. Esposito E. Serotonin-dopamine interaction as a focus of novel antidepressant drugs. Curr Drug Targets. 2006;7: 177–185. doi:10.2174/138945006775515455

641. Moutkine I, Quentin E, Guiard BP, Maroteaux L, Doly S. Heterodimers of serotonin receptor subtypes 2 are driven by 5-HT2C protomers. J Biol Chem. 2017;292: 6352–6368. doi:10.1074/jbc.M117.779041

642. Renner U, Zeug A, Woehler A, Niebert M, Dityatev A, Dityateva G, et al. Heterodimerization of serotonin receptors 5-HT1A and 5-HT7 differentially regulates receptor signalling and trafficking. J Cell Sci. 2012;125: 2486–2499. doi:10.1242/jcs.101337

643. Barnes NM, Sharp T. A review of central 5-HT receptors and their function. Neuropharmacology. 1999;38: 1083–1152. doi:10.1016/s0028-3908(99)00010-6

644. Raymond JR, Mukhin YV, Gettys TW, Garnovskaya MN. The recombinant 5-HT1A receptor: G protein coupling and signalling pathways. Br J Pharmacol. 1999;127: 1751–1764. doi:10.1038/sj.bjp.0702723

645. Li Y-H, Xiang K, Xu X, Zhao X, Li Y, Zheng L, et al. Co-activation of both 5-HT1A and 5-HT7 receptors induced attenuation of glutamatergic synaptic transmission in the rat visual cortex. Neurosci Lett. 2018;686: 122–126. doi:10.1016/j.neulet.2018.09.013

646. Naumenko VS, Popova NK, Lacivita E, Leopoldo M, Ponimaskin EG. Interplay between serotonin 5-HT1A and 5-HT7 receptors in depressive disorders. CNS Neurosci Ther. 2014;20: 582–590. doi:10.1111/cns.12247

647. Łukasiewicz S, Błasiak E, Szafran-Pilch K, Dziedzicka-Wasylewska M. Dopamine D2 and serotonin 5-HT1A receptor interaction in the context of the effects of antipsychotics - in vitro studies. J Neurochem. 2016;137: 549–560. doi:10.1111/jnc.13582

648. Lukasiewicz S, Polit A, Kędracka-Krok S, Wędzony K, Maćkowiak M, Dziedzicka-Wasylewska M. Hetero-dimerization of serotonin 5-HT(2A) and dopamine D(2) receptors. Biochim Biophys Acta. 2010;1803: 1347–1358. doi:10.1016/j.bbamcr.2010.08.010

649. Albizu L, Holloway T, González-Maeso J, Sealfon SC. Functional crosstalk and heteromerization of serotonin 5-HT2A and dopamine D2 receptors. Neuropharmacology. 2011;61: 770–777. doi:10.1016/j.neuropharm.2011.05.023

650. Borroto-Escuela DO, Romero-Fernandez W, Tarakanov AO, Marcellino D, Ciruela F, Agnati LF, et al. Dopamine D2 and 5-hydroxytryptamine 5-HT($_2$A) receptors assemble into functionally interacting heteromers. Biochem Biophys Res Commun. 2010;401: 605–610. doi:10.1016/j.bbrc.2010.09.110

651. Moreira PI, Santos MS, Oliveira CR, Shenk JC, Nunomura A, Smith MA, et al. Alzheimer disease and the role of free radicals in the pathogenesis of the disease. CNS Neurol Disord Drug Targets. 2008;7: 3–10. doi:10.2174/187152708783885156

652. Reimherr FW, Wood DR, Wender PH. The use of MK-801, a novel sympathomimetic, in adults with attention deficit disorder, residual type. Psychopharmacol Bull. 1986;22: 237–242. Available: https://www.ncbi.nlm.nih.gov/pubmed/3523579

653. Gattaz WF, Schummer B, Behrens S. Effects of zotepine, haloperidol and clozapine on MK-801-induced stereotypy and locomotion in rats. J Neural Transm Gen Sect. 1994;96: 227–232. doi:10.1007/BF01294789

654. Borroto-Escuela DO, Narvaez M, Marcellino D, Parrado C, Narvaez JA, Tarakanov AO, et al. Galanin receptor-1 modulates 5-hydroxtryptamine-1A signaling via heterodimerization. Biochem Biophys Res Commun. 2010;393: 767–772. doi:10.1016/j.bbrc.2010.02.078

655. Branchek T, Smith KE, Walker MW. Molecular biology and pharmacology of galanin receptors. Ann N Y Acad Sci. 1998;863: 94–107. doi:10.1111/j.1749-

6632.1998.tb10687.x

656. Fuxe K, Hedlund P, von Euler G, Lundgren K, Martire M, Ögren SO, et al. Galanin/5-HT interactions in the rat central nervous system. Relevance for depression. In: Hökfelt T, Bartfai T, Jacobowitz D, Ottoson D, editors. Galanin: A New Multifunctional Peptide in the Neuro-endocrine System. London: Macmillan Education UK; 1991. pp. 221–235. doi:10.1007/978-1-349-12664-4_16

657. Razani H, Díaz-Cabiale Z, Misane I, Wang FH, Fuxe K, Ogren SO. Prolonged effects of intraventricular galanin on a 5-hydroxytryptamine(1A) receptor mediated function in the rat. Neurosci Lett. 2001;299: 145–149. doi:10.1016/s0304-3940(00)01788-2

658. Fuxe K, von Euler G, Agnati LF, Ogren SO. Galanin selectively modulates 5-hydroxytryptamine 1A receptors in the rat ventral limbic cortex. Neurosci Lett. 1988;85: 163–167. doi:10.1016/0304-3940(88)90448-x

659. Razani H, Diaz-Cabiale Z, Fuxe K, Ogren SO. Intraventricular galanin produces a time-dependent modulation of 5-HT1A receptors in the dorsal raphe of the rat. Neuroreport. 2000;11: 3943–3948. doi:10.1097/00001756-200012180-00008

660. Fuxe K, Ogren SO, Jansson A, Cintra A, Härfstrand A, Agnati LF. Intraventricular injections of galanin reduces 5-HT metabolism in the ventral limbic cortex, the hippocampal formation and the fronto-parietal cortex of the male rat. Acta Physiol Scand. 1988;133: 579–581. doi:10.1111/j.1748-1716.1988.tb08444.x

661. Kehr J, Yoshitake T, Wang F-H, Razani H, Gimenez-Llort L, Jansson A, et al. Galanin is a potent in vivo modulator of mesencephalic serotonergic neurotransmission. Neuropsychopharmacology. 2002;27: 341–356. doi:10.1016/S0893-133X(02)00309-3

662. Chruścicka B, Wallace Fitzsimons SE, Borroto-Escuela DO, Druelle C, Stamou P, Nally K, et al. Attenuation of Oxytocin and Serotonin 2A Receptor Signaling through Novel Heteroreceptor Formation. ACS Chem Neurosci. 2019;10: 3225–3240. doi:10.1021/acschemneuro.8b00665

663. Eaton JL, Roache L, Nguyen KN, Cushing BS, Troyer E, Papademetriou E, et al. Organizational effects of oxytocin on serotonin innervation. Dev Psychobiol. 2012;54: 92–97. doi:10.1002/dev.20566

664. Lefevre A, Richard N, Jazayeri M, Beuriat P-A, Fieux S, Zimmer L, et al. Oxytocin and Serotonin Brain Mechanisms in the Nonhuman Primate. J Neurosci. 2017;37: 6741–6750. doi:10.1523/JNEUROSCI.0659-17.2017

665. Dölen G, Darvishzadeh A, Huang KW, Malenka RC. Social reward requires coordinated activity of nucleus accumbens oxytocin and serotonin. Nature. 2013;501: 179–184. doi:10.1038/nature12518

666. Yoshida M, Takayanagi Y, Inoue K, Kimura T, Young LJ, Onaka T, et al.

Evidence that oxytocin exerts anxiolytic effects via oxytocin receptor expressed in serotonergic neurons in mice. J Neurosci. 2009;29: 2259–2271. doi:10.1523/JNEUROSCI.5593-08.2009

667. Chruścicka B, Cowan CSM, Wallace Fitzsimons SE, Borroto-Escuela DO, Druelle CM, Stamou P, et al. Molecular, biochemical and behavioural evidence for a novel oxytocin receptor and serotonin 2C receptor heterocomplex. Neuropharmacology. 2021;183: 108394. doi:10.1016/j.neuropharm.2020.108394

668. Prosser RA. Melatonin inhibits in vitro serotonergic phase shifts of the suprachiasmatic circadian clock. Brain Res. 1999;818: 408–413. doi:10.1016/s0006-8993(98)01295-5

669. Kamal M, Gbahou F, Guillaume J-L, Daulat AM, Benleulmi-Chaachoua A, Luka M, et al. Convergence of melatonin and serotonin (5-HT) signaling at MT2/5-HT2C receptor heteromers. J Biol Chem. 2015;290: 11537–11546. doi:10.1074/jbc.M114.559542

670. Millan MJ, Gobert A, Lejeune F, Dekeyne A, Newman-Tancredi A, Pasteau V, et al. The novel melatonin agonist agomelatine (S20098) is an antagonist at 5-hydroxytryptamine2C receptors, blockade of which enhances the activity of frontocortical dopaminergic and adrenergic pathways. J Pharmacol Exp Ther. 2003;306: 954–964. doi:10.1124/jpet.103.051797

671. Audinot V, Bonnaud A, Grandcolas L, Rodriguez M, Nagel N, Galizzi J-P, et al. Molecular cloning and pharmacological characterization of rat melatonin MT1 and MT2 receptors. Biochem Pharmacol. 2008;75: 2007–2019. doi:10.1016/j.bcp.2008.02.022

672. Racagni G, Riva MA, Molteni R, Musazzi L, Calabrese F, Popoli M, et al. Mode of action of agomelatine: synergy between melatonergic and 5-HT2C receptors. World J Biol Psychiatry. 2011;12: 574–587. doi:10.3109/15622975.2011.595823

673. Gerbier R, Ndiaye-Lobry D, Martinez de Morentin PB, Cecon E, Heisler LK, Delagrange P, et al. Pharmacological evidence for transactivation within melatonin MT2 and serotonin 5-HT2C receptor heteromers in mouse brain. FASEB J. 2021;35: e21161. doi:10.1096/fj.202000305R

674. Kishimoto K, Koyama S, Akaike N. Synergistic mu-opioid and 5-HT1A presynaptic inhibition of GABA release in rat periaqueductal gray neurons. Neuropharmacology. 2001;41: 529–538. doi:10.1016/s0028-3908(01)00100-9

675. Daval G, Vergé D, Basbaum AI, Bourgoin S, Hamon M. Autoradiographic evidence of serotonin1 binding sites on primary afferent fibres in the dorsal horn of the rat spinal cord. Neurosci Lett. 1987;83: 71–76. doi:10.1016/0304-3940(87)90218-7

676. Pompeiano M, Palacios JM, Mengod G. Distribution and cellular localization of mRNA coding for 5-HT1A receptor in the rat brain: correlation with receptor

binding. J Neurosci. 1992;12: 440–453. doi:10.1523/JNEUROSCI.12-02-00440.1992

677. Law PY, Wong YH, Loh HH. Molecular mechanisms and regulation of opioid receptor signaling. Annu Rev Pharmacol Toxicol. 2000;40: 389–430. doi:10.1146/annurev.pharmtox.40.1.389

678. Cussac D, Rauly-Lestienne I, Heusler P, Finana F, Cathala C, Bernois S, et al. μ-Opioid and 5-HT1A receptors heterodimerize and show signalling crosstalk via G protein and MAP-kinase pathways. Cell Signal. 2012;24: 1648–1657. doi:10.1016/j.cellsig.2012.04.010

679. Milligan G. Insights into ligand pharmacology using receptor-G-protein fusion proteins. Trends Pharmacol Sci. 2000;21: 24–28. doi:10.1016/s0165-6147(99)01404-2

680. Ashton JC, Appleton I, Darlington CL, Smith PF. Immunohistochemical localization of cerebrovascular cannabinoid CB1 receptor protein. J Cardiovasc Pharmacol. 2004;44: 517–519. doi:10.1097/00005344-200411000-00001

681. Smith TH, Sim-Selley LJ, Selley DE. Cannabinoid CB1 receptor-interacting proteins: novel targets for central nervous system drug discovery? Br J Pharmacol. 2010;160: 454–466. doi:10.1111/j.1476-5381.2010.00777.x

682. Munro S, Thomas KL, Abu-Shaar M. Molecular characterization of a peripheral receptor for cannabinoids. Nature. 1993;365: 61–65. doi:10.1038/365061a0

683. Latek D, Kolinski M, Ghoshdastider U, Debinski A, Bombolewski R, Plazinska A, et al. Modeling of ligand binding to G protein coupled receptors: cannabinoid CB1, CB2 and adrenergic β2AR. Journal of Molecular Modeling. 2011. pp. 2353–2366. doi:10.1007/s00894-011-0986-7

684. Callén L, Moreno E, Barroso-Chinea P, Moreno-Delgado D, Cortés A, Mallol J, et al. Cannabinoid receptors CB1 and CB2 form functional heteromers in brain. J Biol Chem. 2012;287: 20851–20865. doi:10.1074/jbc.M111.335273

685. Sierra S, Luquin N, Rico AJ, Gómez-Bautista V, Roda E, Dopeso-Reyes IG, et al. Detection of cannabinoid receptors CB1 and CB2 within basal ganglia output neurons in macaques: changes following experimental parkinsonism. Brain Struct Funct. 2015;220: 2721–2738. doi:10.1007/s00429-014-0823-8

686. Pertwee RG. Pharmacology of cannabinoid CB1 and CB2 receptors. Pharmacol Ther. 1997;74: 129–180. doi:10.1016/s0163-7258(97)82001-3

687. Navarro G, Borroto-Escuela D, Angelats E, Etayo Í, Reyes-Resina I, Pulido-Salgado M, et al. Receptor-heteromer mediated regulation of endocannabinoid signaling in activated microglia. Role of CB1 and CB2 receptors and relevance for Alzheimer's disease and levodopa-induced dyskinesia. Brain Behav Immun. 2018;67: 139–151. doi:10.1016/j.bbi.2017.08.015

688. Beltramo M, de Fonseca FR, Navarro M, Calignano A, Gorriti MA, Grammatikopoulos G, et al. Reversal of dopamine D(2) receptor responses by an anandamide transport inhibitor. J Neurosci. 2000;20: 3401–3407. doi:10.1523/JNEUROSCI.20-09-03401.2000

689. Giuffrida A, Parsons LH, Kerr TM, Rodríguez de Fonseca F, Navarro M, Piomelli D. Dopamine activation of endogenous cannabinoid signaling in dorsal striatum. Nat Neurosci. 1999;2: 358–363. doi:10.1038/7268

690. Kearn CS, Blake-Palmer K, Daniel E, Mackie K, Glass M. Concurrent stimulation of cannabinoid CB1 and dopamine D2 receptors enhances heterodimer formation: a mechanism for receptor cross-talk? Mol Pharmacol. 2005;67: 1697–1704. doi:10.1124/mol.104.006882

691. Herkenham M, Lynn AB, de Costa BR, Richfield EK. Neuronal localization of cannabinoid receptors in the basal ganglia of the rat. Brain Res. 1991;547: 267–274. doi:10.1016/0006-8993(91)90970-7

692. Meschler JP, Howlett AC. Signal transduction interactions between CB1 cannabinoid and dopamine receptors in the rat and monkey striatum. Neuropharmacology. 2001;40: 918–926. doi:10.1016/s0028-3908(01)00012-0

693. van der Stelt M, Di Marzo V. The endocannabinoid system in the basal ganglia and in the mesolimbic reward system: implications for neurological and psychiatric disorders. Eur J Pharmacol. 2003;480: 133–150. doi:10.1016/j.ejphar.2003.08.101

694. Julian MD, Martin AB, Cuellar B, Rodriguez De Fonseca F, Navarro M, Moratalla R, et al. Neuroanatomical relationship between type 1 cannabinoid receptors and dopaminergic systems in the rat basal ganglia. Neuroscience. 2003;119: 309–318. doi:10.1016/s0306-4522(03)00070-8

695. Terzian AL, Drago F, Wotjak CT, Micale V. The Dopamine and Cannabinoid Interaction in the Modulation of Emotions and Cognition: Assessing the Role of Cannabinoid CB1 Receptor in Neurons Expressing Dopamine D1 Receptors. Front Behav Neurosci. 2011;5: 49. doi:10.3389/fnbeh.2011.00049

696. Serrano A, Vadas E, Ferrer B, Bilbao A, Granado N, Suárez J, et al. Genetic deletion of dopamine D1 receptors increases the sensitivity to cannabinoid CB1 receptor antagonist-precipitated withdrawal when compared with wild-type littermates: studies in female mice repeatedly exposed to the Spice cannabinoid HU-210. Psychopharmacology . 2021;238: 551–557. doi:10.1007/s00213-020-05704-8

697. Egertová M, Elphick MR. Localisation of cannabinoid receptors in the rat brain using antibodies to the intracellular C-terminal tail of CB. J Comp Neurol. 2000;422: 159–171. doi:10.1002/(sici)1096-9861(20000626)422:2<159::aid-cne1>3.0.co;2-1

698. Yin HH, Lovinger DM. Frequency-specific and D2 receptor-mediated inhibition

of glutamate release by retrograde endocannabinoid signaling. Proc Natl Acad Sci U S A. 2006;103: 8251–8256. doi:10.1073/pnas.0510797103

699. Pickel VM, Chan J, Kearn CS, Mackie K. Targeting dopamine D2 and cannabinoid-1 (CB1) receptors in rat nucleus accumbens. J Comp Neurol. 2006;495: 299–313. doi:10.1002/cne.20881

700. Bagher AM, Young AP, Laprairie RB, Toguri JT, Kelly MEM, Denovan-Wright EM. Heteromer formation between cannabinoid type 1 and dopamine type 2 receptors is altered by combination cannabinoid and antipsychotic treatments. J Neurosci Res. 2020;98: 2496–2509. doi:10.1002/jnr.24716

701. Bagher AM, Laprairie RB, Toguri JT, Kelly MEM, Denovan-Wright EM. Bidirectional allosteric interactions between cannabinoid receptor 1 (CB1) and dopamine receptor 2 long (D2L) heterotetramers. Eur J Pharmacol. 2017;813: 66–83. doi:10.1016/j.ejphar.2017.07.034

702. Bagher AM, Laprairie RB, Kelly MEM, Denovan-Wright EM. Antagonism of Dopamine Receptor 2 Long Affects Cannabinoid Receptor 1 Signaling in a Cell Culture Model of Striatal Medium Spiny Projection Neurons. Mol Pharmacol. 2016;89: 652–666. doi:10.1124/mol.116.103465

703. Pinna A, Bonaventura J, Farré D, Sánchez M, Simola N, Mallol J, et al. L-DOPA disrupts adenosine A(2A)-cannabinoid CB(1)-dopamine D(2) receptor heteromer cross-talk in the striatum of hemiparkinsonian rats: biochemical and behavioral studies. Exp Neurol. 2014;253: 180–191. doi:10.1016/j.expneurol.2013.12.021

704. Bonaventura J, Rico AJ, Moreno E, Sierra S, Sánchez M, Luquin N, et al. L-DOPA-treatment in primates disrupts the expression of A(2A) adenosine-CB(1) cannabinoid-D(2) dopamine receptor heteromers in the caudate nucleus. Neuropharmacology. 2014;79: 90–100. doi:10.1016/j.neuropharm.2013.10.036

705. Jarrahian A, Watts VJ, Barker EL. D2 dopamine receptors modulate Galpha-subunit coupling of the CB1 cannabinoid receptor. J Pharmacol Exp Ther. 2004;308: 880–886. doi:10.1124/jpet.103.057620

706. Glass M, Felder CC. Concurrent stimulation of cannabinoid CB1 and dopamine D2 receptors augments cAMP accumulation in striatal neurons: evidence for a Gs linkage to the CB1 receptor. J Neurosci. 1997;17: 5327–5333. doi:10.1523/JNEUROSCI.17-14-05327.1997

707. Marcellino D, Carriba P, Filip M, Borgkvist A, Frankowska M, Bellido I, et al. Antagonistic cannabinoid CB1/dopamine D2 receptor interactions in striatal CB1/D2 heteromers. A combined neurochemical and behavioral analysis. Neuropharmacology. 2008;54: 815–823. doi:10.1016/j.neuropharm.2007.12.011

708. Ferré S, Goldberg SR, Lluis C, Franco R. Looking for the role of cannabinoid receptor heteromers in striatal function. Neuropharmacology. 2009;56 Suppl 1: 226–234. doi:10.1016/j.neuropharm.2008.06.076

709. Soria G, Castañé A, Berrendero F, Ledent C, Parmentier M, Maldonado R, et al. Adenosine A2A receptors are involved in physical dependence and place conditioning induced by THC. Eur J Neurosci. 2004;20: 2203–2213. doi:10.1111/j.1460-9568.2004.03682.x

710. Tebano MT, Martire A, Chiodi V, Pepponi R, Ferrante A, Domenici MR, et al. Adenosine A2A receptors enable the synaptic effects of cannabinoid CB1 receptors in the rodent striatum. J Neurochem. 2009;110: 1921–1930. doi:10.1111/j.1471-4159.2009.06282.x

711. Anderson WW, Collingridge GL. The LTP Program: a data acquisition program for on-line analysis of long-term potentiation and other synaptic events. J Neurosci Methods. 2001;108: 71–83. doi:10.1016/s0165-0270(01)00374-0

712. Carriba P, Ortiz O, Patkar K, Justinova Z, Stroik J, Themann A, et al. Striatal adenosine A2A and cannabinoid CB1 receptors form functional heteromeric complexes that mediate the motor effects of cannabinoids. Neuropsychopharmacology. 2007;32: 2249–2259. doi:10.1038/sj.npp.1301375

713. Rodríguez de Fonseca F, Rubio P, Menzaghi F, Merlo-Pich E, Rivier J, Koob GF, et al. Corticotropin-releasing factor (CRF) antagonist [D-Phe12,Nle21,38,C alpha MeLeu37]CRF attenuates the acute actions of the highly potent cannabinoid receptor agonist HU-210 on defensive-withdrawal behavior in rats. J Pharmacol Exp Ther. 1996;276: 56–64. Available: https://www.ncbi.nlm.nih.gov/pubmed/8558457

714. Castellano C, Rossi-Arnaud C, Cestari V, Costanzi M. Cannabinoids and memory: animal studies. Curr Drug Targets CNS Neurol Disord. 2003;2: 389–402. doi:10.2174/1568007033482670

715. Moreira FA, Lutz B. The endocannabinoid system: emotion, learning and addiction. Addict Biol. 2008;13: 196–212. doi:10.1111/j.1369-1600.2008.00104.x

716. Maldonado R, Berrendero F, Ozaita A, Robledo P. Neurochemical basis of cannabis addiction. Neuroscience. 2011;181: 1–17. doi:10.1016/j.neuroscience.2011.02.035

717. Viñals X, Moreno E, Lanfumey L, Cordomí A, Pastor A, de La Torre R, et al. Cognitive Impairment Induced by Delta9-tetrahydrocannabinol Occurs through Heteromers between Cannabinoid CB1 and Serotonin 5-HT2A Receptors. PLoS Biol. 2015;13: e1002194. doi:10.1371/journal.pbio.1002194

718. Gorzalka BB, Hill MN, Sun JC. Functional role of the endocannabinoid system and AMPA/kainate receptors in 5-HT2A receptor-mediated wet dog shakes. Eur J Pharmacol. 2005;516: 28–33. doi:10.1016/j.ejphar.2005.04.019

719. Darmani NA. Cannabinoids of diverse structure inhibit two DOI-induced 5-HT(2A) receptor-mediated behaviors in mice. Pharmacol Biochem Behav. 2001;68: 311–317. doi:10.1016/s0091-3057(00)00477-9

720. Cheer JF, Cadogan AK, Marsden CA, Fone KC, Kendall DA. Modification of 5-HT2 receptor mediated behaviour in the rat by oleamide and the role of cannabinoid receptors. Neuropharmacology. 1999;38: 533–541. doi:10.1016/s0028-3908(98)00208-1

721. de Almeida J, Mengod G. Quantitative analysis of glutamatergic and GABAergic neurons expressing 5-HT(2A) receptors in human and monkey prefrontal cortex. J Neurochem. 2007;103: 475–486. doi:10.1111/j.1471-4159.2007.04768.x

722. Mechoulam R, Parker LA. The endocannabinoid system and the brain. Annu Rev Psychol. 2013;64: 21–47. doi:10.1146/annurev-psych-113011-143739

723. Bombardi C, Di Giovanni G. Functional anatomy of 5-HT2A receptors in the amygdala and hippocampal complex: relevance to memory functions. Exp Brain Res. 2013;230: 427–439. doi:10.1007/s00221-013-3512-6

724. Galindo L, Moreno E, López-Armenta F, Guinart D, Cuenca-Royo A, Izquierdo-Serra M, et al. Cannabis Users Show Enhanced Expression of CB1-5HT2A Receptor Heteromers in Olfactory Neuroepithelium Cells. Mol Neurobiol. 2018;55: 6347–6361. doi:10.1007/s12035-017-0833-7

725. Borroto-Escuela DO, Narvaez M, Di Palma M, Calvo F, Rodriguez D, Millon C, et al. Preferential activation by galanin 1-15 fragment of the GalR1 protomer of a GalR1-GalR2 heteroreceptor complex. Biochem Biophys Res Commun. 2014;452: 347–353. doi:10.1016/j.bbrc.2014.08.061

726. Millón C, Flores-Burgess A, Narváez M, Borroto-Escuela DO, Santín L, Parrado C, et al. A role for galanin N-terminal fragment (1-15) in anxiety- and depression-related behaviors in rats. Int J Neuropsychopharmacol. 2014;18. doi:10.1093/ijnp/pyu064

727. Fuxe K, Borroto-Escuela DO, Romero-Fernandez W, Tarakanov AO, Calvo F, Garriga P, et al. On the existence and function of galanin receptor heteromers in the central nervous system. Front Endocrinol . 2012;3: 127. doi:10.3389/fendo.2012.00127

728. Rivas-Santisteban R, Rodriguez-Perez AI, Muñoz A, Reyes-Resina I, Labandeira-García JL, Navarro G, et al. Angiotensin AT1 and AT2 receptor heteromer expression in the hemilesioned rat model of Parkinson’s disease that increases with levodopa-induced dyskinesia. J Neuroinflammation. 2020;17: 243. doi:10.1186/s12974-020-01908-z

729. Perez-Lloret S, Otero-Losada M, Toblli JE, Capani F. Renin-angiotensin system as a potential target for new therapeutic approaches in Parkinson’s disease. Expert Opin Investig Drugs. 2017;26: 1163–1173. doi:10.1080/13543784.2017.1371133

730. Muñoz A, Garrido-Gil P, Dominguez-Meijide A, Labandeira-Garcia JL. Angiotensin type 1 receptor blockage reduces l-dopa-induced dyskinesia in the 6-

OHDA model of Parkinson's disease. Involvement of vascular endothelial growth factor and interleukin-1β. Exp Neurol. 2014;261: 720–732. doi:10.1016/j.expneurol.2014.08.019

731. Pin J-P, Galvez T, Prézeau L. Evolution, structure, and activation mechanism of family 3/C G-protein-coupled receptors. Pharmacol Ther. 2003;98: 325–354. doi:10.1016/s0163-7258(03)00038-x

732. Rondard P, Goudet C, Kniazeff J, Pin J-P, Prézeau L. The complexity of their activation mechanism opens new possibilities for the modulation of mGlu and GABAB class C G protein-coupled receptors. Neuropharmacology. 2011;60: 82–92. doi:10.1016/j.neuropharm.2010.08.009

733. Urwyler S. Allosteric modulation of family C G-protein-coupled receptors: from molecular insights to therapeutic perspectives. Pharmacol Rev. 2011;63: 59–126. doi:10.1124/pr.109.002501

734. Chun L, Zhang W-H, Liu J-F. Structure and ligand recognition of class C GPCRs. Acta Pharmacol Sin. 2012;33: 312–323. doi:10.1038/aps.2011.186

735. Binet V, Duthey B, Lecaillon J, Vol C, Quoyer J, Labesse G, et al. Common structural requirements for heptahelical domain function in class A and class C G protein-coupled receptors. J Biol Chem. 2007;282: 12154–12163. doi:10.1074/jbc.M611071200

736. Kunishima N, Shimada Y, Tsuji Y, Sato T, Yamamoto M, Kumasaka T, et al. Structural basis of glutamate recognition by a dimeric metabotropic glutamate receptor. Nature. 2000;407: 971–977. doi:10.1038/35039564

737. Tsuchiya D, Kunishima N, Kamiya N, Jingami H, Morikawa K. Structural views of the ligand-binding cores of a metabotropic glutamate receptor complexed with an antagonist and both glutamate and Gd3+. Proc Natl Acad Sci U S A. 2002;99: 2660–2665. doi:10.1073/pnas.052708599

738. Conn PJ, Jeffrey Conn P, Lindsley CW, Jones CK. Activation of metabotropic glutamate receptors as a novel approach for the treatment of schizophrenia. Trends in Pharmacological Sciences. 2009. pp. 25–31. doi:10.1016/j.tips.2008.10.006

739. Bessis A-S, Rondard P, Gaven F, Brabet I, Triballeau N, Prezeau L, et al. Closure of the Venus flytrap module of mGlu8 receptor and the activation process: Insights from mutations converting antagonists into agonists. Proc Natl Acad Sci U S A. 2002;99: 11097–11102. doi:10.1073/pnas.162138699

740. Romano C, Miller JK, Hyrc K, Dikranian S, Mennerick S, Takeuchi Y, et al. Covalent and Noncovalent Interactions Mediate Metabotropic Glutamate Receptor $mGlu_5$Dimerization. Molecular Pharmacology. 2001. pp. 46–53. doi:10.1124/mol.59.1.46

741. Tsuji Y, Shimada Y, Takeshita T, Kajimura N, Nomura S, Sekiyama N, et al. Cryptic dimer interface and domain organization of the extracellular region of metabotropic glutamate receptor subtype 1. J Biol Chem. 2000;275: 28144–28151. doi:10.1074/jbc.M003226200

742. Ray K, Hauschild BC. Cys-140 is critical for metabotropic glutamate receptor-1 dimerization. J Biol Chem. 2000;275: 34245–34251. doi:10.1074/jbc.M005581200

743. Muto T, Tsuchiya D, Morikawa K, Jingami H. Structures of the extracellular regions of the group II/III metabotropic glutamate receptors. Proc Natl Acad Sci U S A. 2007;104: 3759–3764. doi:10.1073/pnas.0611577104

744. Rondard P, Liu J, Huang S, Malhaire F, Vol C, Pinault A, et al. Coupling of agonist binding to effector domain activation in metabotropic glutamate-like receptors. J Biol Chem. 2006;281: 24653–24661. doi:10.1074/jbc.M602277200

745. Hu J, Hauache O, Spiegel AM. Human Ca2+ receptor cysteine-rich domain. Analysis of function of mutant and chimeric receptors. J Biol Chem. 2000;275: 16382–16389. doi:10.1074/jbc.M000277200

746. Brown EM. Clinical lessons from the calcium-sensing receptor. Nat Clin Pract Endocrinol Metab. 2007;3: 122–133. doi:10.1038/ncpendmet0388

747. Deal C. Future therapeutic targets in osteoporosis. Curr Opin Rheumatol. 2009;21: 380–385. doi:10.1097/BOR.0b013e32832cbc2a

748. Brown EM. Anti-parathyroid and anti-calcium sensing receptor antibodies in autoimmune hypoparathyroidism. Endocrinol Metab Clin North Am. 2009;38: 437–45, x. doi:10.1016/j.ecl.2009.01.001

749. Burger A. Progress in Medicinal Chemistry. Journal of Medicinal Chemistry. 1963. pp. 827–827. doi:10.1021/jm00342a061

750. Gao Y, Robertson MJ, Rahman SN, Seven AB, Zhang C, Meyerowitz JG, et al. Asymmetric activation of the calcium-sensing receptor homodimer. Nature. 2021;595: 455–459. doi:10.1038/s41586-021-03691-0

751. Yano S, Brown EM, Chattopadhyay N. Calcium-sensing receptor in the brain. Cell Calcium. 2004;35: 257–264. doi:10.1016/j.ceca.2003.10.008

752. Giudice ML, Mihalik B, Dinnyés A, Kobolák J. The Nervous System Relevance of the Calcium Sensing Receptor in Health and Disease. Molecules. 2019;24. doi:10.3390/molecules24142546

753. Berridge MJ. Neuronal calcium signaling. Neuron. 1998;21: 13–26. doi:10.1016/s0896-6273(00)80510-3

754. Schrank S, Barrington N, Stutzmann GE. Calcium-Handling Defects and Neurodegenerative Disease. Cold Spring Harb Perspect Biol. 2020;12. doi:10.1101/cshperspect.a035212

755. Kawamoto EM, Vivar C, Camandola S. Physiology and pathology of calcium signaling in the brain. Front Pharmacol. 2012;3: 61. doi:10.3389/fphar.2012.00061

756. Khachaturian ZS. Hypothesis on the regulation of cytosol calcium concentration and the aging brain. Neurobiol Aging. 1987;8: 345–346. doi:10.1016/0197-4580(87)90073-x

757. Mattson MP, Pedersen WA, Duan W, Culmsee C, Camandola S. Cellular and molecular mechanisms underlying perturbed energy metabolism and neuronal degeneration in Alzheimer's and Parkinson's diseases. Ann N Y Acad Sci. 1999;893: 154–175. doi:10.1111/j.1749-6632.1999.tb07824.x

758. Surmeier DJ, Schumacker PT, Guzman JD, Ilijic E, Yang B, Zampese E. Calcium and Parkinson's disease. Biochem Biophys Res Commun. 2017;483: 1013–1019. doi:10.1016/j.bbrc.2016.08.168

759. Stutzmann GE, Smith I, Caccamo A, Oddo S, Laferla FM, Parker I. Enhanced ryanodine receptor recruitment contributes to Ca2+ disruptions in young, adult, and aged Alzheimer's disease mice. J Neurosci. 2006;26: 5180–5189. doi:10.1523/JNEUROSCI.0739-06.2006

760. Pchitskaya E, Popugaeva E, Bezprozvanny I. Calcium signaling and molecular mechanisms underlying neurodegenerative diseases. Cell Calcium. 2018;70: 87–94. doi:10.1016/j.ceca.2017.06.008

761. Bettler B, Tiao JY-H. Molecular diversity, trafficking and subcellular localization of GABAB receptors. Pharmacol Ther. 2006;110: 533–543. doi:10.1016/j.pharmthera.2006.03.006

762. Sakamaki K, Nomura M, Hatakenaka S, Miyakubo H, Tanaka J. GABAergic modulation of noradrenaline release in the median preoptic nucleus area in the rat. Neurosci Lett. 2003;342: 77–80. doi:10.1016/s0304-3940(03)00242-8

763. Waldmeier PC, Kaupmann K, Urwyler S. Roles of GABAB receptor subtypes in presynaptic auto- and heteroreceptor function regulating GABA and glutamate release. J Neural Transm. 2008;115: 1401–1411. doi:10.1007/s00702-008-0095-7

764. Jones KA, Borowsky B, Tamm JA, Craig DA, Durkin MM, Dai M, et al. GABA(B) receptors function as a heteromeric assembly of the subunits GABA(B)R1 and GABA(B)R2. Nature. 1998;396: 674–679. doi:10.1038/25348

765. Kaupmann K, Malitschek B, Schuler V, Heid J, Froestl W, Beck P, et al. GABA(B)-receptor subtypes assemble into functional heteromeric complexes. Nature. 1998;396: 683–687. doi:10.1038/25360

766. Fatemi SH, Folsom TD, Thuras PD. Deficits in GABA(B) receptor system in schizophrenia and mood disorders: a postmortem study. Schizophr Res. 2011;128: 37–43. doi:10.1016/j.schres.2010.12.025

767. Nyitrai G, Kékesi KA, Emri Z, Szárics E, Juhász G, Kardos J. GABA(B) receptor

antagonist CGP-36742 enhances somatostatin release in the rat hippocampus in vivo and in vitro. Eur J Pharmacol. 2003;478: 111–119. doi:10.1016/j.ejphar.2003.08.006

768. Galvez T, Parmentier ML, Joly C, Malitschek B, Kaupmann K, Kuhn R, et al. Mutagenesis and modeling of the GABAB receptor extracellular domain support a venus flytrap mechanism for ligand binding. J Biol Chem. 1999;274: 13362–13369. doi:10.1074/jbc.274.19.13362

769. Margeta-Mitrovic M, Jan YN, Jan LY. Function of GB1 and GB2 subunits in G protein coupling of GABA(B) receptors. Proc Natl Acad Sci U S A. 2001;98: 14649–14654. doi:10.1073/pnas.251554498

770. Li C-J, Lu Y, Zhou M, Zong X-G, Li C, Xu X-L, et al. Activation of GABAB receptors ameliorates cognitive impairment via restoring the balance of HCN1/HCN2 surface expression in the hippocampal CA1 area in rats with chronic cerebral hypoperfusion. Mol Neurobiol. 2014;50: 704–720. doi:10.1007/s12035-014-8736-3

771. Kuramoto N, Wilkins ME, Fairfax BP, Revilla-Sanchez R, Terunuma M, Tamaki K, et al. Phospho-dependent functional modulation of GABA(B) receptors by the metabolic sensor AMP-dependent protein kinase. Neuron. 2007;53: 233–247. doi:10.1016/j.neuron.2006.12.015

772. Dave KR, Lange-Asschenfeldt C, Raval AP, Prado R, Busto R, Saul I, et al. Ischemic preconditioning ameliorates excitotoxicity by shifting glutamate/gamma-aminobutyric acid release and biosynthesis. J Neurosci Res. 2005;82: 665–673. doi:10.1002/jnr.20674

773. Tu H, Xu C, Zhang W, Liu Q, Rondard P, Pin J-P, et al. GABAB receptor activation protects neurons from apoptosis via IGF-1 receptor transactivation. J Neurosci. 2010;30: 749–759. doi:10.1523/JNEUROSCI.2343-09.2010

774. Cryan JF, Kaupmann K. Don’t worry “B” happy!: a role for GABA(B) receptors in anxiety and depression. Trends Pharmacol Sci. 2005;26: 36–43. doi:10.1016/j.tips.2004.11.004

775. Bowery NG. GABAB receptor: a site of therapeutic benefit. Curr Opin Pharmacol. 2006;6: 37–43. doi:10.1016/j.coph.2005.10.002

776. Goudet C, Magnaghi V, Landry M, Nagy F, Gereau RW 4th, Pin J-P. Metabotropic receptors for glutamate and GABA in pain. Brain Res Rev. 2009;60: 43–56. doi:10.1016/j.brainresrev.2008.12.007

777. Boczek T, Mackiewicz J, Sobolczyk M, Wawrzyniak J, Lisek M, Ferenc B, et al. The Role of G Protein-Coupled Receptors (GPCRs) and Calcium Signaling in Schizophrenia. Focus on GPCRs Activated by Neurotransmitters and Chemokines. Cells. 2021;10. doi:10.3390/cells10051228

778. Niswender CM, Conn PJ. Metabotropic glutamate receptors: physiology, pharmacology, and disease. Annu Rev Pharmacol Toxicol. 2010;50: 295–322. doi:10.1146/annurev.pharmtox.011008.145533

779. Conn PJ, Pin JP. Pharmacology and functions of metabotropic glutamate receptors. Annu Rev Pharmacol Toxicol. 1997;37: 205–237. doi:10.1146/annurev.pharmtox.37.1.205

780. Nicoletti F, Bockaert J, Collingridge GL, Conn PJ, Ferraguti F, Schoepp DD, et al. Metabotropic glutamate receptors: from the workbench to the bedside. Neuropharmacology. 2011;60: 1017–1041. doi:10.1016/j.neuropharm.2010.10.022

781. Iyer AM, van Scheppingen J, Milenkovic I, Anink JJ, Lim D, Genazzani AA, et al. Metabotropic glutamate receptor 5 in Down's syndrome hippocampus during development: increased expression in astrocytes. Curr Alzheimer Res. 2014;11: 694–705. doi:10.2174/1567205011666140812115423

782. Spampinato SF, Copani A, Nicoletti F, Sortino MA, Caraci F. Metabotropic Glutamate Receptors in Glial Cells: A New Potential Target for Neuroprotection? Front Mol Neurosci. 2018;11: 414. doi:10.3389/fnmol.2018.00414

783. Chen X, Lin R, Chang L, Xu S, Wei X, Zhang J, et al. Enhancement of long-term depression by soluble amyloid β protein in rat hippocampus is mediated by metabotropic glutamate receptor and involves activation of p38MAPK, STEP and caspase-3. Neuroscience. 2013;253: 435–443. doi:10.1016/j.neuroscience.2013.08.054

784. Renner M, Lacor PN, Velasco PT, Xu J, Contractor A, Klein WL, et al. Deleterious effects of amyloid beta oligomers acting as an extracellular scaffold for mGluR5. Neuron. 2010;66: 739–754. doi:10.1016/j.neuron.2010.04.029

785. Caraci F, Molinaro G, Battaglia G, Giuffrida ML, Riozzi B, Traficante A, et al. Targeting group II metabotropic glutamate (mGlu) receptors for the treatment of psychosis associated with Alzheimer's disease: selective activation of mGlu2 receptors amplifies beta-amyloid toxicity in cultured neurons, whereas dual activation of mGlu2 and mGlu3 receptors is neuroprotective. Mol Pharmacol. 2011;79: 618–626. doi:10.1124/mol.110.067488

786. White JH, Wise A, Main MJ, Green A, Fraser NJ, Disney GH, et al. Heterodimerization is required for the formation of a functional GABA(B) receptor. Nature. 1998;396: 679–682. doi:10.1038/25354

787. Stewart GD, Comps-Agrar L, Nørskov-Lauritsen LB, Pin J-P, Kniazeff J. Allosteric interactions between GABAB1 subunits control orthosteric binding sites occupancy within GABAB oligomers. Neuropharmacology. 2018;136: 92–101. doi:10.1016/j.neuropharm.2017.12.042

788. Pin J-P, Kniazeff J, Prézeau L, Liu J-F, Rondard P. GPCR interaction as a possible way for allosteric control between receptors. Mol Cell Endocrinol.

2019;486: 89–95. doi:10.1016/j.mce.2019.02.019

789. Koehl A, Hu H, Feng D, Sun B, Zhang Y, Robertson MJ, et al. Structural insights into the activation of metabotropic glutamate receptors. Nature. 2019;566: 79–84. doi:10.1038/s41586-019-0881-4

790. Ellaithy A, Gonzalez-Maeso J, Logothetis DA, Levitz J. Structural and Biophysical Mechanisms of Class C G Protein-Coupled Receptor Function. Trends Biochem Sci. 2020;45: 1049–1064. doi:10.1016/j.tibs.2020.07.008

791. Ray K, Hauschild BC, Steinbach PJ, Goldsmith PK, Hauache O, Spiegel AM. Identification of the cysteine residues in the amino-terminal extracellular domain of the human Ca(2+) receptor critical for dimerization. Implications for function of monomeric Ca(2+) receptor. J Biol Chem. 1999;274: 27642–27650. doi:10.1074/jbc.274.39.27642

792. Pagano A, Rovelli G, Mosbacher J, Lohmann T, Duthey B, Stauffer D, et al. C-terminal interaction is essential for surface trafficking but not for heteromeric assembly of GABA(b) receptors. J Neurosci. 2001;21: 1189–1202. doi:10.1523/JNEUROSCI.21-04-01189.2001

793. Couve A, Filippov AK, Connolly CN, Bettler B, Brown DA, Moss SJ. Intracellular retention of recombinant GABAB receptors. J Biol Chem. 1998;273: 26361–26367. doi:10.1074/jbc.273.41.26361

794. Duthey B, Caudron S, Perroy J, Bettler B, Fagni L, Pin J-P, et al. A single subunit (GB2) is required for G-protein activation by the heterodimeric GABA(B) receptor. J Biol Chem. 2002;277: 3236–3241. doi:10.1074/jbc.M108900200

795. Robbins MJ, Calver AR, Filippov AK, Hirst WD, Russell RB, Wood MD, et al. GABAB2 is essential for G-protein coupling of the GABAB receptor heterodimer. Journal of Neuroscience. 2001;21: 8043–8052. Available: https://www.jneurosci.org/content/21/20/8043.short

796. Galvez T, Duthey B, Kniazeff J, Blahos J, Rovelli G, Bettler B, et al. Allosteric interactions between GB1 and GB2 subunits are required for optimal GABA(B) receptor function. EMBO J. 2001;20: 2152–2159. doi:10.1093/emboj/20.9.2152

797. Margeta-Mitrovic M, Jan YN, Jan LY. Ligand-induced signal transduction within heterodimeric GABA(B) receptor. Proc Natl Acad Sci U S A. 2001;98: 14643–14648. doi:10.1073/pnas.251554798

798. Fritzius T, Bettler B. The organizing principle of GABAB receptor complexes: Physiological and pharmacological implications. Basic Clin Pharmacol Toxicol. 2020;126 Suppl 6: 25–34. doi:10.1111/bcpt.13241

799. Benke D. GABAB receptor trafficking and interacting proteins: targets for the development of highly specific therapeutic strategies to treat neurological disorders? Biochem Pharmacol. 2013;86: 1525–1530.

doi:10.1016/j.bcp.2013.09.016

800. Calebiro D, Rieken F, Wagner J, Sungkaworn T, Zabel U, Borzi A, et al. Single-molecule analysis of fluorescently labeled G-protein-coupled receptors reveals complexes with distinct dynamics and organization. Proc Natl Acad Sci U S A. 2013;110: 743–748. doi:10.1073/pnas.1205798110

801. Kent CN, Park C, Lindsley CW. Classics in Chemical Neuroscience: Baclofen. ACS Chem Neurosci. 2020;11: 1740–1755. doi:10.1021/acschemneuro.0c00254

802. Agabio R, Sinclair JM, Addolorato G, Aubin H-J, Beraha EM, Caputo F, et al. Baclofen for the treatment of alcohol use disorder: the Cagliari Statement. The lancet. Psychiatry. 2018. pp. 957–960. doi:10.1016/S2215-0366(18)30303-1

803. Pin J-P, Kniazeff J, Liu J, Binet V, Goudet C, Rondard P, et al. Allosteric functioning of dimeric class C G-protein-coupled receptors. FEBS J. 2005;272: 2947–2955. doi:10.1111/j.1742-4658.2005.04728.x

804. El Moustaine D, Granier S, Doumazane E, Scholler P, Rahmeh R, Bron P, et al. Distinct roles of metabotropic glutamate receptor dimerization in agonist activation and G-protein coupling. Proc Natl Acad Sci U S A. 2012;109: 16342–16347. doi:10.1073/pnas.1205838109

805. Morató X, Luján R, Gonçalves N, Watanabe M, Altafaj X, Carvalho AL, et al. Metabotropic glutamate type 5 receptor requires contactin-associated protein 1 to control memory formation. Hum Mol Genet. 2018;27: 3528–3541. doi:10.1093/hmg/ddy264

806. García-Negredo G, Soto D, Llorente J, Morató X, Galenkamp KMO, Gómez-Soler M, et al. Coassembly and coupling of SK2 channels and mGlu5 receptors. J Neurosci. 2014;34: 14793–14802. doi:10.1523/JNEUROSCI.2038-14.2014

807. Fagni L, Chavis P, Ango F, Bockaert J. Complex interactions between mGluRs, intracellular Ca2+ stores and ion channels in neurons. Trends Neurosci. 2000;23: 80–88. doi:10.1016/s0166-2236(99)01492-7

808. Canela L, Fernández-Dueñas V, Albergaria C, Watanabe M, Lluís C, Mallol J, et al. The association of metabotropic glutamate receptor type 5 with the neuronal Ca2+-binding protein 2 modulates receptor function. J Neurochem. 2009;111: 555–567. doi:10.1111/j.1471-4159.2009.06348.x

809. Bockaert J, Perroy J, Bécamel C, Marin P, Fagni L. GPCR interacting proteins (GIPs) in the nervous system: Roles in physiology and pathologies. Annu Rev Pharmacol Toxicol. 2010;50: 89–109. doi:10.1146/annurev.pharmtox.010909.105705

810. Goudet C, Kniazeff J, Hlavackova V, Malhaire F, Maurel D, Acher F, et al. Asymmetric functioning of dimeric metabotropic glutamate receptors disclosed by positive allosteric modulators. J Biol Chem. 2005;280: 24380–24385.

doi:10.1074/jbc.M502642200

811. Kammermeier PJ. Functional and pharmacological characteristics of metabotropic glutamate receptors 2/4 heterodimers. Mol Pharmacol. 2012;82: 438–447. doi:10.1124/mol.112.078501

812. Pandya NJ, Klaassen RV, van der Schors RC, Slotman JA, Houtsmuller A, Smit AB, et al. Group 1 metabotropic glutamate receptors 1 and 5 form a protein complex in mouse hippocampus and cortex. Proteomics. 2016;16: 2698–2705. doi:10.1002/pmic.201500400

813. Hayashi MK, Tang C, Verpelli C, Narayanan R, Stearns MH, Xu R-M, et al. The postsynaptic density proteins Homer and Shank form a polymeric network structure. Cell. 2009;137: 159–171. doi:10.1016/j.cell.2009.01.050

814. Jong Y-JI, Sergin I, Purgert CA, O'Malley KL. Location-dependent signaling of the group 1 metabotropic glutamate receptor mGlu5. Mol Pharmacol. 2014;86: 774–785. doi:10.1124/mol.114.094763

815. Damian M, Martin A, Mesnier D, Pin J-P, Banères J-L. Asymmetric conformational changes in a GPCR dimer controlled by G-proteins. The EMBO Journal. 2006. pp. 5693–5702. doi:10.1038/sj.emboj.7601449

816. Albizu L, Cottet M, Kralikova M, Stoev S, Seyer R, Brabet I, et al. Time-resolved FRET between GPCR ligands reveals oligomers in native tissues. Nat Chem Biol. 2010;6: 587–594. doi:10.1038/nchembio.396

817. Sebastianutto I, Goyet E, Andreoli L, Font-Ingles J, Moreno-Delgado D, Bouquier N, et al. D1-mGlu5 heteromers mediate noncanonical dopamine signaling in Parkinson's disease. J Clin Invest. 2020;130: 1168–1184. doi:10.1172/JCI126361

818. Surmeier DJ, Graves SM, Shen W. Dopaminergic modulation of striatal networks in health and Parkinson's disease. Curr Opin Neurobiol. 2014;29: 109–117. doi:10.1016/j.conb.2014.07.008

819. Bagetta V, Ghiglieri V, Sgobio C, Calabresi P, Picconi B. Synaptic dysfunction in Parkinson's disease. Biochem Soc Trans. 2010;38: 493–497. doi:10.1042/BST0380493

820. Ciruela F, Escriche M, Burgueno J, Angulo E, Casado V, Soloviev MM, et al. Metabotropic glutamate 1alpha and adenosine A1 receptors assemble into functionally interacting complexes. J Biol Chem. 2001;276: 18345–18351. doi:10.1074/jbc.M006960200

821. Kamikubo Y, Tabata T, Sakairi H, Hashimoto Y, Sakurai T. Complex formation and functional interaction between adenosine A1 receptor and type-1 metabotropic glutamate receptor. J Pharmacol Sci. 2015;128: 125–130. doi:10.1016/j.jphs.2015.06.002

822. Kamikubo Y, Shimomura T, Fujita Y, Tabata T, Kashiyama T, Sakurai T, et al. Functional cooperation of metabotropic adenosine and glutamate receptors regulates postsynaptic plasticity in the cerebellum. J Neurosci. 2013;33: 18661–18671. doi:10.1523/JNEUROSCI.5567-12.2013

823. Klinger M, Freissmuth M, Nanoff C. Adenosine receptors: G protein-mediated signalling and the role of accessory proteins. Cell Signal. 2002;14: 99–108. doi:10.1016/s0898-6568(01)00235-2

824. Moreno JL, Muguruza C, Umali A, Mortillo S, Holloway T, Pilar-Cuéllar F, et al. Identification of three residues essential for 5-hydroxytryptamine 2A-metabotropic glutamate 2 (5-HT2A·mGlu2) receptor heteromerization and its psychoactive behavioral function. J Biol Chem. 2012;287: 44301–44319. doi:10.1074/jbc.M112.413161

825. González-Maeso J, Ang RL, Yuen T, Chan P, Weisstaub NV, López-Giménez JF, et al. Identification of a serotonin/glutamate receptor complex implicated in psychosis. Nature. 2008;452: 93–97. doi:10.1038/nature06612

826. González-Maeso J, Weisstaub NV, Zhou M, Chan P, Ivic L, Ang R, et al. Hallucinogens recruit specific cortical 5-HT(2A) receptor-mediated signaling pathways to affect behavior. Neuron. 2007;53: 439–452. doi:10.1016/j.neuron.2007.01.008

827. Fribourg M, Moreno JL, Holloway T, Provasi D, Baki L, Mahajan R, et al. Decoding the signaling of a GPCR heteromeric complex reveals a unifying mechanism of action of antipsychotic drugs. Cell. 2011;147: 1011–1023. doi:10.1016/j.cell.2011.09.055

828. Schröder H, Wu DF, Seifert A, Rankovic M, Schulz S, Höllt V, et al. Allosteric modulation of metabotropic glutamate receptor 5 affects phosphorylation, internalization, and desensitization of the micro-opioid receptor. Neuropharmacology. 2009;56: 768–778. doi:10.1016/j.neuropharm.2008.12.010

829. Neugebauer V, Li W, Bird GC, Han JS. The amygdala and persistent pain. Neuroscientist. 2004;10: 221–234. doi:10.1177/1073858403261077

830. Spooren WP, Gasparini F, Salt TE, Kuhn R. Novel allosteric antagonists shed light on mglu(5) receptors and CNS disorders. Trends Pharmacol Sci. 2001;22: 331–337. doi:10.1016/s0165-6147(00)01694-1

831. Dickenson AH. Central acute pain mechanisms. Ann Med. 1995;27: 223–227. doi:10.3109/07853899509031963

832. Lee HJ, Choi HS, Ju JS, Bae YC, Kim SK, Yoon YW, et al. Peripheral mGluR5 antagonist attenuated craniofacial muscle pain and inflammation but not mGluR1 antagonist in lightly anesthetized rats. Brain Res Bull. 2006;70: 378–385. doi:10.1016/j.brainresbull.2005.09.021

833. Gabra BH, Smith FL, Navarro HA, Carroll FI, Dewey WL. mGluR5 antagonists that block calcium mobilization in vitro also reverse (S)-3,5-DHPG-induced hyperalgesia and morphine antinociceptive tolerance in vivo. Brain Res. 2008;1187: 58–66. doi:10.1016/j.brainres.2007.10.007

834. Fuxe K, Marcellino D, Borroto-Escuela DO, Frankowska M, Ferraro L, Guidolin D, et al. The changing world of G protein-coupled receptors: from monomers to dimers and receptor mosaics with allosteric receptor-receptor interactions. J Recept Signal Transduct Res. 2010;30: 272–283. doi:10.3109/10799893.2010.506191

835. Agnati LF, Guidolin D, Albertin G, Trivello E, Ciruela F, Genedani S, et al. An integrated view on the role of receptor mosaics at perisynaptic level: focus on adenosine A(2A), dopamine D(2), cannabinoid CB(1), and metabotropic glutamate mGlu(5) receptors. J Recept Signal Transduct Res. 2010;30: 355–369. doi:10.3109/10799893.2010.487492

836. Agnati LF, Guidolin D, Vilardaga JP, Ciruela F, Fuxe K. On the expanding terminology in the GPCR field: the meaning of receptor mosaics and receptor heteromers. J Recept Signal Transduct Res. 2010;30: 287–303. doi:10.3109/10799891003786226

837. Agnati LF, Fuxe K, Zoli M, Rondanini C, Ogren SO. New vistas on synaptic plasticity: the receptor mosaic hypothesis of the engram. Med Biol. 1982;60: 183–190. Available: https://www.ncbi.nlm.nih.gov/pubmed/6128444

838. Fuxe K, Canals M, Torvinen M, Marcellino D, Terasmaa A, Genedani S, et al. Intramembrane receptor-receptor interactions: a novel principle in molecular medicine. J Neural Transm. 2007;114: 49–75. doi:10.1007/s00702-006-0589-0

839. Agnati LF, Guidolin D, Leo G, Carone C, Genedani S, Fuxe K. Receptor-receptor interactions: A novel concept in brain integration. Prog Neurobiol. 2010;90: 157–175. doi:10.1016/j.pneurobio.2009.10.004

840. Agnati LF, Franzen O, Ferré S, Leo G, Franco R, Fuxe K. Possible role of intramembrane receptor-receptor interactions in memory and learning via formation of long-lived heteromeric complexes: focus on motor learning in the basal ganglia. J Neural Transm Suppl. 2003; 1–28. doi:10.1007/978-3-7091-0643-3_1

841. Denning DW, Follansbee SE, Scolaro M, Norris S, Edelstein H, Stevens DA. Pulmonary aspergillosis in the acquired immunodeficiency syndrome. N Engl J Med. 1991;324: 654–662. doi:10.1056/NEJM199103073241003

842. Navarro G, Carriba P, Gandía J, Ciruela F, Casadó V, Cortés A, et al. Detection of heteromers formed by cannabinoid CB1, dopamine D2, and adenosine A2A G-protein-coupled receptors by combining bimolecular fluorescence complementation and bioluminescence energy transfer. ScientificWorldJournal. 2008;8: 1088–1097. doi:10.1100/tsw.2008.136

843. Dean B, Sundram S, Bradbury R, Scarr E, Copolov D. Studies on [3H]CP-55940 binding in the human central nervous system: regional specific changes in density of cannabinoid-1 receptors associated with schizophrenia and cannabis use. Neuroscience. 2001;103: 9–15. doi:10.1016/s0306-4522(00)00552-2

844. Guillin O, Abi-Dargham A, Laruelle M. Neurobiology of dopamine in schizophrenia. Int Rev Neurobiol. 2007;78: 1–39. doi:10.1016/S0074-7742(06)78001-1

845. Kerppola TK. Bimolecular fluorescence complementation: visualization of molecular interactions in living cells. Methods Cell Biol. 2008;85: 431–470. doi:10.1016/S0091-679X(08)85019-4

846. Carriba P, Navarro G, Ciruela F, Ferré S, Casadó V, Agnati L, et al. Detection of heteromerization of more than two proteins by sequential BRET-FRET. Nat Methods. 2008;5: 727–733. doi:10.1038/nmeth.1229

847. Deckert J, Brenner M, Durany N, Zöchling R, Paulus W, Ransmayr G, et al. Up-regulation of striatal adenosine A(2A) receptors in schizophrenia. Neuroreport. 2003;14: 313–316. doi:10.1097/00001756-200303030-00003

848. Sundram S, Copolov D, Dean B. Clozapine decreases [3H] CP 55940 binding to the cannabinoid 1 receptor in the rat nucleus accumbens. Naunyn Schmiedebergs Arch Pharmacol. 2005;371: 428–433. doi:10.1007/s00210-005-1074-2

849. Urigüen L, García-Fuster MJ, Callado LF, Morentin B, La Harpe R, Casadó V, et al. Immunodensity and mRNA expression of A2A adenosine, D2 dopamine, and CB1 cannabinoid receptors in postmortem frontal cortex of subjects with schizophrenia: effect of antipsychotic treatment. Psychopharmacology . 2009;206: 313–324. doi:10.1007/s00213-009-1608-2

850. Cabello N, Gandía J, Bertarelli DCG, Watanabe M, Lluís C, Franco R, et al. Metabotropic glutamate type 5, dopamine D2 and adenosine A2a receptors form higher-order oligomers in living cells. J Neurochem. 2009;109: 1497–1507. doi:10.1111/j.1471-4159.2009.06078.x

851. Popoli P, Pèzzola A, Torvinen M, Reggio R, Pintor A, Scarchilli L, et al. The selective mGlu(5) receptor agonist CHPG inhibits quinpirole-induced turning in 6-hydroxydopamine-lesioned rats and modulates the binding characteristics of dopamine D(2) receptors in the rat striatum: interactions with adenosine A(2a) receptors. Neuropsychopharmacology. 2001;25: 505–513. doi:10.1016/S0893-133X(01)00256-1

852. Díaz-Cabiale Z, Vivó M, Del Arco A, O'Connor WT, Harte MK, Müller CE, et al. Metabotropic glutamate mGlu5 receptor-mediated modulation of the ventral striopallidal GABA pathway in rats. Interactions with adenosine A(2A) and dopamine D(2) receptors. Neurosci Lett. 2002;324: 154–158. doi:10.1016/s0304-3940(02)00179-9

853. Schwarzschild MA, Agnati L, Fuxe K, Chen J-F, Morelli M. Targeting adenosine A2A receptors in Parkinson's disease. Trends Neurosci. 2006;29: 647–654. doi:10.1016/j.tins.2006.09.004

854. Bockaert J, Fagni L, Dumuis A, Marin P. GPCR interacting proteins (GIP). Pharmacol Ther. 2004;103: 203–221. doi:10.1016/j.pharmthera.2004.06.004

855. Fagni L, Ango F, Perroy J, Bockaert J. Identification and functional roles of metabotropic glutamate receptor-interacting proteins. Semin Cell Dev Biol. 2004;15: 289–298. doi:10.1016/j.semcdb.2003.12.018

856. Kamal M, Maurice P, Jockers R. Expanding the Concept of G Protein-Coupled Receptor (GPCR) Dimer Asymmetry towards GPCR-Interacting Proteins. Pharmaceuticals . 2011;4: 273–284. doi:10.3390/ph4020273

857. Bockaert J, Dumuis A, Fagni L, Marin P. GPCR-GIP networks: a first step in the discovery of new therapeutic drugs? Curr Opin Drug Discov Devel. 2004;7: 649–657. Available: https://www.ncbi.nlm.nih.gov/pubmed/15503867

858. Kowalsman N, Niv MY. GPCR & company: databases and servers for GPCRs and interacting partners. Adv Exp Med Biol. 2014;796: 185–204. doi:10.1007/978-94-007-7423-0_9

859. Maurice P, Guillaume J-L, Benleulmi-Chaachoua A, Daulat AM, Kamal M, Jockers R. GPCR-interacting proteins, major players of GPCR function. Adv Pharmacol. 2011;62: 349–380. doi:10.1016/B978-0-12-385952-5.00001-4

860. Magalhaes AC, Dunn H, Ferguson SS. Regulation of GPCR activity, trafficking and localization by GPCR-interacting proteins. Br J Pharmacol. 2012;165: 1717–1736. doi:10.1111/j.1476-5381.2011.01552.x

861. Ritter SL, Hall RA. Fine-tuning of GPCR activity by receptor-interacting proteins. Nat Rev Mol Cell Biol. 2009;10: 819–830. doi:10.1038/nrm2803

862. Shaw AS, Filbert EL. Scaffold proteins and immune-cell signalling. Nat Rev Immunol. 2009;9: 47–56. doi:10.1038/nri2473

863. Wong W, Scott JD. AKAP signalling complexes: focal points in space and time. Nat Rev Mol Cell Biol. 2004;5: 959–970. doi:10.1038/nrm1527

864. Maurice P, Daulat AM, Turecek R, Ivankova-Susankova K, Zamponi F, Kamal M, et al. Molecular organization and dynamics of the melatonin MT_1 receptor/RGS20/G(i) protein complex reveal asymmetry of receptor dimers for RGS and G(i) coupling. EMBO J. 2010;29: 3646–3659. doi:10.1038/emboj.2010.236

865. Neitzel KL, Hepler JR. Cellular mechanisms that determine selective RGS protein regulation of G protein-coupled receptor signaling. Semin Cell Dev Biol. 2006;17: 383–389. doi:10.1016/j.semcdb.2006.03.002

866. Xie G-X, Palmer PP. How regulators of G protein signaling achieve selective regulation. J Mol Biol. 2007;366: 349–365. doi:10.1016/j.jmb.2006.11.045

867. Bockaert J, Perroy J, Ango F. The Complex Formed by Group I Metabotropic Glutamate Receptor (mGluR) and Homer1a Plays a Central Role in Metaplasticity and Homeostatic Synaptic Scaling. J Neurosci. 2021;41: 5567–5578. doi:10.1523/JNEUROSCI.0026-21.2021

868. Ango F, Prézeau L, Muller T, Tu JC, Xiao B, Worley PF, et al. Agonist-independent activation of metabotropic glutamate receptors by the intracellular protein Homer. Nature. 2001;411: 962–965. doi:10.1038/35082096

869. Kammermeier PJ, Xiao B, Tu JC, Worley PF, Ikeda SR. Homer proteins regulate coupling of group I metabotropic glutamate receptors to N-type calcium and M-type potassium channels. J Neurosci. 2000;20: 7238–7245. doi:10.1523/JNEUROSCI.20-19-07238.2000

870. Xiao B, Tu JC, Worley PF. Homer: a link between neural activity and glutamate receptor function. Curr Opin Neurobiol. 2000;10: 370–374. doi:10.1016/s0959-4388(00)00087-8

871. Ehlers MD. Synapse structure: glutamate receptors connected by the shanks. Curr Biol. 1999;9: R848–50. doi:10.1016/s0960-9822(00)80043-3

872. Bockaert J, Fagni L, Perroy J. Chapter 13. Functional crosstalk between group I metabotropic glutamate receptors and ionotropic glutamate receptors controls synaptic transmission. Drug Discovery. Cambridge: Royal Society of Chemistry; 2011. pp. 269–283. doi:10.1039/9781849733441-00269

873. Ferré S, Ciruela F, Dessauer CW, González-Maeso J, Hébert TE, Jockers R, et al. G protein-coupled receptor-effector macromolecular membrane assemblies (GEMMAs). Pharmacol Ther. 2022;231: 107977. doi:10.1016/j.pharmthera.2021.107977

874. Erez M, Takemori AE, Portoghese PS. Narcotic antagonistic potency of bivalent ligands which contain beta-naltrexamine. Evidence for bridging between proximal recognition sites. J Med Chem. 1982;25: 847–849. doi:10.1021/jm00349a016

875. Portoghese PS, Ronsisvalle G, Larson DL, Yim CB, Sayre LM, Takemori AE. Opioid agonist and antagonist bivalent ligands as receptor probes. Life Sci. 1982;31: 1283–1286. doi:10.1016/0024-3205(82)90362-9

876. Huang B, St Onge CM, Ma H, Zhang Y. Design of bivalent ligands targeting putative GPCR dimers. Drug Discov Today. 2021;26: 189–199. doi:10.1016/j.drudis.2020.10.006

877. Shonberg J, Scammells PJ, Capuano B. Design strategies for bivalent ligands targeting GPCRs. ChemMedChem. 2011;6: 963–974. doi:10.1002/cmdc.201100101

878. Budzinski J, Maschauer S, Kobayashi H, Couvineau P, Vogt H, Gmeiner P, et al. Bivalent ligands promote endosomal trafficking of the dopamine D3 receptor-neurotensin receptor 1 heterodimer. Commun Biol. 2021;4: 1062. doi:10.1038/s42003-021-02574-4

879. Qian M, Wouters E, Dalton JAR, Risseeuw MDP, Crans RAJ, Stove C, et al. Synthesis toward Bivalent Ligands for the Dopamine D2 and Metabotropic Glutamate 5 Receptors. J Med Chem. 2018;61: 8212–8225. doi:10.1021/acs.jmedchem.8b00671

880. Nasrallah C, Cannone G, Briot J, Rottier K, Berizzi AE, Huang C-Y, et al. Agonists and allosteric modulators promote signaling from different metabotropic glutamate receptor 5 conformations. Cell Rep. 2021;36: 109648. doi:10.1016/j.celrep.2021.109648

881. Bock A, Bermudez M. Allosteric coupling and biased agonism in G protein-coupled receptors. FEBS J. 2021;288: 2513–2528. doi:10.1111/febs.15783

882. Ma N, Nivedha AK, Vaidehi N. Allosteric communication regulates ligand-specific GPCR activity. FEBS J. 2021;288: 2502–2512. doi:10.1111/febs.15826

883. Romantini N, Alam S, Dobitz S, Spillmann M, De Foresta M, Schibli R, et al. Exploring the signaling space of a GPCR using bivalent ligands with a rigid oligoproline backbone. Proc Natl Acad Sci U S A. 2021;118. doi:10.1073/pnas.2108776118

884. Haubrich J, Font J, Quast RB, Goupil-Lamy A, Scholler P, Nevoltris D, et al. A nanobody activating metabotropic glutamate receptor 4 discriminates between homo- and heterodimers. Proc Natl Acad Sci U S A. 2021;118. doi:10.1073/pnas.2105848118

885. Wagner TR, Rothbauer U. Nanobodies - Little helpers unravelling intracellular signaling. Free Radic Biol Med. 2021;176: 46–61. doi:10.1016/j.freeradbiomed.2021.09.005

886. Hamers-Casterman C, Atarhouch T, Muyldermans S, Robinson G, Hamers C, Songa EB, et al. Naturally occurring antibodies devoid of light chains. Nature. 1993;363: 446–448. doi:10.1038/363446a0

887. Che T, English J, Krumm BE, Kim K, Pardon E, Olsen RHJ, et al. Nanobody-enabled monitoring of kappa opioid receptor states. Nat Commun. 2020;11: 1145. doi:10.1038/s41467-020-14889-7

888. Stoeber M, Jullié D, Li J, Chakraborty S, Majumdar S, Lambert NA, et al. Agonist-selective recruitment of engineered protein probes and of GRK2 by opioid receptors in living cells. Elife. 2020;9. doi:10.7554/eLife.54208

889. Stoeber M, Jullié D, Lobingier BT, Laeremans T, Steyaert J, Schiller PW, et al. A Genetically Encoded Biosensor Reveals Location Bias of Opioid Drug Action.

Neuron. 2018;98: 963–976.e5. doi:10.1016/j.neuron.2018.04.021

890. Che T, Majumdar S, Zaidi SA, Ondachi P, McCorvy JD, Wang S, et al. Structure of the Nanobody-Stabilized Active State of the Kappa Opioid Receptor. Cell. 2018;172: 55–67.e15. doi:10.1016/j.cell.2017.12.011

891. Johnson GP, Agwuegbo U, Jonas KC. New insights into the functional impact of G protein–coupled receptor oligomerization. Current Opinion in Endocrine and Metabolic Research. 2021;16: 43–50. doi:10.1016/j.coemr.2020.08.005

892. De Groof TWM, Bobkov V, Heukers R, Smit MJ. Nanobodies: New avenues for imaging, stabilizing and modulating GPCRs. Mol Cell Endocrinol. 2019;484: 15–24. doi:10.1016/j.mce.2019.01.021

893. Dolgin E. First GPCR-directed antibody passes approval milestone. Nat Rev Drug Discov. 2018;17: 457–459. doi:10.1038/nrd.2018.103

894. Han L, Liu Y, Xiong H, Hong P. CGRP monoclonal antibody for preventive treatment of chronic migraine: An update of meta-analysis. Brain Behav. 2019;9: e01215. doi:10.1002/brb3.1215

895. Glatt SJ, Faraone SV, Lasky-Su JA, Kanazawa T, Hwu H-G, Tsuang MT. Family-based association testing strongly implicates DRD2 as a risk gene for schizophrenia in Han Chinese from Taiwan. Mol Psychiatry. 2009;14: 885–893. doi:10.1038/mp.2008.30

896. So CH, Varghese G, Curley KJ, Kong MMC, Alijaniaram M, Ji X, et al. D1 and D2 dopamine receptors form heterooligomers and cointernalize after selective activation of either receptor. Mol Pharmacol. 2005;68: 568–578. doi:10.1124/mol.105.012229

897. DelaCuesta-Barrutia J, Peñagarikano O, Erdozain AM. G Protein-Coupled Receptor Heteromers as Putative Pharmacotherapeutic Targets in Autism. Front Cell Neurosci. 2020;14: 588662. doi:10.3389/fncel.2020.588662

898. Franco R, Ferré S, Agnati L, Torvinen M, Ginés S, Hillion J, et al. Evidence for adenosine/dopamine receptor interactions: indications for heteromerization. Neuropsychopharmacology. 2000;23: S50–9. doi:10.1016/S0893-133X(00)00144-5

899. Torvinen M, Ginés S, Hillion J, Latini S, Canals M, Ciruela F, et al. Interactions among adenosine deaminase, adenosine A(1) receptors and dopamine D(1) receptors in stably cotransfected fibroblast cells and neurons. Neuroscience. 2002;113: 709–719. doi:10.1016/s0306-4522(02)00058-1

900. Cao Y, Xie K-Q, Zhu X-Z. The enhancement of dopamine D1 receptor desensitization by adenosine A1 receptor activation. Eur J Pharmacol. 2007;562: 34–38. doi:10.1016/j.ejphar.2007.01.090

901. Soriano A, Ventura R, Molero A, Hoen R, Casadó V, Cortés A, et al. Adenosine

A2A receptor-antagonist/dopamine D2 receptor-agonist bivalent ligands as pharmacological tools to detect A2A-D2 receptor heteromers. J Med Chem. 2009;52: 5590–5602. doi:10.1021/jm900298c

902. Fuxe K, Ferré S, Canals M, Torvinen M, Terasmaa A, Marcellino D, et al. Adenosine A2A and dopamine D2 heteromeric receptor complexes and their function. J Mol Neurosci. 2005;26: 209–220. doi:10.1385/JMN:26:2-3:209

903. Ciruela F, Burgueño J, Casadó V, Canals M, Marcellino D, Goldberg SR, et al. Combining mass spectrometry and pull-down techniques for the study of receptor heteromerization. Direct epitope-epitope electrostatic interactions between adenosine A2A and dopamine D2 receptors. Anal Chem. 2004;76: 5354–5363. doi:10.1021/ac049295f

904. Bara-Jimenez W, Sherzai A, Dimitrova T, Favit A, Bibbiani F, Gillespie M, et al. Adenosine A(2A) receptor antagonist treatment of Parkinson's disease. Neurology. 2003;61: 293–296. doi:10.1212/01.wnl.0000073136.00548.d4

905. Rocheville M, Lange DC, Kumar U, Patel SC, Patel RC, Patel YC. Receptors for dopamine and somatostatin: formation of hetero-oligomers with enhanced functional activity. Science. 2000;288: 154–157. doi:10.1126/science.288.5463.154

906. Damian M, Pons V, Renault P, M'Kadmi C, Delort B, Hartmann L, et al. GHSR-D2R heteromerization modulates dopamine signaling through an effect on G protein conformation. Proc Natl Acad Sci U S A. 2018;115: 4501–4506. doi:10.1073/pnas.1712725115

907. Cordisco Gonzalez S, Mustafá ER, Rodriguez SS, Perello M, Raingo J. Dopamine Receptor Type 2 and Ghrelin Receptor Coexpression Alters CaV2.2 Modulation by G Protein Signaling Cascades. ACS Chem Neurosci. 2020;11: 3–13. doi:10.1021/acschemneuro.9b00426

908. Morales-Figueroa G-E, Rivera-Ramírez N, González-Pantoja R, Escamilla-Sánchez J, García-Hernández U, Galván EJ, et al. Adenosine A2A and histamine H3 receptors interact at the cAMP/PKA pathway to modulate depolarization-evoked [3H]-GABA release from rat striato-pallidal terminals. Purinergic Signal. 2019;15: 85–93. doi:10.1007/s11302-018-9638-z

909. Lenard NR, Daniels DJ, Portoghese PS, Roerig SC. Absence of conditioned place preference or reinstatement with bivalent ligands containing mu-opioid receptor agonist and delta-opioid receptor antagonist pharmacophores. Eur J Pharmacol. 2007;566: 75–82. doi:10.1016/j.ejphar.2007.02.040

910. Daniels DJ, Lenard NR, Etienne CL, Law P-Y, Roerig SC, Portoghese PS. Opioid-induced tolerance and dependence in mice is modulated by the distance between pharmacophores in a bivalent ligand series. Proc Natl Acad Sci U S A. 2005;102: 19208–19213. doi:10.1073/pnas.0506627102

911. Zhang YQ, Limbird LE. Hetero-oligomers of alpha2A-adrenergic and mu-opioid receptors do not lead to transactivation of G-proteins or altered endocytosis profiles. Biochem Soc Trans. 2004;32: 856–860. doi:10.1042/BST0320856

912. Jordan BA, Gomes I, Rios C, Filipovska J, Devi LA. Functional interactions between mu opioid and alpha 2A-adrenergic receptors. Mol Pharmacol. 2003;64: 1317–1324. doi:10.1124/mol.64.6.1317

913. Glass MJ, Pickel VM. Alpha(2A)-adrenergic receptors are present in mu-opioid receptor containing neurons in rat medial nucleus tractus solitarius. Synapse. 2002;43: 208–218. doi:10.1002/syn.10036

914. Gabilondo AM, Meana JJ, Barturen F, Sastre M, García-Sevilla JA. mu-Opioid receptor and alpha 2-adrenoceptor agonist binding sites in the postmortem brain of heroin addicts. Psychopharmacology . 1994;115: 135–140. doi:10.1007/BF02244763

915. Fongang B, Cunningham KA, Rowicka M, Kudlicki A. Coevolution of Residues Provides Evidence of a Functional Heterodimer of 5-HT2AR and 5-HT2CR Involving Both Intracellular and Extracellular Domains. Neuroscience. 2019;412: 48–59. doi:10.1016/j.neuroscience.2019.05.013

916. Cunningham KA, Anastasio NC, Fox RG, Stutz SJ, Bubar MJ, Swinford SE, et al. Synergism between a serotonin 5-HT2A receptor (5-HT2AR) antagonist and 5-HT2CR agonist suggests new pharmacotherapeutics for cocaine addiction. ACS Chem Neurosci. 2013;4: 110–121. doi:10.1021/cn300072u

917. Martín AB, Fernandez-Espejo E, Ferrer B, Gorriti MA, Bilbao A, Navarro M, et al. Expression and function of CB1 receptor in the rat striatum: localization and effects on D1 and D2 dopamine receptor-mediated motor behaviors. Neuropsychopharmacology. 2008;33: 1667–1679. doi:10.1038/sj.npp.1301558

918. Charles-Messance H, Blot G, Couturier A, Vignaud L, Touhami S, Beguier F, et al. IL-1β induces rod degeneration through the disruption of retinal glutamate homeostasis. J Neuroinflammation. 2020;17: 1. doi:10.1186/s12974-019-1655-5

919. Doumazane E, Scholler P, Zwier JM, Trinquet E, Rondard P, Pin J-P. A new approach to analyze cell surface protein complexes reveals specific heterodimeric metabotropic glutamate receptors. FASEB J. 2011;25: 66–77. doi:10.1096/fj.10-163147

920. Nieto A, Bailey T, Kaczanowska K, McDonald P. GABAB Receptor Chemistry and Pharmacology: Agonists, Antagonists, and Allosteric Modulators. Curr Top Behav Neurosci. 2022;52: 81–118. doi:10.1007/7854_2021_232

921. Delille HK, Becker JM, Burkhardt S, Bleher B, Terstappen GC, Schmidt M, et al. Heterocomplex formation of 5-HT2A-mGlu2 and its relevance for cellular signaling cascades. Neuropharmacology. 2012;62: 2184–2191. doi:10.1016/j.neuropharm.2012.01.010

922. Shah UH, González-Maeso J. Serotonin and Glutamate Interactions in Preclinical Schizophrenia Models. ACS Chem Neurosci. 2019;10: 3068–3077. doi:10.1021/acschemneuro.9b00044

923. Yasi EA, Kruyer NS, Peralta-Yahya P. Advances in G protein-coupled receptor high-throughput screening. Curr Opin Biotechnol. 2020;64: 210–217. doi:10.1016/j.copbio.2020.06.004

924. Macarron R, Banks MN, Bojanic D, Burns DJ, Cirovic DA, Garyantes T, et al. Impact of high-throughput screening in biomedical research. Nat Rev Drug Discov. 2011;10: 188–195. doi:10.1038/nrd3368

925. Sykes DA, Stoddart LA, Kilpatrick LE, Hill SJ. Binding kinetics of ligands acting at GPCRs. Mol Cell Endocrinol. 2019;485: 9–19. doi:10.1016/j.mce.2019.01.018

926. Neubig RR, Spedding M, Kenakin T, Christopoulos A. International Union of Pharmacology Committee on Receptor Nomenclature and Drug Classification. XXXVIII. Update on terms and symbols in quantitative pharmacology. Pharmacol Rev. 2003;55: 597–606. Available: https://pharmrev.aspetjournals.org/content/55/4/597.short?casa_token=qy3dFKKbUG0AAAAA:4RmoxVzrcYIuqg9w5Y6FLLbdnxi1FXbIynVTA8QbS8BXdxJmhiCieLRl0V_uTixTDdMPoo8NGQs

927. Kenakin T. Drug efficacy at G protein-coupled receptors. Annu Rev Pharmacol Toxicol. 2002;42: 349–379. doi:10.1146/annurev.pharmtox.42.091401.113012

928. Zhao X, Jones A, Olson KR, Peng K, Wehrman T, Park A, et al. A homogeneous enzyme fragment complementation-based beta-arrestin translocation assay for high-throughput screening of G-protein-coupled receptors. J Biomol Screen. 2008;13: 737–747. doi:10.1177/1087057108321531

929. Ren X-R, Reiter E, Ahn S, Kim J, Chen W, Lefkowitz RJ. Different G protein-coupled receptor kinases govern G protein and beta-arrestin-mediated signaling of V2 vasopressin receptor. Proc Natl Acad Sci U S A. 2005;102: 1448–1453. doi:10.1073/pnas.0409534102

930. Yin H, Chu A, Li W, Wang B, Shelton F, Otero F, et al. Lipid G protein-coupled receptor ligand identification using beta-arrestin PathHunter assay. J Biol Chem. 2009;284: 12328–12338. doi:10.1074/jbc.M806516200

931. Quoyer J, Janz JM, Luo J, Ren Y, Armando S, Lukashova V, et al. Pepducin targeting the C-X-C chemokine receptor type 4 acts as a biased agonist favoring activation of the inhibitory G protein. Proc Natl Acad Sci U S A. 2013;110: E5088–97. doi:10.1073/pnas.1312515110

932. Namkung Y, Le Gouill C, Lukashova V, Kobayashi H, Hogue M, Khoury E, et al. Monitoring G protein-coupled receptor and β-arrestin trafficking in live cells using enhanced bystander BRET. Nat Commun. 2016;7: 12178. doi:10.1038/ncomms12178

933. Dixon AS, Schwinn MK, Hall MP, Zimmerman K, Otto P, Lubben TH, et al. NanoLuc Complementation Reporter Optimized for Accurate Measurement of Protein Interactions in Cells. ACS Chem Biol. 2016;11: 400–408. doi:10.1021/acschembio.5b00753

934. Hauge Pedersen M, Pham J, Mancebo H, Inoue A, Asher WB, Javitch JA. A novel luminescence-based β-arrestin recruitment assay for unmodified receptors. J Biol Chem. 2021;296: 100503. doi:10.1016/j.jbc.2021.100503

935. Kroeze WK, Sassano MF, Huang X-P, Lansu K, McCorvy JD, Giguère PM, et al. PRESTO-Tango as an open-source resource for interrogation of the druggable human GPCRome. Nat Struct Mol Biol. 2015;22: 362–369. doi:10.1038/nsmb.3014

936. von Degenfeld G, Wehrman TS, Hammer MM, Blau HM. A universal technology for monitoring G-protein-coupled receptor activation in vitro and noninvasively in live animals. FASEB J. 2007;21: 3819–3826. doi:10.1096/fj.07-9597com

937. Yan Y-X, Boldt-Houle DM, Tillotson BP, Gee MA, D'Eon BJ, Chang X-J, et al. Cell-based high-throughput screening assay system for monitoring G protein-coupled receptor activation using beta-galactosidase enzyme complementation technology. J Biomol Screen. 2002;7: 451–459. doi:10.1177/108705702237677

938. Weis WI, Kobilka BK. The Molecular Basis of G Protein-Coupled Receptor Activation. Annu Rev Biochem. 2018;87: 897–919. doi:10.1146/annurev-biochem-060614-033910

939. Hamm HE. How activated receptors couple to G proteins. Proceedings of the National Academy of Sciences of the United States of America. 2001. pp. 4819–4821. doi:10.1073/pnas.011099798

940. Tian X, Kang DS, Benovic JL. β-arrestins and G protein-coupled receptor trafficking. Handb Exp Pharmacol. 2014;219: 173–186. doi:10.1007/978-3-642-41199-1_9

941. Bronstein I, Edwards B, Voyta JC. 1,2-dioxetanes: novel chemiluminescent enzyme substrates. Applications to immunoassays. J Biolumin Chemilumin. 1989;4: 99–111. doi:10.1002/bio.1170040116

942. Van Munster EB, Kremers GJ, Adjobo-Hermans MJW, Gadella TWJ Jr. Fluorescence resonance energy transfer (FRET) measurement by gradual acceptor photobleaching. J Microsc. 2005;218: 253–262. doi:10.1111/j.1365-2818.2005.01483.x

943. Karpova T, McNally JG. Detecting protein-protein interactions with CFP-YFP FRET by acceptor photobleaching. Curr Protoc Cytom. 2006;Chapter 12: Unit12.7. doi:10.1002/0471142956.cy1207s35

944. Perrin F. Théorie quantique des transferts d'activation entre molécules de

même espèce. Cas des solutions fluorescentes. Ann Phys . 1932;10: 283–314. doi:10.1051/anphys/193210170283

945. Förster T. Zwischenmolekulare energiewanderung und fluoreszenz. Ann Phys. 1948;437: 55–75. doi:10.1002/andp.19484370105

946. Vilardaga J-P. Studying ligand efficacy at G protein-coupled receptors using FRET. Methods Mol Biol. 2011;756: 133–148. doi:10.1007/978-1-61779-160-4_6

947. Bajar BT, Wang ES, Zhang S, Lin MZ, Chu J. A Guide to Fluorescent Protein FRET Pairs. Sensors . 2016;16. doi:10.3390/s16091488

948. Lam AJ, St-Pierre F, Gong Y, Marshall JD, Cranfill PJ, Baird MA, et al. Improving FRET dynamic range with bright green and red fluorescent proteins. Nat Methods. 2012;9: 1005–1012. doi:10.1038/nmeth.2171

949. Miyawaki A. Development of probes for cellular functions using fluorescent proteins and fluorescence resonance energy transfer. Annu Rev Biochem. 2011;80: 357–373. doi:10.1146/annurev-biochem-072909-094736

950. Piston DW, Kremers G-J. Fluorescent protein FRET: the good, the bad and the ugly. Trends Biochem Sci. 2007;32: 407–414. doi:10.1016/j.tibs.2007.08.003

951. Balla T. Green light to illuminate signal transduction events. Trends Cell Biol. 2009;19: 575–586. doi:10.1016/j.tcb.2009.08.001

952. Vilardaga J-P, Bünemann M, Krasel C, Castro M, Lohse MJ. Measurement of the millisecond activation switch of G protein–coupled receptors in living cells. Nat Biotechnol. 2003;21: 807–812. doi:10.1038/nbt838

953. Hoffmann C, Gaietta G, Bünemann M, Adams SR, Oberdorff-Maass S, Behr B, et al. A FlAsH-based FRET approach to determine G protein-coupled receptor activation in living cells. Nat Methods. 2005;2: 171–176. doi:10.1038/nmeth742

954. Ferrandon S, Feinstein TN, Castro M, Wang B, Bouley R, Potts JT, et al. Sustained cyclic AMP production by parathyroid hormone receptor endocytosis. Nat Chem Biol. 2009;5: 734–742. doi:10.1038/nchembio.206

955. Hoppe A, Christensen K, Swanson JA. Fluorescence resonance energy transfer-based stoichiometry in living cells. Biophys J. 2002;83: 3652–3664. doi:10.1016/S0006-3495(02)75365-4

956. LeGendre N. Immobilon-P transfer membrane: applications and utility in protein biochemical analysis. Biotechniques. 1990;9: 788–805. Available: https://www.ncbi.nlm.nih.gov/pubmed/2271178

957. Renart J, Reiser J, Stark GR. Transfer of proteins from gels to diazobenzyloxymethyl-paper and detection with antisera: a method for studying antibody specificity and antigen structure. Proc Natl Acad Sci U S A. 1979;76: 3116–3120. doi:10.1073/pnas.76.7.3116

958. Mahmood T, Yang P-C. Western blot: technique, theory, and trouble shooting. N Am J Med Sci. 2012;4: 429–434. doi:10.4103/1947-2714.100998

959. Al-Tubuly AA. SDS-PAGE and Western Blotting. Methods Mol Med. 2000;40: 391–405. doi:10.1385/1-59259-076-4:391

960. Towbin H, Staehelin T, Gordon J. Electrophoretic transfer of proteins from polyacrylamide gels to nitrocellulose sheets: procedure and some applications. Proc Natl Acad Sci U S A. 1979;76: 4350–4354. doi:10.1073/pnas.76.9.4350

961. Laemmli UK. Cleavage of Structural Proteins during the Assembly of the Head of Bacteriophage T4. Nature. 1970;227: 680–685. doi:10.1038/227680a0

962. Kurien BT, Scofield RH. Western blotting. Methods. 2006;38: 283–293. doi:10.1016/j.ymeth.2005.11.007

963. Kurien BT, Scofield RH. Western blotting: an introduction. Methods Mol Biol. 2015;1312: 17–30. doi:10.1007/978-1-4939-2694-7_5

964. Goldman A, Harper S, Speicher DW. Detection of Proteins on Blot Membranes. Curr Protoc Protein Sci. 2016;86: 10.8.1–10.8.11. doi:10.1002/cpps.15

965. Salinovich O, Montelaro RC. Reversible staining and peptide mapping of proteins transferred to nitrocellulose after separation by sodium dodecylsulfate-polyacrylamide gel electrophoresis. Anal Biochem. 1986;156: 341–347. doi:10.1016/0003-2697(86)90263-0

966. Im K, Mareninov S, Diaz MFP, Yong WH. An Introduction to Performing Immunofluorescence Staining. Methods Mol Biol. 2019;1897: 299–311. doi:10.1007/978-1-4939-8935-5_26

967. Gold ER, Peacock DB. Antigen-antibody reactions. Basic Immunology. 2014; 183. Available: https://books.google.com/books?hl=en&lr=&id=boviBQAAQBAJ&oi=fnd&pg=PA183&dq=Antigen-Antibody+Reactions+2014&ots=TtDVmpR5N8&sig=0N2Vd_GMPLPOz3VQ-I7qQQvF0ig

968. Foxman B. Chapter 5 - A Primer of Molecular Biology. In: Foxman B, editor. Molecular Tools and Infectious Disease Epidemiology. San Diego: Academic Press; 2012. pp. 53–78. doi:10.1016/B978-0-12-374133-2.00005-8

969. Karatani H. Luminol–hydrogen peroxide–horseradish peroxidase chemiluminescence intensification by kosmotrope ammonium sulfate. Anal Sci. 2022;38: 613–621. doi:10.1007/s44211-022-00069-8

970. Easton PM, Simmonds AC, Rakishev A, Egorov AM, Candeias LP. Quantitative Model of the Enhancement of Peroxidase-Induced Luminol Luminescence. J Am Chem Soc. 1996;118: 6619–6624. doi:10.1021/ja9605073

971. Costanzi S. Homology modeling of class a G protein-coupled receptors. Methods Mol Biol. 2012;857: 259–279. doi:10.1007/978-1-61779-588-6_11

972. Bender BJ, Marlow B, Meiler J. Improving homology modeling from low-sequence identity templates in Rosetta: A case study in GPCRs. PLoS Comput Biol. 2020;16: e1007597. doi:10.1371/journal.pcbi.1007597

973. Palczewski K, Kumasaka T, Hori T, Behnke CA, Motoshima H, Fox BA, et al. Crystal structure of rhodopsin: A G protein-coupled receptor. Science. 2000;289: 739–745. doi:10.1126/science.289.5480.739

974. Cherezov V, Rosenbaum DM, Hanson MA, Rasmussen SGF, Thian FS, Kobilka TS, et al. High-resolution crystal structure of an engineered human beta2-adrenergic G protein-coupled receptor. Science. 2007;318: 1258–1265. doi:10.1126/science.1150577

975. Rasmussen SGF, Choi H-J, Rosenbaum DM, Kobilka TS, Thian FS, Edwards PC, et al. Crystal structure of the human beta2 adrenergic G-protein-coupled receptor. Nature. 2007;450: 383–387. doi:10.1038/nature06325

976. García-Nafría J, Tate CG. Structure determination of GPCRs: cryo-EM compared with X-ray crystallography. Biochem Soc Trans. 2021;49: 2345–2355. doi:10.1042/BST20210431

977. Pándy-Szekeres G, Munk C, Tsonkov TM, Mordalski S, Harpsøe K, Hauser AS, et al. GPCRdb in 2018: adding GPCR structure models and ligands. Nucleic Acids Res. 2018;46: D440–D446. doi:10.1093/nar/gkx1109

978. Zhang K, Wu H, Hoppe N, Manglik A, Cheng Y. Fusion protein strategies for cryo-EM study of G protein-coupled receptors. Nat Commun. 2022;13: 4366. doi:10.1038/s41467-022-32125-2

979. Sun B, Feng D, Chu ML-H, Fish I, Lovera S, Sands ZA, et al. Crystal structure of dopamine D1 receptor in complex with G protein and a non-catechol agonist. Nat Commun. 2021;12: 3305. doi:10.1038/s41467-021-23519-9

980. Rasmussen SGF, Choi H-J, Fung JJ, Pardon E, Casarosa P, Chae PS, et al. Structure of a nanobody-stabilized active state of the β(2) adrenoceptor. Nature. 2011;469: 175–180. doi:10.1038/nature09648

981. Huang W, Manglik A, Venkatakrishnan AJ, Laeremans T, Feinberg EN, Sanborn AL, et al. Structural insights into µ-opioid receptor activation. Nature. 2015;524: 315–321. doi:10.1038/nature14886

982. Scheerer P, Park JH, Hildebrand PW, Kim YJ, Krauss N, Choe H-W, et al. Crystal structure of opsin in its G-protein-interacting conformation. Nature. 2008;455: 497–502. doi:10.1038/nature07330

983. Kruse AC, Ring AM, Manglik A, Hu J, Hu K, Eitel K, et al. Activation and allosteric modulation of a muscarinic acetylcholine receptor. Nature. 2013;504:

101–106. doi:10.1038/nature12735

984. Carpenter B, Nehmé R, Warne T, Leslie AGW, Tate CG. Structure of the adenosine A(2A) receptor bound to an engineered G protein. Nature. 2016;536: 104–107. doi:10.1038/nature18966

985. Tsai C-J, Pamula F, Nehmé R, Mühle J, Weinert T, Flock T, et al. Crystal structure of rhodopsin in complex with a mini-Go sheds light on the principles of G protein selectivity. Sci Adv. 2018;4: eaat7052. doi:10.1126/sciadv.aat7052

986. Bai X-C, McMullan G, Scheres SHW. How cryo-EM is revolutionizing structural biology. Trends Biochem Sci. 2015;40: 49–57. doi:10.1016/j.tibs.2014.10.005

987. Cheng Y. Single-particle cryo-EM-How did it get here and where will it go. Science. 2018;361: 876–880. doi:10.1126/science.aat4346

988. Lyumkis D. Challenges and opportunities in cryo-EM single-particle analysis. J Biol Chem. 2019;294: 5181–5197. doi:10.1074/jbc.REV118.005602

989. Danev R, Belousoff M, Liang Y-L, Zhang X, Eisenstein F, Wootten D, et al. Routine sub-2.5 Å cryo-EM structure determination of GPCRs. Nat Commun. 2021;12: 4333. doi:10.1038/s41467-021-24650-3

990. Liang Y-L, Khoshouei M, Radjainia M, Zhang Y, Glukhova A, Tarrasch J, et al. Phase-plate cryo-EM structure of a class B GPCR-G-protein complex. Nature. 2017;546: 118–123. doi:10.1038/nature22327

991. Smyth MS, Martin JH. x ray crystallography. Mol Pathol. 2000;53: 8–14. doi:10.1136/mp.53.1.8

992. Kobilka B, Schertler GFX. New G-protein-coupled receptor crystal structures: insights and limitations. Trends Pharmacol Sci. 2008;29: 79–83. doi:10.1016/j.tips.2007.11.009

993. Opella SJ. Structure determination of membrane proteins by nuclear magnetic resonance spectroscopy. Annu Rev Anal Chem . 2013;6: 305–328. doi:10.1146/annurev-anchem-062012-092631

994. Teng Q. Structural Biology: Practical NMR Applications. Springer Science & Business Media; 2012. Available: https://play.google.com/store/books/details?id=zLnzmoj6HqkC

995. Yang L, Liu D, Wüthrich K. GPCR structural characterization by NMR spectroscopy in solution. Acta Biochim Biophys Sin . 2022;54: 1207–1212. doi:10.3724/abbs.2022106

996. Doerr A. Cryo-electron tomography. Nat Methods. 2016;14: 34–34. doi:10.1038/nmeth.4115

997. Nakane T, Kotecha A, Sente A, McMullan G, Masiulis S, Brown PMGE, et al.

Single-particle cryo-EM at atomic resolution. Nature. 2020;587: 152–156. doi:10.1038/s41586-020-2829-0

998. Wang H-W, Wang J-W. How cryo-electron microscopy and X-ray crystallography complement each other. Protein Sci. 2017;26: 32–39. doi:10.1002/pro.3022

999. Callaway E. Revolutionary cryo-EM is taking over structural biology. Nature. 2020;578: 201. doi:10.1038/d41586-020-00341-9

1000. Cheng Y. Single-Particle Cryo-EM at Crystallographic Resolution. Cell. 2015;161: 450–457. doi:10.1016/j.cell.2015.03.049

1001. Cheng Y, Grigorieff N, Penczek PA, Walz T. A primer to single-particle cryo-electron microscopy. Cell. 2015;161: 438–449. doi:10.1016/j.cell.2015.03.050

1002. Punjani A, Fleet DJ. 3D Flexible Refinement: Structure and Motion of Flexible Proteins from Cryo-EM. bioRxiv. 2021. p. 2021.04.22.440893. doi:10.1101/2021.04.22.440893

1003. Kühlbrandt W. Biochemistry. The resolution revolution. Science. 2014. pp. 1443–1444. doi:10.1126/science.1251652

1004. Yip KM, Fischer N, Paknia E, Chari A, Stark H. Atomic-resolution protein structure determination by cryo-EM. Nature. 2020;587: 157–161. doi:10.1038/s41586-020-2833-4

1005. Sun Z, Liu Q, Qu G, Feng Y, Reetz MT. Utility of B-Factors in Protein Science: Interpreting Rigidity, Flexibility, and Internal Motion and Engineering Thermostability. Chem Rev. 2019;119: 1626–1665. doi:10.1021/acs.chemrev.8b00290

1006. Carugo O. How large B-factors can be in protein crystal structures. BMC Bioinformatics. 2018;19: 61. doi:10.1186/s12859-018-2083-8

1007. Vihinen M, Torkkila E, Riikonen P. Accuracy of protein flexibility predictions. Proteins. 1994;19: 141–149. doi:10.1002/prot.340190207

1008. Parthasarathy S, Murthy MR. Analysis of temperature factor distribution in high-resolution protein structures. Protein Sci. 1997;6: 2561–2567. doi:10.1002/pro.5560061208

1009. Parthasarathy S, Murthy MR. On the correlation between the main-chain and side-chain atomic displacement parameters (B values) in high-resolution protein structures. Acta Crystallogr D Biol Crystallogr. 1999;55: 173–180. doi:10.1107/S0907444998006611

1010. de Brevern AG, Bornot A, Craveur P, Etchebest C, Gelly J-C. PredyFlexy: flexibility and local structure prediction from sequence. Nucleic Acids Res. 2012;40: W317–22. doi:10.1093/nar/gks482

1011. Smith DK, Radivojac P, Obradovic Z, Dunker AK, Zhu G. Improved amino acid flexibility parameters. Protein Sci. 2003;12: 1060–1072. doi:10.1110/ps.0236203

1012. Liu Q, Li Z, Li J. Use B-factor related features for accurate classification between protein binding interfaces and crystal packing contacts. BMC Bioinformatics. 2014;15 Suppl 16: S3. doi:10.1186/1471-2105-15-S16-S3

1013. Fowler NJ, Sljoka A, Williamson MP. A method for validating the accuracy of NMR protein structures. Nat Commun. 2020;11: 6321. doi:10.1038/s41467-020-20177-1

1014. Szwabowski GL, Baker DL, Parrill AL. Application of computational methods for class A GPCR Ligand discovery. J Mol Graph Model. 2023;121: 108434. doi:10.1016/j.jmgm.2023.108434

1015. Jones DT, Taylor WR, Thornton JM. A new approach to protein fold recognition. Nature. 1992;358: 86–89. doi:10.1038/358086a0

1016. Sali A, Blundell TL. Comparative protein modelling by satisfaction of spatial restraints. J Mol Biol. 1993;234: 779–815. doi:10.1006/jmbi.1993.1626

1017. Yang J, Zhang W, He B, Walker SE, Zhang H, Govindarajoo B, et al. Template-based protein structure prediction in CASP11 and retrospect of I-TASSER in the last decade. Proteins. 2016;84 Suppl 1: 233–246. doi:10.1002/prot.24918

1018. Costanzi S. Modeling G Protein-Coupled Receptors: a Concrete Possibility. Chim Oggi. 2010;28: 26–31. Available: https://www.ncbi.nlm.nih.gov/pubmed/21253444

1019. Worth CL, Kleinau G, Krause G. Comparative sequence and structural analyses of G-protein-coupled receptor crystal structures and implications for molecular models. PLoS One. 2009;4: e7011. doi:10.1371/journal.pone.0007011

1020. Mobarec JC, Sanchez R, Filizola M. Modern homology modeling of G-protein coupled receptors: which structural template to use? J Med Chem. 2009;52: 5207–5216. doi:10.1021/jm9005252

1021. Hanson MA, Stevens RC. Discovery of new GPCR biology: one receptor structure at a time. Structure. 2009;17: 8–14. doi:10.1016/j.str.2008.12.003

1022. Sievers F, Wilm A, Dineen D, Gibson TJ, Karplus K, Li W, et al. Fast, scalable generation of high-quality protein multiple sequence alignments using Clustal Omega. Mol Syst Biol. 2011;7: 539. doi:10.1038/msb.2011.75

1023. Song Y, DiMaio F, Wang RY-R, Kim D, Miles C, Brunette T, et al. High-resolution comparative modeling with RosettaCM. Structure. 2013;21: 1735–1742. doi:10.1016/j.str.2013.08.005

1024. Raman S, Vernon R, Thompson J, Tyka M, Sadreyev R, Pei J, et al. Structure prediction for CASP8 with all-atom refinement using Rosetta. Proteins. 2009;77

Suppl 9: 89–99. doi:10.1002/prot.22540

1025. Nguyen ED, Norn C, Frimurer TM, Meiler J. Assessment and challenges of ligand docking into comparative models of G-protein coupled receptors. PLoS One. 2013;8: e67302. doi:10.1371/journal.pone.0067302

1026. Webb B, Sali A. Comparative Protein Structure Modeling Using MODELLER. Curr Protoc Bioinformatics. 2016;54: 5.6.1–5.6.37. doi:10.1002/cpbi.3

1027. Fiser A, Do RK, Sali A. Modeling of loops in protein structures. Protein Sci. 2000;9: 1753–1773. doi:10.1110/ps.9.9.1753

1028. Land H, Humble MS. YASARA: A Tool to Obtain Structural Guidance in Biocatalytic Investigations. Methods Mol Biol. 2018;1685: 43–67. doi:10.1007/978-1-4939-7366-8_4

1029. Krieger E, Vriend G. YASARA View—molecular graphics for all devices—from smartphones to workstations. Bioinformatics. 2014;30: 2981–2982. doi:10.1093/bioinformatics/btu426

1030. Jumper J, Evans R, Pritzel A, Green T, Figurnov M, Ronneberger O, et al. Highly accurate protein structure prediction with AlphaFold. Nature. 2021;596: 583–589. doi:10.1038/s41586-021-03819-2

1031. Pearce R, Li Y, Omenn GS, Zhang Y. Fast and accurate Ab Initio Protein structure prediction using deep learning potentials. PLoS Comput Biol. 2022;18: e1010539. doi:10.1371/journal.pcbi.1010539

1032. Lee J, Freddolino PL, Zhang Y. Ab Initio Protein Structure Prediction. In: J. Rigden D, editor. From Protein Structure to Function with Bioinformatics. Dordrecht: Springer Netherlands; 2017. pp. 3–35. doi:10.1007/978-94-024-1069-3_1

1033. Varadi M, Anyango S, Deshpande M, Nair S, Natassia C, Yordanova G, et al. AlphaFold Protein Structure Database: massively expanding the structural coverage of protein-sequence space with high-accuracy models. Nucleic Acids Res. 2022;50: D439–D444. doi:10.1093/nar/gkab1061

1034. Halgren TA, Murphy RB, Friesner RA, Beard HS, Frye LL, Pollard WT, et al. Glide: a new approach for rapid, accurate docking and scoring. 2. Enrichment factors in database screening. J Med Chem. 2004;47: 1750–1759. doi:10.1021/jm030644s

1035. Salmas RE, Yurtsever M, Stein M, Durdagi S. Modeling and protein engineering studies of active and inactive states of human dopamine D2 receptor (D2R) and investigation of drug/receptor interactions. Mol Divers. 2015;19: 321–332. doi:10.1007/s11030-015-9569-3

1036. Kufareva I, Rueda M, Katritch V, Stevens RC, Abagyan R, GPCR Dock 2010 participants. Status of GPCR modeling and docking as reflected by community-

wide GPCR Dock 2010 assessment. Structure. 2011;19: 1108–1126. doi:10.1016/j.str.2011.05.012

1037. Bueschbell B, Preto AJ, Barreto CAV, Schiedel AC, Moreira IS. Creating a valid in silico Dopamine D2-receptor model for small molecular docking studies. MOL2NET, International Conference Series on Multidisciplinary Sciences. SCIFORUM Basel, Switzerland; 2017. pp. 1–6. Available: https://www.researchgate.net/profile/Irina-Moreira/publication/321878815_Creating_a_valid_in_silico_Dopamine_D2-receptor_model_for_small_molecular_docking_studies/links/5a38f75a0f7e9b7c48708d02/Creating-a-valid-in-silico-Dopamine-D2-receptor-model-for-small-molecular-docking-studies.pdf

1038. Cristobal S, Zemla A, Fischer D, Rychlewski L, Elofsson A. A study of quality measures for protein threading models. BMC Bioinformatics. 2001;2: 5. doi:10.1186/1471-2105-2-5

1039. Hou J, Charron CL, Fowkes MM, Luyt LG. Bridging computational modeling with amino acid replacements to investigate GHS-R1a-peptidomimetic recognition. Eur J Med Chem. 2016;123: 822–833. doi:10.1016/j.ejmech.2016.07.078

1040. Wiederstein M, Sippl MJ. ProSA-web: interactive web service for the recognition of errors in three-dimensional structures of proteins. Nucleic Acids Res. 2007;35: W407–10. doi:10.1093/nar/gkm290

1041. Wallner B, Elofsson A. Can correct protein models be identified? Protein Sci. 2003;12: 1073–1086. doi:10.1110/ps.0236803

1042. Wallner B, Elofsson A. Identification of correct regions in protein models using structural, alignment, and consensus information. Protein Sci. 2006;15: 900–913. doi:10.1110/ps.051799606

1043. Shen M-Y, Sali A. Statistical potential for assessment and prediction of protein structures. Protein Sci. 2006;15: 2507–2524. doi:10.1110/ps.062416606

1044. Anfinsen CB. The formation and stabilization of protein structure. Biochem J. 1972;128: 737–749. doi:10.1042/bj1280737

1045. Sippl MJ. Recognition of errors in three-dimensional structures of proteins. Proteins. 1993;17: 355–362. doi:10.1002/prot.340170404

1046. Sippl MJ. Calculation of conformational ensembles from potentials of mean force. An approach to the knowledge-based prediction of local structures in globular proteins. J Mol Biol. 1990;213: 859–883. doi:10.1016/s0022-2836(05)80269-4

1047. Sippl MJ. Knowledge-based potentials for proteins. Curr Opin Struct Biol. 1995;5: 229–235. doi:10.1016/0959-440x(95)80081-6

1048. Sippl MJ. Boltzmann’s principle, knowledge-based mean fields and protein

folding. An approach to the computational determination of protein structures. J Comput Aided Mol Des. 1993;7: 473–501. doi:10.1007/BF02337562

1049. Siew N, Elofsson A, Rychlewski L, Fischer D. MaxSub: an automated measure for the assessment of protein structure prediction quality. Bioinformatics. 2000;16: 776–785. doi:10.1093/bioinformatics/16.9.776

1050. Levitt M, Gerstein M. A unified statistical framework for sequence comparison and structure comparison. Proc Natl Acad Sci U S A. 1998;95: 5913–5920. doi:10.1073/pnas.95.11.5913

1051. McGuffin LJ, Bryson K, Jones DT. The PSIPRED protein structure prediction server. Bioinformatics. 2000;16: 404–405. doi:10.1093/bioinformatics/16.4.404

1052. Pagadala NS, Syed K, Tuszynski J. Software for molecular docking: a review. Biophys Rev. 2017;9: 91–102. doi:10.1007/s12551-016-0247-1

1053. Shoichet BK, McGovern SL, Wei B, Irwin JJ. Lead discovery using molecular docking. Curr Opin Chem Biol. 2002;6: 439–446. doi:10.1016/s1367-5931(02)00339-3

1054. Salmaso V, Moro S. Bridging Molecular Docking to Molecular Dynamics in Exploring Ligand-Protein Recognition Process: An Overview. Front Pharmacol. 2018;9: 923. doi:10.3389/fphar.2018.00923

1055. Dnyandev KM, Babasaheb GV, Chandrashekhar KV, Chandrakant MA, Vasant OK. A Review on Molecular Docking. IRJPAC. 2021; 60–68. doi:10.9734/irjpac/2021/v22i330396

1056. Salmaso V, Sturlese M, Cuzzolin A, Moro S. Combining self- and cross-docking as benchmark tools: the performance of DockBench in the D3R Grand Challenge 2. J Comput Aided Mol Des. 2018;32: 251–264. doi:10.1007/s10822-017-0051-4

1057. Leach AR. Molecular Modelling: Principles and Applications. Pearson Education; 2001. Available: https://play.google.com/store/books/details?id=kB7jsbV-uhkC

1058. Adcock SA, McCammon JA. Molecular dynamics: survey of methods for simulating the activity of proteins. Chem Rev. 2006;106: 1589–1615. doi:10.1021/cr040426m

1059. Ceperley DM, Libby SB. Berni Julian Alder, theoretical physicist and inventor of molecular dynamics, 1925-2020. Proc Natl Acad Sci U S A. 2021;118. doi:10.1073/pnas.2024252118

1060. Schmidt T, Bergner A, Schwede T. Modelling three-dimensional protein structures for applications in drug design. Drug Discov Today. 2014;19: 890–897. doi:10.1016/j.drudis.2013.10.027

1061. Schwede T, Sali A, Honig B, Levitt M, Berman HM, Jones D, et al. Outcome of

a workshop on applications of protein models in biomedical research. Structure. 2009;17: 151–159. doi:10.1016/j.str.2008.12.014

1062. Khoury GA, Smadbeck J, Kieslich CA, Floudas CA. Protein folding and de novo protein design for biotechnological applications. Trends Biotechnol. 2014;32: 99–109. doi:10.1016/j.tibtech.2013.10.008

1063. Wang T, Wu M-B, Zhang R-H, Chen Z-J, Hua C, Lin J-P, et al. Advances in Computational Structure-Based Drug Design and Application in Drug Discovery. Curr Top Med Chem. 2016;16: 901–916. doi:10.2174/1568026615666150825142002

1064. Vendruscolo M, Dobson CM. Protein dynamics: Moore's law in molecular biology. Curr Biol. 2011;21: R68–70. doi:10.1016/j.cub.2010.11.062

1065. Gray JJ, Moughon S, Wang C, Schueler-Furman O, Kuhlman B, Rohl CA, et al. Protein–Protein Docking with Simultaneous Optimization of Rigid-body Displacement and Side-chain Conformations. J Mol Biol. 2003;331: 281–299. doi:10.1016/S0022-2836(03)00670-3

1066. Tozzini V. Coarse-grained models for proteins. Curr Opin Struct Biol. 2005;15: 144–150. doi:10.1016/j.sbi.2005.02.005

1067. Clementi C. Coarse-grained models of protein folding: toy models or predictive tools? Curr Opin Struct Biol. 2008;18: 10–15. doi:10.1016/j.sbi.2007.10.005

1068. Kamerlin SCL, Vicatos S, Dryga A, Warshel A. Coarse-grained (multiscale) simulations in studies of biophysical and chemical systems. Annu Rev Phys Chem. 2011;62: 41–64. doi:10.1146/annurev-physchem-032210-103335

1069. Kmiecik S, Gront D, Kolinski M, Wieteska L, Dawid AE, Kolinski A. Coarse-Grained Protein Models and Their Applications. Chem Rev. 2016;116: 7898–7936. doi:10.1021/acs.chemrev.6b00163

1070. Levitt M, Warshel A. Computer simulation of protein folding. Nature. 1975;253: 694–698. doi:10.1038/253694a0

1071. Warshel A, Levitt M. Theoretical studies of enzymic reactions: dielectric, electrostatic and steric stabilization of the carbonium ion in the reaction of lysozyme. J Mol Biol. 1976;103: 227–249. doi:10.1016/0022-2836(76)90311-9

1072. Levitt M. Birth and future of multiscale modeling for macromolecular systems (Nobel Lecture). Angew Chem Int Ed Engl. 2014;53: 10006–10018. doi:10.1002/anie.201403691

1073. Kolinski A, Skolnick J. Reduced models of proteins and their applications. Polymer . 2004;45: 511–524. doi:10.1016/j.polymer.2003.10.064

1074. Warshel A. Multiscale modeling of biological functions: from enzymes to molecular machines (Nobel Lecture). Angew Chem Int Ed Engl. 2014;53: 10020–

10031. doi:10.1002/anie.201403689

1075. Phillips DC. Symposium on Three-Dimensional Structure of Macromolecules of Biological Origin. by Invitation of the Committee on Arrangements for the Autumn Meeting. Presented before the Academy on October 19, 1966. Chairman, Walter Kauzmann: THE HEN EGG-WHITE LYSOZYME MOLECULE. Proc Natl Acad Sci U S A. 1967;57: 483. Available: https://www.ncbi.nlm.nih.gov/pmc/articles/PMC335535/

1076. Roel-Touris J, Bonvin AMJJ. Coarse-grained (hybrid) integrative modeling of biomolecular interactions. Comput Struct Biotechnol J. 2020;18: 1182–1190. doi:10.1016/j.csbj.2020.05.002

1077. Levinthal C. How to fold graciously. Mossbauer spectroscopy in.

1078. Levitt M. A simplified representation of protein conformations for rapid simulation of protein folding. J Mol Biol. 1976;104: 59–107. doi:10.1016/0022-2836(76)90004-8

1079. Lodish HB, Berk A. A., Zipursky, SL, Matsudaira, P., Baltimore, D., Darnell, J. Mol Cell Biol Res Commun.

1080. Anslyn EV, Dougherty DA. Modern Physical Organic Chemistry. University Science Books; 2006. Available: https://play.google.com/store/books/details?id=gY-Sxijk_tMC

1081. Frenkel D, Smit B, Ratner MA. Understanding molecular simulation: From algorithms to applications. Phys Today. 1997;50: 66–66. doi:10.1063/1.881812

1082. Stephan S, Horsch MT, Vrabec J, Hasse H. MolMod – an open access database of force fields for molecular simulations of fluids. Mol Simul. 2019;45: 806–814. doi:10.1080/08927022.2019.1601191

1083. González MA. Force fields and molecular dynamics simulations. Éc thémat Soc Fr Neutron. 2011;12: 169–200. doi:10.1051/sfn/201112009

1084. Robustelli P, Piana S, Shaw DE. Developing a molecular dynamics force field for both folded and disordered protein states. Proc Natl Acad Sci U S A. 2018;115: E4758–E4766. doi:10.1073/pnas.1800690115

1085. Nordholm S, Bacskay G. The Basics of Covalent Bonding in Terms of Energy and Dynamics. Molecules. 2020;25. doi:10.3390/molecules25112667

1086. Lewis GN. THE ATOM AND THE MOLECULE. J Am Chem Soc. 1916;38: 762–785. doi:10.1021/ja02261a002

1087. Feynman RP, Leighton RB, Sands M. Quantenmechanik. Walter de Gruyter GmbH & Co KG; 2015. Available: https://play.google.com/store/books/details?id=L6C1CgAAQBAJ

1088. Riniker S. Fixed-Charge Atomistic Force Fields for Molecular Dynamics Simulations in the Condensed Phase: An Overview. J Chem Inf Model. 2018;58: 565–578. doi:10.1021/acs.jcim.8b00042

1089. Schmidt MW, Ivanic J, Ruedenberg K. Covalent bonds are created by the drive of electron waves to lower their kinetic energy through expansion. J Chem Phys. 2014;140: 204104. doi:10.1063/1.4875735

1090. Frenking G, Shaik S. The Chemical Bond: Fundamental Aspects of Chemical Bonding. John Wiley & Sons; 2014. Available: https://play.google.com/store/books/details?id=gw7VAwAAQBAJ

1091. Hayek SI. Mechanical Vibration and Damping. digital Encyclopedia of Applied Physics. Weinheim, Germany: Wiley-VCH Verlag GmbH & Co. KGaA; 2003. doi:10.1002/3527600434.eap231

1092. van der Waals forces. The IUPAC Compendium of Chemical Terminology. Research Triangle Park, NC: International Union of Pure and Applied Chemistry (IUPAC); 2014. doi:10.1351/goldbook.v06597

1093. Abrikosov AA, Lev P. Gor'kov, and Igor E. Dzyaloshinskii. Methods of quantum field theory in statistical physics.

1094. Garrett RH, Grisham CM. Biochemistry. Cengage Learning; 2016. Available: https://play.google.com/store/books/details?id=G99bzgEACAAJ

1095. Wu X, Brooks BR. A double exponential potential for van der Waals interaction. AIP Adv. 2019;9: 065304. doi:10.1063/1.5107505

1096. Jones JE. On the determination of molecular fields. —II. From the equation of state of a gas. Proc R Soc Lond A Math Phys Sci. 1924;106: 463–477. doi:10.1098/rspa.1924.0082

1097. Mecke M, Müller A, Winkelmann J, Vrabec J, Fischer J, Span R, et al. An accurate van der Waals-type equation of state for the Lennard-Jones fluid. Int J Thermophys. 1996;17: 391–404. Available: https://www.researchgate.net/profile/Jadran-Vrabec-2/publication/226878949_An_Accurate_Van_der_Waals-Type_Equation_of_State_for_the_Lennard-Jones_Fluid/links/615f3108ae47db4e57a46d56/An-Accurate-Van-der-Waals-Type-Equation-of-State-for-the-Lennard-Jones-Fluid.pdf

1098. Dion M, Rydberg H, Schröder E, Langreth DC, Lundqvist BI. van der Waals density functional for general geometries. Phys Rev Lett. 2004;92: 246401. doi:10.1103/PhysRevLett.92.246401

1099. London F. The general theory of molecular forces. Trans Faraday Soc. 1937;33: 8b–26. doi:10.1039/TF937330008B

1100. Thonhauser T, Cooper VR, Li S, Puzder A, Hyldgaard P, Langreth DC. Van der

Waals density functional: Self-consistent potential and the nature of the van der Waals bond. Phys Rev B Condens Matter. 2007;76: 125112. doi:10.1103/PhysRevB.76.125112

1101. Van Oss CJ, Chaudhury MK, Good RJ. Interfacial Lifshitz-van der Waals and polar interactions in macroscopic systems. Chem Rev. 1988;88: 927–941. doi:10.1021/cr00088a006

1102. de Hond J, Cisternas N, Spreeuw RJC, van den Heuvell HB van L, van Druten NJ. Interplay between van der Waals and dipole–dipole interactions among Rydberg atoms. J Phys B At Mol Opt Phys. 2020;53: 084007. doi:10.1088/1361-6455/ab752b

1103. Zhang P, Bao P, Gao J. Dipole preserving and polarization consistent charges. J Comput Chem. 2011;32: 2127–2139. doi:10.1002/jcc.21795

1104. Tuttle T, Thiel W. OMx-D: semiempirical methods with orthogonalization and dispersion corrections. Implementation and biochemical application. Phys Chem Chem Phys. 2008;10: 2159–2166. doi:10.1039/B718795E

1105. Thole BT, van Duijnen PT. A general population analysis preserving the dipole moment. Theor Chim Acta. 1983;63: 209–221. doi:10.1007/BF00569246

1106. Jorge M, Barrera MC, Milne AW, Ringrose C, Cole DJ. What is the Optimal Dipole Moment for Nonpolarizable Models of Liquids? J Chem Theory Comput. 2023;19: 1790–1804. doi:10.1021/acs.jctc.2c01123

1107. Ciferri A, Perico A. Ionic Interactions in Natural and Synthetic Macromolecules. John Wiley & Sons; 2012. Available: https://play.google.com/store/books/details?id=nHTXkrJ0GvUC

1108. Schneider H-J. Binding mechanisms in supramolecular complexes. Angew Chem Int Ed Engl. 2009;48: 3924–3977. doi:10.1002/anie.200802947

1109. Kolafa J, Perram JW. Cutoff Errors in the Ewald Summation Formulae for Point Charge Systems. Mol Simul. 1992;9: 351–368. doi:10.1080/08927029208049126

1110. Wells BA, Chaffee AL. Ewald Summation for Molecular Simulations. J Chem Theory Comput. 2015;11: 3684–3695. doi:10.1021/acs.jctc.5b00093

1111. Di Pierro M, Elber R, Leimkuhler B. A Stochastic Algorithm for the Isobaric-Isothermal Ensemble with Ewald Summations for All Long Range Forces. J Chem Theory Comput. 2015;11: 5624–5637. doi:10.1021/acs.jctc.5b00648

1112. Quinn JJ, Ferrell RA. Electron Self-Energy Approach to Correlation in a Degenerate Electron Gas. Phys Rev. 1958;112: 812–827. doi:10.1103/PhysRev.112.812

1113. Darden T, York D, Pedersen L. Particle mesh Ewald: An N·log(N) method for Ewald sums in large systems. J Chem Phys. 1993;98: 10089–10092.

doi:10.1063/1.464397

1114. Essmann U, Perera L, Berkowitz ML, Darden T, Lee H, Pedersen LG. A smooth particle mesh Ewald method. J Chem Phys. 1995;103: 8577–8593. doi:10.1063/1.470117

1115. Wang H, Zhang P, Schütte C. On the Numerical Accuracy of Ewald, Smooth Particle Mesh Ewald, and Staggered Mesh Ewald Methods for Correlated Molecular Systems. J Chem Theory Comput. 2012;8: 3243–3256. doi:10.1021/ct300343y

1116. Case DA, Cheatham TE 3rd, Darden T, Gohlke H, Luo R, Merz KM Jr, et al. The Amber biomolecular simulation programs. J Comput Chem. 2005;26: 1668–1688. doi:10.1002/jcc.20290

1117. Van Der Spoel D, Lindahl E, Hess B, Groenhof G, Mark AE, Berendsen HJC. GROMACS: fast, flexible, and free. J Comput Chem. 2005;26: 1701–1718. doi:10.1002/jcc.20291

1118. Hess B, Kutzner C, van der Spoel D, Lindahl E. GROMACS 4: Algorithms for Highly Efficient, Load-Balanced, and Scalable Molecular Simulation. J Chem Theory Comput. 2008;4: 435–447. doi:10.1021/ct700301q

1119. Heideman M, Johnson D, Burrus C. Gauss and the history of the fast fourier transform. IEEE ASSP Magazine. 1984;1: 14–21. doi:10.1109/MASSP.1984.1162257

1120. Giese TJ, Panteva MT, Chen H, York DM. Multipolar Ewald methods, 1: theory, accuracy, and performance. J Chem Theory Comput. 2015;11: 436–450. doi:10.1021/ct5007983

1121. Cerutti DS, Duke RE, Darden TA, Lybrand TP. Staggered Mesh Ewald: An extension of the Smooth Particle-Mesh Ewald method adding great versatility. J Chem Theory Comput. 2009;5: 2322. doi:10.1021/ct9001015

1122. Cerutti DS, Case DA. Multi-Level Ewald: A hybrid multigrid / Fast Fourier Transform approach to the electrostatic particle-mesh problem. J Chem Theory Comput. 2010;6: 443–458. doi:10.1021/ct900522g

1123. Timmer BJJ, Mooibroek TJ. Intermolecular π–π Stacking Interactions Made Visible. J Chem Educ. 2021;98: 540–545. doi:10.1021/acs.jchemed.0c01252

1124. Hunter CA, Lawson KR, Perkins J, Urch CJ. Aromatic interactions. J Chem Soc Perkin Trans 2. 2001; 651–669. doi:10.1039/B008495F

1125. Hwang SB, Lee CJ, Lee S, Ma S, Kang Y-M, Cho KH, et al. PMFF: Development of a Physics-Based Molecular Force Field for Protein Simulation and Ligand Docking. J Phys Chem B. 2020;124: 974–989. doi:10.1021/acs.jpcb.9b10339

1126. Momany FA, McGuire RF, Burgess AW, Scheraga HA. Energy parameters in polypeptides. VII. Geometric parameters, partial atomic charges, nonbonded interactions, hydrogen bond interactions, and intrinsic torsional potentials for the naturally occurring amino acids. J Phys Chem. 1975;79: 2361–2381. doi:10.1021/j100589a006

1127. Sippl MJ, Nemethy G, Scheraga HA. Intermolecular potentials from crystal data. 6. Determination of empirical potentials for O-H...O = C hydrogen bonds from packing configurations. J Phys Chem. 1984;88: 6231–6233. doi:10.1021/j150669a035

1128. Arnautova YA, Jagielska A, Scheraga HA. A new force field (ECEPP-05) for peptides, proteins, and organic molecules. J Phys Chem B. 2006;110: 5025–5044. doi:10.1021/jp054994x

1129. Allinger NL, Yuh YH, Lii JH. Molecular mechanics. The MM3 force field for hydrocarbons. 1. J Am Chem Soc. 1989;111: 8551–8566. doi:10.1021/ja00205a001

1130. Lii JH, Allinger NL. Molecular mechanics. The MM3 force field for hydrocarbons. 2. Vibrational frequencies and thermodynamics. J Am Chem Soc. 1989;111: 8566–8575. doi:10.1021/ja00205a002

1131. Lii JH, Allinger NL. Molecular mechanics. The MM3 force field for hydrocarbons. 3. The van der Waals' potentials and crystal data for aliphatic and aromatic hydrocarbons. J Am Chem Soc. 1989;111: 8576–8582. doi:10.1021/ja00205a003

1132. MacKerell AD, Bashford D, Bellott M, Dunbrack RL, Evanseck JD, Field MJ, et al. All-atom empirical potential for molecular modeling and dynamics studies of proteins. J Phys Chem B. 1998;102: 3586–3616. doi:10.1021/jp973084f

1133. Brooks BR, Bruccoleri RE, Olafson BD, States DJ, Swaminathan S, Karplus M. CHARMM: A program for macromolecular energy, minimization, and dynamics calculations. J Comput Chem. 1983;4: 187–217. doi:10.1002/jcc.540040211

1134. Vanommeslaeghe K, MacKerell AD Jr. Automation of the CHARMM General Force Field (CGenFF) I: bond perception and atom typing. J Chem Inf Model. 2012;52: 3144–3154. doi:10.1021/ci300363c

1135. Patel S, Mackerell AD Jr, Brooks CL 3rd. CHARMM fluctuating charge force field for proteins: II protein/solvent properties from molecular dynamics simulations using a nonadditive electrostatic model. J Comput Chem. 2004;25: 1504–1514. doi:10.1002/jcc.20077

1136. Cornell WD, Cieplak P, Bayly CI, Gould IR, Merz KM, Ferguson DM, et al. A Second Generation Force Field for the Simulation of Proteins, Nucleic Acids, and Organic Molecules. J Am Chem Soc. 1995;117: 5179–5197. doi:10.1021/ja00124a002

1137. Weiner SJ, Kollman PA, Case DA, Singh UC, Ghio C, Alagona G, et al. A new force field for molecular mechanical simulation of nucleic acids and proteins. J Am Chem Soc. 1984;106: 765–784. doi:10.1021/ja00315a051

1138. Peters MB, Yang Y, Wang B, Füsti-Molnár L, Weaver MN, Merz KM Jr. Structural Survey of Zinc Containing Proteins and the Development of the Zinc AMBER Force Field (ZAFF). J Chem Theory Comput. 2010;6: 2935–2947. doi:10.1021/ct1002626

1139. Dickson CJ, Rosso L, Betz RM, Walker RC, Gould IR. GAFFlipid: a General Amber Force Field for the accurate molecular dynamics simulation of phospholipid. Soft Matter. 2012;8: 9617–9627. doi:10.1039/C2SM26007G

1140. Oostenbrink C, Villa A, Mark AE, van Gunsteren WF. A biomolecular force field based on the free enthalpy of hydration and solvation: the GROMOS force-field parameter sets 53A5 and 53A6. J Comput Chem. 2004;25: 1656–1676. doi:10.1002/jcc.20090

1141. Rappe AK, Casewit CJ, Colwell KS, Goddard WA III, Skiff WM. UFF, a full periodic table force field for molecular mechanics and molecular dynamics simulations. J Am Chem Soc. 1992;114: 10024–10035. doi:10.1021/ja00051a040

1142. Cossio P, Granata D, Laio A, Seno F, Trovato A. A simple and efficient statistical potential for scoring ensembles of protein structures. Sci Rep. 2012;2: 1–8. doi:10.1038/srep00351

1143. Ciemny MP, Badaczewska-Dawid AE, Pikuzinska M, Kolinski A, Kmiecik S. Modeling of Disordered Protein Structures Using Monte Carlo Simulations and Knowledge-Based Statistical Force Fields. Int J Mol Sci. 2019;20. doi:10.3390/ijms20030606

1144. Tanaka S, Scheraga HA. Medium- and long-range interaction parameters between amino acids for predicting three-dimensional structures of proteins. Macromolecules. 1976;9: 945–950. doi:10.1021/ma60054a013

1145. Kolinski A. Protein modeling and structure prediction with a reduced representation. Acta Biochim Pol. 2004;51: 349–371. Available: https://www.ncbi.nlm.nih.gov/pubmed/15218533

1146. Tsai J, Bonneau R, Morozov AV, Kuhlman B, Rohl CA, Baker D. An improved protein decoy set for testing energy functions for protein structure prediction. Proteins. 2003;53: 76–87. doi:10.1002/prot.10454

1147. Ovchinnikov S, Park H, Kim DE, Liu Y, Wang RY-R, Baker D. Structure prediction using sparse simulated NOE restraints with Rosetta in CASP11. Proteins. 2016;84 Suppl 1: 181–188. doi:10.1002/prot.25006

1148. Ovchinnikov S, Kim DE, Wang RY-R, Liu Y, DiMaio F, Baker D. Improved de novo structure prediction in CASP11 by incorporating coevolution information into

Rosetta. Proteins. 2016;84 Suppl 1: 67–75. doi:10.1002/prot.24974

1149. Alexander NS, Stein RA, Koteiche HA, Kaufmann KW, McHaourab HS, Meiler J. RosettaEPR: rotamer library for spin label structure and dynamics. PLoS One. 2013;8: e72851. doi:10.1371/journal.pone.0072851

1150. Martin RM. Electronic Structure: Basic Theory and Practical Methods. Cambridge University Press; 2020. Available: https://play.google.com/store/books/details?id=Gun_DwAAQBAJ

1151. Spiegelman F, Tarrat N, Cuny J, Dontot L, Posenitskiy E, Martí C, et al. Density-functional tight-binding: basic concepts and applications to molecules and clusters. Adv Phys X. 2020;5: 1710252. doi:10.1080/23746149.2019.1710252

1152. Husch T, Vaucher AC, Reiher M. Semiempirical molecular orbital models based on the neglect of diatomic differential overlap approximation. Int J Quantum Chem. 2018;118: e25799. doi:10.1002/qua.25799

1153. Shi Y, Xia Z, Zhang J, Best R, Wu C, Ponder JW, et al. The Polarizable Atomic Multipole-based AMOEBA Force Field for Proteins. J Chem Theory Comput. 2013;9: 4046–4063. doi:10.1021/ct4003702

1154. Senftle TP, Hong S, Islam MM, Kylasa SB, Zheng Y, Shin YK, et al. The ReaxFF reactive force-field: development, applications and future directions. npj Computational Materials. 2016;2: 1–14. doi:10.1038/npjcompumats.2015.11

1155. van Mourik T, Bühl M, Gaigeot M-P. Density functional theory across chemistry, physics and biology. Philos Trans A Math Phys Eng Sci. 2014;372: 20120488. doi:10.1098/rsta.2012.0488

1156. Kohn W. Nobel Lecture: Electronic structure of matter---wave functions and density functionals. Rev Mod Phys. 1999;71: 1253–1266. doi:10.1103/RevModPhys.71.1253

1157. Cremer D. Møller-Plesset perturbation theory: from small molecule methods to methods for thousands of atoms. Wiley Interdiscip Rev Comput Mol Sci. 2011;1: 509–530. doi:10.1002/wcms.58

1158. Vakser IA. Protein-protein docking: from interaction to interactome. Biophys J. 2014;107: 1785–1793. doi:10.1016/j.bpj.2014.08.033

1159. Naga Madhavilatha K, Rama Mohan Babu G. Systematic approach for enrichment of docking outcome using consensus scoring functions. J Phys Conf Ser. 2019;1228: 012019. doi:10.1088/1742-6596/1228/1/012019

1160. Di Filippo JI, Cavasotto CN. Guided structure-based ligand identification and design via artificial intelligence modeling. Expert Opin Drug Discov. 2022;17: 71–78. doi:10.1080/17460441.2021.1979514

1161. Abagyan R, Totrov M. High-throughput docking for lead generation. Curr Opin

Chem Biol. 2001;5: 375–382. doi:10.1016/s1367-5931(00)00217-9

1162. Kitchen DB, Decornez H, Furr JR, Bajorath J. Docking and scoring in virtual screening for drug discovery: methods and applications. Nat Rev Drug Discov. 2004;3: 935–949. doi:10.1038/nrd1549

1163. Huang S-Y, Zou X. Advances and challenges in protein-ligand docking. Int J Mol Sci. 2010;11: 3016–3034. doi:10.3390/ijms11083016

1164. van der Lubbe SCC, Fonseca Guerra C. The nature of hydrogen bonds: A delineation of the role of different energy components on hydrogen bond strengths and lengths. Chem Asian J. 2019;14: 2760–2769. doi:10.1002/asia.201900717

1165. Rarey M, Kramer B, Lengauer T, Klebe G. A fast flexible docking method using an incremental construction algorithm. J Mol Biol. 1996;261: 470–489. doi:10.1006/jmbi.1996.0477

1166. Halperin I, Ma B, Wolfson H, Nussinov R. Principles of docking: An overview of search algorithms and a guide to scoring functions. Proteins. 2002;47: 409–443. doi:10.1002/prot.10115

1167. May A, Eisenhardt S, Schmidt-Ehrenberg J, Cordes F. Rigid body docking for Virtual Screening. 2003 [cited 27 May 2023]. Available: https://opus4.kobv.de/opus4-zib/frontdoor/index/index/docId/769

1168. Xu M, Lill MA. Induced fit docking, and the use of QM/MM methods in docking. Drug Discov Today Technol. 2013;10: e411–8. doi:10.1016/j.ddtec.2013.02.003

1169. Koshland DE Jr. CORRELATION OF STRUCTURE AND FUNCTION IN ENZYME ACTION. Science. 1963;142: 1533–1541. doi:10.1126/science.142.3599.1533

1170. Yuriev E, Ramsland PA. Latest developments in molecular docking: 2010-2011 in review. J Mol Recognit. 2013;26: 215–239. doi:10.1002/jmr.2266

1171. Brint AT, Willett P. Algorithms for the identification of three-dimensional maximal common substructures. J Chem Inf Comput Sci. 1987;27: 152–158. doi:10.1021/ci00056a002

1172. Fischer D, Norel R, Wolfson H, Nussinov R. Surface motifs by a computer vision technique: searches, detection, and implications for protein-ligand recognition. Proteins. 1993;16: 278–292. doi:10.1002/prot.340160306

1173. Norel R, Fischer D, Wolfson HJ, Nussinov R. Molecular surface recognition by a computer vision-based technique. Protein Eng. 1994;7: 39–46. doi:10.1093/protein/7.1.39

1174. Meng X-Y, Zhang H-X, Mezei M, Cui M. Molecular docking: a powerful approach for structure-based drug discovery. Curr Comput Aided Drug Des. 2011;7: 146–157. doi:10.2174/157340911795677602

1175. Kuntz ID, Blaney JM, Oatley SJ, Langridge R, Ferrin TE. A geometric approach to macromolecule-ligand interactions. J Mol Biol. 1982;161: 269–288. doi:10.1016/0022-2836(82)90153-x

1176. Lee B, Richards FM. The interpretation of protein structures: estimation of static accessibility. J Mol Biol. 1971;55: 379–400. doi:10.1016/0022-2836(71)90324-x

1177. Shrake A, Rupley JA. Environment and exposure to solvent of protein atoms. Lysozyme and insulin. J Mol Biol. 1973;79: 351–371. doi:10.1016/0022-2836(73)90011-9

1178. Zhang Z, Schindler CEM, Lange OF, Zacharias M. Application of Enhanced Sampling Monte Carlo Methods for High-Resolution Protein-Protein Docking in Rosetta. PLoS One. 2015;10: e0125941. doi:10.1371/journal.pone.0125941

1179. Goodsell DS, Olson AJ. Automated docking of substrates to proteins by simulated annealing. Proteins. 1990;8: 195–202. doi:10.1002/prot.340080302

1180. Gupta A, Gandhimathi A, Sharma P, Jayaram B. ParDOCK: an all atom energy based Monte Carlo docking protocol for protein-ligand complexes. Protein Pept Lett. 2007;14: 632–646. doi:10.2174/092986607781483831

1181. Alam N, Schueler-Furman O. Modeling Peptide-Protein Structure and Binding Using Monte Carlo Sampling Approaches: Rosetta FlexPepDock and FlexPepBind. Methods Mol Biol. 2017;1561: 139–169. doi:10.1007/978-1-4939-6798-8_9

1182. Morris GM, Goodsell DS, Halliday RS, Huey R, Hart WE, Belew RK, et al. Automated docking using a Lamarckian genetic algorithm and an empirical binding free energy function. J Comput Chem. 1998;19: 1639–1662. doi:10.1002/(sici)1096-987x(19981115)19:14<1639::aid-jcc10>3.0.co;2-b

1183. Jones G, Willett P, Glen RC, Leach AR, Taylor R. Development and validation of a genetic algorithm for flexible docking. J Mol Biol. 1997;267: 727–748. doi:10.1006/jmbi.1996.0897

1184. Oshiro CM, Kuntz ID, Dixon JS. Flexible ligand docking using a genetic algorithm. J Comput Aided Mol Des. 1995;9: 113–130. doi:10.1007/BF00124402

1185. Guan B, Zhang C, Ning J. Genetic algorithm with a crossover elitist preservation mechanism for protein-ligand docking. AMB Express. 2017;7: 174. doi:10.1186/s13568-017-0476-0

1186. Ördög R, Grolmusz V. Evaluating Genetic Algorithms in Protein-Ligand Docking. Bioinformatics Research and Applications. Springer Berlin Heidelberg; 2008. pp. 402–413. doi:10.1007/978-3-540-79450-9_37

1187. Fuhrmann J, Rurainski A, Lenhof H-P, Neumann D. A new Lamarckian genetic algorithm for flexible ligand-receptor docking. J Comput Chem. 2010;31: 1911–1918. doi:10.1002/jcc.21478

1188. Verdonk ML, Cole JC, Hartshorn MJ, Murray CW, Taylor RD. Improved protein-ligand docking using GOLD. Proteins. 2003;52: 609–623. doi:10.1002/prot.10465

1189. Taylor JS, Burnett RM. DARWIN: a program for docking flexible molecules. Proteins. 2000;41: 173–191. Available: https://www.ncbi.nlm.nih.gov/pubmed/10966571

1190. Gardiner EJ, Willett P, Artymiuk PJ. Protein docking using a genetic algorithm. Proteins. 2001;44: 44–56. doi:10.1002/prot.1070

1191. Liwo A. Computational Methods to Study the Structure and Dynamics of Biomolecules and Biomolecular Processes: From Bioinformatics to Molecular Quantum Mechanics. Springer; 2018. Available: https://play.google.com/store/books/details?id=9HWADwAAQBAJ

1192. Kollman P. Free energy calculations: Applications to chemical and biochemical phenomena. Chem Rev. 1993;93: 2395–2417. doi:10.1021/cr00023a004

1193. Åqvist J, Luzhkov VB, Brandsdal BO. Ligand Binding Affinities from MD Simulations. Acc Chem Res. 2002;35: 358–365. doi:10.1021/ar010014p

1194. Carlson HA, Jorgensen WL. An Extended Linear Response Method for Determining Free Energies of Hydration. J Phys Chem. 1995;99: 10667–10673. doi:10.1021/j100026a034

1195. Leach AR, Kuntz ID. Conformational analysis of flexible ligands in macromolecular receptor sites. J Comput Chem. 1992;13: 730–748. doi:10.1002/jcc.540130608

1196. Ewing TJ, Makino S, Skillman AG, Kuntz ID. DOCK 4.0: search strategies for automated molecular docking of flexible molecule databases. J Comput Aided Mol Des. 2001;15: 411–428. doi:10.1023/a:1011115820450

1197. Shoichet BK, Stroud RM, Santi DV, Kuntz ID, Perry KM. Structure-based discovery of inhibitors of thymidylate synthase. Science. 1993;259: 1445–1450. doi:10.1126/science.8451640

1198. Michel J, Verdonk ML, Essex JW. Protein-ligand binding affinity predictions by implicit solvent simulations: a tool for lead optimization? J Med Chem. 2006;49: 7427–7439. doi:10.1021/jm061021s

1199. Briggs JM, Marrone TJ, McCammon JA. Computational science new horizons and relevance to pharmaceutical design. Trends Cardiovasc Med. 1996;6: 198–203. doi:10.1016/S1050-1738(96)00068-0

1200. Rifai EA, van Dijk M, Geerke DP. Recent Developments in Linear Interaction Energy Based Binding Free Energy Calculations. Front Mol Biosci. 2020;7: 114. doi:10.3389/fmolb.2020.00114

1201. Aqvist J, Medina C, Samuelsson JE. A new method for predicting binding

affinity in computer-aided drug design. Protein Eng. 1994;7: 385–391. doi:10.1093/protein/7.3.385

1202. Lee FS, Chu ZT, Bolger MB, Warshel A. Calculations of antibody-antigen interactions: microscopic and semi-microscopic evaluation of the free energies of binding of phosphorylcholine analogs to McPC603. Protein Eng. 1992;5: 215–228. doi:10.1093/protein/5.3.215

1203. Zhu F, Bourguet FA, Bennett WFD, Lau EY, Arrildt KT, Segelke BW, et al. Large-scale application of free energy perturbation calculations for antibody design. Sci Rep. 2022;12: 12489. doi:10.1038/s41598-022-14443-z

1204. Beveridge DL, DiCapua FM. Free energy via molecular simulation: applications to chemical and biomolecular systems. Annu Rev Biophys Biophys Chem. 1989;18: 431–492. doi:10.1146/annurev.bb.18.060189.002243

1205. Jespers W, Åqvist J, Gutiérrez-de-Terán H. Free Energy Calculations for Protein-Ligand Binding Prediction. Methods Mol Biol. 2021;2266: 203–226. doi:10.1007/978-1-0716-1209-5_12

1206. Wang L, Deng Y, Knight JL, Wu Y, Kim B, Sherman W, et al. Modeling Local Structural Rearrangements Using FEP/REST: Application to Relative Binding Affinity Predictions of CDK2 Inhibitors. J Chem Theory Comput. 2013;9: 1282–1293. doi:10.1021/ct300911a

1207. Lee T-S, Allen BK, Giese TJ, Guo Z, Li P, Lin C, et al. Alchemical Binding Free Energy Calculations in AMBER20: Advances and Best Practices for Drug Discovery. J Chem Inf Model. 2020;60: 5595–5623. doi:10.1021/acs.jcim.0c00613

1208. Zwanzig RW. High-temperature equation of state by a perturbation method. I. nonpolar gases. J Chem Phys. 1954;22: 1420–1426. doi:10.1063/1.1740409

1209. Böhm HJ. Prediction of binding constants of protein ligands: a fast method for the prioritization of hits obtained from de novo design or 3D database search programs. J Comput Aided Mol Des. 1998;12: 309–323. doi:10.1023/a:1007999920146

1210. Verkhivker GM, Bouzida D, Gehlhaar DK, Rejto PA, Arthurs S, Colson AB, et al. Deciphering common failures in molecular docking of ligand-protein complexes. J Comput Aided Mol Des. 2000;14: 731–751. doi:10.1023/a:1008158231558

1211. Jain AN. Scoring noncovalent protein-ligand interactions: a continuous differentiable function tuned to compute binding affinities. J Comput Aided Mol Des. 1996;10: 427–440. doi:10.1007/BF00124474

1212. Eldridge MD, Murray CW, Auton TR, Paolini GV, Mee RP. Empirical scoring functions: I. The development of a fast empirical scoring function to estimate the binding affinity of ligands in receptor complexes. J Comput Aided Mol Des. 1997;11: 425–445. doi:10.1023/a:1007996124545

1213. Muegge I, Martin YC. A general and fast scoring function for protein-ligand interactions: a simplified potential approach. J Med Chem. 1999;42: 791–804. doi:10.1021/jm980536j

1214. Ishchenko AV, Shakhnovich EI. SMall Molecule Growth 2001 (SMoG2001): an improved knowledge-based scoring function for protein-ligand interactions. J Med Chem. 2002;45: 2770–2780. doi:10.1021/jm0105833

1215. Feher M, Deretey E, Roy S. BHB: a simple knowledge-based scoring function to improve the efficiency of database screening. J Chem Inf Comput Sci. 2003;43: 1316–1327. doi:10.1021/ci030006i

1216. Verkhivker G, Appelt K, Freer ST, Villafranca JE. Empirical free energy calculations of ligand-protein crystallographic complexes. I. Knowledge-based ligand-protein interaction potentials applied to the prediction of human immunodeficiency virus 1 protease binding affinity. Protein Eng Des Sel. 1995;8: 677–691. Available: https://academic.oup.com/peds/article-abstract/8/7/677/1465466

1217. Gohlke H, Hendlich M, Klebe G. Knowledge-based scoring function to predict protein-ligand interactions. J Mol Biol. 2000;295: 337–356. doi:10.1006/jmbi.1999.3371

1218. DeWitte RS, Ishchenko AV, Shakhnovich EI. SMoG: de Novo Design Method Based on Simple, Fast, and Accurate Free Energy Estimates. 2. Case Studies in Molecular Design. J Am Chem Soc. 1997;119: 4608–4617. doi:10.1021/ja963689+

1219. Mitchell JBO, Laskowski RA, Alex A, Thornton JM. BLEEP?potential of mean force describing protein-ligand interactions: I. Generating potential. J Comput Chem. 1999;20: 1165–1176. doi:10.1002/(sici)1096-987x(199908)20:11<1165::aid-jcc7>3.0.co;2-a

1220. Feher M. Consensus scoring for protein–ligand interactions. Drug Discov Today. 2006;11: 421–428. doi:10.1016/j.drudis.2006.03.009

1221. Clark RD, Strizhev A, Leonard JM, Blake JF, Matthew JB. Consensus scoring for ligand/protein interactions. J Mol Graph Model. 2002;20: 281–295. doi:10.1016/s1093-3263(01)00125-5

1222. Kollman PA, Massova I, Reyes C, Kuhn B, Huo S, Chong L, et al. Calculating structures and free energies of complex molecules: combining molecular mechanics and continuum models. Acc Chem Res. 2000;33: 889–897. doi:10.1021/ar000033j

1223. Still WC, Tempczyk A, Hawley RC, Hendrickson T. Semianalytical treatment of solvation for molecular mechanics and dynamics. J Am Chem Soc. 1990;112: 6127–6129. doi:10.1021/ja00172a038

1224. Reulecke I, Lange G, Albrecht J, Klein R, Rarey M. Towards an integrated

description of hydrogen bonding and dehydration: decreasing false positives in virtual screening with the HYDE scoring function. ChemMedChem. 2008;3: 885–897. doi:10.1002/cmdc.200700319

1225. Schneider N, Lange G, Hindle S, Klein R, Rarey M. A consistent description of HYdrogen bond and DEhydration energies in protein-ligand complexes: methods behind the HYDE scoring function. J Comput Aided Mol Des. 2013;27: 15–29. doi:10.1007/s10822-012-9626-2

1226. Samish I, Gu J, Klein ML. Protein Motion: Simulation. Structural Bioinformatics. 2009;2: 907–936. Available: https://www.academia.edu/download/37449016/2009_c37_Samish_Klein_Protein_Simulation.pdf

1227. Berg HC. Random Walks in Biology. Princeton University Press; 1993. Available: https://play.google.com/store/books/details?id=DjdgXGLoJY8C

1228. Lemons DS, Gythiel A. Paul Langevin's 1908 paper "On the Theory of Brownian Motion" ["Sur la théorie du mouvement brownien," C. R. Acad. Sci. (Paris) 146, 530–533 (1908)]. Am J Phys. 1997;65: 1079–1081. doi:10.1119/1.18725

1229. Born M, Oppenheimer R. Zur Quantentheorie der Molekeln. Ann Phys. 1927;389: 457–484. doi:10.1002/andp.19273892002

1230. Bird K, Sherwin MJ. American Prometheus: The Triumph and Tragedy of J. Robert Oppenheimer. Atlantic Books; 2021. Available: https://play.google.com/store/books/details?id=F79LEAAAQBAJ

1231. Hairer E, Lubich C, Wanner G. Geometric numerical integration illustrated by the Störmer–Verlet method. Acta Numer. 2003;12: 399–450. doi:10.1017/S0962492902000144

1232. Verlet L. Computer "Experiments" on Classical Fluids. I. Thermodynamical Properties of Lennard-Jones Molecules. Phys Rev. 1967;159: 98–103. doi:10.1103/PhysRev.159.98

1233. Streett WB, Tildesley DJ, Saville G. Multiple time-step methods in molecular dynamics. Mol Phys. 1978;35: 639–648. doi:10.1080/00268977800100471

1234. Batcho PF, Case DA, Schlick T. Optimized particle-mesh Ewald/multiple-time step integration for molecular dynamics simulations. J Chem Phys. 2001;115: 4003–4018. doi:10.1063/1.1389854

1235. Yeh I-C, Hummer G. System-Size Dependence of Diffusion Coefficients and Viscosities from Molecular Dynamics Simulations with Periodic Boundary Conditions. J Phys Chem B. 2004;108: 15873–15879. doi:10.1021/jp0477147

1236. Barclay PL, Zhang DZ. Periodic boundary conditions for arbitrary deformations in molecular dynamics simulations. J Comput Phys. 2021;435: 110238. doi:10.1016/j.jcp.2021.110238

1237. Lippert RA, Predescu C, Ierardi DJ, Mackenzie KM, Eastwood MP, Dror RO, et al. Accurate and efficient integration for molecular dynamics simulations at constant temperature and pressure. J Chem Phys. 2013;139: 164106. doi:10.1063/1.4825247

1238. Ke Q, Gong X, Liao S, Duan C, Li L. Effects of thermostats/barostats on physical properties of liquids by molecular dynamics simulations. J Mol Liq. 2022;365: 120116. doi:10.1016/j.molliq.2022.120116

1239. Tschopp MA, Bouvard JL, Ward DK, Bammann DJ, Horstemeyer MF. Influence of ensemble boundary conditions (thermostat and barostat) on the deformation of amorphous polyethylene by molecular dynamics. arXiv [cond-mat.mtrl-sci]. 2013. Available: http://arxiv.org/abs/1310.0728

1240. Ahn S-H, Ojha AA, Amaro RE, McCammon JA. Gaussian-Accelerated Molecular Dynamics with the Weighted Ensemble Method: A Hybrid Method Improves Thermodynamic and Kinetic Sampling. J Chem Theory Comput. 2021;17: 7938–7951. doi:10.1021/acs.jctc.1c00770

1241. Hess B. P-LINCS: A Parallel Linear Constraint Solver for Molecular Simulation. J Chem Theory Comput. 2008;4: 116–122. doi:10.1021/ct700200b

1242. Abraham MJ, Murtola T, Schulz R, Páll S, Smith JC, Hess B, et al. GROMACS: High performance molecular simulations through multi-level parallelism from laptops to supercomputers. SoftwareX. 2015;1-2: 19–25. doi:10.1016/j.softx.2015.06.001

1243. Perez A, MacCallum JL, Coutsias EA, Dill KA. Constraint methods that accelerate free-energy simulations of biomolecules. J Chem Phys. 2015;143: 243143. doi:10.1063/1.4936911

1244. Likhachev IV, Balabaev NK, Galzitskaya OV. Available Instruments for Analyzing Molecular Dynamics Trajectories. Open Biochem J. 2016;10: 1–11. doi:10.2174/1874091X01610010001

1245. De Filippo E, Schiedel AC, Manga P. Interaction between G Protein-Coupled Receptor 143 and Tyrosinase: Implications for Understanding Ocular Albinism Type 1. J Invest Dermatol. 2017;137: 457–465. doi:10.1016/j.jid.2016.09.022

1246. Smith LN, Bachus SE, McDonald CG, Smith RF. Role of the D3 dopamine receptor in nicotine sensitization. Behav Brain Res. 2015;289: 92–104. doi:10.1016/j.bbr.2015.04.025

1247. Liu F, Wan Q, Pristupa ZB, Yu XM, Wang YT, Niznik HB. Direct protein-protein coupling enables cross-talk between dopamine D5 and gamma-aminobutyric acid A receptors. Nature. 2000;403: 274–280. doi:10.1038/35002014

1248. Hillefors M, Hedlund PB, von Euler G. Effects of adenosine A(2A) receptor stimulation in vivo on dopamine D3 receptor agonist binding in the rat brain.

Biochem Pharmacol. 1999;58: 1961–1964. doi:10.1016/s0006-2952(99)00276-2

1249. Borroto-Escuela DO, Ferraro L, Narvaez M, Tanganelli S, Beggiato S, Liu F, et al. Multiple Adenosine-Dopamine (A2A-D2 Like) Heteroreceptor Complexes in the Brain and Their Role in Schizophrenia. Cells. 2020;9. doi:10.3390/cells9051077

1250. De Filippo E, Manga P, Schiedel AC. Identification of Novel G Protein–Coupled Receptor 143 Ligands as Pharmacologic Tools for Investigating X-Linked Ocular Albinism. Invest Ophthalmol Vis Sci. 2017;58: 3118–3126. doi:10.1167/iovs.16-21128

1251. Schwinn G. Schwarck H, McIntosh C, Milstrey HR, Willms B, and Kobberling J. pimozide on the growth hormone response to arginine ….

1252. Freedman SB, Patel S, Marwood R, Emms F, Seabrook GR, Knowles MR, et al. Expression and pharmacological characterization of the human D3 dopamine receptor. J Pharmacol Exp Ther. 1994;268: 417–426. Available: https://www.ncbi.nlm.nih.gov/pubmed/8301582

1253. Sokoloff P, Andrieux M, Besançon R, Pilon C, Martres MP, Giros B, et al. Pharmacology of human dopamine D3 receptor expressed in a mammalian cell line: comparison with D2 receptor. Eur J Pharmacol. 1992;225: 331–337. doi:10.1016/0922-4106(92)90107-7

1254. Sokoloff P, Giros B, Martres MP, Bouthenet ML, Schwartz JC. Molecular cloning and characterization of a novel dopamine receptor (D3) as a target for neuroleptics. Nature. 1990;347: 146–151. doi:10.1038/347146a0

1255. Masukawa D, Nakamura F, Koga M, Kamiya M, Chen S, Yamashita N, et al. Localization of ocular albinism-1 gene product GPR143 in the rat central nervous system. Neurosci Res. 2014;88: 49–57. doi:10.1016/j.neures.2014.07.008

1256. Fukuda N, Naito S, Masukawa D, Kaneda M, Miyamoto H, Abe T, et al. Expression of ocular albinism 1 (OA1), 3, 4- dihydroxy- L-phenylalanine (DOPA) receptor, in both neuronal and non-neuronal organs. Brain Res. 2015;1602: 62–74. doi:10.1016/j.brainres.2015.01.020

1257. Hiroshima Y, Miyamoto H, Nakamura F, Masukawa D, Yamamoto T, Muraoka H, et al. The protein Ocular albinism 1 is the orphan GPCR GPR143 and mediates depressor and bradycardic responses to DOPA in the nucleus tractus solitarii. Br J Pharmacol. 2014;171: 403–414. doi:10.1111/bph.12459

1258. Schiaffino MV, Tacchetti C. The ocular albinism type 1 (OA1) protein and the evidence for an intracellular signal transduction system involved in melanosome biogenesis. Pigment Cell Res. 2005;18: 227–233. doi:10.1111/j.1600-0749.2005.00240.x

1259. O'Donnell FE Jr, Hambrick GW Jr, Green WR, Iliff WJ, Stone DL. X-linked ocular albinism. An oculocutaneous macromelanosomal disorder. Arch

Ophthalmol. 1976;94: 1883–1892. doi:10.1001/archopht.1976.03910040593001

1260. Samaraweera P, Shen B, Newton JM, Barsh GS, Orlow SJ. The mouse ocular albinism 1 gene product is an endolysosomal protein. Exp Eye Res. 2001;72: 319–329. doi:10.1006/exer.2000.0962

1261. van Dorp DB. Albinism, or the NOACH syndrome (the book of Enoch c.v. 1-20). Clin Genet. 1987;31: 228–242. doi:10.1111/j.1399-0004.1987.tb02801.x

1262. Charles SJ, Green JS, Grant JW, Yates JR, Moore AT. Clinical features of affected males with X linked ocular albinism. Br J Ophthalmol. 1993;77: 222–227. doi:10.1136/bjo.77.4.222

1263. Creel DJ, Summers CG, King RA. Visual anomalies associated with albinism. Ophthalmic Paediatr Genet. 1990;11: 193–200. doi:10.3109/13816819009020979

1264. Giordano F, Bonetti C, Surace EM, Marigo V, Raposo G. The ocular albinism type 1 (OA1) G-protein-coupled receptor functions with MART-1 at early stages of melanogenesis to control melanosome identity and composition. Hum Mol Genet. 2009;18: 4530–4545. doi:10.1093/hmg/ddp415

1265. Palmisano I, Bagnato P, Palmigiano A, Innamorati G, Rotondo G, Altimare D, et al. The ocular albinism type 1 protein, an intracellular G protein-coupled receptor, regulates melanosome transport in pigment cells. Hum Mol Genet. 2008;17: 3487–3501. doi:10.1093/hmg/ddn241

1266. Young A, Jiang M, Wang Y, Ahmedli NB, Ramirez J, Reese BE, et al. Specific interaction of Gαi3 with the Oa1 G-protein coupled receptor controls the size and density of melanosomes in retinal pigment epithelium. PLoS One. 2011;6: e24376. doi:10.1371/journal.pone.0024376

1267. Masukawa D, Koga M, Sezaki A, Nakao Y, Kamikubo Y, Hashimoto T, et al. L-DOPA sensitizes vasomotor tone by modulating the vascular alpha1-adrenergic receptor. JCI Insight. 2017;2. doi:10.1172/jci.insight.90903

1268. Innamorati G, Piccirillo R, Bagnato P, Palmisano I, Schiaffino MV. The melanosomal/lysosomal protein OA1 has properties of a G protein-coupled receptor. Pigment Cell Res. 2006;19: 125–135. doi:10.1111/j.1600-0749.2006.00292.x

1269. Sone M, Orlow SJ. The ocular albinism type 1 gene product, OA1, spans intracellular membranes 7 times. Exp Eye Res. 2007;85: 806–816. doi:10.1016/j.exer.2007.08.016

1270. Shen B, Rosenberg B, Orlow SJ. Intracellular distribution and late endosomal effects of the ocular albinism type 1 gene product: consequences of disease-causing mutations and implications for melanosome biogenesis. Traffic. 2001;2: 202–211. doi:10.1034/j.1600-0854.2001.020306.x

1271. Staleva L, Orlow SJ. Ocular albinism 1 protein: trafficking and function when

expressed in Saccharomyces cerevisiae. Exp Eye Res. 2006;82: 311–318. doi:10.1016/j.exer.2005.07.003

1272. Neumann A, Engel V, Mahardhika AB, Schoeder CT, Namasivayam V, Kieć-Kononowicz K, et al. Computational Investigations on the Binding Mode of Ligands for the Cannabinoid-Activated G Protein-Coupled Receptor GPR18. Biomolecules. 2020;10. doi:10.3390/biom10050686

1273. Gu Y, Di WL, Kelsell DP, Zicha D. Quantitative fluorescence resonance energy transfer (FRET) measurement with acceptor photobleaching and spectral unmixing. J Microsc. 2004;215: 162–173. doi:10.1111/j.0022-2720.2004.01365.x

1274. Wilson MC, Meredith D, Halestrap AP. Fluorescence resonance energy transfer studies on the interaction between the lactate transporter MCT1 and CD147 provide information on the topology and stoichiometry of the complex in situ. J Biol Chem. 2002;277: 3666–3672. doi:10.1074/jbc.M109658200

1275. Mott AM, Nunes EJ, Collins LE, Port RG, Sink KS, Hockemeyer J, et al. The adenosine A2A antagonist MSX-3 reverses the effects of the dopamine antagonist haloperidol on effort-related decision making in a T-maze cost/benefit procedure. Psychopharmacology . 2009;204: 103–112. doi:10.1007/s00213-008-1441-z

1276. Romero-Fernandez W, Zhou Z, Beggiato S, Wydra K, Filip M, Tanganelli S, et al. Acute cocaine treatment enhances the antagonistic allosteric adenosine A2A-dopamine D2 receptor-receptor interactions in rat dorsal striatum without increasing significantly extracellular dopamine levels. Pharmacol Rep. 2020;72: 332–339. doi:10.1007/s43440-020-00069-3

1277. Lee FJS, Xue S, Pei L, Vukusic B, Chéry N, Wang Y, et al. Dual regulation of NMDA receptor functions by direct protein-protein interactions with the dopamine D1 receptor. Cell. 2002;111: 219–230. doi:10.1016/s0092-8674(02)00962-5

1278. Niewiarowska-Sendo A, Polit A, Piwowar M, Tworzydło M, Kozik A, Guevara-Lora I. Bradykinin B2 and dopamine D2 receptors form a functional dimer. Biochim Biophys Acta Mol Cell Res. 2017;1864: 1855–1866. doi:10.1016/j.bbamcr.2017.07.012

1279. Schwinn G, Schwarck H, McIntosh C, Milstrey HR, Willms B, Köbberling J. Effect of the dopamine receptor blocking agent pimozide on the growth hormone response to arginine and exercise and on the spontaneous growth hormone fluctuations. J Clin Endocrinol Metab. 1976;43: 1183–1185. doi:10.1210/jcem-43-5-1183

1280. Jung JM, Kim SY, Lee WJ, Hwang JS, Chang SE. Dopamine D4 receptor antagonist inhibits melanogenesis through transcriptional downregulation of MITF via ERK signalling. Exp Dermatol. 2016;25: 325–328. doi:10.1111/exd.12943

1281. Incerti B, Cortese K, Pizzigoni A, Surace EM, Varani S, Coppola M, et al. Oa1 knock-out: new insights on the pathogenesis of ocular albinism type 1. Hum Mol

Genet. 2000;9: 2781–2788. doi:10.1093/hmg/9.19.2781

1282. Cortese K, Giordano F, Surace EM, Venturi C, Ballabio A, Tacchetti C, et al. The ocular albinism type 1 (OA1) gene controls melanosome maturation and size. Invest Ophthalmol Vis Sci. 2005;46: 4358–4364. doi:10.1167/iovs.05-0834

1283. Burgoyne T, Jolly R, Martin-Martin B, Seabra MC, Piccirillo R, Schiaffino MV, et al. Expression of OA1 limits the fusion of a subset of MVBs with lysosomes - a mechanism potentially involved in the initial biogenesis of melanosomes. J Cell Sci. 2013;126: 5143–5152. doi:10.1242/jcs.128561

1284. Carr R 3rd, Benovic JL. From biased signalling to polypharmacology: unlocking unique intracellular signalling using pepducins. Biochem Soc Trans. 2016;44: 555–561. doi:10.1042/BST20150230

1285. Falletta P, Bagnato P, Bono M, Monticone M, Schiaffino MV, Bennett DC, et al. Melanosome-autonomous regulation of size and number: the OA1 receptor sustains PMEL expression. Pigment Cell Melanoma Res. 2014;27: 565–579. doi:10.1111/pcmr.12239

1286. Vetrini F, Auricchio A, Du J, Angeletti B, Fisher DE, Ballabio A, et al. The microphthalmia transcription factor (Mitf) controls expression of the ocular albinism type 1 gene: link between melanin synthesis and melanosome biogenesis. Mol Cell Biol. 2004;24: 6550–6559. doi:10.1128/MCB.24.15.6550-6559.2004

1287. Masukawa D, Nishizawa D, Kanai K, Kitamura S, Kasahara Y, Hashimoto T, et al. Genetic associations of single nucleotide polymorphisms in the l-DOPA receptor (GPR143) gene with severity of nicotine dependence in Japanese individuals, and attenuation of nicotine reinforcement in Gpr143 gene-deficient mice. J Pharmacol Sci. 2020;144: 89–93. doi:10.1016/j.jphs.2020.07.003

1288. Schiaffino MV, d'Addio M, Alloni A, Baschirotto C, Valetti C, Cortese K, et al. Ocular albinism: evidence for a defect in an intracellular signal transduction system. Nat Genet. 1999;23: 108–112. doi:10.1038/12715

1289. Lopez VM, Decatur CL, Stamer WD, Lynch RM, McKay BS. L-DOPA is an endogenous ligand for OA1. PLoS Biol. 2008;6: e236. doi:10.1371/journal.pbio.0060236

1290. Levoye A, Dam J, Ayoub MA, Guillaume J-L, Jockers R. Do orphan G-protein-coupled receptors have ligand-independent functions? New insights from receptor heterodimers. EMBO Rep. 2006;7: 1094–1098. doi:10.1038/sj.embor.7400838

1291. Levoye A, Dam J, Ayoub MA, Guillaume J-L, Couturier C, Delagrange P, et al. The orphan GPR50 receptor specifically inhibits MT1 melatonin receptor function through heterodimerization. EMBO J. 2006;25: 3012–3023. doi:10.1038/sj.emboj.7601193

1292. Chen T, Hu Y, Lin X, Huang X, Liu B, Leung P, et al. Dopamine signaling

regulates the projection patterns in the mouse chiasm. Brain Res. 2015;1625: 324–336. doi:10.1016/j.brainres.2015.08.026

1293. Marchese A, Paing MM, Temple BRS, Trejo J. G protein-coupled receptor sorting to endosomes and lysosomes. Annu Rev Pharmacol Toxicol. 2008;48: 601–629. doi:10.1146/annurev.pharmtox.48.113006.094646

1294. Hanyaloglu AC. Chapter Four - Advances in Membrane Trafficking and Endosomal Signaling of G Protein-Coupled Receptors. In: Shukla AK, editor. International Review of Cell and Molecular Biology. Academic Press; 2018. pp. 93–131. doi:10.1016/bs.ircmb.2018.03.001

1295. Jensen DD, Lieu T, Halls ML, Veldhuis NA, Imlach WL, Mai QN, et al. Neurokinin 1 receptor signaling in endosomes mediates sustained nociception and is a viable therapeutic target for prolonged pain relief. Sci Transl Med. 2017;9. doi:10.1126/scitranslmed.aal3447

1296. Sriram K, Insel PA. G Protein-Coupled Receptors as Targets for Approved Drugs: How Many Targets and How Many Drugs? Mol Pharmacol. 2018;93: 251–258. doi:10.1124/mol.117.111062

1297. Caniceiro AB, Bueschbell B, Schiedel AC, Moreira IS. Class A and C GPCR dimers in neurodegenerative diseases. Curr Neuropharmacol. 2022. doi:10.2174/1570159X20666220327221830

1298. Hiller C, Kühhorn J, Gmeiner P. Class A G-protein-coupled receptor (GPCR) dimers and bivalent ligands. J Med Chem. 2013;56: 6542–6559. doi:10.1021/jm4004335

1299. Quitterer U, AbdAlla S. Discovery of Pathologic GPCR Aggregation. Front Med. 2019;6: 9. doi:10.3389/fmed.2019.00009

1300. Sarasola LI, Del Torrent CL, Pérez-Arévalo A, Argerich J, Casajuana-Martín N, Chevigné A, et al. The ADORA1 mutation linked to early-onset Parkinson's disease alters adenosine A1-A2A receptor heteromer formation and function. Biomed Pharmacother. 2022;156: 113896. doi:10.1016/j.biopha.2022.113896

1301. Borroto-Escuela DO, Brito I, Romero-Fernandez W, Di Palma M, Oflijan J, Skieterska K, et al. The G protein-coupled receptor heterodimer network (GPCR-HetNet) and its hub components. Int J Mol Sci. 2014;15: 8570–8590. doi:10.3390/ijms15058570

1302. Kaczor AA, Jörg M, Capuano B. The dopamine D2 receptor dimer and its interaction with homobivalent antagonists: homology modeling, docking and molecular dynamics. J Mol Model. 2016;22: 203. doi:10.1007/s00894-016-3065-2

1303. Guo W, Shi L, Javitch JA. The fourth transmembrane segment forms the interface of the dopamine D2 receptor homodimer. J Biol Chem. 2003;278: 4385–4388. doi:10.1074/jbc.C200679200

1304. Guo W, Urizar E, Kralikova M, Mobarec JC, Shi L, Filizola M, et al. Dopamine D2 receptors form higher order oligomers at physiological expression levels. EMBO J. 2008;27: 2293–2304. doi:10.1038/emboj.2008.153

1305. Lee SP, O'Dowd BF, Rajaram RD, Nguyen T, George SR. D2 dopamine receptor homodimerization is mediated by multiple sites of interaction, including an intermolecular interaction involving transmembrane domain 4. Biochemistry. 2003;42: 11023–11031. doi:10.1021/bi0345539

1306. Jiang L-H. Cysteine-based cross-linking approach to study inter-domain interactions in ion channels. Methods Mol Biol. 2013;998: 267–276. doi:10.1007/978-1-62703-351-0_21

1307. Cottet M, Faklaris O, Maurel D, Scholler P, Doumazane E, Trinquet E, et al. BRET and Time-resolved FRET strategy to study GPCR oligomerization: from cell lines toward native tissues. Front Endocrinol . 2012;3: 92. doi:10.3389/fendo.2012.00092

1308. Chen J, Cai X, Yan M, Wang Z, Lv Z, Wang C. A method for identifying G protein-coupled receptor dimers and their interfaces. Biochim Biophys Acta Mol Cell Res. 2021;1868: 118887. doi:10.1016/j.bbamcr.2020.118887

1309. Borroto-Escuela DO, Brito I, Romero-Fernandez W, Di Palma M, Oflijan J, Skieterska K, et al. The G protein-coupled receptor heterodimer network (GPCR-HetNet) and its hub components. Int J Mol Sci. 2014;15: 8570–8590. doi:10.3390/ijms15058570

1310. Kaczor AA, Jörg M, Capuano B. The dopamine D2 receptor dimer and its interaction with homobivalent antagonists: homology modeling, docking and molecular dynamics. J Mol Model. 2016;22: 203. doi:10.1007/s00894-016-3065-2

1311. Rangel-Barajas C, Coronel I, Florán B. Dopamine Receptors and Neurodegeneration. Aging Dis. 2015;6: 349–368. doi:10.14336/AD.2015.0330

1312. Blagotinšek Cokan K, Mavri M, Rutland CS, Glišić S, Senćanski M, Vrecl M, et al. Critical Impact of Different Conserved Endoplasmic Retention Motifs and Dopamine Receptor Interacting Proteins (DRIPs) on Intracellular Localization and Trafficking of the D2 Dopamine Receptor (D2-R) Isoforms. Biomolecules. 2020;10. doi:10.3390/biom10101355

1313. Andersen PH, Gingrich JA, Bates MD, Dearry A, Falardeau P, Senogles SE, et al. Dopamine receptor subtypes: beyond the D1/D2 classification. Trends Pharmacol Sci. 1990;11: 231–236. doi:10.1016/0165-6147(90)90249-8

1314. Carli M, Kolachalam S, Aringhieri S, Rossi M, Giovannini L, Maggio R, et al. Dopamine D2 Receptors Dimers: How can we Pharmacologically Target Them? Curr Neuropharmacol. 2018;16: 222–230. doi:10.2174/1570159X15666170518151127

1315. Wang M, Pei L, Fletcher PJ, Kapur S, Seeman P, Liu F. Schizophrenia, amphetamine-induced sensitized state and acute amphetamine exposure all show a common alteration: increased dopamine D2 receptor dimerization. Mol Brain. 2010;3: 25. doi:10.1186/1756-6606-3-25

1316. Bagalkot TR, Jin H-M, Prabhu VV, Muna SS, Cui Y, Yadav BK, et al. Chronic social defeat stress increases dopamine D2 receptor dimerization in the prefrontal cortex of adult mice. Neuroscience. 2015;311: 444–452. doi:10.1016/j.neuroscience.2015.10.024

1317. Congreve M, de Graaf C, Swain NA, Tate CG. Impact of GPCR Structures on Drug Discovery. Cell. 2020;181: 81–91. doi:10.1016/j.cell.2020.03.003

1318. Mansoor S, Kayık G, Durdagi S, Sensoy O. Mechanistic insight into the impact of a bivalent ligand on the structure and dynamics of a GPCR oligomer. Comput Struct Biotechnol J. 2022;20: 925–936. doi:10.1016/j.csbj.2022.01.016

1319. Simpson LM, Taddese B, Wall ID, Reynolds CA. Bioinformatics and molecular modelling approaches to GPCR oligomerization. Curr Opin Pharmacol. 2010;10: 30–37. doi:10.1016/j.coph.2009.11.001

1320. Armstrong D, Strange PG. Dopamine D2 receptor dimer formation: evidence from ligand binding. J Biol Chem. 2001;276: 22621–22629. doi:10.1074/jbc.M006936200

1321. Xue L, Rovira X, Scholler P, Zhao H, Liu J, Pin J-P, et al. Major ligand-induced rearrangement of the heptahelical domain interface in a GPCR dimer. Nat Chem Biol. 2015;11: 134–140. doi:10.1038/nchembio.1711

1322. Marsango S, Caltabiano G, Pou C, Varela Liste MJ, Milligan G. Analysis of Human Dopamine D3 Receptor Quaternary Structure. J Biol Chem. 2015;290: 15146–15162. doi:10.1074/jbc.M114.630681

1323. Wang S, Che T, Levit A, Shoichet BK, Wacker D, Roth BL. Structure of the D2 dopamine receptor bound to the atypical antipsychotic drug risperidone. Nature. 2018;555: 269–273. doi:10.1038/nature25758

1324. Yin J, Chen K-YM, Clark MJ, Hijazi M, Kumari P, Bai X-C, et al. Structure of a D2 dopamine receptor-G-protein complex in a lipid membrane. Nature. 2020;584: 125–129. doi:10.1038/s41586-020-2379-5

1325. Kaczor AA, Bartuzi D, Stępniewski TM, Matosiuk D, Selent J. Protein–Protein Docking in Drug Design and Discovery. In: Gore M, Jagtap UB, editors. Computational Drug Discovery and Design. New York, NY: Springer New York; 2018. pp. 285–305. doi:10.1007/978-1-4939-7756-7_15

1326. Karaca E, Prévost C, Sacquin-Mora S. Modeling the Dynamics of Protein-Protein Interfaces, How and Why? Molecules. 2022;27. doi:10.3390/molecules27061841

1327. Erol I, Cosut B, Durdagi S. Toward Understanding the Impact of Dimerization Interfaces in Angiotensin II Type 1 Receptor. J Chem Inf Model. 2019;59: 4314–4327. doi:10.1021/acs.jcim.9b00294

1328. Wang L, Yuan Y, Chen X, Chen J, Guo Y, Li M, et al. Probing the cooperative mechanism of the μ–δ opioid receptor heterodimer by multiscale simulation. Phys Chem Chem Phys. 2018;20: 29969–29982. doi:10.1039/C8CP06652C

1329. Elez K, Bonvin AMJJ, Vangone A. Distinguishing crystallographic from biological interfaces in protein complexes: role of intermolecular contacts and energetics for classification. BMC Bioinformatics. 2018;19: 438. doi:10.1186/s12859-018-2414-9

1330. Jiménez-García B, Elez K, Koukos PI, Bonvin AM, Vangone A. PRODIGY-crystal: a web-tool for classification of biological interfaces in protein complexes. Bioinformatics. 2019;35: 4821–4823. doi:10.1093/bioinformatics/btz437

1331. Xue LC, Rodrigues JP, Kastritis PL, Bonvin AM, Vangone A. PRODIGY: a web server for predicting the binding affinity of protein-protein complexes. Bioinformatics. 2016;32: 3676–3678. doi:10.1093/bioinformatics/btw514

1332. Leioatts N, Suresh P, Romo TD, Grossfield A. Structure-based simulations reveal concerted dynamics of GPCR activation. Proteins. 2014;82: 2538–2551. doi:10.1002/prot.24617

1333. Ballesteros, Jensen, Liapakis. Activation of the β2-adrenergic receptor involves disruption of an ionic lock between the cytoplasmic ends of transmembrane segments 3 and 6. Boll Soc Ital Biol Sper. Available: https://www.jbc.org/article/S0021-9258(20)80383-4/abstract

1334. Vogel R, Mahalingam M, Lüdeke S, Huber T, Siebert F, Sakmar TP. Functional role of the “ionic lock”--an interhelical hydrogen-bond network in family A heptahelical receptors. J Mol Biol. 2008;380: 648–655. doi:10.1016/j.jmb.2008.05.022

1335. Han X, Feng Y, Chen X, Gerard C, Boisvert WA. Characterization of G protein coupling mediated by the conserved D134(3.49) of DRY motif, M241(6.34), and F251(6.44) residues on human CXCR1. FEBS Open Bio. 2015;5: 182–190. doi:10.1016/j.fob.2015.03.001

1336. Fleetwood O, Matricon P, Carlsson J, Delemotte L. Energy Landscapes Reveal Agonist Control of G Protein-Coupled Receptor Activation via Microswitches. Biochemistry. 2020;59: 880–891. doi:10.1021/acs.biochem.9b00842

1337. Latorraca NR, Venkatakrishnan AJ, Dror RO. GPCR Dynamics: Structures in Motion. Chem Rev. 2017;117: 139–155. doi:10.1021/acs.chemrev.6b00177

1338. Fleetwood O, Carlsson J, Delemotte L. Identification of ligand-specific G protein-coupled receptor states and prediction of downstream efficacy via data-

driven modeling. Elife. 2021;10. doi:10.7554/eLife.60715

1339. Lu S, He X, Yang Z, Chai Z, Zhou S, Wang J, et al. Activation pathway of a G protein-coupled receptor uncovers conformational intermediates as targets for allosteric drug design. Nature Communications. 2021. doi:10.1038/s41467-021-25020-9

1340. Floresca CZ, Schetz JA. Dopamine receptor microdomains involved in molecular recognition and the regulation of drug affinity and function. J Recept Signal Transduct Res. 2004;24: 207–239. doi:10.1081/rrs-200032088

1341. Ranganathan A, Dror RO, Carlsson J. Insights into the Role of Asp792.50 in β2 Adrenergic Receptor Activation from Molecular Dynamics Simulations. Biochemistry. 2014. pp. 7283–7296. doi:10.1021/bi5008723

1342. Zou R, Wang X, Li S, Chan HCS, Vogel H, Yuan S. The role of metal ions in G protein-coupled receptor signalling and drug discovery. Wiley Interdiscip Rev Comput Mol Sci. 2022;12. doi:10.1002/wcms.1565

1343. Gutiérrez-de-Terán H, Massink A, Rodríguez D, Liu W, Han GW, Joseph JS, et al. The Role of a Sodium Ion Binding Site in the Allosteric Modulation of the A2A Adenosine G Protein-Coupled Receptor. Structure. 2013;21: 2175–2185. doi:10.1016/j.str.2013.09.020

1344. Miller-Gallacher JL, Nehmé R, Warne T, Edwards PC, Schertler GFX, Leslie AGW, et al. The 2.1 Å resolution structure of cyanopindolol-bound β1-adrenoceptor identifies an intramembrane Na+ ion that stabilises the ligand-free receptor. PLoS One. 2014;9: e92727. doi:10.1371/journal.pone.0092727

1345. Dror RO, Arlow DH, Maragakis P, Mildorf TJ, Pan AC, Xu H, et al. Activation mechanism of the β2-adrenergic receptor. Proc Natl Acad Sci U S A. 2011;108: 18684–18689. doi:10.1073/pnas.1110499108

1346. Gorinski N, Kowalsman N, Renner U, Wirth A, Reinartz MT, Seifert R, et al. Computational and Experimental Analysis of the Transmembrane Domain 4/5 Dimerization Interface of the Serotonin 5-HT1A Receptor. Mol Pharmacol. 2012;82: 448–463. doi:10.1124/mol.112.079137

1347. Prasanna X, Sengupta D, Chattopadhyay A. Cholesterol-dependent Conformational Plasticity in GPCR Dimers. Sci Rep. 2016;6: 31858. doi:10.1038/srep31858

1348. Carrillo JJ, López-Giménez JF, Milligan G. Multiple Interactions between Transmembrane Helices Generate the Oligomeric α1b-Adrenoceptor. Molecular Pharmacology. 2004. pp. 1123–1137. doi:10.1124/mol.104.001586

1349. Lopez-Gimenez JF, Canals M, Pediani JD, Milligan G. The α1b-Adrenoceptor Exists as a Higher-Order Oligomer: Effective Oligomerization Is Required for Receptor Maturation, Surface Delivery, and Function. Mol Pharmacol. 2007;71:

1015–1029. doi:10.1124/mol.106.033035

1350. Mancia F, Assur Z, Herman AG, Siegel R, Hendrickson WA. Ligand sensitivity in dimeric associations of the serotonin 5HT2c receptor. EMBO Rep. 2008;9: 363–369. doi:10.1038/embor.2008.27

1351. Huang J, Chen S, Zhang JJ, Huang X-Y. Crystal structure of oligomeric β1-adrenergic G protein–coupled receptors in ligand-free basal state. Nat Struct Mol Biol. 2013;20: 419–425. doi:10.1038/nsmb.2504

1352. Filizola M. Increasingly accurate dynamic molecular models of G-protein coupled receptor oligomers: Panacea or Pandora's box for novel drug discovery? Life Sci. 2010;86: 590–597. doi:10.1016/j.lfs.2009.05.004

1353. Perreault ML, Hasbi A, O'Dowd BF, George SR. Heteromeric dopamine receptor signaling complexes: emerging neurobiology and disease relevance. Neuropsychopharmacology. 2014;39: 156–168. doi:10.1038/npp.2013.148

1354. Liu J, Tang H, Xu C, Zhou S, Zhu X, Li Y, et al. Biased signaling due to oligomerization of the G protein-coupled platelet-activating factor receptor. Nat Commun. 2022;13: 6365. doi:10.1038/s41467-022-34056-4

1355. Wu B, Chien EYT, Mol CD, Fenalti G, Liu W, Katritch V, et al. Structures of the CXCR4 chemokine GPCR with small-molecule and cyclic peptide antagonists. Science. 2010;330: 1066–1071. doi:10.1126/science.1194396

1356. Guidolin D, Marcoli M, Tortorella C, Maura G, Agnati LF. G protein-coupled receptor-receptor interactions give integrative dynamics to intercellular communication. Rev Neurosci. 2018;29: 703–726. doi:10.1515/revneuro-2017-0087

1357. Dijkman PM, Castell OK, Goddard AD, Munoz-Garcia JC, de Graaf C, Wallace MI, et al. Dynamic tuneable G protein-coupled receptor monomer-dimer populations. Nat Commun. 2018;9: 1710. doi:10.1038/s41467-018-03727-6

1358. Cordomí A, Navarro G, Aymerich MS, Franco R. Structures for G-Protein-Coupled Receptor Tetramers in Complex with G Proteins. Trends Biochem Sci. 2015;40: 548–551. doi:10.1016/j.tibs.2015.07.007

1359. Vafabakhsh R, Levitz J, Isacoff EY. Conformational dynamics of a class C G-protein-coupled receptor. Nature. 2015;524: 497–501. doi:10.1038/nature14679

1360. Pulido D, Casadó-Anguera V, Pérez-Benito L, Moreno E, Cordomí A, López L, et al. Design of a True Bivalent Ligand with Picomolar Binding Affinity for a G Protein-Coupled Receptor Homodimer. J Med Chem. 2018;61: 9335–9346. doi:10.1021/acs.jmedchem.8b01249

1361. Gahbauer S, Böckmann RA. Membrane-Mediated Oligomerization of G Protein Coupled Receptors and Its Implications for GPCR Function. Front Physiol. 2016;7: 494. doi:10.3389/fphys.2016.00494

1362. Gurevich VV, Gurevich EV. How and why do GPCRs dimerize? Trends Pharmacol Sci. 2008;29: 234–240. doi:10.1016/j.tips.2008.02.004

1363. Jackson SN, Wang H-YJ, Yergey A, Woods AS. Phosphate stabilization of intermolecular interactions. J Proteome Res. 2006;5: 122–126. doi:10.1021/pr0503578

1364. Woods AS, Ferré S. Amazing stability of the arginine-phosphate electrostatic interaction. J Proteome Res. 2005;4: 1397–1402. doi:10.1021/pr050077s

1365. Johnston JM, Aburi M, Provasi D, Bortolato A, Urizar E, Lambert NA, et al. Making structural sense of dimerization interfaces of delta opioid receptor homodimers. Biochemistry. 2011;50: 1682–1690. doi:10.1021/bi101474v

1366. Teng X, Chen S, Wang Q, Chen Z, Wang X, Huang N, et al. Structural insights into G protein activation by D1 dopamine receptor. Sci Adv. 2022;8: eabo4158. doi:10.1126/sciadv.abo4158

1367. Borroto-Escuela DO, Romero-Fernandez W, Tarakanov AO, Gómez-Soler M, Corrales F, Marcellino D, et al. Characterization of the A2AR–D2R interface: Focus on the role of the C-terminal tail and the transmembrane helices. Biochem Biophys Res Commun. 2010;402: 801–807. doi:10.1016/j.bbrc.2010.10.122

1368. Perreault ML, Hasbi A, Alijaniaram M, Fan T, Varghese G, Fletcher PJ, et al. The Dopamine D1-D2 Receptor Heteromer Localizes in Dynorphin/Enkephalin Neurons. Journal of Biological Chemistry. 2010. pp. 36625–36634. doi:10.1074/jbc.m110.159954

1369. Brock C, Oueslati N, Soler S, Boudier L, Rondard P, Pin J-P. Activation of a dimeric metabotropic glutamate receptor by intersubunit rearrangement. J Biol Chem. 2007;282: 33000–33008. doi:10.1074/jbc.M702542200

1370. Caniceiro AB, Bueschbell B, Barreto CAV, Preto AJ, Moreira IS. MUG: a mutation overview of GPCR subfamily A17 receptors. Computational and Structural Biotechnology Journal. 2022. doi:10.1016/j.csbj.2022.12.031

1371. Zhang R, Li D, Mao H, Wei X, Xu M, Zhang S, et al. Disruption of 5-hydroxytryptamine 1A receptor and orexin receptor 1 heterodimer formation affects novel G protein-dependent signaling pathways and has antidepressant effects in vivo. Transl Psychiatry. 2022;12: 122. doi:10.1038/s41398-022-01886-1

1372. Lira SS, Ahammad I. A comprehensive in silico investigation into the nsSNPs of Drd2 gene predicts significant functional consequences in dopamine signaling and pharmacotherapy. Sci Rep. 2021;11: 23212. doi:10.1038/s41598-021-02715-z

1373. Mondal S, Johnston JM, Wang H, Khelashvili G, Filizola M, Weinstein H. Membrane driven spatial organization of GPCRs. Sci Rep. 2013;3: 2909. doi:10.1038/srep02909

1374. Sankararamakrishnan R, Weinstein H. Positioning and Stabilization of

Dynorphin Peptides in Membrane Bilayers: the Mechanistic Role of Aromatic and Basic Residues Revealed from Comparative MD Simulations. The Journal of Physical Chemistry B. 2002. pp. 209–218. doi:10.1021/jp012174o

1375. Ma X, Hu Y, Batebi H, Heng J, Xu J, Liu X, et al. Analysis of β2AR-Gs and β2AR-Gi complex formation by NMR spectroscopy. Proc Natl Acad Sci U S A. 2020;117: 23096–23105. doi:10.1073/pnas.2009786117

1376. Wang X, Cheng X, Zhao L, Wang Y, Ye C, Zou X, et al. Molecular insights into differentiated ligand recognition of the human parathyroid hormone receptor 2. Proc Natl Acad Sci U S A. 2021;118. doi:10.1073/pnas.2101279118

1377. Ma X, Segura MA, Zarzycka B, Vischer HF, Leurs R. Analysis of Missense Variants in the Human Histamine Receptor Family Reveals Increased Constitutive Activity of E4106.30×30K Variant in the Histamine H1 Receptor. Int J Mol Sci. 2021;22. doi:10.3390/ijms22073702

1378. Cai X, Wang D, Zhang R, Chen Y, Chen J. The transmembrane domains of GPCR dimers as targets for drug development. Drug Discov Today. 2022;28: 103419. doi:10.1016/j.drudis.2022.103419

1379. Lipiński PFJ, Jarończyk M, Dobrowolski JC, Sadlej J. Molecular dynamics of fentanyl bound to μ-opioid receptor. J Mol Model. 2019;25: 144. doi:10.1007/s00894-019-3999-2

1380. Zou Y, Ewalt J, Ng H-L. Recent Insights from Molecular Dynamics Simulations for G Protein-Coupled Receptor Drug Discovery. Int J Mol Sci. 2019;20. doi:10.3390/ijms20174237

1381. Wu Y, Li X, Hua T, Liu Z-J, Liu H, Zhao S. MD Simulations Revealing Special Activation Mechanism of Cannabinoid Receptor 1. Front Mol Biosci. 2022;9: 860035. doi:10.3389/fmolb.2022.860035

1382. Preto AJ, Barreto CAV, Baptista SJ, Almeida JG de, Lemos A, Melo A, et al. Understanding the Binding Specificity of G-Protein Coupled Receptors toward G-Proteins and Arrestins: Application to the Dopamine Receptor Family. J Chem Inf Model. 2020;60: 3969–3984. doi:10.1021/acs.jcim.0c00371

1383. Staus DP, Hu H, Robertson MJ, Kleinhenz ALW, Wingler LM, Capel WD, et al. Structure of the M2 muscarinic receptor-β-arrestin complex in a lipid nanodisc. Nature. 2020;579: 297–302. doi:10.1038/s41586-020-1954-0

1384. Humphrey W, Dalke A, Schulten K. VMD: visual molecular dynamics. J Mol Graph. 1996;14: 33–8, 27–8. doi:10.1016/0263-7855(96)00018-5

1385. Kaufmann KW, Lemmon GH, Deluca SL, Sheehan JH, Meiler J. Practically useful: what the Rosetta protein modeling suite can do for you. Biochemistry. 2010;49: 2987–2998. doi:10.1021/bi902153g

1386. Prodigy Webserver. [cited 7 Jul 2022]. Available:

https://bianca.science.uu.nl/prodigy/

1387. Vangone A, Bonvin AM. Contacts-based prediction of binding affinity in protein-protein complexes. Elife. 2015;4: e07454. doi:10.7554/eLife.07454

1388. Lomize MA, Pogozheva ID, Joo H, Mosberg HI, Lomize AL. OPM database and PPM web server: resources for positioning of proteins in membranes. Nucleic Acids Res. 2012;40: D370–6. doi:10.1093/nar/gkr703

1389. Jo S, Kim T, Iyer VG, Im W. CHARMM-GUI: a web-based graphical user interface for CHARMM. J Comput Chem. 2008;29: 1859–1865. doi:10.1002/jcc.20945

1390. Lee J, Cheng X, Jo S, MacKerell AD, Klauda JB, Im W. CHARMM-GUI Input Generator for NAMD, Gromacs, Amber, Openmm, and CHARMM/OpenMM Simulations using the CHARMM36 Additive Force Field. Biophysical Journal. 2016. p. 641a. doi:10.1016/j.bpj.2015.11.3431

1391. Wu EL, Cheng X, Jo S, Rui H, Song KC, Dávila-Contreras EM, et al. CHARMM-GUI Membrane Builder toward realistic biological membrane simulations. J Comput Chem. 2014;35: 1997–2004. doi:10.1002/jcc.23702

1392. Jo S, Cheng X, Islam SM, Huang L, Rui H, Zhu A, et al. Chapter Eight - CHARMM-GUI PDB Manipulator for Advanced Modeling and Simulations of Proteins Containing Nonstandard Residues. In: Karabencheva-Christova T, editor. Advances in Protein Chemistry and Structural Biology. Academic Press; 2014. pp. 235–265. doi:10.1016/bs.apcsb.2014.06.002

1393. Kim S, Lee J, Jo S, Brooks CL 3rd, Lee HS, Im W. CHARMM-GUI ligand reader and modeler for CHARMM force field generation of small molecules. J Comput Chem. 2017;38: 1879–1886. doi:10.1002/jcc.24829

1394. Brooks BR, Brooks CL 3rd, Mackerell AD Jr, Nilsson L, Petrella RJ, Roux B, et al. CHARMM: the biomolecular simulation program. J Comput Chem. 2009;30: 1545–1614. doi:10.1002/jcc.21287

1395. Lindahl E, Hess B, van der Spoel D. GROMACS 3.0: a package for molecular simulation and trajectory analysis. Molecular modeling annual. 2001;7: 306–317. doi:10.1007/s008940100045

1396. Bussi G, Donadio D, Parrinello M. Canonical sampling through velocity rescaling. J Chem Phys. 2007;126: 014101. doi:10.1063/1.2408420

1397. Nosé S, Klein ML. Constant pressure molecular dynamics for molecular systems. Mol Phys. 1983;50: 1055–1076. doi:10.1080/00268978300102851

1398. Parrinello M, Rahman A. Polymorphic transitions in single crystals: A new molecular dynamics method. J Appl Phys. 1981;52: 7182–7190. doi:10.1063/1.328693

1399. Páll S, Hess B. A flexible algorithm for calculating pair interactions on SIMD architectures. Comput Phys Commun. 2013;184: 2641–2650. doi:10.1016/j.cpc.2013.06.003

1400. Luenberger DG, Ye Y. Linear and Nonlinear Programming. Springer International Publishing; doi:10.1007/978-3-030-85450-8

1401. De Las Rivas J, Alonso-López D, Arroyo MM. Human Interactomics: Comparative Analysis of Different Protein Interaction Resources and Construction of a Cancer Protein-Drug Bipartite Network. Adv Protein Chem Struct Biol. 2018;111: 263–282. doi:10.1016/bs.apcsb.2017.09.002

1402. Szklarczyk D, Kirsch R, Koutrouli M, Nastou K, Mehryary F, Hachilif R, et al. The STRING database in 2023: protein-protein association networks and functional enrichment analyses for any sequenced genome of interest. Nucleic Acids Res. 2023;51: D638–D646. doi:10.1093/nar/gkac1000

1403. Burke DF, Bryant P, Barrio-Hernandez I, Memon D, Pozzati G, Shenoy A, et al. Towards a structurally resolved human protein interaction network. Nat Struct Mol Biol. 2023;30: 216–225. doi:10.1038/s41594-022-00910-8

1404. Martinez-Garcia M, Trujillo-Tiebas MJ, Villaverde C, López-Martínez MA, Ayuso C. Novel human pathological mutations. Gene symbol: OA1. Disease: albinism, ocular. Hum Genet. 2009;125: 349. Available: https://www.ncbi.nlm.nih.gov/pubmed/19320034

1405. Young A, Powelson EB, Whitney IE, Raven MA, Nusinowitz S, Jiang M, et al. Involvement of OA1, an intracellular GPCR, and G alpha i3, its binding protein, in melanosomal biogenesis and optic pathway formation. Invest Ophthalmol Vis Sci. 2008;49: 3245–3252. doi:10.1167/iovs.08-1806

1406. Goshima Y, Masukawa D, Kasahara Y, Hashimoto T, Aladeokin AC. l-DOPA and Its Receptor GPR143: Implications for Pathogenesis and Therapy in Parkinson's Disease. Front Pharmacol. 2019;10: 1119. doi:10.3389/fphar.2019.01119

1407. Strange PG. Oligomers of D2 dopamine receptors. J Mol Neurosci. 2005;26: 155–160. doi:10.1385/JMN:26:2-3:155

1408. Kasai RS, Kusumi A. Single-molecule imaging revealed dynamic GPCR dimerization. Current Opinion in Cell Biology. 2014. pp. 78–86. doi:10.1016/j.ceb.2013.11.008

1409. Hern JA, Baig AH, Mashanov GI, Birdsall B, Corrie JET, Lazareno S, et al. Formation and dissociation of M1 muscarinic receptor dimers seen by total internal reflection fluorescence imaging of single molecules. Proc Natl Acad Sci U S A. 2010;107: 2693–2698. doi:10.1073/pnas.0907915107

1410. Kasai RS, Suzuki KGN, Prossnitz ER, Koyama-Honda I, Nakada C, Fujiwara

TK, et al. Full characterization of GPCR monomer–dimer dynamic equilibrium by single molecule imaging. J Cell Biol. 2011;192: 463–480. doi:10.1083/jcb.201009128

1411. Tabor A, Weisenburger S, Banerjee A, Purkayastha N, Kaindl JM, Hübner H, et al. Visualization and ligand-induced modulation of dopamine receptor dimerization at the single molecule level. Sci Rep. 2016;6: 33233. doi:10.1038/srep33233

1412. Sun Y, Huang J, Xiang Y, Bastepe M, Jüppner H, Kobilka BK, et al. Dosage-dependent switch from G protein-coupled to G protein-independent signaling by a GPCR. EMBO J. 2007;26: 53–64. doi:10.1038/sj.emboj.7601502

1413. Rovira X, Pin J-P, Giraldo J. The asymmetric/symmetric activation of GPCR dimers as a possible mechanistic rationale for multiple signalling pathways. Trends Pharmacol Sci. 2010;31: 15–21. doi:10.1016/j.tips.2009.10.008

1414. Zhou B, Giraldo J. An operational model for GPCR homodimers and its application in the analysis of biased signaling. Drug Discov Today. 2018;23: 1591–1595. doi:10.1016/j.drudis.2018.04.004

1415. Schwartz TW, Frimurer TM, Holst B, Rosenkilde MM, Elling CE. Molecular mechanism of 7TM receptor activation--a global toggle switch model. Annu Rev Pharmacol Toxicol. 2006;46: 481–519. doi:10.1146/annurev.pharmtox.46.120604.141218

1416. Shi L, Liapakis G, Xu R, Guarnieri F, Ballesteros JA, Javitch JA. Beta2 adrenergic receptor activation. Modulation of the proline kink in transmembrane 6 by a rotamer toggle switch. J Biol Chem. 2002;277: 40989–40996. doi:10.1074/jbc.M206801200

1417. Mertz B, Struts AV, Feller SE, Brown MF. Molecular simulations and solid-state NMR investigate dynamical structure in rhodopsin activation. Biochim Biophys Acta. 2012;1818: 241–251. doi:10.1016/j.bbamem.2011.08.003

1418. Kling RC, Tschammer N, Lanig H, Clark T, Gmeiner P. Active-state model of a dopamine D2 receptor-Gαi complex stabilized by aripiprazole-type partial agonists. PLoS One. 2014;9: e100069. doi:10.1371/journal.pone.0100069

1419. Plazinska A, Plazinski W, Luchowski R, Wnorowski A, Grudzinski W, Gruszecki WI. Ligand-induced action of the W2866.48 rotamer toggle switch in the β2-adrenergic receptor. Phys Chem Chem Phys. 2017;20: 581–594. doi:10.1039/c7cp04808d

6. Appendices

6.1. Additional introductory information on: The world of GPCR dimers - mapping dopamine receptor D2 homodimers in different activation states and configuration arrangements

In contrast to the proposed TM4-TM5-TM4-TM5 interface firstly described by Guo et al. (Guo, Shi, and Javitch 2003; Guo et al. 2005), a study by Wouters et al. (2019) used complementation-based NanoLuciferase® Binary Technology (NanoBiT® assay) to investigate the effect of antagonists on the formation of D_2R-homodimers (D_{2long}), with a focus on the TM5-TM6-TM5-TM6 interface (Wouters et al. 2019). Dimer formation was observed over time in the presence of spiperones. Although the D_{2long} dimer was significantly decreased by 40-60% in real time, $A_{2A}R$-D_{2long}-dimer formation was not altered. The other antagonists (clozapine, risperidone, and droperidol) appeared to have no effect. In molecular modelling studies, Tyr199$^{5.48}$ and Phe390$^{6.52}$ were found to be crucial residues that may determine D_2R-homodimerization (Wouters et al. 2019). This was further supported by a study by Guitart et al. showing that D_1R-homodimerization was reduced by D_1R TM5- or TM6-derived single peptides (Guitart et al. 2014). Therefore, a potential TM5-TM6-TM5-TM6 interface is also possible in The D_2R-homodimer, as has been reported for other GPCRs (Wouters et al. 2019). The D_2R-homodimer without a bound antagonist was modelled from the original crystal structure with a TM5-TM6-TM5-TM6 interface and was used for protein docking studies (Pulido et al. 2018). When the model was subjected to MD, rapid cis to trans conversion occurred at Tyr199$^{5.48}$, and Phe390$^{6.52}$, suggesting that these residues were relevant for the D_2R-homodimer interface. The removal of these aromatic interactions (by alanine mutation) results in a less favorable average interface energy (Guitart et al. 2014).

An *in silico* study by Kaczor et al. generated a D_2R-homodimer model with a TM4-TM5-TM7-TM1 interface to investigate the role of homo-bivalent antagonists (Kaczor, Jörg, and Capuano 2016). They developed a protocol for building dimers suitable for molecular dynamics simulations and ligand docking, which we used as the basis of our study (Kaczor et al. 2015; Kaczor, Jörg, and Capuano 2016). Multiple higher-order D_2R oligomers consisting of at least four monomers were reported in combined Forster Resonance Energy Transfer (FRET) and Bioluminescence Resonance Energy Transfer (BRET) assays (Wouters et al. 2019; Guo et al. 2008; Strange 2005). These findings support the hypothesis that D_2R can undergo multiple cycles of monomeric and dimeric states at different interfaces (Wouters et al. 2019; Kasai and Kusumi 2014). The dimerization process itself should be considered a dynamic process between monomers and dimers, suggesting that this process is transient (Kasai and Kusumi 2014; Kasai et al. 2018).

The nature of GPCR dimers has been described as dynamic and fast-moving, and whether the formation of such dimers is transient or constitutive has been controversial and might be different for different GPCRs (Guo, Shi, and Javitch 2003; Kasai et al. 2018;

Ng et al. 1996). Previous studies showed that the half-life of a dimer was approximately $t_{1/2}$= 0.1–5.0 s (Hern et al. 2010; Kasai et al. 2011; Calebiro et al. 2013; Dijkman et al. 2018) and that there can be an equilibrium between monomeric and dimeric species (Tabor et al. 2016). It is known to D_2R forms transient homodimers that could be prolonged in their lifetime by a factor of 1.5 upon agonist binding (e.g., dopamine, quinpirole) (Kasai et al. 2018). Although it has been reported for several heterodimers that partnered monomers can have different conformations to pharmacologically influence one another, this has not yet been well described for homodimers (Caniceiro et al. 2022; Cordomí et al. 2020). Nevertheless, some theoretical models attempt to explain the phenomenon of biphasic curves for the same receptor and ligand by homodimerization (Sun et al. 2007; Rovira, Pin, and Giraldo 2010; B. Zhou and Giraldo 2018).

2. Results

2.1. Predicted interface in models

The entire subset of very frequent residues was found in the **in-in** configuration in both monomers as well as in the **in-monomer** of the **in-ar** configuration. Fewest ac monomers were also found. The other symmetric dimer configuration, **ar-ar**, lacked Ile$^{3.48}$, Tyr$^{3.51}$, Thr$^{3.52}$, Ala$^{3.55}$, Val$^{5.49}$, Ile$^{5.52}$, Val$^{5.53}$, and Leu$^{5.56}$ in one monomer and Ala$^{3.55}$, Arg$^{4.40}$, Val$^{4.44}$, Ile$^{4.48}$, Leu$^{4.52}$, and Thr$^{4.55}$. Different situations were observed for asymmetric dimer configurations. For the **in-ar** configuration, all 19 very frequent residues were found in the **in-monomer**; only Val$^{4.44}$, Thr$^{4.55}$ and Pro$^{4.59}$ were found on the **ar-monomer**. This was also true for the **in-monomer ac-in** configuration, except for Ile$^{3.48}$, Thr$^{3.52}$, Thr$^{4.55}$, Pro$^{4.59}$, and Val$^{5.53}$. None of the 19 residues were found in the **ac-monomer**. Finally, the **ac monomer** lacked Tyr$^{3.51}$, Thr$^{3.52}$, Ile$^{4.48}$, Thr$^{4.55}$, Ile$^{5.52}$, Val$^{5.53}$, and Leu$^{5.56}$, whereas the **ar monomer** lacked Arg$^{4.40}$, Va$^{4.44}$l, and Ile$^{5.52}$.

Guo et al. did not specify if Cys$^{4.58}$ was found for both monomers and if the presence of one was sufficient for crosstalk (Guo et al. 2005). Interestingly, Cys$^{4.58}$ was only considered 1x an interfacial residue for the **ac-** and **ar-monomers** (**Table S2**). Regarding other residues suggested by Guo et al., Pro$^{4.59}$, Thr$^{4.55}$, Val$^{4.51}$, Ile$^{4.48}$, Val$^{4.44}$, and Arg$^{4.41}$ were found to be present in the inactive conformation, whereas Cys$^{4.58}$, Phe$^{4.54}$, Trp$^{4.50}$, Ser$^{4.47}$, Thr$^{4.43}$, and Arg$^{4.40}$ were proposed for the active conformation of the dimer (Guo et al. 2005).

The pattern of amino acids assigned to the inactive conformation (Pro$^{4.59}$, Thr$^{4.55}$, Val$^{4.51}$, Ile$^{4.48}$, Val$^{4.44}$, and Arg$^{4.41}$) was found for both monomers in the **in-in** conformation, the **in-monomer** of the **ac-in** dimer (only comprising Arg$^{4.41}$, Val$^{4.44}$, and Ile$^{4.48}$), and the **in-monomer** of the **in-ar** configuration (only Val$^{4.51}$ missing) (**Table S2**). Furthermore, **ar-ar** comprised one monomer with all six residues, whereas the other monomer possessed only Arg$^{4.41}$ and Pro$^{4.59}$. The **ar-monomers** of the **in-ar** accounted for Val$^{4.44}$, Val$^{4.51}$, Thr$^{4.55}$, and Pro$^{4.59}$. The **ac-ar** showed four residues in each monomer (Arg$^{4.41}$, Val$^{4.44}$, Val$^{4.51}$, Thr$^{4.55}$ in the **ac-monomer**; Arg$^{4.41}$, Ile$^{4.48}$, Thr$^{4.55}$, and Pro$^{4.59}$ in the **ar-monomer**). One monomer of the **ac-ac** dimer comprised all six residues, while the other comprised Val$^{4.44}$, Ile$^{4.48}$, Thr$^{4.55}$, and Pro$^{4.59}$. Interestingly, the **ac-monomer** in the **ac-in**

configuration appeared to be the only monomer without any residues assigned to the inactive conformation.

The active set of amino acids was described by Guo et al. (Cys$^{4.58}$, Phe$^{4.54}$, Trp$^{4.50}$, Ser$^{4.47}$, Thr$^{4.43}$, and Arg$^{4.40}$) and only five were found per monomer (**Table S2**) (Guo et al. 2005). In the **ac-ar** dimer, Arg$^{4.40}$, Phe$^{4.54}$ and Cys$^{4.58}$ were found on the **ac-monomer**. The **ac-monomer** in **ac-in** contains Thr$^{4.43}$, Ser$^{4.47}$, Trp$^{4.50}$, and Phe$^{4.54}$. The **in-in** dimer contains Arg$^{4.40}$ (2x), Thr$^{4.43}$ (2x), and Ser$^{4.47}$. Arg$^{4.40}$ was also found in one monomer of **ar-ar**, in the **in-monomer** of **ac-in**, and in the **in-ar** dimer. All six residues were found in the ar-monomer of in-ar, except for Arg$^{4.40}$. Finally, Cys$^{4.58}$ was found in the **ar-monomer** of the **ac-ar** configuration.

2.2. The D_2R-homodimer interface

2.2.1. Interaction type established for the different interfaces

For the in-in configuration, H-bond contacts were distributed along TM4-ICL2, ICL2-ICL2, TM3-TM4, ECL2-ECL3, ICL2-TM6, and ECL3-ECL2 with an occurrence of 5-22% (first structure from monomer 1, second structure from monomer 2; M1-M2). Regarding salt bridges, 75% occurred between TM4-TM3 and 25% between TM3-TM4. π-cation interactions for the in-in configuration were found between ECL3-ECL2, ECL2-ECL3, TM4-ICL2, ICL2-ICL2 and ICL2-TM6, ranging from 14-36%, while π-stacking interactions were mainly found between ICL2-ICL2 (66%) and ECL2-ECL3 (32%). In contrast, this was the case for T-stacking interactions, in which 64% occurred for ECL3-ECL2 and 33% for ICL2-ICL2.

In the **ar-ar** configuration, TM5 was involved in most of the interactions analyzed. No salt bridges were found for **ar-ar** and π-cation interactions, which were concentrated to 98% between ECL2-ECL3 and only 1-2% between TM4 and ECL3. π-stacking interactions were also concentrated between TM5-TM5 (95%), and few were found between ECL2-ECL3 (4%) and TM5-ECL2 (1%). T-stacking interactions were also found between TM5-TM5 (45%) and between ECL2-ECL3 (55%). Finally, H-bond interactions were mostly found for the TMs, particular between TM5-TM4, TM5-ECL2, TM5-TM5 and TM4-TM5, ranging from 15-29%.

No salt bridges were observed in the ac–ac configuration. However, H-bond interactions were widely distributed between TM4-TM3, TM4-ICL2, TM5-TM4, TM5-TM5, ECL2-TM5 and TM4-TM5, ranging between 6-29%. π-cation interactions were mostly concentrated in the ECL2-ECL3 regions (46%), with a few in ICL2-TM6 (23%) and TM3-TM4 (25%). Most π-stacking interactions could be determined between TM5-TM5 (60%) and TM5-ECL2 (34%), and very few could be determined between ECL2-ECL3 (2%) and TM4-TM5 (3%). The **in-ar** configuration formed dimer along TM3-TM4 and TM4-TM5. Hence, different areas were involved in the establishment of interfacial interactions. TM3-TM1, TM3-ICL1, TM4-ICL1, ECL2-TM4, ECL2-ECL2, and TM4-TM4 were relevant for establishing H-bonds, ranging between 9-17%. Salt bridges were mostly found between TM3-ICL1 (81%) and ECL3-TM3 (15%), ECL3-ECL2 (2%), TM6-ICL1 (1%) and TM4-ICL1 (1%). The π-cation interactions were mainly observed in ECL4-TM3 (81%), TM5-HX8 (27%), TM4-ICL2 (12%), and TM3-TM1 (13%). π-stacking interactions were located

between TM5-TM4 (75%) and ECL3-TM3 (25%). Finally, the T-stacking interactions involved 67% of TM5-ECL2 and 33% of TM5-TM4.

In the **ac-ar** configuration, a highly conserved salt bridge is found between TM4 and TM3. Furthermore, H-bond interactions were distributed along TM4-TM3 (41%), ECL2-ECL2 (23%) and TM5-ECL2 (23%), with few between TM4-TM5 (9%) and TM3-TM4 (8%). For this configuration, π-cation interactions were also found to be conserved between TM4-TM3 (73%) and TM3-TM4 (26%) and 1% between ICL2-TM5. For π-stacking interactions, 94% were found in ECL2-TM5, 5% in TM5-ECL2, and 1% were found in TM5-TM4. Finally, T-stacking interactions were distributed between TM5-TM4 (67%) and between ECL2-TM5 (33%).

The **ac-in** configuration possessed an interface comprising TM1-TM2-TM4-TM5. Relevant H-bonds were formed between HX8-TM5, ECL2-ECL2, ICL2-TM3, ICL2-ICL2, TM3-ECL2, TM2-TM3, TM2-ICL2, TM2-TM5, and TM1-TM3 (range 5-14%). TM1, TM2, and ICL2 from the **in-monomer** domain were the domains most involved in the establishment of H-bonds. Salt bridges could be determined not only between ICL2-TM3 (73%) but also between ICL1-TM5 (23%), TM3-ECL2 (24%), and some between ICL1-TM6 (1%) for the **ac-in**. π-cation interactions were mainly concentrated in ICL2-ICL2 (73%) but also–HX8-TM5 (24%), TM4-TM4 (1%) and TM1-TM5 (1%). Finally, π-stacking and T-stacking interactions were found between the same regions:70% or 60% between ICL2-ICL2 and 30% or 40% between ECL2-ECL2, respectively.

2.3. Macro- and microswitches upon dimerization

The activation mechanism of class A GPCRs has been intensively studied (Leioatts et al. 2014; Nygaard et al. 2009; Trzaskowski et al. 2012; Schwartz et al. 2006; Shi et al. 2002; Mertz et al. 2012), and was recently generalized and summarized in a holistic study by Zhou et al. (**Figure S8**) (Q. Zhou et al. 2019). According to Zhou et al., the GPCR class A activation mechanism involves 34 residue pairs, which rearrange known but spatially apart structural motifs such as CWxP, PIF, Na^+ pocket, NPxxY, and DRY, including the ionic lock (Q. Zhou et al. 2019). This conserved rearrangement of residue contacts takes place from the extracellular ligand-binding domain to the intracellular space where the G protein binds (Q. Zhou et al. 2019). Briefly: (i.) The conserved signal initiation step, where the CWxP motif (especially $Trp^{6.48}$) senses the binding of a ligand (also known as rotamer toggle switch),((Leioatts et al. 2014)) which then leads to a transmission switch by repacking the PIF motif (5.51, 6.44, 3.40) and collapse of the Na^+ pocket (2.50, 7.45, 3.39, 7.49); (ii.) Breaking of critical hydrophobic contacts, such as opening of the hydrophobic lock (3.43, 6.40, 6.41); (iii) rewiring of microswitch residues 6.37 and 7.53, (.) the release of 3.50 and G protein-contacting positions (5.61, 6.33, 3.54, and 3.53) to become prone to binding to the G protein (Figure 3 of (Q. Zhou et al. 2019)).

To further determine the conformational changes involving the outward movement of TM6, inward movement of TM7, and disruption of the ionic lock, the distances between the Cα atoms of residues $Arg^{3.50}$ and $Thr^{6.34}$ (TM3-TM6) and between $Ser^{5.46}$ and $Leu^{7.41}$ (TM5-TM7) were measured to determine their relevance in the activation process. Here, $Ser^{5.46}$ and $Leu^{7.41}$ were chosen because the inward movement of TM7 upon activation

also leads to a structural movement towards TM5 (Fleetwood et al. 2020). According to Fleetwood et al., ligand binding to 5.46 (in their work it was the catechol group of adrenaline binding to the β_2-adrenergic receptor that would form hydrogen bonds) leads to an inward bugle of TM5, causing structural rearrangement of the PIF motif and several other conserved motifs (Fleetwood et al. 2020). Additionally, the DRs residue $Ser^{5.46}$ is part of the conserved serine microdomain, which, together with $Ser^{5.42}$ and $Ser^{5.43}$, are known to form hydrogen bonds with the catechol hydroxyls of dopamine (Bueschbell et al. 2019; Floresca and Schetz 2004; Salmas et al. 2015; Kling et al. 2014). According to Fleetwood et al., micro-switching of residue 7.41 and approach towards TM5 leads to a conformational change in a so-called connector region involving the PIF motif (5.51-3.40-6.44) (Fleetwood et al. 2020)**.**

2.3.1. Outward movement of TM6, inward movement of TM7 and disruption of the ionic lock

The rotamer toggle switch of $Trp^{6.48}$ (part of the CWxP motif) and $Tyr^{7.53}$ (NPxxY) has been shown to result in a final outward movement of TM6 and inward movement of TM7 simultaneously after ligand binding (Plazinska et al. 2017; Bueschbell et al. 2019). The CWxP motif, carrying the conserved tryptophan 6.48 additionally is part of the binding pocket of many aminergic GPCRs, including DRs.(Floresca and Schetz 2004) This so-called aromatic microdomain sterically collapses uponligand bindingg and repacks intra-helical contacts between $Trp^{6.48}$ and $Phe^{6.44}$, increasingthe contact between $Ile^{3.40}$ and $Trp^{6.48}$ towards $Phe^{6.44}$, which then leads to rotation of the cytoplasmic end of TM6 and consequently to the disruption of the ionic lock involving $Arg^{3.50}$ and $Thr^{6.34}$ (Q. Zhou et al. 2019; Bueschbell et al. 2019; Ballesteros et al. 2001; Vogel et al. 2008). At the same time, the collapse of the Na^+ pocket would lead to tighter packing of the relevant residues ($Asp^{2.50}$, $Val^{3.29}$, $Asn^{7.45}$, $Asn^{7.49}$) and movement of TM7 towards TM3 and TM5 (Q. Zhou et al. 2019; Vogel et al. 2008). In our study, we captured this process by measuring the distances between the relevant residues on the different TMs.

References

Ballesteros, J. A., A. D. Jensen, G. Liapakis, S. G. Rasmussen, L. Shi, U. Gether, and J. A. Javitch. 2001. “Activation of the Beta 2-Adrenergic Receptor Involves Disruption of an Ionic Lock between the Cytoplasmic Ends of Transmembrane Segments 3 and 6.” *The Journal of Biological Chemistry* 276 (31): 29171–77.

Bueschbell, Beatriz, Carlos A. V. Barreto, António J. Preto, Anke C. Schiedel, and Irina S. Moreira. 2019. “A Complete Assessment of Dopamine Receptor- Ligand Interactions through Computational Methods.” *Molecules* 24 (7). https://doi.org/10.3390/molecules24071196.

Calebiro, Davide, Finn Rieken, Julia Wagner, Titiwat Sungkaworn, Ulrike Zabel, Alfio Borzi, Emanuele Cocucci, Alexander Zürn, and Martin J. Lohse. 2013. “Single-Molecule Analysis of Fluorescently Labeled G-Protein-Coupled Receptors Reveals Complexes with Distinct Dynamics and Organization.” *Proceedings of the National Academy of Sciences of the United States of America* 110 (2): 743–48.

Caniceiro, Ana B., Beatriz Bueschbell, Anke C. Schiedel, and Irina S. Moreira. 2022. “Class A and C GPCR Dimers in Neurodegenerative Diseases.” *Current Neuropharmacology*, March. https://doi.org/10.2174/1570159X20666220327221830.

Cordomí, Arnau, Gemma Navarro, Leonardo Pardo, and Rafael Franco. 2020. “Chapter 7 - Structure of G-Protein-Coupled Receptor Heteromers.” In *GPCRs*, edited by Beata Jastrzebska and Paul S-H Park, 109–19. Academic Press.

Dijkman, Patricia M., Oliver K. Castell, Alan D. Goddard, Juan C. Munoz-Garcia, Chris de Graaf, Mark I. Wallace, and Anthony Watts. 2018. “Dynamic Tuneable G Protein-Coupled Receptor Monomer-Dimer Populations.” *Nature Communications* 9 (1): 1710.

Fleetwood, Oliver, Pierre Matricon, Jens Carlsson, and Lucie Delemotte. 2020. “Energy Landscapes Reveal Agonist Control of G Protein-Coupled Receptor Activation via Microswitches.” *Biochemistry* 59 (7): 880–91.

Floresca, Christina Z., and John A. Schetz. 2004. “Dopamine Receptor Microdomains Involved in Molecular Recognition and the Regulation of Drug Affinity and Function.” *Journal of Receptor and Signal Transduction Research* 24 (3): 207–39.

Guitart, Xavier, Gemma Navarro, Estefania Moreno, Hideaki Yano, Ning-Sheng Cai, Marta Sánchez-Soto, Sandeep Kumar-Barodia, et al. 2014. “Functional Selectivity of Allosteric Interactions within G Protein-Coupled Receptor Oligomers: The Dopamine D1-D3 Receptor Heterotetramer.” *Molecular Pharmacology* 86 (4): 417–29.

Guo, Wen, Lei Shi, Marta Filizola, Harel Weinstein, and Jonathan A. Javitch. 2005. “Crosstalk in G Protein-Coupled Receptors: Changes at the Transmembrane Homodimer Interface Determine Activation.” *Proceedings of the National Academy of Sciences of the United States of America* 102 (48): 17495–500.

Guo, Wen, Lei Shi, and Jonathan A. Javitch. 2003. “The Fourth Transmembrane Segment Forms the Interface of the Dopamine D2 Receptor Homodimer.” *The Journal of Biological Chemistry* 278 (7): 4385–88.

Guo, Wen, Eneko Urizar, Michaela Kralikova, Juan Carlos Mobarec, Lei Shi, Marta Filizola, and Jonathan A. Javitch. 2008. “Dopamine D2 Receptors Form Higher Order Oligomers at Physiological Expression Levels.” *The EMBO Journal* 27 (17): 2293–2304.

Hern, Jonathan A., Asma H. Baig, Gregory I. Mashanov, Berry Birdsall, John E. T. Corrie, Sebastian Lazareno, Justin E. Molloy, and Nigel J. M. Birdsall. 2010. “Formation and Dissociation of M1 Muscarinic Receptor Dimers Seen by Total Internal Reflection Fluorescence Imaging of Single Molecules.” *Proceedings of the National Academy of Sciences of the United States of America* 107 (6): 2693–98.

Kaczor, Agnieszka A., Ramon Guixà-González, Pau Carrió, Antti Poso, Stefan Dove, Manuel Pastor, and Jana Selent. 2015. “Multi-Component Protein - Protein Docking Based Protocol with External Scoring for Modeling Dimers of G Protein-Coupled Receptors.” *Molecular Informatics* 34 (4): 246–55.

Kaczor, Agnieszka A., Manuela Jörg, and Ben Capuano. 2016. “The Dopamine D2 Receptor Dimer and Its Interaction with Homobivalent Antagonists: Homology Modeling, Docking and Molecular Dynamics.” *Journal of Molecular Modeling* 22 (9): 203.

Kasai, Rinshi S., Shuichi V. Ito, Ryo M. Awane, Takahiro K. Fujiwara, and Akihiro Kusumi. 2018. “The Class-A GPCR Dopamine D2 Receptor Forms Transient Dimers Stabilized by Agonists: Detection by Single-Molecule Tracking.” *Cell Biochemistry and Biophysics* 76 (1-2): 29–37.

Kasai, Rinshi S., and Akihiro Kusumi. 2014. “Single-Molecule Imaging Revealed Dynamic GPCR Dimerization.” *Current Opinion in Cell Biology*. https://doi.org/10.1016/j.ceb.2013.11.008.

Kasai, Rinshi S., Kenichi G. N. Suzuki, Eric R. Prossnitz, Ikuko Koyama-Honda, Chieko Nakada, Takahiro K. Fujiwara, and Akihiro Kusumi. 2011. “Full Characterization of GPCR Monomer–dimer Dynamic Equilibrium by Single Molecule Imaging.” *The Journal of Cell Biology* 192 (3): 463–80.

Kling, Ralf C., Nuska Tschammer, Harald Lanig, Timothy Clark, and Peter Gmeiner. 2014. “Active-State Model of a Dopamine D2 Receptor-Gαi Complex Stabilized by Aripiprazole-Type Partial Agonists.” *PloS One* 9 (6): e100069.

Leioatts, Nicholas, Pooja Suresh, Tod D. Romo, and Alan Grossfield. 2014. “Structure-Based Simulations Reveal Concerted Dynamics of GPCR Activation.” *Proteins* 82 (10): 2538–51.

Mertz, Blake, Andrey V. Struts, Scott E. Feller, and Michael F. Brown. 2012. “Molecular Simulations and Solid-State NMR Investigate Dynamical Structure in Rhodopsin Activation.” *Biochimica et Biophysica Acta* 1818 (2): 241–51.

Ng, G. Y., B. F. O’Dowd, S. P. Lee, H. T. Chung, M. R. Brann, P. Seeman, and S. R. George. 1996. “Dopamine D2 Receptor Dimers and Receptor-Blocking Peptides.” *Biochemical and Biophysical Research Communications* 227 (1): 200–204.

Nygaard, Rie, Thomas M. Frimurer, Birgitte Holst, Mette M. Rosenkilde, and Thue W. Schwartz. 2009. “Ligand Binding and Micro-Switches in 7TM Receptor Structures.” *Trends in Pharmacological Sciences* 30 (5): 249–59.

Plazinska, Anita, Wojciech Plazinski, Rafal Luchowski, Artur Wnorowski, Wojciech Grudzinski, and Wieslaw I. Gruszecki. 2017. “Ligand-Induced Action of the W2866.48 Rotamer Toggle Switch in the β2-Adrenergic Receptor.” *Physical Chemistry Chemical Physics: PCCP* 20 (1): 581–94.

Pulido, Daniel, Verònica Casadó-Anguera, Laura Pérez-Benito, Estefanía Moreno, Arnau Cordomí, Laura López, Antoni Cortés, et al. 2018. “Design of a True Bivalent Ligand with Picomolar Binding Affinity for a G Protein-Coupled Receptor Homodimer.” *Journal of Medicinal Chemistry* 61 (20): 9335–46.

Rovira, Xavier, Jean-Philippe Pin, and Jesús Giraldo. 2010. “The Asymmetric/symmetric Activation of GPCR Dimers as a Possible Mechanistic Rationale for Multiple Signalling Pathways.” *Trends in Pharmacological Sciences* 31 (1): 15–21.

Salmas, Ramin Ekhteiari, Mine Yurtsever, Matthias Stein, and Serdar Durdagi. 2015. “Modeling and Protein Engineering Studies of Active and Inactive States of Human Dopamine D2 Receptor (D2R) and Investigation of Drug/receptor Interactions.” *Molecular Diversity* 19 (2): 321–32.

Schwartz, Thue W., Thomas M. Frimurer, Birgitte Holst, Mette M. Rosenkilde, and Christian E. Elling. 2006. “Molecular Mechanism of 7TM Receptor Activation--a Global Toggle Switch Model.” *Annual Review of Pharmacology and Toxicology* 46: 481–519.

Shi, Lei, George Liapakis, Rui Xu, Frank Guarnieri, Juan A. Ballesteros, and Jonathan A. Javitch. 2002. “Beta2 Adrenergic Receptor Activation. Modulation of the Proline Kink in Transmembrane 6 by a Rotamer Toggle Switch.” *The Journal of Biological Chemistry* 277 (43): 40989–96.

Strange, Philip G. 2005. “Oligomers of D2 Dopamine Receptors.” *Journal of Molecular Neuroscience: MN* 26 (2): 155–60.

Sun, Yutong, Jianyun Huang, Yang Xiang, Murat Bastepe, Harald Jüppner, Brian K. Kobilka, J. Jillian Zhang, and Xin-Yun Huang. 2007. “Dosage-Dependent Switch from G Protein-Coupled to G Protein-Independent Signaling by a GPCR.” *The EMBO Journal* 26 (1): 53–64.

Tabor, Alina, Siegfried Weisenburger, Ashutosh Banerjee, Nirupam Purkayastha, Jonas M. Kaindl, Harald Hübner, Luxi Wei, et al. 2016. “Visualization and Ligand-Induced Modulation of Dopamine Receptor Dimerization at the Single Molecule Level.” *Scientific Reports* 6 (September): 33233.

Trzaskowski, B., D. Latek, S. Yuan, U. Ghoshdastider, A. Debinski, and S. Filipek. 2012. “Action of Molecular Switches in GPCRs--Theoretical and Experimental Studies.” *Current Medicinal Chemistry* 19 (8): 1090–1109.

Vogel, Reiner, Mohana Mahalingam, Steffen Lüdeke, Thomas Huber, Friedrich Siebert, and Thomas P. Sakmar. 2008. “Functional Role of the ‘Ionic Lock’--an Interhelical Hydrogen-Bond Network in Family A Heptahelical Receptors.” *Journal of Molecular Biology* 380 (4): 648–55.

Wouters, Elise, Adrián Ricarte Marín, James Andrew Rupert Dalton, Jesús Giraldo, and Christophe Stove. 2019. “Distinct Dopamine D_2 Receptor Antagonists Differentially Impact D_2 Receptor Oligomerization.” *International Journal of Molecular Sciences* 20 (7). https://doi.org/10.3390/ijms20071686.

Zhou, Bin, and Jesús Giraldo. 2018. “An Operational Model for GPCR Homodimers and Its Application in the Analysis of Biased Signaling.” *Drug Discovery Today* 23 (9): 1591–95.

Zhou, Qingtong, Dehua Yang, Meng Wu, Yu Guo, Wanjing Guo, Li Zhong, Xiaoqing Cai, et al. 2019. “Common Activation Mechanism of Class A GPCRs.” *eLife* 8 (December). https://doi.org/10.7554/eLife.50279

7. Supplemental material

7.1. Supplemental information of the research article: Evidence for Protein–Protein Interaction between Dopamine Receptors and the G Protein-Coupled Receptor 143

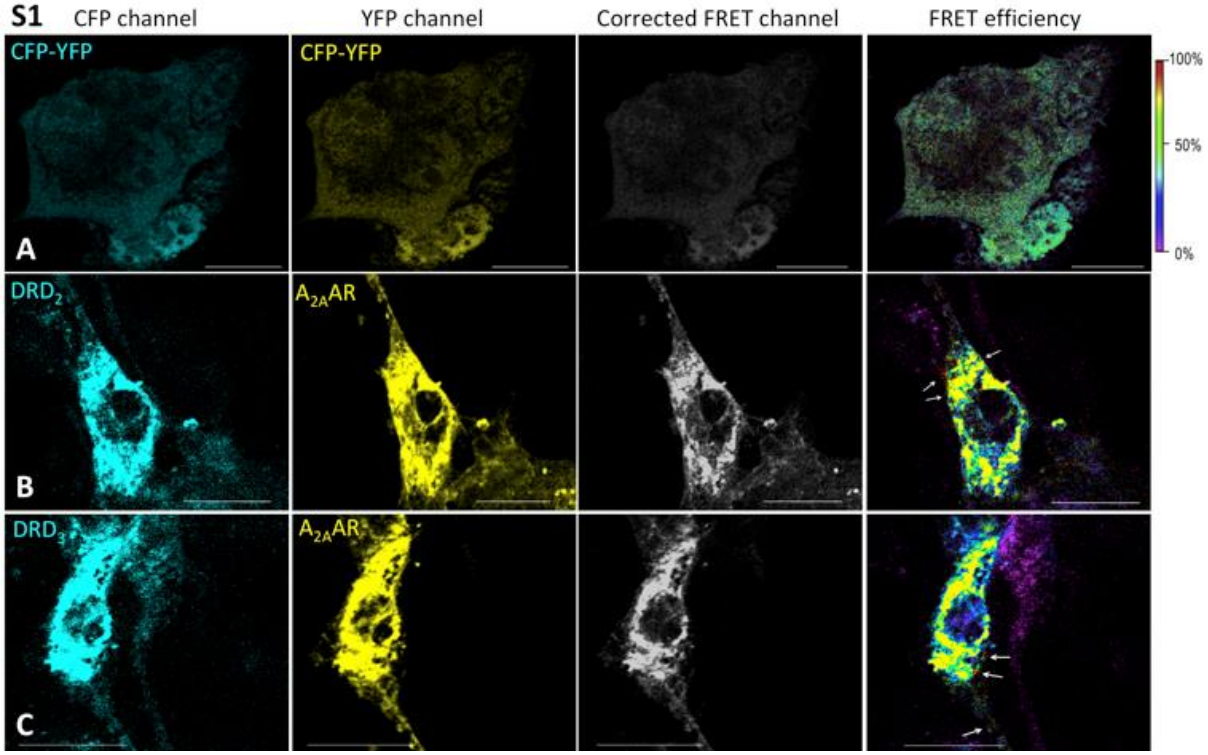

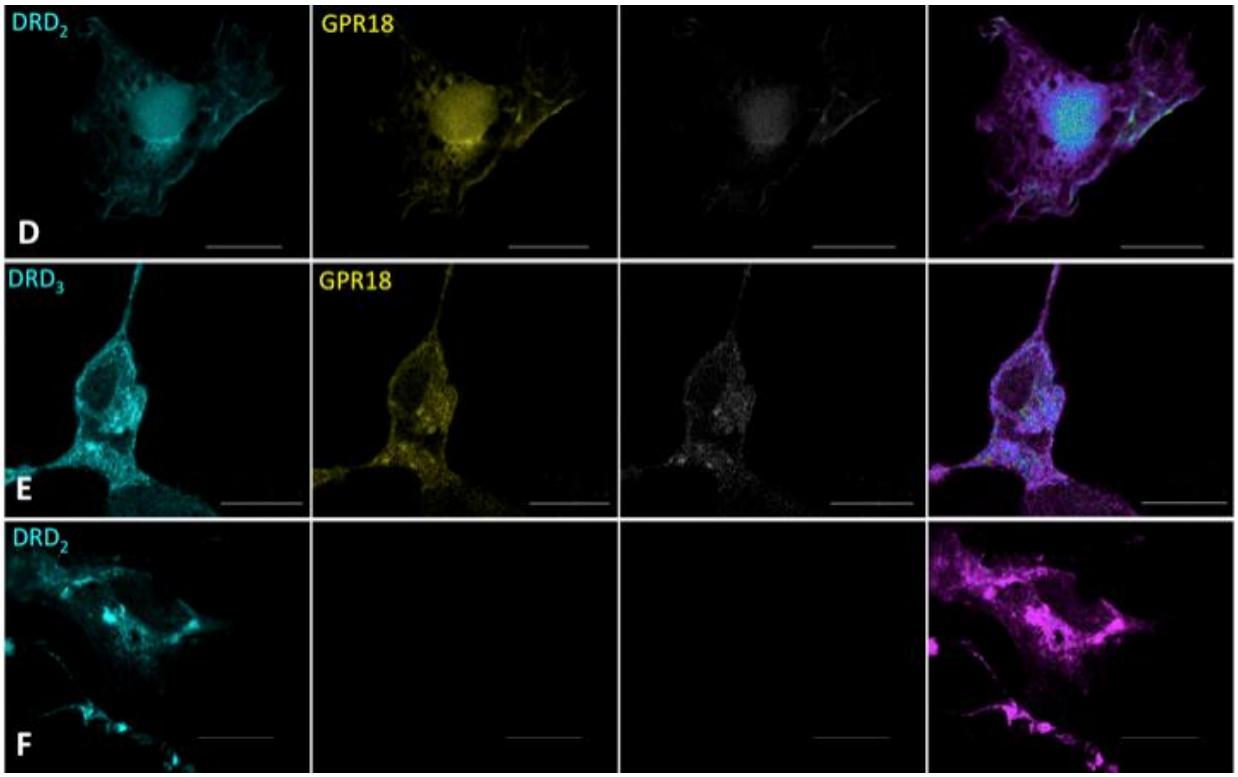
DRD2
GPR18
D
DRD3
GPR18
E
DRD2
F

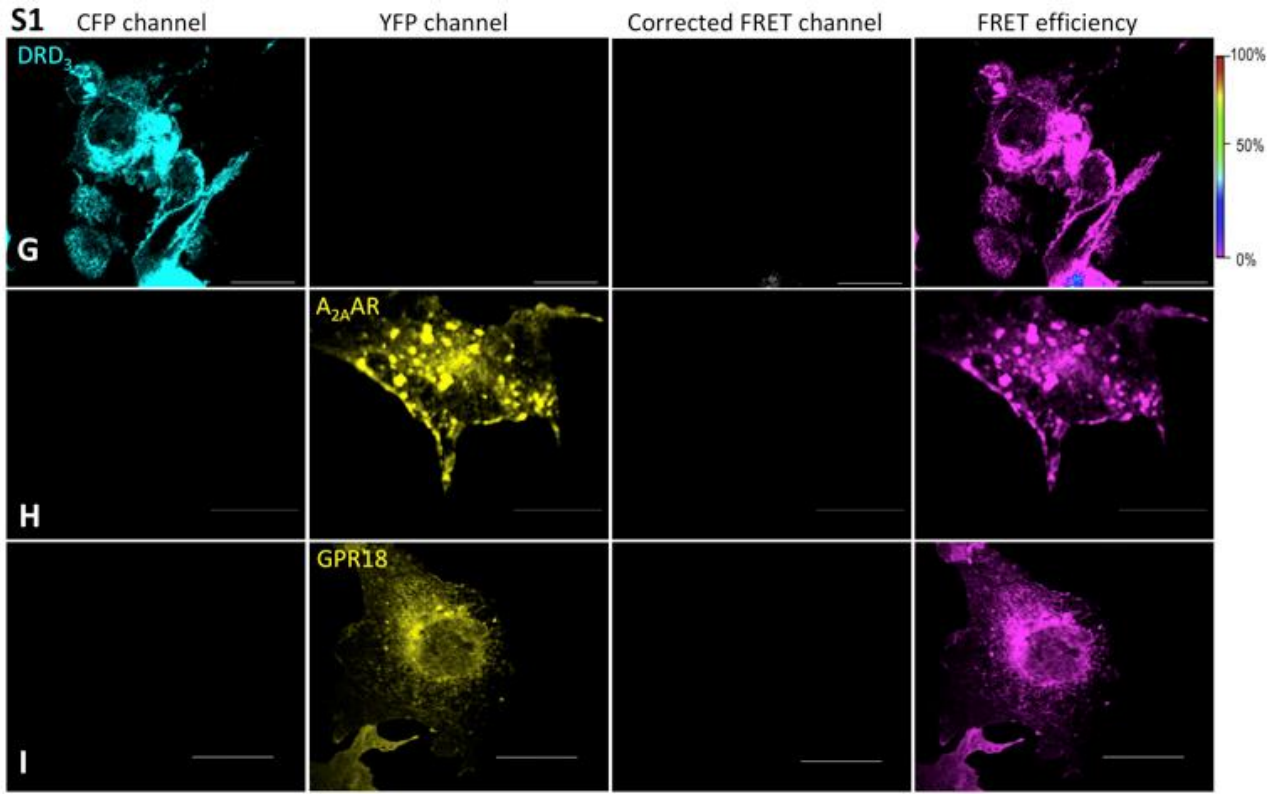
S1
CFP channel
YFP channel
Corrected FRET channel
FRET efficiency
DRD3
G
100%
50%
0%
A2AAR
H
GPR18
I

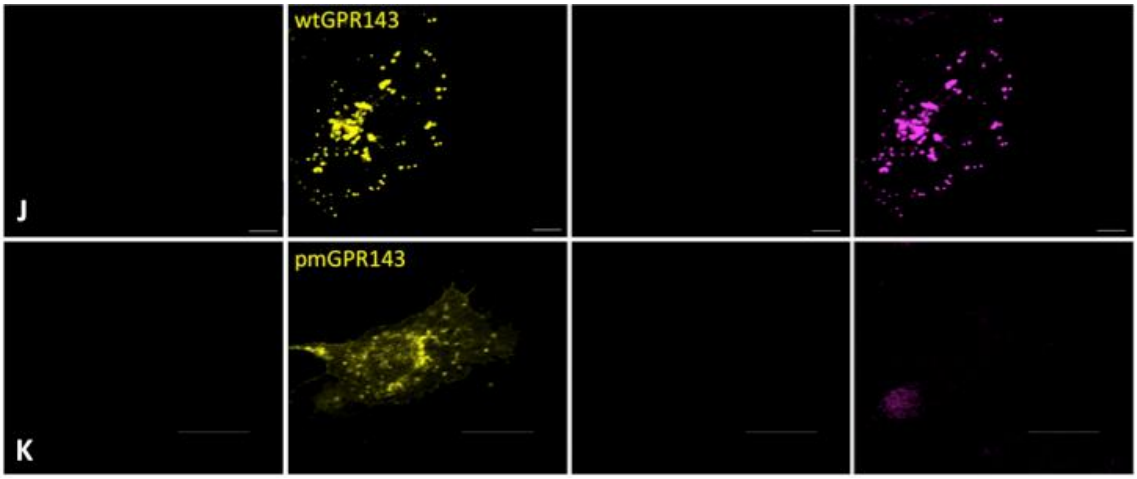

Figure S1. Control images of sensitized emission FRET. Sensitized emission method was used to detect interaction of GPR143 (YFP channel) and DRs (CFP channel) in COS7s transfected either with (**A**) CFP-YFP fusion protein, (**B**) DRD_2-CFP and A_{2A}AR-YFP, (**C**) DRD_3-CFP and A_{2A}AR-YFP as positive controls, (**D**) DRD_2-CFP and GPR18-YFP, (**E**) DRD_3-CFP and GPR18-YFP as negative controls (**F**) DRD_2-CFP, (**G**) DRD_3-CFP, (**H**) A_{2A}AR-YFP, (**I**) GPR18-YFP, (**J**) wtGPR143-YFP or (**K**) pmGPR143-YFP. FRET signal, corrected by CoA and CoB parameters, and FRET efficiency (color scale on the far right) are shown. Scale bar = 20 μm. FRET, fluorescence resonance energy transfer; wt, wildtype, pm, plasma membrane.

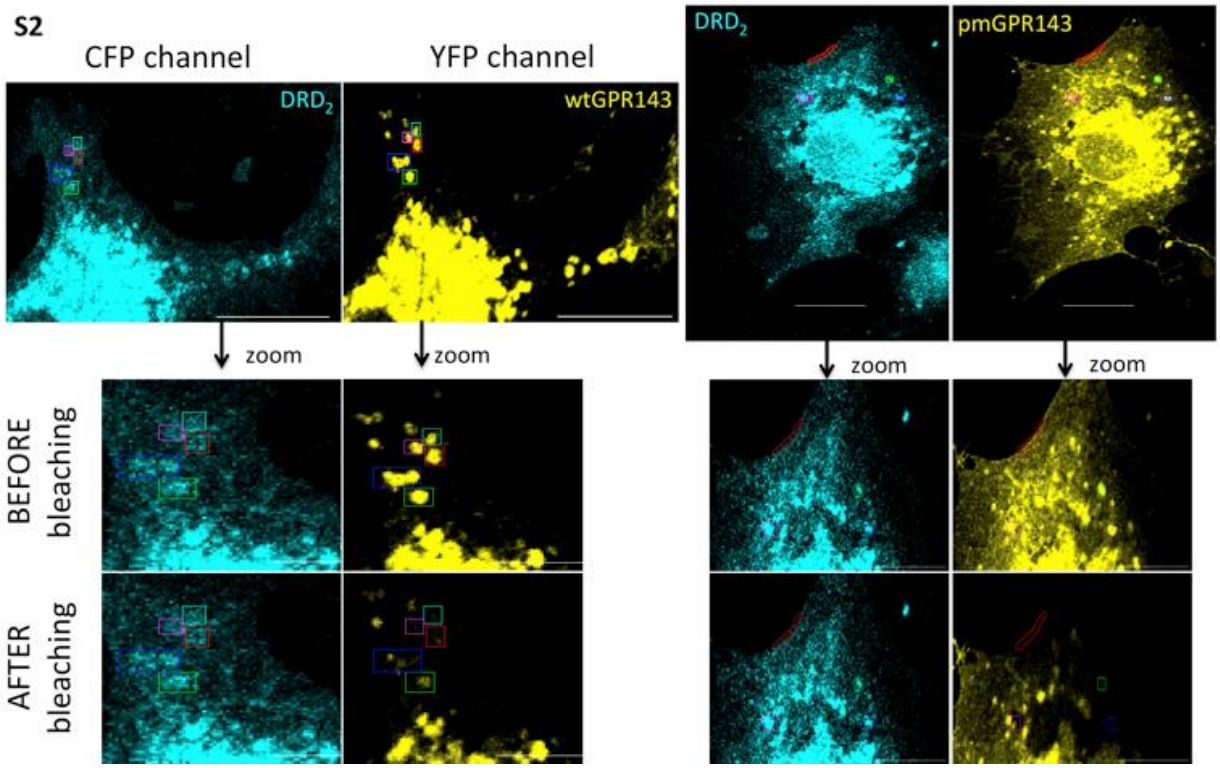
S2
CFP channel
YFP channel
DRD2
wtGPR143
zoom
zoom
BEFORE bleaching
AFTER bleaching
DRD2
pmGPR143
zoom
zoom

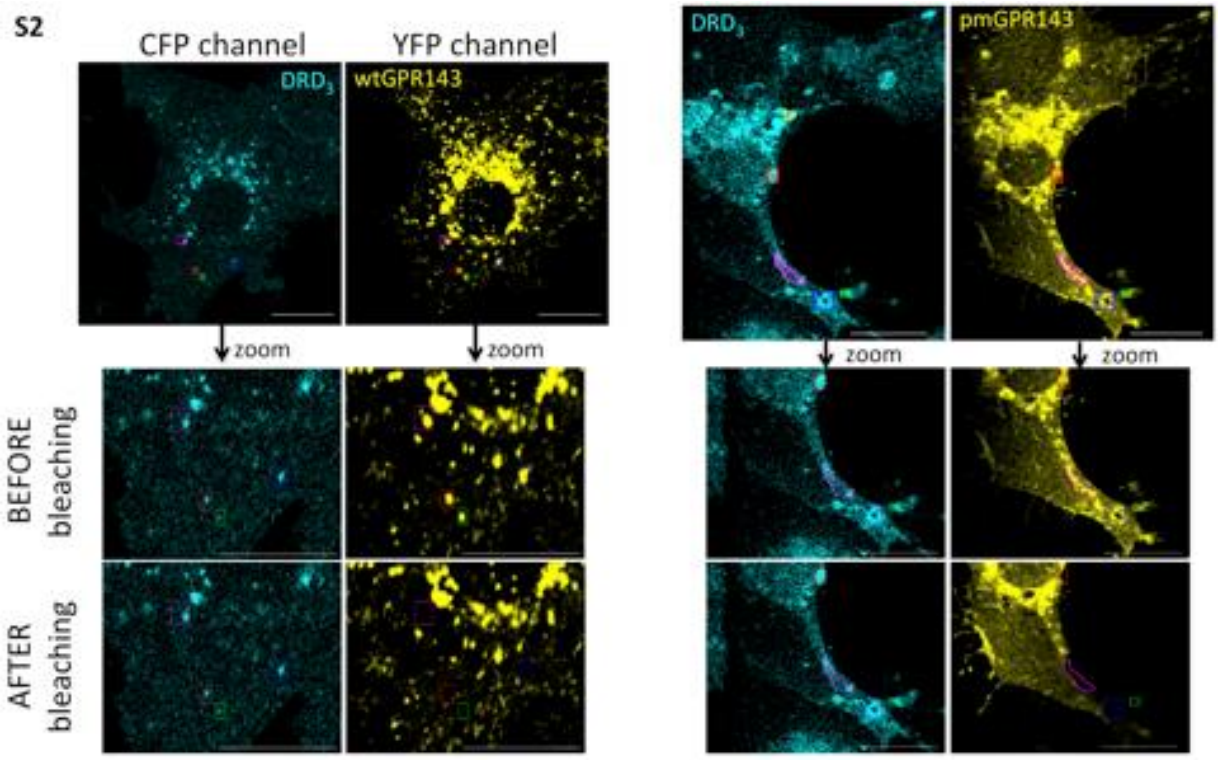
S2
CFP channel
YFP channel
DRD3
wtGPR143
zoom
zoom
BEFORE bleaching
AFTER bleaching
DRD3
pmGPR143
zoom
zoom

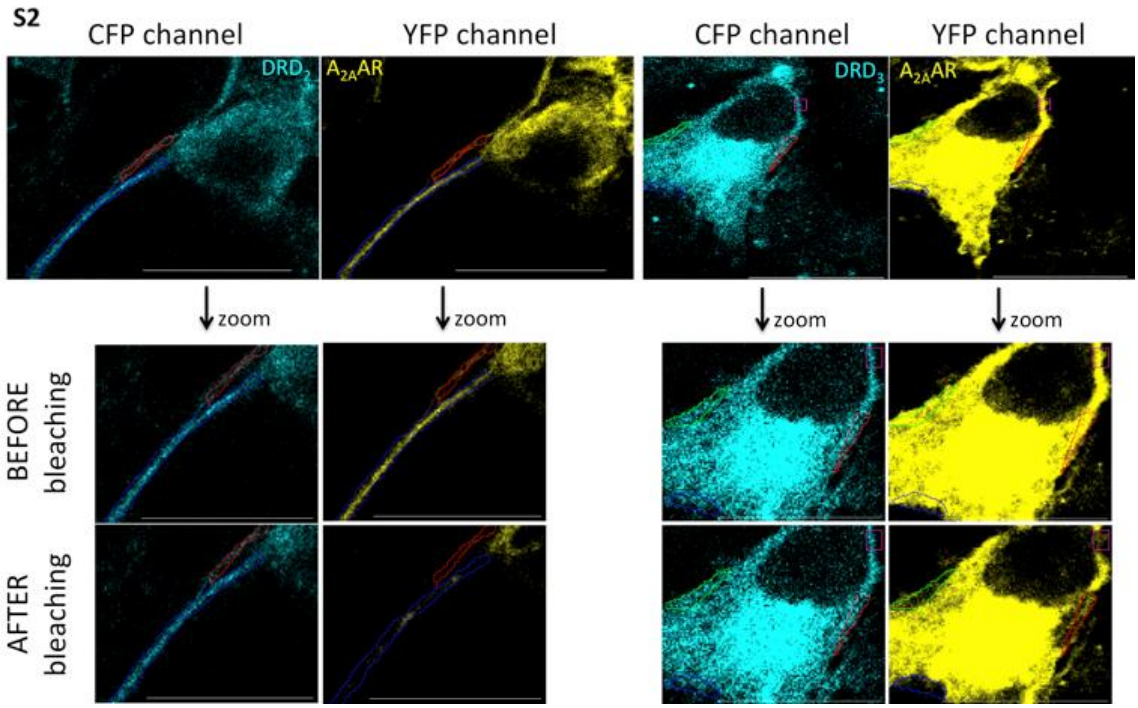

Figure S2. Acceptor photobleaching FRET in COS7 cells. COS7s were co-transfected with wt or pmGPR143-YFP or A_{2A}AR-YFP and DRs-CFP. The YFP photobleaching was performed and detected in delimited regions (highlighted and zoomed in the pictures). The fluorescence of GPR143 (YFP channel) and DRs (DRD_2 or DRD_3; CFP channel) were detected before and immediately after the acceptor photobleaching. Controls are shown in Figure S5. Scale bar = 20 µm.

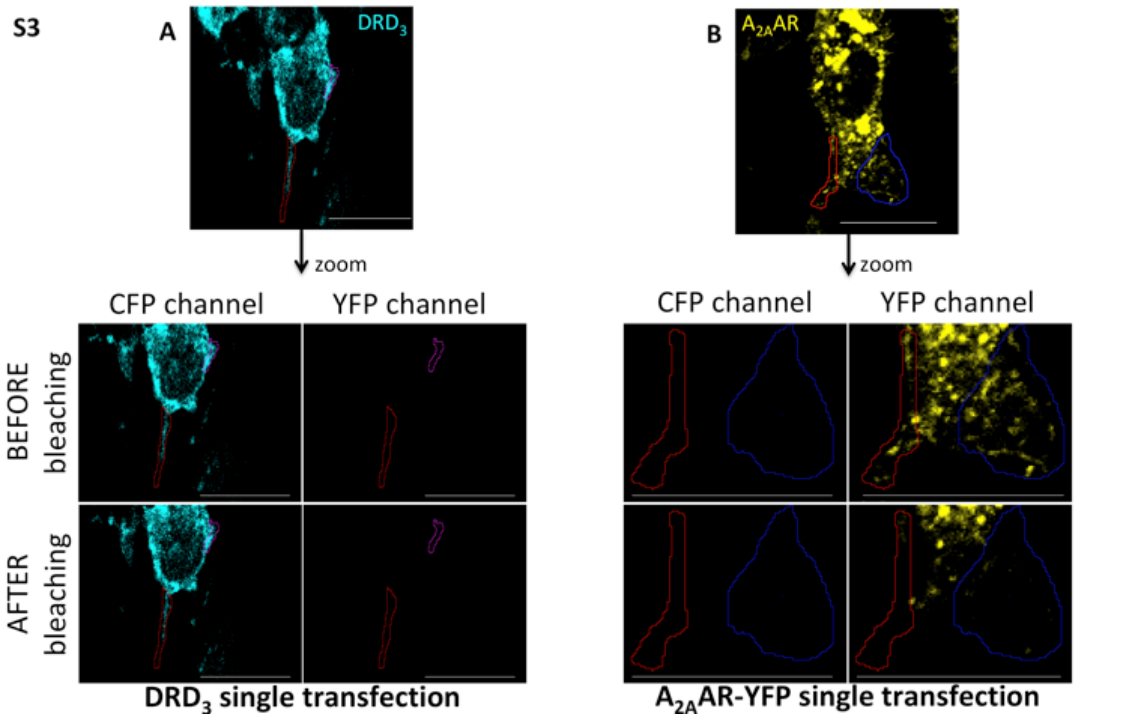
S3
A
DRD3
zoom
CFP channel
YFP channel
BEFORE bleaching
AFTER bleaching
DRD3 single transfection
B
A2AAR
zoom
CFP channel
YFP channel
A2AAR-YFP single transfection

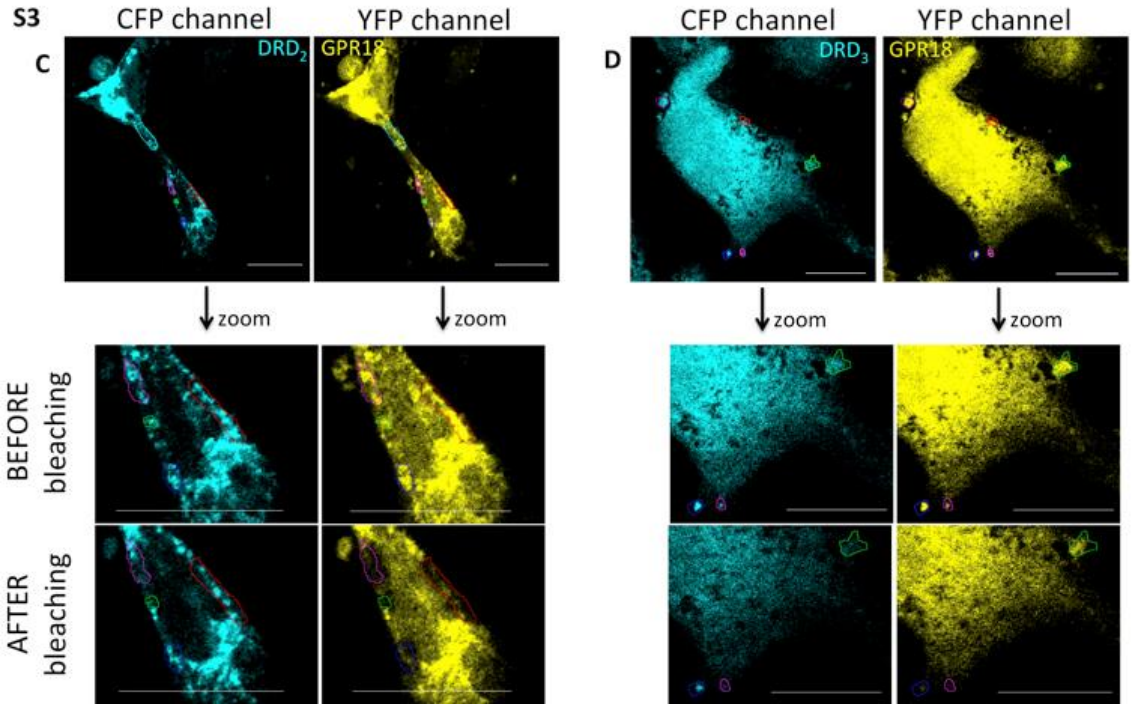
S3
C
CFP channel
YFP channel
DRD2
GPR18
zoom
zoom
BEFORE bleaching
AFTER bleaching
D
CFP channel
YFP channel
DRD3
GPR18
zoom
zoom

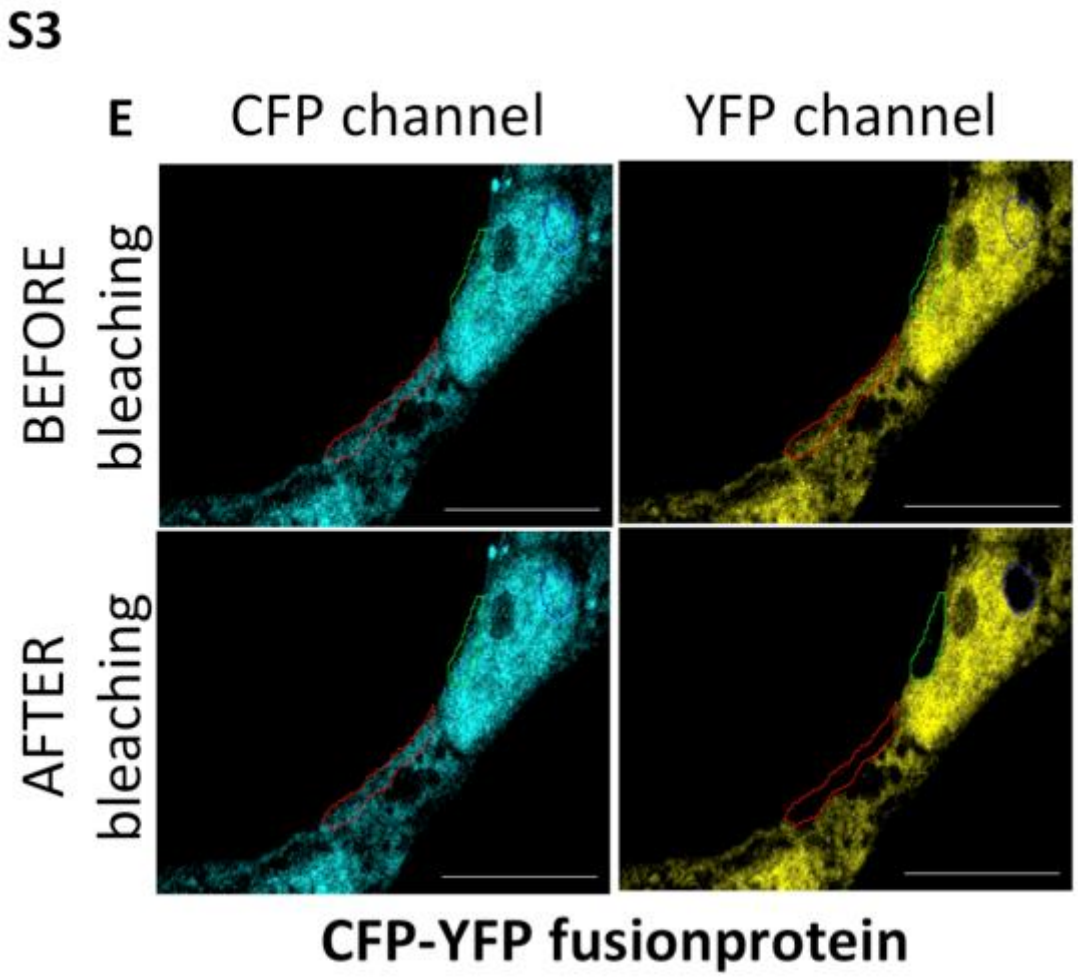

Figure S3. Control images of FRET acceptor photobleaching. The YFP photobleaching was performed and detected in delimited regions (highlighted and zoomed in the pictures) of COS7s transfected with either DRs-CFP, here DRD_3 as representative (**A**) or GPCR-YFP (**B**), here $A_{2A}AR$ as representative. CFP-YFP was used as positive control (E), while co-transfections with GPR18 (**C**, **D**) were used as negative controls. Images of all sample fluorescence are shown before and immediately after the acceptor photobleaching for CFP and YFP channels. For corresponding FRET efficacies see Figure 3. Scale bar = 20 µm.

S4

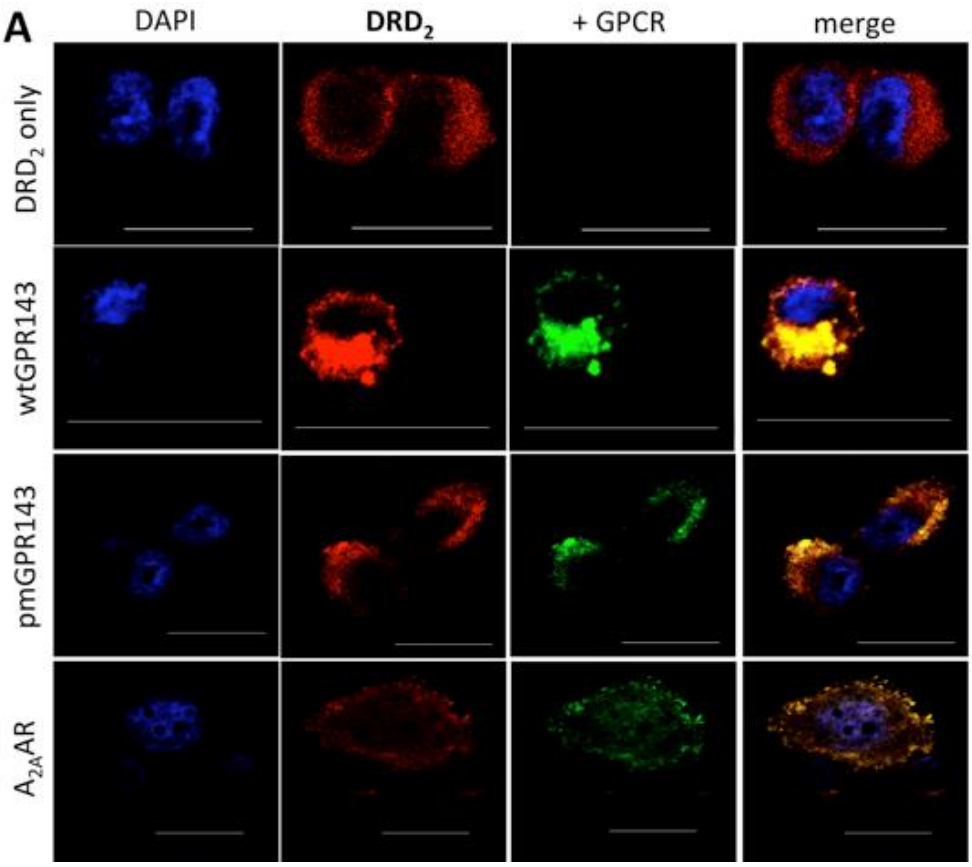

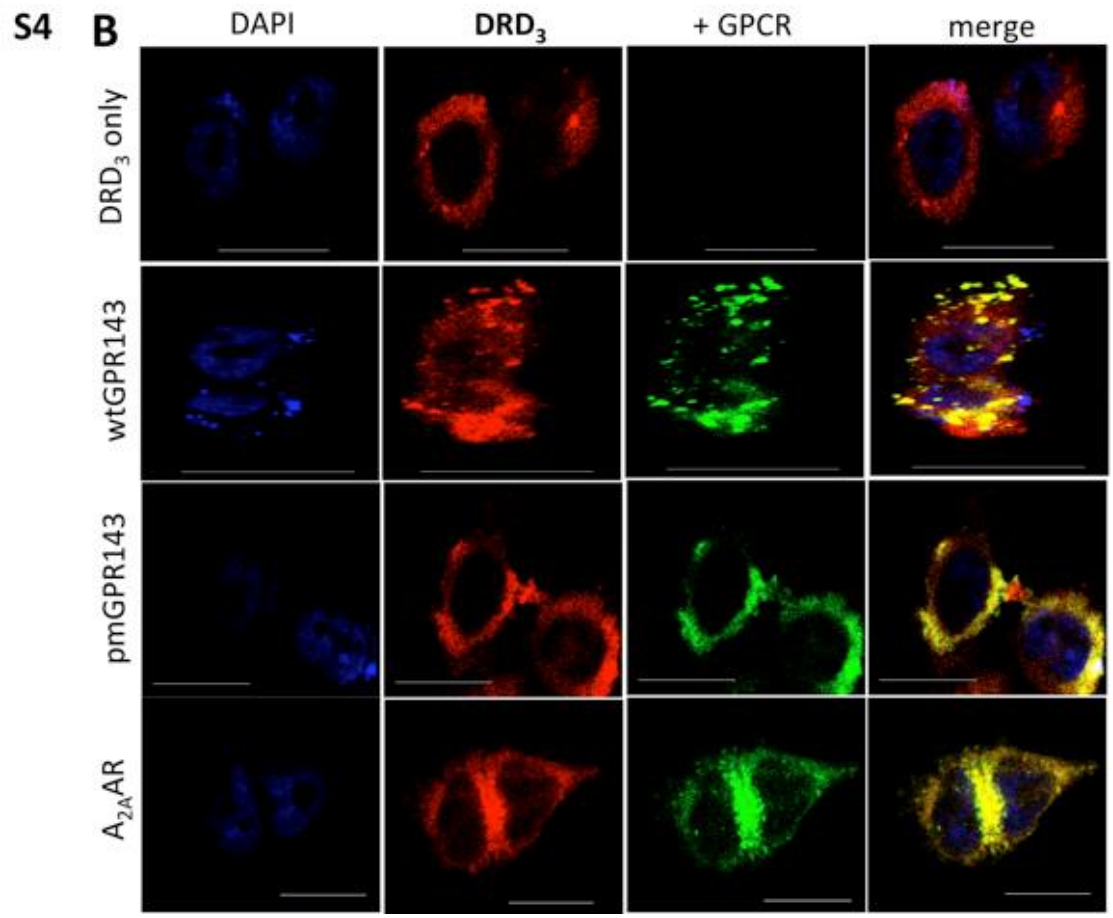

Figure S4. Colocalization of GPR143 and DRs by immunofluorescence in CHO cells. A: CHO DRD_2 cells were co-transfected with wt or pmGPR143-YFP, or $A_{2A}AR$ -YFP, fixed and stained with anti-ProLink (against PL tagged-DRD_2) and DAPI (nuclei). AlexaFluor594 was used as secondary antibody. **B:** CHO DRD_3 cells were co-transfected with wt or pmGPR143-YFP, or $A_{2A}AR$-YFP, fixed and stained with anti-ProLink (against PL tagged-DRD_3) and DAPI (nuclei). AlexaFluor594 was used as secondary antibody. DR only samples are shown in the first row of A and B**.** Scale bar = 20 µm.

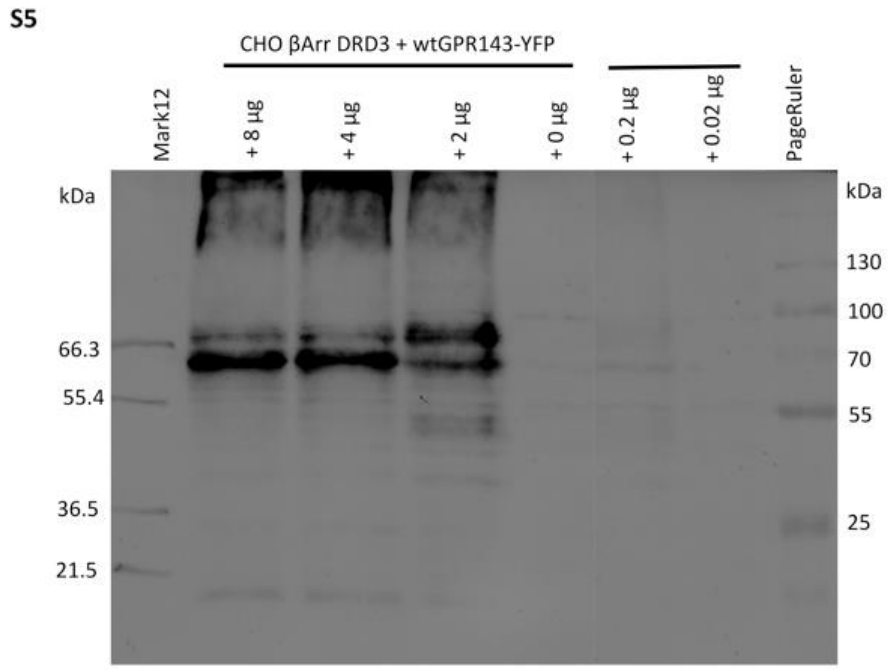

Figure S5. Western Blot Analysis shown as example for wtGPR143+DRD$_3$. CHO b-arrestin cells stable expressing DRD_2 or DRD_3 were co-transfected with wt or pmGPR143-YFP, A_{2A}AR-YFP or GPR18-YFP in different concentrations (8, 4, 2, 0.2 or 0.02 µg). Untransfected CHO b-arrestin cells were used as control. 30 µg lysates were separated in 10% SDS-PAGE and transferred onto nitrocellulose. The anti-GFP tag (mouse monoclonal) antibody was used as primary and rabbit anti-mouse horseradish peroxidase–coupled antibody was used as secondary antibody, both in 1:5000 dilutions.

7.2. Supplemental information of the research article: The world of GPCR dimers - mapping dopamine receptor D_2 homodimers in different activation states and configuration arrangements

S6-I

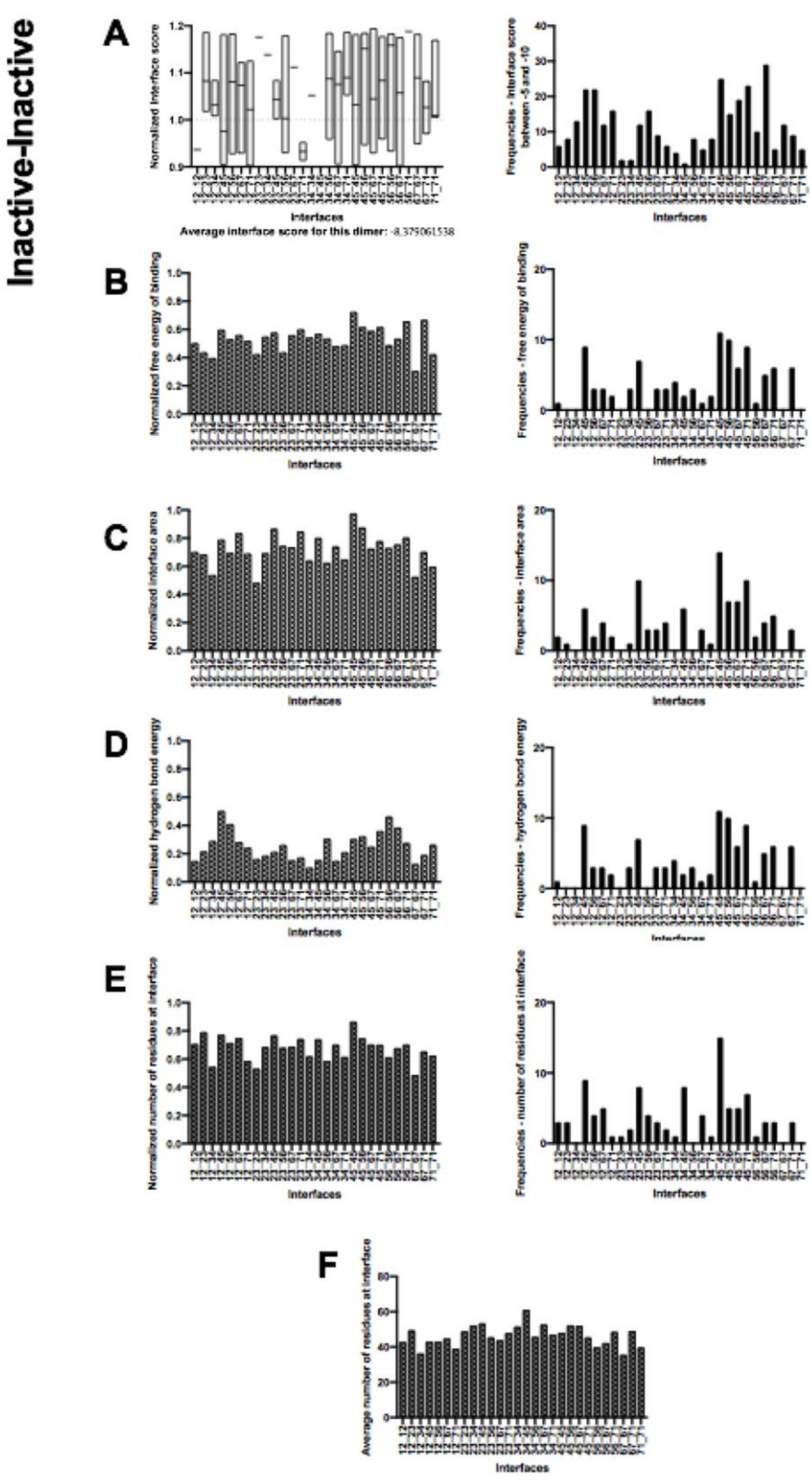
Inactive-Inactive
A
Normalized interface score
Interfaces
Average interface score for this dimer: -8.379061538
Frequencies - interface score between -5 and -10
Interfaces
B
Normalized free energy of binding
Interfaces
Frequencies - free energy of binding
Interfaces
C
Normalized interface area
Interfaces
Frequencies - interface area
Interfaces
D
Normalized hydrogen bond energy
Interfaces
Frequencies - hydrogen bond energy
Interfaces
E
Normalized number of residues at interface
Interfaces
Frequencies - number of residues at interface
Interfaces
F
Average number of residues at interface
Interfaces

S6-II

Active-Active

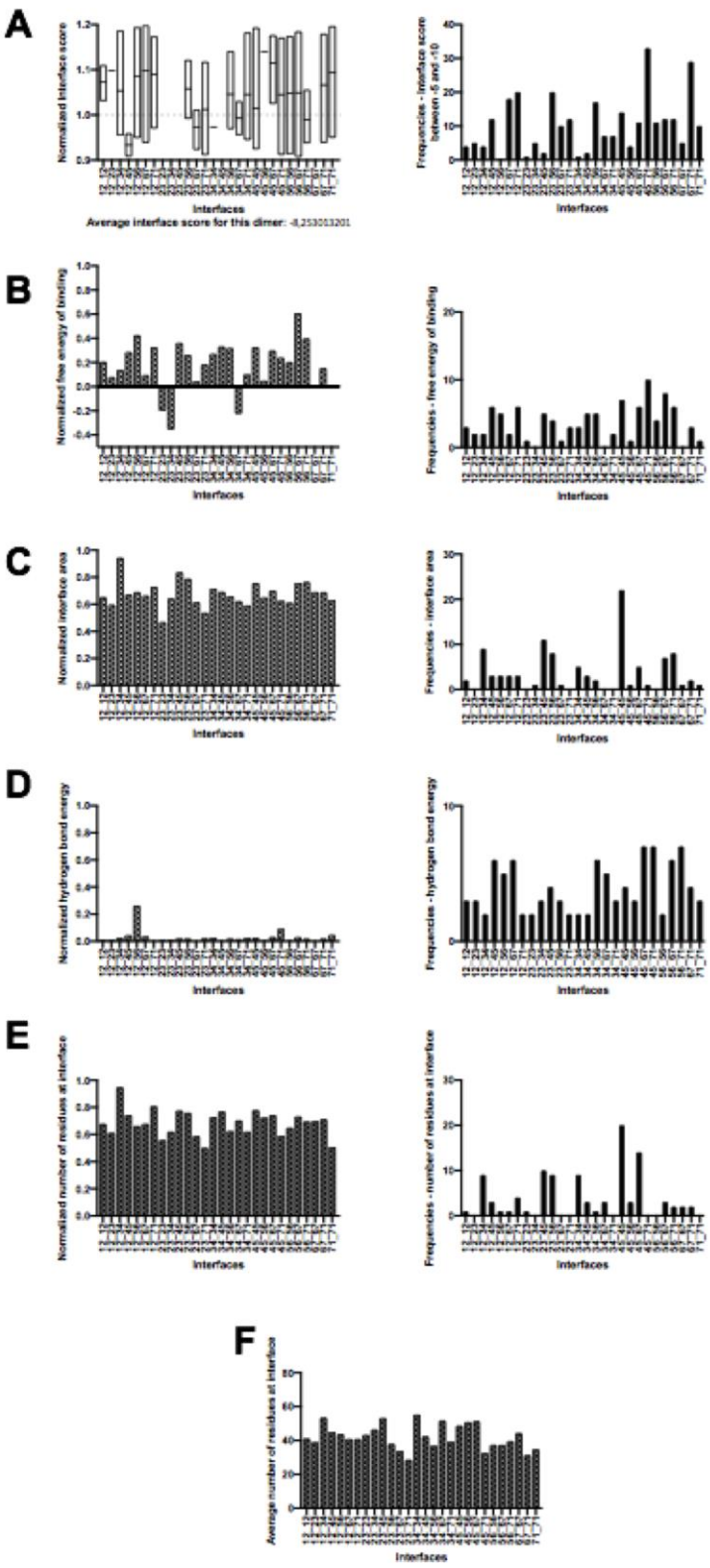

S6-III

Arr-Arr

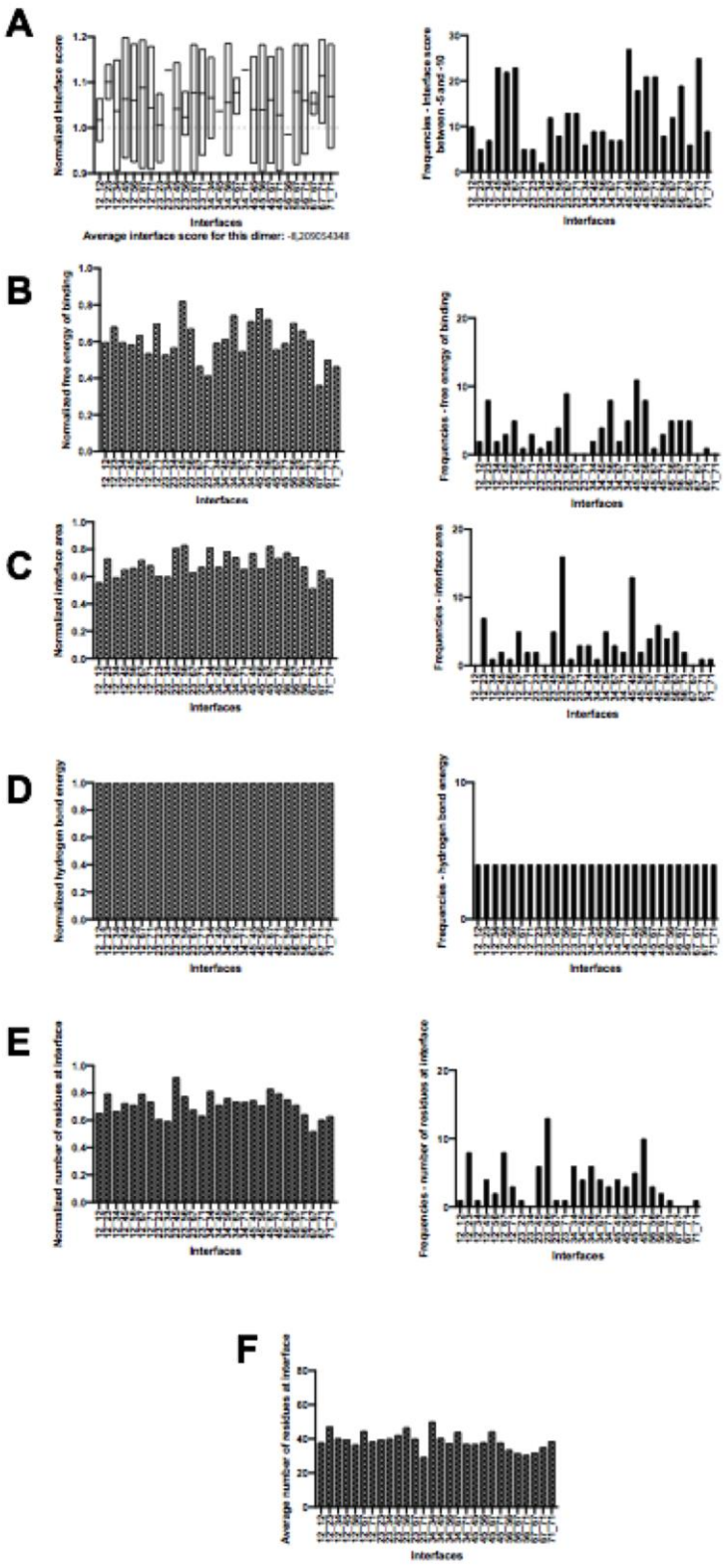

S6-IV

Active-Inactive

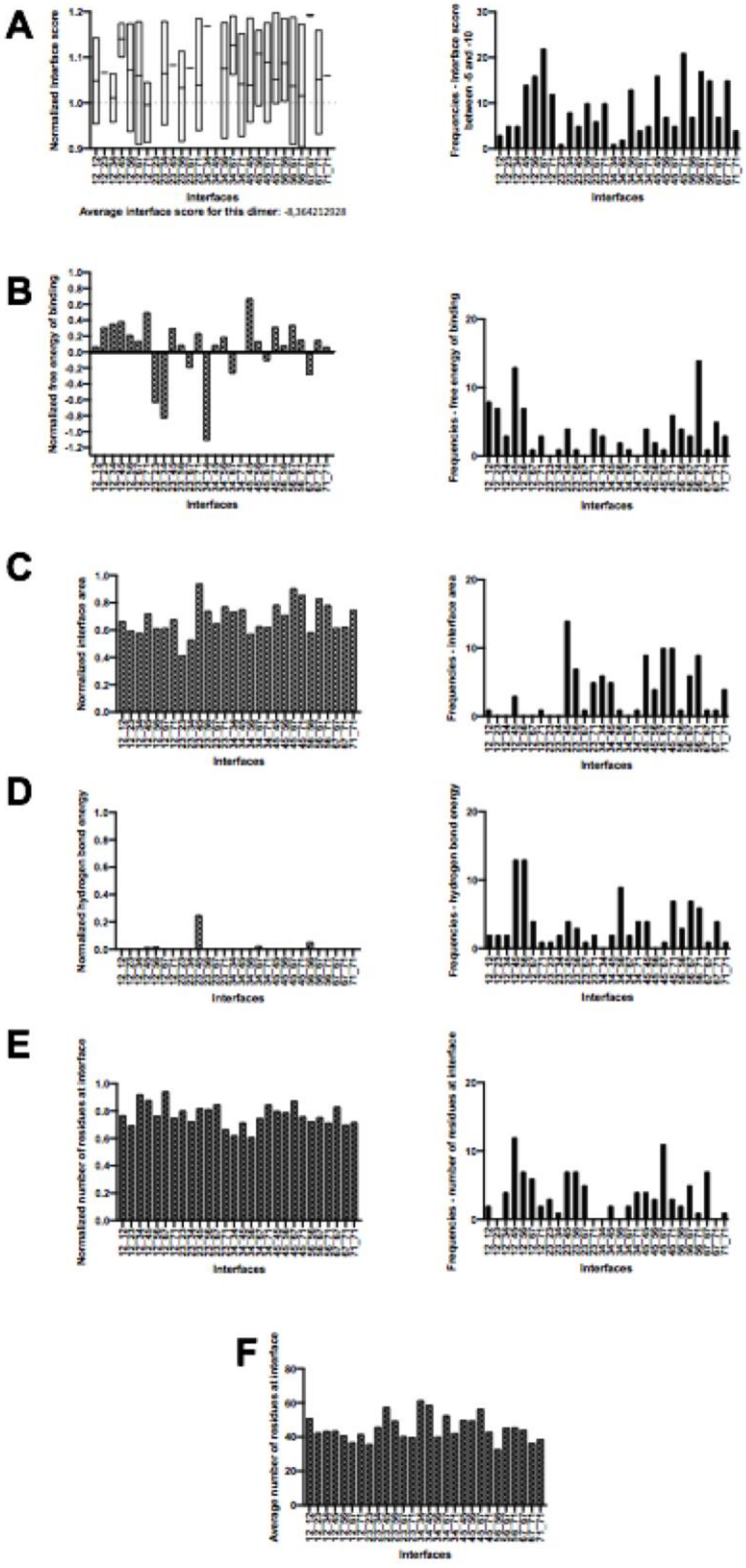

S6-V

Inactive-Arr

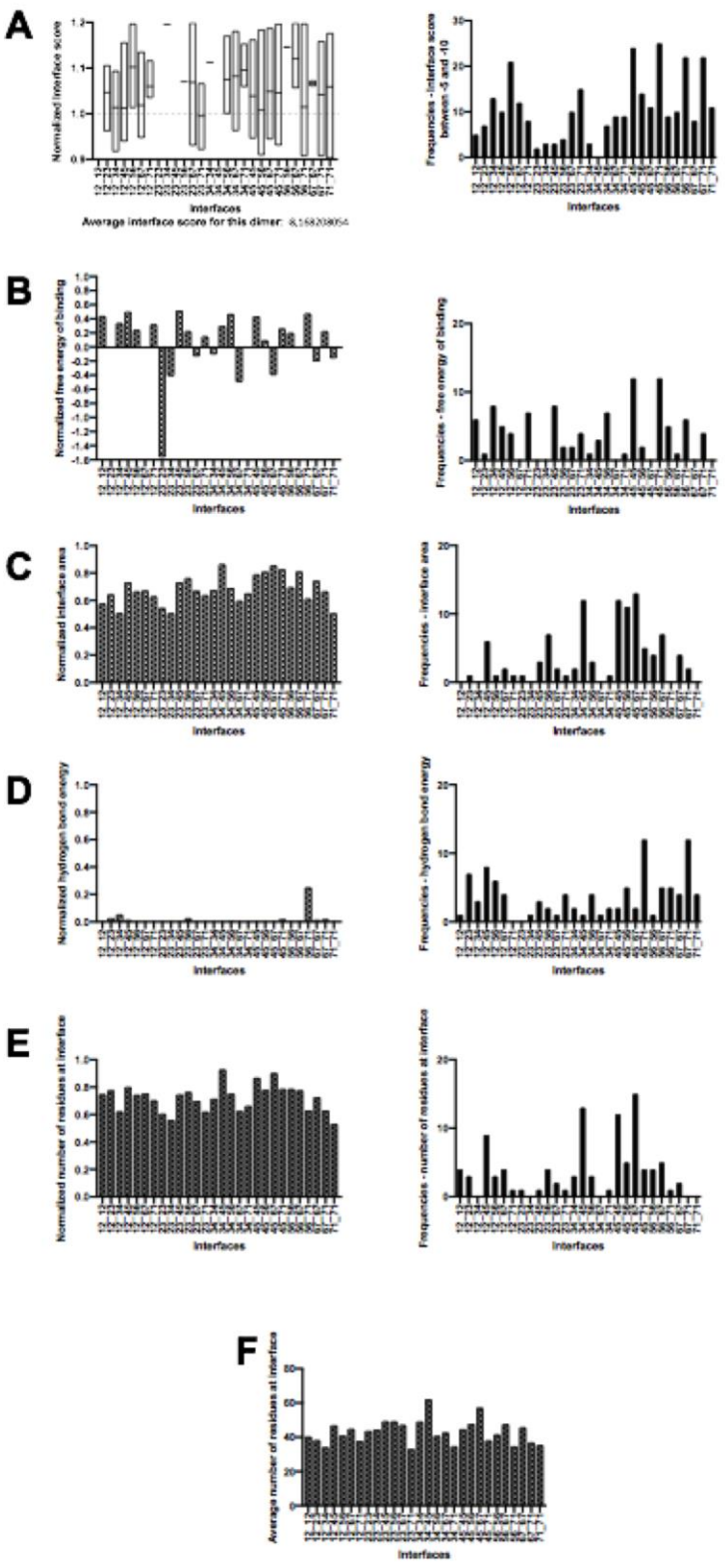

S6-VI

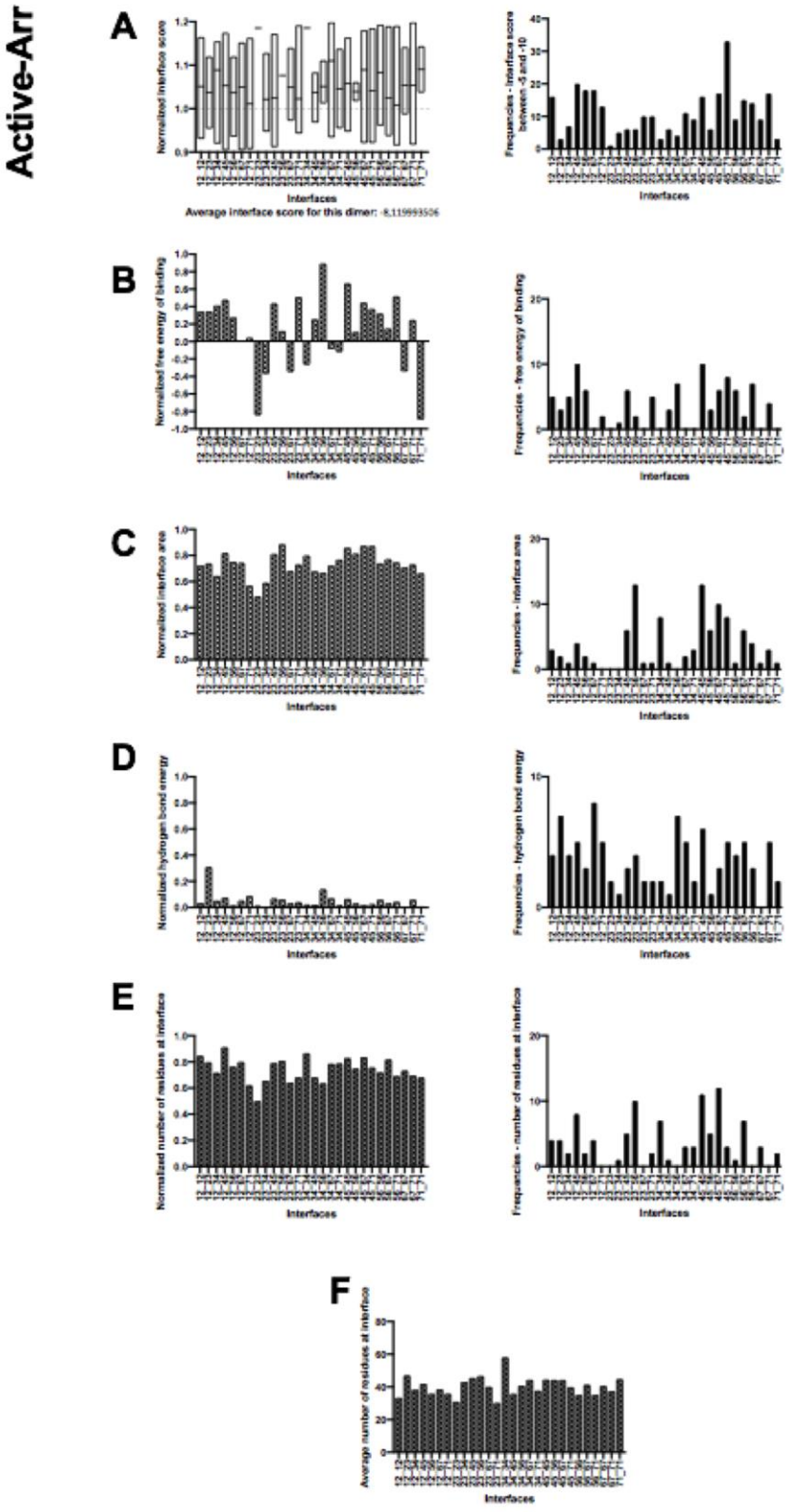
Active-Arr
A
Normalized interface score
Interfaces
Average interface score for this dimer: -8,119993506
Frequencies - interface score between -5 and +10
Interfaces
B
Normalized free energy of binding
Interfaces
Frequencies - free energy of binding
Interfaces
C
Normalized interface area
Interfaces
Frequencies - interface area
Interfaces
D
Normalized hydrogen bond energy
Interfaces
Frequencies - hydrogen bond energy
Interfaces
E
Normalized number of residues at interface
Interfaces
Frequencies - number of residues at interface
Interfaces
F
Average number of residues at interface
Interfaces

Figure S6. Dimer protocol – model selection. Consensus scoring of normalized values (**left plots**) and frequencies of best interfaces (**right plots**) for the different D_2R-homodimer configurations for interface score (**A**), free energy of binding (**B**), interface area (**C**), hydrogen bond energy (**D**) and number of residues at interface (**E**). Scoring was performed for 28 interfaces (x-axis) and labelled according to transmembrane (TM) helices forming the interface, e.g., 12_12 for the interface formed by TM1 and TM2 from one protomer, and TM1 and TM2 from the other protomer. Y-axis indicates the parameter analysed Graph F represents the average number of residues per interface. I: Inactive-Inactive (in-in), II: Active-Active (ac-ac), III: Arrestin-arrestin (ar-ar), IV: Active-Inactive (ac-in), V: Inactive-arrestin (in-ar), VI: Active-arrestin (ac-ar).

S7

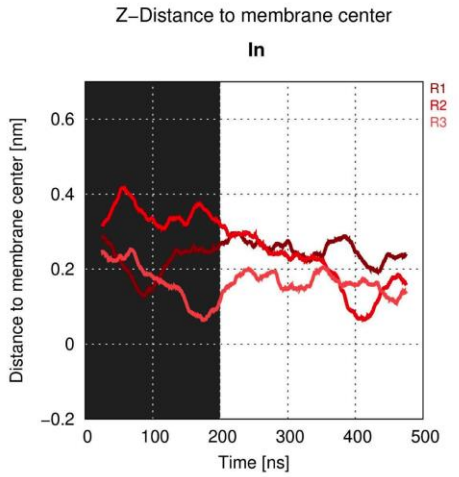
Z–Distance to membrane center
In
R1
R2
R3
Distance to membrane center [nm]
0.6
0.4
0.2
0
−0.2
0
100
200
300
400
500
Time [ns]

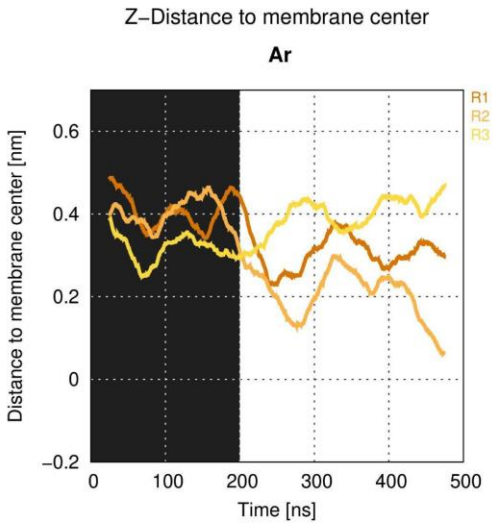
Z–Distance to membrane center
Ar
R1
R2
R3
Distance to membrane center [nm]
0.6
0.4
0.2
0
−0.2
0
100
200
300
400
500
Time [ns]

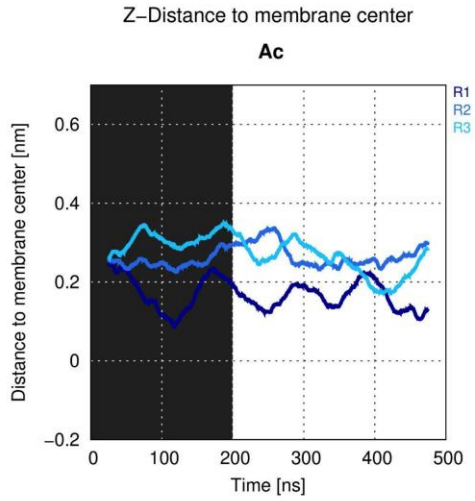
Z–Distance to membrane center
Ac
R1
R2
R3
Distance to membrane center [nm]
0.6
0.4
0.2
0
−0.2
0
100
200
300
400
500
Time [ns]

S7

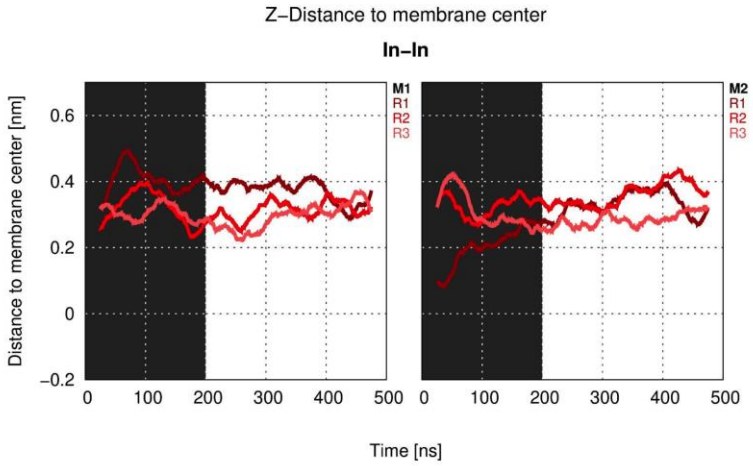
Z–Distance to membrane center
In–In
M1
R1
R2
R3
M2
R1
R2
R3
Distance to membrane center [nm]
0.6
0.4
0.2
0
−0.2
0
100
200
300
400
500
Time [ns]

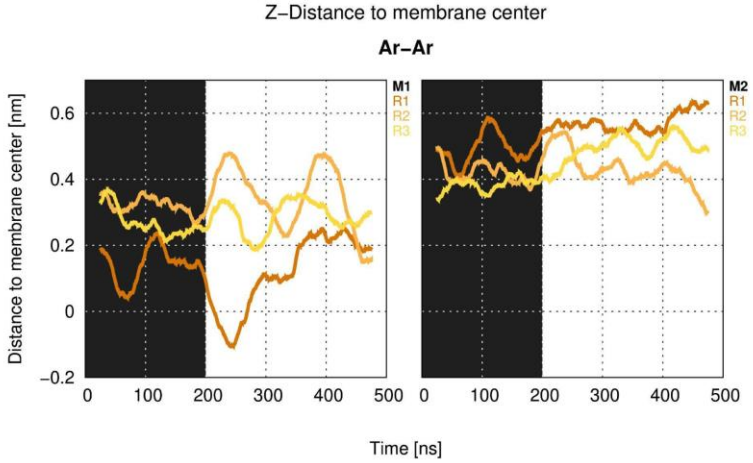
Z–Distance to membrane center
Ar–Ar
M1
R1
R2
R3
M2
R1
R2
R3
Distance to membrane center [nm]
0.6
0.4
0.2
0
−0.2
0
100
200
300
400
500
Time [ns]

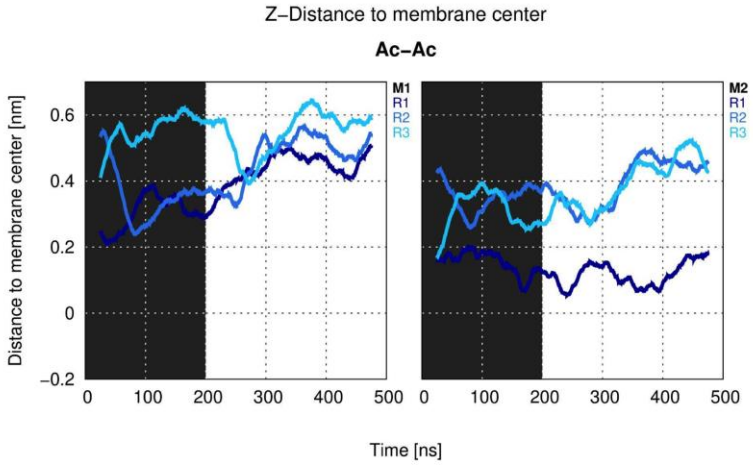
Z–Distance to membrane center
Ac–Ac
M1
R1
R2
R3
M2
R1
R2
R3
Distance to membrane center [nm]
0.6
0.4
0.2
0
−0.2
0
100
200
300
400
500
Time [ns]

S7

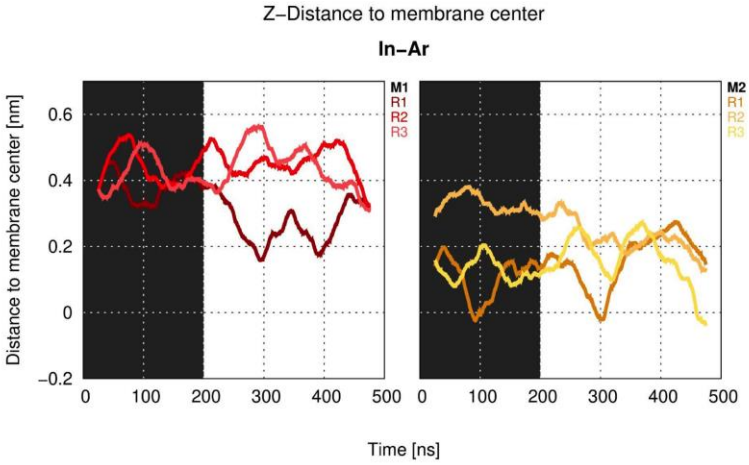
Z–Distance to membrane center
In–Ar
Distance to membrane center [nm]
0.6
0.4
0.2
0
−0.2
0
100
200
300
400
500
M1
R1
R2
R3
M2
R1
R2
R3
Time [ns]

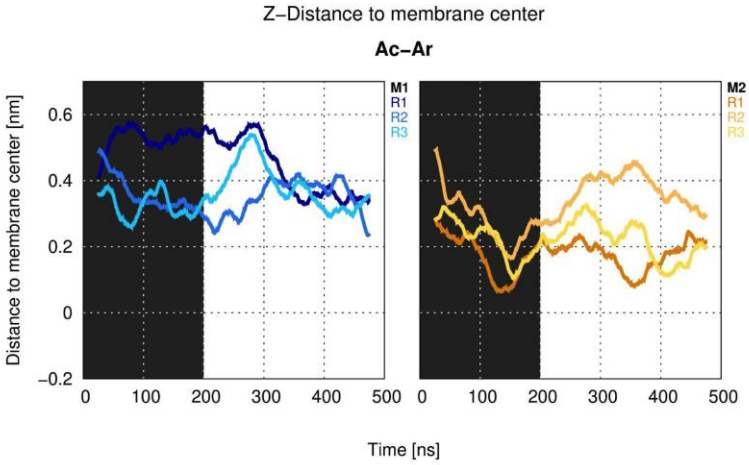
Z–Distance to membrane center
Ac–Ar
Distance to membrane center [nm]
0.6
0.4
0.2
0
−0.2
0
100
200
300
400
500
M1
R1
R2
R3
M2
R1
R2
R3
Time [ns]

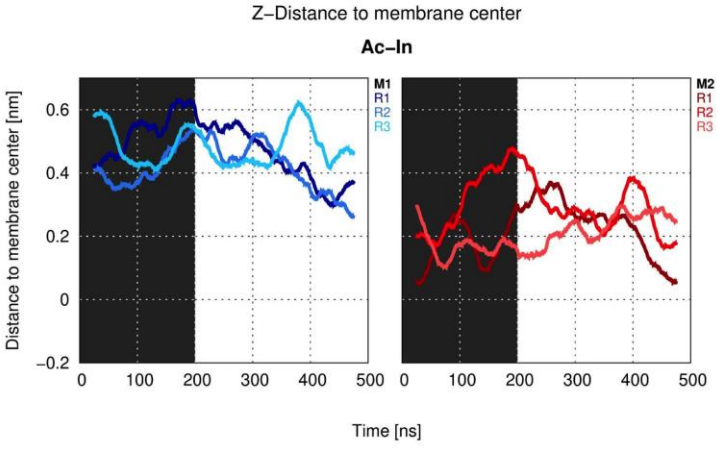
Z–Distance to membrane center
Ac–In
Distance to membrane center [nm]
0.6
0.4
0.2
0
−0.2
0
100
200
300
400
500
M1
R1
R2
R3
M2
R1
R2
R3
Time [ns]

Figure S7. Equilibration of the systems. Distance of the phospholipids of the lipid bilayer and a geometric membrane center, comprising 2 residues per transmembrane helix (TM) at the same height. TM1: 1.44 and 1.45, TM2: 2.52 and 2.53, TM3: 3.37 and 3.38, TM4: 4.51 and 4.52, TM5: 5.49 and 5.50, TM6: 6.44 and 6.45 and TM7: 7.49 and 7.50. Conformations are colour-coded: inactive - red, arrestin - yellow, active - blue. For these representations the total 500 ns of the simulations were utilized. For instance, one of the **ac-ac** D_2R homodimer configurations, **ac-ac-B**, was already disrupted upon initialization of the system and therefore was excluded from further analysis. This may be due to the predicted interface involving TM4-TM5-TM7-TM1, where HX8 at TM7 consequently generated a larger gap between the monomeric entities and leaves room for water molecules to enter the interface and disrupt the dimer (Filizola, 2010).
Reference:
Filizola M. Increasingly accurate dynamic molecular models of G-protein coupled receptor oligomers: Panacea or Pandora's box for novel drug discovery? Life Sci. 2010 Apr 10;86(15-16):590-7. DOI: 10.1016/j.lfs.2009.05.004.

S8-Transmembrane helices (TMs)

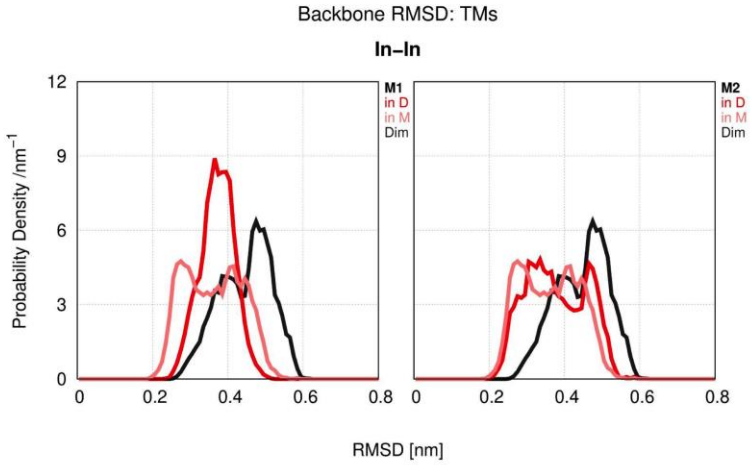

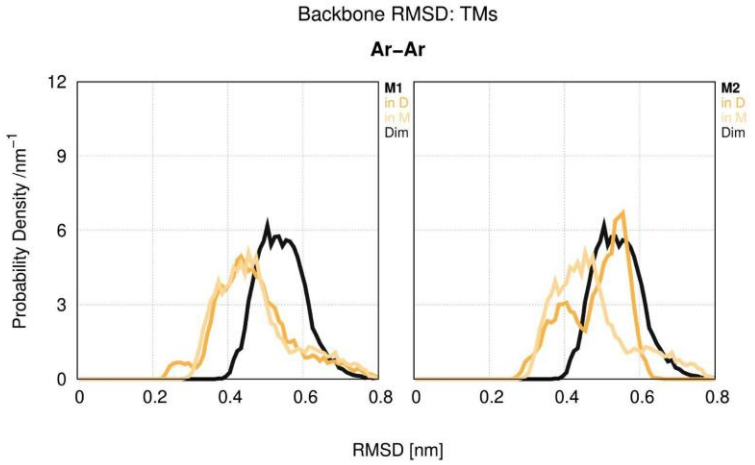

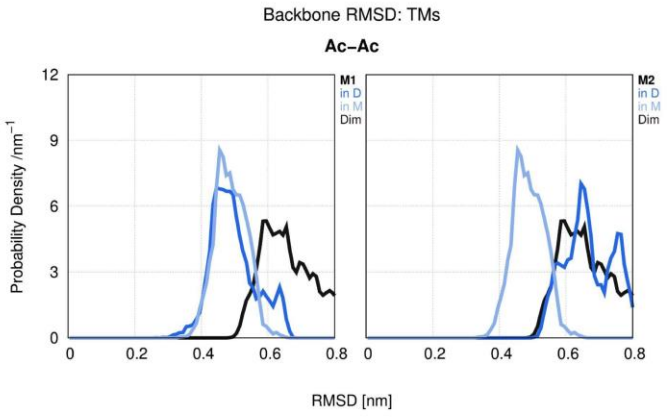

S8-Transmembrane helices (TMs)

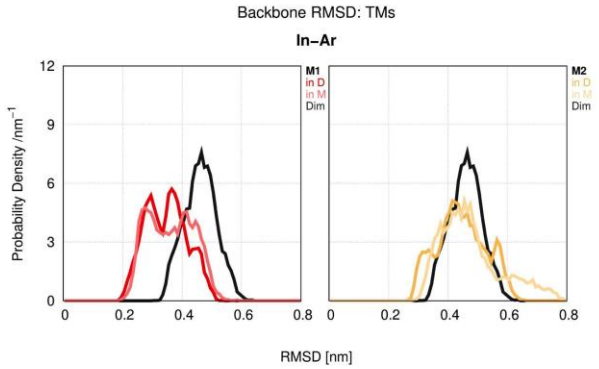

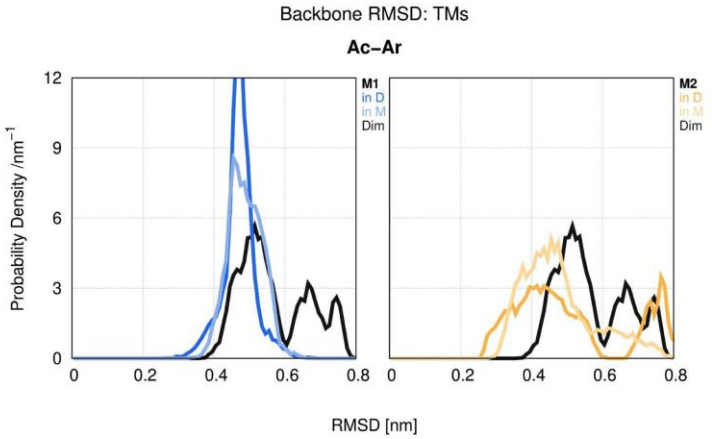

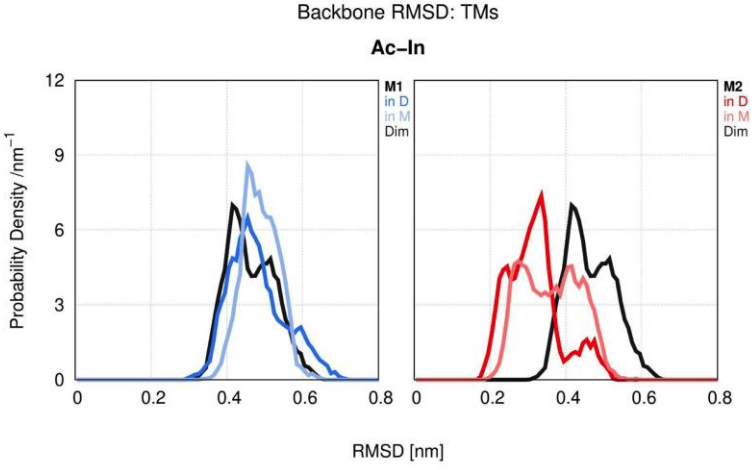

S8-Intra- and extracellular loops

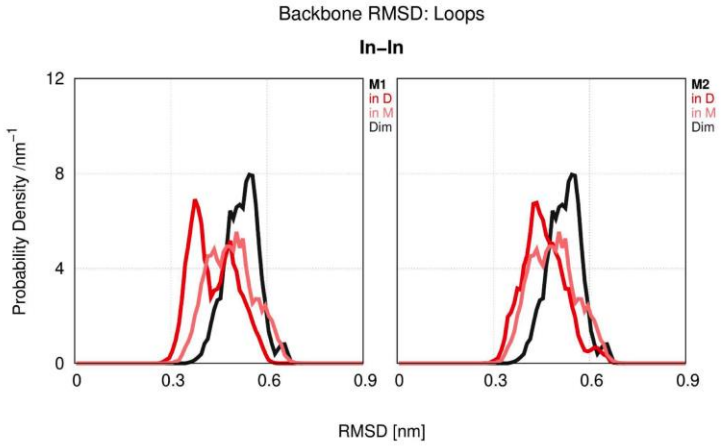

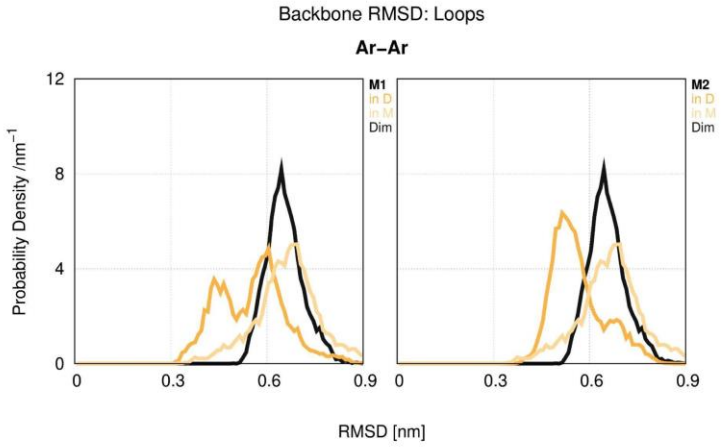

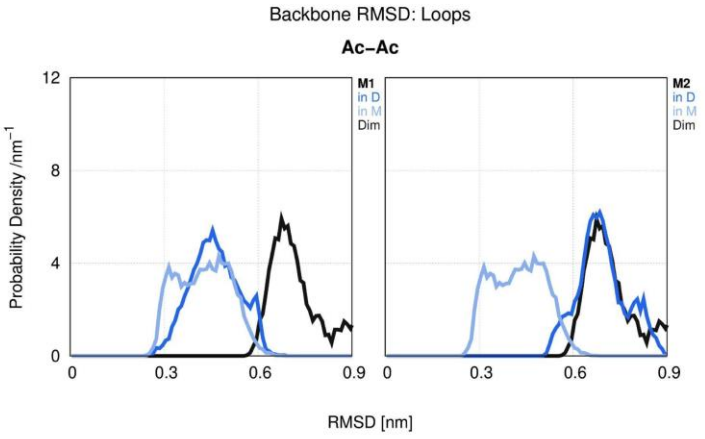

S8-Intra- and extracellular loops

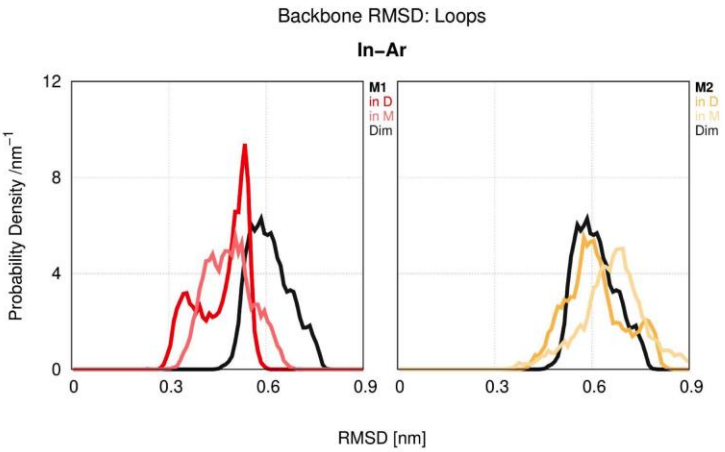

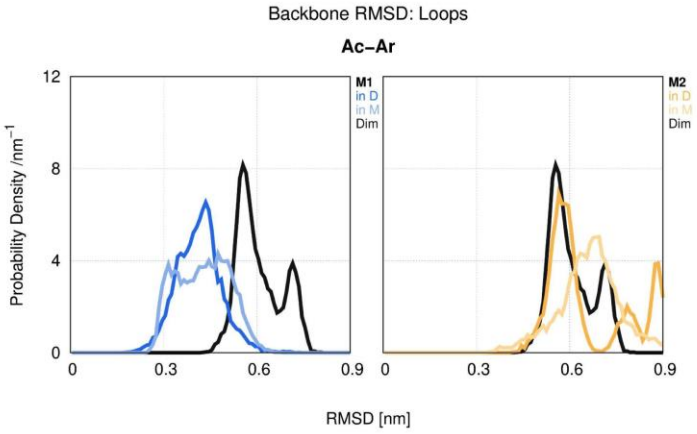

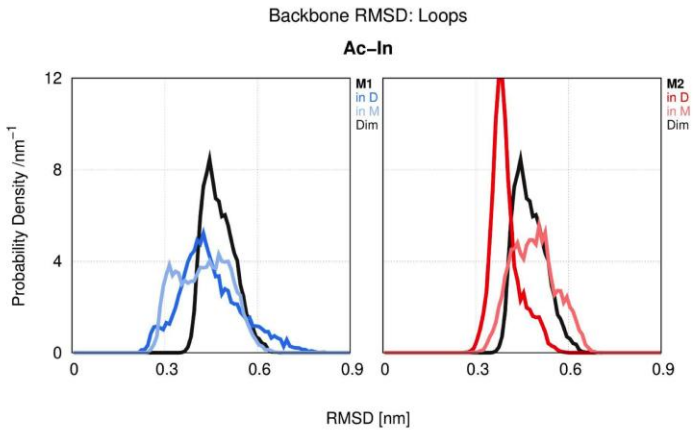

S8-DRY motif

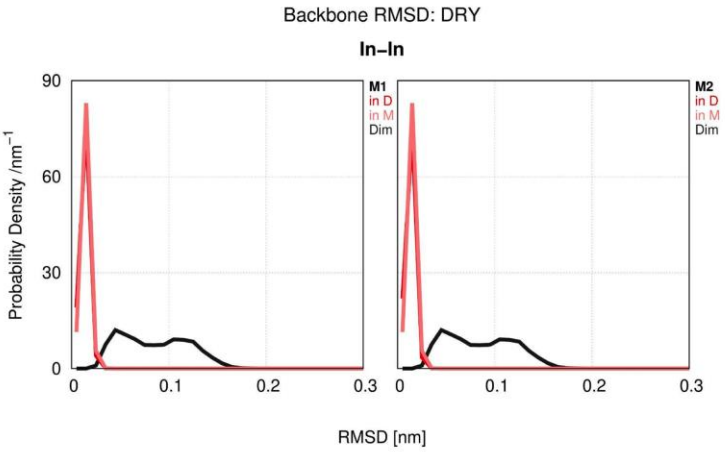
Backbone RMSD: DRY
In–In
Probability Density /nm^{-1}
RMSD [nm]
M1
in D
in M
Dim
M2
in D
in M
Dim

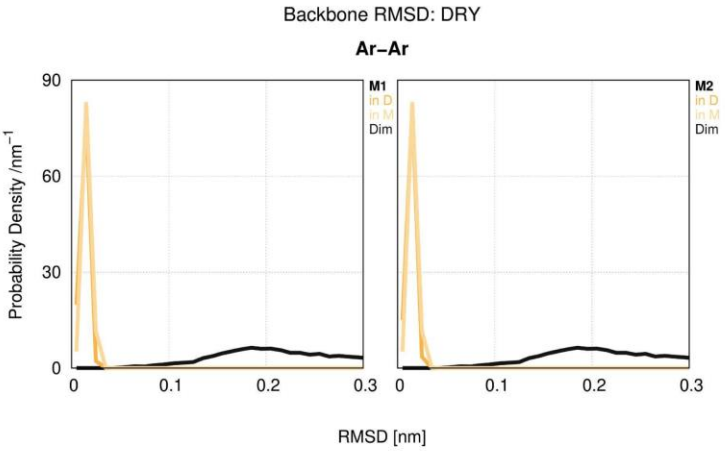
Backbone RMSD: DRY
Ar–Ar
Probability Density /nm^{-1}
RMSD [nm]
M1
in D
in M
Dim
M2
in D
in M
Dim

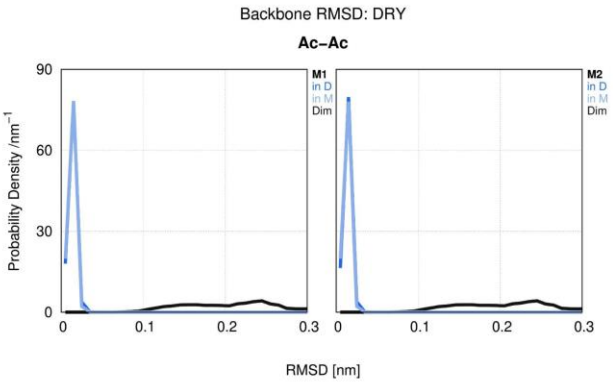
Backbone RMSD: DRY
Ac–Ac
Probability Density /nm^{-1}
RMSD [nm]
M1
in D
in M
Dim
M2
in D
in M
Dim

S8-DRY motif

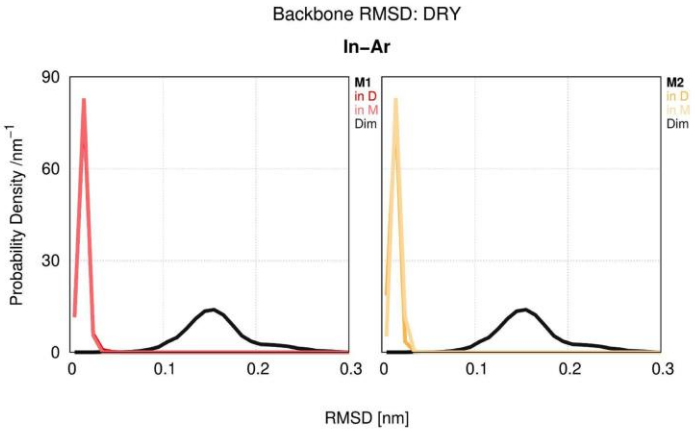
Backbone RMSD: DRY
In–Ar
M1
in D
in M
Dim
M2
in D
in M
Dim
Probability Density /nm⁻¹
90
60
30
0
0
0.1
0.2
0.3
RMSD [nm]

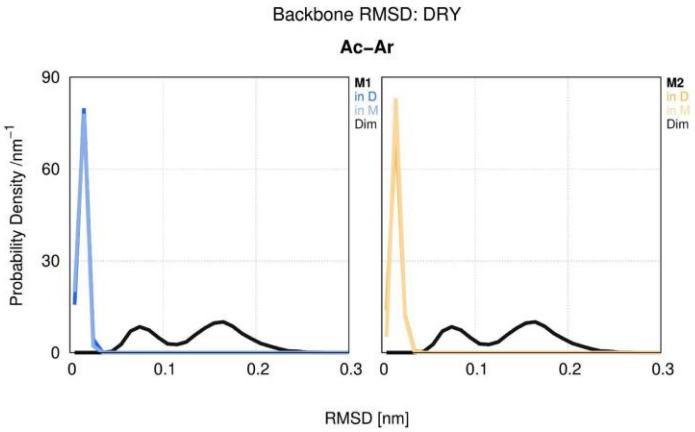
Backbone RMSD: DRY
Ac–Ar
M1
in D
in M
Dim
M2
in D
in M
Dim
Probability Density /nm⁻¹
90
60
30
0
0
0.1
0.2
0.3
RMSD [nm]

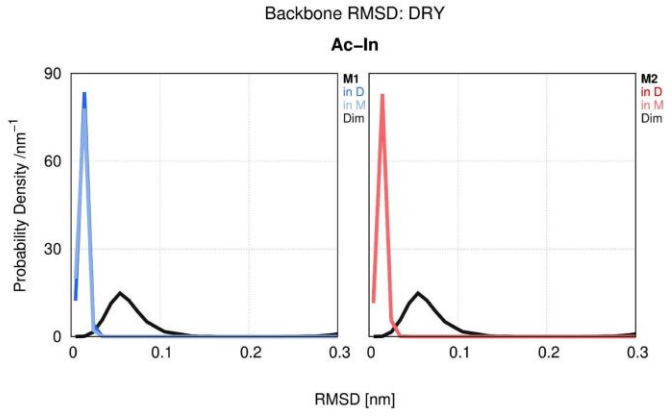
Backbone RMSD: DRY
Ac–In
M1
in D
in M
Dim
M2
in D
in M
Dim
Probability Density /nm⁻¹
90
60
30
0
0
0.1
0.2
0.3
RMSD [nm]

S8-CWxP motif

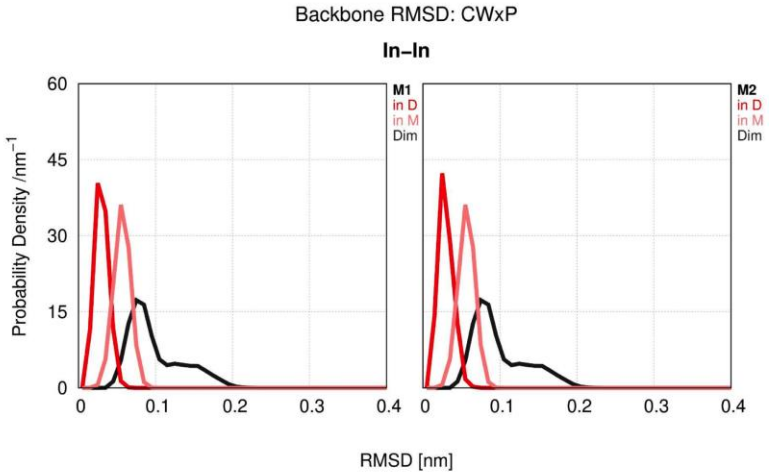

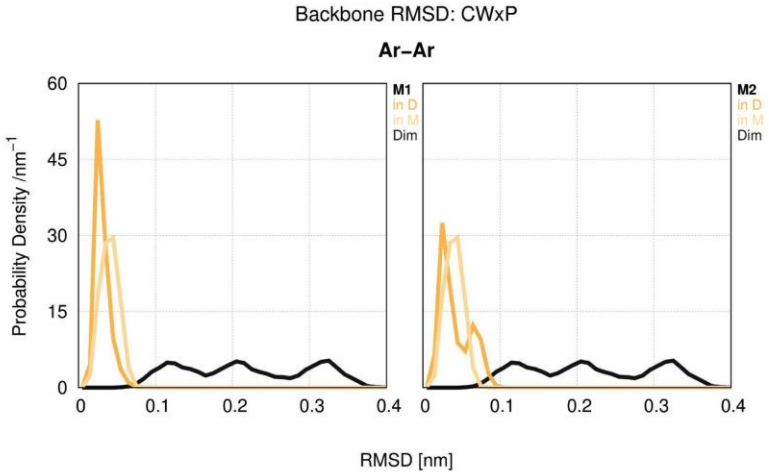

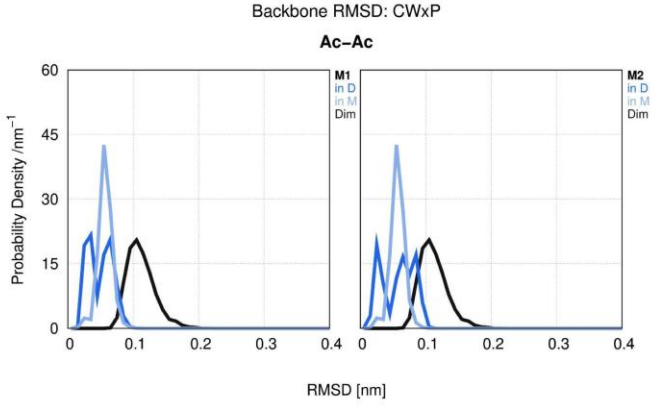

S8-CWxP motif

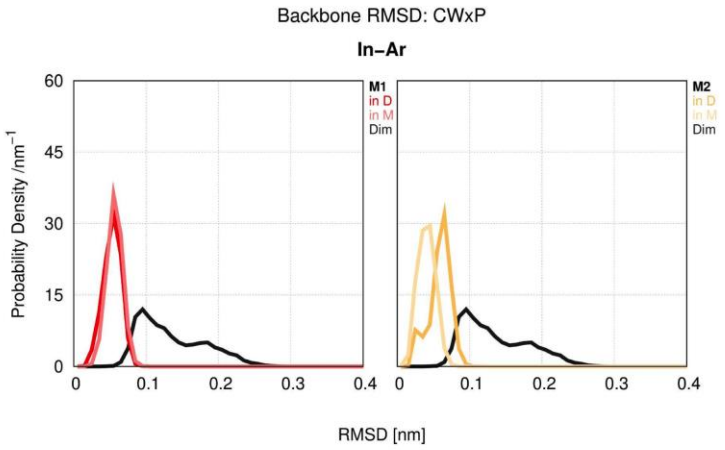

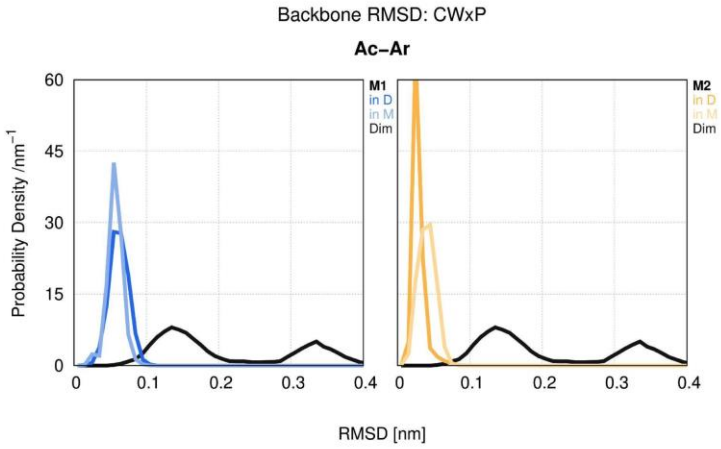

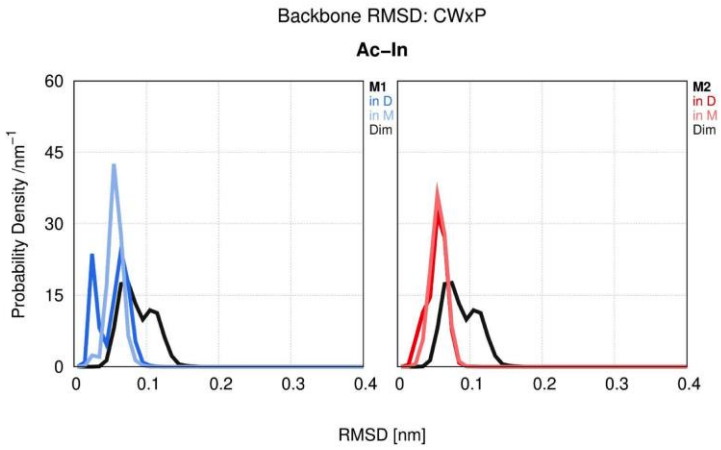

S8-Ionic lock

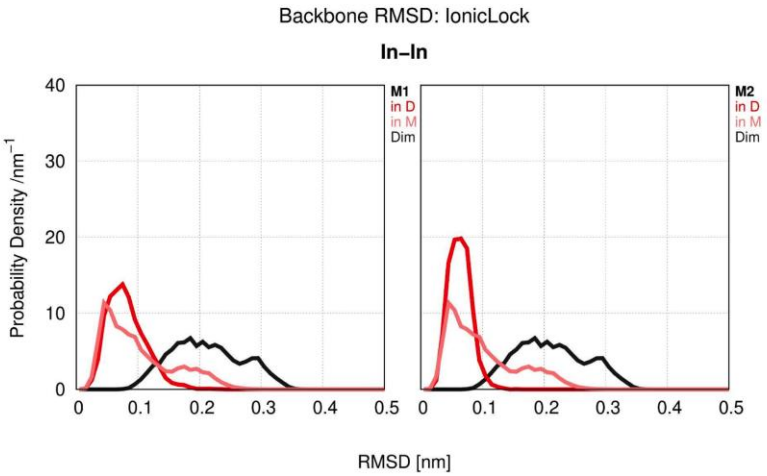

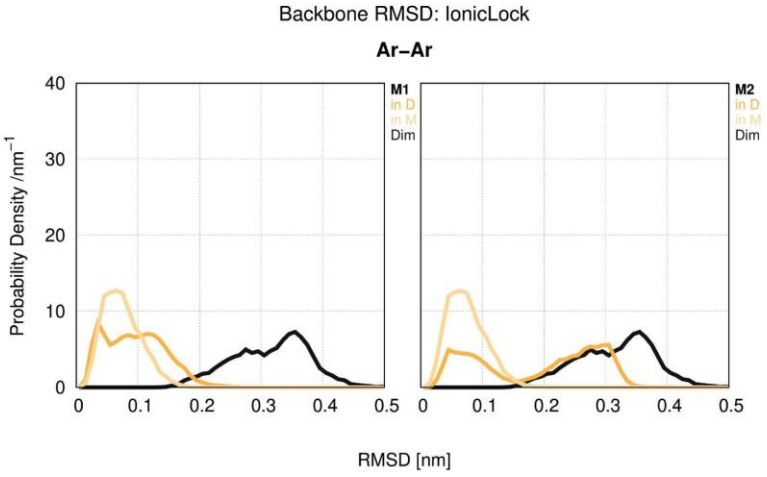

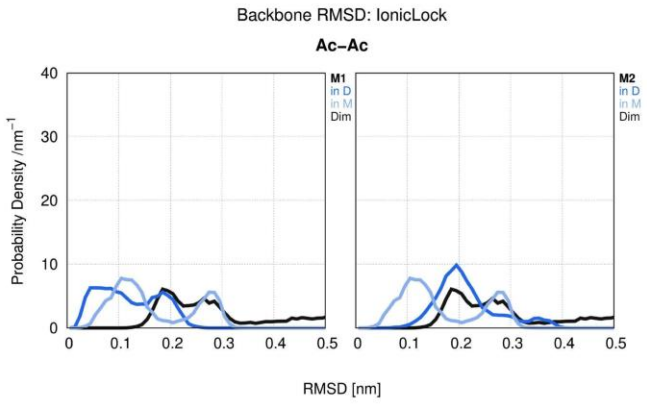

S8-Ionic lock

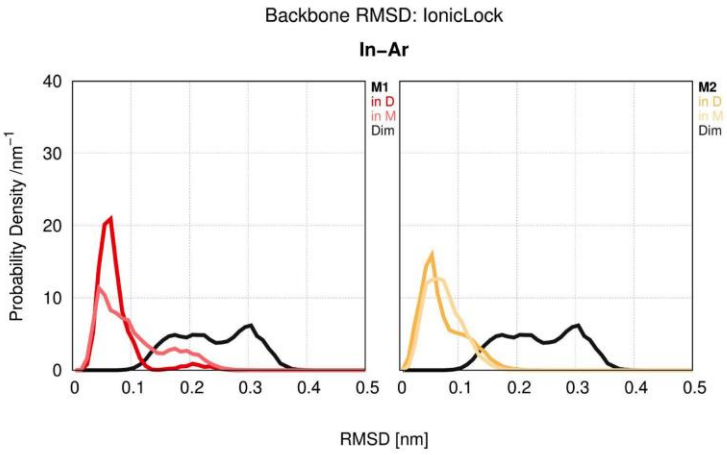

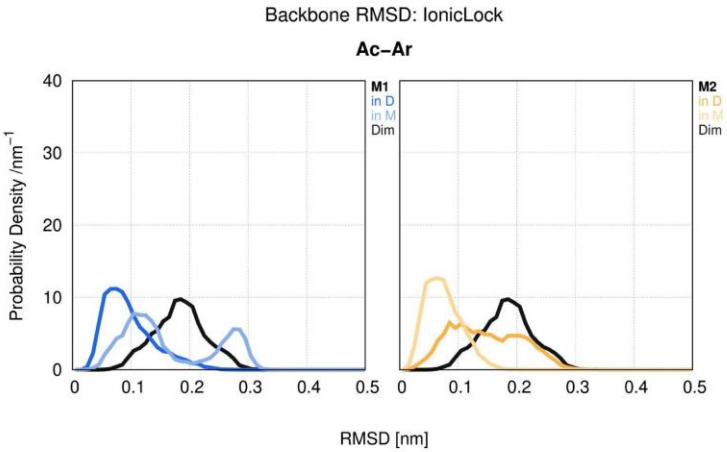

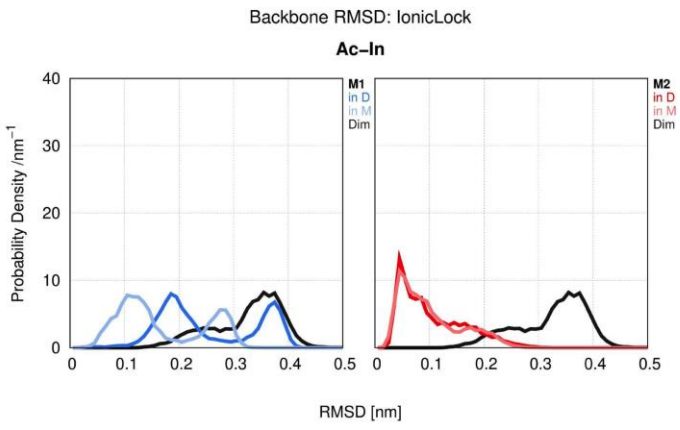

S8-NPxxY motif

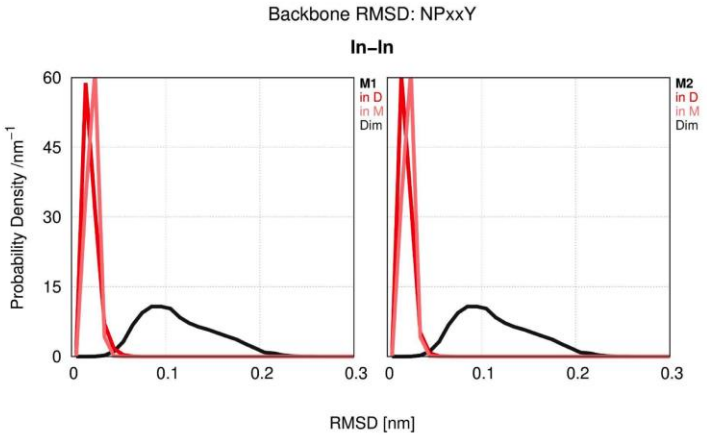

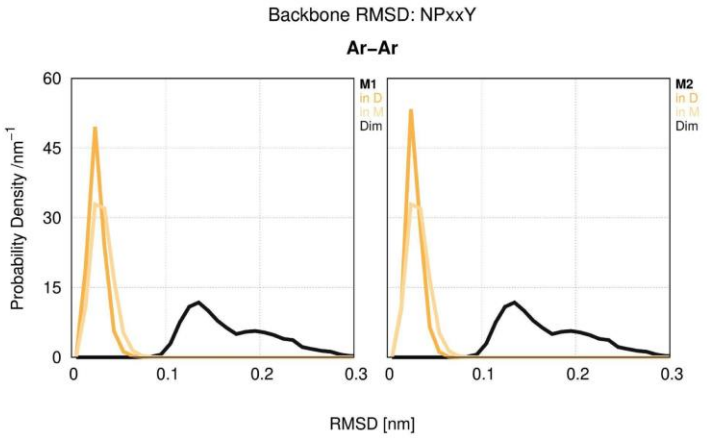

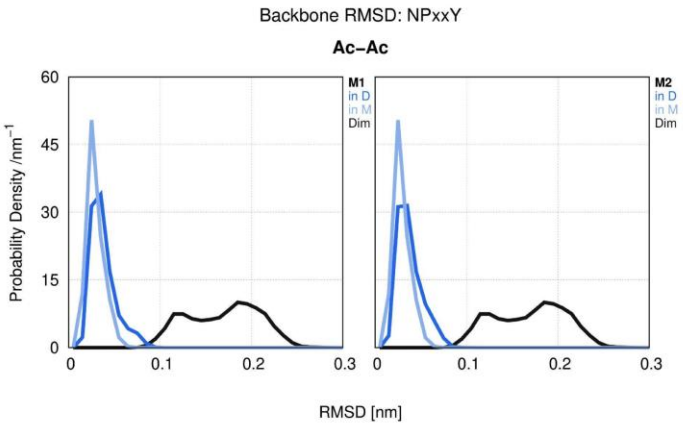

S8-NPxxY motif

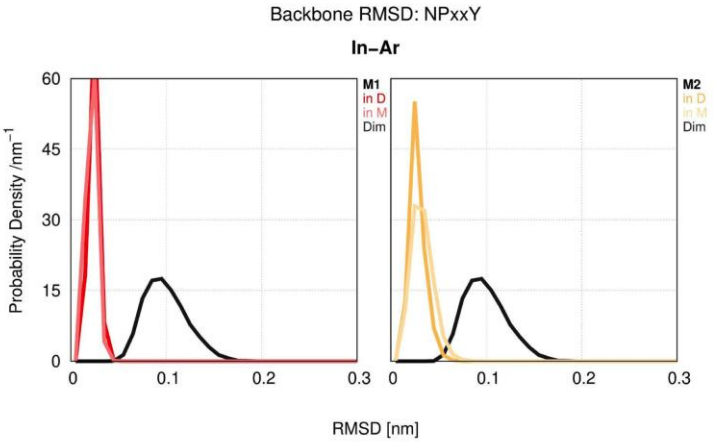

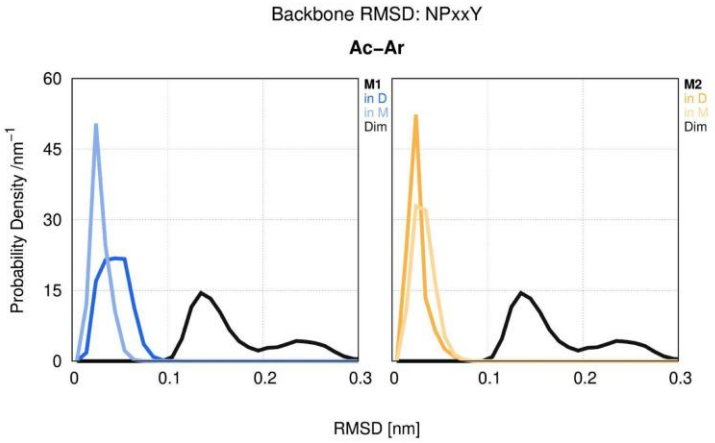

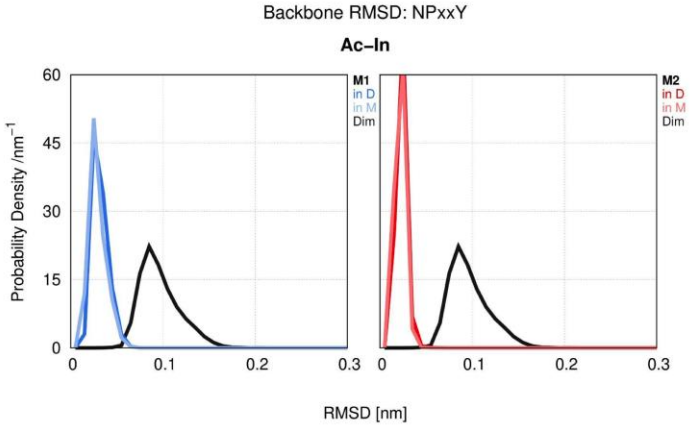

S8-PIF motif

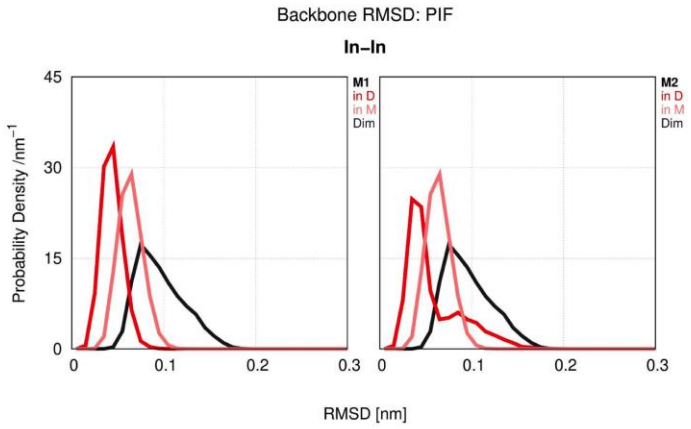
Backbone RMSD: PIF
In–In
M1
in D
in M
Dim
M2
in D
in M
Dim
Probability Density /nm^{-1}
45
30
15
0
0
0.1
0.2
0.3
RMSD [nm]

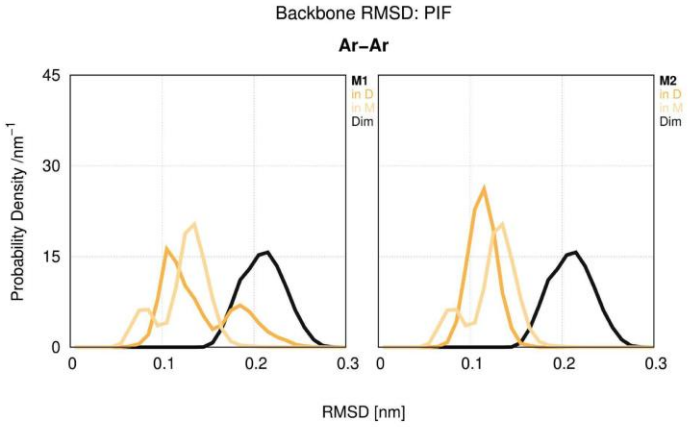
Backbone RMSD: PIF
Ar–Ar
M1
in D
in M
Dim
M2
in D
in M
Dim
Probability Density /nm^{-1}
45
30
15
0
0
0.1
0.2
0.3
RMSD [nm]

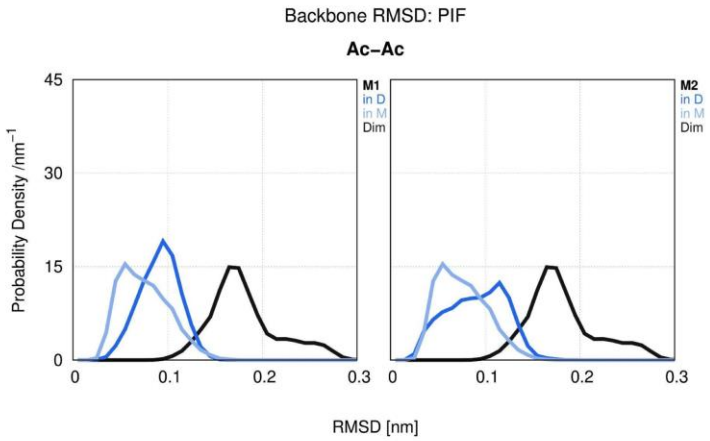
Backbone RMSD: PIF
Ac–Ac
M1
in D
in M
Dim
M2
in D
in M
Dim
Probability Density /nm^{-1}
45
30
15
0
0
0.1
0.2
0.3
RMSD [nm]

S8-PIF motif

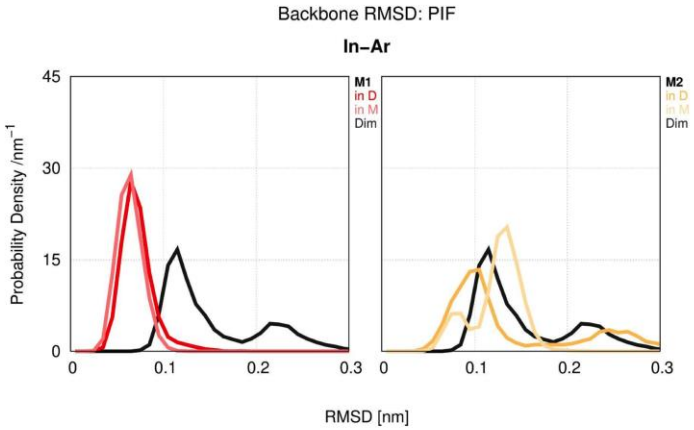
Backbone RMSD: PIF
In–Ar
Probability Density /nm⁻¹
RMSD [nm]
M1
in D
in M
Dim
M2
in D
in M
Dim

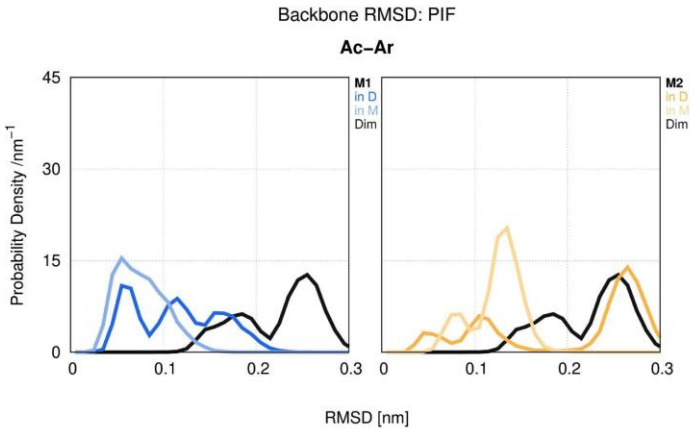
Backbone RMSD: PIF
Ac–Ar
Probability Density /nm⁻¹
RMSD [nm]
M1
in D
in M
Dim
M2
in D
in M
Dim

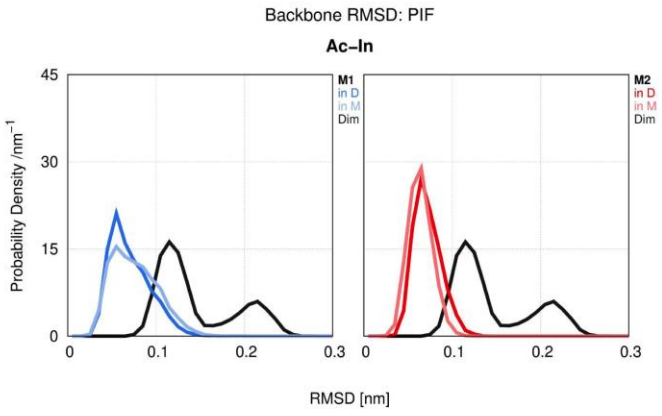
Backbone RMSD: PIF
Ac–In
Probability Density /nm⁻¹
RMSD [nm]
M1
in D
in M
Dim
M2
in D
in M
Dim

S8-Arginine cage motif

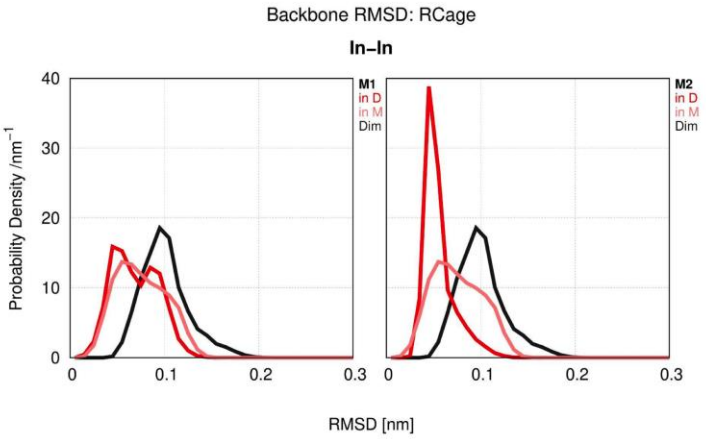

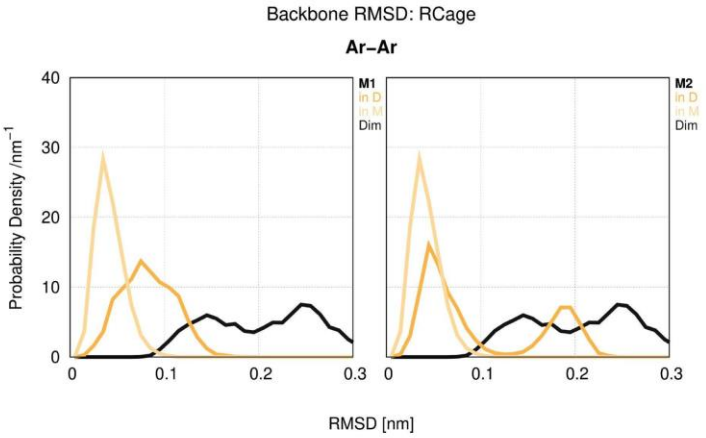

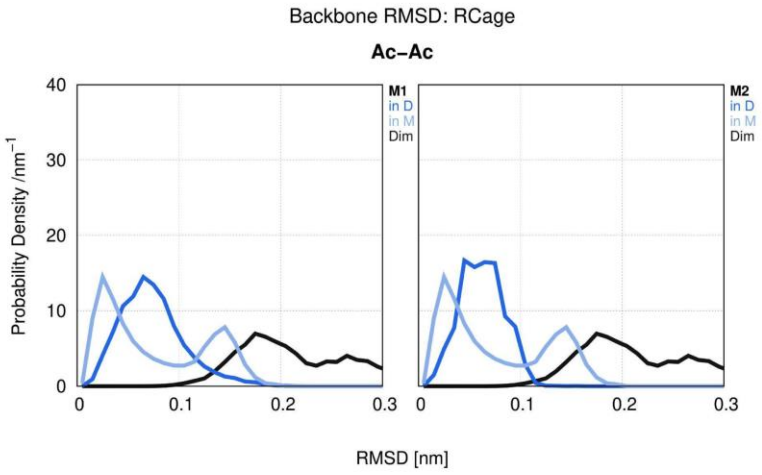

S8-Arginine cage motif

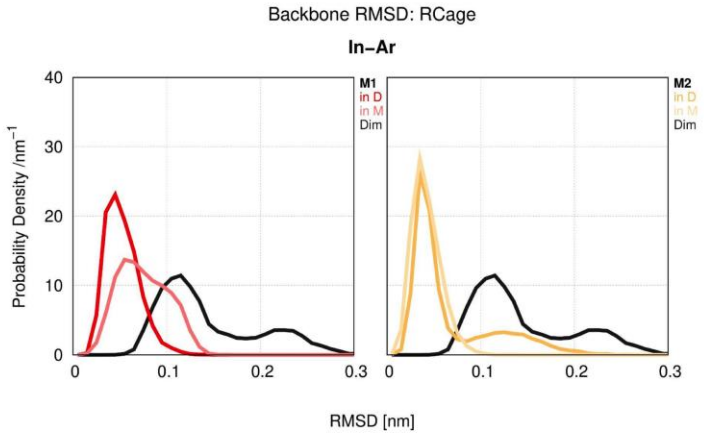

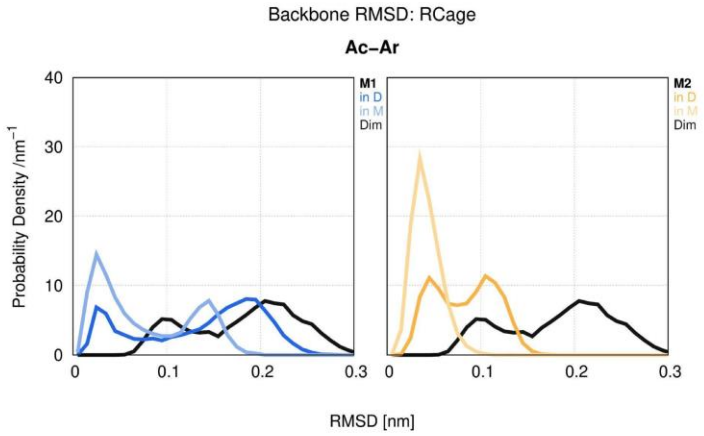

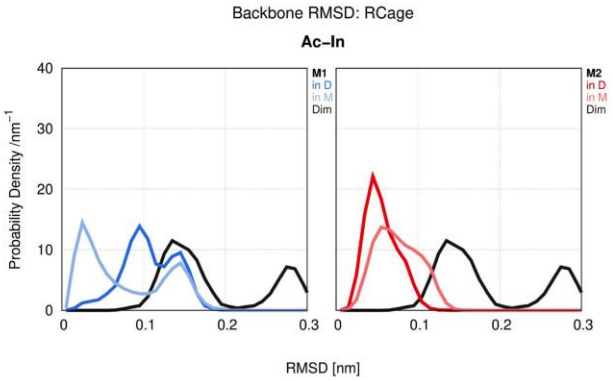

S8-Serine microdomain

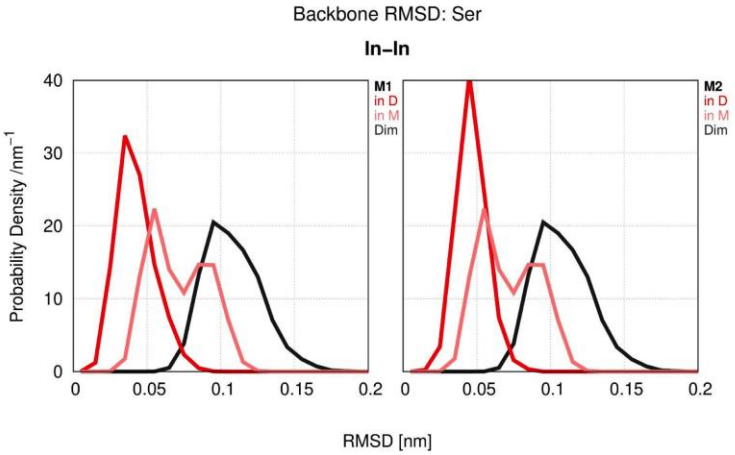

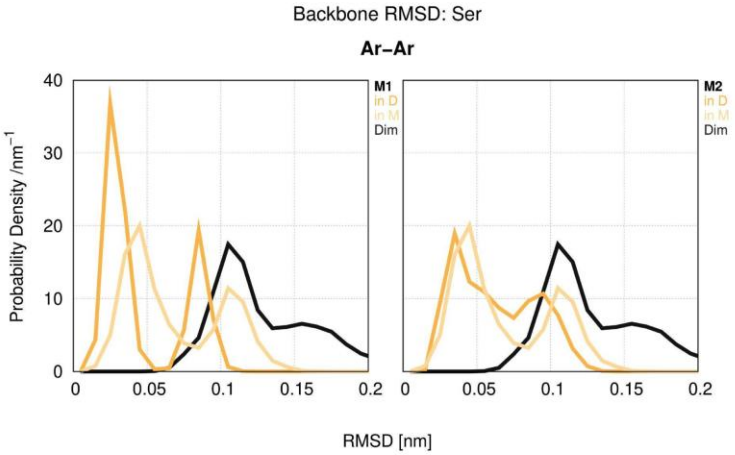

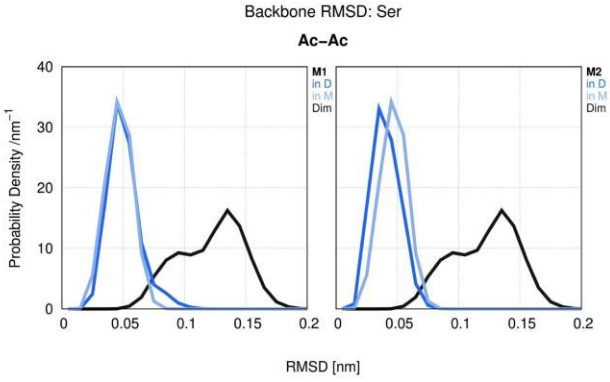

S8-Serine microdomain

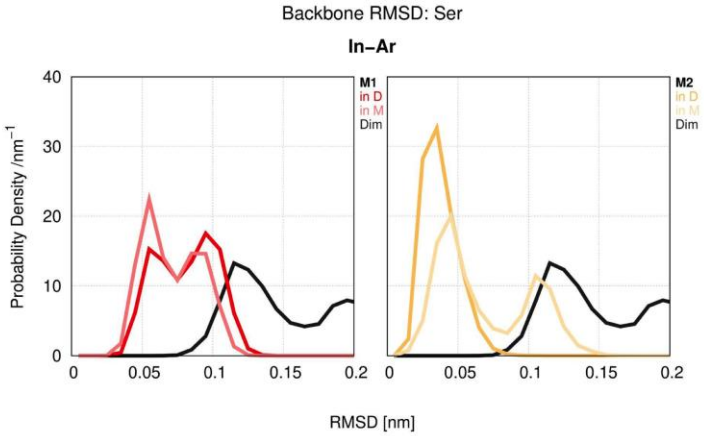

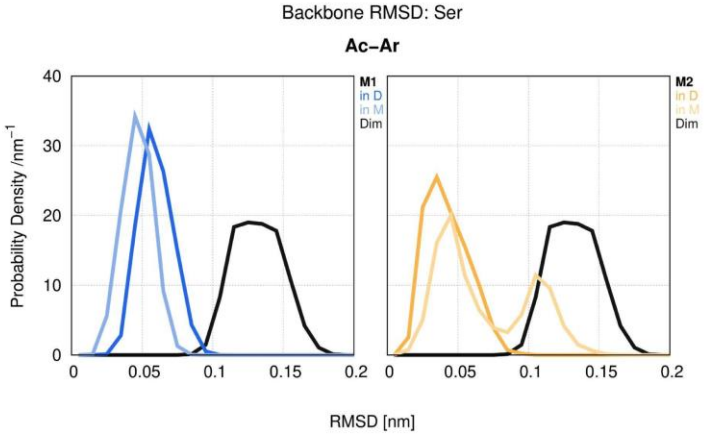

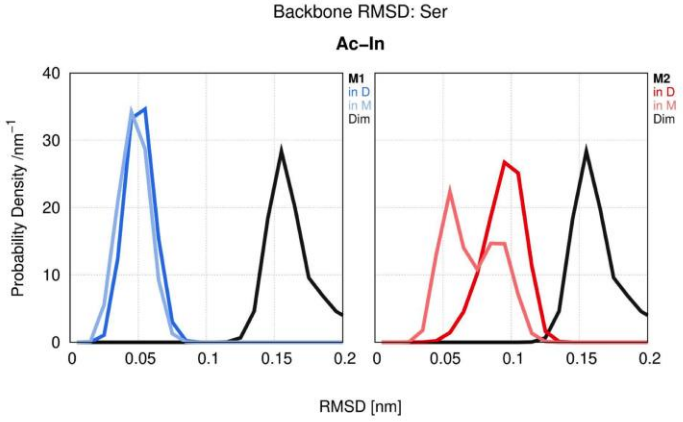

S8-Rotamer toggle switch

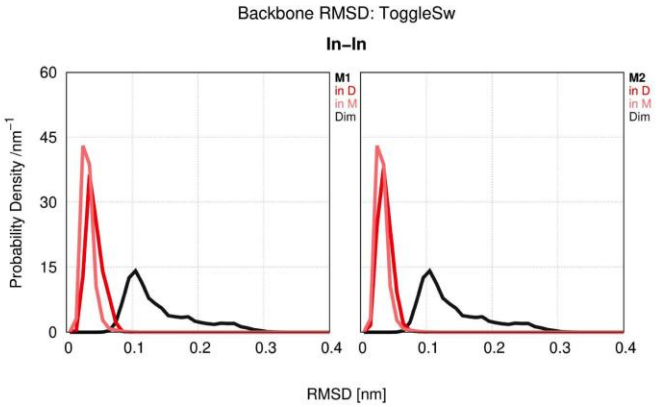

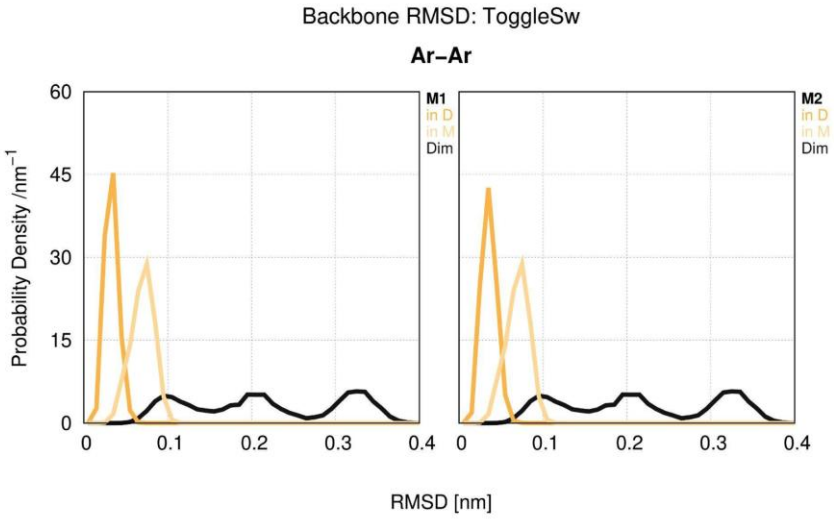

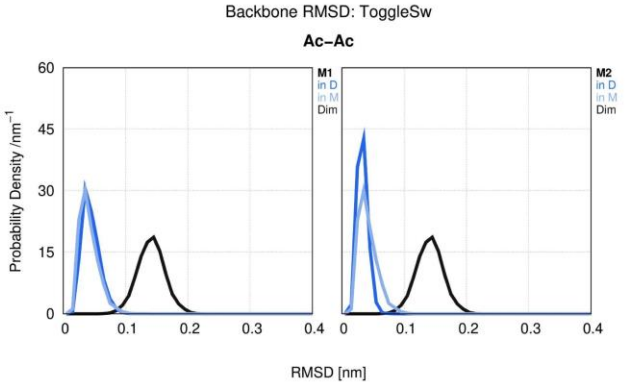

S8-Rotamer toggle switch

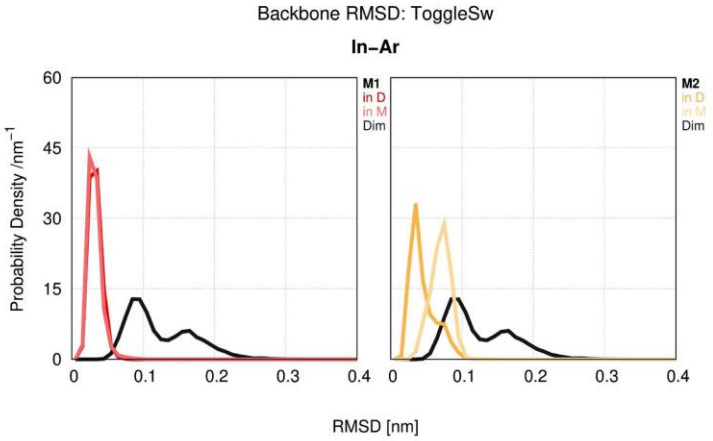

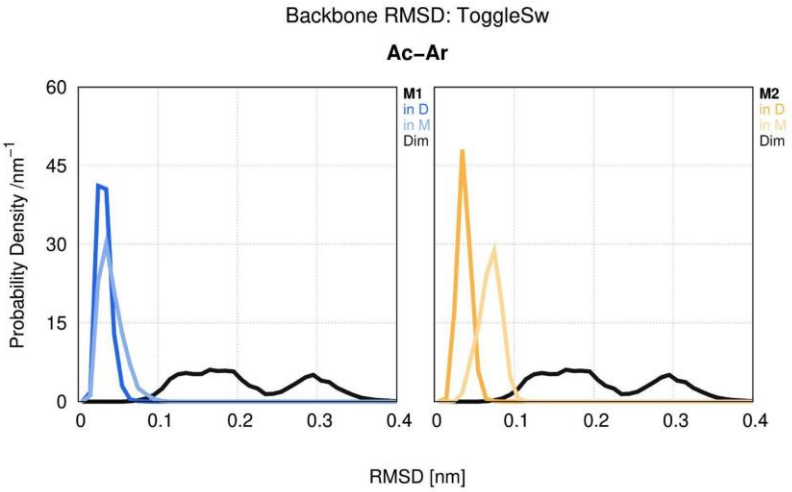

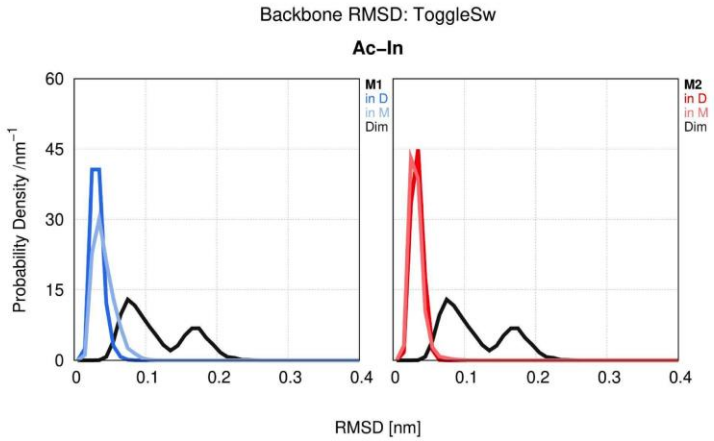

Figure S8. Equilibration of the systems. The equilibration status of the systems was verified using root-mean-square deviations (RMSD) calculated for the backbone of the transmembrane helices (TMs), the loops and structural motifs including DRY (3.49, 3.50 and 3.51), CWxP (6.47, 6.48, 6.49 and 6.50), the ionic lock (3.50 and 6.30), NPxxY (7.49, 7.50, 7.51, 7.52 and 7.53), PIF (5.50, 3.40 and 6.44), arginine cage (3.46 and 6.37), serine microdomain (5.42, 5.43 and 5.46), rotamer toggle switch (6.48, 6.51, 6.52 and 6.55). For these representations the total 500 ns of the simulations were utilized. The black lines represent the dimers in total (Dim), while dark colours represent the monomers within the dimer (M1/M2 in D) and the light colours represent the monomers alone (M1/M2 in M). Conformations are colour-coded: inactive - red, arrestin - yellow, active - blue.

S9

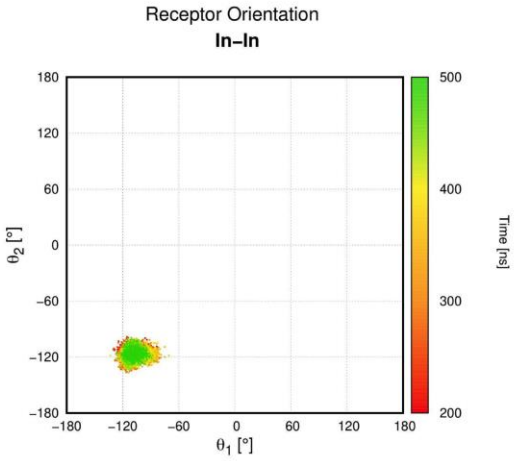
Receptor Orientation
In–In
180
120
60
0
−60
−120
−180
θ2 [°]
−180 −120 −60 0 60 120 180
θ1 [°]
500
400
300
200
Time [ns]

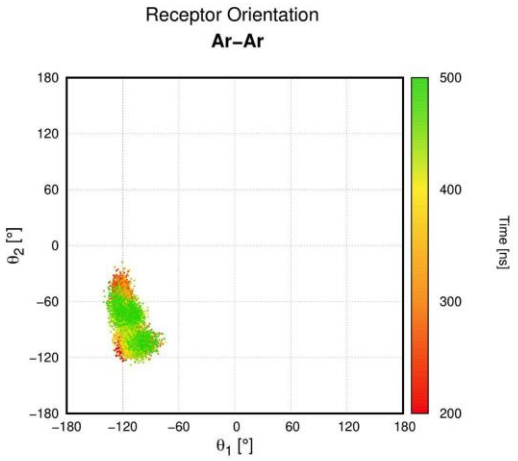
Receptor Orientation
Ar–Ar
180
120
60
0
−60
−120
−180
θ2 [°]
−180 −120 −60 0 60 120 180
θ1 [°]
500
400
300
200
Time [ns]

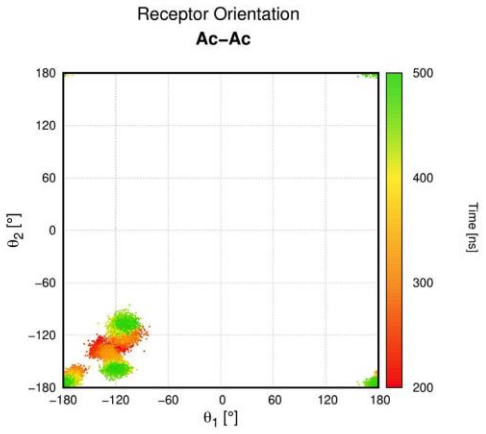
Receptor Orientation
Ac–Ac
180
120
60
0
−60
−120
−180
θ2 [°]
−180 −120 −60 0 60 120 180
θ1 [°]
500
400
300
200
Time [ns]

S9

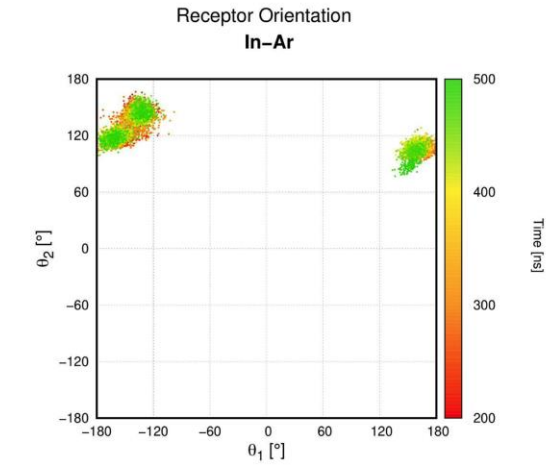
Receptor Orientation
In–Ar
180
120
60
0
−60
−120
−180
θ2 [°]
−180 −120 −60 0 60 120 180
θ1 [°]
500
400
300
200
Time [ns]

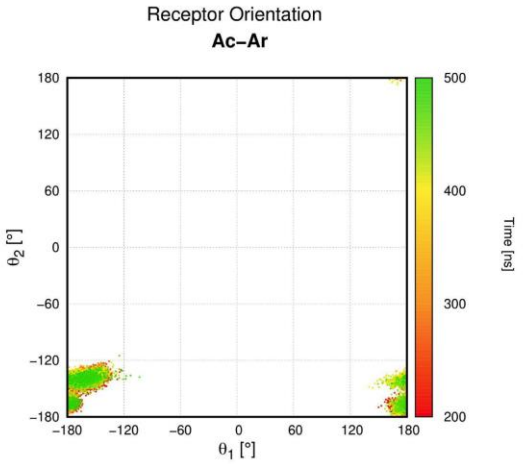
Receptor Orientation
Ac–Ar
180
120
60
0
−60
−120
−180
θ2 [°]
−180 −120 −60 0 60 120 180
θ1 [°]
500
400
300
200
Time [ns]

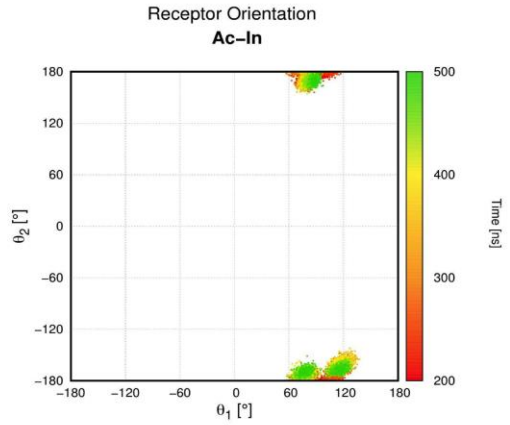
Receptor Orientation
Ac–In
180
120
60
0
−60
−120
−180
θ2 [°]
−180 −120 −60 0 60 120 180
θ1 [°]
500
400
300
200
Time [ns]

Figure S9. Orientation of the systems. Conformational plasticity of the D_2R-homodimer configurations was verified according to Prasanna et al. (2016). The following angles were observed along the MD simulations: θ1 consisting of residues 1.48, 4.53, 4.56 from protomer 1 and 4.56 from protomer 2; and θ2, consisting of residues 1.48, 4.53, 4.56 from protomer 2 and 4.56 from protomer 1. Conformer B (Figures 2 and S2 of Prasanna et al., 2016) corresponds to the interface of the D_2R homodimer and was used as reference with θ1 and θ2 between -50 and -150°. Residues for θ1 and θ2 in the D_2R homodimer configurations were identified according to Paila et al. (2010).
References:

- Prasanna, X., Sengupta, D. & Chattopadhyay, A. Cholesterol-dependent Conformational Plasticity in GPCR Dimers. *Sci Rep* 6, 31858 (2016). DOI: 10.1038/srep31858
- Paila, Y. D., Kombrabail, M., Krishnamoorthy, G. & Chattopadhyay, A. Oligomerization of the serotonin1A receptor in live cells: a time-resolved fluorescence anisotropy approach. J. Phys. Chem. B. 115, 11439–11447 (2011). DOI: 10.1021/jp201458h

S10

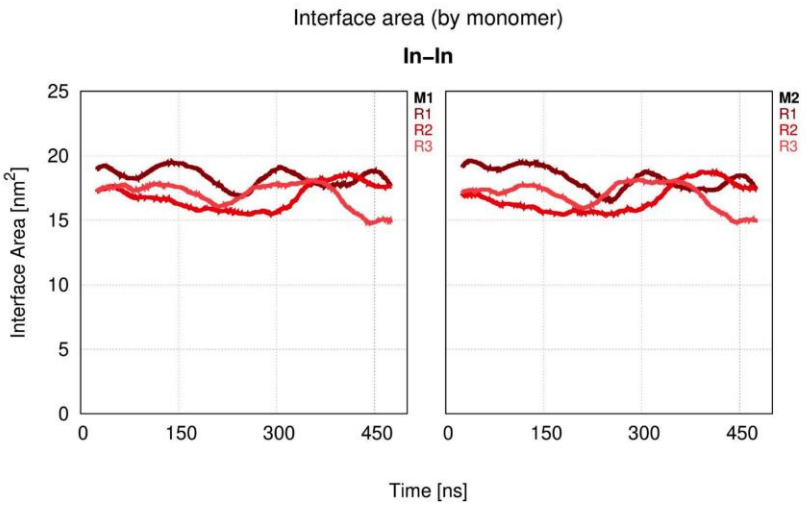
Interface area (by monomer)
In–In
Interface Area [nm^2]
Time [ns]
M1
R1
R2
R3
M2
R1
R2
R3

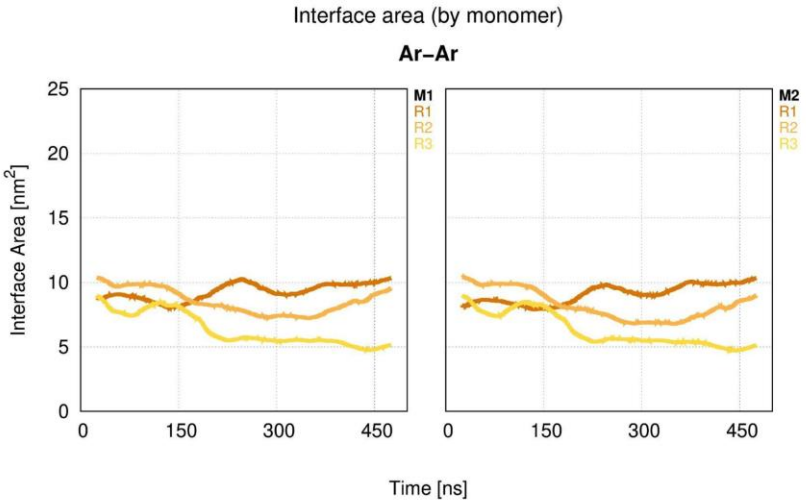
Interface area (by monomer)
Ar–Ar
Interface Area [nm^2]
Time [ns]
M1
R1
R2
R3
M2
R1
R2
R3

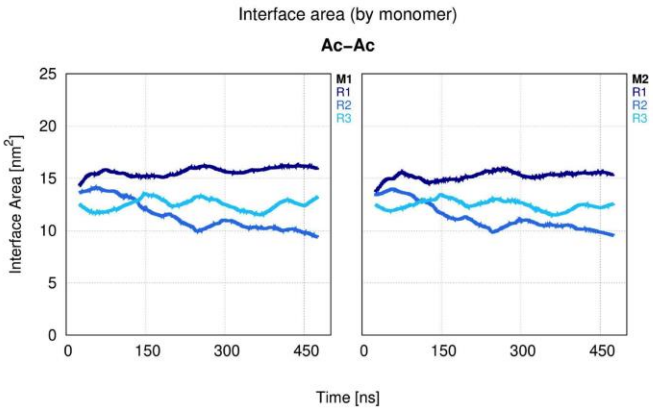
Interface area (by monomer)
Ac–Ac
Interface Area [nm^2]
Time [ns]
M1
R1
R2
R3
M2
R1
R2
R3

S10

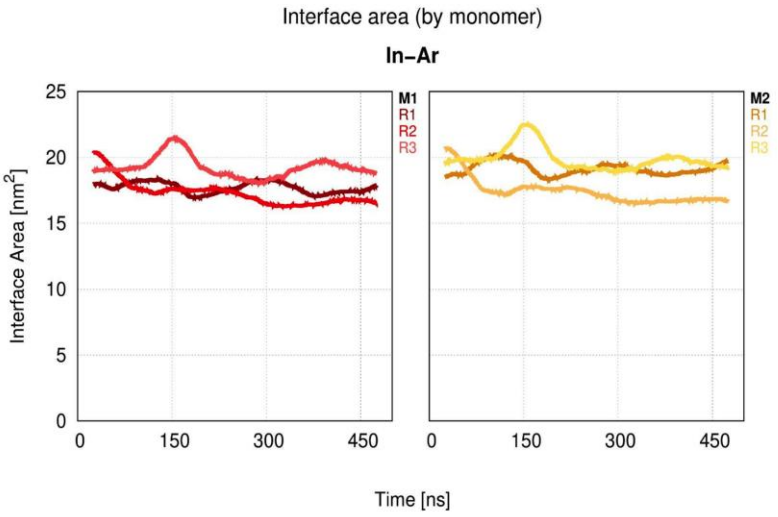
Interface area (by monomer)
In–Ar
Interface Area [nm^2]
Time [ns]
M1
R1
R2
R3
M2
R1
R2
R3

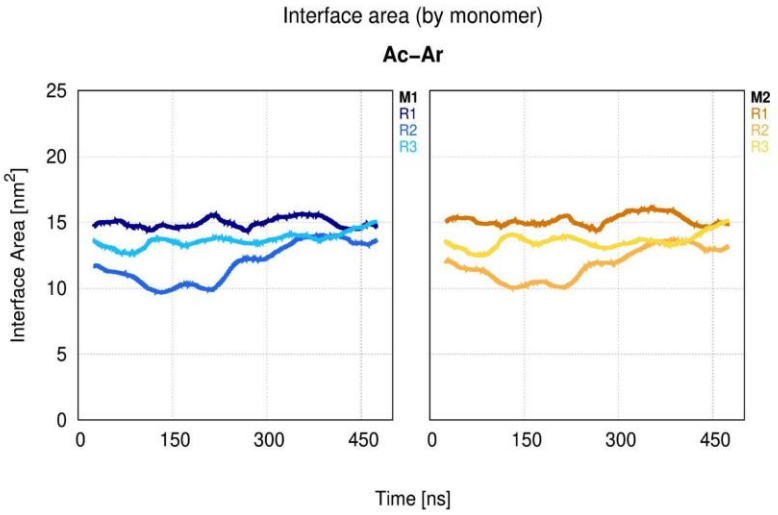
Interface area (by monomer)
Ac–Ar
Interface Area [nm^2]
Time [ns]
M1
R1
R2
R3
M2
R1
R2
R3

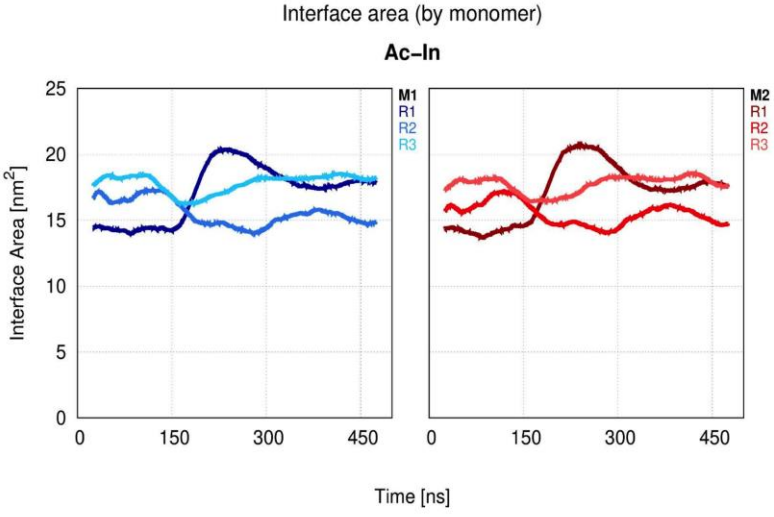
Interface area (by monomer)
Ac–In
Interface Area [nm^2]
Time [ns]
M1
R1
R2
R3
M2
R1
R2
R3

Figure S10. Interface area over time. Interface area of the D_2R homodimer configurations was followed over time. The interface area was calculated using the solvent accessible surface area (SASA). The difference (DSASA) between a residue in monomeric and dimeric state was calculated using $DSASA=(SASA_{monomer}-SASA_{dimer})$. Precisely, the SASA of each monomer was determined in the presence and absence of the partnered monomer. Then the average was calculated: $A_{Interface}=(A_{Interface\ monomer1}+A_{Interface\ monomer2})/2$. Conformations are colour-coded: inactive - red, arrestin - yellow, active - blue.

S11

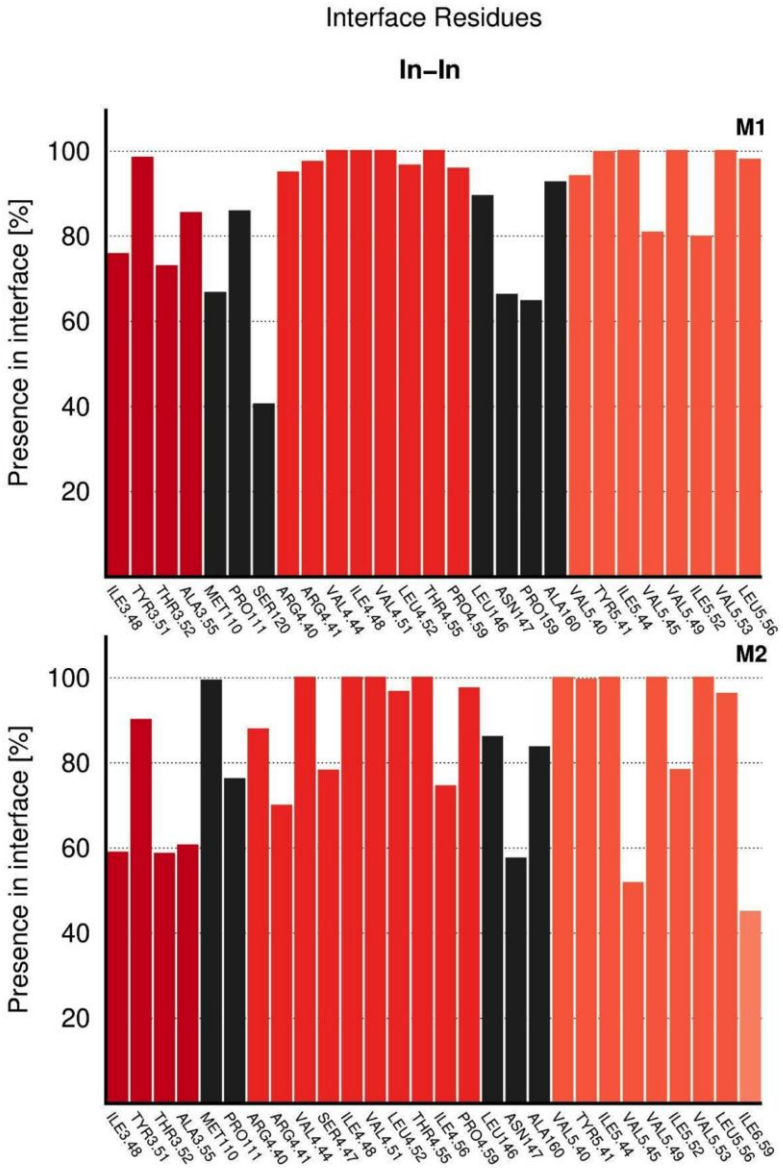
Interface Residues
In–In
M1
Presence in interface [%]
100
80
60
40
20
ILE3.48
TYR3.51
THR3.52
ALA3.55
MET110
PRO111
SER120
ARG4.40
ARG4.41
VAL4.44
ILE4.48
VAL4.51
LEU4.52
THR4.55
PRO4.59
LEU146
ASN147
PRO159
ALA160
VAL5.40
TYR5.41
ILE5.44
VAL5.45
VAL5.49
ILE5.52
VAL5.53
LEU5.56
M2
Presence in interface [%]
100
80
60
40
20
ILE3.48
TYR3.51
THR3.52
ALA3.55
MET110
PRO111
ARG4.40
ARG4.41
VAL4.44
SER4.47
ILE4.48
VAL4.51
LEU4.52
THR4.55
ILE4.56
PRO4.59
LEU146
ASN147
ALA160
VAL5.40
TYR5.41
ILE5.44
VAL5.45
VAL5.49
ILE5.52
VAL5.53
LEU5.56
ILE6.59

S11

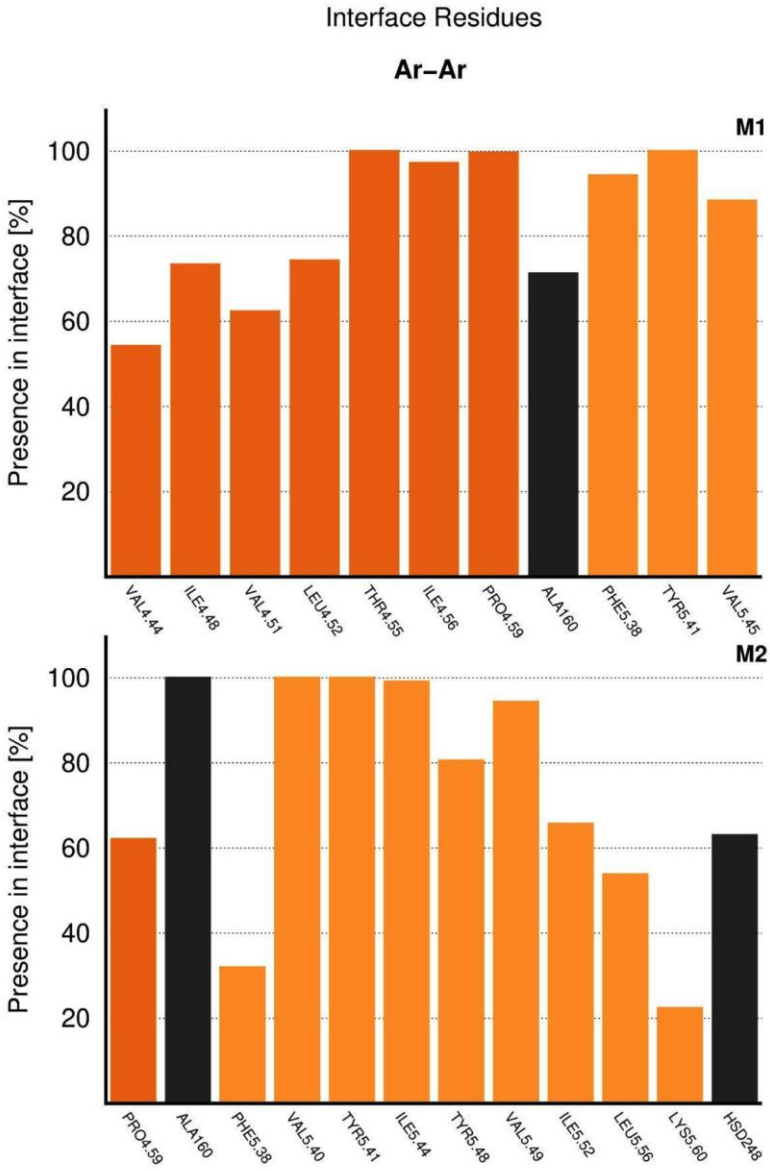
Interface Residues
Ar–Ar
M1
Presence in interface [%]
100
80
60
40
20
VAL4.44
ILE4.48
VAL4.51
LEU4.52
THR4.55
ILE4.56
PRO4.59
ALA160
PHE5.38
TYR5.41
VAL5.45
M2
Presence in interface [%]
100
80
60
40
20
PRO4.59
ALA160
PHE5.38
VAL5.40
TYR5.41
ILE5.44
TYR5.48
VAL5.49
ILE5.52
LEU5.56
LYS5.60
HSD248

S11

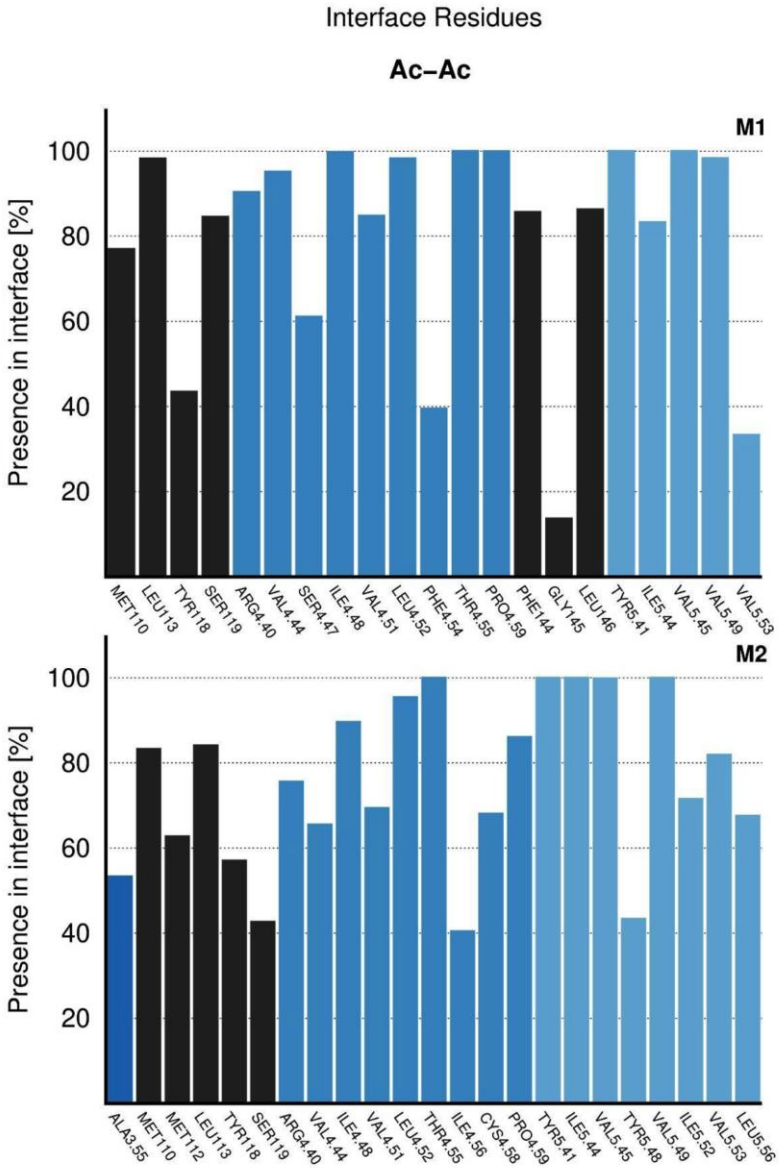
Interface Residues
Ac–Ac
M1
Presence in interface [%]
100
80
60
40
20
MET110
LEU113
TYR118
SER119
ARG4.40
VAL4.44
SER4.47
ILE4.48
VAL4.51
LEU4.52
PHE4.54
THR4.55
PRO4.59
PHE144
GLY145
LEU146
TYR5.41
ILE5.44
VAL5.45
VAL5.49
VAL5.53
M2
Presence in interface [%]
100
80
60
40
20
ALA3.55
MET110
MET112
LEU113
TYR118
SER119
ARG4.40
VAL4.44
ILE4.48
VAL4.51
LEU4.52
THR4.55
ILE4.56
CYS4.58
PRO4.59
TYR5.41
ILE5.44
VAL5.45
TYR5.48
VAL5.49
ILE5.52
VAL5.53
LEU5.56

S11

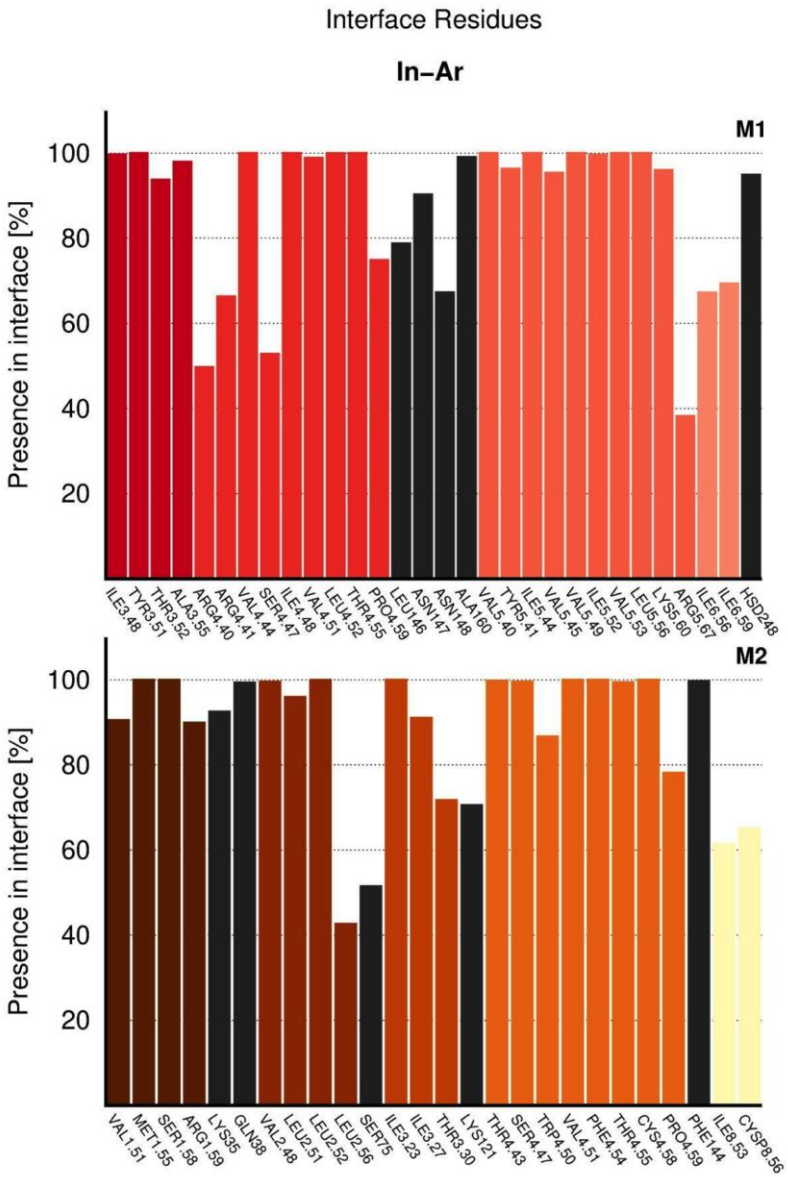
Interface Residues
In–Ar
M1
Presence in interface [%]
100
80
60
40
20
ILE3.48
TYR3.51
THR3.52
ALA3.55
ARG4.40
ARG4.41
VAL4.44
SER4.47
ILE4.48
VAL4.51
LEU4.52
THR4.55
PRO4.59
LEU146
ASN147
ASN148
ALA160
VAL5.40
TYR5.41
ILE5.44
VAL5.45
ILE5.49
ILE5.52
VAL5.53
LEU5.56
LYS5.60
ARG5.67
ILE6.56
ILE6.59
HSD248
M2
Presence in interface [%]
100
80
60
40
20
VAL1.51
MET1.55
SER1.58
ARG1.59
LYS95
GLN98
VAL2.48
LEU2.51
LEU2.52
LEU2.56
SER75
ILE3.23
ILE3.27
THR3.30
LYS121
THR4.43
SER4.47
TRP4.50
VAL4.51
PHE4.54
THR4.55
CYS4.58
PRO4.59
PHE144
ILE8.53
CYSP8.56

S11

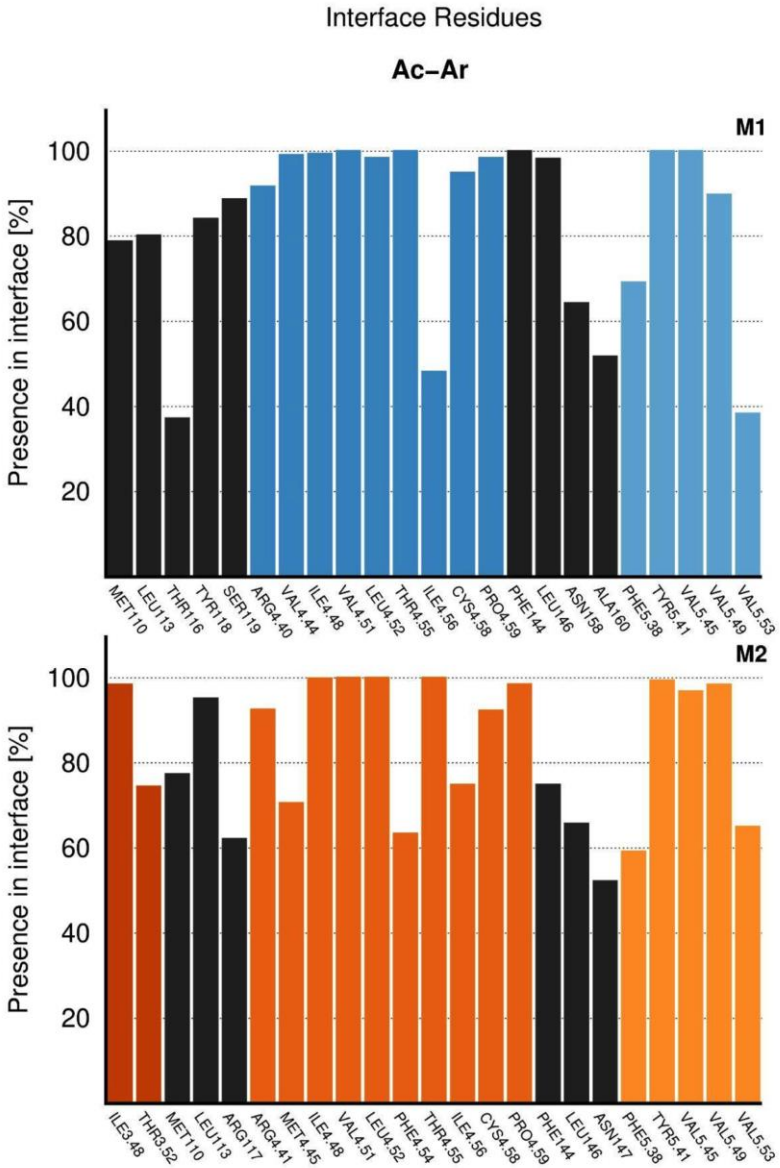
Interface Residues
Ac–Ar
M1
Presence in interface [%]
100
80
60
40
20
MET110
LEU113
THR116
TYR118
SER119
ARG4.40
VAL4.44
ILE4.48
VAL4.51
LEU4.52
THR4.55
ILE4.56
CYS4.58
PRO4.59
PHE144
LEU146
ASN158
ALA160
PHE5.38
TYR5.41
VAL5.45
VAL5.49
VAL5.53
M2
Presence in interface [%]
100
80
60
40
20
ILE3.48
THR3.52
MET110
LEU113
ARG117
ARG4.41
MET4.45
ILE4.48
VAL4.51
LEU4.52
PHE4.54
THR4.55
ILE4.56
CYS4.58
PRO4.59
PHE144
LEU146
ASN147
PHE5.38
TYR5.41
VAL5.45
VAL5.49
VAL5.53

S11

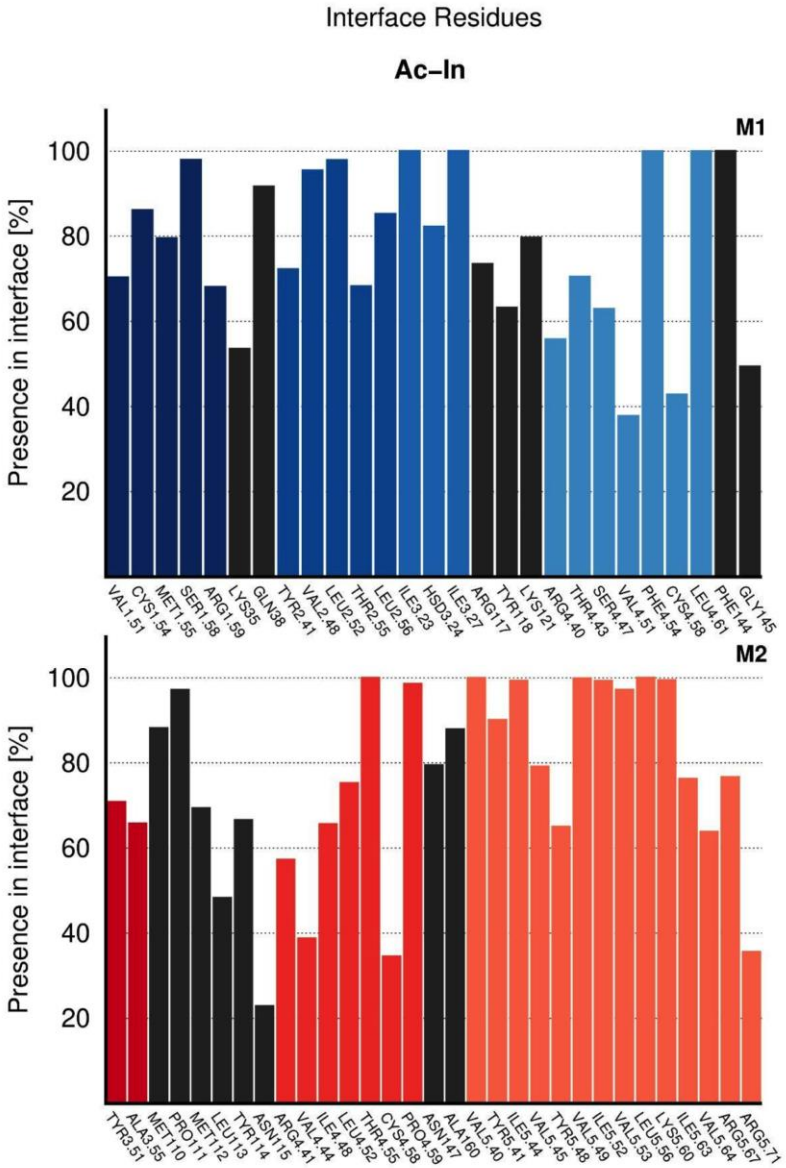
Interface Residues
Ac–In
M1
Presence in interface [%]
100
80
60
40
20
VAL1.51
CYS1.54
MET1.55
SER1.58
ARG1.59
LYS35
GLN38
TYR2.41
VAL2.48
LEU2.52
THR2.55
LEU2.56
ILE3.23
HSD3.24
ILE3.27
ARG117
TYR118
LYS121
ARG4.40
THR4.43
SER4.47
VAL4.51
PHE4.54
CYS4.58
LEU4.61
PHE144
GLY145
M2
Presence in interface [%]
100
80
60
40
20
TYR3.51
ALA3.55
MET110
PRO111
MET112
LEU113
TYR114
ASN115
ARG4.41
VAL4.44
ILE4.48
LEU4.52
THR4.55
CYS4.58
PRO4.59
ASN147
ALA160
VAL5.40
TYR5.41
ILE5.44
VAL5.45
TYR5.48
VAL5.49
ILE5.52
VAL5.53
LEU5.56
LYS5.60
ILE5.63
VAL5.64
ARG5.67
ARG5.71

Figure S11. Decoy original interfacial residues for the D_2R-homodimer configurations. Relevant residues were calculated the ΔSASA of each residue at the start of the simulation, where ΔSASA = ($SASA_m$ - $SASA_d$). $SASA_m$ is the SASA of a residue in the monomeric form and $SASA_d$ is the SASA in the dimeric form. Residues with a ΔSASA of 0 have the same exposure in both the dimeric and monomeric form, and as such, are not part of the initial interface. In addition to the requirement of a ΔSASA >0, another set of criteria to further narrow down this list was employed: residues should have a positive ΔSASA in at least 2/3 replicates, and this value had to be at least >0.05. ΔSASA was calculated over time for each residue on this list and normalized by dividing it by $SASA_{max}$, defined as the maximum SASA value for that residue type (i.e., when fully exposed). Only residues with a normalised ΔSASA >10% were considered to truly belong to the initial interface. Conformations are colour-coded: inactive - red, arrestin - yellow, active - blue. Black was used for the loop residues.

S12-Inactive-inactive

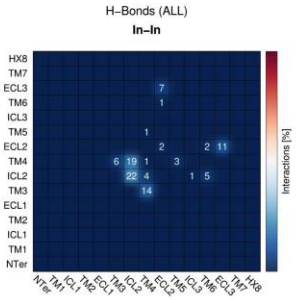

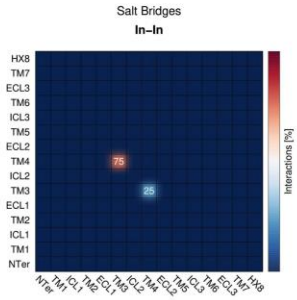

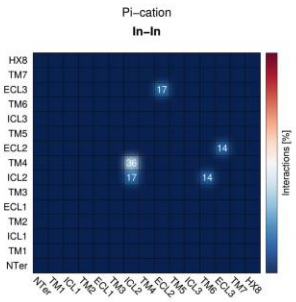

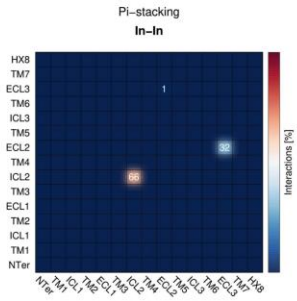

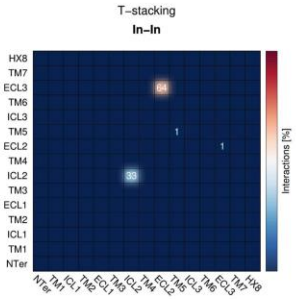

S12-Arrestin-Arrestin

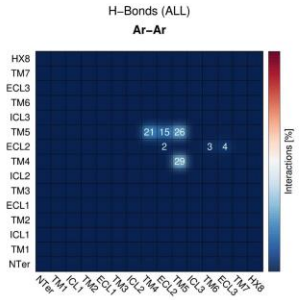

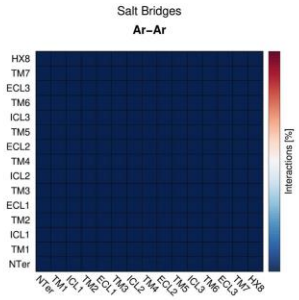

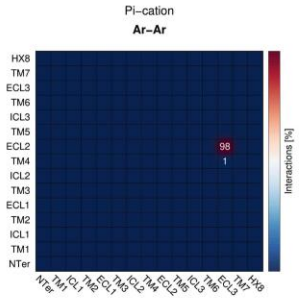

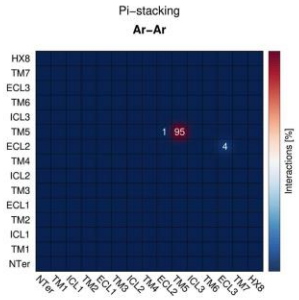

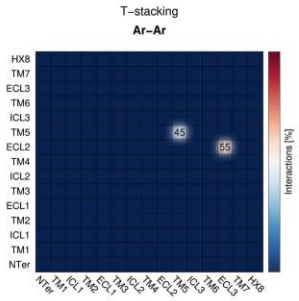

S12-Active-Active

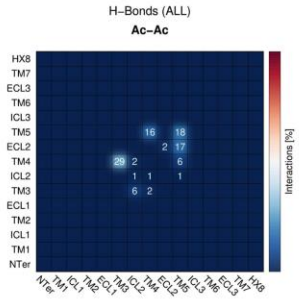

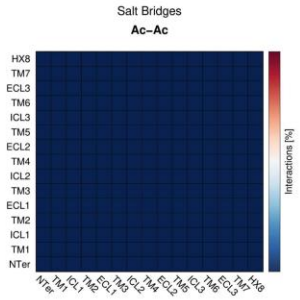

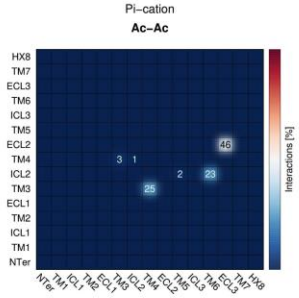

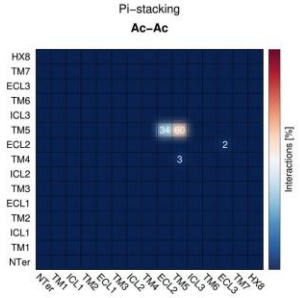

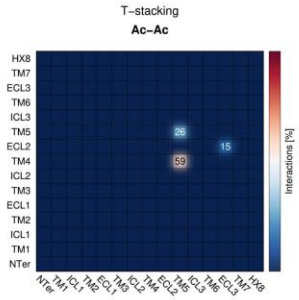

S12-Inactive-Arrestin

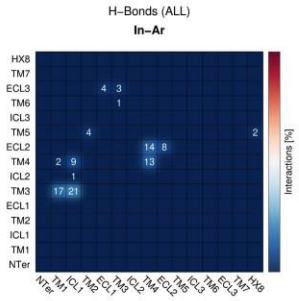

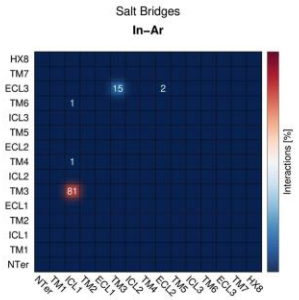

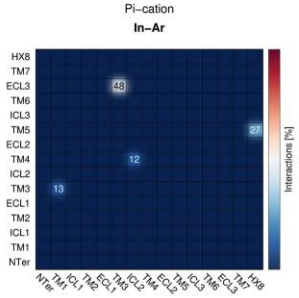

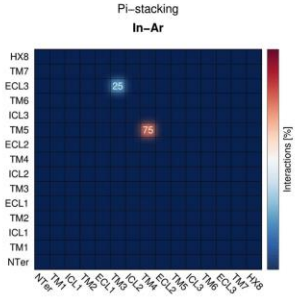

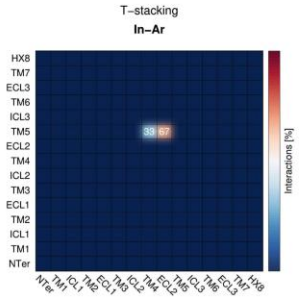

S12-Active-Arrestin

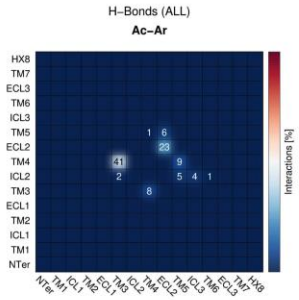

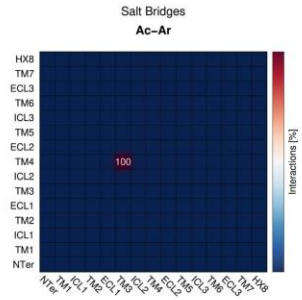

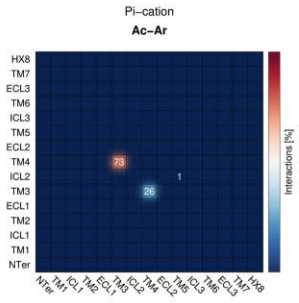

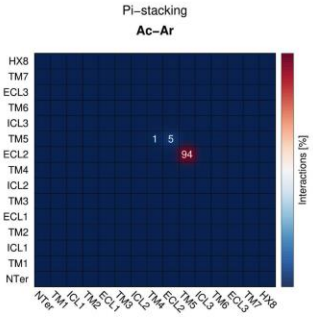

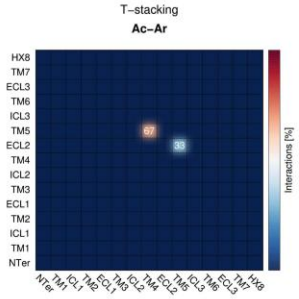

S12-Active-Inactive

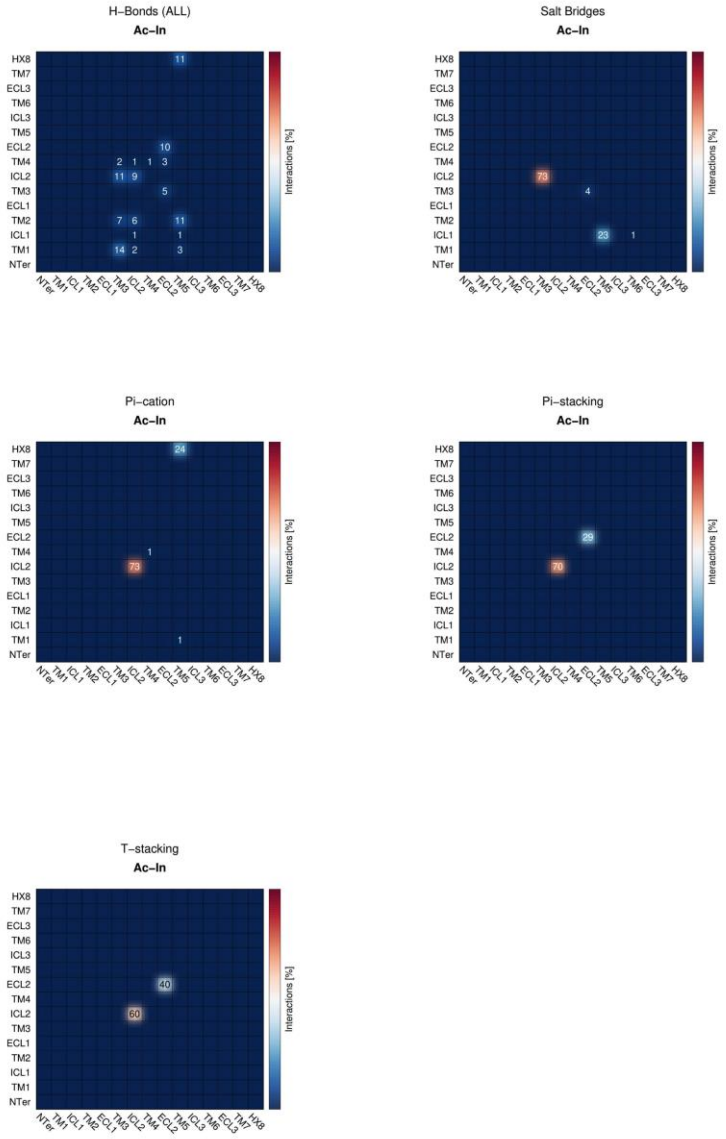

Figure

S12. Types of interaction of the original interface. The type of pairwise interaction established by the residues of the original interface of the D_2R homodimer configurations was determined and quantified using the GetContacts (https://getcontacts.github.io/index.html) application. For each system the average number and location of H-bonds, salt-bridges, π-cation, π-stacking, and T-stacking interactions were determined among the 3 replicates and simulation time (% interactions). Left axis: protomer 1, bottom axis: protomer 2.

S13

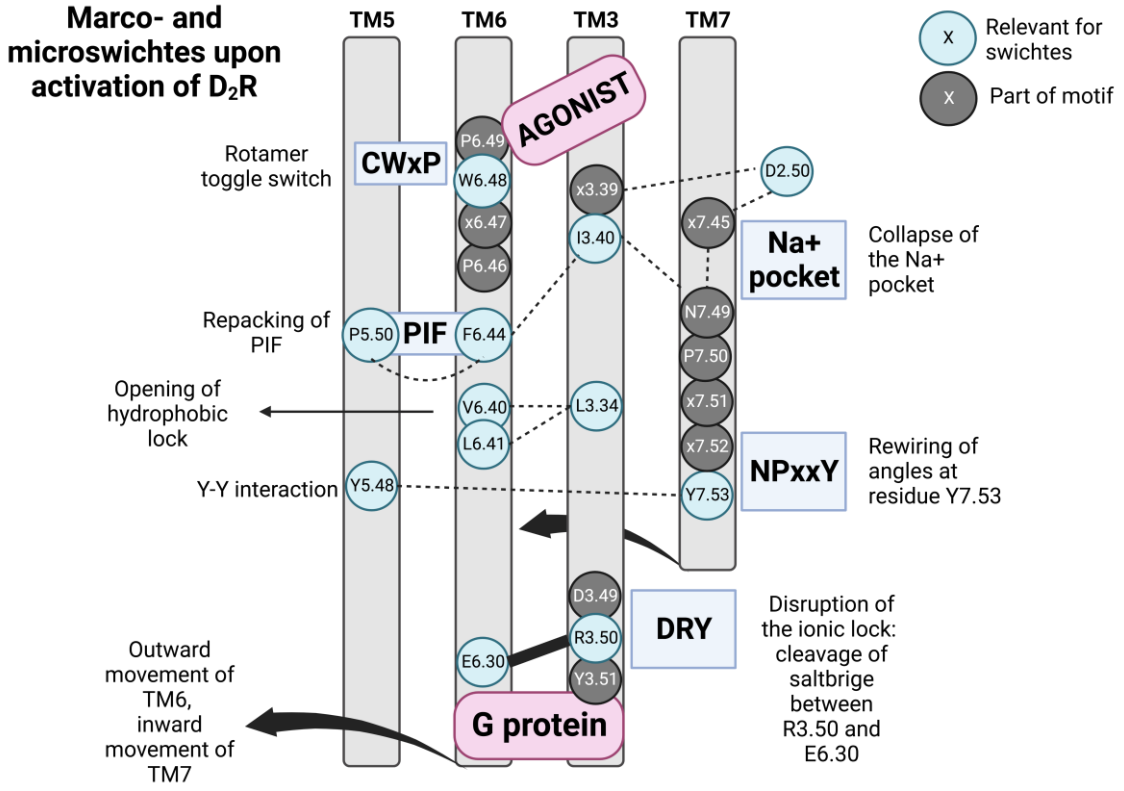

Figure S13. Most important macro- and microswichtes upon acitvation of class A GPCRs. Residues which are part of conserved structural motifs are colored grey, while residues which are involved in conformational swichtes are colored blue.

S14

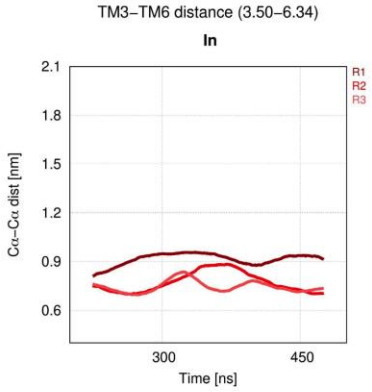
TM3–TM6 distance (3.50–6.34)
In
2.1
1.8
1.5
1.2
0.9
0.6
Cα–Cα dist [nm]
300
450
Time [ns]
R1
R2
R3

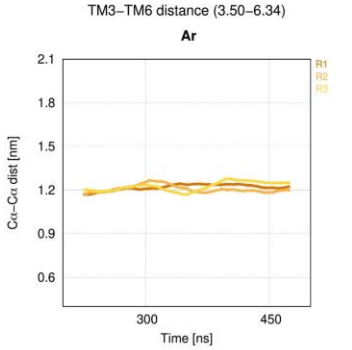
TM3–TM6 distance (3.50–6.34)
Ar
2.1
1.8
1.5
1.2
0.9
0.6
Cα–Cα dist [nm]
300
450
Time [ns]
R1
R2
R3

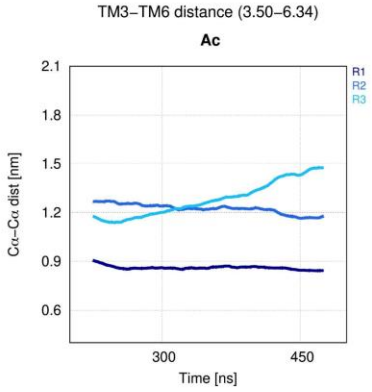
TM3–TM6 distance (3.50–6.34)
Ac
2.1
1.8
1.5
1.2
0.9
0.6
Cα–Cα dist [nm]
300
450
Time [ns]
R1
R2
R3

S14

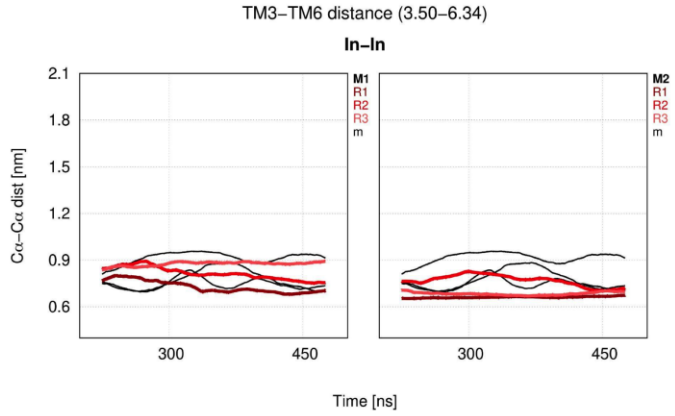
TM3–TM6 distance (3.50–6.34)
In–In
Cα–Cα dist [nm]
2.1
1.8
1.5
1.2
0.9
0.6
M1
R1
R2
R3
m
M2
R1
R2
R3
m
300
450
300
450
Time [ns]

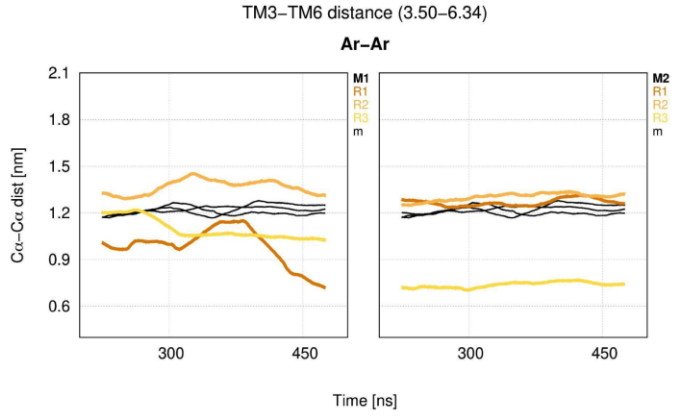
TM3–TM6 distance (3.50–6.34)
Ar–Ar
Cα–Cα dist [nm]
2.1
1.8
1.5
1.2
0.9
0.6
M1
R1
R2
R3
m
M2
R1
R2
R3
m
300
450
300
450
Time [ns]

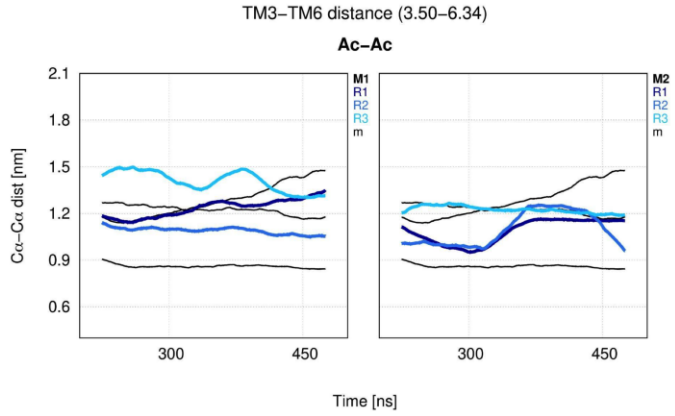
TM3–TM6 distance (3.50–6.34)
Ac–Ac
Cα–Cα dist [nm]
2.1
1.8
1.5
1.2
0.9
0.6
M1
R1
R2
R3
m
M2
R1
R2
R3
m
300
450
300
450
Time [ns]

S14

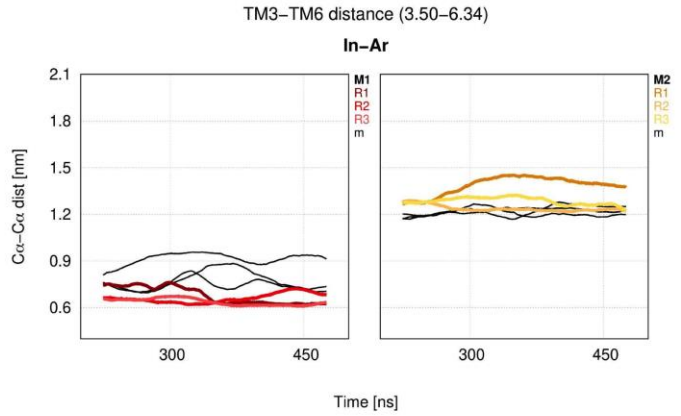
TM3–TM6 distance (3.50–6.34)
In–Ar
Cα–Cα dist [nm]
2.1
1.8
1.5
1.2
0.9
0.6
M1
R1
R2
R3
m
M2
R1
R2
R3
m
300
450
300
450
Time [ns]

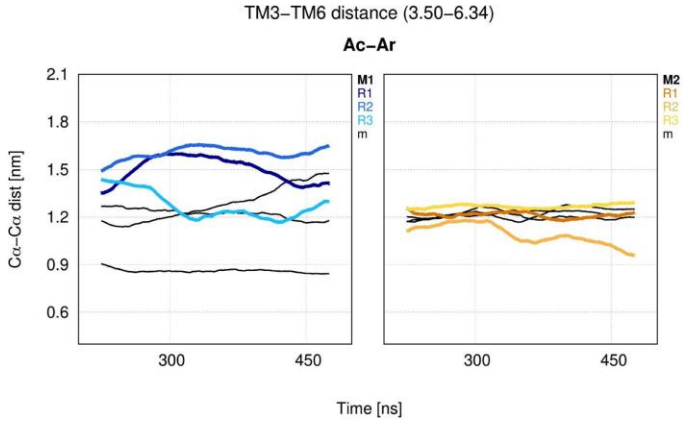
TM3–TM6 distance (3.50–6.34)
Ac–Ar
Cα–Cα dist [nm]
2.1
1.8
1.5
1.2
0.9
0.6
M1
R1
R2
R3
m
M2
R1
R2
R3
m
300
450
300
450
Time [ns]

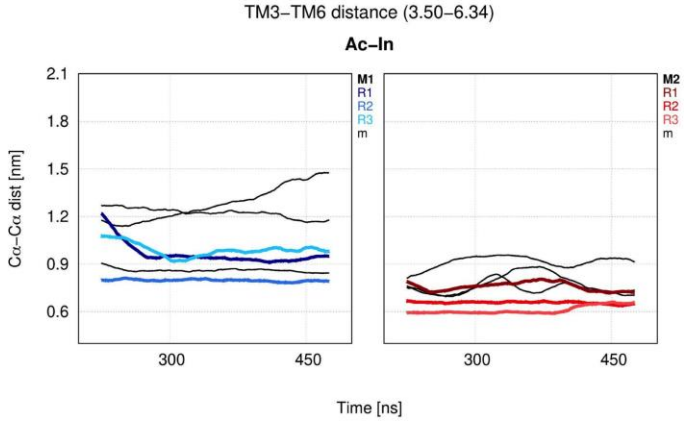
TM3–TM6 distance (3.50–6.34)
Ac–In
Cα–Cα dist [nm]
2.1
1.8
1.5
1.2
0.9
0.6
M1
R1
R2
R3
m
M2
R1
R2
R3
m
300
450
300
450
Time [ns]

Figure S14. Distance between TM3 and TM6. Distance [nM] between Cα-atoms of residues 3.50 and 6.34 for each dimer configuration over time [ns]. Replicates are color-coded and distance is compared to the distance of the replicates of the uncomplexed monomers (black lines) for each protomer. Conformations are colour-coded: inactive - red, arrestin - yellow, active - blue.

S15

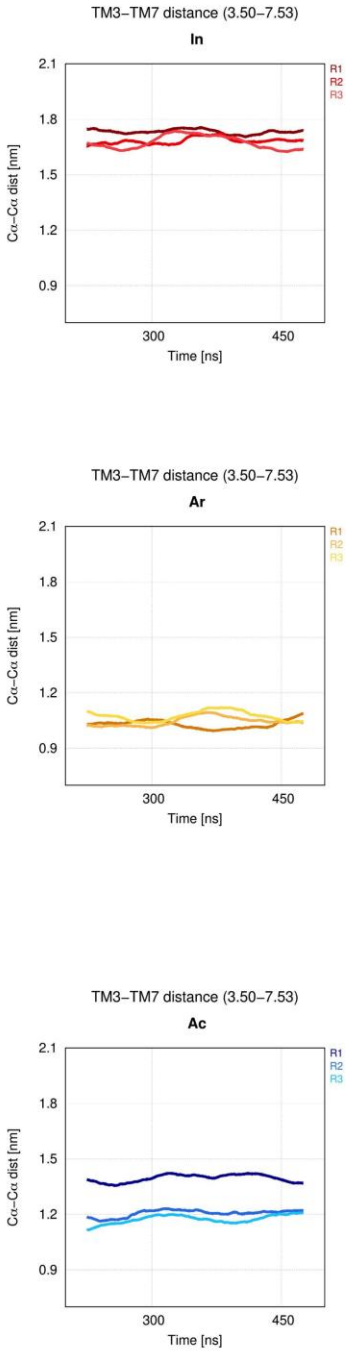
TM3–TM7 distance (3.50–7.53)
In
Cα–Cα dist [nm]
2.1
1.8
1.5
1.2
0.9
300
450
Time [ns]
R1
R2
R3
TM3–TM7 distance (3.50–7.53)
Ar
Cα–Cα dist [nm]
2.1
1.8
1.5
1.2
0.9
300
450
Time [ns]
R1
R2
R3
TM3–TM7 distance (3.50–7.53)
Ac
Cα–Cα dist [nm]
2.1
1.8
1.5
1.2
0.9
300
450
Time [ns]
R1
R2
R3

S15

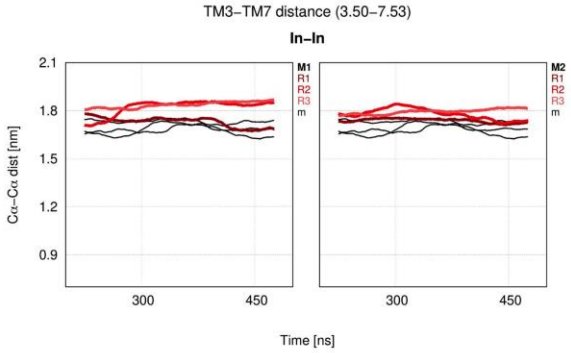
TM3–TM7 distance (3.50–7.53)
In–In
Cα–Cα dist [nm]
2.1
1.8
1.5
1.2
0.9
M1
R1
R2
R3
m
M2
R1
R2
R3
m
300
450
300
450
Time [ns]

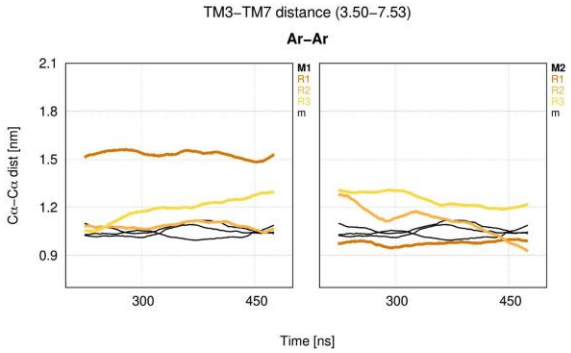
TM3–TM7 distance (3.50–7.53)
Ar–Ar
Cα–Cα dist [nm]
2.1
1.8
1.5
1.2
0.9
M1
R1
R2
R3
m
M2
R1
R2
R3
m
300
450
300
450
Time [ns]

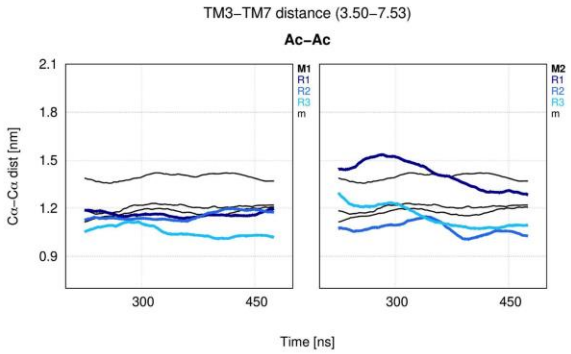
TM3–TM7 distance (3.50–7.53)
Ac–Ac
Cα–Cα dist [nm]
2.1
1.8
1.5
1.2
0.9
M1
R1
R2
R3
m
M2
R1
R2
R3
m
300
450
300
450
Time [ns]

S15

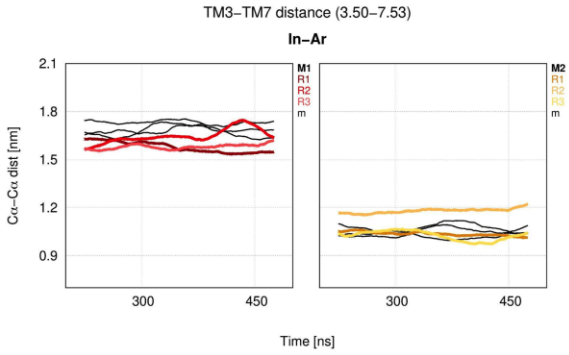
TM3–TM7 distance (3.50–7.53)
In–Ar
Cα–Cα dist [nm]
2.1
1.8
1.5
1.2
0.9
M1
R1
R2
R3
m
M2
R1
R2
R3
m
300
450
300
450
Time [ns]

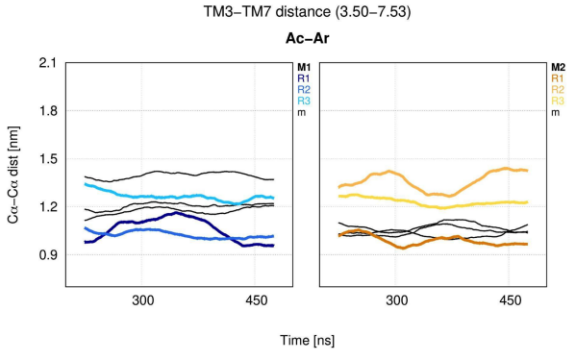
TM3–TM7 distance (3.50–7.53)
Ac–Ar
Cα–Cα dist [nm]
2.1
1.8
1.5
1.2
0.9
M1
R1
R2
R3
m
M2
R1
R2
R3
m
300
450
300
450
Time [ns]

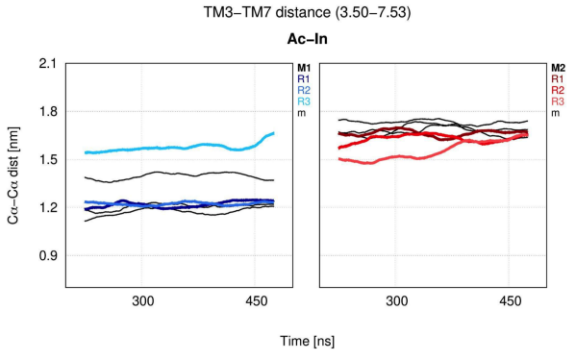
TM3–TM7 distance (3.50–7.53)
Ac–In
Cα–Cα dist [nm]
2.1
1.8
1.5
1.2
0.9
M1
R1
R2
R3
m
M2
R1
R2
R3
m
300
450
300
450
Time [ns]

Figure S15. Distance between TM3 and TM7. Distance [nM] between Cα-atoms of residues 3.50 and 7.53 for each dimer configuration over time [ns]. Replicates are color-coded and distance is compared to the distance of the replicates of the uncomplexed monomers (black lines) for each protomer. Conformations are colour-coded: inactive - red, arrestin - yellow, active - blue.

S16

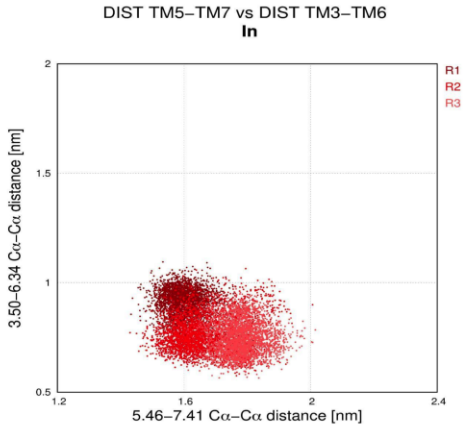
DIST TM5–TM7 vs DIST TM3–TM6
In
R1
R2
R3
3.50–6.34 Cα–Cα distance [nm]
5.46–7.41 Cα–Cα distance [nm]
0.5
1
1.5
2
1.2
1.6
2
2.4

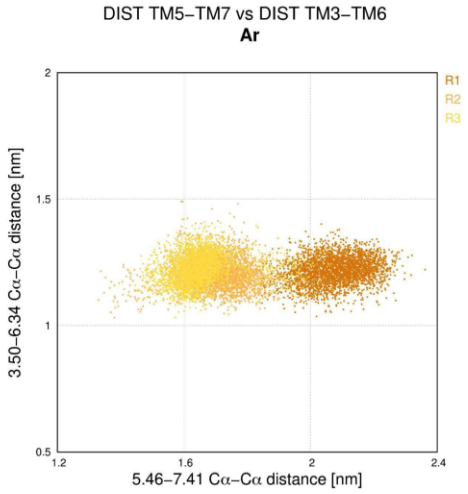
DIST TM5–TM7 vs DIST TM3–TM6
Ar
R1
R2
R3
3.50–6.34 Cα–Cα distance [nm]
5.46–7.41 Cα–Cα distance [nm]
0.5
1
1.5
2
1.2
1.6
2
2.4

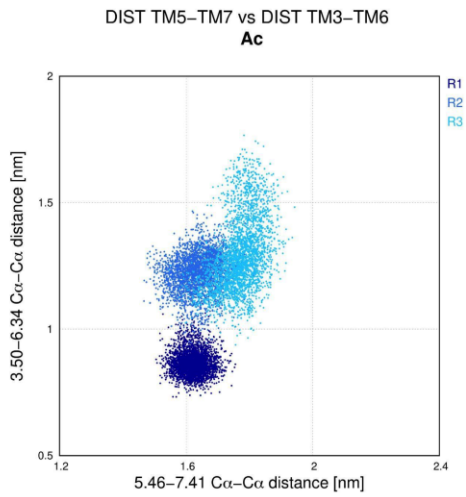
DIST TM5–TM7 vs DIST TM3–TM6
Ac
R1
R2
R3
3.50–6.34 Cα–Cα distance [nm]
5.46–7.41 Cα–Cα distance [nm]
0.5
1
1.5
2
1.2
1.6
2
2.4

Figure S16. Distance TM3-TM6 vs. distance TM5-TM7. Comparison of Cα-atom distances between TM3-TM6 (3.50-6.34) and TM5-TM7 (5.46-7.41) as scatter plots for the replicates of the monomers over time. Conformations are colour-coded: inactive - red, arrestin - yellow, active - blue. This data was used as background for **Figure S17.**

S17

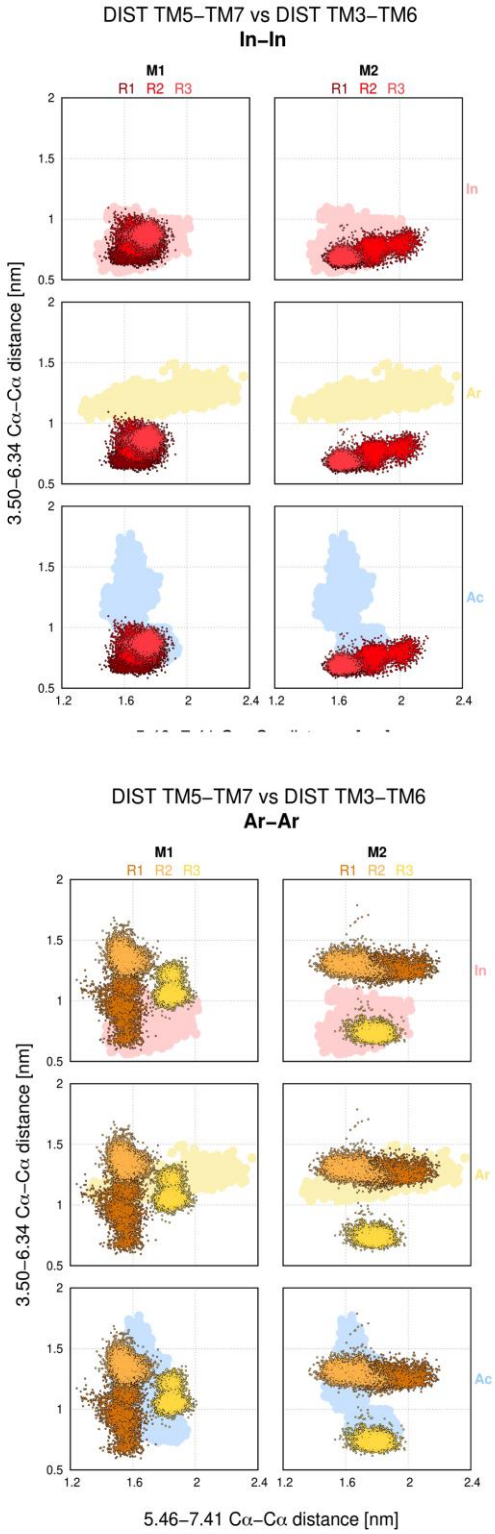
DIST TM5–TM7 vs DIST TM3–TM6
In–In
M1
M2
R1 R2 R3
In
Ar
Ac
3.50–6.34 Cα–Cα distance [nm]
DIST TM5–TM7 vs DIST TM3–TM6
Ar–Ar
5.46–7.41 Cα–Cα distance [nm]

S17

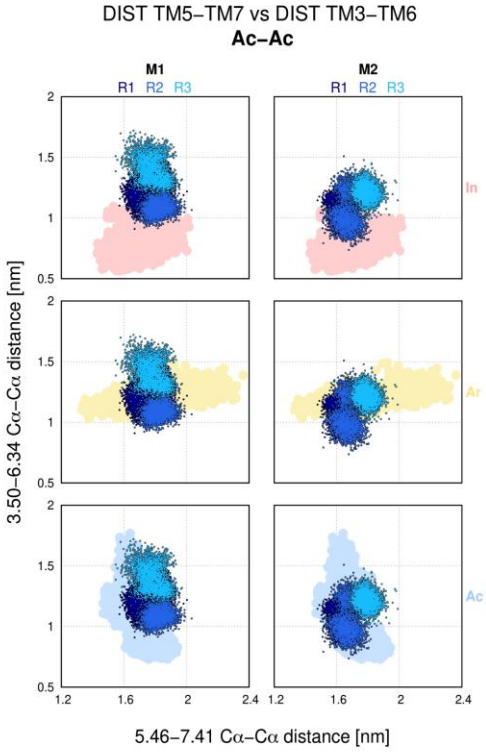
DIST TM5–TM7 vs DIST TM3–TM6
Ac–Ac
M1
R1 R2 R3
M2
R1 R2 R3
In
Ar
Ac
3.50–6.34 Cα–Cα distance [nm]
5.46–7.41 Cα–Cα distance [nm]

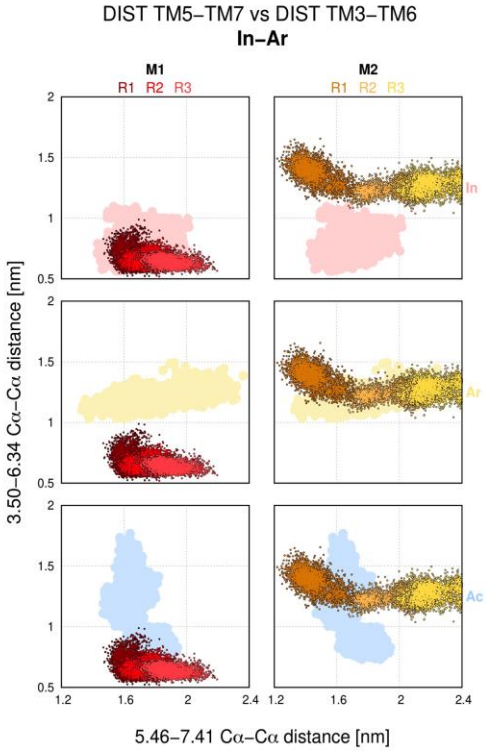
DIST TM5–TM7 vs DIST TM3–TM6
In–Ar
M1
R1 R2 R3
M2
R1 R2 R3
In
Ar
Ac
3.50–6.34 Cα–Cα distance [nm]
5.46–7.41 Cα–Cα distance [nm]

S17

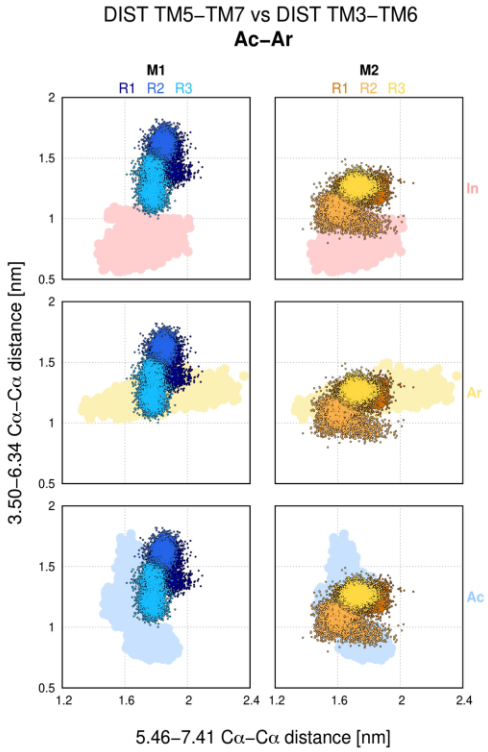
DIST TM5–TM7 vs DIST TM3–TM6
Ac–Ar
M1
R1 R2 R3
M2
R1 R2 R3
In
Ar
Ac
3.50–6.34 Cα–Cα distance [nm]
5.46–7.41 Cα–Cα distance [nm]

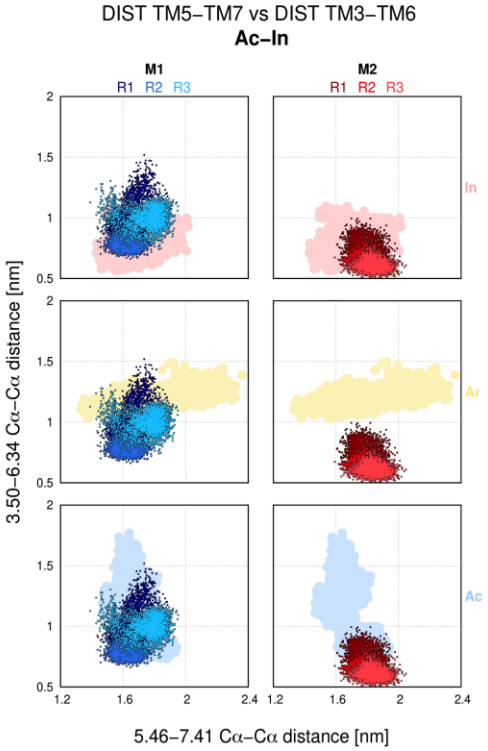
DIST TM5–TM7 vs DIST TM3–TM6
Ac–In
M1
R1 R2 R3
M2
R1 R2 R3
In
Ar
Ac
3.50–6.34 Cα–Cα distance [nm]
5.46–7.41 Cα–Cα distance [nm]

Figure S17. Comparison of transmembrane movement for the D_2R homodimer configurations. Comparison of Cα-distances between 3.50-6.34 [nm] and 5.46-7.41 [nm] (TM3-TM6 vs TM5-TM7) were measured for all monomers and replicates over time. The distances of the individual monomers in the three activation states (**in-**, **ar-** and **ac-monomers**) are shown as light-coloured clouds in the background in three different lines for easier comparison. Conformations are colour-coded: inactive - red, arrestin - yellow, active – blue.

S18

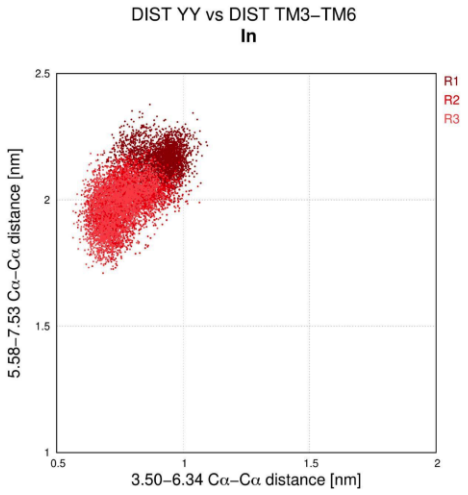
DIST YY vs DIST TM3–TM6
In
R1
R2
R3
5.58–7.53 Cα–Cα distance [nm]
3.50–6.34 Cα–Cα distance [nm]

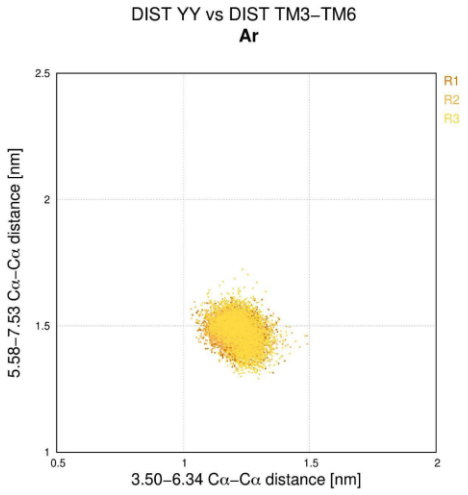
DIST YY vs DIST TM3–TM6
Ar
R1
R2
R3
5.58–7.53 Cα–Cα distance [nm]
3.50–6.34 Cα–Cα distance [nm]

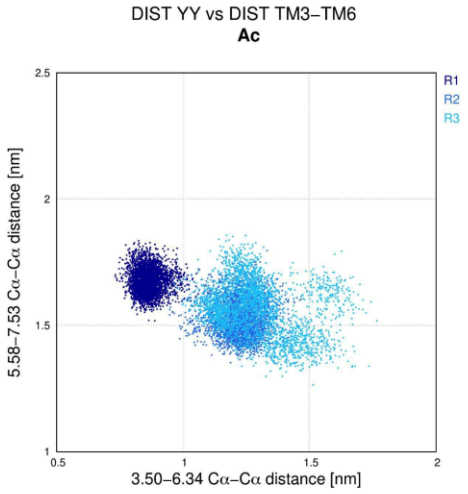
DIST YY vs DIST TM3–TM6
Ac
R1
R2
R3
5.58–7.53 Cα–Cα distance [nm]
3.50–6.34 Cα–Cα distance [nm]

Figure S18. Distance TM3-TM6 vs. distance TM5-TM7 (YY). Comparison of Cα-atom distances between TM3-TM6 (3.50-6.34) and TM5-TM7 (5.58-7.41), which are two tyrosines known as the **Y-Y motif,** as scatter plots for the replicates of the uncomplexed monomers over time. Conformations are colour-coded: inactive - red, arrestin - yellow, active - blue. This data was used as background for **Figure S19.**

S19

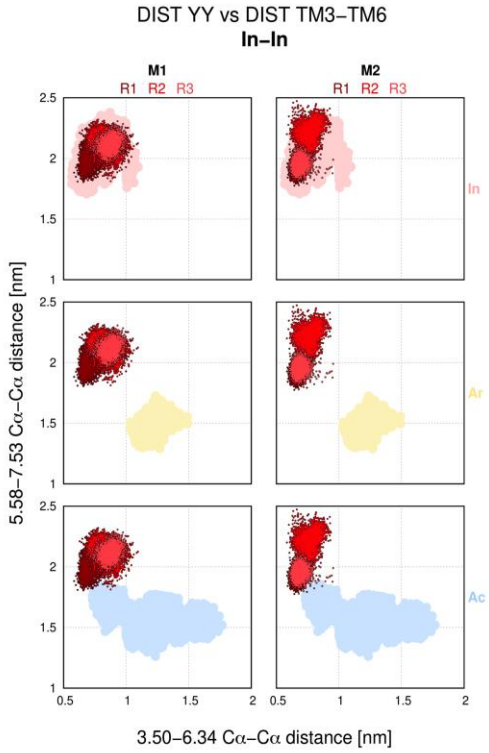
DIST YY vs DIST TM3–TM6
In–In
M1
M2
R1 R2 R3
In
Ar
Ac
5.58–7.53 Cα–Cα distance [nm]
3.50–6.34 Cα–Cα distance [nm]

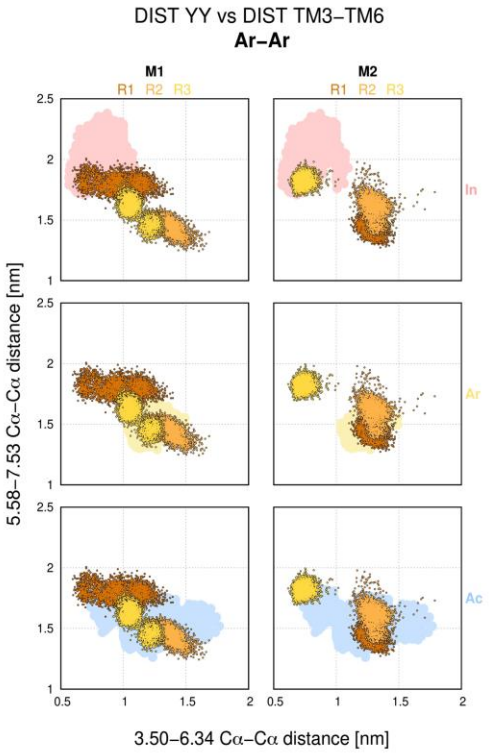
DIST YY vs DIST TM3–TM6
Ar–Ar
M1
M2
R1 R2 R3
In
Ar
Ac
5.58–7.53 Cα–Cα distance [nm]
3.50–6.34 Cα–Cα distance [nm]

S19

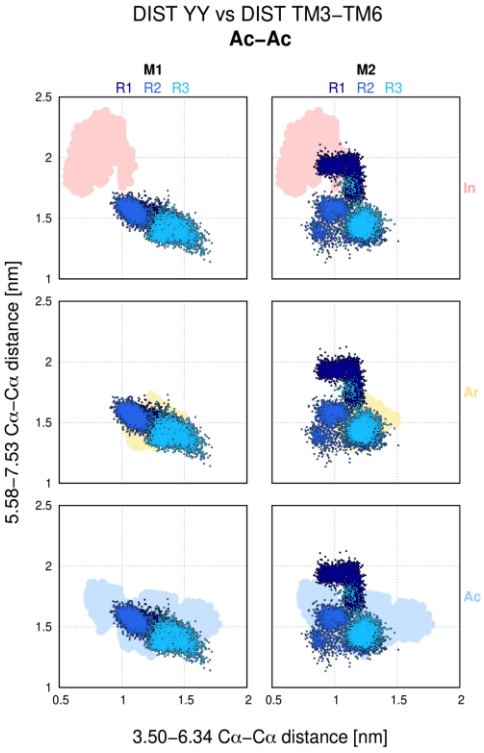
DIST YY vs DIST TM3–TM6
Ac–Ac
M1
R1 R2 R3
M2
R1 R2 R3
In
Ar
Ac
5.58–7.53 Cα–Cα distance [nm]
3.50–6.34 Cα–Cα distance [nm]

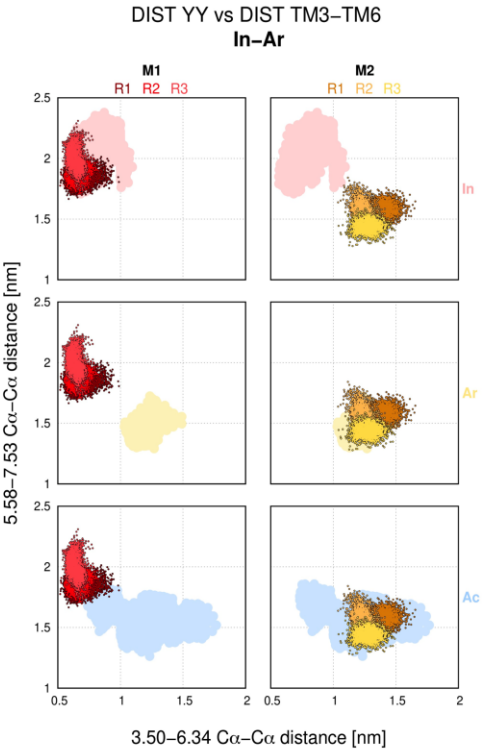
DIST YY vs DIST TM3–TM6
In–Ar
M1
R1 R2 R3
M2
R1 R2 R3
In
Ar
Ac
5.58–7.53 Cα–Cα distance [nm]
3.50–6.34 Cα–Cα distance [nm]

S19

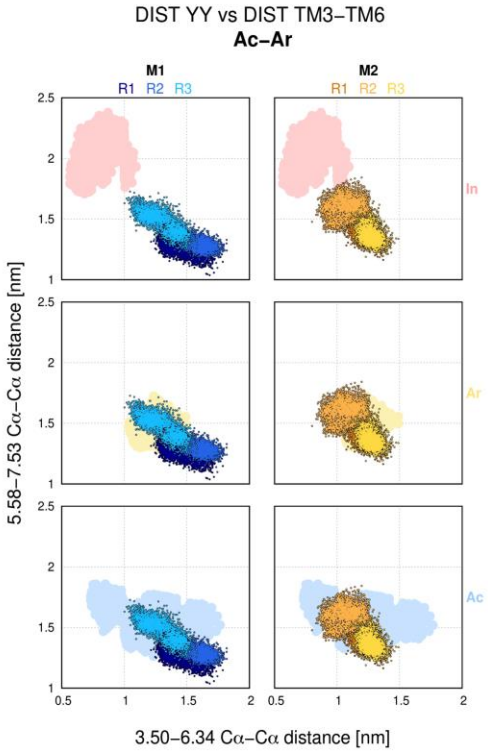
DIST YY vs DIST TM3–TM6
Ac–Ar
M1
R1 R2 R3
M2
R1 R2 R3
In
Ar
Ac
5.58–7.53 Cα–Cα distance [nm]
3.50–6.34 Cα–Cα distance [nm]

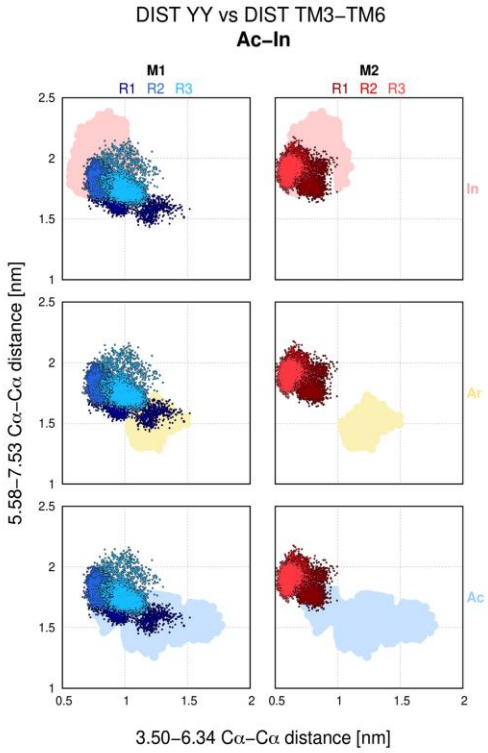
DIST YY vs DIST TM3–TM6
Ac–In
M1
R1 R2 R3
M2
R1 R2 R3
In
Ar
Ac
5.58–7.53 Cα–Cα distance [nm]
3.50–6.34 Cα–Cα distance [nm]

Figure S19. Distance TM3-TM6 vs. distance TM5-TM7 (YY). Comparison of transmembrane movement for the D_2R homodimer configurations captured. Comparison of Cα-distances between 5.58-7.53 [nm] and 3.50-6.34 [nm] (TM5-TM7 vs TM3-TM6) were measured for all monomers and replicates over time. The distances of the individual monomers in the three activation states (**in-**, **ar-** and **ac-monomers**) are shown as light-coloured clouds in the background in three different lines for easier comparison. Conformations are colour-coded: inactive - red, arrestin - yellow, active - blue.

S20

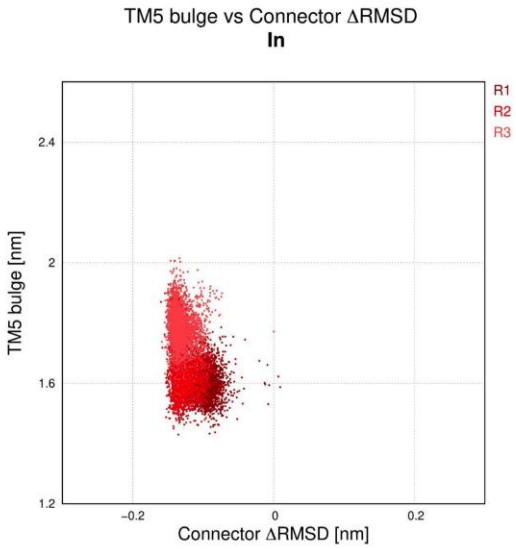
TM5 bulge vs Connector ΔRMSD
In
R1
R2
R3
TM5 bulge [nm]
2.4
2
1.6
1.2
−0.2
0
0.2
Connector ΔRMSD [nm]

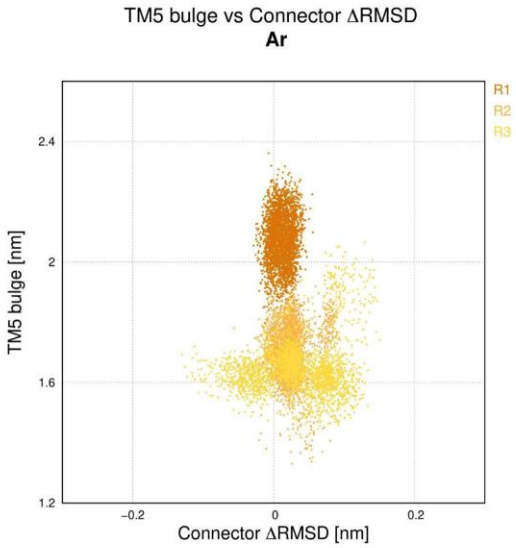
TM5 bulge vs Connector ΔRMSD
Ar
R1
R2
R3
TM5 bulge [nm]
2.4
2
1.6
1.2
−0.2
0
0.2
Connector ΔRMSD [nm]

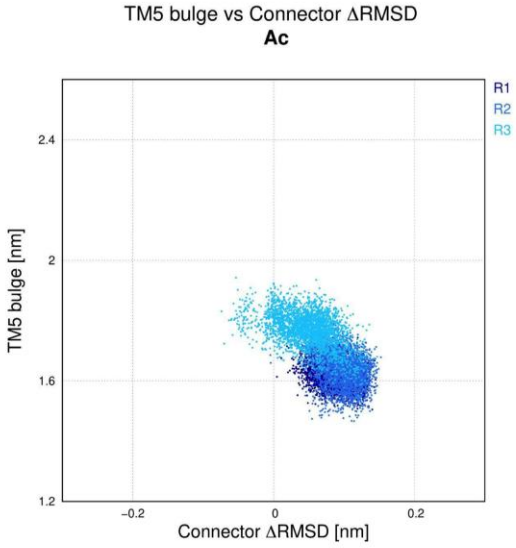
TM5 bulge vs Connector ΔRMSD
Ac
R1
R2
R3
TM5 bulge [nm]
2.4
2
1.6
1.2
−0.2
0
0.2
Connector ΔRMSD [nm]

Figure S20. TM5 bugle vs. connector RMSD. Comparison of Cα-atom distances between TM5-TM7 (5.58-7.41) and the ΔRMSD of a connector module, consisting of residues Phe$^{3.40}$ (F of PIF motif) and Ile$^{6.44}$ (I of PIF motif) as scatter plots for the replicates of the uncomplexed monomers. Conformations are colour-coded: inactive - red, arrestin - yellow, active - blue. This data was used as background for **Figure 16.**

S21

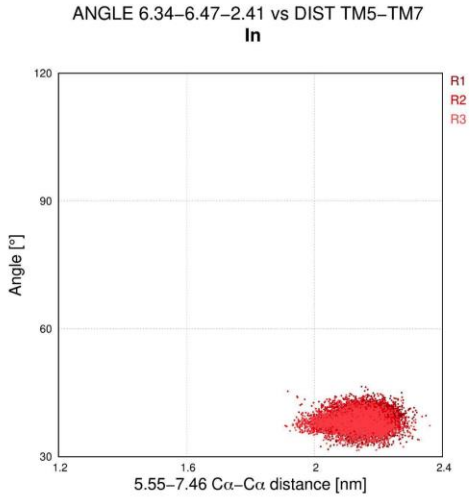
ANGLE 6.34–6.47–2.41 vs DIST TM5–TM7
In
R1
R2
R3
120
90
60
30
Angle [°]
1.2
1.6
2
2.4
5.55–7.46 Cα–Cα distance [nm]

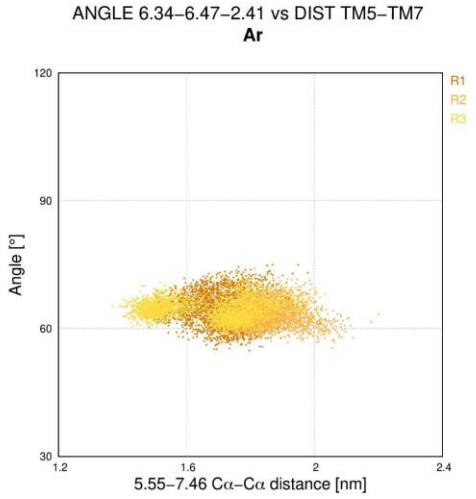
ANGLE 6.34–6.47–2.41 vs DIST TM5–TM7
Ar
R1
R2
R3
120
90
60
30
Angle [°]
1.2
1.6
2
2.4
5.55–7.46 Cα–Cα distance [nm]

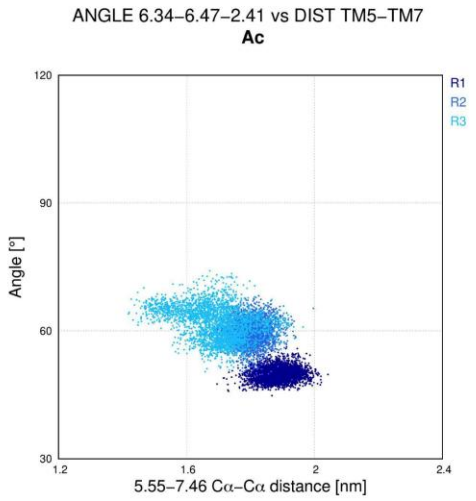
ANGLE 6.34–6.47–2.41 vs DIST TM5–TM7
Ac
R1
R2
R3
120
90
60
30
Angle [°]
1.2
1.6
2
2.4
5.55–7.46 Cα–Cα distance [nm]

Figure S21. Distance TM5-TM7 vs. angle of Cα-atoms of 6.34-6.47-2.41. Comparison of Cα-atom distances between TM5-TM7 (5.55-7.46) [nm] and the angle consisting Cα-atoms of residues 6.34, 6.47 and 2.41 [°] as scatter plots for the replicates of the uncomplexed monomers. Conformations are colour-coded: inactive - red, arrestin - yellow, active - blue. This data was used as background for **Figure S22.**

S22

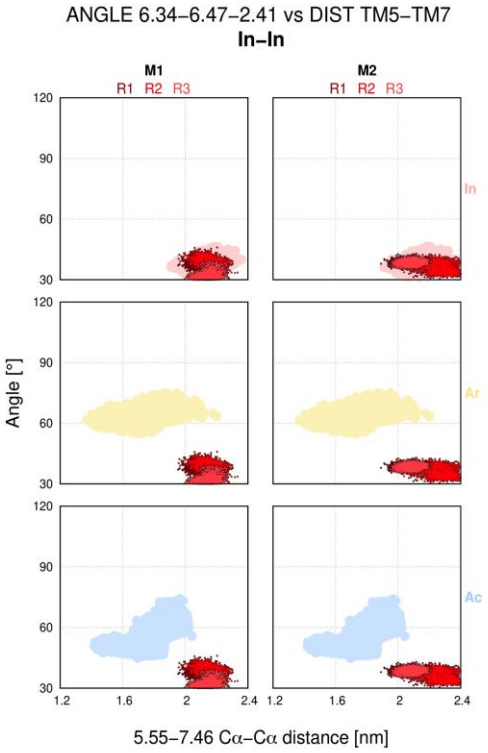
ANGLE 6.34–6.47–2.41 vs DIST TM5–TM7
In–In
M1
R1 R2 R3
M2
R1 R2 R3
In
Ar
Ac
Angle [°]
120
90
60
30
1.2
1.6
2
2.4
5.55–7.46 Cα–Cα distance [nm]

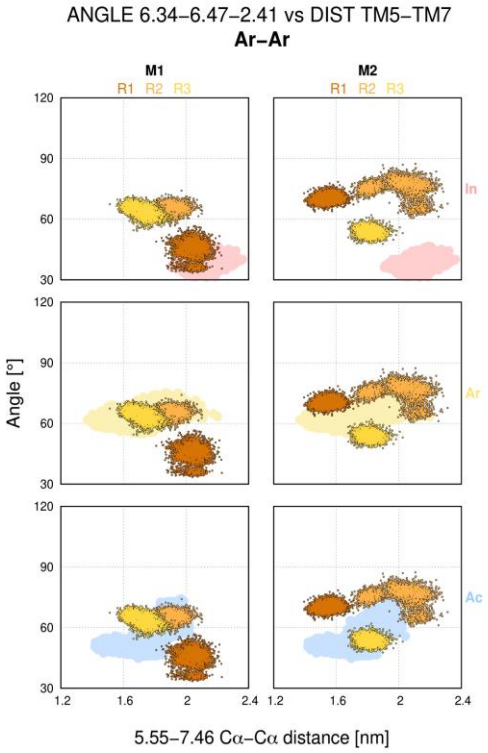
ANGLE 6.34–6.47–2.41 vs DIST TM5–TM7
Ar–Ar
M1
R1 R2 R3
M2
R1 R2 R3
In
Ar
Ac
Angle [°]
120
90
60
30
1.2
1.6
2
2.4
5.55–7.46 Cα–Cα distance [nm]

S22

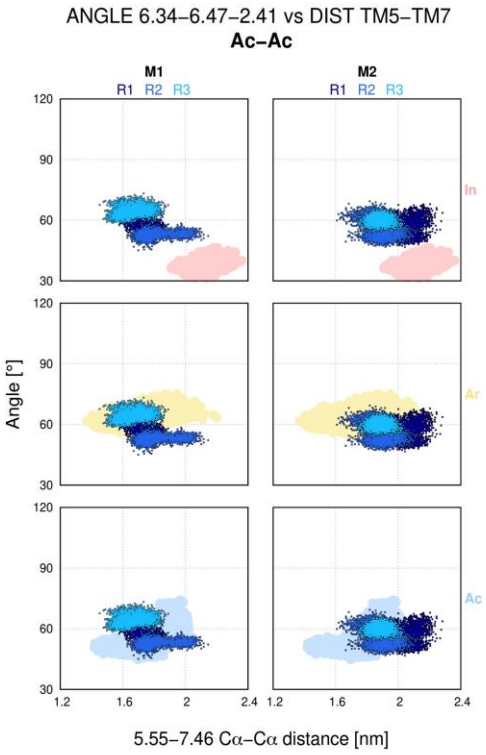
ANGLE 6.34–6.47–2.41 vs DIST TM5–TM7
Ac–Ac
M1
R1 R2 R3
M2
R1 R2 R3
In
Ar
Ac
Angle [°]
120
90
60
30
1.2
1.6
2
2.4
5.55–7.46 Cα–Cα distance [nm]

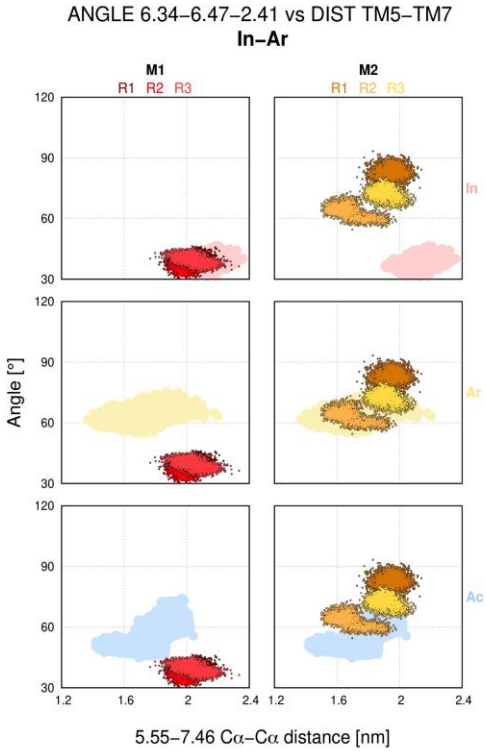
ANGLE 6.34–6.47–2.41 vs DIST TM5–TM7
In–Ar
M1
R1 R2 R3
M2
R1 R2 R3
In
Ar
Ac
Angle [°]
120
90
60
30
1.2
1.6
2
2.4
5.55–7.46 Cα–Cα distance [nm]

S22

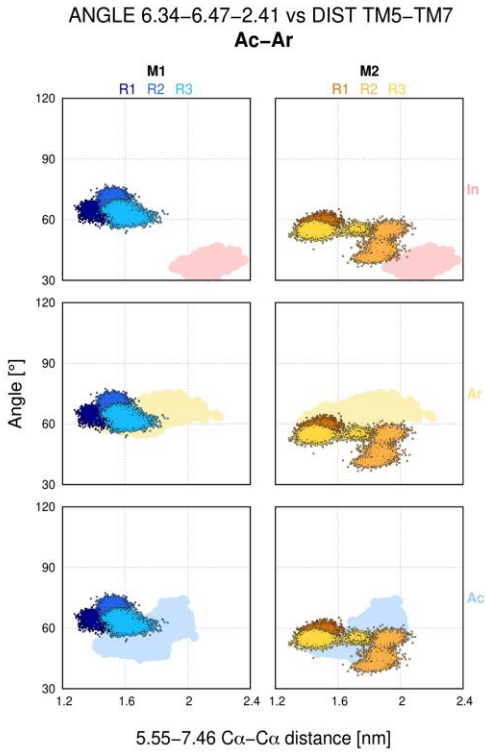
ANGLE 6.34–6.47–2.41 vs DIST TM5–TM7
Ac–Ar
M1
R1 R2 R3
M2
R1 R2 R3
In
Ar
Ac
Angle [°]
120
90
60
30
1.2
1.6
2
2.4
5.55–7.46 Cα–Cα distance [nm]

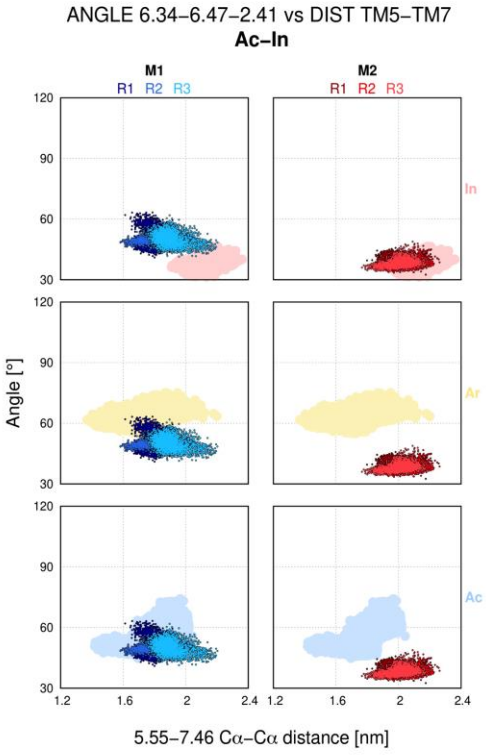
ANGLE 6.34–6.47–2.41 vs DIST TM5–TM7
Ac–In
M1
R1 R2 R3
M2
R1 R2 R3
In
Ar
Ac
Angle [°]
120
90
60
30
1.2
1.6
2
2.4
5.55–7.46 Cα–Cα distance [nm]

Figure S22. Distance TM5-TM7 vs. angle of Cα-atoms of 6.34-6.47-2.41. Comparison of the angle between residues 6.34-6.47-2.41 [°] and the distance between the Cα-atoms of residues 5.55 and 7.46 [nm]. Comparison of the angle between residues 6.34-6.47-2.41 [°] and the distance between the Cα-atoms of residues 5.55 and 7.46 [nm], which were measured for all monomers and replicates over time. The distances of the individual monomers are shown as light-coloured clouds in the background. Conformations are colour-coded: inactive - red, arrestin - yellow, active – blue.

S23

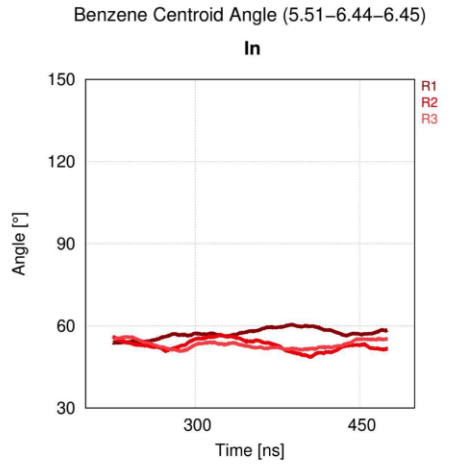
Benzene Centroid Angle (5.51–6.44–6.45)
In
150
120
90
60
30
Angle [°]
300
450
Time [ns]
R1
R2
R3

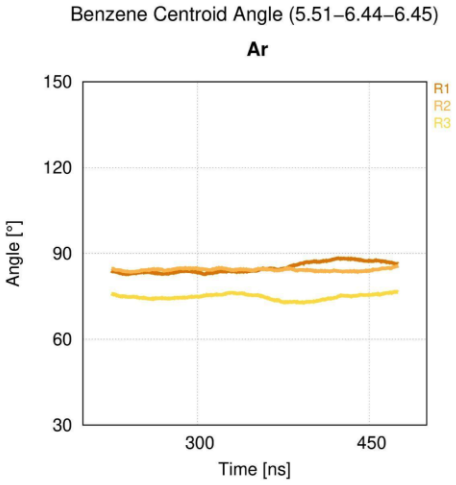
Benzene Centroid Angle (5.51–6.44–6.45)
Ar
150
120
90
60
30
Angle [°]
300
450
Time [ns]
R1
R2
R3

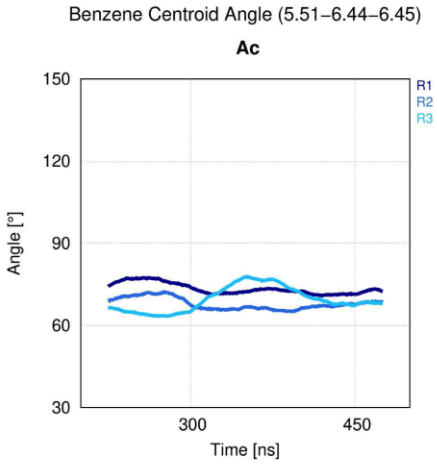
Benzene Centroid Angle (5.51–6.44–6.45)
Ac
150
120
90
60
30
Angle [°]
300
450
Time [ns]
R1
R2
R3

S23

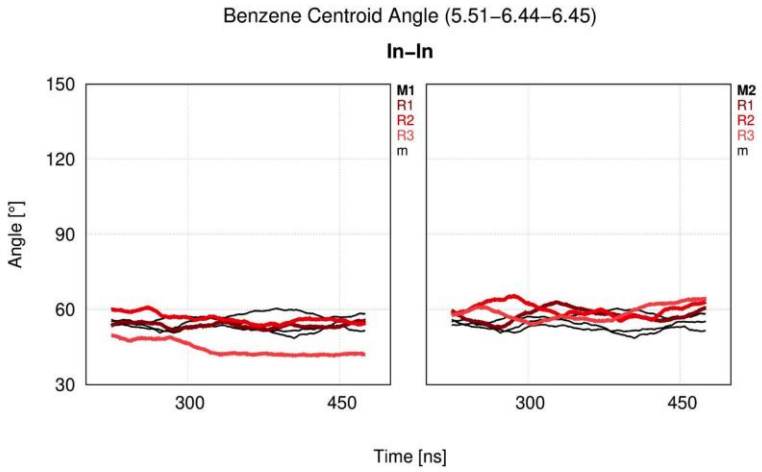
Benzene Centroid Angle (5.51–6.44–6.45)
In–In
M1
R1
R2
R3
m
M2
R1
R2
R3
m
Angle [°]
150
120
90
60
30
300
450
300
450
Time [ns]

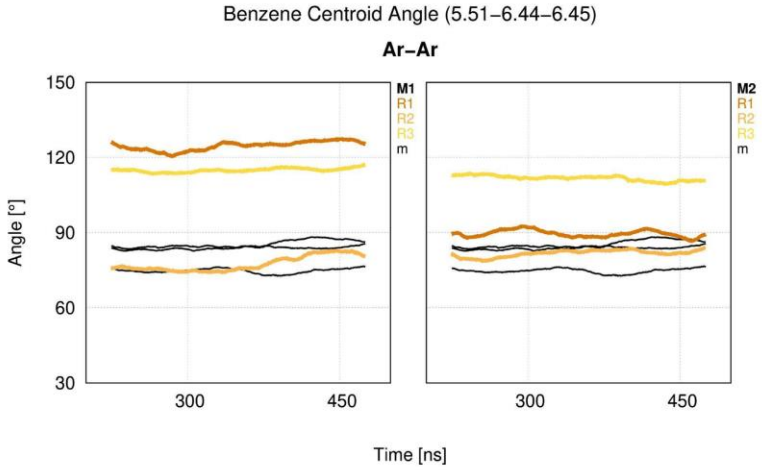
Benzene Centroid Angle (5.51–6.44–6.45)
Ar–Ar
M1
R1
R2
R3
m
M2
R1
R2
R3
m
Angle [°]
150
120
90
60
30
300
450
300
450
Time [ns]

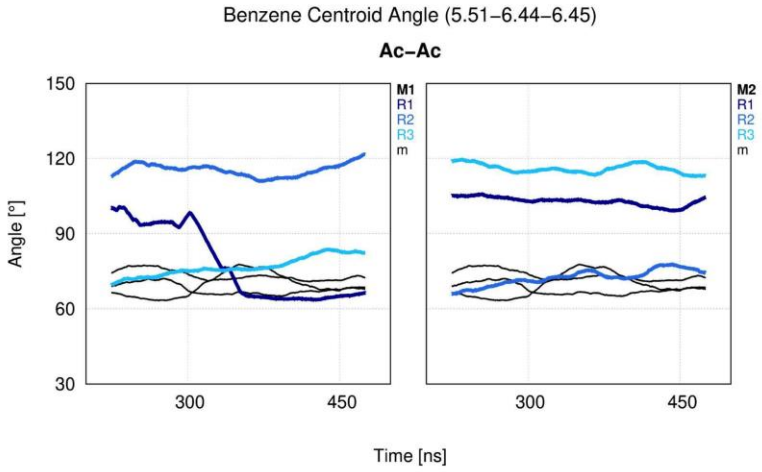
Benzene Centroid Angle (5.51–6.44–6.45)
Ac–Ac
M1
R1
R2
R3
m
M2
R1
R2
R3
m
Angle [°]
150
120
90
60
30
300
450
300
450
Time [ns]

S23

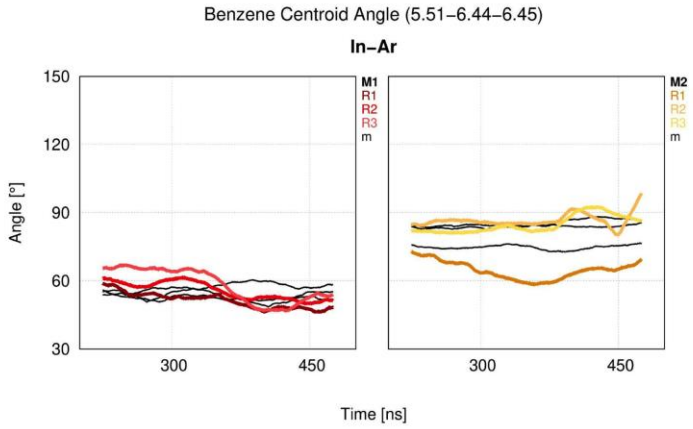
Benzene Centroid Angle (5.51–6.44–6.45)
In–Ar
M1
R1
R2
R3
m
M2
R1
R2
R3
m
150
120
90
60
30
Angle [°]
300
450
300
450
Time [ns]

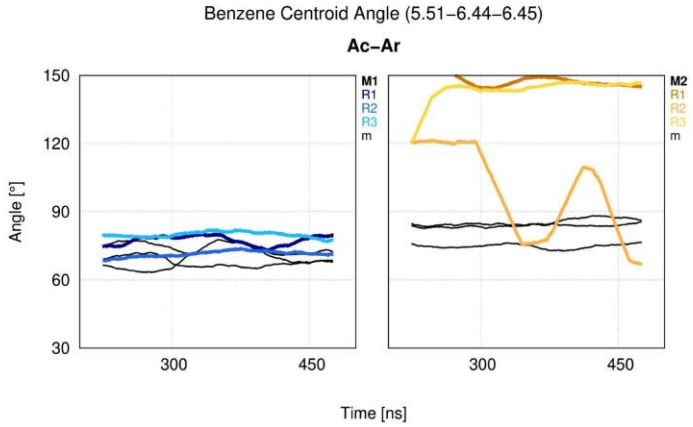
Benzene Centroid Angle (5.51–6.44–6.45)
Ac–Ar
M1
R1
R2
R3
m
M2
R1
R2
R3
m
150
120
90
60
30
Angle [°]
300
450
300
450
Time [ns]

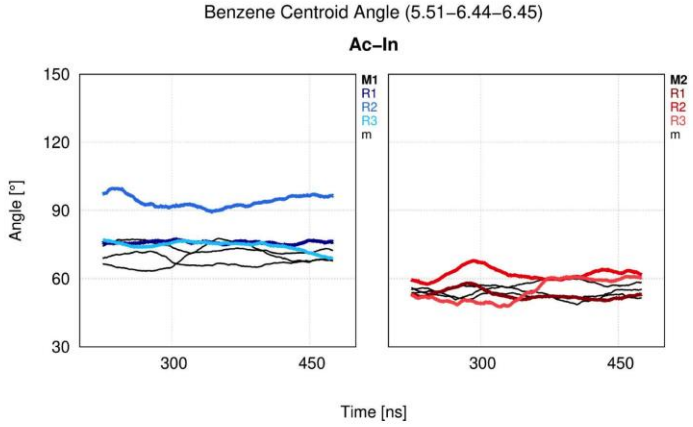
Benzene Centroid Angle (5.51–6.44–6.45)
Ac–In
M1
R1
R2
R3
m
M2
R1
R2
R3
m
150
120
90
60
30
Angle [°]
300
450
300
450
Time [ns]

Figure S23. Angle among the centroids of the benzene ring of residues Phe$^{5.51}$, Phe$^{6.44}$ and Ile$^{6.45}$ over time. Angle of benzene centroids [°] of residues Phe$^{5.51}$, Phe$^{6.44}$ and Ile$^{6.45}$ measured over time [ns]. Replicates are color-coded and distance is compared to the distance of the replicates of the uncomplexed monomers (black lines) for each protomer. Conformations are colour-coded: inactive - red, arrestin - yellow, active - blue.

S24

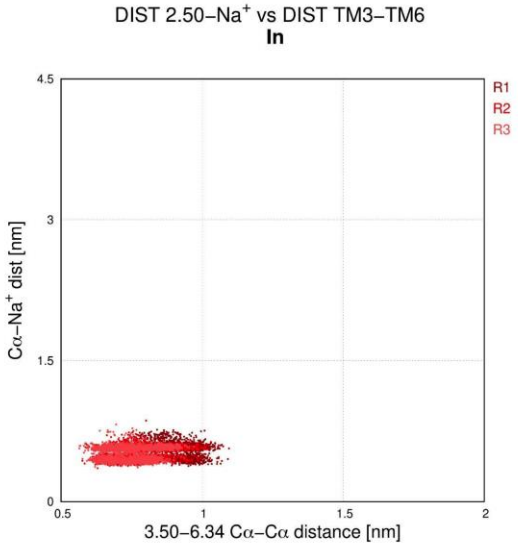
DIST 2.50–Na+ vs DIST TM3–TM6
In
R1
R2
R3
Cα–Na+ dist [nm]
3.50–6.34 Cα–Cα distance [nm]
0
0.5
1
1.5
2
3
4.5

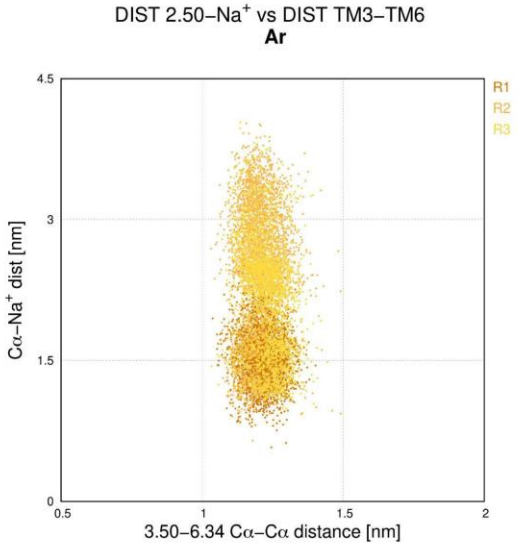
DIST 2.50–Na+ vs DIST TM3–TM6
Ar
R1
R2
R3
Cα–Na+ dist [nm]
3.50–6.34 Cα–Cα distance [nm]
0
0.5
1
1.5
2
3
4.5

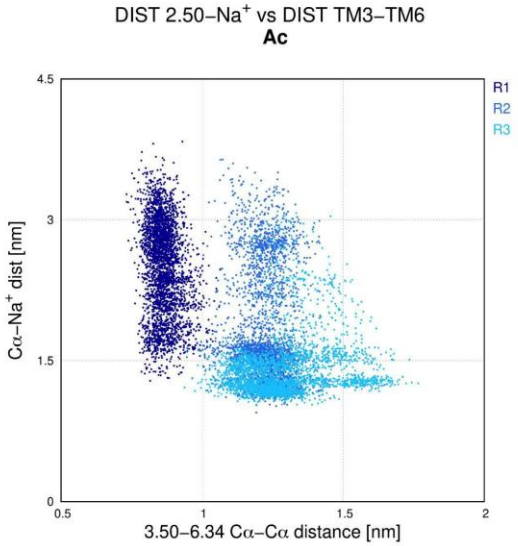
DIST 2.50–Na+ vs DIST TM3–TM6
Ac
R1
R2
R3
Cα–Na+ dist [nm]
3.50–6.34 Cα–Cα distance [nm]
0
0.5
1
1.5
2
3
4.5

Figure S24. Ionic lock vs. distance between Asp$^{2.50}$ and sodium. Comparison of Cα-atom distances between 3.50 and 6.34 (TM3-TM6) representing the ionic lock and between Asp$^{2.50}$ and the closest sodium atom as scatter plots for the replicates of the uncomplexed monomers. Conformations are colour-coded: inactive - red, arrestin - yellow, active - blue. This data was used as background for **Figure 17.**

S25

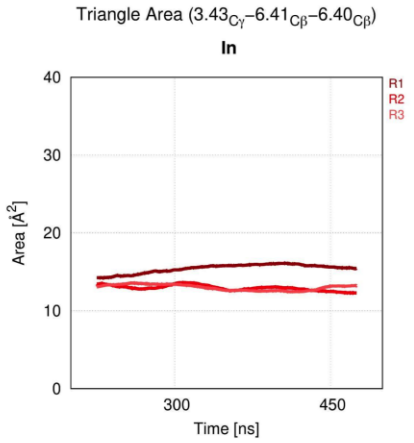
Triangle Area (3.43Cγ–6.41Cβ–6.40Cβ)
In
R1
R2
R3
Area [Å2]
0
10
20
30
40
300
450
Time [ns]

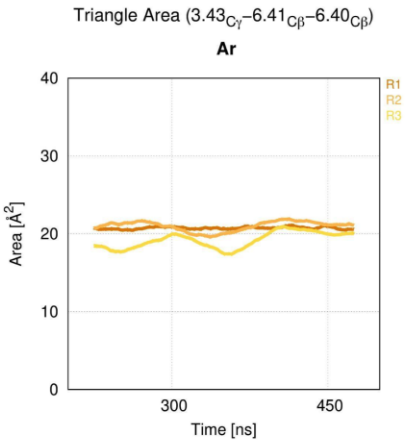
Triangle Area (3.43Cγ–6.41Cβ–6.40Cβ)
Ar
R1
R2
R3
Area [Å2]
0
10
20
30
40
300
450
Time [ns]

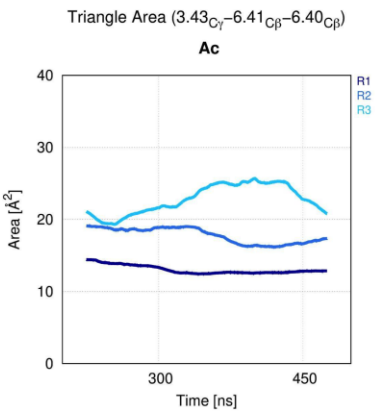
Triangle Area (3.43Cγ–6.41Cβ–6.40Cβ)
Ac
R1
R2
R3
Area [Å2]
0
10
20
30
40
300
450
Time [ns]

S25

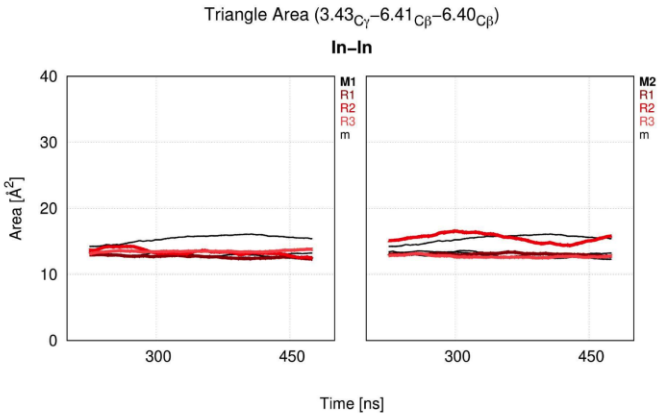
Triangle Area (3.43Cγ–6.41Cβ–6.40Cβ)
In–In
M1
R1
R2
R3
m
M2
R1
R2
R3
m
Area [Å2]
0
10
20
30
40
300
450
300
450
Time [ns]

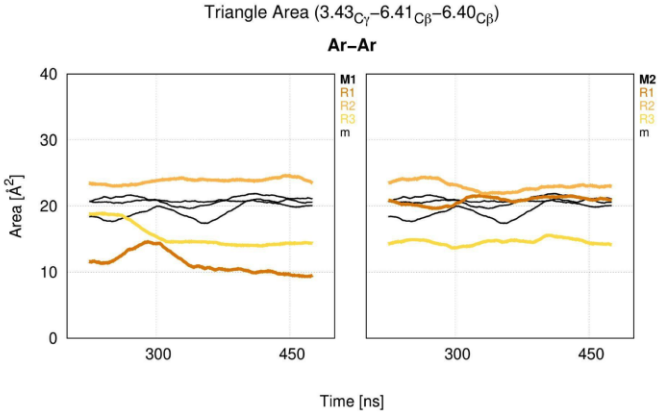
Triangle Area (3.43Cγ–6.41Cβ–6.40Cβ)
Ar–Ar
M1
R1
R2
R3
m
M2
R1
R2
R3
m
Area [Å2]
0
10
20
30
40
300
450
300
450
Time [ns]

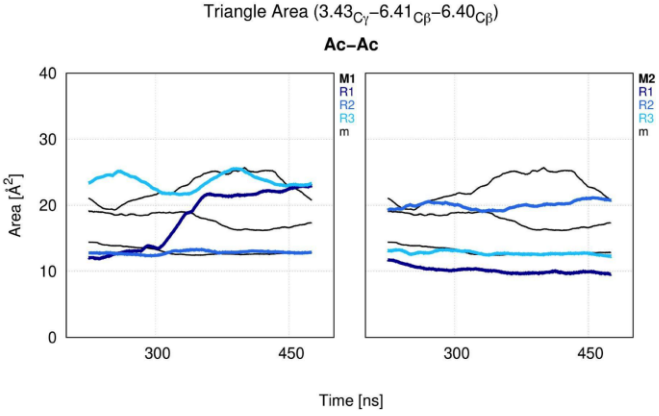
Triangle Area (3.43Cγ–6.41Cβ–6.40Cβ)
Ac–Ac
M1
R1
R2
R3
m
M2
R1
R2
R3
m
Area [Å2]
0
10
20
30
40
300
450
300
450
Time [ns]

S25

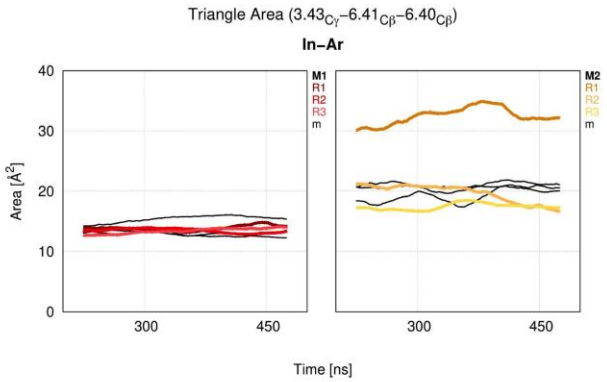
Triangle Area (3.43Cγ–6.41Cβ–6.40Cβ)
In–Ar
M1
R1
R2
R3
m
M2
R1
R2
R3
m
Area [Å2]
0
10
20
30
40
300
450
300
450
Time [ns]

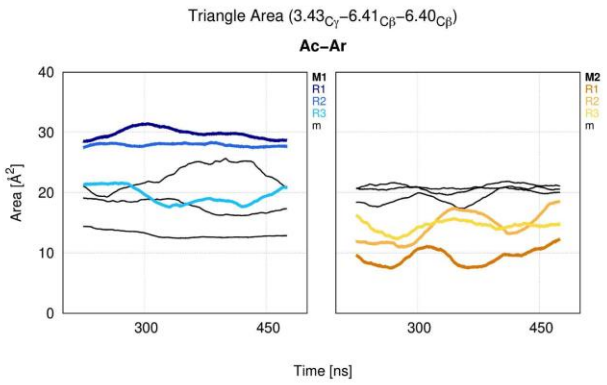
Triangle Area (3.43Cγ–6.41Cβ–6.40Cβ)
Ac–Ar
M1
R1
R2
R3
m
M2
R1
R2
R3
m
Area [Å2]
0
10
20
30
40
300
450
300
450
Time [ns]

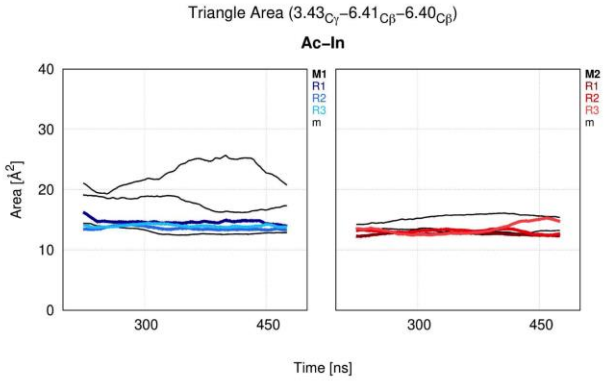
Triangle Area (3.43Cγ–6.41Cβ–6.40Cβ)
Ac–In
M1
R1
R2
R3
m
M2
R1
R2
R3
m
Area [Å2]
0
10
20
30
40
300
450
300
450
Time [ns]

Figure S25. Opening of the hydrophobic lock. Opening of the hydrophobic lock was measured by calculating the area of the angle [$Å^2$] composed by the Cγ atom of residue 3.43, the Cβ of residue 6.41 and 6.40 over simulation time [ns]. Replicates are color-coded and distance is compared to the distance of the replicates of the uncomplexed monomers (black lines) for each protomer. Conformations are colour-coded: inactive - red, arrestin - yellow, active - blue.

S26

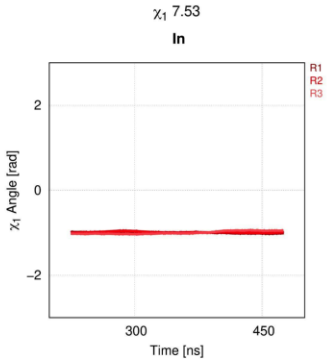
χ1 7.53
In
R1
R2
R3
2
0
−2
χ1 Angle [rad]
300
450
Time [ns]

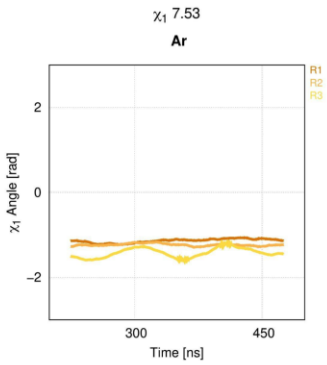
χ1 7.53
Ar
R1
R2
R3
2
0
−2
χ1 Angle [rad]
300
450
Time [ns]

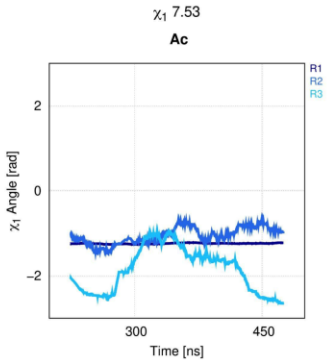
χ1 7.53
Ac
R1
R2
R3
2
0
−2
χ1 Angle [rad]
300
450
Time [ns]

S26

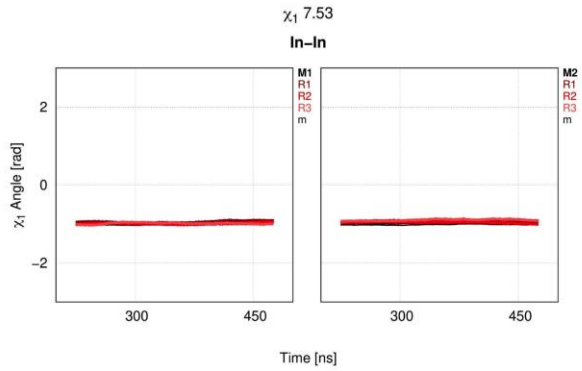
χ1 7.53
In–In
M1
R1
R2
R3
m
M2
R1
R2
R3
m
χ1 Angle [rad]
2
0
−2
300
450
300
450
Time [ns]

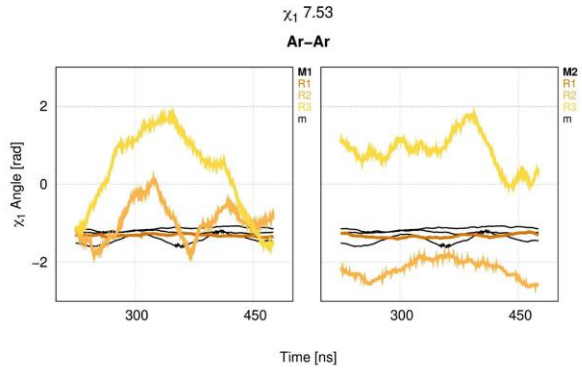
χ1 7.53
Ar–Ar
M1
R1
R2
R3
m
M2
R1
R2
R3
m
χ1 Angle [rad]
2
0
−2
300
450
300
450
Time [ns]

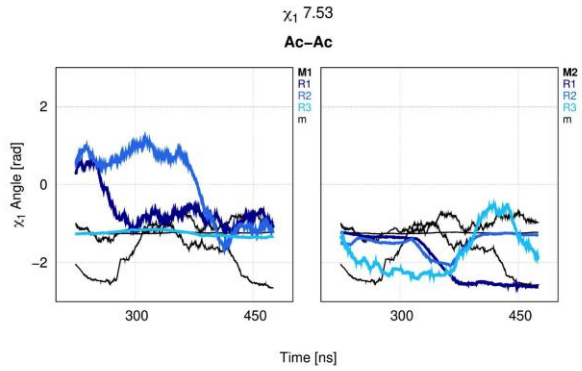
χ1 7.53
Ac–Ac
M1
R1
R2
R3
m
M2
R1
R2
R3
m
χ1 Angle [rad]
2
0
−2
300
450
300
450
Time [ns]

S26

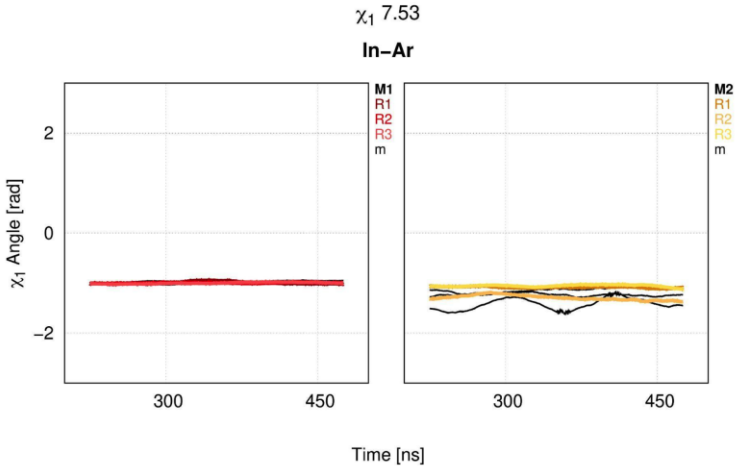
χ1 7.53
In–Ar
M1
R1
R2
R3
m
M2
R1
R2
R3
m
χ1 Angle [rad]
2
0
−2
300
450
300
450
Time [ns]

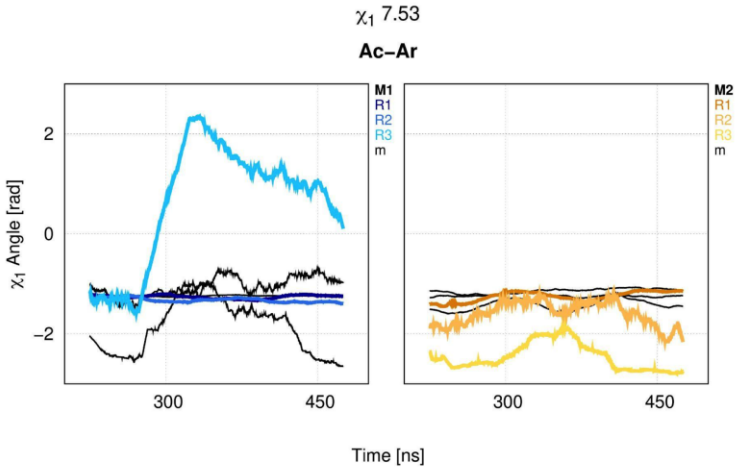
χ1 7.53
Ac–Ar
M1
R1
R2
R3
m
M2
R1
R2
R3
m
χ1 Angle [rad]
2
0
−2
300
450
300
450
Time [ns]

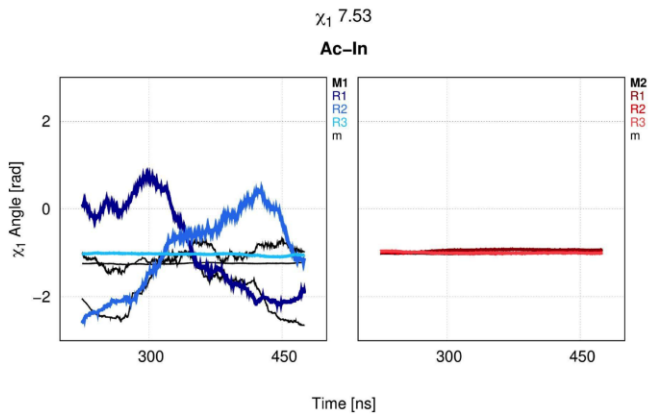
χ1 7.53
Ac–In
M1
R1
R2
R3
m
M2
R1
R2
R3
m
χ1 Angle [rad]
2
0
−2
300
450
300
450
Time [ns]

Figure S26. . Angle χ_1 of the conserved tyrosine 7.53 ($Tyr^{7.53}$) over time. Angle χ_1 [rad] of the conserved $Tyr^{7.53}$ observed over simulation time [ns]. Replicates are color-coded and distance is compared to the distance of the replicates of the uncomplexed monomers (black lines) for each protomer. Conformations are colour-coded: inactive - red, arrestin - yellow, active - blue.

S27

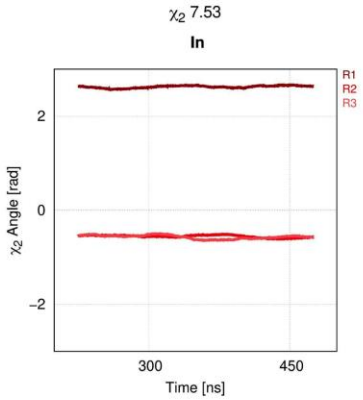
χ2 7.53
In
R1
R2
R3
2
0
−2
χ2 Angle [rad]
300
450
Time [ns]

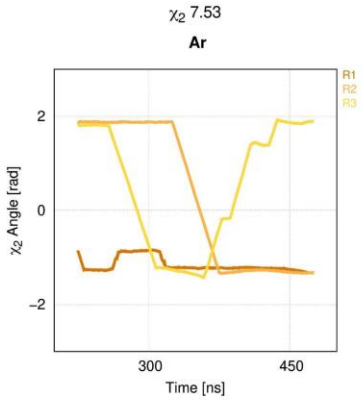
χ2 7.53
Ar
R1
R2
R3
2
0
−2
χ2 Angle [rad]
300
450
Time [ns]

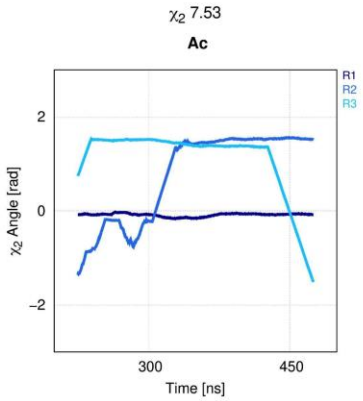
χ2 7.53
Ac
R1
R2
R3
2
0
−2
χ2 Angle [rad]
300
450
Time [ns]

S27

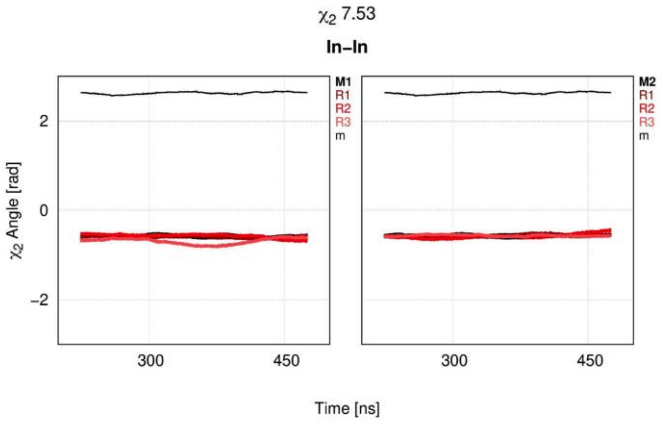
χ2 7.53
In–In
M1
R1
R2
R3
m
M2
R1
R2
R3
m
χ2 Angle [rad]
2
0
−2
300
450
300
450
Time [ns]

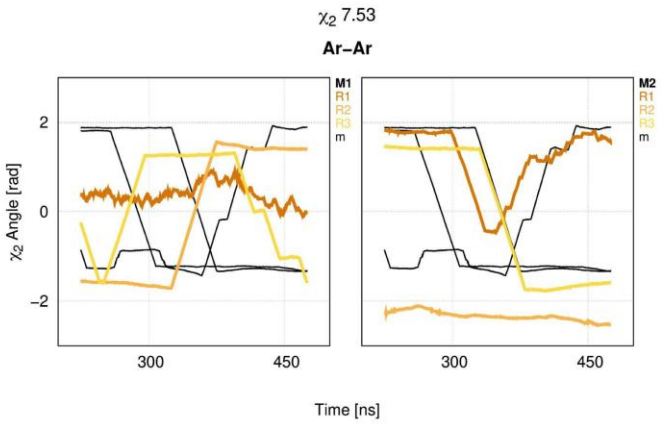
χ2 7.53
Ar–Ar
M1
R1
R2
R3
m
M2
R1
R2
R3
m
χ2 Angle [rad]
2
0
−2
300
450
300
450
Time [ns]

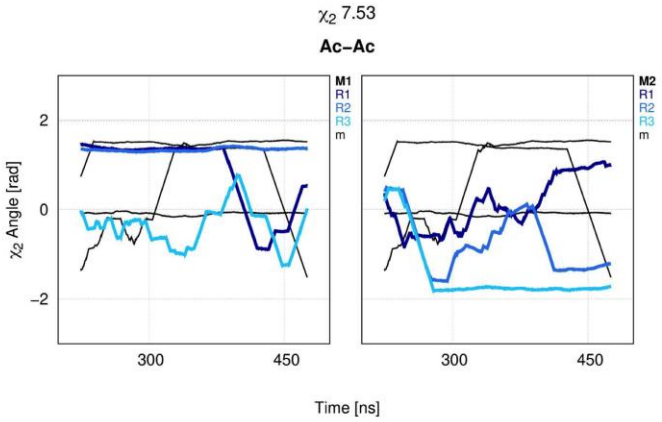
χ2 7.53
Ac–Ac
M1
R1
R2
R3
m
M2
R1
R2
R3
m
χ2 Angle [rad]
2
0
−2
300
450
300
450
Time [ns]

S27

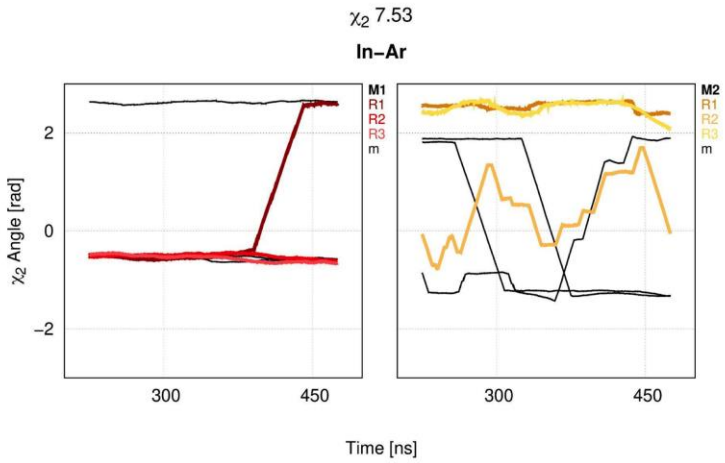
χ2 7.53
In–Ar
M1
R1
R2
R3
m
M2
R1
R2
R3
m
χ2 Angle [rad]
2
0
−2
300
450
300
450
Time [ns]

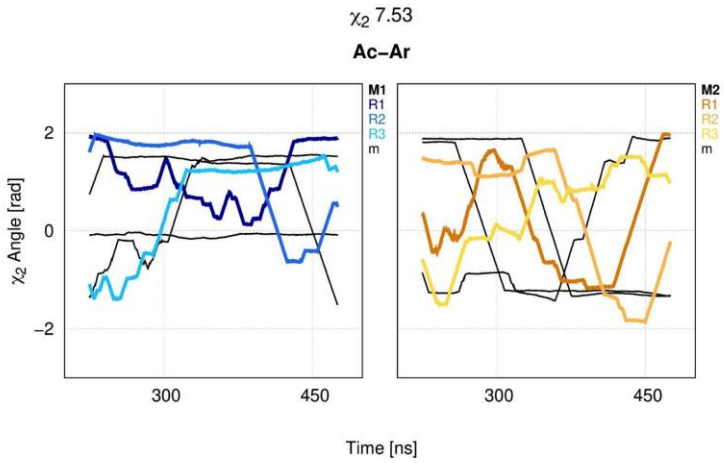
χ2 7.53
Ac–Ar
M1
R1
R2
R3
m
M2
R1
R2
R3
m
χ2 Angle [rad]
2
0
−2
300
450
300
450
Time [ns]

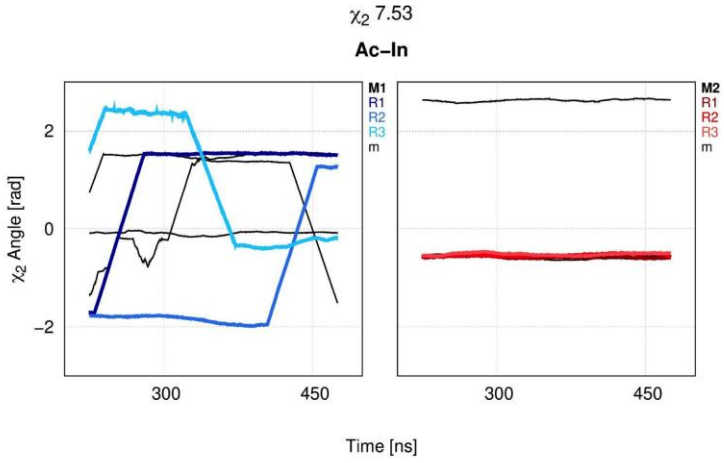
χ2 7.53
Ac–In
M1
R1
R2
R3
m
M2
R1
R2
R3
m
χ2 Angle [rad]
2
0
−2
300
450
300
450
Time [ns]

Figure S27. Angle χ_2 of the conserved tyrosine 7.53 ($Tyr^{7.53}$) over time. Angle χ_2 [rad] of the conserved $Tyr^{7.53}$ observed over simulation time [ns]. Replicates are color-coded and distance is compared to the distance of the replicates of the uncomplexed monomers (black lines) for each protomer. Conformations are colour-coded: inactive - red, arrestin - yellow, active - blue.

S28

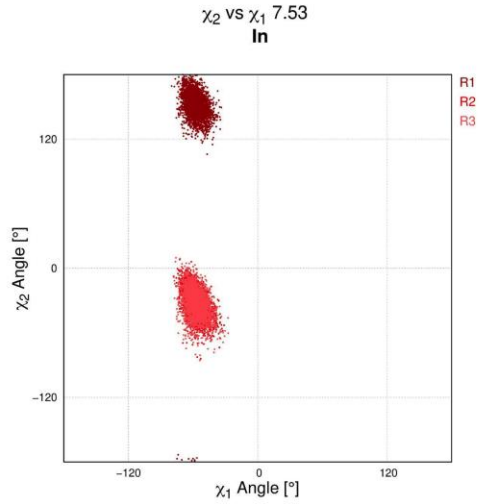
χ2 vs χ1 7.53
In
R1
R2
R3
120
0
−120
χ2 Angle [°]
−120
0
120
χ1 Angle [°]

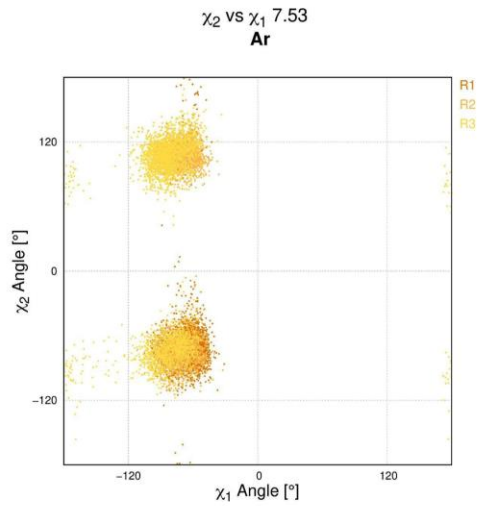
χ2 vs χ1 7.53
Ar
R1
R2
R3
120
0
−120
χ2 Angle [°]
−120
0
120
χ1 Angle [°]

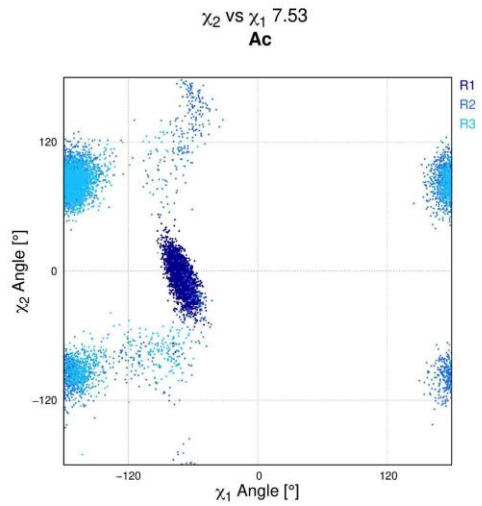
χ2 vs χ1 7.53
Ac
R1
R2
R3
120
0
−120
χ2 Angle [°]
−120
0
120
χ1 Angle [°]

Figure S28. Angles χ_1 and χ_2 [°] of tyrosine 7.53 ($Tyr^{7.53}$) compared. The angles χ_1 and χ_2 [°] of $Tyr^{7.53}$ were observed over time and averaged for each replicate of the uncomplexed monomers. Conformations are colour-coded: inactive - red, arrestin - yellow, active - blue. This data was used as background for **Figure S29**.

S29

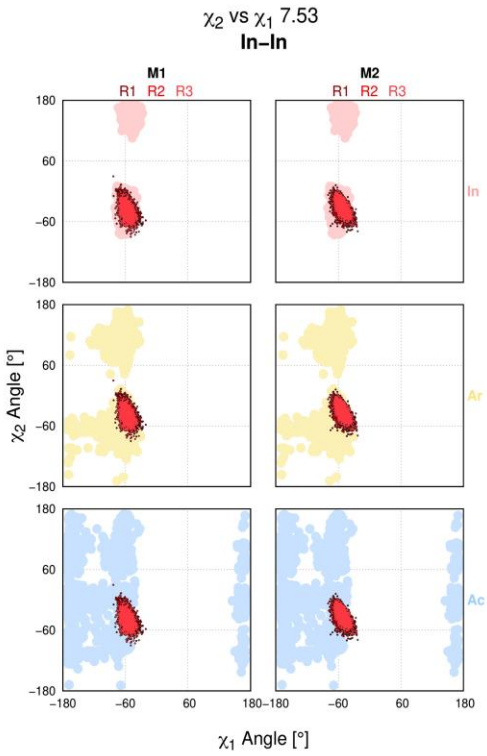
χ2 vs χ1 7.53
In–In
M1
M2
R1 R2 R3
In
Ar
Ac
χ2 Angle [°]
χ1 Angle [°]
180
60
−60
−180

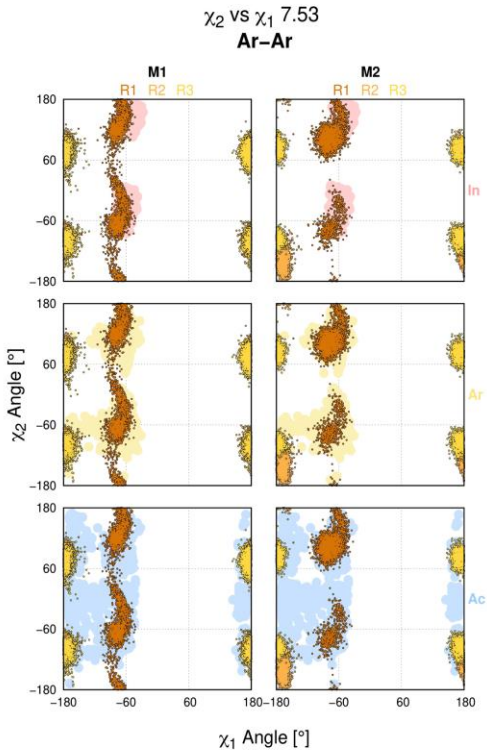
χ2 vs χ1 7.53
Ar–Ar
M1
M2
R1 R2 R3
In
Ar
Ac
χ2 Angle [°]
χ1 Angle [°]
180
60
−60
−180

S29

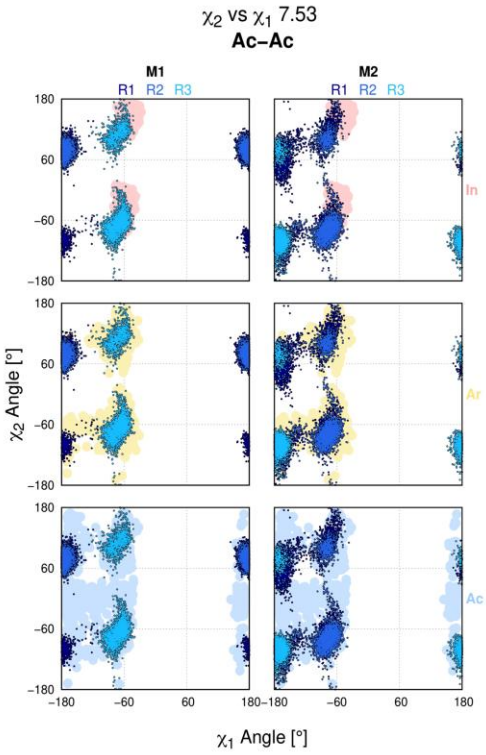
χ2 vs χ1 7.53
Ac–Ac
M1
M2
R1 R2 R3
In
Ar
Ac
χ2 Angle [°]
χ1 Angle [°]

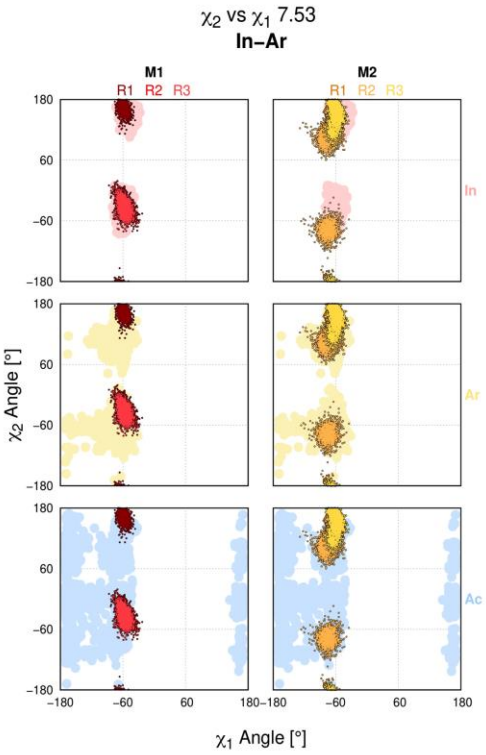
χ2 vs χ1 7.53
In–Ar
M1
M2
R1 R2 R3
In
Ar
Ac
χ2 Angle [°]
χ1 Angle [°]

S29

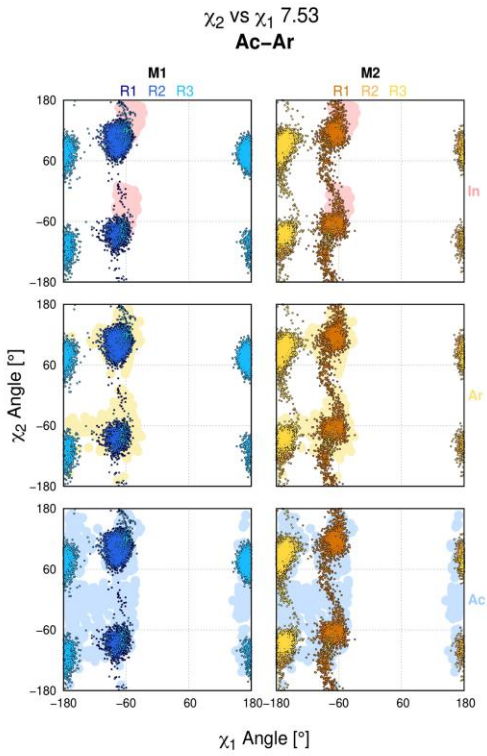
χ2 vs χ1 7.53
Ac–Ar
M1
M2
R1 R2 R3
R1 R2 R3
In
Ar
Ac
χ2 Angle [°]
χ1 Angle [°]
180
60
−60
−180

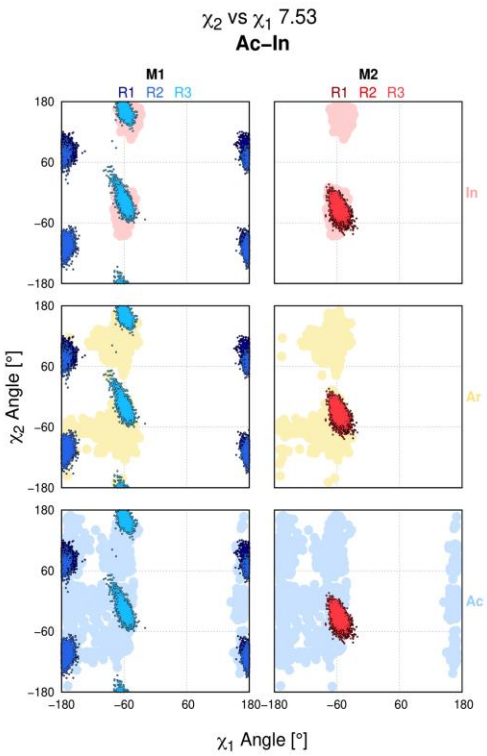
χ2 vs χ1 7.53
Ac–In
M1
M2
R1 R2 R3
R1 R2 R3
In
Ar
Ac
χ2 Angle [°]
χ1 Angle [°]
180
60
−60
−180

Figure S29. Angles χ_1 and χ_2 of tyrosine 7.53 ($Tyr^{7.53}$) compared in the dimers. Comparison of dihedral angles χ_1 and χ_2 of the conserved residue $Tyr^{7.53}$, which were measured for all monomers and replicates over time. The angles [°] of the monomers only are shown as light-coloured clouds in the background. Conformations are colour-coded: inactive - red, arrestin - yellow, active - blue.

S30

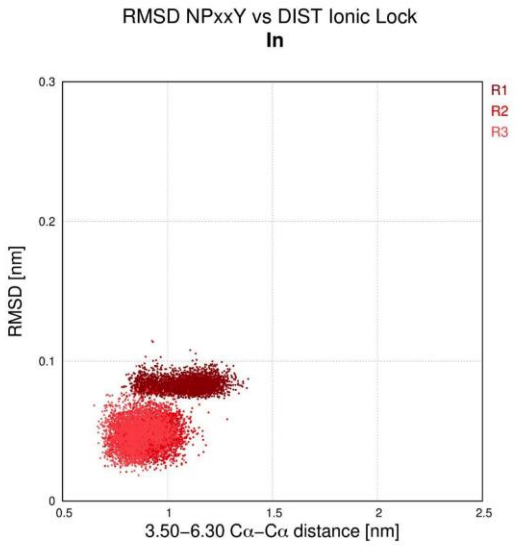
RMSD NPxxY vs DIST Ionic Lock
In
R1
R2
R3
RMSD [nm]
0.3
0.2
0.1
0
0.5
1
1.5
2
2.5
3.50–6.30 Cα–Cα distance [nm]

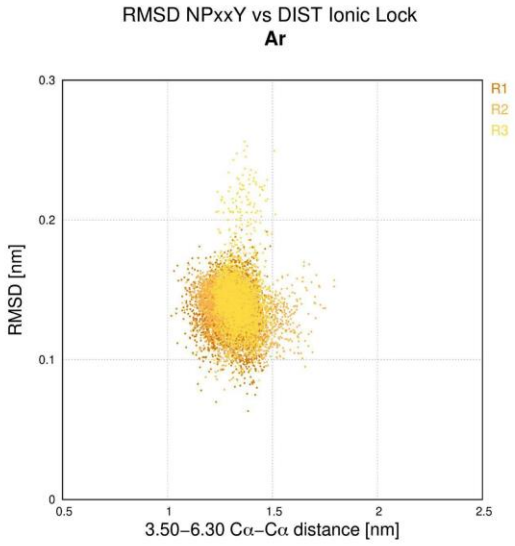
RMSD NPxxY vs DIST Ionic Lock
Ar
R1
R2
R3
RMSD [nm]
0.3
0.2
0.1
0
0.5
1
1.5
2
2.5
3.50–6.30 Cα–Cα distance [nm]

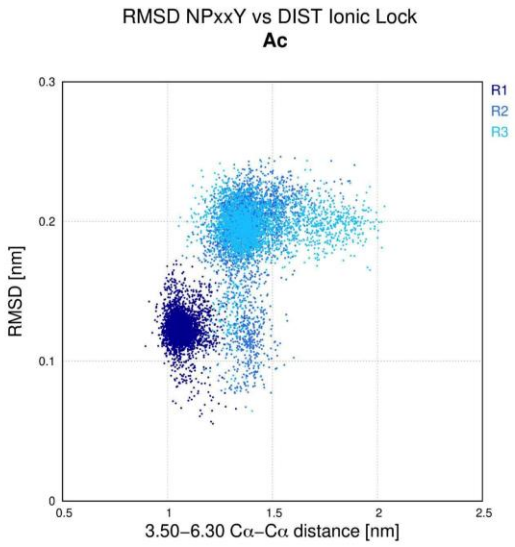
RMSD NPxxY vs DIST Ionic Lock
Ac
R1
R2
R3
RMSD [nm]
0.3
0.2
0.1
0
0.5
1
1.5
2
2.5
3.50–6.30 Cα–Cα distance [nm]

Figure S30. Distance of ionic lock vs. RMSD of NPxxY motif. Comparison of the distance between residues of the ionic lock and the RMSD of the NPxxY motif. The RMSD of the NPxxY motif [nm] was compared to the distance between the Cα-atoms of residues 3.50 and 6.30 [nm], which are part of the ionic lock. Conformations are colour-coded: inactive - red, arrestin - yellow, active - blue. This data was used as background for **Figure 19**.

S31

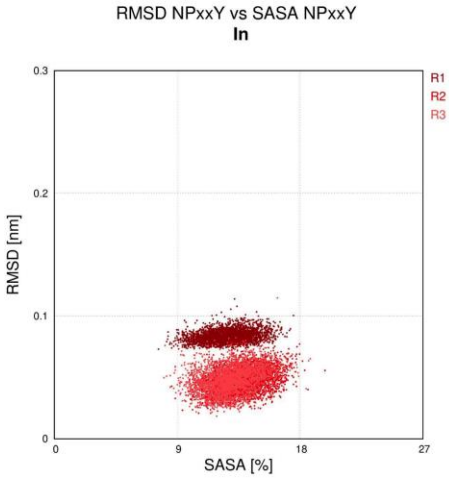
RMSD NPxxY vs SASA NPxxY
In
R1
R2
R3
RMSD [nm]
SASA [%]
0
0.1
0.2
0.3
9
18
27

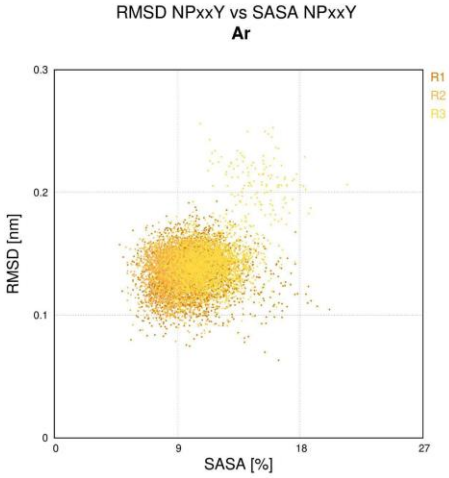
RMSD NPxxY vs SASA NPxxY
Ar
R1
R2
R3
RMSD [nm]
SASA [%]
0
0.1
0.2
0.3
9
18
27

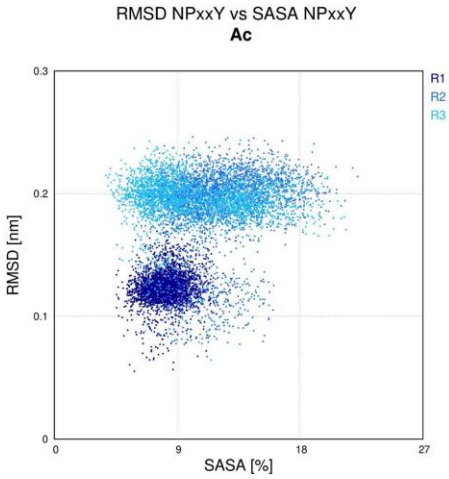
RMSD NPxxY vs SASA NPxxY
Ac
R1
R2
R3
RMSD [nm]
SASA [%]
0
0.1
0.2
0.3
9
18
27

Figure S31. RMSD of NPxxY motif vs ΔSASA NPxxY. Comparison of the NPxxY motif using RMSD and DSASA. The RMSD [nm] and ΔSASA [%] was calculated for all systems separately. DSASA was determined as previously described. Conformations are colour-coded: inactive - red, arrestin - yellow, active - blue. This data was used as background for **Figure S32**.

S32

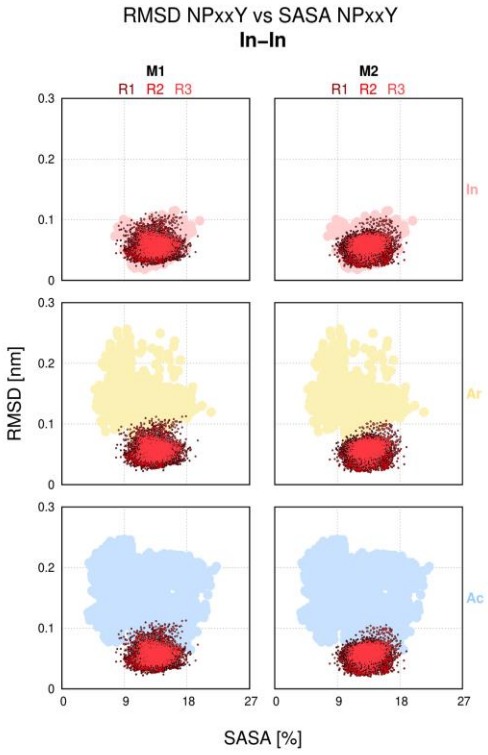
RMSD NPxxY vs SASA NPxxY
In–In
M1
M2
R1 R2 R3
In
Ar
Ac
RMSD [nm]
SASA [%]

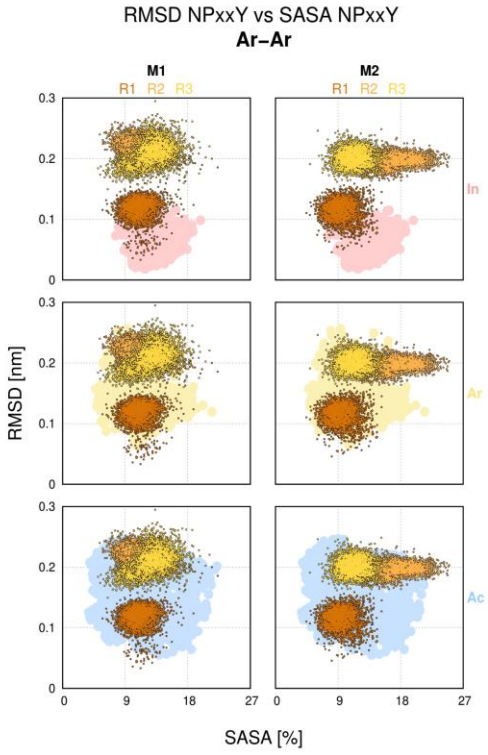
RMSD NPxxY vs SASA NPxxY
Ar–Ar
M1
M2
R1 R2 R3
In
Ar
Ac
RMSD [nm]
SASA [%]

S32

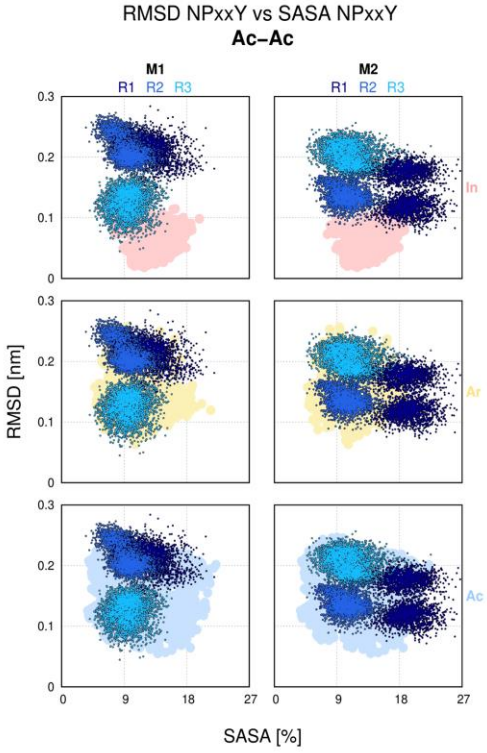
RMSD NPxxY vs SASA NPxxY
Ac–Ac
M1
R1 R2 R3
M2
R1 R2 R3
In
Ar
Ac
RMSD [nm]
SASA [%]
0
0.1
0.2
0.3
0
9
18
27

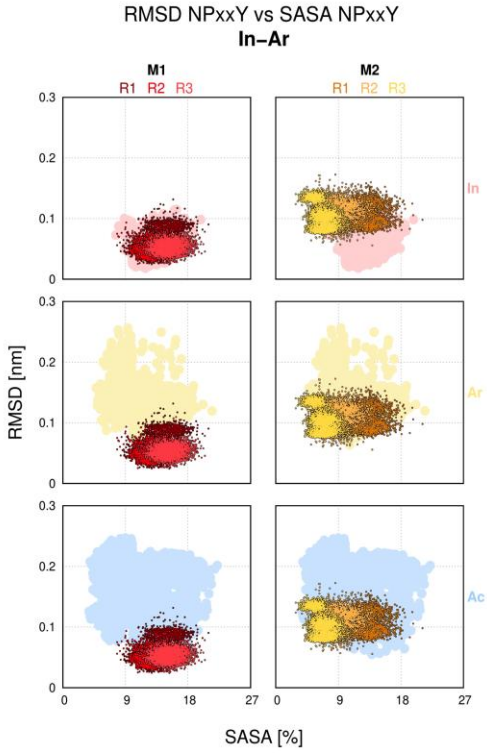
RMSD NPxxY vs SASA NPxxY
In–Ar
M1
R1 R2 R3
M2
R1 R2 R3
In
Ar
Ac
RMSD [nm]
SASA [%]
0
0.1
0.2
0.3
0
9
18
27

S32

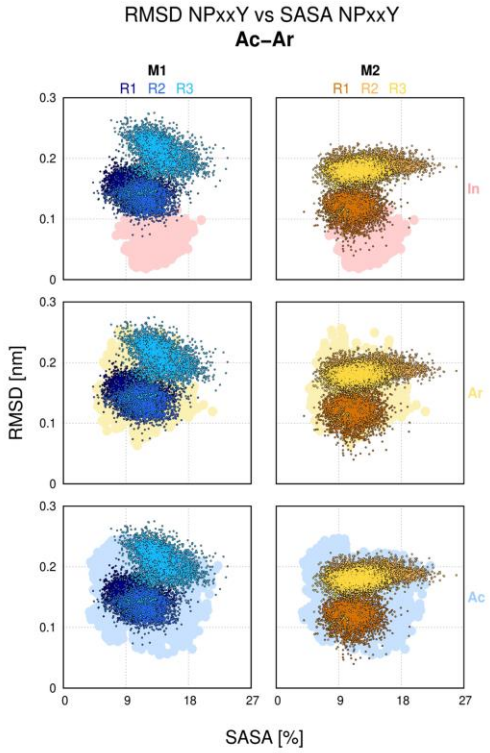
RMSD NPxxY vs SASA NPxxY
Ac–Ar
M1
R1 R2 R3
M2
R1 R2 R3
In
Ar
Ac
RMSD [nm]
SASA [%]

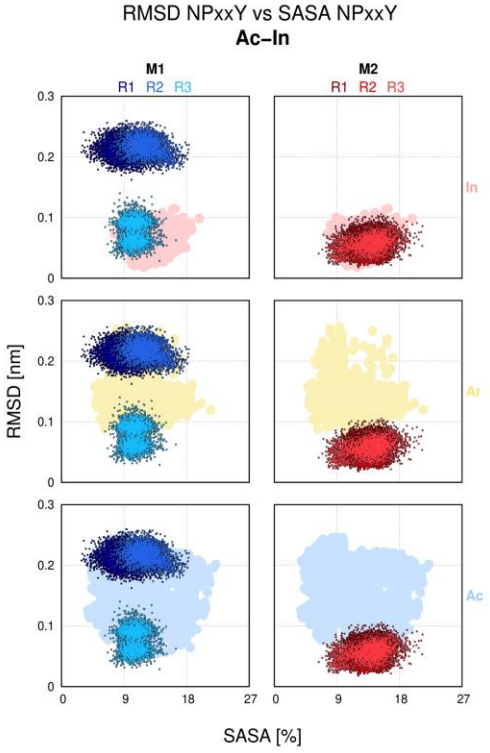
RMSD NPxxY vs SASA NPxxY
Ac–In
M1
R1 R2 R3
M2
R1 R2 R3
In
Ar
Ac
RMSD [nm]
SASA [%]

Figure S32. Comparison of RMSD and ΔSASA of the NPxxY motif. Comparison of RMSD and dSASA of the NPxxY motif of the D_2R-homodimer configurations. The RMSD [nm] and ΔSASA [%] was calculated for all systems separately and then joined in the scatter plot. ΔSASA was calculated as previously described. The distances of the individual monomers in the three activation states (**in-**, **ar-** and **ac-monomers**) are shown as light-coloured clouds in the background in three different lines for easier comparison Conformations are colour-coded: inactive - red, arrestin - yellow, active - blue.

S33

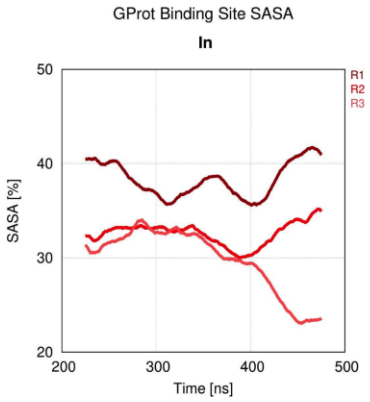
GProt Binding Site SASA
In
R1
R2
R3
SASA [%]
50
40
30
20
200
300
400
500
Time [ns]

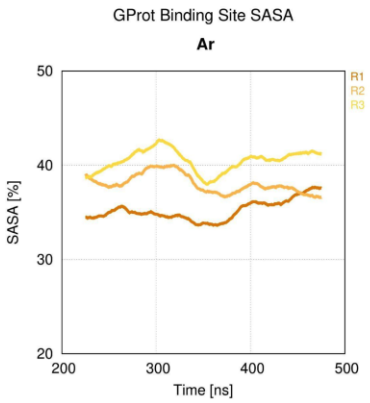
GProt Binding Site SASA
Ar
R1
R2
R3
SASA [%]
50
40
30
20
200
300
400
500
Time [ns]

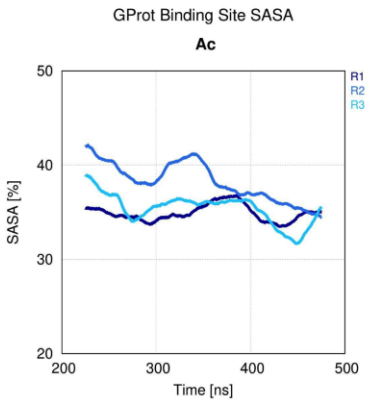
GProt Binding Site SASA
Ac
R1
R2
R3
SASA [%]
50
40
30
20
200
300
400
500
Time [ns]

S33

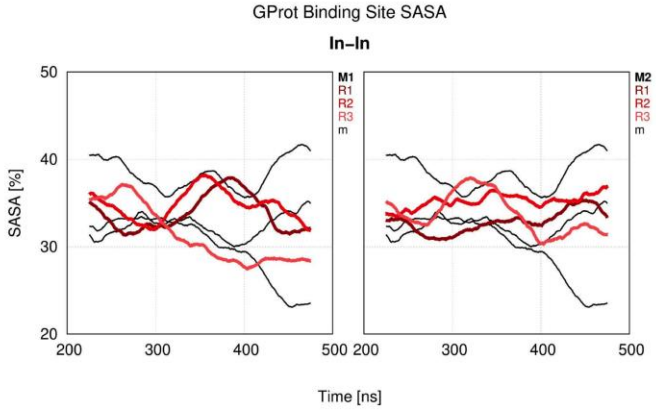
GProt Binding Site SASA
In–In
SASA [%]
Time [ns]
M1
M2
R1
R2
R3
m

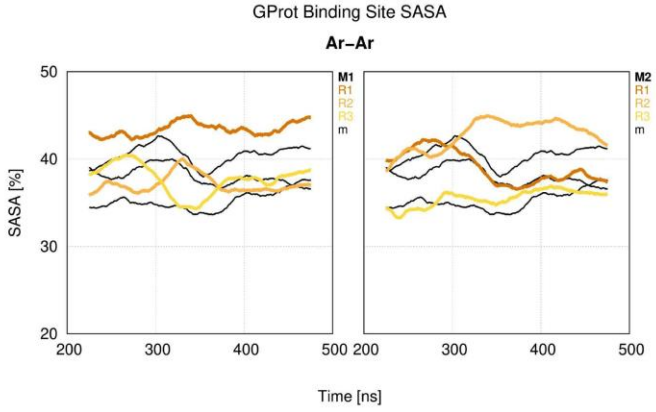
GProt Binding Site SASA
Ar–Ar
SASA [%]
Time [ns]
M1
M2
R1
R2
R3
m

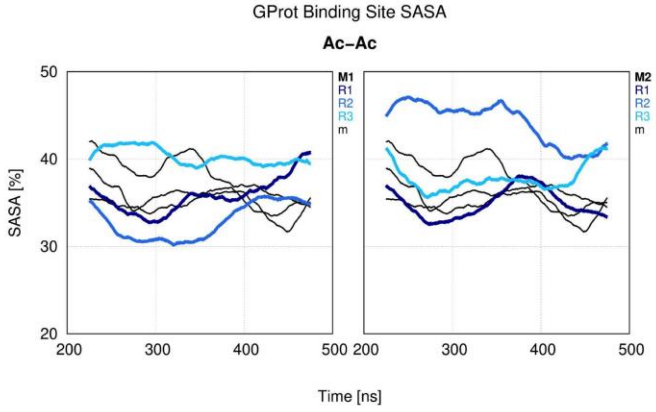
GProt Binding Site SASA
Ac–Ac
SASA [%]
Time [ns]
M1
M2
R1
R2
R3
m

S33

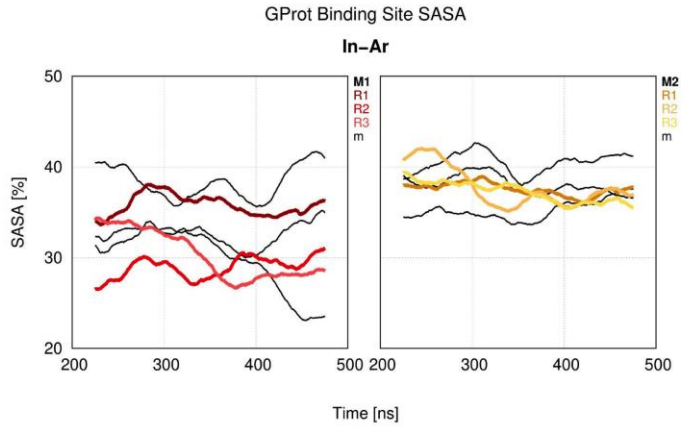
GProt Binding Site SASA
In–Ar
SASA [%]
Time [ns]
M1
R1
R2
R3
m
M2
R1
R2
R3
m

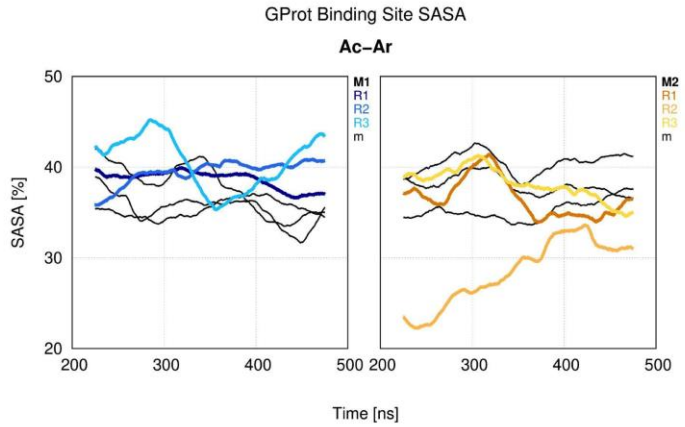
GProt Binding Site SASA
Ac–Ar
SASA [%]
Time [ns]
M1
R1
R2
R3
m
M2
R1
R2
R3
m

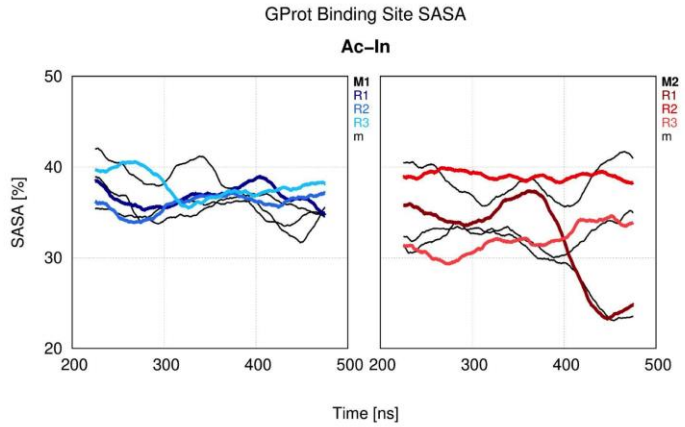
GProt Binding Site SASA
Ac–In
SASA [%]
Time [ns]
M1
R1
R2
R3
m
M2
R1
R2
R3
m

Figure S33. Size of binding site for G protein over time. Sizes of binding site for the G protein were determined over time [ns] for all D_2R-homodimer configurations using the SASA for a known subset of interacting residues (Preto et al., 2020). These values were then normalized to $SASA_{max}$.

G protein-relevant residues: 39THR, 2.39THR, 3.50ARG, 3.53ALA, 3.54VAL, 202ARG, 210ARG, 212LYS, 213LEU, 214SER, 215GLN, 6.29LYS, 6.30GLU, 6.32LYS, 6.33ALA, 7.56PHE, 8.43ASN, 8.44ILE, 8.45GLU, 8.46PHE.

Conformations are colour-coded: inactive - red, arrestin - yellow, active - blue.

Reference:
Preto AJ, Barreto CAV, Baptista SJ, Almeida JG, Lemos A, Melo A, Cordeiro MNDS, Kurkcuoglu Z, Melo R, Moreira IS. Understanding the Binding Specificity of G-Protein Coupled Receptors toward G-Proteins and Arrestins: Application to the Dopamine Receptor Family. *J Chem Inf Model.* 2020 Aug 24;60(8):3969-3984. DOI: 10.1021/acs.jcim.0c00371.

S34

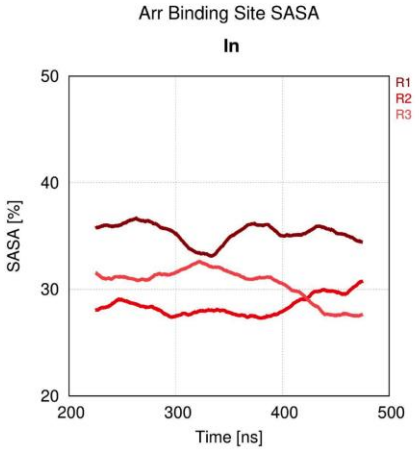
Arr Binding Site SASA
In
R1
R2
R3
SASA [%]
50
40
30
20
200
300
400
500
Time [ns]

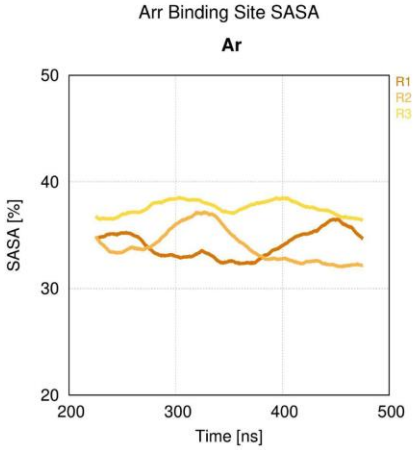
Arr Binding Site SASA
Ar
R1
R2
R3
SASA [%]
50
40
30
20
200
300
400
500
Time [ns]

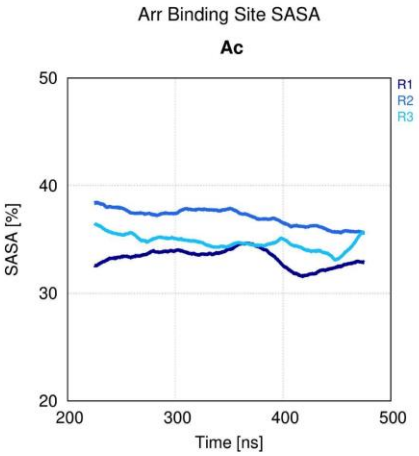
Arr Binding Site SASA
Ac
R1
R2
R3
SASA [%]
50
40
30
20
200
300
400
500
Time [ns]

S34

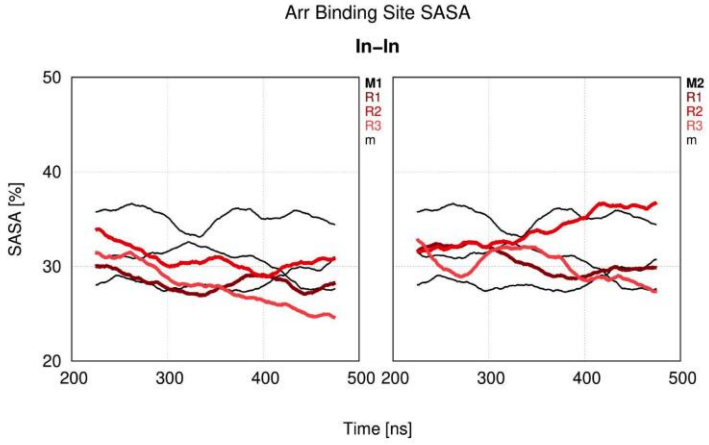
Arr Binding Site SASA
In–In
SASA [%]
Time [ns]
M1
R1
R2
R3
m
M2
R1
R2
R3
m

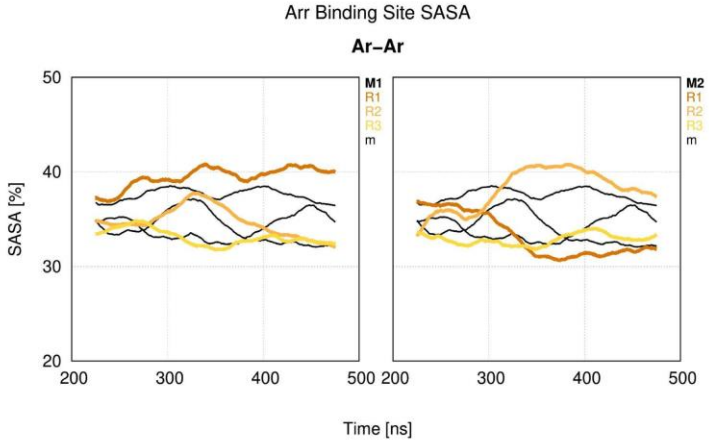
Arr Binding Site SASA
Ar–Ar
SASA [%]
Time [ns]
M1
R1
R2
R3
m
M2
R1
R2
R3
m

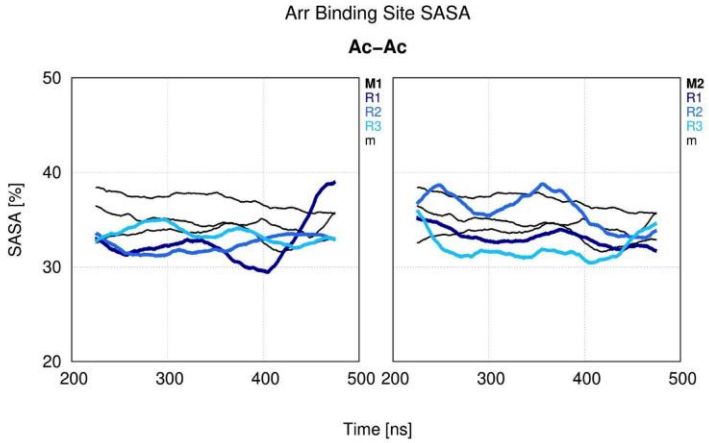
Arr Binding Site SASA
Ac–Ac
SASA [%]
Time [ns]
M1
R1
R2
R3
m
M2
R1
R2
R3
m

S34

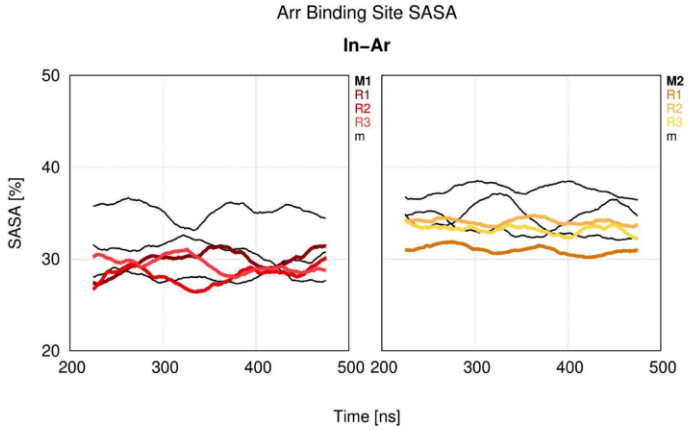
Arr Binding Site SASA
In–Ar
M1
R1
R2
R3
m
M2
R1
R2
R3
m
SASA [%]
50
40
30
20
200
300
400
500
Time [ns]

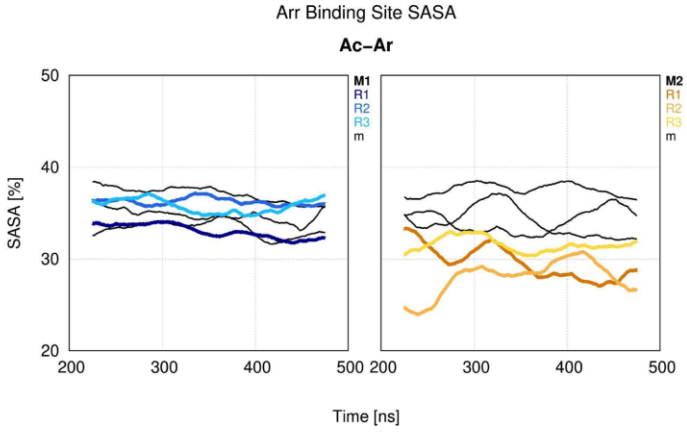
Arr Binding Site SASA
Ac–Ar
M1
R1
R2
R3
m
M2
R1
R2
R3
m
SASA [%]
50
40
30
20
200
300
400
500
Time [ns]

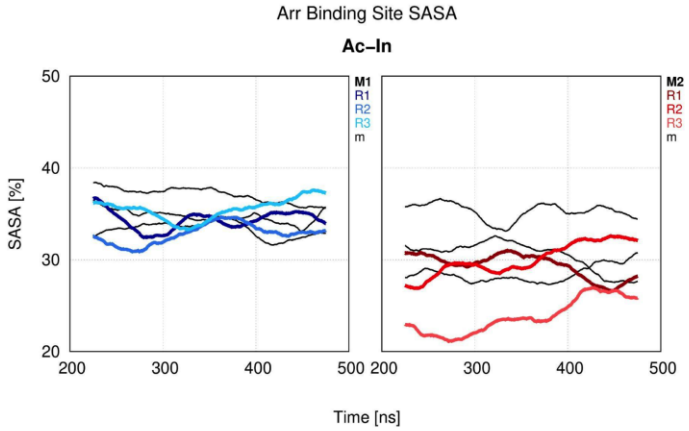
Arr Binding Site SASA
Ac–In
M1
R1
R2
R3
m
M2
R1
R2
R3
m
SASA [%]
50
40
30
20
200
300
400
500
Time [ns]

Figure S34. Size of binding site for β-arrestin over time. Sizes of binding site for β-arrestin were determined over time [ns] for all D_2R homodimer configurations using the SASA for a known subset of interacting residues (Preto et al., 2020). These values were then normalized to $SASA_{max}$.

β-arrestin-relevant residues: 36ALA, 37LEU, 38GLN, 39THR, 2.39THR, 2.40ASN, 3.50ARG, 3.53ALA, 3.54VAL, 11PRO, 112MET, 113LEU, 115ASN, 116THR, 119SER, 5.64VAL, 5.65LEU, 5.67ARG, 5.68ARG, 5.72VAL, 5.75LYS, 199ARG, 200SER 201SER, 214SER, 6.29LYS, 6.30GLU 6.31LYS, 6.32LYS, 6.33ALA, 6.34THR, 6.36MET, 7.56PHE, 8.43ASN, 8.44ILE.

Conformations are colour-coded: inactive - red, arrestin - yellow, active - blue.

Reference:
Preto AJ, Barreto CAV, Baptista SJ, Almeida JG, Lemos A, Melo A, Cordeiro MNDS, Kurkcuoglu Z, Melo R, Moreira IS. Understanding the Binding Specificity of G-Protein Coupled Receptors toward G-Proteins and Arrestins: Application to the Dopamine Receptor Family. *J Chem Inf Model.* 2020 Aug 24;60(8):3969-3984. DOI: 10.1021/acs.jcim.0c00371.

Table S1. PRODIGY-CRYSTAL and PRODIGY results for the final modeled structures of the dimer configurations.

Dimer variant	Proposed interface	Binding affinity (ΔG) [kcal mol-1]	Dissociation constant (Kd) [M] at 37.0 °C	Total number of interfacial contacts (ICs) per property	Non Interacting Surface (NIS) per property	Link density	Prodigy-crystal prediction [>0.5]
in-in	TM4-TM5-TM4-TM5	-11.4	9.1E-09	79 (1x charged-charged, 7x charged-polar, 8x charged-apolar, 0x polar-polar, 28x polar-apolar, 35x apolar-apolar)	17.09% (charged); 50.42% (apolar)	0.074	0.940
ac-ac-B	TM4-TM5-TM7-TM1	-4.6	5.9E-04	5 (0x charged-charged, 0x charged-polar, 4x charged-apolar, 0x polar-polar, 0x polar-apolar, 1x apolar-apolar)	15.38% (charged); 51.62% (apolar)	0.417	0.552
ac-ac	TM4-TM5-TM4-TM5	-8.5	1.0E-06	42 (1x charged-charged, 1x polar, 8x charged-apolar, 0x polar-polar, 10x polar-apolar, 22x apolar-apolar)	15.34% (charged); 51.91% (apolar)	0.095	0.684
ar-ar	TM4-TM5-TM4-TM5	-7.3	7.7E-06	38 (1x charged-charged, 1x charged-polar, 10x charged-apolar, 0x polar-polar, 6x polar-apolar, 20x apolar-apolar)	15.96% (charged); 53.08% (apolar)	0.102	0.536
ac-in	TM1-TM2-TM4-TM5	-9.0	4.7E-07	58 (4x charged-charged, 4x charged-polar, 11x charged-apolar, 0x polar-polar, 11x polar-apolar, 28x apolar-apolar)	16.19% (charged); 51.02% (apolar)	0.069	0.868
in-ar	TM3-TM4-TM4-TM5	-8.3	1.5E-06	49 (2x charged-charged, 2x charged-polar, 12x charged-apolar, 3x polar-polar, 10x polar-apolar, 20x apolar-apolar)	16.73% (charged); 51.41% (apolar)	0.063	0.720
ac-ar	TM4-TM5-TM4-TM5	-7.3	6.6E-06	39 (2x charged-charged, 1x charged-polar, 6x charged-apolar, 0x polar-polar, 7x polar-apol, 23x apolar-apolar)	16.10% (charged); 52.09% (apolar)	0.087	0.656

Table S2. Interfacial residues determined by PRODIGY. Interfacial residues were either sorted by appearance within the partnered monomers (bold/italic) and frequency across all configurations (colors).

Dimer	in-in		ac-ac-B		ac-ac		ar-ar		ac-in		in-ar		ac-ar	
Interface	TM4-TM5-TM4-TM5		TM4-TM5-TM7-TM1		TM4-TM5-TM4-TM5		TM4-TM5-TM4-TM5		TM1-TM2-TM4-TM5		TM3-TM4-TM4-TM5		TM4-TM5-TM4-TM5	
Monomer	A	B	A	B	A	B	A	B	A	B	A	B	A	B
Template	6CM4	6CM4	6VMS	6VMS	6VMS	6VMS	6U1N	6U1N	6VMS	6CM4	6CM4	6U1N	6VMS	6U1N
	3.48ILE	**3.48ILE**	112MET (ICL2)	*4PRO (Nterm)*	**3.48ILE**	**3.48ILE**	**110MET (ICL2**	3.48ILE	1.51VAL	3.51TYR	3.48ILE	1.51VAL	**3.48ILE**	*3.47SER*
	3.51TYR	**3.51TYR**	160ALA (ECL2	*5HIS (Nterm)*	**3.51TYR**	**3.51TYR**	**113LEU (ICL2)**	3.51TYR	*1.54CYS*	3.55ALA	3.51TYR	1.55MET	**3.52THR**	**3.48ILE**
	3.52THR	**3.52THR**	5.41TYR	*1.34TYR*	3.52THR	*3.54VAL*	116THR (ICL2)	3.52THR	1.55MET	110MET (ICL2)	3.52THR	1.57VAL	**110MET (ICL2**	3.51TYR
	3.55ALA	**3.55ALA**		*1.35TYR*	**3.55ALA**	**3.55ALA**	**117ARG (ICL2**	**110MET (ICL2**	1.57VAL	111PRO (ICL2)	3.55ALA	1.58SER	112MET (ICL2)	**3.52THR**
	110MET (ICL2	**110MET (ICL2)**		*6.23ARG*	**110MET (ICL2**	**110MET (ICL2**	118TYR (ICL2)	**113LEU (ICL2)**	1.58SER	112MET (ICL2)	110MET (ICL2)	1.59ARG	**113LEU (ICL2)**	3.55ALA
	111PRO (ICL2	**111PRO (ICL2)**		*6.24LYS*	**111PRO (ICL2**	**111PRO (ICL2**	119SER (ICL2)	**117ARG (ICL2**	1.59ARG	*114TYR (ICL2*	111PRO (ICL2)	35LYS (ICL1)	116THR (ICL2)	**110MET (ICL2**
	120SER (ICL2	**120SER (ICL2)**			**112MET (ICL2**	**112MET (ICL2**	4.40ARG	**4.41ARG**	*34GLU (ICL1)*	*115ASN (ICL2*	112MET (ICL2)	2.41TYR	118TYR (ICL2)	**113LEU (ICL2)**
	4.40ARG	**4.40ARG**			**113LEU (ICL2**	**113LEU (ICL2)**	**4.41ARG**	**4.56ILE**	35LYS (ICL1)	4.40ARG	4.40ARG	2.48VAL	119SER (ICL2)	117ARG (ICL2
	4.41ARG	**4.41ARG**			**116THR (ICL2**	**116THR (ICL2)**	4.44VAL	**4.59PRO**	*37LEU (ICL1)*	4.41ARG	4.41ARG	2.51LEU	4.40ARG	**4.41ARG**
	4.43THR	**4.43THR**			**119SER (ICL2**	**119SER (ICL2)**	4.48ILE	.58ASN (ECL2	*37GLN (ICL1)*	4.44VAL	**4.44VAL**	2.52LEU	**4.41ARG**	4.48ILE
	4.44VAL	**4.44VAL**			**4.40ARG**	**4.40ARG**	4.51VAL	59PRO (ECL2	2.41TYR	4.48ILE	4.48ILE	2.56LEU	4.44VAL	**4.52LEU**
	4.48ILE	4.47SER			4.41ARG	**4.44VAL**	4.52LEU	**.60ALA (ECL2**	2.48VAL	4.52LEU	4.52LEU	75SER (ECL1)	4.51VAL	**4.55THR**
	4.51VAL	**4.48ILE**			*4.42VAL*	**4.48ILE**	4.55THR	**5.38PHE**	2.51LEU	.46LEU (ECL2	**4.55THR**	3.22ARG	**4.52LEU**	4.56ILE
	4.52LEU	**4.51VAL**			4.43THR	**4.52LEU**	**4.56ILE**	5.40VAL	2.52LEU	.47ASN (ECL2	**4.59PRO**	3.23ILE	4.54PHE	**4.58CYS**
	4.55THR	**4.52LEU**			**4.44VAL**	**4.55THR**	**4.59PRO**	**5.41TYR**	2.56LEU	.48ASN (ECL2	46LEU (ECL2	3.27ILE	**4.55THR**	**4.59PRO**
	4.56ILE	**4.55THR**			4.47SER	**4.58CYS**	**.60ALA (ECL2**	**5.42SER**	*2.60TRP*	160ALA (ECL2	47ASN (ECL2	3.31LEU	**4.58CYS**	**.44PHE (ECL2**
	4.59PRO	**4.56ILE**			**4.48ILE**	**4.59PRO**	**5.38PHE**	5.44ILE	75SER (ECL1)	5.40VAL	.48ASN (ECL2	*3.34MET*	**4.59PRO**	**.60ALA (ECL2**
	146LEU (ECL2	**4.59PRO**			4.51VAL	**5.41TYR**	**5.41TYR**	**5.45VAL**	3.22ARG	5.41TYR	*149ALA (ECL2*	121LYS (ICL2)	4.61LEU	**5.38PHE**
	147ASN (ECL2	**146LEU (ECL2)**			**4.52LEU**	5.44ILE	**5.42SER**	5.48TYR	3.23ILE	5.44ILE	160ALA (ECL2	4.43THR	**.44PHE (ECL2**	**5.41TYR**
	148ASN (ECL2	**147ASN (ECL2)**			**4.55THR**	**5.45VAL**	**5.45VAL**	5.49VAL	*3.24HIS*	5.45VAL	5.40VAL	**4.44VAL**	145GLY (ECL2	5.42SER
	151GLN (ECL2	**148ASN (ECL2)**			**4.58CYS**	5.48TYR	*5.46SER*	5.52ILE	3.27ILE	5.48TYR	5.41TYR	4.47SER	146LEU (ECL2	**5.45VAL**
	159PRO (ECL2	**159PRO (ECL2)**			**4.59PRO**	**5.49VAL**		5.53VAL	3.31LEU	5.49VAL	5.44ILE	4.50TRP	.58ASN (ECL2	**5.49VAL**
	160ALA (ECL2	**160ALA (ECL2)**			144PHE (ECL2	**5.52ILE**		5.56LEU	118TYR (ICL2)	5.52ILE	5.45VAL	4.51VAL	**.60ALA (ECL2**	5.53VAL
	5.40VAL	**5.40VAL**			145GLY (ECL2	**5.53VAL**		5.57VAL	121LYS (ICL2)	5.56LEU	5.48TYR	4.54PHE	**5.38PHE**	5.56LEU
	5.41TYR	**5.41TYR**			146LEU (ECL2	**5.56LEU**		5.60LYS	4.43THR	5.60LYS	5.49VAL	**4.55THR**	**5.41TYR**	5.57VAL
	5.44ILE	**5.44ILE**			**5.41TYR**	5.60LYS		6.59ILE	4.47SER	*5.63ILE*	5.52ILE	4.58CYS	**5.45VAL**	5.60LYS
	5.45VAL	**5.45VAL**			**5.45VAL**	5.64VAL			4.50TRP	5.64VAL	5.53VAL	**4.59PRO**	**5.49VAL**	
	5.48TYR	**5.48TYR**			**5.49VAL**	5.67ARG			4.54PHE	5.67ARG	5.56LEU	4.61LEU		
	5.49VAL	**5.49VAL**			**5.52ILE**	5.68ARG			4.61LEU	5.68ARG	5.57VAL	.44PHE (ECL2)		
	5.52ILE	**5.52ILE**			**5.53VAL**				144PHE (ECL2	*5.70LYS*	5.60LYS	8.53ILE		
	5.53VAL	**5.53VAL**			**5.56LEU**				8.53ILE	5.71ARG	5.67ARG	8.55HIS		
	5.56LEU	**5.56LEU**							8.55HIS	*5.74THR*	5.68ARG	8.56CYS		
	5.60LYS	**6.59ILE**							8.56CYS		5.71ARG			
	6.59ILE	**248HIS (ECL3)**									6.59ILE			
	248HIS (ECL3)										248HIS (ECL3)			
Total number of interfacing residues	35	34	3	6	31	29	21	26	33	32	35	32	27	26

Bold residues: Double residues within dimers
Italic residues: Unique residues across all dimers
Green: Very frequent residues (8-12x)
Orange: Moderate frequent residues (3-7x)
Pink: Rare residues (1-2x)

Table S3. Frequency of common interfacial residues for dimer configurations determined by PRODIGY.

	Frequency		
	1-2 times: rare	3-7 times: moderate	8-12 times: very frequent
	4PRO (N-terminus)	111PRO (ICL2)	110MET (ICL2)
	5HIS (N-terminus)	112MET (ICL2)	160ALA (ECL2)
	34GLU (ICL1)	113LEU (ICL2)	3.48ILE
	35LYS (ICL1)	116THR (ICL2)	3.51TYR
	37LEU (ICL1)	117ARG (ICL2)	3.52THR
	38GLN (ICL1)	118TYR (ICL2)	3.55ALA
	75SER (ECL1)	119SER (ICL2)	4.40ARG
	114TYR (ICL2)	144PHE(ECL2)	4.41ARG
	115ASN (ICL2)	146LEU (ECL2)	4.44VAL
	120SER (ICL2)	147ASN (ECL2)	4.48ILE
	121LYS (ICL2)	148ASN (ECL2)	4.52LEU
	145GLY (ECL2)	159PRO (ECL2)	4.55THR
	149ALA (ECL2)	248HIS (ECL3)	4.59PRO
	151GLN (ECL2)	4.43THR	5.41TYR
	158ASN (ECL2)	4.47SER	5.45VAL
	1.34TYR	4.51VAL	5.49VAL
	1.35TYR	4.54PHE	5.52ILE
	1.51VAL	4.56ILE	5.53VAL
	1.54CYS	4.58CYS	5.56LEU
	1.55MET	4.61LEU	
	1.57VAL	5.38PHE	
	1.58SER	5.40VAL	
	1.59ARG	5.42SER	
	2.41TYR	5.44ILE	
	2.48VAL	5.48TYR	
	2.51LEU	5.57VAL	
	2.52LEU	5.60LYS	
	2.56LEU	5.67ARG	
	2.60TRP	5.68ARG	
	3.22ARG	6.59ILE	
	3.23ILE		
	3.24HIS		
	3.27ILE		
	3.31LEU		
	3.34MET		
	3.47SER		
	3.54VAL		
	4.42VAL		
	4.50TRP		
	5.46SER		
	5.63ILE		
	5.64VAL		
	5.70LYS		
	5.71ARG		
	5.74THR		
	6.23ARG		
	6.24LYS		
	8.53ILE		
	8.55HIS		
	8.56CYS		
Total	50	30	19

Table S4. Original interface residues determined by solvent accessible surface area (SASA) colored by location. Summary of Figure S11.

Dimer	in-in		ac-ac		ar-ar		ac-in		in-ar		ac-ar	
Interface	TM4-TM5-TM4-TM5		TM4-TM5-TM4-TM5		TM4-TM5-TM4-TM5		TM1-TM2-TM4-TM5		TM3-TM4-TM4-TM5		TM4-TM5-TM4-TM5	
Monomer	A	B	A	B	A	B	A	B	A	B	A	B
Template	6CM4	6CM4	6VMS	6VMS	6U1N	6U1N	6VMS	6CM4	6CM4	6U1N	6VMS	6U1N
	3.48ILE	3.48ILE	110MET	3.55ALA	4.40ARG	4.59PRO	1.51VAL	3.51TYR	3.48ILE	1.51VAL	110MET	3.48ILE
	3.51TYR	3.51TYR	113LEU	110MET	4.44VAL	160ALA	1.54CYS	3.55ALA	3.51TYR	1.55MET	113LEU	3.52THR
	3.52THR	3.52THR	118TYR	112MET	4.48ILE	5.38PHE	1.55MET	110MET	3.52THR	1.58SER	116THR	110MET
	3.55ALA	3.55ALA	119SER	113LEU	4.51VAL	5.40VAL	1.58SER	111PRO	3.55ALA	1.59ARG	118TYR	113LEU
	110MET	110MET	4.40ARG	118TYR	4.52LEU	5.41TYR	1.59ARG	112MET	4.40ARG	35LYS	119SER	117ARG
	111PRO	111PRO	4.44VAL	119SER	4.55THR	5.44ILE	35LYS	113LEU	4.41ARG	38GLN	4.40ARG	4.41ARG
	120SER	4.40ARG	4.47SER	4.40ARG	4.56ILE	5.48TYR	38GLN	114TYR	4.44VAL	2.48VAL	4.44VAL	4.45MET
	4.40ARG	4.41ARG	4.48ILE	4.44VAL	4.59PRO	5.49VAL	2.41TYR	115ASN	4.47SER	2.51LEU	4.51VAL	4.48ILE
	4.41ARG	4.44VAL	4.51VAL	4.48ILE	160ALA	5.52ILE	2.48VAL	4.41ARG	4.48ILE	2.52LEU	4.52LEU	4.51VAL
	4.44VAL	4.47SER	4.52LEU	4.51VAL	5.38PHE	5.56LEU	2.52LEU	4.44VAL	4.51VAL	2.56LEU	4.55THR	4.52LEU
	4.48ILE	4.48ILE	4.54PHE	4.52LEU	5.41TYR	5.60LYS	2.55THR	4.48ILE	4.52LEU	75SER	4.58CYS	4.54PHE
	4.51VAL	4.51VAL	4.55THR	4.55THR	5.45VAL	248HIS	2.56LEU	4.52LEU	4.55THR	3.23ILE	4.59PRO	4.55THR
	4.52LEU	4.52LEU	4.59PRO	4.56ILE			3.23ILE	4.55THR	4.59PRO	3.27ILE	144PHE	4.56ILE
	4.55THR	4.55THR	144PHE	4.58CYS			3.24HIS	4.58CYS	146LEU	3.30THR	146LEU	4.58CYS
	4.59PRO	4.56ILE	145GLY	4.59PRO			3.27ILE	4.59PRO	147ASN	121LYS	158ASN	4.59PRO
	146LEU	4.59PRO	146LEU	5.41TYR			117ARG	147ASN	148ASN	4.43THR	160ALA	144PHE
	147ASN	146LEU	5.41TYR	5.44ILE			118TYR	160ALA	160ALA	4.47SER	5.38PHE	146LEU
	159PRO	147ASN	5.44ILE	5.45VAL			121LYS	5.40VAL	5.40VAL	4.50TRP	5.41TYR	147ASN
	160ALA	160ALA	5.45VAL	5.48TYR			4.40ARG	5.41TYR	5.41TYR	4.51VAL	5.45VAL	5.38PHE
	5.40VAL	5.40VAL	5.49VAL	5.49VAL			4.43THR	5.44ILE	5.44ILE	4.54PHE	5.49VAL	5.41TYR
	5.41TYR	5.41TYR	5.53VAL	5.52ILE			4.47SER	5.45VAL	5.45VAL	4.55THR	5.53VAL	5.45VAL
	5.44ILE	5.44ILE		5.53VAL			4.51VAL	5.48TYR	5.49VAL	4.58CYS		5.49VAL
	5.45VAL	5.45VAL		5.56LEU			4.54PHE	5.49VAL	5.52ILE	4.59PRO		5.53VAL
	5.49VAL	5.49VAL					4.58CYS	5.52ILE	5.53VAL	144PHE		
	5.52ILE	5.52ILE					4.61LEU	5.53VAL	5.56LEU	8.53ILE		
	5.53VAL	5.53VAL					144PHE	5.56LEU	5.60LYS	8.56CYS		
	5.56LEU	5.56LEU					145GLY	5.60LYS	5.67ARG			
		6.59ILE						5.63ILE	6.56ILE			
								5.64VAL	6.59ILE			
								5.67ARG	248HIS			
								5.71ARG				

TM1: rose
ICL1: cyan
TM2: blue
ECL1: ocher
TM3: red
ICL2: dark blue
TM4: green
ECL2: pink
TM5: yellow
ICL3: N/A
TM6: orange
ECL3: dark green
TM7: N/A
HX8: purple

Table S5. Original interface residues determined by solvent accessible surface area (SASA) and compared to PRODIGY-predicted residues.

Dimer	Inactive-Inactive		Active-Active		Arrestin-Arrestin		Active-Inactive		Inactive-Arrestin		Active-Arrestin	
Interface	TM4-TM5-TM4-TM5		TM4-TM5-TM4-TM5		TM4-TM5-TM4-TM5		TM1-TM2-TM4-TM5		TM3-TM4-TM4-TM5		TM4-TM5-TM4-TM5	
Monomer	A	B	A	B	A	B	A	B	A	B	A	B
Template	6CM4	6CM4	6VMS	6VMS	6U1N	6U1N	6VMS	6CM4	6CM4	6U1N	6VMS	6U1N
	3.48ILE	3.48ILE	3.48ILE	3.48ILE	110MET	3.48ILE	1.51VAL	3.51TYR	3.48ILE	1.51VAL	3.48ILE	3.47SER
	3.51TYR	3.51TYR	3.51TYR	3.51TYR	113LEU	3.51TYR	1.54CYS	3.55ALA	3.51TYR	1.55MET	3.52THR	3.48ILE
	3.52THR	3.52THR	3.52THR	3.54VAL	116THR	3.52THR	1.55MET	110MET	3.52THR	1.57VAL	110MET	3.51TYR
	3.55ALA	3.55ALA	3.55ALA	3.55ALA	117ARG	110MET	1.57VAL	111PRO	3.55ALA	1.58SER	112MET	3.52THR
	110MET	110MET	110MET	110MET	118TYR	113LEU	1.58SER	112MET	110MET	1.59ARG	113LEU	3.55ALA
	111PRO	111PRO	111PRO	111PRO	119SER	117ARG	1.59ARG	113LEU	111PRO	35LYS	116THR	110MET
	120SER	120SER	112MET	112MET	4.40ARG	4.41ARG	34GLU	114TYR	112MET	38GLN	118TYR	113LEU
	4.40ARG	4.40ARG	113LEU	113LEU	4.41ARG	4.56ILE	35LYS	115ASN	4.40ARG	2.41TYR	119SER	117ARG
	4.41ARG	4.41ARG	116THR	116THR	4.44VAL	4.59PRO	37LEU	4.40ARG	4.41ARG	2.48VAL	4.40ARG	4.41ARG
	4.43THR	4.43THR	TYR118	TYR118	4.48ILE	158ASN	38GLN	4.41ARG	4.44VAL	2.51LEU	4.41ARG	4.45MET
	4.44VAL	4.44VAL	119SER	119SER	4.51VAL	159PRO	2.41TYR	4.44VAL	4.47SER	2.52LEU	4.44VAL	4.48ILE
	4.48ILE	4.47SER	4.40ARG	4.40ARG	4.52LEU	160ALA	2.48VAL	4.48ILE	4.48ILE	2.56LEU	4.51VAL	4.51VAL
	4.51VAL	4.48ILE	4.41ARG	4.44VAL	4.55THR	5.38PHE	2.51LEU	4.52LEU	4.51VAL	75SER	4.52LEU	4.52LEU
	4.52LEU	4.51VAL	4.42VAL	4.48ILE	4.56ILE	5.40VAL	2.52LEU	4.55THR	4.52LEU	3.22ARG	4.54PHE	4.54PHE
	4.55THR	4.52LEU	4.43THR	4.51VAL	4.59PRO	5.41TYR	2.55THR	4.58CYS	4.55THR	3.23ILE	4.55THR	4.55THR
	4.56ILE	4.55THR	4.44VAL	4.52LEU	160ALA	5.42SER	2.56LEU	4.59PRO	4.59PRO	3.27ILE	4.56ILE	4.56ILE
	4.59PRO	4.56ILE	4.47SER	4.55THR	5.38PHE	5.44ILE	2.60TRP	146LEU	146LEU	3.30THR	4.58CYS	4.58CYS
	146LEU	4.59PRO	4.48ILE	4.56ILE	5.41TYR	5.45VAL	75SER	147ASN	147ASN	3.31LEU	4.59PRO	4.59PRO
	147ASN	146LEU	4.51VAL	4.58CYS	5.42SER	5.48TYR	3.22ARG	148ASN	148ASN	3.34MET	4.61LEU	L44PHE(ECL2)
	148ASN	147ASN	4.52LEU	4.59PRO	5.45VAL	5.49VAL	3.23ILE	160ALA	149ALA	121LYS	L44PHE(ECL2)	146LEU
	151GLN	148ASN	4.54PHE	5.41TYR	5.46SER	5.52ILE	3.24HIS	5.40VAL	160ALA	4.43THR	145GLY	147ASN
	159PRO	159PRO	4.55THR	5.44ILE		5.53VAL	3.27ILE	5.41TYR	5.40VAL	4.44VAL	146LEU	160ALA
	160ALA	160ALA	4.58CYS	5.45VAL		5.56LEU	3.31LEU	5.44ILE	5.41TYR	4.47SER	158ASN	5.38PHE
	5.40VAL	5.40VAL	4.59PRO	5.48TYR		5.57VAL	117ARG	5.45VAL	5.44ILE	4.50TRP	160ALA	5.41TYR
	5.41TYR	5.41TYR	L44PHE(ECL2)	5.49VAL		5.60LYS	118TYR	5.48TYR	5.45VAL	4.51VAL	5.38PHE	5.42SER
	5.44ILE	5.44ILE	145GLY	5.52ILE		6.59ILE	121LYS	5.49VAL	5.48TYR	4.54PHE	5.41TYR	5.45VAL
	5.45VAL	5.45VAL	146LEU	5.53VAL		248HIS	4.40ARG	5.52ILE	5.49VAL	4.55THR	5.45VAL	5.49VAL
	5.48TYR	5.48TYR	5.41TYR	5.56LEU			4.43THR	5.53VAL	5.52ILE	4.58CYS	5.49VAL	5.53VAL
	5.49VAL	5.49VAL	5.44ILE	5.60LYS			4.47SER	5.56LEU	5.53VAL	4.59PRO	5.53VAL	5.56LEU
	5.52ILE	5.52ILE	5.45VAL	5.64VAL			4.50TRP	5.60LYS	5.56LEU	4.61LEU		5.57VAL
	5.53VAL	5.53VAL	5.49VAL	5.67ARG			4.51VAL	5.63ILE	5.57VAL	L44PHE(ECL2)		5.60LYS
	5.56LEU	5.56LEU	5.52ILE	5.68ARG			4.54PHE	5.64VAL	5.60LYS	8.53ILE		
	5.60LYS	6.59ILE	5.53VAL				4.58CYS	5.67ARG	5.67ARG	8.55HIS		
	6.59ILE	248HIS	5.56LEU				4.61LEU	5.68ARG	5.68ARG	8.56CYS		
	248HIS						144PHE	5.70LYS	5.71ARG			
							145GLY	5.71ARG	6.56ILE			
							8.53ILE	5.74THR	6.59ILE			
							8.55HIS		248HIS			
							8.56CYS					

Green residues: Residues predicted by PRODIGY + part Green residues: predicted by PRODIGY + part of SASA-based original interface
Orange residues: Residues predicted only by PRODIGY
Purple residues: Residues only part of SASA-based original interface

Table S6. Key residues and unique residues of the original interface determined by solvent accessible surface area (SASA).

Dimer	Inactive-Inactive		Active-Active		Arrestin-Arrestin		Active-Inactive		Inactive-Arrestin		Active-Arrestin	
Interface	TM4-TM5-TM4-TM5		TM4-TM5-TM4-TM5		TM4-TM5-TM4-TM5		TM1-TM2-TM4-TM5		TM3-TM4-TM4-TM5		TM4-TM5-TM4-TM5	
Monomer	A	B	A	B	A	B	A	B	A	B	A	B
Template	6CM4	6CM4	6VMS	6VMS	6U1N	6U1N	6VMS	6CM4	6CM4	6U1N	6VMS	6U1N
	3.48ILE	3.48ILE	110MET	3.55ALA	4.40ARG	4.59PRO	1.51VAL	3.51TYR	3.48ILE	1.51VAL	110MET	3.48ILE
	3.51TYR	3.51TYR	113LEU	110MET	4.44VAL	160ALA	1.54CYS	3.55ALA	3.51TYR	1.55MET	113LEU	3.52THR
	3.52THR	3.52THR	118TYR	112MET	4.48ILE	5.38PHE	1.55MET	110MET	3.52THR	1.58SER	116THR	110MET
	3.55ALA	3.55ALA	119SER	113LEU	4.51VAL	5.40VAL	1.58SER	111PRO	3.55ALA	1.59ARG	118TYR	113LEU
	110MET	110MET	4.40ARG	118TYR	4.52LEU	5.41TYR	1.59ARG	112MET	4.40ARG	35LYS	119SER	117ARG
	111PRO	111PRO	4.44VAL	119SER	4.55THR	5.44ILE	35LYS	113LEU	4.41ARG	38GLN	4.40ARG	4.41ARG
	120SER	4.40ARG	4.47SER	4.40ARG	4.56ILE	5.48TYR	38GLN	114TYR	4.44VAL	2.48VAL	4.44VAL	4.45MET
	4.40ARG	4.41ARG	4.48ILE	4.44VAL	4.59PRO	5.49VAL	2.41TYR	115ASN	4.47SER	2.51LEU	4.51VAL	4.48ILE
	4.41ARG	4.44VAL	4.51VAL	4.48ILE	160ALA	5.52ILE	2.48VAL	4.41ARG	4.48ILE	2.52LEU	4.52LEU	4.51VAL
	4.44VAL	4.47SER	4.52LEU	4.51VAL	5.38PHE	5.56LEU	2.52LEU	4.44VAL	4.51VAL	2.56LEU	4.55THR	4.52LEU
	4.48ILE	4.48ILE	4.54PHE	4.52LEU	5.41TYR	5.60LYS	2.55THR	4.48ILE	4.52LEU	75SER	4.58CYS	4.54PHE
	4.51VAL	4.51VAL	4.55THR	4.55THR	5.45VAL	248HIS	2.56LEU	4.52LEU	4.55THR	3.23ILE	4.59PRO	4.55THR
	4.52LEU	4.52LEU	4.59PRO	4.56ILE			3.23ILE	4.55THR	4.59PRO	3.27ILE	144PHE	4.56ILE
	4.55THR	4.55THR	144PHE	4.58CYS			3.24HIS	4.58CYS	146LEU	3.30THR	146LEU	4.58CYS
	4.59PRO	4.56ILE	145GLY	4.59PRO			3.27ILE	4.59PRO	147ASN	121LYS	158ASN	4.59PRO
	146LEU	4.59PRO	146LEU	5.41TYR			117ARG	147ASN	148ASN	4.43THR	160ALA	144PHE
	147ASN	146LEU	5.41TYR	5.44ILE			118TYR	160ALA	160ALA	4.47SER	5.38PHE	146LEU
	159PRO	147ASN	5.44ILE	5.45VAL			121LYS	5.40VAL	5.40VAL	4.50TRP	5.41TYR	147ASN
	160ALA	160ALA	5.45VAL	5.48TYR			4.40ARG	5.41TYR	5.41TYR	4.51VAL	5.45VAL	5.38PHE
	5.40VAL	5.40VAL	5.49VAL	5.49VAL			4.43THR	5.44ILE	5.44ILE	4.54PHE	5.49VAL	5.41TYR
	5.41TYR	5.41TYR	5.53VAL	5.52ILE			4.47SER	5.45VAL	5.45VAL	4.55THR	5.53VAL	5.45VAL
	5.44ILE	5.44ILE		5.53VAL			4.51VAL	5.48TYR	5.49VAL	4.58CYS		5.49VAL
	5.45VAL	5.45VAL		5.56LEU			4.54PHE	5.49VAL	5.52ILE	4.59PRO		5.53VAL
	5.49VAL	5.49VAL					4.58CYS	5.52ILE	5.53VAL	144PHE		
	5.52ILE	5.52ILE					4.61LEU	5.53VAL	5.56LEU	8.53ILE		
	5.53VAL	5.53VAL					144PHE	5.56LEU	5.60LYS	8.56CYS		
	5.56LEU	5.56LEU					145GLY	5.60LYS	5.67ARG			
		6.59ILE						5.63ILE	6.56ILE			
								5.64VAL	6.59ILE			
								5.67ARG	248HIS			
								5.71ARG				

Green: Very frequent residues (8-12x)
Orange: Moderate frequent residues (3-7x)
Pink: Rare residues (1-2x)